# ENGINEERING BEHAVIOUR OF THANET SAND

by

KONSTANTINOS VENTOURAS

Supervised by:

Dr Matthew R. Coop

October 2005

A thesis submitted to the University of London

(Imperial College of Science, Technology & Medicine)

In partial fulfilment of the requirements for the degree of

Doctor of Philosophy in the Faculty of Engineering

# ABSTRACT

Thanet sand is a soil stratum that lies deep enough within the central London area not to have been the topic of extensive research to date, as most foundation works, foundation designs and tunnels have mainly been focused on the London Clay stratum. Recently, as buildings and construction works in general tend to get bigger and heaver and as tunnelling techniques are constantly being improved, Thanet sand has attracted increasingly larger scientific interest.

The research programme primarily consisted of an extensive series of triaxial tests. Most of the intact samples available were rotary cored and the rest were extracted using block sampling. Intact samples were compared with reconstituted sample formed in the lab in an attempt to locate and quantify the effect of structure within Thanet sand. Additionally, by cutting samples in different directions from the extracted block, the effects of anisotropy within the soil were also examined.

To run these tests, three different triaxial cells were used out of which one was modified with pressure multipliers. This, along with some previously conducted experiments, allowed the full stress range to be covered from a starting effective pressure of 125kPa till 20MPa. It had previousely been suggested by others that Thanet sand could be divided into two sub-strata based on its particle size distribution curves as well as based on findings from insitu testing and large scale on-site pile tests. The work in this Thesis has established that two parallel CSLs, one per sub-stratum, can been found which has a significant influence on its behaviour in laboratory tests and in-situ. Thanet sand was shown to be a cross-anisotropic material with a distinct effect of structure, even though the soil is neither cemented nor does it have a locked fabric.

# ACKNOWLEDGEMENTS

Firstly and primarily I would like to thank my supervisor, Dr M. Coop for his guidance, contribution, encouragement but mostly for his endless patience when it came to experiment and/or equipment failures and draft corrections. One of the greatest assets of a PhD student is knowing that his supervisor is there for him and can, in most cases, be contacted if any consulting/support is needed.

I would also like to thank the staff and research group of Imperial College soil mechanics section for their support.

I would also like to thank my parents who funded and supported me during the course of the PhD.

Special thanks to A. Qadimi, P. Ferreira, L. Gasparre, R. Monroy, A. Takahashi, S. Nishimura and A. Jotisankasa who apart from valuable colleagues were great friends.

Last but not least, I would like to express my gratitude to anyone that should be here and has been forgotten and left out. This has certainly been a great experience.

# TABLE OF CONTENTS

ABSTRACT ..... i

ACKNOWLEDGEMENTS ..... ii

TABLE OF CONTENTS ..... iii

LIST OF FIGURES ..... vi

LIST OF TABLES ..... xix

LIST OF SYMBOLS AND ABBREVIATIONS ..... xx

1 INTRODUCTION ..... 1

1.1 Background of the Research ..... 1

1.2 Objectives ..... 1

1.3 Thesis Structure ..... 2

2 LITERATURE REVIEW ..... 4

2.1 Introduction ..... 4

2.2 Compression Behaviour Of Sands ..... 4

2.3 Monotonic Shearing Behaviour Of Sands ..... 5

2.3.1 Monotonic shearing of sands ..... 6

2.3.2 Effects of structure ..... 11

2.3.3 Yielding of sands ..... 15

2.3.4 Sample barrelling and strain localisation ..... 16

2.4 Anisotropy ..... 17

2.4.1 Anisotropy subdivisions ..... 18

2.4.2 Effects of α and b in soil response ..... 19

2.5 Particle Breakage ..... 19

2.6 State Concept For Sands ..... 21

3 APPARATUS DESCRIPTION & PROCEDURES ..... 67

3.1 Bishop & Wesley Triaxial Cell And Instrumentation ..... 67

3.1.1 General structure ..... 67

3.1.2 Measuring stresses ..... 68

3.1.3 Measuring strains ..... 69

3.1.4 Modifications to the apparatus ..... 69
3.2 High Pressure Triaxial Cell And Instrumentation ..... 70
3.2.1 General structure ..... 70
3.2.2 Measuring stresses ..... 71
3.2.3 Measuring strains ..... 72
3.2.4 Bender elements ..... 72
3.3 100mm Triaxial Cell And Instrumentation ..... 73
3.3.1 General structure ..... 73
3.3.2 Measuring stresses ..... 75
3.3.3 Measuring strains ..... 75
3.3.4 Bender elements ..... 76
3.4 Test Procedures ..... 76
3.4.1 Sample preparation – Intact cored samples ..... 76
3.4.2 Sample preparation – Intact block samples ..... 78
a) Block sample extraction in CTRL tunnel at Stratford ..... 78
b) Laboratory triaxial sample preparation ..... 79
3.4.3 Reconstituted samples ..... 79
3.5 Test Phase Description ..... 81
3.5.1 Saturation ..... 81
3.5.2 Isotropic compression ..... 82
3.5.3 Shearing ..... 83
a) Shearing in compression ..... 83
b) Shearing in extension ..... 83
3.5.4 Y1 and Y2 probing ..... 84
3.6 Formulae Used For The Data Analysis ..... 85
3.7 Right Cylinder Assumption & Strain Localisation ..... 91
4 THANET SAND DESCRIPTION & EXPERIMENTS PERFORMED ..... 117
4.1 Thanet Sand Description & Existing Field Data ..... 117
4.2 Testing Programme And Description Of The Sand ..... 119
5 LARGE STRAIN BEHAVIOUR ..... 160
5.1 Introduction ..... 160
5.2 Isotropic Compression Behaviour ..... 160
5.3 Critical States Of Thanet Sand ..... 162
5.4 Stress – Strain Behaviour ..... 166
5.4.1 Silt content effect ..... 166
5.4.2 Intact – reconstituted effect ..... 168
5.4.3 Glauconite effect ..... 171
5.4.4 Influence of effective confining stress ..... 171
5.4.5 Influence of site location ..... 173
5.5 Normalised Stress Paths ..... 173

5.6 Influence Of Anisotropy ..... 175
5.6.1 Drained compression tests ..... 175
5.6.2 Undrained compression tests ..... 176
5.6.3 Drained extension tests ..... 177
5.6.4 Overview ..... 177
5.7 Particle Breakage ..... 179
5.8 Pile And Pressuremeter Test Data ..... 180
6 SMALL STRAIN BEHAVIOUR ..... 227
6.1 Introduction ..... 227
6.2 Bender Element Tests – Dynamic Shear Moduli ..... 227
6.3 Equivalent Monotonic Shear Moduli ..... 229
6.3.1 Trends ..... 229
6.3.2 Silt content effect ..... 230
6.3.3 Intact – reconstituted effect ..... 231
6.3.4 Glauconite effect ..... 233
6.3.5 Material Anisotropy ..... 233
6.4 Stiffness – Influence of Effective Confining Stress ..... 235
6.5 Yielding behaviour ..... 238
7 SUMMARY, CONCLUSIONS & FURTHER RESEARCH ..... 268
7.1 Summary & Conclusions ..... 268
7.1.1 Silt Content effect ..... 268
7.1.2 Effect of structure ..... 269
7.1.3 Glauconite effect ..... 271
7.1.4 Influence of site location ..... 271
7.1.5 Anisotropy ..... 271
7.1.6 State parameter effect on stress-dilatancy ..... 273
7.2 Future Research ..... 273
REFERENCES ..... 276

# LIST OF FIGURES

Figure 2-1 Grading curves for the three sands tested by Coop & Lee (1993) ..... 24
Figure 2-2 Isotropic compression & critical state data for three sands (after Coop & Lee, 1993) ..... 25
Figure 2-3 $K_0$ compression for Dogs Bay sand (after Coop & Lee, 1993) ..... 25
Figure 2-4 Measurements of $G_0$ for Dogs Bay Sand (after Jovicic & Coop, 1997) ..... 26
Figure 2-5 $G_0$ on the NCL for various sands (after Jovicic & Coop, 1999) ..... 26
Figure 2-6 Critical state and normal compression lines for various sands (after Cuccovillo & Coop, 1999). ..... 27
Figure 2-7 Typical stress-strain behaviour of Dogs Bay sand (after Coop, 1990) 27
Figure 2-8 Critical States for Dogs Bay Sand (after Coop, 1990) ..... 28
Figure 2-9 Effects of incomplete testing on the identification of the CSL (after Coop, 1999) ..... 28
Figure 2-10 Curvature of the CSL at lower confining stresses for Leighton Buzzard sand (after Klotz & Coop, 2001) ..... 29
Figure 2-11 Schematic diagram illustrating CSL and NCL over the full range of stresses (after Coop, 1999) ..... 29
Figure 2-12 Stress-strain behaviour of Toyoura sand in triaxial tests ($\sigma_0$'=0.1MPa) (after Verdugo & Ishihara, 1996) ..... 30
Figure 2-13 Stress-strain behaviour of Toyoura sand in triaxial tests ($\sigma_0$'=0.5MPa) (after Verdugo & Ishihara, 1996) ..... 30
Figure 2-14 State diagram for Toyoura sand evaluated from both drained and undrained tests (after Verdugo & Ishihara, 1996) ..... 31
Figure 2-15 Isotropic compression curves for Toyoura sand samples prepared using three different methods (after Verdugo & Ishihara, 1996) ..... 31
Figure 2-16 Effect on sample preparation on critical states (after Been et al., 1991) ..... 32

Figure 2-17 Effect of stress path on critical state of Erksak 330/07 sand (after Been et al., 1991) ..... 32
Figure 2-18 Effect of stress path on critical states of Toyoura sand (after Been et al., 1991) ..... 33
Figure 2-19 Isotropic compression of reconstituted carbonate sand samples with and without fines (after Coop & Atkinson, 1993) ..... 33
Figure 2-20 Ultimate failure of uncemented and cemented samples of carbonate sands (after Coop & Atkinson, 1993) ..... 34
Figure 2-21 Definition of normalizing parameters ..... 34
Figure 2-22 Normalised shearing data for three sands (after Coop & Lee, 1993) 35
Figure 2-23 Stress dilatancy data for Dogs Bay sand (after Coop, 1990) ..... 35
Figure 2-24 Development of stress ratio with dilatancy for sand with different confining pressures (after Yang and Li, 2004) ..... 36
Figure 2-25 Development of stress ratio with dilatancy for sand with different densities (after Yang and Li, 2004) ..... 36
Figure 2-26 Experimental data for stress-dilatancy relationship (data from Verdugo and Ishihara, 1996) (after Yang and Li, 2004) ..... 37
Figure 2-27 Undrained tests on Dogs Bay sand (after Coop, 1990) ..... 38
Figure 2-28 Correlation between voids ratio and age of material (after Coop, 2003 using data from Barton & Palmer, 1989) ..... 38
Figure 2-29 Inter-particle cementing of a Rankin calcarenite (after Coop, 2003) 39
Figure 2-30 Particle interlocking and inter-particle cementing of Lower Greensand (after Coop, 2003) ..... 39
Figure 2-31 Compression data for Rankin calcarenite (after Cuccovillo & Coop, 1999) ..... 40
Figure 2-32 Compression data for Lower Greensand (after Cuccovillo & Coop, 1999) ..... 40
Figure 2-33 Comparison between the shear moduli of intact and reconstituted silica sandstone (after Cuccovillo & Coop, 1997) ..... 41
Figure 2-34 Comparison between stress-dilatancy relationships of intact and reconstituted silica sandstone samples (after Cuccovillo & Coop, 1999) ..... 41
Figure 2-35 Influence of state on dilatancy for the intact and reconstituted silica sandstone (a) using the same CSL (b) using an offset CSL for the intact soil (after Cuccovillo & Coop, 1999) ..... 42

Figure 2-36 Typical stress: strain data for an intact sample of Reigate silver sand at an effective cell pressure of 50kPa (after Cresswell & Powrie, 2004) ..... 43
Figure 2-37 Typical stress: strain data for an intact sample of Reigate silver sand at an effective cell pressure of 200kPa (after Cresswell & Powrie, 2004) ... 43
Figure 2-38 Rate of dilation d, at the maximum stress ratio, $\eta_{max}$, for tests on both intact and pluviated A4 sand at different cell pressures (after Cresswell & Powrie, 2004) ..... 44
Figure 2-39 Shear modulus G and volumetric strain $\varepsilon_{vol}$ plotted against average local axial strain for intact and pluviated samples of A4 sand (effective cell pressure 100kPa) (after Cresswell & Powrie, 2004) ..... 44
Figure 2-40 Stress-strain behaviour prior to and after grout injection (after Dano & Hicher, 2003) ..... 45
Figure 2-41 Stress-strain relationships for drained triaxial compression tests of natural and reconstituted sands (after Mimura, 2003) ..... 46
Figure 2-42 Angles of shearing resistance for three sands (after Mimura, 2003). 46
Figure 2-43 Axial strain - volumetric strain behaviour for four natural Japanese sands (after Mimura, 2003) ..... 47
Figure 2-44 Normalised shearing data for a reservoir sand (after Coop & Wilson, 2003) ..... 48
Figure 2-45 Normalised shearing behaviour for Rankin calcarenite at lower stress levels (after Cuccovillo & Coop, 1999) ..... 48
Figure 2-46 Normalised shearing behaviour for Rankin calcarenite at higher stress levels (after Cuccovillo & Coop, 1999) ..... 49
Figure 2-47 Normalised shearing data for Greensand (after Cuccovillo & Coop, 1999) ..... 49
Figure 2-48 Multiple sub-yield surfaces and plastic strain increment vectors for anisotropically consolidated loose HRS (OCR=1.3) (after Kuwano, 1999). 50
Figure 2-49 Multiple sub-yield surfaces and plastic strain increment vectors for isotropically consolidated loose HRS (OCR=2) (after Kuwano, 1999)..... 51
Figure 2-50 Right cylinder assumption..... 52
Figure 2-51 Details of the lubricated end platens (adapted from Head (1985), by Klotz (2000) and Qadimi (2004)) ..... 52
Figure 2-52 Effects of strain localisation (after Klotz and Coop, 2001)..... 53

Figure 2-53 Dilatancy in recent and old shear bands: towards a limiting void ratio (after Desrues et al., 1991) ..... 53
Figure 2-54 Schematic of major principal stress inclination relative to the soil depositional direction ..... 54
Figure 2-55 Dependency of stress ratio at failure on α and b in isotropically consolidated HRS (OCR=1) (after Symes, 1983) ..... 54
Figure 2-56 Effect of b on the stress-strain response of isotropically consolidated medium-loose HRS (OCR=1) (after Symes, 1983) ..... 55
Figure 2-57 Effect of b on the ultimate φ' of isotropically consolidated medium-loose HRS (OCR=1) ($\alpha = 45^0$) (after Symes, 1983) ..... 55
Figure 2-58 Influence of shearing mode and sample orientation on α and b. ..... 56
Figure 2-59 Definition of relative breakage, Br (Hardin, 1985) ..... 57
Figure 2-60 One-dimensional compression curves for uniformly and well graded sands (after Nakata et al., 2001) ..... 57
Figure 2-61 Particle breakage for isotropically compressed and sheared samples of three sands (after Coop & Lee, 1993) ..... 58
Figure 2-62 Particle breakage for compacted and overconsolidated samples of decomposed granite (after Lee & Coop, 1993) ..... 58
Figure 2-63 Compression curves for petroleum coke (after McDowell & Bolton, 1998) ..... 59
Figure 2-64 Evolving particle breakage for petroleum coke (after McDowell & Bolton, 1998) ..... 59
Figure 2-65 Evolving particle size distribution curves for one-dimensionally compressed Ottawa sand (after Fukumoto, 1992) ..... 60
Figure 2-66 Evolving particle size distributions for ring shear tests on Dogs Bay sand with $\sigma_v$ in range 650-930 kPa (after Coop et al., 2004) ..... 60
Figure 2-67 Particle breakage for ring shear tests on Dogs Bay sand in stress range 650-930 kPa (after Coop et al., 2004) ..... 61
Figure 2-68 Volumetric strain behaviour with increasing levels of shear strain for ring shear tests on Dogs Bay sand (after Coop et al., 2004) ..... 61
Figure 2-69 Schematic showing the influence of state (after Qadimi, 2005) ..... 62
Figure 2-70 Definition of State parameters (after Klotz & Coop, 2001) ..... 62

Figure 2-71 Normalised CPT data for three different sands (after Been et al., 2001) ..... 63
Figure 2-72 Unit base resistance during pile installation (a) Leighton Buzzard sand, (b)Dogs Bay sand (after Klotz & Coop, 2001) ..... 64
Figure 2-73 Normalised base resistance for (a) Leighton Buzzard sand using a non-linear CSL, (b) Leighton Buzzard sand using a linear CSL, (c)Dogs Bay sand (after Klotz & Coop, 2001) ..... 65
Figure 2-74 Peak dilation rate as a function of: (a) state parameter; (after Been & Jefferies, 1986) (b) Normalised state parameter for several sands (after Konrad, 1988) ..... 66
Figure 2-75 DMT test results on Ottawa sand in terms of normalised state parameter (after Konrad, 1988) ..... 66
Figure 3-1 Schematic diagram of the Bishop & Wesley (1975) triaxial cell (after Qadimi, 2005) ..... 95
Figure 3-2 Submersible load cell (after Head, 1985) ..... 96
Figure 3-3 Sources of error in external axial deformation measurements (after Burland et al., 1984) ..... 96
Figure 3-4 of electrolevel inclinometer (after Kuwano, 1999) ..... 97
Figure 3-5 Multiplier used on the Bishop & Wesley triaxial cell ..... 98
Figure 3-6 Schematic diagram of the high pressure apparatus (after Qadimi, 2005) ..... 99
Figure 3-7 The high pressure apparatus ..... 100
Figure 3-8 Motorised hydraulic pump ..... 100
Figure 3-9 Schematic diagram of the motorised hydraulic pump (after Qadimi, 2005) ..... 101
Figure 3-10 Oil submersible LVDT for measuring internal axial strains ..... 102
Figure 3-11 Oil submersible LVDT for directly measuring internal radial strains on the high pressure triaxial apparatus (after Qadimi, 2005) ..... 102
Figure 3-12 Bender element equipment setup on the high pressure system (after Qadimi, 2005) ..... 103
Figure 3-13 Schematic diagram of the bender elements (after Jovicic, 1997).... 104
Figure 3-14 Measurement of the arrival time from the screen of the oscilloscope (after Jovicic, 1997) ..... 104
Figure 3-15 Hydraulic triaxial cell for 100mm diameter samples ..... 105

Figure 3-16 Mid-height pore pressure probe (after Hight, 1983) ..... 105
Figure 3-17 Axial LVDT with adjustable screw (after Rolo, 2003) ..... 106
Figure 3-18 Schematic diagram of the lateral bender elements (after Gasparre, 2005) ..... 106
Figure 3-19 Borehole log - map of area & list of boreholes (after Soil Mechanics, 2003) ..... 107
Figure 3-20 Borehole log - 0.00 to 9.80m (after Soil Mechanics, 2003) ..... 108
Figure 3-21 Borehole log - 10.00 to 20.00m (after Soil Mechanics, 2003) ..... 109
Figure 3-22 Borehole log - 20.00 to 30.00m (after Soil Mechanics, 2003) ..... 110
Figure 3-23 Borehole log - 30.00 to 40.50m (after Soil Mechanics, 2003) ..... 111
Figure 3-24 Borehole log - 40.50 to 46.50m (after Soil Mechanics, 2003) ..... 112
Figure 3-25 Block sample being trimmed ..... 113
Figure 3-26 Sample cut to correct dimensions ..... 113
Figure 3-27 Block sample wrapped in cling film & wax ..... 113
Figure 3-28 Voids between sample and box filled with expansive foam ..... 113
Figure 3-29 Top of box end sealed ..... 113
Figure 3-30 Block samples left for foam to set ..... 113
Figure 3-31 Directions of samples extracted from sand blocks ..... 114
Figure 3-32 Typical Thanet sand in-situ conditions ..... 115
Figure 3-33 Y1 and Y2 selected probe directions ..... 116
Figure 4-1 Back analysed Nq* against pile base penetration into Thanet sand (after Nicholson et al., 2002) ..... 126
Figure 4-2 Corrected SPT "N" values (after Nicholson et al., 2002) ..... 126
Figure 4-3 Calculated Nq* versus height above Chalk at Heron Quays (after ARUP Geotechnics) ..... 127
Figure 4-4 Pressuremeter results for Thanet sand (after Nicholson et al., 2002) 128
Figure 4-5 Conductivity versus depth from top of Thanet sand at Heron Quays (after ARUP Geotechnics) ..... 129
Figure 4-6 Resistivity versus depth at North Quay (after after Nicholson et al., 2002) ..... 130
Figure 4-7 Conductivity data for Thanet sand (after Pascal, 2002 – personal communication) ..... 131
Figure 4-8 Comparison of resistivity and SPT N at Heron Quays (after ARUP Geotechnics) ..... 132

Figure 4-9 Comparison of Gamma ray and conductivity logs at Heron Quays (after ARUP Geotechnics) ..... 133
Figure 4-10 Wireline conductivity measurements at Heron Quays. (after ARUP Geotechnics) ..... 134
Figure 4-11 Comparison of fines content with conductivity at Heron Quays (after ARUP Geotechnics) ..... 135
Figure 4-12 Map of the four sites within London ..... 136
Figure 4-13 Particle size distribution curves for all available sites ..... 137
Figure 4-14 Glauconite extracted from high silt content Thanet sand ..... 138
Figure 4-15 Thin section of intact Thanet sand under plain transmitted light ..... 139
Figure 4-16 Thin section of intact Thanet sand under cross-polarised light ..... 139
Figure 4-17 Isotropic Compression data for Millennium Tower ..... 140
Figure 4-18 Isotropic Compression data for Moore House ..... 140
Figure 4-19 Isotropic Compression data for Moore House ..... 141
Figure 4-20 Isotropic Compression data for River Side ..... 141
Figure 4-21 Isotropic Compression data for River Side ..... 142
Figure 4-22 Isotropic Compression data for River Side ..... 142
Figure 4-23 Isotropic Compression data for River Side ..... 143
Figure 4-24 Isotropic Compression data for River Side ..... 143
Figure 4-25 Isotropic Compression data for CTRL Stratford ..... 144
Figure 4-26 Isotropic Compression data for CTRL Stratford ..... 144
Figure 4-27 Isotropic Compression data for CTRL Stratford ..... 145
Figure 4-28 Isotropic Compression data for undrained experiments ..... 145
Figure 4-29 Isotropic Compression data for extension tests ..... 146
Figure 4-30 Stress-strain data for Millennium Tower ..... 147
Figure 4-31 Volumetric strain Data for Millennium Tower ..... 147
Figure 4-32 Stress-strain data for Moore House ..... 148
Figure 4-33 Volumetric strain data for Moore House ..... 148
Figure 4-34 Stress-strain data for Moore House ..... 149
Figure 4-35 Volumetric strain data for Moore House ..... 149
Figure 4-36 Stress-strain data for Rive Side ..... 150
Figure 4-37 Volumetric strain data for River Side ..... 150
Figure 4-38 Stress-strain data for River Side ..... 151
Figure 4-39 Volumetric strain data for River Side ..... 151

Figure 4-40 Stress-strain data for River Side ..... 152
Figure 4-41 Volumetric strain data for River Side ..... 152
Figure 4-42 Stress-strain data for River Side ..... 153
Figure 4-43 Volumetric strain data for River Side ..... 153
Figure 4-44 Stress-strain data for River Side ..... 154
Figure 4-45 Volumetric strain data for River Side ..... 154
Figure 4-46 Stress-strain data for CTRL Stratford ..... 155
Figure 4-47 Volumetric strain data for CTRL Stratford ..... 155
Figure 4-48 Stress-strain data for CTRL Stratford ..... 156
Figure 4-49 Volumetric strain data for CTRL Stratford ..... 156
Figure 4-50 Stress-strain data for CTRL Stratford ..... 157
Figure 4-51 Volumetric strain data for CTRL Stratford ..... 157
Figure 4-52 Stress-strain data for all undrained tests ..... 158
Figure 4-53 Pore pressure response for all undrained tests ..... 158
Figure 4-54 Stress-strain data for both extension tests ..... 159
Figure 4-55 Volumetric strain data for both extension tests ..... 159
Figure 5-1 High/low silt content comparison for isotropic compression of the intact material ..... 183
Figure 5-2 High/low silt content comparison for isotropic compression of the reconstituted material ..... 183
Figure 5-3 Sample type comparison for isotropic compression of high silt content material (rotary cored sample from River Side) ..... 184
Figure 5-4 Sample type comparison for isotropic compression of high silt content material (block sample from CTRL Stratford) ..... 184
Figure 5-5 Sample type comparison for isotropic compression of low silt content material (rotary cored sample from River Side) ..... 185
Figure 5-6 Effect of sampling method on isotropic compression of high silt content material ..... 185
Figure 5-7 Extrapolation of volumetric strains to a Critical State for test CTRL1 ..... 186
Figure 5-8 Critical States – high/low silt content comparison ..... 187
Figure 5-9 Identification of critical state lines for high and low silt content material ..... 187
Figure 5-10 Site comparison for high silt content material ..... 188

Figure 5-11 Site comparison for low silt content material ..... 188
Figure 5-12 Sample type comparison for critical states of high silt material ..... 189
Figure 5-13 Sample type comparison for critical states of low silt content ..... 189
Figure 5-14 High/low silt content comparison for critical states in the q-p' plane ..... 190
Figure 5-15 Site comparison for critical states in the q-p' plane ..... 190
Figure 5-16 Sample type comparison for critical states in the q-p' plane ..... 191
Figure 5-17 Sample type comparison for critical states in the q-p' plane including the chosen CSL ..... 191
Figure 5-18 High/low silt content comparison for stress:strain behaviour of intact material ..... 192
Figure 5-19 High/low silt content comparison for volumetric strain behaviour of intact material ..... 192
Figure 5-20 High/low silt comparison for stress:dilatancy of intact material ..... 193
Figure 5-21 High/low silt comparison for stress:strain behaviour of reconstituted material ..... 194
Figure 5-22 High/low silt content comparison for volumetric strain behaviour of reconstituted material ..... 194
Figure 5-23 High/low silt comparison for stress:dilatancy of reconstituted material ..... 195
Figure 5-24 Sample type comparison for stress:strain behaviour of high silt content material ..... 196
Figure 5-25 Sample type comparison for volumetric strain behaviour of high silt content material ..... 196
Figure 5-26 Sample type comparison for stress:dilatancy of high silt content material ..... 197
Figure 5-27 Sample type comparison for stress:strain behaviour of high silt content material ..... 198
Figure 5-28 Sample type comparison for volumetric strain behaviour of high silt content material ..... 198
Figure 5-29 Sample type comparison for stress:dilatancy of high silt content material ..... 199
Figure 5-30 Sample type comparison for stress:strain behaviour of low silt content material ..... 200

Figure 5-31 Sample type comparison for volumetric strain behaviour of low silt content material ..... 200
Figure 5-32 Sample type comparison for stress:dilatancy of low silt content material ..... 201
Figure 5-33 Glauconite effect for stress:strain behaviour of high silt content material ..... 202
Figure 5-34 Glauconite effect for volumetric strain behaviour of high silt content material ..... 202
Figure 5-35 Glauconite effect for stress:dilatancy behaviour of high silt content material ..... 203
Figure 5-36 Influence of effective confining stress on stress:strain behaviour – intact low silt content samples ..... 204
Figure 5-37 Influence of effective confining stress on volumetric strain behaviour – intact low silt content samples ..... 204
Figure 5-38 Influence of effective confining stress on stress:strain behaviour – reconstituted low silt content samples ..... 206
Figure 5-39 Influence of effective confining stress on volumetric strain behaviour – reconstituted low silt content samples ..... 206
Figure 5-40 Influence of effective confining stress on stress:dilatancy relationship for reconstituted low silt content samples ..... 207
Figure 5-41 Influence of effective confining stress on stress:strain behaviour – intact high silt content samples ..... 208
Figure 5-42 Influence of effective confining stress on volumetric strain behaviour – intact high silt content samples ..... 208
Figure 5-43 Influence of effective confining stress on stress:dilatancy relationship for intact high silt content samples ..... 209
Figure 5-44 Influence of effective confining stress on stress:strain behaviour – reconstituted high silt content samples ..... 210
Figure 5-45 Influence of effective confining stress on volumetric strain behaviour – reconstituted high silt content samples ..... 210
Figure 5-46 Influence of effective confining stress on stress:dilatancy relationship for reconstituted high silt content samples ..... 211
Figure 5-47 Effect of site location on stress:strain behaviour ..... 212
Figure 5-48 Effect of site location on volumetric strain behaviour ..... 212

Figure 5-49 Effect of site location on stress:dilation behaviour ..... 213
Figure 5-50 Effect of sample type on normalised stress paths for high silt content material ..... 214
Figure 5-51 Effect of sampling method on normalised stress paths for high silt content material ..... 214
Figure 5-52 Effect of sample type on normalised stress paths for low silt content material ..... 215
Figure 5-53 Effect of glauconite on normalised stress paths for high silt content material ..... 215
Figure 5-54 Effect of site location on normalised stress paths for high silt content material ..... 216
Figure 5-55 Effect of site location on normalised stress paths for low silt content material ..... 216
Figure 5-56 Effect of silt content on normalised stress paths ..... 217
Figure 5-57 Effect of silt content on normalised stress path space – State Boundary Surface ..... 217
Figure 5-58 Influence of anisotropy on stress:strain behaviour of drained tests 218
Figure 5-59 Influence of anisotropy on volumetric strain behaviour ..... 218
Figure 5-60 Effect of anisotropy on stress:dilatancy behaviour ..... 219
Figure 5-61 Influence of anisotropy on stress:strain behaviour of undrained tests ..... 220
Figure 5-62 Influence of anisotropy on generated pore pressure behaviour..... 220
Figure 5-63 Effect of anisotropy – all compression tests..... 221
Figure 5-64 Influence of anisotropy –extension tests plotted with external strains ..... 222
Figure 5-65 Influence of anisotropy –extension tests plotted with internal strains ..... 222
Figure 5-66 Influence of anisotropy –extension tests plotted with external strains ..... 223
Figure 5-67 Influence of anisotropy –extension tests plotted with external strains ..... 223
Figure 5-68 Material anisotropy comparison – all tests..... 224
Figure 5-69 Particle breakage – high silt content soil (experiment RS5) ..... 225
Figure 5-70 Particle breakage – low silt content soil (Experiment RS1)..... 225

Figure 5-71 Comparison of normalised pile end bearing capacities with trends from Klotz & Coop (2001) ..... 226
Figure 5-72 Normalised Limit Pressures ..... 226
Figure 6-1 Effect of structure – Cored sample – High Silt content material ..... 241
Figure 6-2 Effect of structure – Cored sample – Low Silt content material ..... 241
Figure 6-3 Effect of structure – Block sample – High silt content material ..... 242
Figure 6-4 Effect of structure – All bender element results ..... 243
Figure 6-5 Effect of structure –Bender element results with trends ..... 243
Figure 6-6 Shear modulus trend for RS1 ..... 244
Figure 6-7 Shear modulus trend for RS2 ..... 244
Figure 6-8 Shear modulus trend for RS5 ..... 245
Figure 6-9 Shear modulus trend for RS9 ..... 245
Figure 6-10 Shear modulus trend for RS10 ..... 246
Figure 6-11 Shear modulus trend for CTRL16 ..... 246
Figure 6-12 Shear modulus trend for CTRL17 ..... 247
Figure 6-13 Shear modulus trend for CTRL4 ..... 247
Figure 6-14 Shear modulus trend for CTRL6 ..... 248
Figure 6-15 Shear modulus trend for CTRL10 ..... 248
Figure 6-16 Shear modulus trend for CTRL11 ..... 249
Figure 6-17 Shear modulus trend for CTRL12 ..... 249
Figure 6-18 Shear modulus trend for CTRL15 ..... 250
Figure 6-19 High/low silt content comparison of stiffness for intact (cored) material ..... 251
Figure 6-20 High/low silt content comparison of stiffness for reconstituted material ..... 251
Figure 6-21 Sample type comparison of stiffness for a high silt content cored sample ..... 252
Figure 6-22 Sample type comparison of stiffness for a high silt block sample .. 252
Figure 6-23 Sample type comparison for stiffness of low silt cored sample ..... 253
Figure 6-24 Glauconite effect on stiffness for High silt content material ..... 253
Figure 6-25 Material anisotropy comparison – Drained Compression tests ..... 254
Figure 6-26 Material anisotropy comparison – Undrained Compression tests ... 254
Figure 6-27 Material anisotropy comparison – Drained Extension tests ..... 255
Figure 6-28 Monotonic shear moduli @ 0.01% $\varepsilon_s$ – Silt content comparison .... 256

Figure 6-29 Monotonic shear moduli @ 0.01% $\varepsilon_s$ – Silt content comparison – dynamic and monotonic stiffness trends added ..... 256
Figure 6-30 Monotonic shear moduli @ 0.1% $\varepsilon_s$ – Silt content comparison..... 257
Figure 6-31 Monotonic shear moduli @ 0.1% $\varepsilon_s$ – Silt content comparison - dynamic and monotonic stiffness trends added ..... 257
Figure 6-32 Monotonic shear moduli @ 0.1% $\varepsilon_\varsigma$ and 0.01% $\varepsilon_s$ – Silt content comparison - dynamic and monotonic stiffness trends added ..... 258
Figure 6-33 Monotonic shear moduli @ 0.01% $\varepsilon_s$ – Sample type comparison .. 259
Figure 6-34 Monotonic shear moduli @ 0.01% $\varepsilon_s$ – Sample type comparison - dynamic and monotonic stiffness trends added ..... 259
Figure 6-35 Monotonic shear moduli @ 0.1% $\varepsilon_s$ – Sample type comparison .... 260
Figure 6-36 Monotonic shear moduli @ 0.1% $\varepsilon_s$ – Sample type comparison - dynamic and monotonic stiffness trends added ..... 260
Figure 6-37 Monotonic shear moduli @ 0.1% $\varepsilon_\varsigma$ and 0.01% $\varepsilon_s$ – Sample type comparison - dynamic and monotonic stiffness trends added ..... 261
Figure 6-38 Y1 location for probe A..... 262
Figure 6-39 Y1 location for probe C..... 262
Figure 6-40 Y1 location for probe E..... 263
Figure 6-41 Y1 location for probe E –Vertical Young's Modulus calculation... 263
Figure 6-42 Possible Y2 location for probe E..... 264
Figure 6-43 Y2 location for probe H..... 264
Figure 6-44 Y1 location for probe J..... 265
Figure 6-45 Y1 location for probe J–Vertical Young's Modulus calculation .... 265
Figure 6-46 Y2 location for probe J..... 266
Figure 6-47 Y2 location for probe K..... 266
Figure 6-48 Location of all Y1 points on stress-space..... 267
Figure 6-49 Location of all Y1 & Y2 pSoints on stress-space ..... 267
Figure 7-1 High pressure odometer tests – silt comparison..... 275

# LIST OF TABLES

Table 3-1 Summarizing table of approximate instrumentation accuracies ..... 93
Table 3-2 Summarizing table of approximate instrumentation resolution – 100mm apparatus (after Gasparre, 2005) ..... 94
Table 4-1 Summary table of experiments ..... 125
Table 5-1 Summary table of anisotropy influence ..... 182
Table 6-1 Summary table of Y1 & Y2 probes ..... 240

# LIST OF SYMBOLS AND ABBREVIATIONS

| | |
|---|---|
| $A_0$, $n_0$ | *Stiffness constants for a given soil as defined by Viggiani & Atkinson (1995)* |
| $A_{Current}$ | *Current sample cross-sectional area* |
| $B = \frac{\text{pore pressure increase}}{\text{cell pressure increase}} \times 100\%$ | *B-factor used to ensure sample saturation* |
| Bp | *Breakage potential (after Hardin, 1985)* |
| Br | *Relative Breakage factor (after Hardin, 1985)* |
| Bt | *Total breakage (after Hardin, 1985)* |
| $E_h$ | *Horizontal Young's Modulus* |
| $E_v$ | *Vertical Young's Modulus* |
| $G_0$ or $G_{VH}$ | *Dynamic shear modulus vertical propagation – horizontal polarisation* |
| $G_{EQ}$ | *Equivalent monotonic shear modulus* |
| $G_{HH}$ | *Dynamic shear modulus horizontal propagation – horizontal polarisation* |
| $G_{HV}$ | *Dynamic shear modulus horizontal propagation – vertical polarisation* |
| Gs | *Spesific Gravity* |
| L | *Length of triaxial sample* |
| M | *CSL gradient* |
| N | *Value of v on the NCL for p'=1 kPa* |
| $R_s = p_0' / p_{cs}'$ | *State parameter stress ratio* |
| T | *Time required for the shear wave to travel through the sample* |
| $V_0$ | *Initial sample volume at thebeginning of a certain test stage* |
| Vs | *Elastic shear wave velocity* |
| $b = \frac{\sigma_2 - \sigma_3}{\sigma_1 - \sigma_3}$ | *Intermediate stress factor* |
| $e_0$ | *Void ratio at the beginning of the test* |
| e | *Void ratio* |
| $e_{max}$ | *Maximum void ratio* |

| | |
|---|---|
| $e_{min}$ | *Minimum void ratio* |
| $e_s$ | *Void ratio at the beginning of the shearing stage* |
| g | Acceleration of gravity typically taken as $9.81 m/sec^2$ |
| $l_0$ | *Initial axial sample length at thebeginning of a certain test stage* |
| $p' = \frac{\sigma_1' + \sigma_2' + \sigma_3'}{3}$ | *Mean normal effective stress* |
| $p'_{cs}$ | *Normalising mean effective stress based on CSL* |
| $p'_e$ | *Normalising mean effective stress based on NCL* |
| $p'_p$ | *Normalising preconsolidation pressure based on NCL* |
| $p_r$ | *Reference pressure as defined by Viggiani & Atkinson (1995)* |
| $q = \sigma_1' - \sigma_3' = F/A_{Current}$ | *Deviatoric stress* |
| u or pwp | *Pore water pressure* |
| $v_0$ | *Specific Volume at the beginning of the test* |
| v | *Specific Volume* |
| $\Gamma$ | *Intercept of the CSL in v:lnp' space at p' = 1kPa* |
| $\Delta$ or $\delta$ | *symbon denoting change* |
| $\alpha$ | *Inclination of the major principal stress to the bedding plane* |
| $\gamma_b$ | *Initial sample bulk unit weight* |
| $\gamma_d$ | *Initial sample dry unit weight* |
| $\varepsilon_a = \frac{\Delta l}{l_0}$ | *Axial strain* |
| $\varepsilon_v = \frac{\Delta V}{V_0}$ | *Volumetric strain* |
| $\varepsilon_r$ | *Radial strain* |
| $\varepsilon_s = \varepsilon_a - \frac{\varepsilon_v}{3}$ | *Triaxial shear strain* |
| $\lambda$ | *NCL and CSL gradient* |
| $\nu_{vh}$ | *Vertical Poisson's Ratio* |

| | |
|---|---|
| $\nu_{hh}$ | *Horizontal Poisson's Ratio* |
| $\rho$ | *Soil Mass density* |
| $\sigma_v^{'}$ | *Vertical effective stress* |
| $\sigma_h^{'}$ | *Horizontal effective stress* |
| $\sigma_1^{'}$ | *Major principal effective stress* |
| $\sigma_2^{'}$ | *Intermediate principal effective stress* |
| $\sigma_3^{'}$ | *Minor principal effective stress* |
| $\varphi'$ | *Angle of shearing resistance* |
| $\varphi_{cs}^{'}$ | *Angle of shearing resistance ay critical state* |
| $\varphi_{peak}^{'}$ | *Peak angle of shearing resistance* |
| $\psi$ | *State parameter* |
| $\psi_N = \frac{\psi}{e_{\max} - e_{\min}}$ | *Normalised state parameter* |

| | |
|---|---|
| CRSP | *Constant rate strain pump* |
| CSL | *Critical State Line* |
| ICL | *Intrinsic Compression Line* |
| $K_0$NCL | *Normal Compression Line under $K_0$ conditions* |
| LVDT | *Linear variable differential transducer* |
| NCL | *Normal Compression Line* |
| OCR | *Overconsolidation Ratio* |

1 INTRODUCTION ..... 1

1.1 Background of the Research ..... 1

1.2 Objectives ..... 1

1.3 Thesis Structure ..... 2

# 1 INTRODUCTION

## 1.1 Background of the Research

Thanet sand is a soil stratum that lies deep enough within the central London area not to have been the topic of extensive research to date, as most foundation works, foundation designs and tunnels have mainly been focused on the London Clay stratum. Recently, as buildings and construction works in general tend to get bigger and heaver and as tunnelling techniques are constantly being improved, Thanet sand has attracted increasingly larger scientific interest.

## 1.2 Objectives

The primary aim of this research was to investigate the engineering behaviour of Thanet sand. This has been attempted by subdividing and examining separately the influencing factors on the soil's behaviour into four main groups; the effect of structure within the soil, the effect of the relative depth within the Thanet sand stratum which in turn translates into the effect of silt content within Thanet sand, the effect of site location that the specific sample tested originated from and finally, the effect of anisotropy in Thanet sand. For this purpose, a series of triaxial tests has been performed, analysed and compared, as shall be explained in detail in Chapters 4, 5 and 6. By using the critical state soil mechanics framework as a background for the analysis of these comparisons, a series of concluding remarks considering the soils behaviour has been drawn.

## *1.3 Thesis Structure*

This thesis consists of a total of seven chapters. Following the introduction which is Chapter 1, Chapter 2 contains the literature review section of the thesis where general background theory for the behaviour of sands is presented. Among the various factors discussed are the critical states of different sands, soil structure by cementation, bonding and particle interlocking, the effects of particle breakage and effective confining pressure as well as the state concept for sands.

In Chapter 3, details of the construction, layout as well as the limitations of the three triaxial cells used to run the soil experiments are presented. The preparation processes used for the formation of the different types of samples tested are explained. A full description of the testing procedures used is also given. Finally, the formulae and the assumptions used for the data analyses are also presented.

Chapter 4 consists of a description of Thanet sand coupled with a presentation of all the field data that were available to the project at the time. Also, a table with details of all tests conducted is presented. The raw data for all experiments used for the analysis are also presented at the end of the chapter in the form of isotropic compression curves, and stress-strain and volumetric strain or pore pressure change plots for shearing.

Chapter 5 presents the large strain behaviour of the soil. The chapter starts off by discussing the isotropic compression behaviour of Thanet sand and assessing the various factors affecting it. Then, the critical state behaviour of the soil is addressed and two different critical state lines of the material are derived. The stress-strain behaviour of Thanet sand is then examined and the effect of the various factors is identified. The anisotropy of the soil is also examined with a series of test comparisons. Finally, the particle breakage of Thanet sand is briefly assessed.

In Chapter 6 the small strain behaviour of Thanet sand is discussed. Again, the various factors affecting the soil's behaviour are distinguished by a series of cross-comparisons, starting from the dynamic shear moduli, in turn looking at the equivalent monotonic shear moduli and finally examining the effect of confining pressure on the soil's behaviour. The elastic parameters of the soil have also been derived and are presented at the end of this chapter.

Chapter 7 is the last chapter of the thesis. Here, conclusions of all the work that has been preformed are presented. The various factors that govern both small strain as well as the large strain behaviour of Thanet sand are summarised. The limitations the project has been faced with are also discussed. Finally, the chapter ends with a brief section on future suggested research; here, additional potential points of interest regarding the further understanding of the soil's behaviour are also presented.

2 LITERATURE REVIEW ..... 4

2.1 Introduction ..... 4

2.2 Compression Behaviour Of Sands ..... 4

2.3 Monotonic Shearing Behaviour Of Sands ..... 5

2.3.1 Monotonic shearing of sands ..... 6
2.3.2 Effects of structure ..... 11
2.3.3 Yielding of sands ..... 15
2.3.4 Sample barrelling and strain localisation ..... 16

2.4 Anisotropy ..... 17

2.4.1 Anisotropy subdivisions ..... 18
2.4.2 Effects of α and b in soil response ..... 19

2.5 Particle Breakage ..... 19

2.6 State Concept For Sands ..... 21

# 2 LITERATURE REVIEW

## 2.1 Introduction

In this chapter, the behaviour of various sands under compression and monotonic shearing will be discussed. Findings from previous researchers are cross-compared and examined in an attempt to present a general background to the mechanics of sands against which the behaviour of Thanet sand will be examined as shall be later seen in Chapters 5 and 6.

## 2.2 Compression Behaviour Of Sands

The two most important factors that control the behaviour of any sand in compression are the initial particle size distribution and the strength of the individual particles the sand consists of. Coop & Lee (1993) studied the behaviour of three different sands; Dogs Bay sand - a carbonate sand from western Ireland, Ham River sand - a quartz or silica sand and thirdly a decomposed granite. The decomposed granite was well graded in comparison to the first two types of sand that were poorly graded (Figure 2-1).

The behaviour of these three different sands in isotropic compression can be seen in Figure 2-2. For all three sands, tests from a range of initial specific volumes were presented. As the tests progress and a high enough pressure is reached, all the different compression curves for the different initial densities converge to a unique line that is defined as the Normal Compression Line (NCL). The equation of the NCL in v-lnp' space is as follows:

$$v = N - \lambda \ln p' \qquad (2\text{-}1)$$

where N is the value of v if the NCL is projected to an effective stress p'=1kPa and $\lambda$ is its gradient.

The same principle also applies to the $K_0$ compression behaviour of sands. In Figure 2-3 data from $K_0$ compression tests on Dogs Bay sand are presented. Again, even though all tests start off from different initial specific volumes, as the mean effective stress is increased, all soil samples tend to converge to a unique line, the $K_0$ compression line, which is parallel to the isotropic NCL and slightly below it.

The volumetric strain that occurs during compression is related to particle breakage but this will be discussed in Section 2.5 which follows. During "virgin" compression sand does not have a well defined yield point; the slight curving that can be observed is related to the gradual onset of particle breakage due to high interparticle contact forces. Once a sand has reached its NCL and it is subjected to an unload-reload path (swelling), since the particles within the sand are not being mechanically rearranged or broken the material shows a much stiffer response. As soon as the preconsolidation pressure is reached on the reloading path, a clear yield point is formed between the two phases of the test. This is due to the particle breakage recommencing at the exact same stress level that the "virgin" compression had previously reached. Additionally, it must be noted that a sand can reach a particular state via either compaction, or overconsolidation, as can be seen in Figure 2-2 where experiments P and Q are shown to reach the same state by different routes.

## 2.3 *Monotonic Shearing Behaviour Of Sands*

For convenience, when examining the shearing behaviour of sands, the information available has been subdivided into two sections; the general monotonic behaviour of reconstituted sands and the results from various comparative studies investigating the effects of structure in forms of interlocking and/or cementation of natural sands.

### 2.3.1 *Monotonic shearing of sands*

Jovicic & Coop (1997) have studied the very small strain behaviour of the same three different sands examined by Coop & Lee using bender element tests to measure the elastic shear wave velocity "$V_s$" and hence calculate the very small strain shear modulus "$G_0$" as follows:

$$G_0 = \rho V_s^2 \qquad (2\text{-}2)$$

where $\rho$ is the mass density of the soil.

In Figure 2-4, small strain shear modulus measurements for Dogs Bay sand during both isotropic first loading and unload-reload are presented. The samples start at different initial specific volumes with denser samples being initially stiffer. As p' increases, the tests tend to a unique line in terms of $\log G_0$:logp' that corresponds to NCL in v:lnp' space. The data on the NCL can be represented by the same equation that was derived by Viggiani & Atkinson (1995) for normally consolidated clays:

$$\left(\frac{G_0}{p_r}\right) = A_0\left(\frac{p'}{p_r}\right)^{n_0} \qquad (2\text{-}3)$$

where $p_r$ is a reference pressure and $A_0$ and $n_0$ are constants for a given soil.

The stiffnesses on the unload-reload paths are significantly higher than those during first loading, so that the unload and reload behaviour follows a pattern that is equivalent to a swelling line in v:lnp' space.

Dynamic shear moduli from different sands are presented in Figure 2-5. All sands show fairly similar stiffnesses on the NCL, regardless of the differences in mineralogy and grading. This is in contrast with the variety of CSLs and NCLs locations in v-lnp' plane, as shown in Figure 2-6.

Results from shearing tests on Dogs Bay sand are shown in Figure 2-7. These data are typical of the experimental stress-strain behaviour of most sands. A soil reaches its Critical State once either the deviatoric stress and volumetric strain or the deviatoric stress and pore pressure have reached a plateau, depending on whether the experiment conducted is drained or undrained. For the Critical State to be reached, large strains are required for sands, which usually exceed 30% shear strain on a triaxial sample.

By conducting a series of tests and combining all the final Critical State points in q-p' space, the gradient M of the CSL can be derived. Figure 2-8 is based on results from experiments on Dogs Bay sand; the CSL does not seem to change gradient even at high pressures, despite the particle breakage that occurs during shearing, providing the soil is sheared to large enough strains.

In Figure 2-9 a schematic stress – strain behaviour of sands for various stress levels is presented. In v-lnp' space, the behaviour could be directly associated with the starting point of the test relative to the location of the CSL. Therefore, if a sand initially lies on the left of the CSL in v-lnp' space then, when tested, it will dilate and reach a peak angle of shearing resistance prior to reaching its Critical State while, if it lies on the right of the CSL, it will have a compressive behaviour with a monotonically increasing strength until the Critical State is reached. This though will be discussed in greater detail in Section 2.6.

In v-lnp' space, the isotropic NCL, the $K_0$NCL and the CSL are parallel having the same inclination but different offsets at p'=1kPa (e.g. Figure 2-2 & Figure 2-3), so that for the CSL:

$$v = \Gamma - \lambda \ln p' \qquad (2\text{-}4)$$

where $\Gamma$ is the specific volume at p'=1kPa and $\lambda$ is again the slope of the line.

While at high pressures the CSL is straight and parallel to the NCL, at low confining pressures, the CSL does tend to curve towards the horizontal (e.g. Lee & Seed, 1967; Verdugo & Ishihara, 1996). In Figure 2-10 the results from lower-

pressure triaxial experiments on Leighton-Buzzard sand are presented along with the CSL for Toyoura sand (Ishihara, 1996) as well as an earlier interpretation for the Thanet sand CSL by Coop & Cuccovillo (1997). The curvature and/or straightness of the CSL for Thanet sand is discussed in detail in Section 5.3.

Coop (1999) suggested that the curvature of the CSL at low pressures can be partially attributed to experimental incompleteness (Figure 2-9). As can be seen in Figure 2-7, the overall shear strain required for a true CS to be reached typically ranges from 35% to 45% for sands. In reality, however, triaxial cells can often provide shear strains of only about 25%. This means that the soil would not yet have reached its Critical State, leading to incorrect identification of the CSL location as illustrated. The experimental data then need to be extrapolated for the true Critical State of individual experiments to be calculated and in turn, the real CSL of the soil to be derived. Nevertheless, according to Coop (1999), the CSL and NCL must be curved at either end as shown in Figure 2-11 considering that at very high pressures the soil must tend to a specific volume equal to 1 (void ratio = 0), whereas at very low pressures the maximum value of specific volume should be governed by the loosest packing possible for the soil in question.

Verdugo & Ishihara (1996) performed a series of drained and undrained triaxial tests on Toyoura sand, a typical quartz sand, for various initial densities as well as different confining stresses. They found that at large strains (25% or higher), the soil tested developed a unique shearing resistance, regardless of the initial void ratio the samples had been set up at (Figure 2-12 & Figure 2-13). Additionally, when combining all experiments performed at different stress levels, it was found that the void ratios of the samples converged to a unique curve in e-p' space, as shown in Figure 2-14. The location of this curve was not affected by the different initial void ratios and fabrics of the samples that, in turn gave offsets to the isotropic compression curves of the samples tested, depending on the preparation method used (Figure 2-15). Nevertheless, it should be noted that the pressures that were reached were not sufficiently high to reach the NCL. It is possible that if p' had been high enough, the initial fabrics from the different preparation methods used in Figure 2-15 might also have been erased in compression as well as in shearing to a Critical State.

Been, Jefferies and Hachey (1991) performed an extensive triaxial tests on Erksak sand along with some experiments on Leighton Buzzard and Toyoura sands. They too determined that sample preparation method was not a major influence on the critical state of the soil. As shown on Figure 2-16, they found a bi-linear critical state line; one for stresses up to 1,000kPa and another for higher stresses. They also found that for Erksak sand as well as Toyoura sand, the stress path followed during testing had no effect on the location of the CSL in e-lnp' space (Figure 2-17 & Figure 2-18).

Coop and Atkinson (1993) studied the mechanics of cemented carbonate sands. During their study they were able to determine that grading has a large impact on both the location of the CSL as well as the NCL of reconstituted sands in v-lnp' space, as shown in Figure 2-19 and Figure 2-20. In the latter figure, ultimate state data are presented for the various different materials examined where the fines content effect on the CSL location for reconstituted sands is illustrated.

Figure 2-21 shows three distinct methods that can be used for a set of shearing data to be normalised. Normalisation for volume by means of equivalent pressure is used to reduce the three dimensional plot q:p':v to two dimensions. The equivalent pressure $p'_{cs}$ is based on the CSL whereas $p'_p$ and $p'_e$ are both based on the NCL.

In Figure 2-22, a set of normalized shearing data for all three different sands studied by Coop & Lee (1993) is presented. After the normalization, both the CSL and NCL are each reduced to a single point. Each soil forms a unique State Boundary Surface. However, the CSL does not lie at the top of the SBS for sands. This was predicted by Chandler (1985) for materials with deformable grains (agricultural grains) so it is not surprising that it can be seen for soils with crushable grains. This also means that normality principal does not apply to sands. Additionally, another implication is that the spacing of the NCL and CSL is very much greater than what is seen for clays (e.g. Modified Cam Clay assumes a ratio of 2.0). In Figure 2-22 we have a spacing ratio of approximately 4.5. Another

difference in the behaviour of sands is that, it is not possible for undrained tests to identify the SBS either on the "wet side" or the "dry side" as the paths of undrained tests plot below the SBS identified by drained tests.

In Figure 2-23 stress-dilatancy data for drained tests on Dogs Bay sand are shown. The data confirm that at large strains a linear relationship between the stress ratio q/p' and the rate of dilation $\delta\varepsilon_v/\delta\varepsilon_s$ exists and the representative equation is as follows:

$$\frac{q}{p'} = M - a\left(\frac{\delta\varepsilon_v}{\delta\varepsilon_s}\right) \qquad (2\text{-}5)$$

where α is a constant.

From a stress-dilatancy point of view, if Equation 2-5 is accepted then when $\frac{\delta\varepsilon_v}{\delta\varepsilon_s} = 0$ one would expect $\frac{q}{p'} = M$. By analogy, one could expect $\frac{q}{p'} = M$ for $\frac{\delta u}{\delta\varepsilon_s} = 0$ for an undrained test, which is the point of phase transformation. It must be noted that some models for sands such as that suggested by Yang and Li (2004) assume a stress-dilatancy relationship that is dependant on the state parameter (i.e. specific volume and density) (Figure 2-24 & Figure 2-25). Yang and Li based their model on stress-dilatancy data that were taken from Verdugo and Ishihara (1996), as shown in Figure 2-26. However, this neither agrees with the data presented in Figure 2-23 which shows a relationship that is independent of stress level and initial density, nor with any of the data from tests on Thanet sand presented later in this Thesis (see Section 5.4).

In Figure 2-27, undrained stress paths are shown for tests on Dogs Bay sand isotropically loaded to states that had not yet reached the NCL. In each case, the point of phase transformation which lies at the reversal of the stress path, occurs at the critical state stress ratio determined from drained tests.

### 2.3.2 *Effects of structure*

The influence of structure on the engineering behaviour of sands has recently become a key point of interest in research. From what is known until the present, structure itself can be subdivided into two major categories, based on the nature of the soil in question; sand particles can have developed bonds between them (i.e. cementation) that results in a bonded structure, or can be interlocked, forming a fabric (e.g. Barton, 1993).

Barton & Palmer (1989) examined the in situ dry density for various different British sands and correlated their relative densities with their geological age. Their data were replotted by Coop (2003), as shown in Figure 2-28. Barton & Palmer examined uncemented poorly graded sands with low fines contents that were based on quartz. They also assumed a uniform specific gravity of 2.65 for all sands examined. The trend that was identified was attributed to the development of a locked fabric. Nevertheless, it must be noted that age can only be an approximate indicator as it is not the sole factor influencing the development of fabric. In addition to the original Barton & Palmer data Figure 2-28 contains data from other sands as well as the data obtained from intact Thanet sand samples from earlier tests. The data points for the Thanet sand plot higher than the points of other sands which is perhaps an indication that it does not have locked fabric.

Thin sections of both a calcarenite and Greensand (a quartzitic sandstone) tested by Cuccovillo & Coop (1997) are shown in Figure 2-29 and Figure 2-30 respectively. Looking at Figure 2-29, the picture of this thin section of calcarenite was taken with cross-polarised light and therefore, the voids appear as black. The particles calcarenite consists of are shells (i.e. $CaCO_3$) with high angularity and it therefore as a high initial specific volume. The cement for calcarenite is the white fringe of crystals around each particle (calcium carbonate) as can be seen in Figure 2-29 and is abundant. The cement was deposited soon after the particle deposition in warm shallow sea. The early deposition of cement preserved the high specific volume, even though this soil was buried at an approximate depth of

150m. This is due to the fact that the burial did not reach sufficiently high stresses for the bonds to be damaged and broken down. Moving now to Figure 2-30, this image of Greensand is a SEM photograph with voids appearing as black, particles of solid quartz appearing as dark grey and iron oxide cement appearing as white. In Greensand, the cement is sparse when compared to the calcarenite. Greensand has a well-developed locked fabric caused by pressure solution i.e. quartz at the particle contacts dissolved under high contact pressures over very long periods of time. In Greensand the cement was deposited rather recently, after the soil was buried to a great depth and after erosion had brought the soil back near the surface. Therefore, in Greensand cementing took place after a locked fabric had already been created.

Compression data for the calcarenite and the Lower Greensand are presented in Figure 2-31 and Figure 2-32 respectively. The calcarenite is highly cemented and has a high initial specific volume and therefore reaches states outside the Intrinsic Compression Line (ICL) defined by the reconstituted soil. On the other hand, the Greensand is lightly cemented and is very dense and therefore does not reach states outside the ICL. As can be seen in Figure 2-32, the very high density of the intact Greensand samples caused by the locked fabric could not be reproduced when setting up reconstituted samples and the minimum specific volume of about 1.65 that could be created by compaction was well above the specific volume of the intact soil that was about 1.44.

Cuccovillo & Coop (1997) conducted comparative tests between intact and reconstituted samples of the Greensand. The influence of the cementation of the material is made clear when looking at the equivalent monotonic shear moduli presented in Figure 2-33 for both intact and reconstituted samples. For samples with the same initial specific volume the intact sample gives a stiffer behaviour by almost a factor of three at small strains, even if the stress level for the test on the reconstituted sample was slightly higher.

Cuccovillo & Coop also produced a stress-dilatancy plot (Figure 2-34) indicating the divergence in shearing behaviour between intact and reconstituted sandstone samples. The reconstituted soil obeys the standard stress-dilatancy relationship as

presented in Equation 2-5. The dilation on the other hand for the intact samples was delayed by the cementing and the fabric. When finally the cementing and locked fabric were broken, the dilation rate was very high and it was also associated with very high peak strengths. As can be seen from the graph, these peak strengths still plot on the same relationship as for the reconstituted soil, but with much higher corresponding rates of dilation.

In Figure 2-35 the peak states of dilation are presented for the Lower Greensand. The figure shows how state in v-lnp' plane affects the rate of dilation and therefore the peak strength. The first part of the figure (a) shows that at a given state $d_{max}$ is much greater for the natural sandstone compared to the reconstituted sandstone. Additionally, Figure 2-35(a) shows that the CSL for the natural soil cannot be the same as the CSL for the reconstituted sandstone as $\frac{\delta\varepsilon_v}{\delta\varepsilon_s}$ should be zero on the CSL but the intercepts on Figure 2-35(a) are different. To avoid that conflict, different CSLs were selected for the intact and reconstituted sandstone and then the diagram was re-plotted based on the new CSL locations, as shown in Figure 2-35(b). What must be noted is that even when using different CSLs, $d_{max}$ is is still greater at a given state for the natural sandstone compared to the reconstituted material.

Cresswell and Powrie (2004) performed a series of tests investigating the influence of fabric on Reigate silver sand. This is a locked sand also from the Greensand sequence but with minimal cement content. Two stress ratio and volumetric strain plots against axial deformation are presented in Figure 2-36 and Figure 2-37, each for a different level of effective cell pressure. Even though the stress-dilatancy plots were not available for a direct observation in this case, a similar pattern to what was observed by Cuccovillo & Coop can be seen here as well. Dilation is again delayed by the particle interlocking within the material. In both plots, two vertical lines have been inserted; line (a) and line (b) as well as a horizontal line that corresponds to the Critical State stress ratio, M. Line (a) corresponds to the point of minimum volume but does not coincide with a stress ratio equal to M as would be expected if the dilation behaviour followed the pattern described in Equation 2-5. This is equivalent to what was shown by

Cuccovillo & Coop in Figure 2-34. The interesting difference between the two materials tested is that the Reigate silver sand contains no cementing within its structure but still shows similar dilation behaviour to the cemented sandstone examined before. Therefore, it can be argued that the locked fabric was indeed the primary reason for the delayed dilation that was observed in both cases whereas the role of the cementing present in the sandstone tested by Cuccovillo & Coop is yet to be clearly identified.

Figure 2-38 from Cresswell and Powrie is a similar plot to the one previously presented in Figure 2-35. It shows a clear difference in behaviour between the intact and reconstituted samples with the corresponding trends having been marked on the plot. Again, the intact samples are associated with much higher dilation rates compared to the reconstituted samples. Furthermore, from Figure 2-39 it can be seen that the intact sand gave much higher equivalent monotonic shear moduli than the reconstituted sand. However, the intact samples were consistently denser than the reconstituted samples, so it is not known to what extent the difference seen is a result of the effect of structure.

Dano and Hicher (2003) observed a similar pattern in terms of stiffness behaviour, when comparing tests on uncemented sands and grouted sands. The effect of cementation is made clear by the stress-strain diagrams shown in Figure 2-40

Mimura (2003) performed a series of comparative tests between intact samples of sand that had been sampled by freezing and reconstituted samples for various different Japanese sands. In all cases, the reconstituted sample was set up at the same void ratio as the intact sample. The stress-strain relationships observed are presented in Figure 2-41. Here it is clear that the intact samples have a much stiffer behaviour compared to the reconstituted samples. At larger strains though, the intact and reconstituted samples show little difference in shearing behaviour. The angles of shearing resistance (Figure 2-42) are similar, with the intact angles being slightly higher in two of the three cases. Finally, the axial strain - volumetric strain data for the four different sand comparisons are presented in Figure 2-43. Again, they are fairly similar for the intact and the reconstituted samples.

To illustrate the effect of various levels of sand cementation on the normalised shearing behaviour, three distinctly different sands are compared; an uncemented reservoir sand, a calcarenite, which is a heavily cemented sand with strong bonds and finally Greensand, a medium cemented sand with weak bonds. Starting with the uncemented reservoir sand, its behaviour is presented in Figure 2-44. Here, there is no obvious effect of structure for the intact sand as the normalised shearing data resemble the behaviour one would expect from a reconstituted sand without the presence of structure. The calcarenite on the other hand, being a heavily cemented sand, reaches states well outside the intrinsic SBS on the wet sideof the CSL, as shown in Figure 2-45 and Figure 2-46 and as was also seen in Figure 2-31. The intrinsic SBS for each soil was derived from tests on reconstituted samples. Finally, normalised shearing data for the Greensand are presented in Figure 2-47. The weak bonding of Greensand gives yield points and hence a yield locus that is almost completely inside the intrinsic SBS. The Greensand reaches states outside the intrinsic SBS only on the dry side due to the additionally dilation and higher peak strength of the natural soil, compared to the reconstituted, due to the locked fabric and cementing.

### 2.3.3 *Yielding of sands*

When small strain yielding is examined, a Y1 envelope is defined as the envelope that encloses a region where the soil in question has a linear elastic response. When the soil crosses this envelope, a linear elastic response can only be observed when the soil state re-enters the Y1 envelope. A Y2 yield point as was defined by Jardine (1992) is the point at which the vectors relating increments of volumetric to shear strain starts to change direction. A Y2 envelope is the envelope defined by all Y2 points. The Y2 envelope includes the Y1 envelope described above (Y1<Y2) and within which the soil in question has a non-linear or otherwise hysteretic elastic response. Finally, a Y3 envelope is defined as the locus of points where large strain yielding of the soil commences and an elastic soil response (linear or hysteretic) no longer applies (Y1<Y2<Y3). Two examples of Y1 and Y2 yield loci measured by Kuwano (1999) are shown in Figure 2-48 and Figure

2-49. She extensively studied the anisotropy of reconstituted Ham River sand for various different loading cases and overconsolidation ratios. Here, two specific plots are shown for OCRs of 1.3 and 2 with the former being anisotropically and the latter isotropically compressed. In both cases Kuwano presents highly asymmetrical envelopes, with the Y1 envelope reaching a radius of about 15kPa and Y2 reaching values of up to 70kPa. In Section 6.5, the yield loci produced for Thanet sand shall be compared with those presented here.

### *2.3.4 Sample barrelling and strain localisation*

In order for the cross-sectional area of a sample tested to be calculated, the standard right cylinder assumption is typically adopted. In reality though, as large strains accumulate in the sample, its behaviour deviates from this idealised adopted geometry and the sample barrels (Figure 2-50). Barrelling and localisation both have a direct impact on volumetric strain calculations. Internal volumetric strains based on internal axial and radial measurements may indicate completely different soil behaviour to the measurements derived from the external volume gauge which considers the overall sample behaviour. Therefore, the internal strain readings are typically only considered until a relatively small axial strain (for example 5%). Past that point, the sample does not truly follow the right cylinder deformation pattern and the volumetric strains calculated based on the combined readings of the internal axial and radial instrumentation deviate from the global volumetric strains measured by the volume gauge (e.g. Klotz and Coop, 2002).

On a highly structured soil sheared under low effective confining stress, strain localisations will be observed with the formation of shear bands. On the other hand, if a soil sample is sheared under high effective stress, only barrelling will be observed. For many sands at standard engineering stresses, failure may involve a combination of barrelling and strain localisation (e.g. Klotz and Coop, 2002).

One method of reducing the effects of strain localisation and also barrelling in a triaxial test is the adoption of lubricated end platens. Triaxial experiments using

lubricated end platens have shown increased accuracy and better correlation of internal measured volumetric strains with the externally measured global volumetric strain. A schematic of a typical example of a triaxial apparatus modified to accommodate the use of lubricated end platens is shown in Figure 2-51.

Klotz and Coop (2001) assessed the errors introduced by both strain localisation and sample barrelling. The triaxial cell that they used was equipped with lubricated end platens as well as a full set of internal strain instrumentation (Figure 2-52). Even so, the volumetric strains obtained from the internal instrumentation still showed large deviations from the global measurements. Once clear shear bands had formed in the sample, the internal and external volumetric strains did not show any tendency to converge. This was partly due to barrelling and partly due to the rigid body movement on the shear planes indicated in Figure 2-52 at large strains giving unrealistic radial strain data. Desrues et al. (1996) investigated the formation of shear bands and their characteristics using computed tomography. They found that the limit void ratio was reached within the localisation zone (Figure 2-53), that is the void ratio when the system reaches an equilibrium at end of test is significantly different to the global void ratio calculated based on global sample measurements giving rise to significant doubt in the lower stress range of the location of the critical state line in the v:lnp' plane. Also, they found that strain localisations may start taking place even if they cannot be directly observed on the outside of a soil sample.

## 2.4 *Anisotropy*

The deposition and consolidation of the particles that form uncemented sediments influences the potential fabrics that develop within the soil mass. Because sedimentary soils are gravity driven, the particle contacts formed are directionally dependant or in other words anisotropic. Anisotropy is subdivided into two components: "Inherent" and "Induced". The anisotropy in a real soil in the ground is most likely to be a combination of the two.

### *2.4.1 Anisotropy subdivisions*

"Inherent" anisotropy as defined by Casagrande and Carrillo (1944) is a physical characteristic inherent in the material and entirely independent of the applied strains. "Inherent" anisotropy is created by and during the depositional process of the soil. Examples of cases where "inherent" anisotropy can be found are in laminated and bedded soils. Arthur & Menzies (1972) showed on their tests on Leighton Buzzard sand that a rotation of $90^0$ of the direction of pouring at setup relative to the principal stress axis resulted in a change in stress ratio at failure of 10% for the same porosity. They also found that the rotation of the pouring direction resulted in differences of over 200% in the axial strains required to reach a given prefailure stress ratio.

"Induced" anisotropy is caused by particle contact re-distribution due to stresses applied to and strains induced in the soil (Casagrande and Carrillo, 1944). As can be directly observed by photoelastic experiments, soil particles form load-carrying internal paths (otherwise called "columns") that are orientated primarily parallel to the major principal stresses imposed on the soil mass (Oda, 1972). Therefore, if a soil that was initially isotropic and has been subjected to anisotropic stresses until equilibrium within the soil mass is reached, it will have developed "Induced" anisotropic structure. In order to examine Induced anisotropy, Arthur et al. (1977) subjected dense sand samples to sudden rotations of the principal axis directions. These rotations varied from $0^0$ to $90^0$. It was established that even though induced anisotropy does not significantly affect the angle of shearing resistance $\varphi'$, it has a large influence on the strains required to achieve a given stress ratio.

As mentioned previously, in nature, the behaviour of and structure of a soil mass is dependent on both the mode of soil deposition ("Inherent" anisotropy) as well as the stress changes (geological or other) it has been subjected to since deposition was completed ("Induced" anisotropy).

### 2.4.2 *Effects of α and b in soil response*

The parameter α is defined as the inclination of the major principal stress with respect to the depositional direction of the soil (Figure 2-54) and b shows the relative magnitude of the intermediate principal stress: $b = \frac{\sigma_2 - \sigma_3}{\sigma_1 - \sigma_3}$. Hollow Cylinder apparatuses are used to examine the effects of α and b on soil response. Symes (1983) has performed a series of experiments on Ham River sand and has been able to quantify the effects of those two factors, as shown in Figure 2-55 to Figure 2-57 from which it can be seen that both α and b have a significant effect on the soil behaviour. The possible variations of intermediate stress factor "b" as well as the angle of major principal stress to the bedding plane "α" that can be accommodated in a triaxial cell are four pairs of values at either end of the ranges, as shown in Figure 2-58. It must be emphasised that while α only has an effect on anisotropic soils, b would have have an effect even on an isotropic soil, although the b effect on an anisotropic soil might differ to that seen on an isotropic soil.

## 2.5 *Particle Breakage*

During either isotropic or $K_0$ compression, sand does not have a well defined yield point. The gradual curving that can be observed is related to the gradual onset of particle breakage due to high inter-particle contact forces. For the unload-reload path, the material shows a much stiffer response (Figure 2-2). However, as soon as the pre-consolidation pressure is reached on the reload path, a clear yield point is formed between the two phases of the test. This is due to the particle breakage recommencing at the exactly same stress level that the compression had previously reached.

In an attempt to quantify the shift of a material's grading curve once a test has been performed, Hardin (1985) defined Relative Breakage "Br" (Figure 2-59). It

should be emphasized that sand behaviour is controlled by the initial material grading. Therefore, if sand that has already been tested to high pressures is reconstituted and tested again, it will not give the same behaviour, since the initial particle size distribution for the new test will be different to that of the first experiment. This was verified by Nakata et al. (2001) when they subjected artificially graded silica to one dimensional compression. They found that, even for the same material, the yielding characteristics are dependant on the initial grading curve with the uniformly graded samples giving a much more marked yielding than the well graded samples tested (Figure 2-60).

In Figure 2-61 particle breakage results for triaxial experiments conducted by Coop & Lee (1993) on Dogs Bay sand, decomposed granite sand and Ham River sand have been presented. In this plot it can be seen that the different sand behaviours in terms of breakage can be primarily attributed to the soil particle strength and the effective confining stress, with the quartzitic sand being able to withstand much higher stresses for given breakage factor. At higher stresses, a linear relationship can be seen between breakage factor and logp' for both the CSL and NCL.

Coop & Lee (1993) also investigated the effect that the stress path followed has on sand particle breakage. When the breakage factors from a series of compacted samples (not yet having reached the NCL) were compared with those of a series of overconsolidated samples (unloaded from the NCL), they found that at higher stresses a unique linear relationship is formed between Br and logp' (Figure 2-62). This means that the stress path followed does not affect the final breakage factor of the soil when it has reached its critical state.

An alternative approach in the interpretation of oedometer data has been adopted by McDowell & Bolton (1998) who have simulated the evolving particle breakage during virgin compression using fractal geometry. Their results (Figure 2-63 & Figure 2-64) clearly correlate the evolving particle breakage with the increasing confining pressure. Their predictions agree with the experimental data obtained by Fukumoto (1992) when he subjected Ottawa sand to one-dimensional compression until different final stress levels. The particle size distribution curves

obtained from the various tests were combined to highlight the evolution of the particle size distribution curve with pressure (Figure 2-65).

Particle breakage is also associated with shearing. Coop et al. (2004) ran a series of ring shear tests on Dogs Bay sand in an attempt to find the strains at witch the particle breakage would cease to continue. This would allow the true critical state of a sand to be found, when no additional particle breakage should take place. Figure 2-66 shows the evolving particle size distributions with double logarithmic axes. Experiment RS4 is the first one to form an almost straight relationship between percentage passing and particle size. This happens at around 1,400% shear strain. Figure 2-67 shows the breakage factor evolution with shear strain. Zone 2 is the middle thirdof the sample where most of the shearing is consentrated, whereas zones 1 and 3 are the top and bottom third of the sample respectively. The breakage factor stabilises and therefore true Critical State is achieved only after 1,500% to 2,000% shear strain. Similarly, Figure 2-68 shows the volumetric strain evolution with shear strain. Again, the volumetric strain of the samples can be considered to have reached a plateau at strain levels greater than 1,500% to 2,000%. Such a strain cannot be applied in a triaxial test due to apparatus and geometric sample restrictions. Therefore, the critical states found from triaxial tests can only be an approximation.

## 2.6 *State Concept For Sands*

The "State" of a sand is considered to be the combination of a sand's current void ratio and stress level. If either of these two factors were to be considered separately, their influence would not yield a consistent pattern of behaviour. To illustrate this, Figure 2-69 shows three experiments with different stress and void ratio characteristics. As all soil when sheared tends towards the CSL, if experiments A and B were to be sheared, experiment A would compress whereas experiment B would dialate, even though they started off from the same specific volume. Similarly, experiments A and C starting from the same stress level, would again show different behaviours with C dilating and A compressing.

The state parameter "ψ" has been used by many researchers (e.g. Been & Jefferies, 1985) in an attempt to quantify this phenomenon. The state parameter is defined as the vertical distance of the soil sample in question from its CSL, as sown in Figure 2-70. Klotz & Coop (2001) introduced the stress ratio $R_s = p_0' / p_{cs}'$ which is the ratio of the current mean effective stress $p_0'$ to that projected on the CSL at the same void ratio, as shown in Figure 2-70. Both state parameter and stress ratio Rs quantify the state of the soil in similar ways. If one though considers bi-linear or curved CSL at lower pressures then by definition, ψ will then become more sensitive to the choice of the CSL location at lower stresses where difficulties may be encountered because of strain localisation.

Beet et al. (1987) used the state parameter "ψ" to normalise data from cone penetration tests performed on several sands. Figure 2-71 shows the resulting plots for three different sands tested. Linear trends with the normalised data can be seen in all three cases.

Klotz & Coop (2001) used the state approach to quantify the capacity of driven model piles in centrifuge tests. In addition to the centrifuge tests, a series of triaxial tests were performed in order for the CSL of the two sand used to be determined. This allowed the normalization of base resistance data shown in Figure 2-72 based on the stress ratio Rs, as shown in Figure 2-73. In the latter figure, a linear tred is seen for increasing penetration.

In an attempt to further reduce the scatter arising from data normalisation with ψ, Konrad (1988) introduced a normalised state parameter: $\psi_N = \frac{\psi}{e_{max} - e_{min}}$. According to Konrad, the scatter was arising due to the different fabrics of the various sands tested. By dividing the state parameter by the difference between the maximum and minimum void ratio of every sand, the fabric as well as the particle size distributions of the materials were included in the normalisation. In Figure 2-74 the improvement in the normalisation with the use of $\psi_N$ is evident

as the scatter seen in Figure 2-74 is greately reduced in Figure 2-74(b). Konrad also used $\psi_N$ to analyse dialatometer tests (DMT) on Ottowa sand. The results are presented in Figure 2-75 where a very good correlation of the normalised data has been achieved.

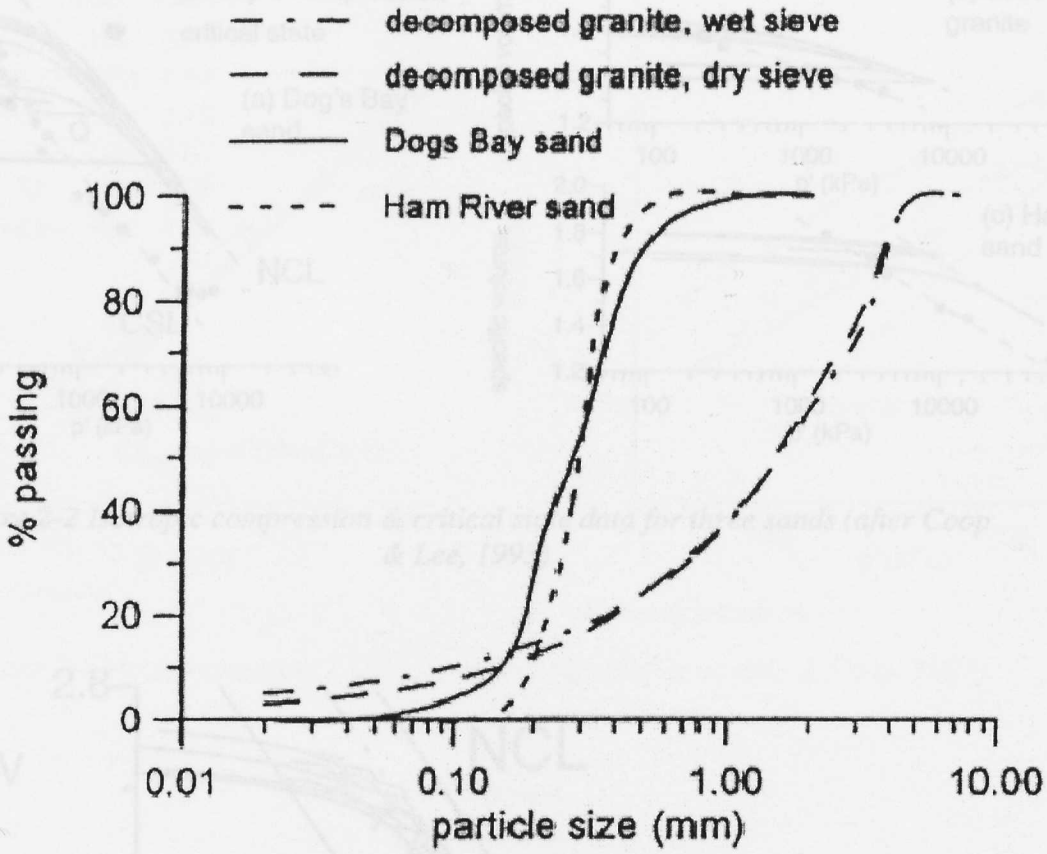


***Figure 2-1*** *Grading curves for the three sands tested by Coop & Lee (1993)*

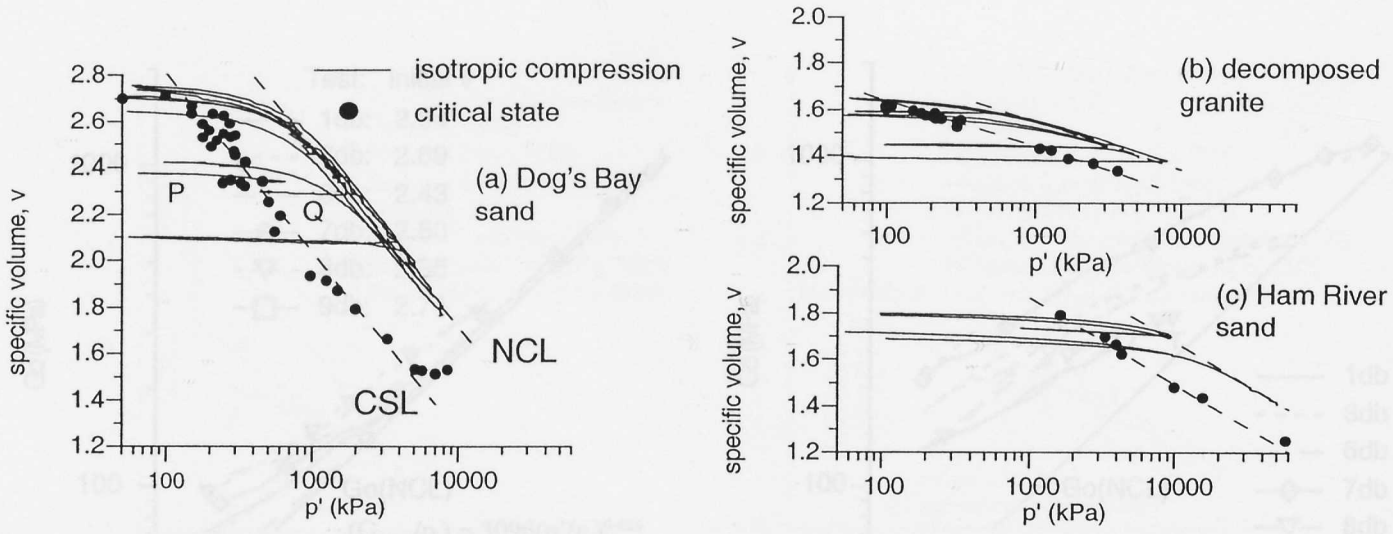


*Figure 2-2 Isotropic compression & critical state data for three sands (after Coop & Lee, 1993)*

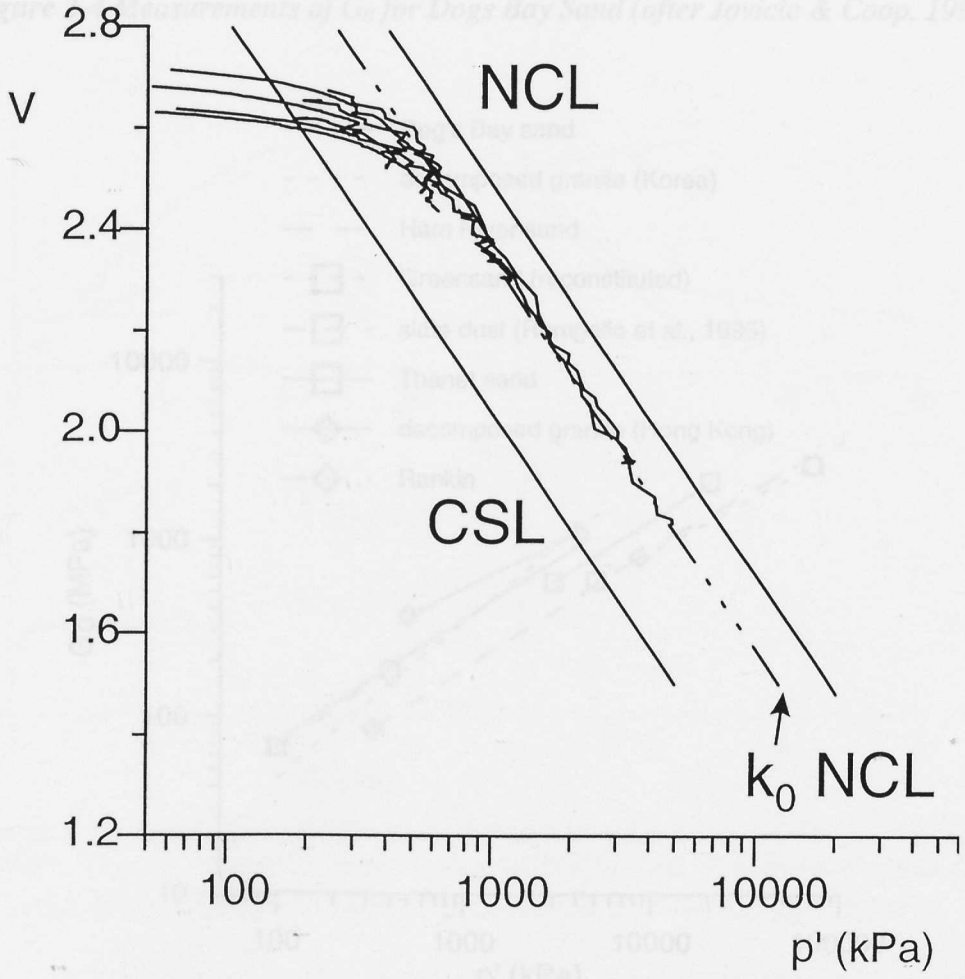


*Figure 2-3 $K_0$ compression for Dogs Bay sand (after Coop & Lee, 1993)*

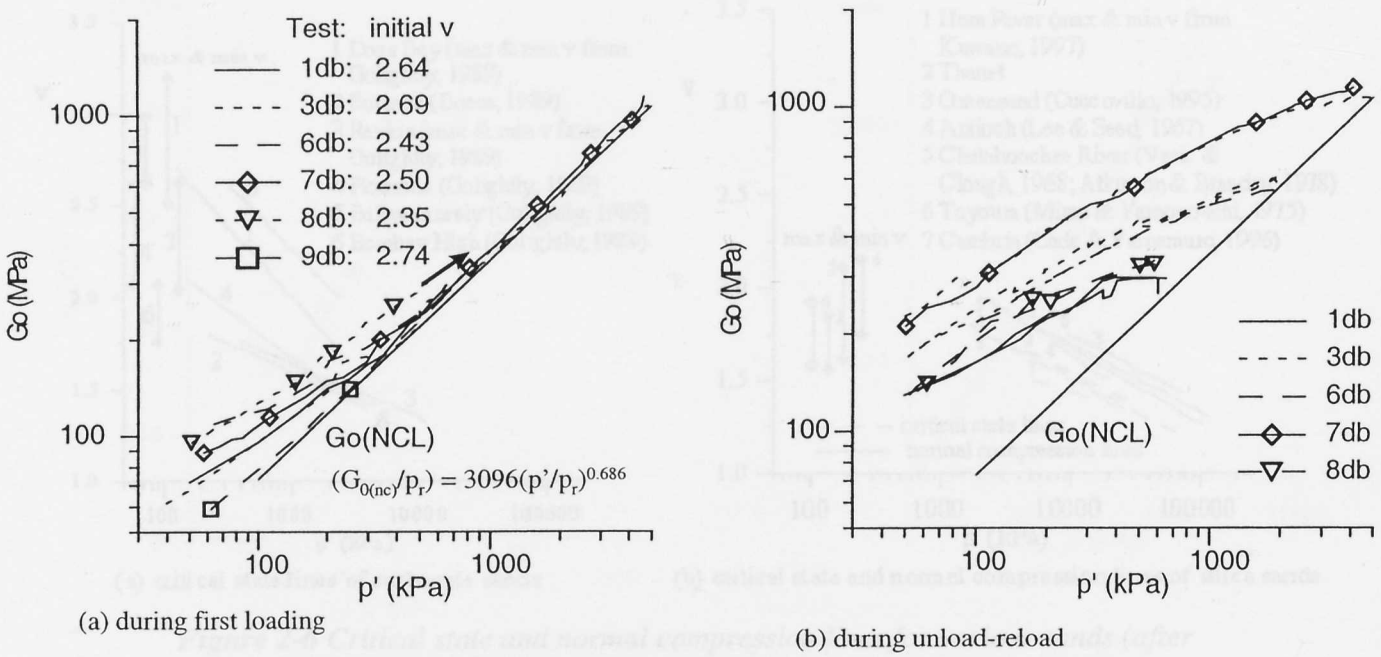


***Figure 2-4** Measurements of $G_0$ for Dogs Bay Sand (after Jovicic & Coop, 1997)*

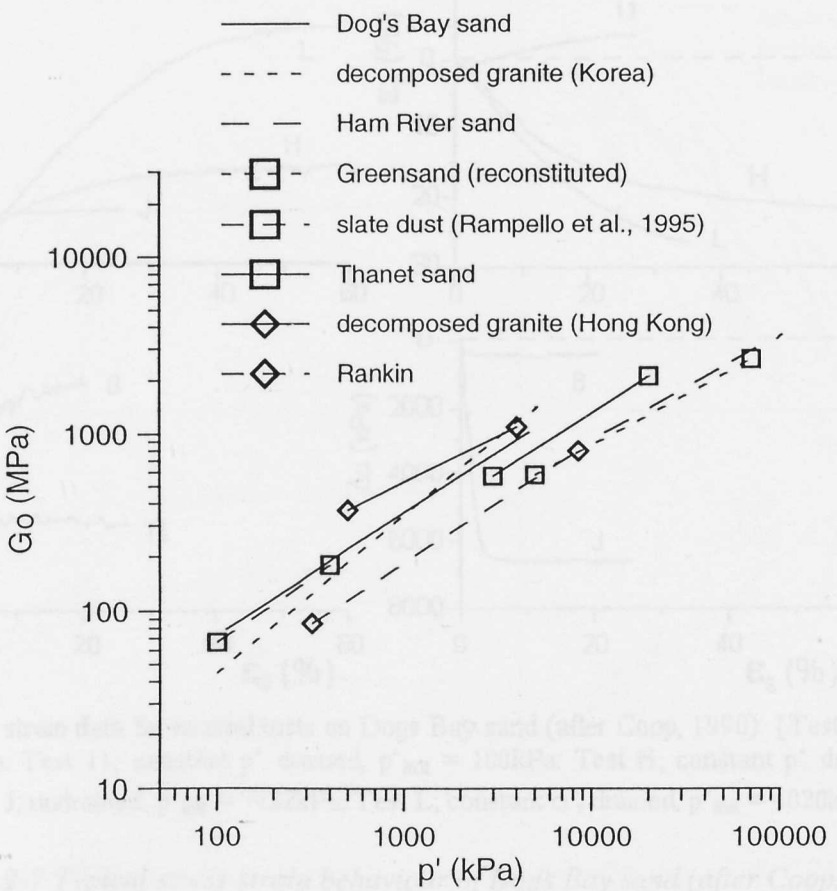


***Figure 2-5** $G_0$ on the NCL for various sands (after Jovicic & Coop, 1999)*

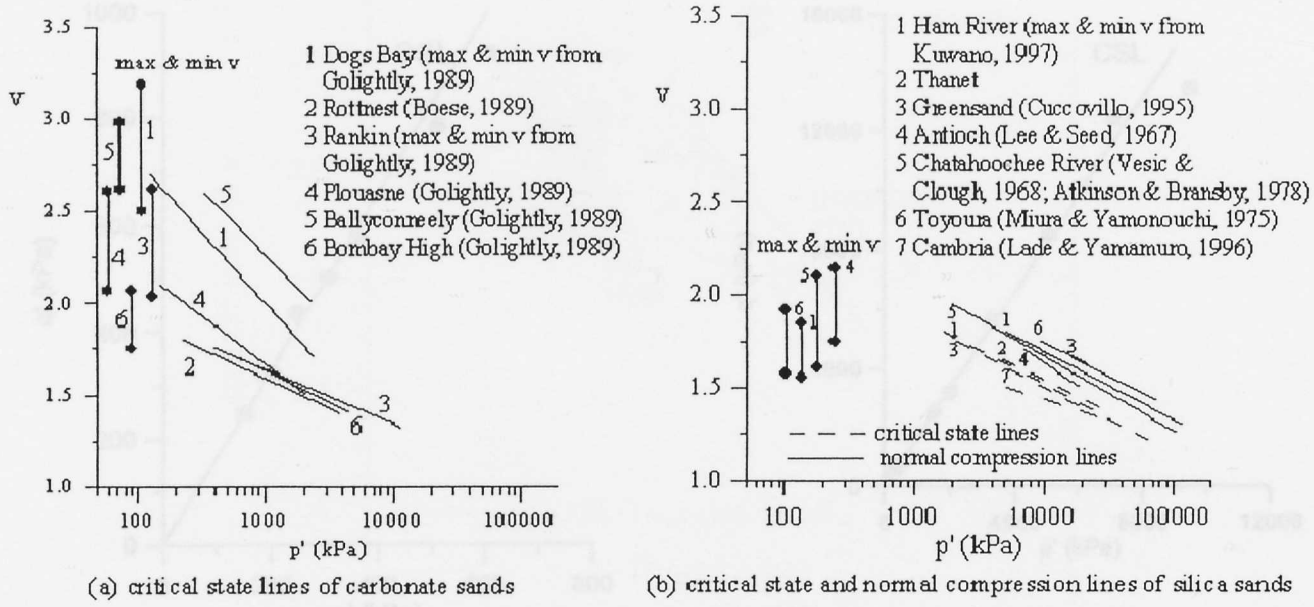


(a) critical state lines of carbonate sands (b) critical state and normal compression lines of silica sands

***Figure 2-6*** *Critical state and normal compression lines for various sands (after Cuccovillo & Coop, 1999).*

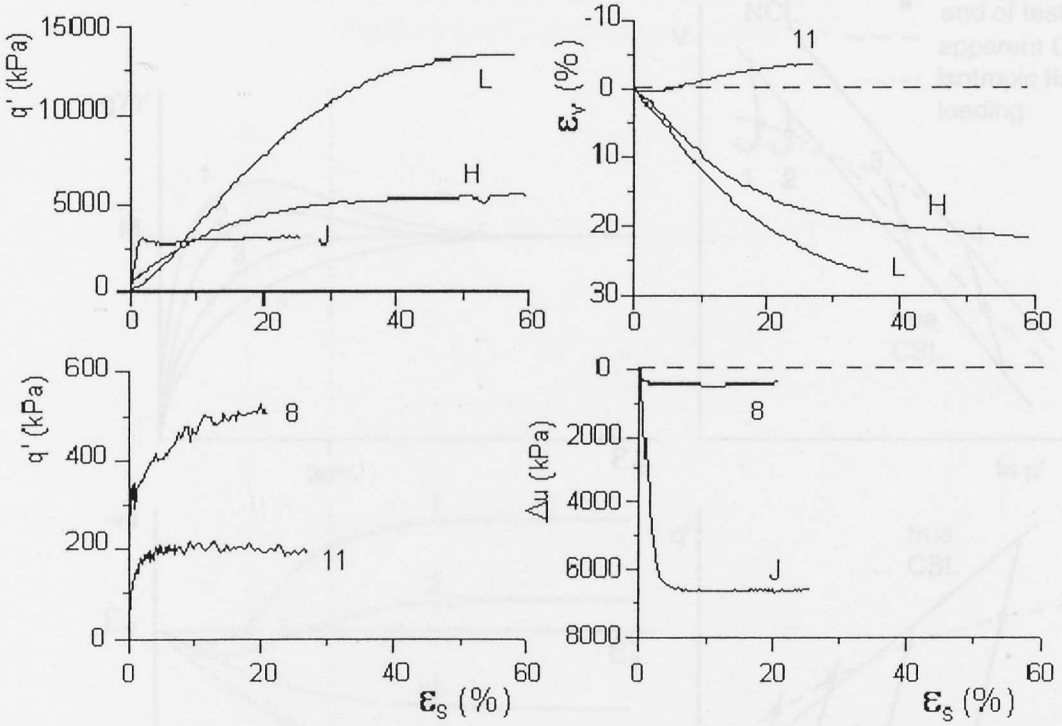


Typical stress: strain data for triaxial tests on Dogs Bay sand (after Coop, 1990). (Test 8; undrained, $p'_{init}$ = 500kPa: Test 11; constant p' drained, $p'_{init}$ = 100kPa: Test H; constant p' drained, $p'_{init}$ = 3286kPa: Test J; undrained, $p'_{init}$ = 7422kPa: Test L; constant $\sigma'_r$ drained, $p'_{init}$ = 4020kPa)

***Figure 2-7*** *Typical stress-strain behaviour of Dogs Bay sand (after Coop, 1990)*

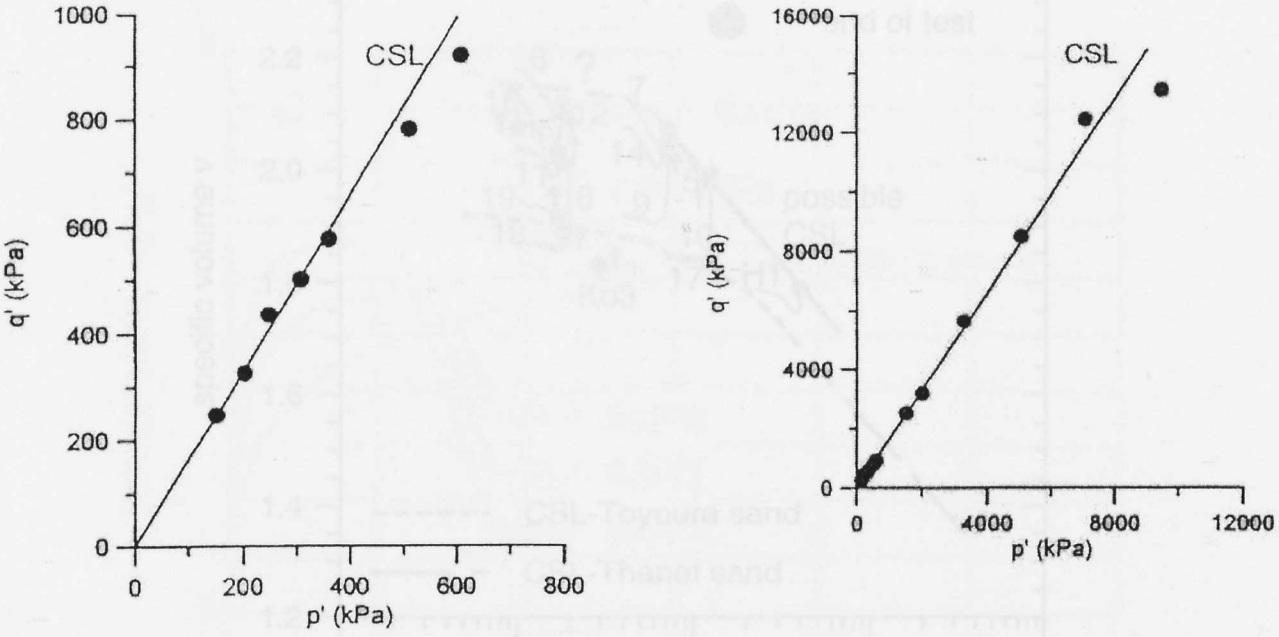


*Figure 2-8 Critical States for Dogs Bay Sand (after Coop, 1990)*

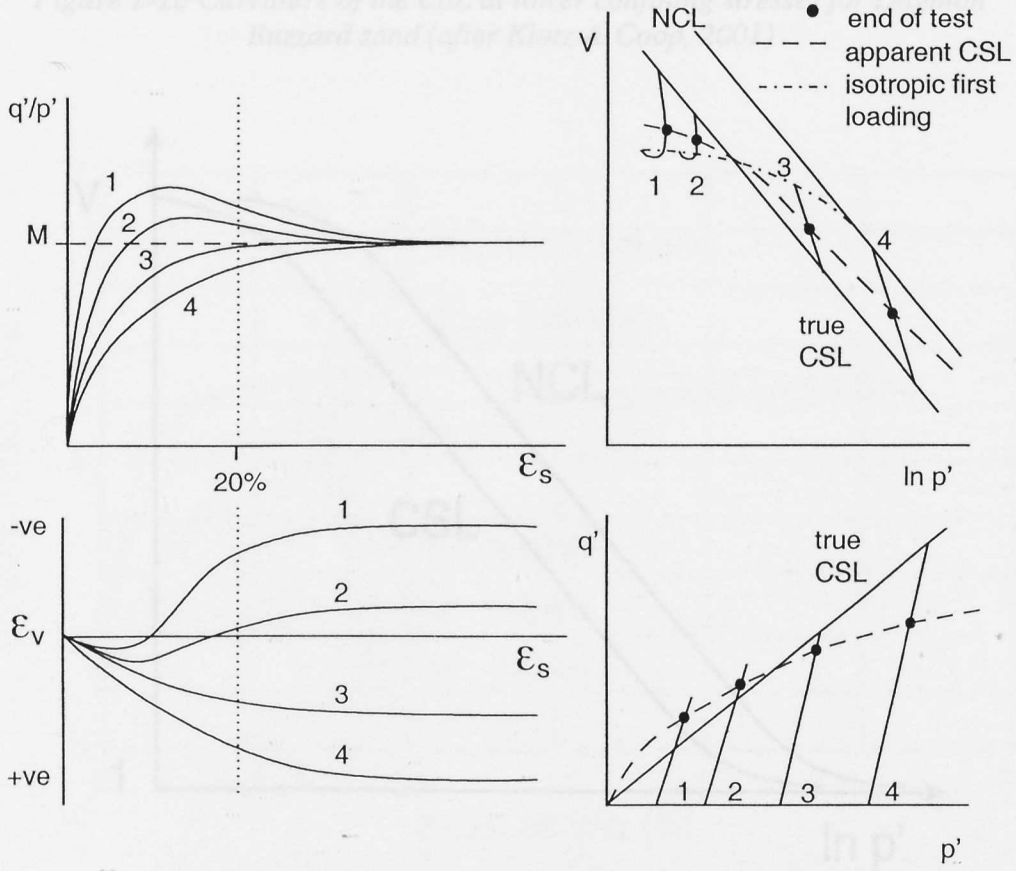


*Figure 2-9 Effects of incomplete testing on the identification of the CSL (after Coop, 1999)*

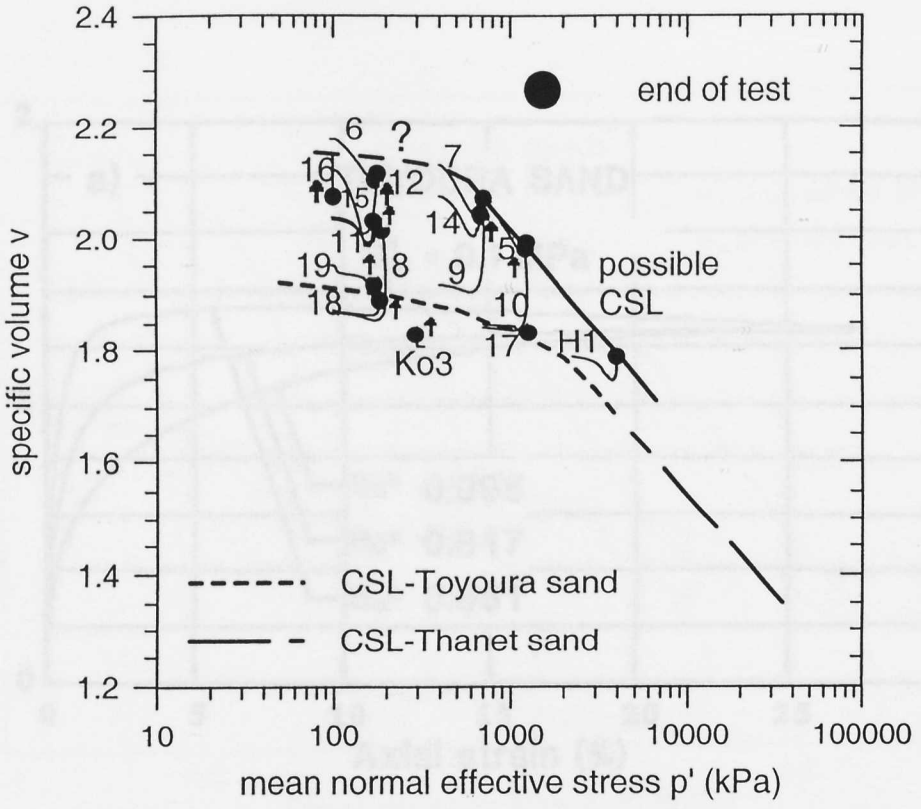


***Figure 2-10*** *Curvature of the CSL at lower confining stresses for Leighton Buzzard sand (after Klotz & Coop, 2001)*

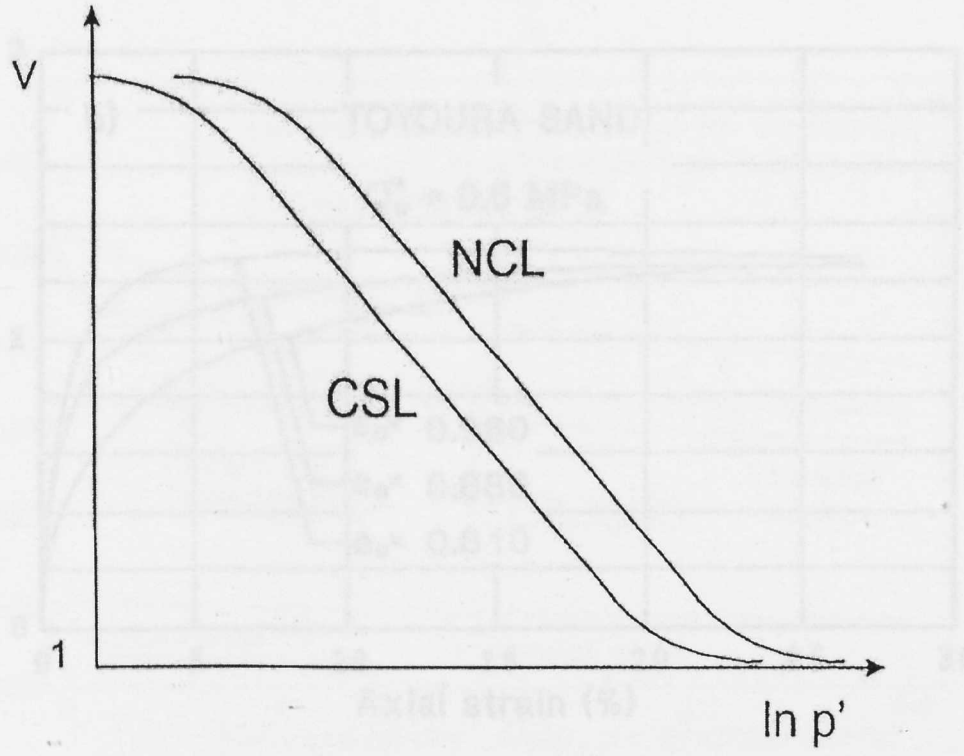


***Figure 2-11*** *Schematic diagram illustrating CSL and NCL over the full range of stresses (after Coop, 1999)*

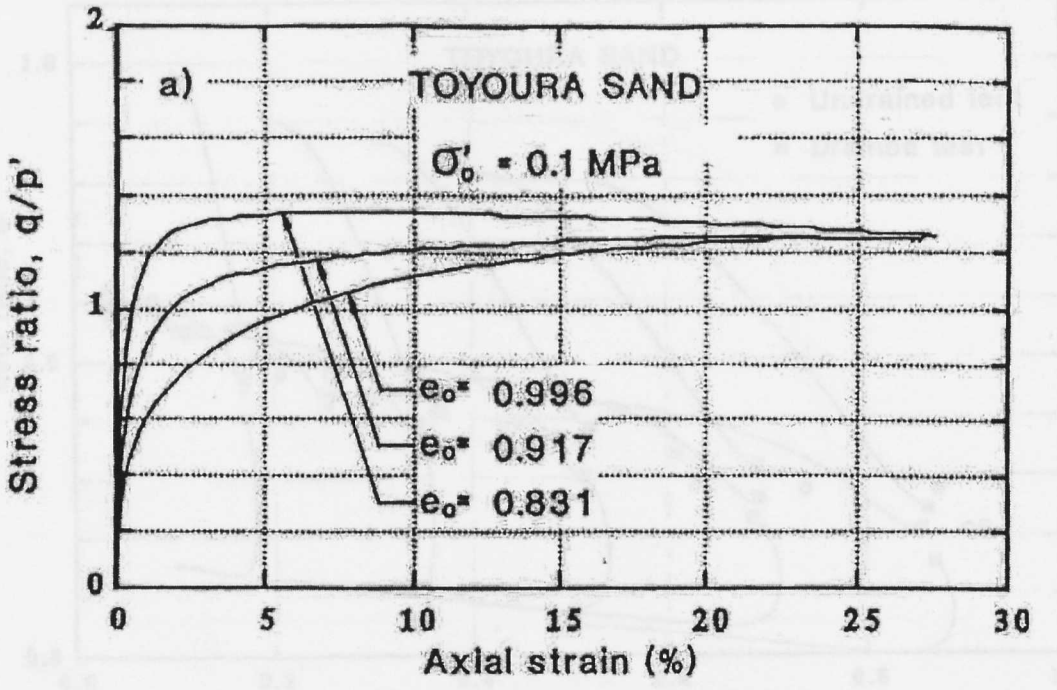


*Figure 2-12 Stress-strain behaviour of Toyoura sand in triaxial tests ($\sigma_0$'=0.1MPa) (after Verdugo & Ishihara, 1996)*

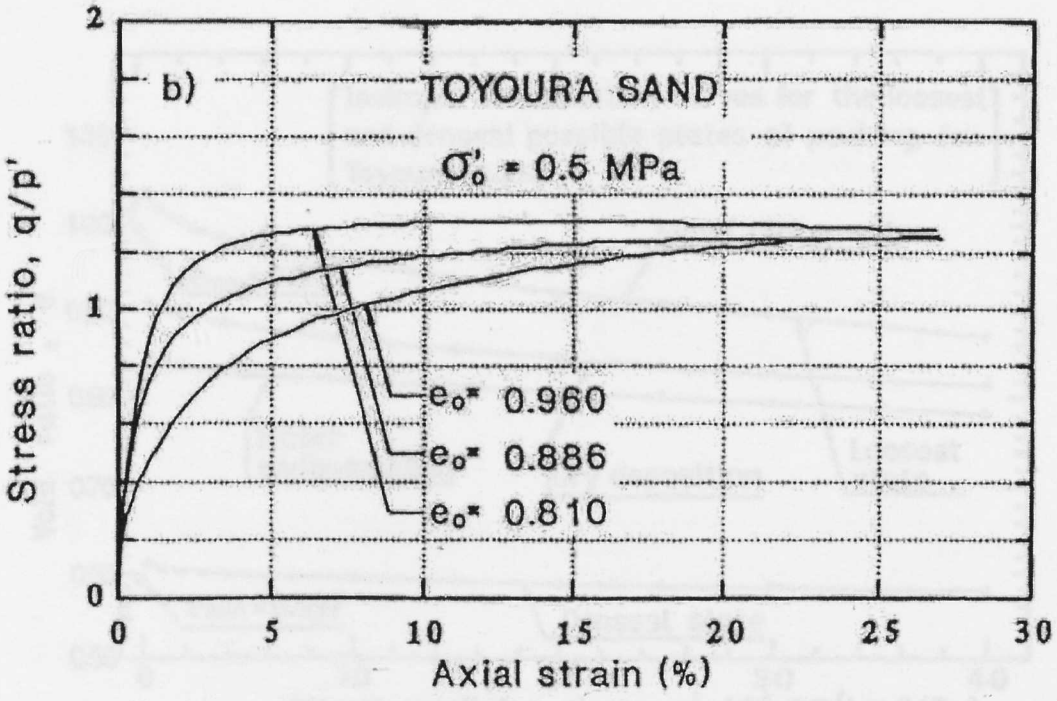


*Figure 2-13 Stress-strain behaviour of Toyoura sand in triaxial tests ($\sigma_0$'=0.5MPa) (after Verdugo & Ishihara, 1996)*

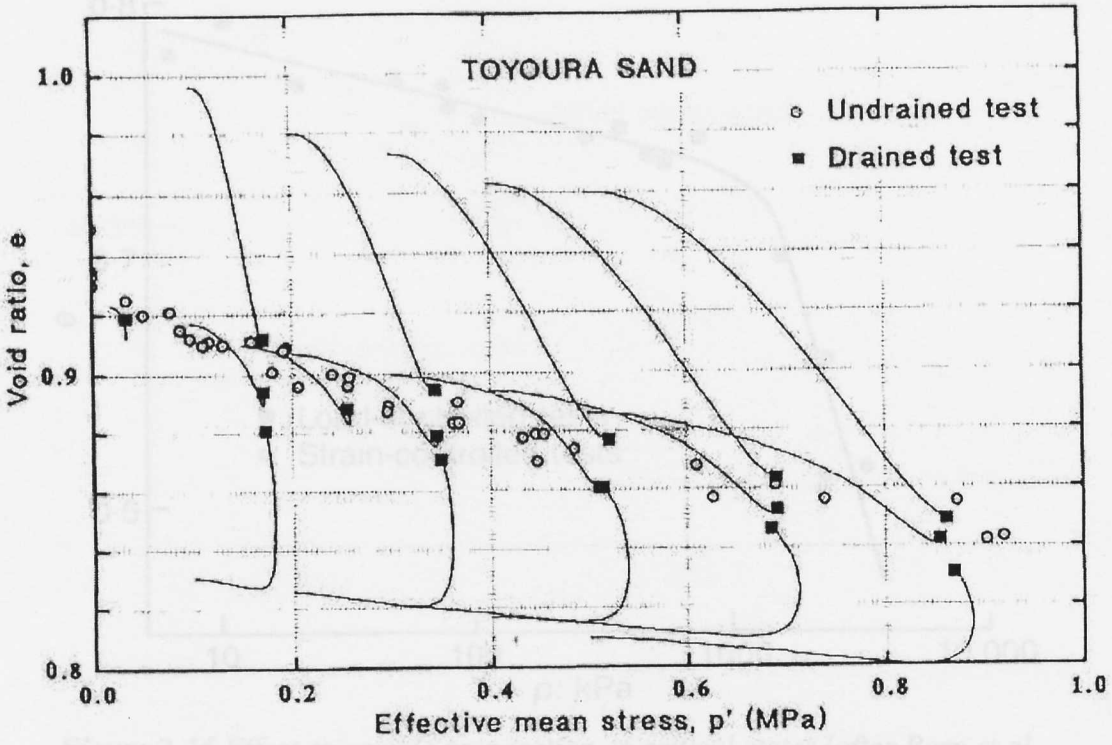


*Figure 2-14 State diagram for Toyoura sand evaluated from both drained and undrained tests (after Verdugo & Ishihara, 1996)*

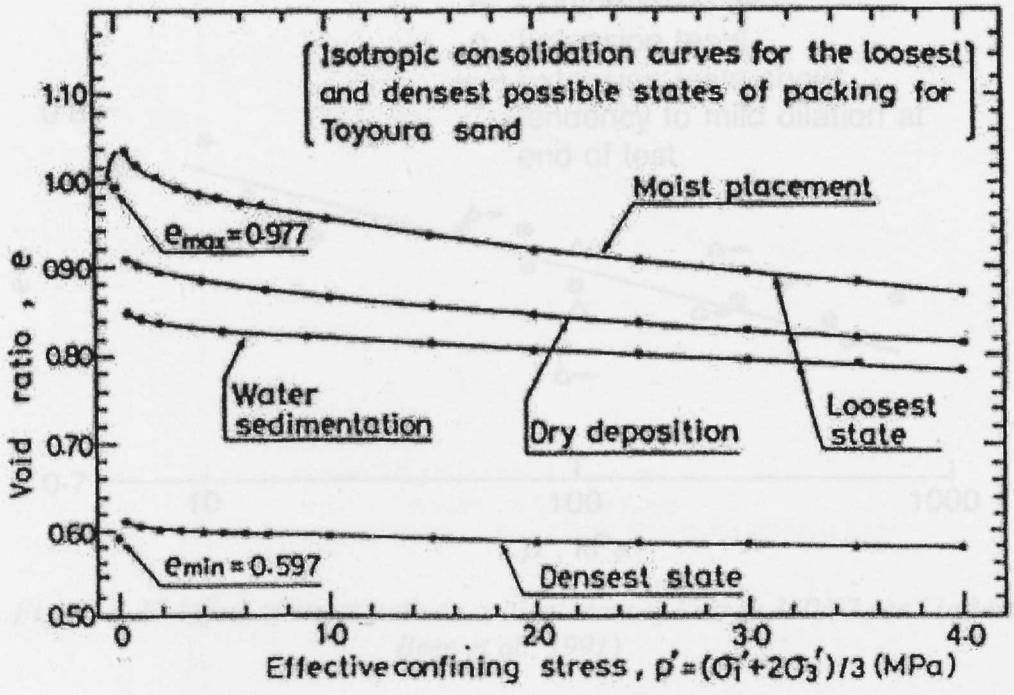


*Figure 2-15 Isotropic compression curves for Toyoura sand samples prepared using three different methods (after Verdugo & Ishihara, 1996)*

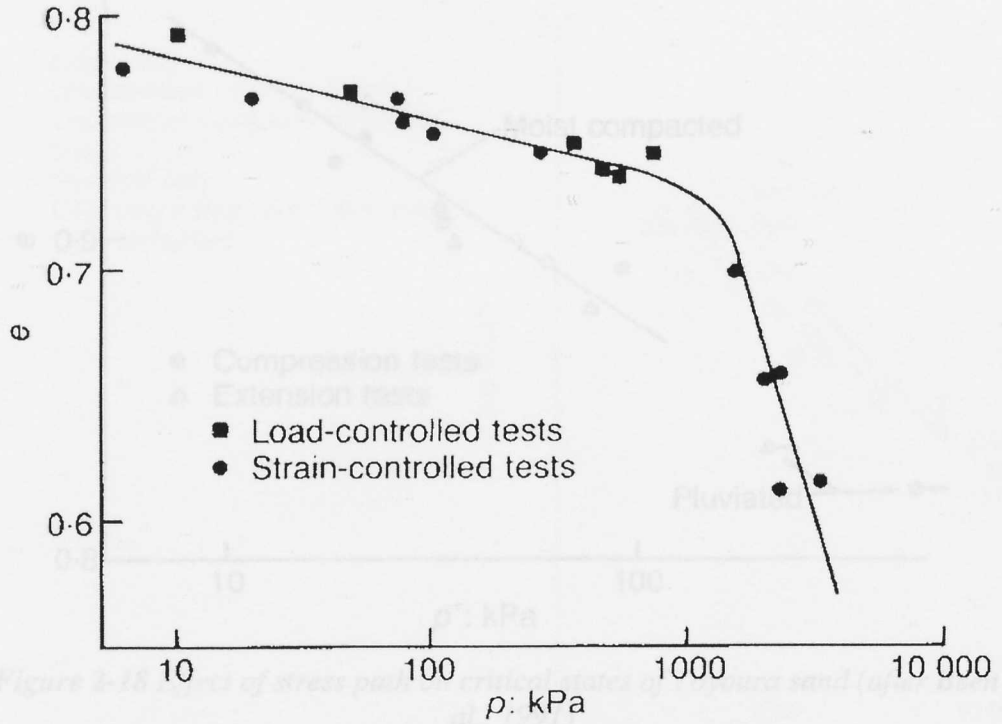


***Figure 2-16*** *Effect on sample preparation on critical states (after Been et al., 1991)*

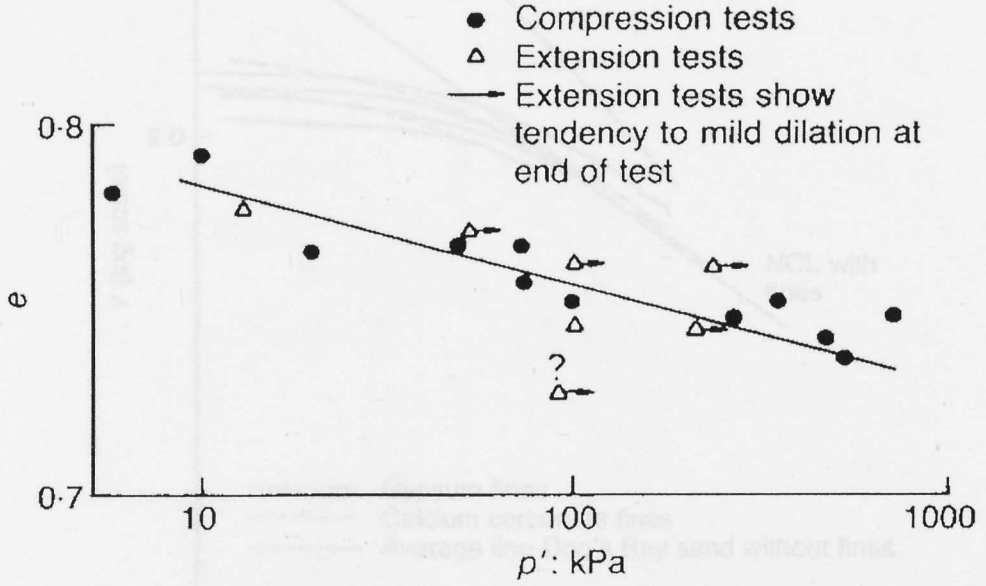


***Figure 2-17*** *Effect of stress-path on critical state of Erksak 330/07 sand (after Been et al., 1991)*

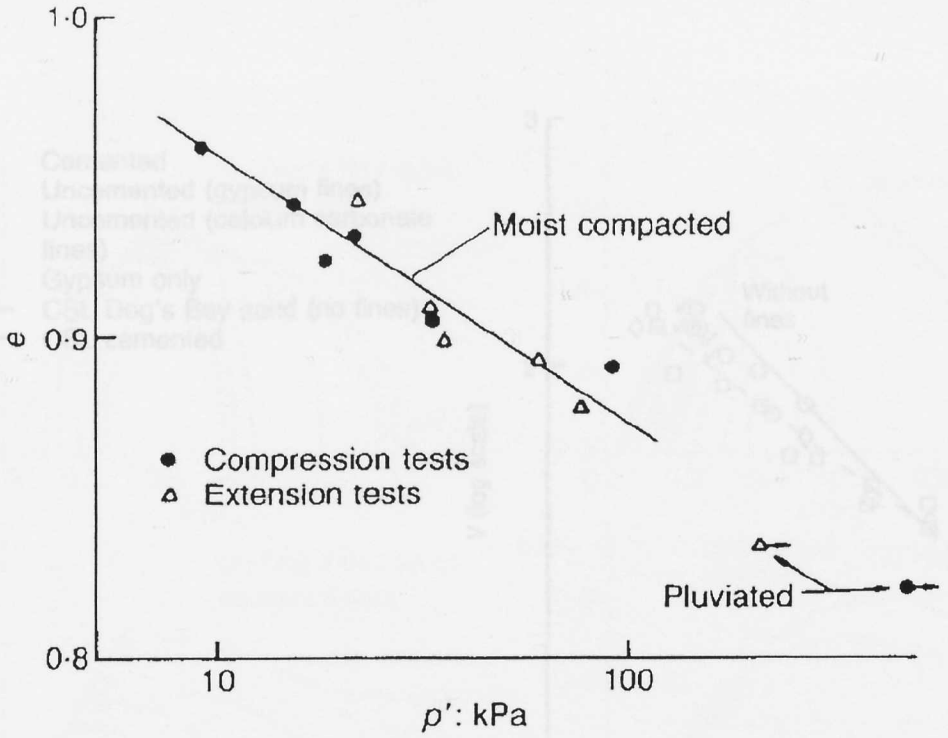


*Figure 2-18 Effect of stress path on critical states of Toyoura sand (after Been et al., 1991)*

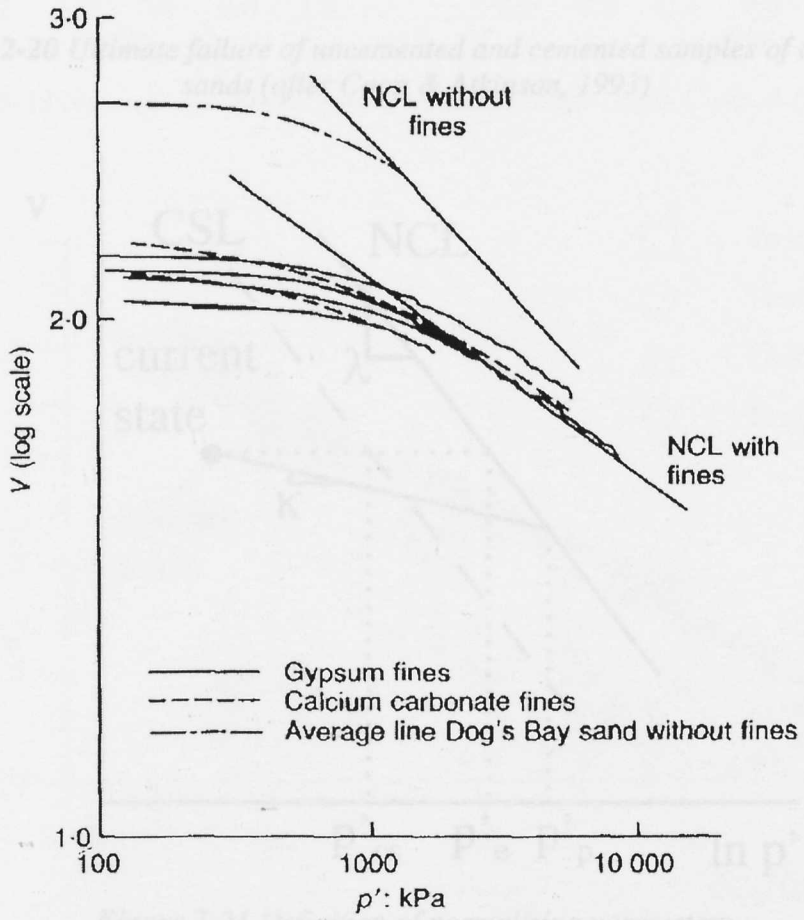


*Figure 2-19 Isotropic compression of reconstituted carbonate sand samples with and without fines (after Coop & Atkinson, 1993)*

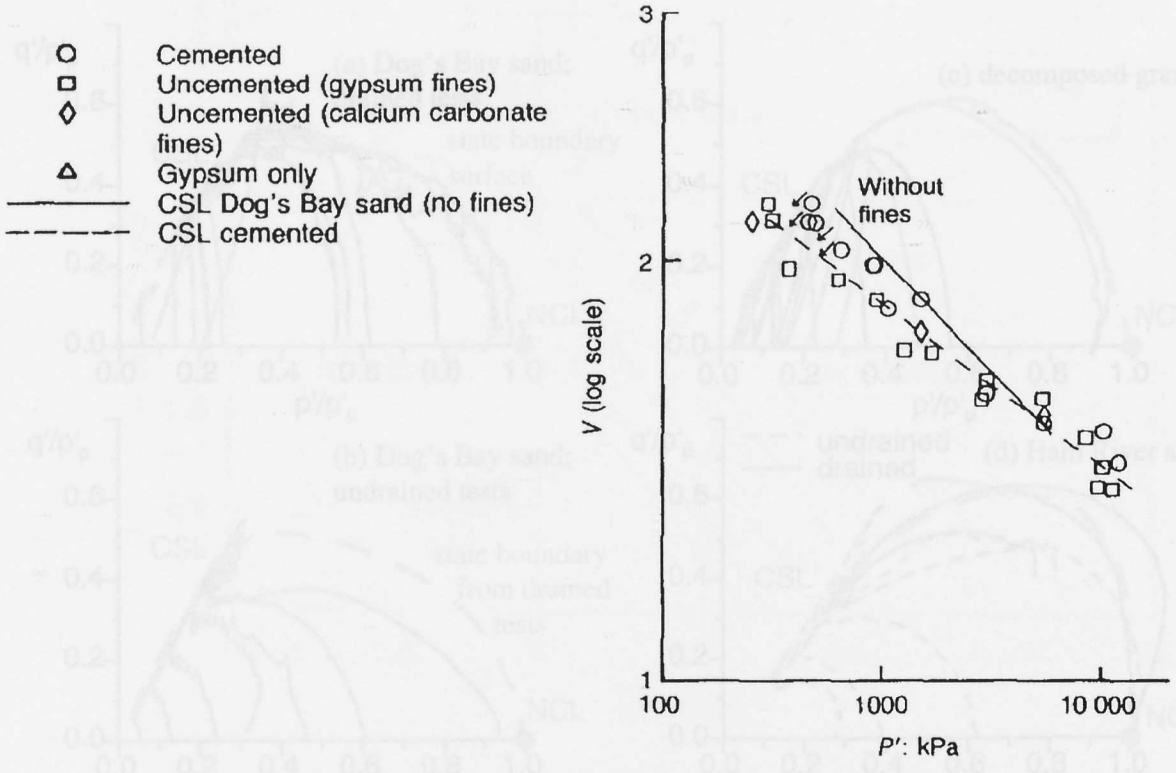


*Figure 2-20 Ultimate failure of uncemented and cemented samples of carbonate sands (after Coop & Atkinson, 1993)*

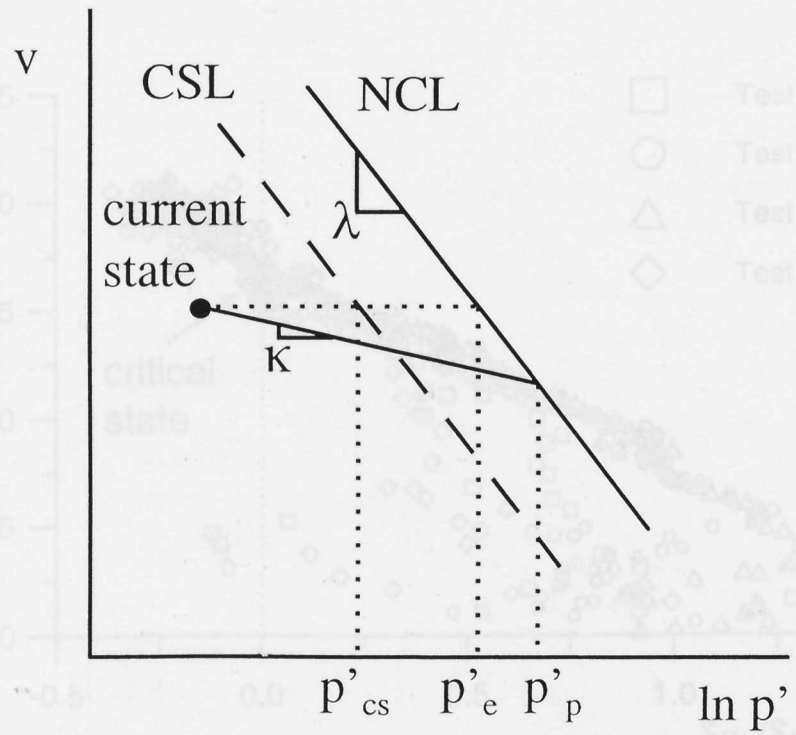


*Figure 2-21 Definition of normalizing parameters*

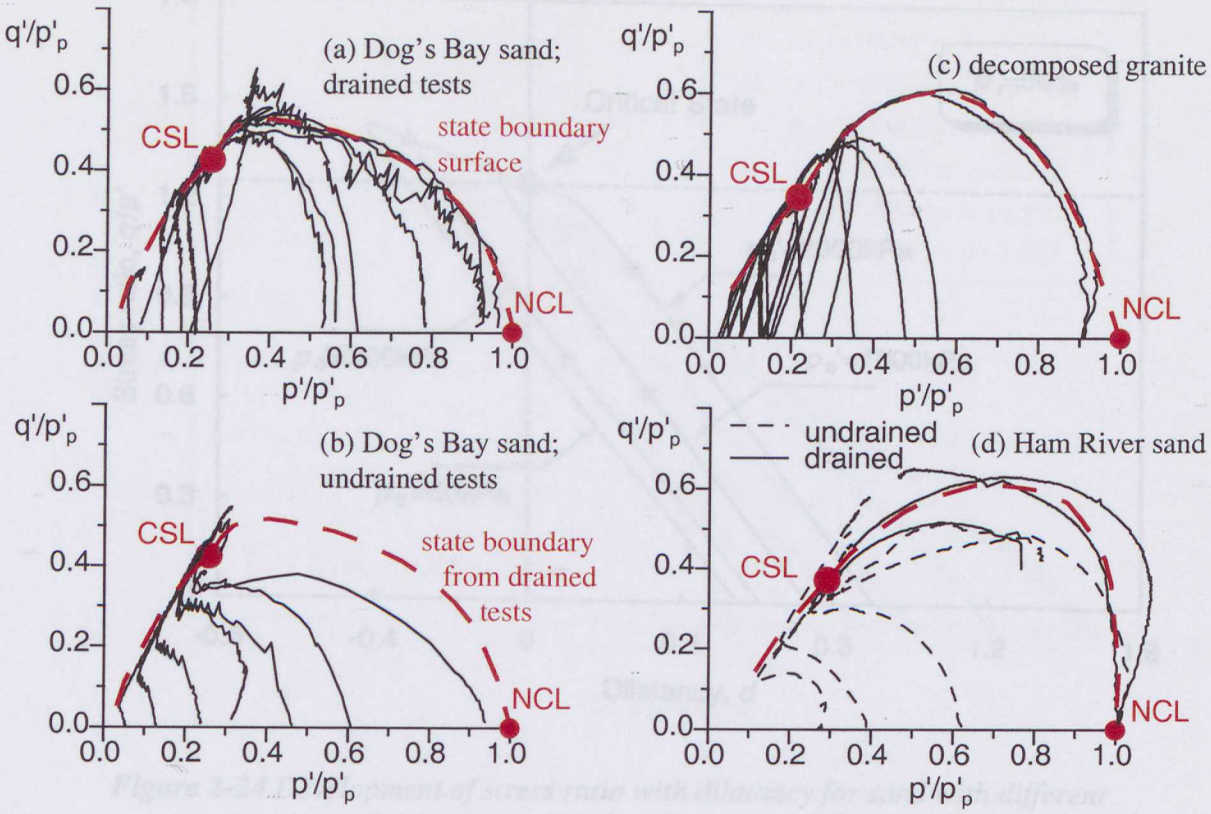


***Figure 2-22*** *Normalised shearing data for three sands (after Coop & Lee, 1993)*

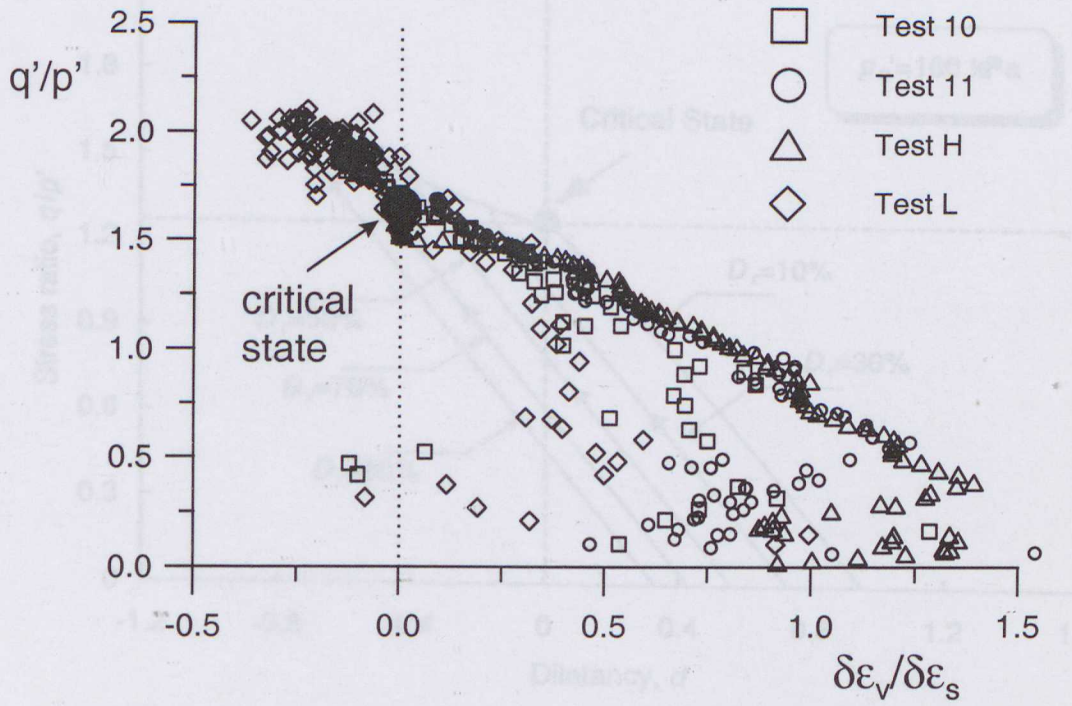


***Figure 2-23*** *Stress dilatancy data for Dogs Bay sand (after Coop, 1990)*

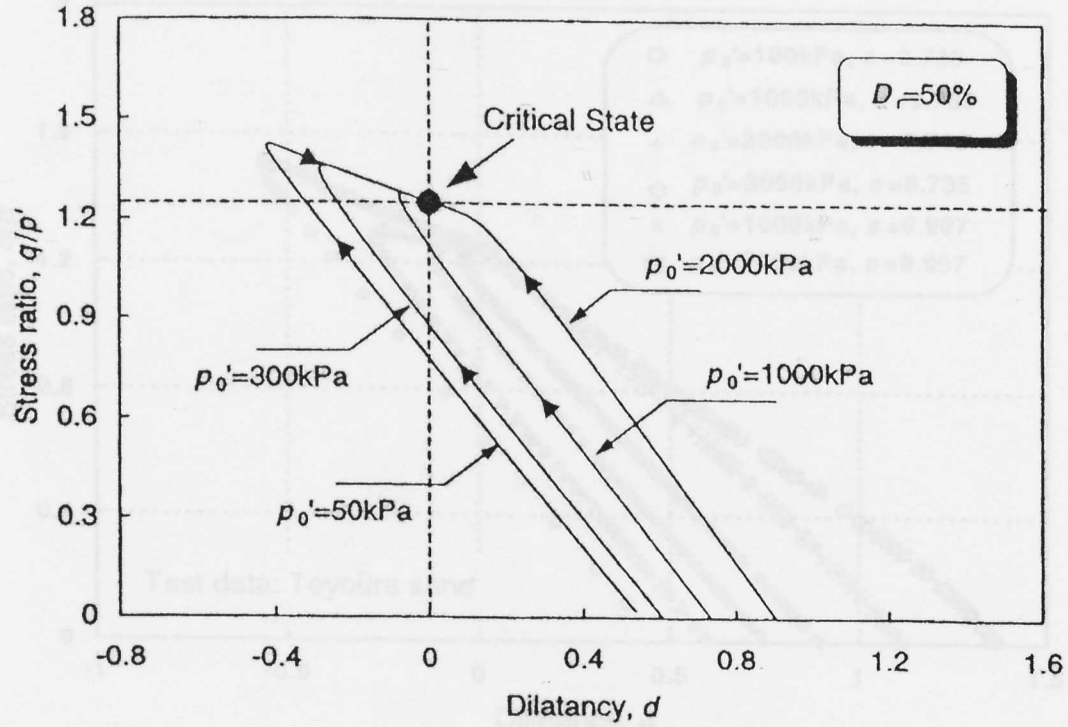


*Figure 2-24 Development of stress ratio with dilatancy for sand with different confining pressures (after Yang and Li, 2004)*

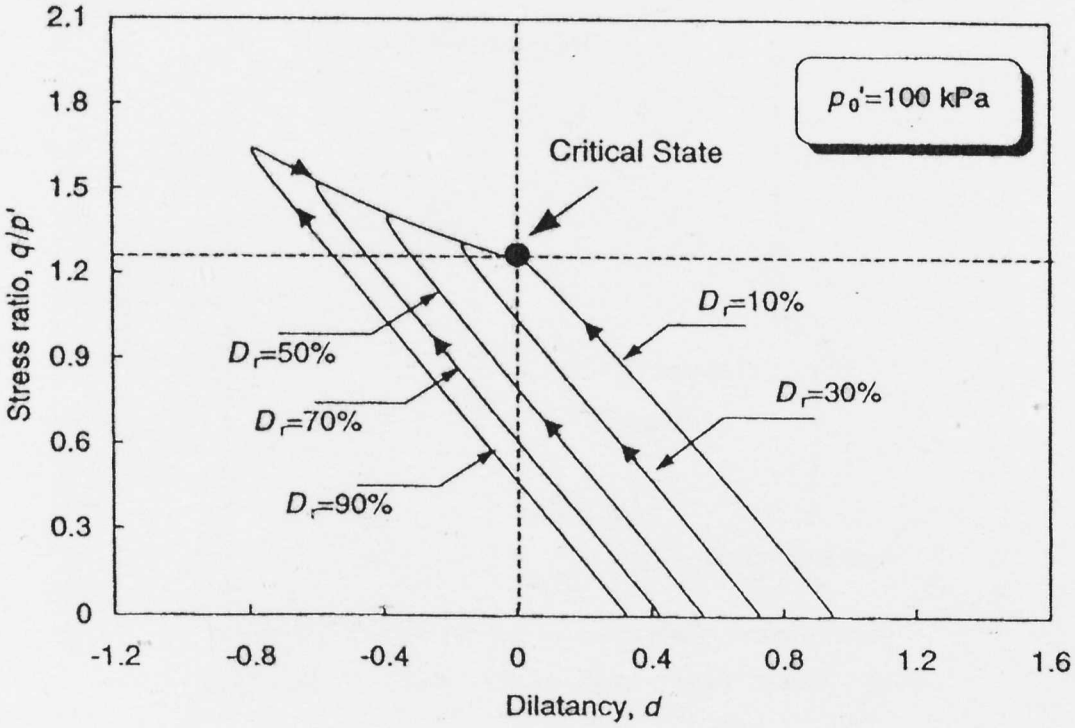


*Figure 2-25 Development of stress ratio with dilatancy for sand with different densities (after Yang and Li, 2004)*

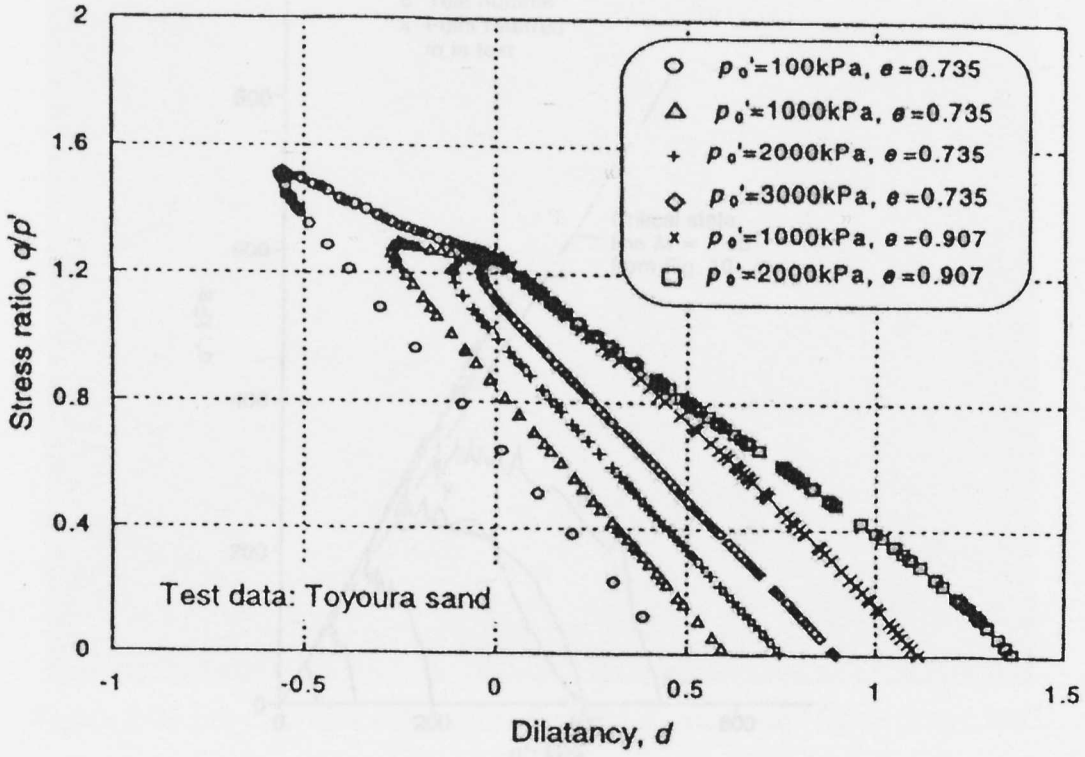


***Figure 2-26*** *Experimental data for stress-dilatancy relationship (data from Verdugo and Ishihara, 1996) (after Yang and Li, 2004)*

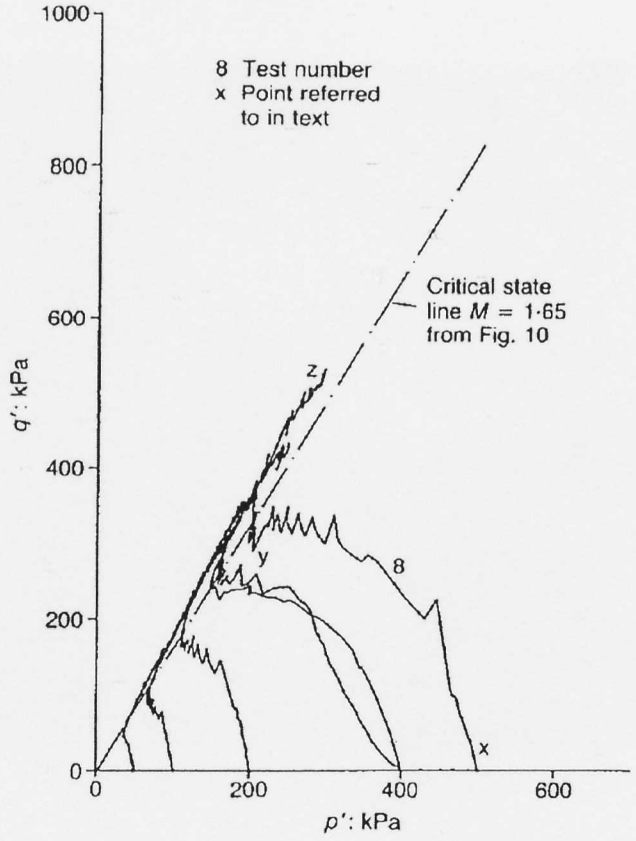


*Figure 2-27 Undrained tests on Dogs Bay sand (after Coop, 1990)*

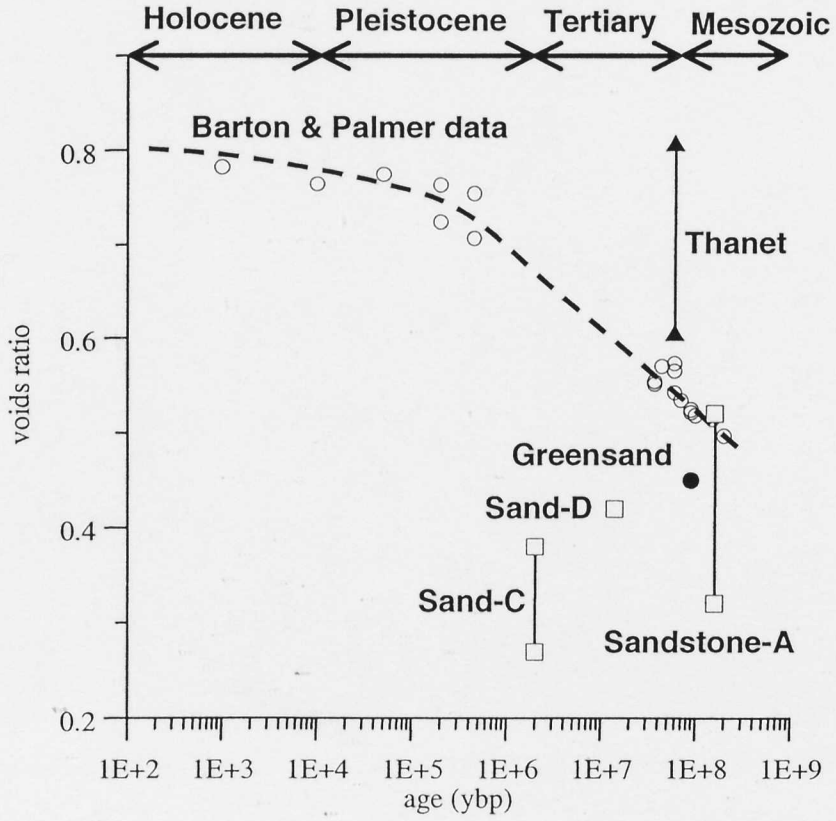


*Figure 2-28 Correlation between voids ratio and age of material (after Coop, 2003 using data from Barton & Palmer, 1989)*

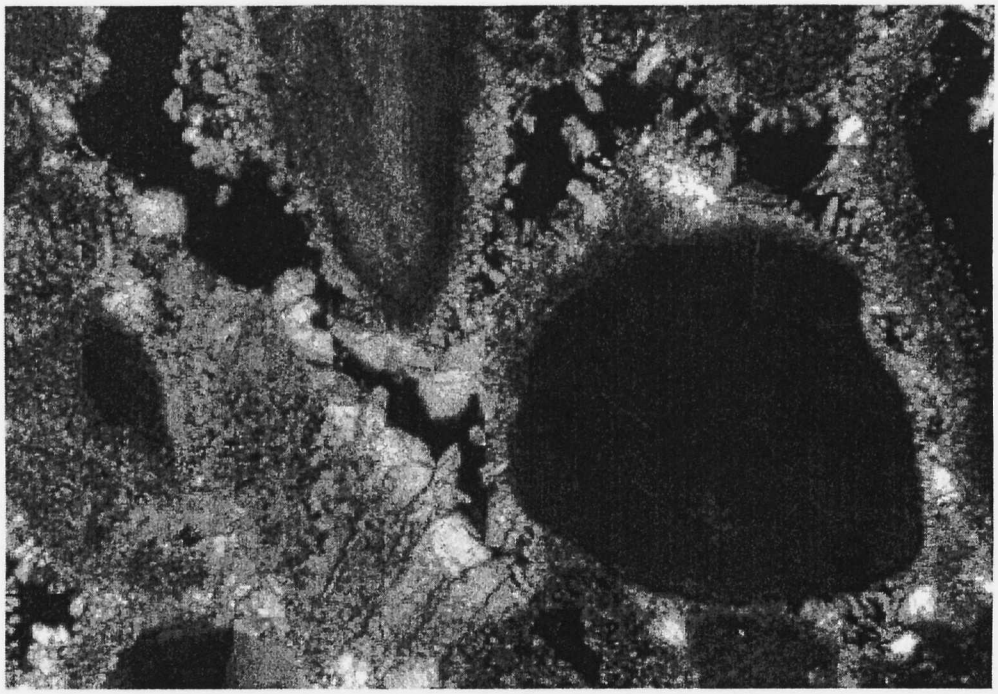

***Figure 2-29*** *Inter-particle cementing of a Rankin calcarenite (after Coop, 2003)*

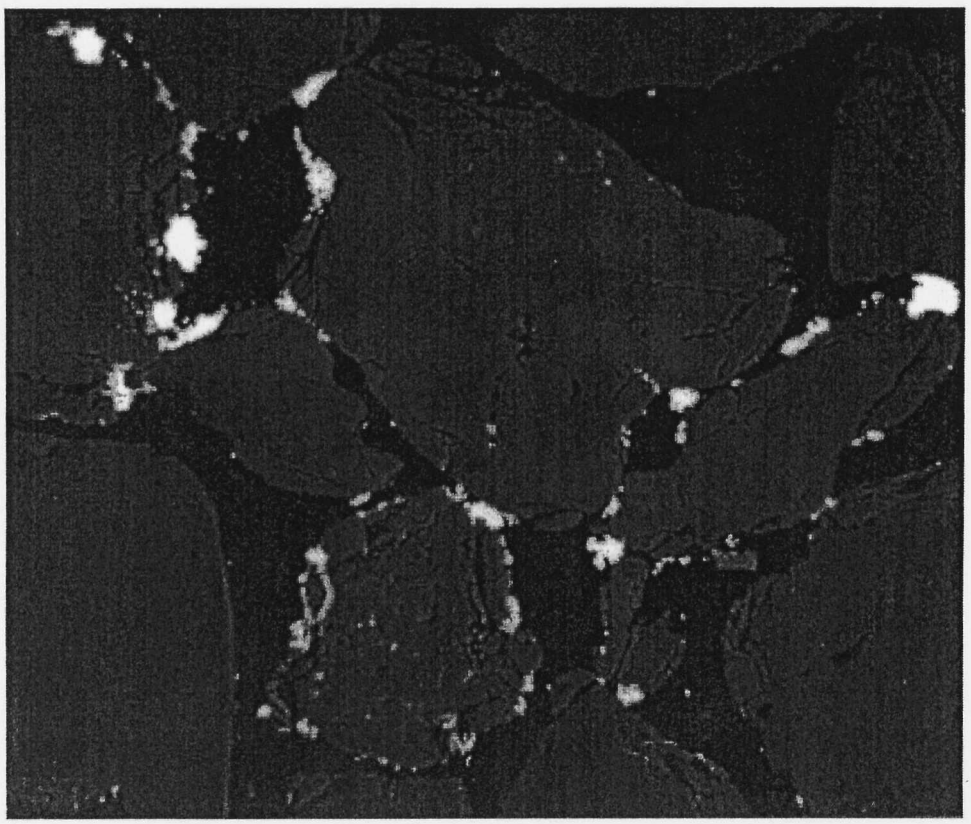

***Figure 2-30*** *Particle interlocking and inter-particle cementing of Lower Greensand (after Coop, 2003)*

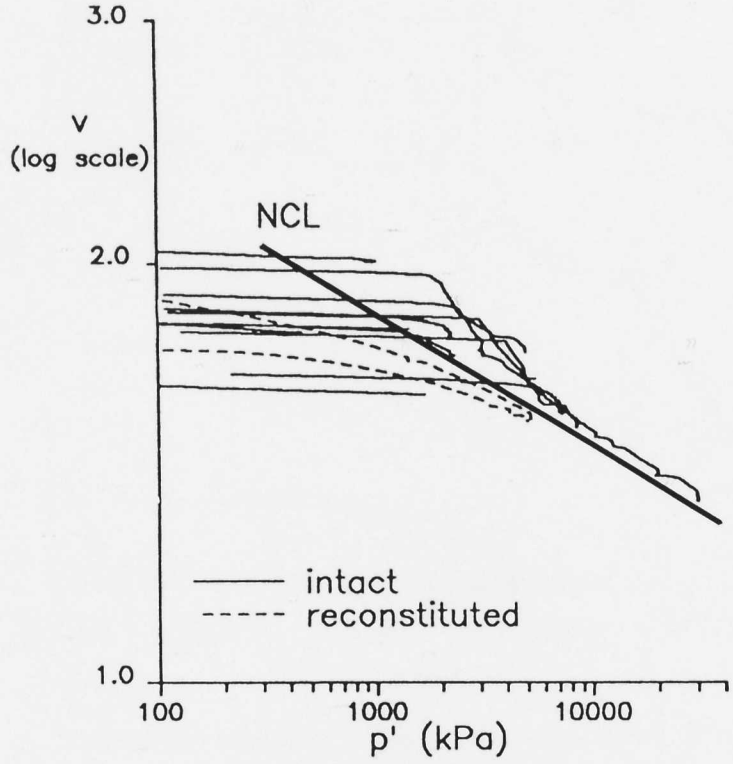


***Figure 2-31*** *Compression data for Rankin calcarenite (after Cuccovillo & Coop, 1999)*

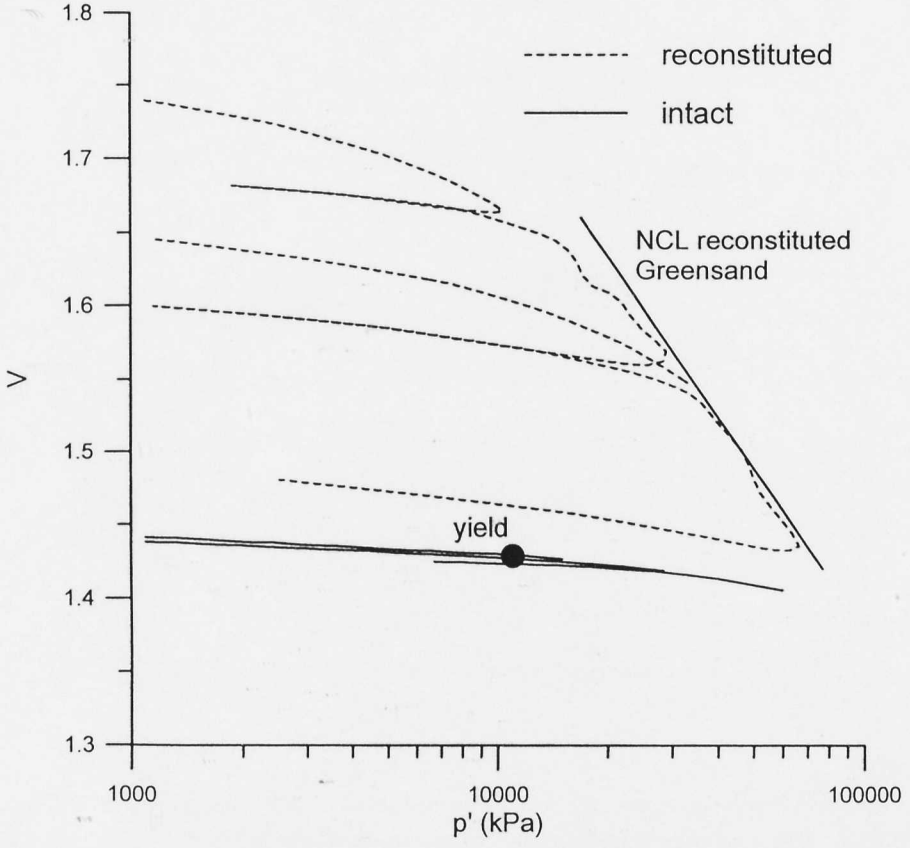


***Figure 2-32*** *Compression data for Lower Greensand (after Cuccovillo & Coop, 1999)*

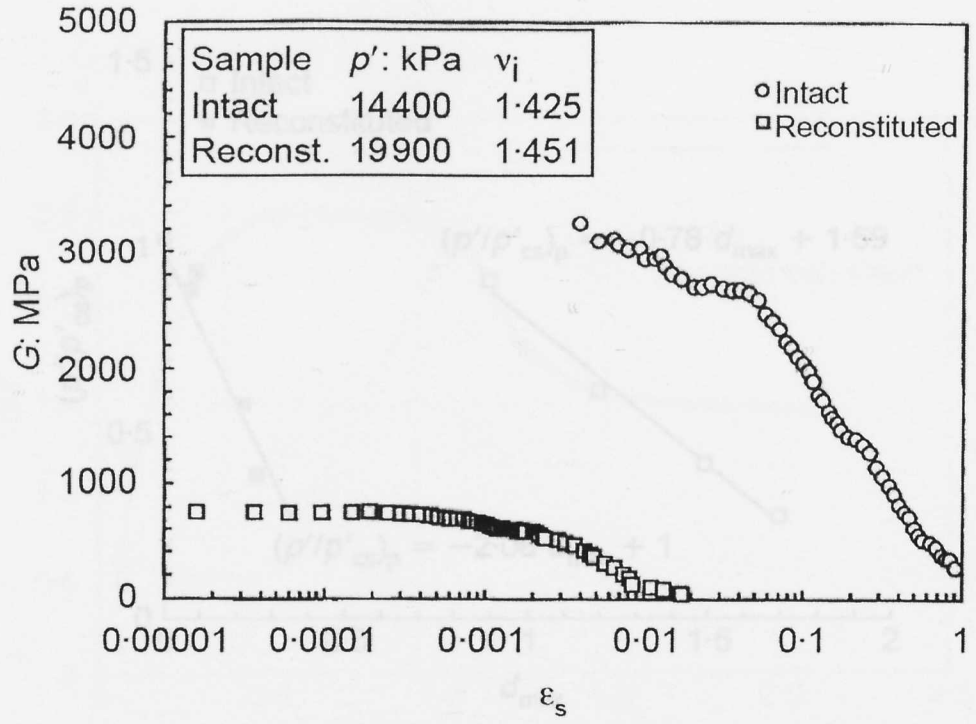


***Figure 2-33*** *Comparison between the shear moduli of intact and reconstituted silica sandstone (after Cuccovillo & Coop, 1997)*

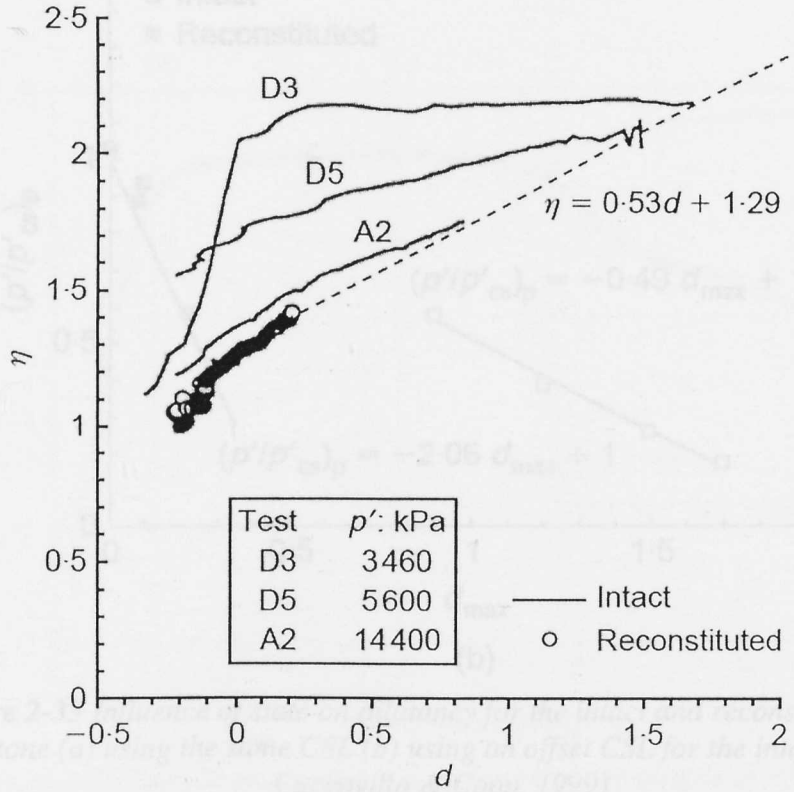


***Figure 2-34*** *Comparison between stress-dilatancy relationships of intact and reconstituted silica sandstone samples (after Cuccovillo & Coop, 1999)*

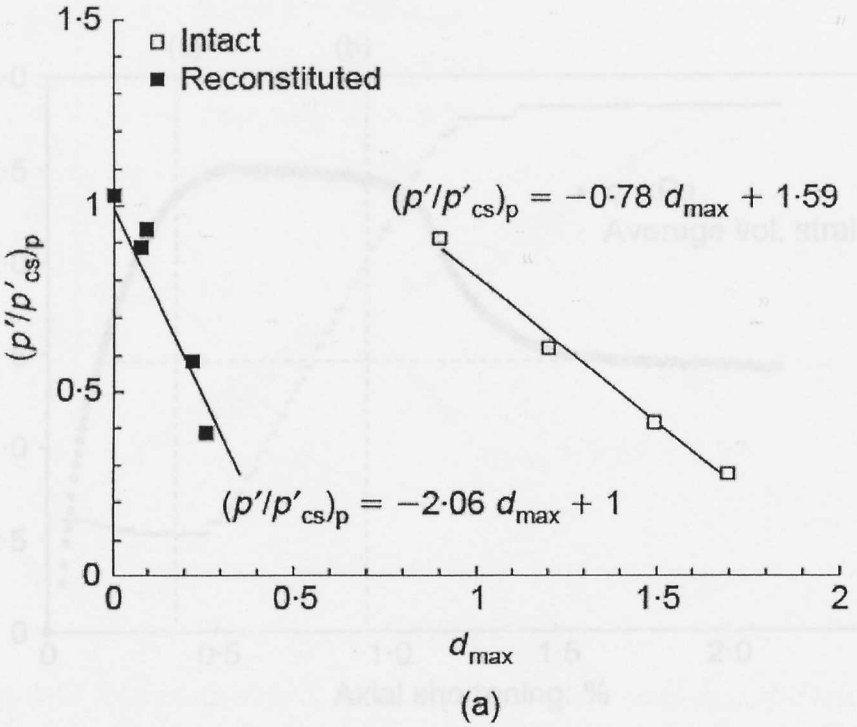


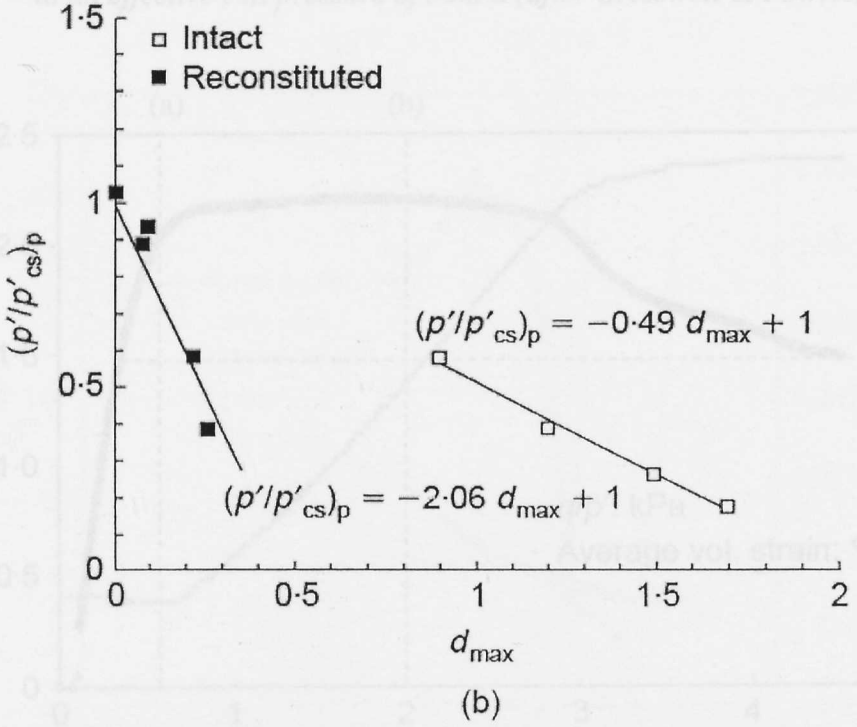


***Figure 2-35*** *Influence of state on dilatancy for the intact and reconstituted silica sandstone (a) using the same CSL (b) using an offset CSL for the intact soil (after Cuccovillo & Coop, 1999)*

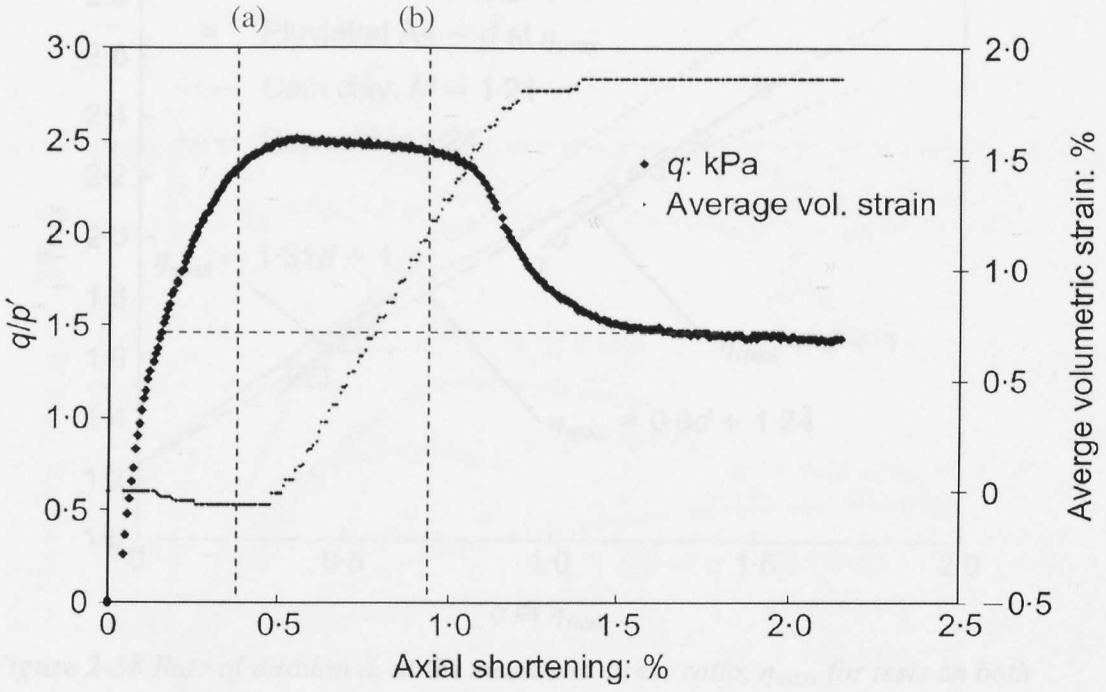


***Figure 2-36*** *Typical stress: strain data for an intact sample of Reigate silver sand at an effective cell pressure of 50kPa (after Cresswell & Powrie, 2004)*

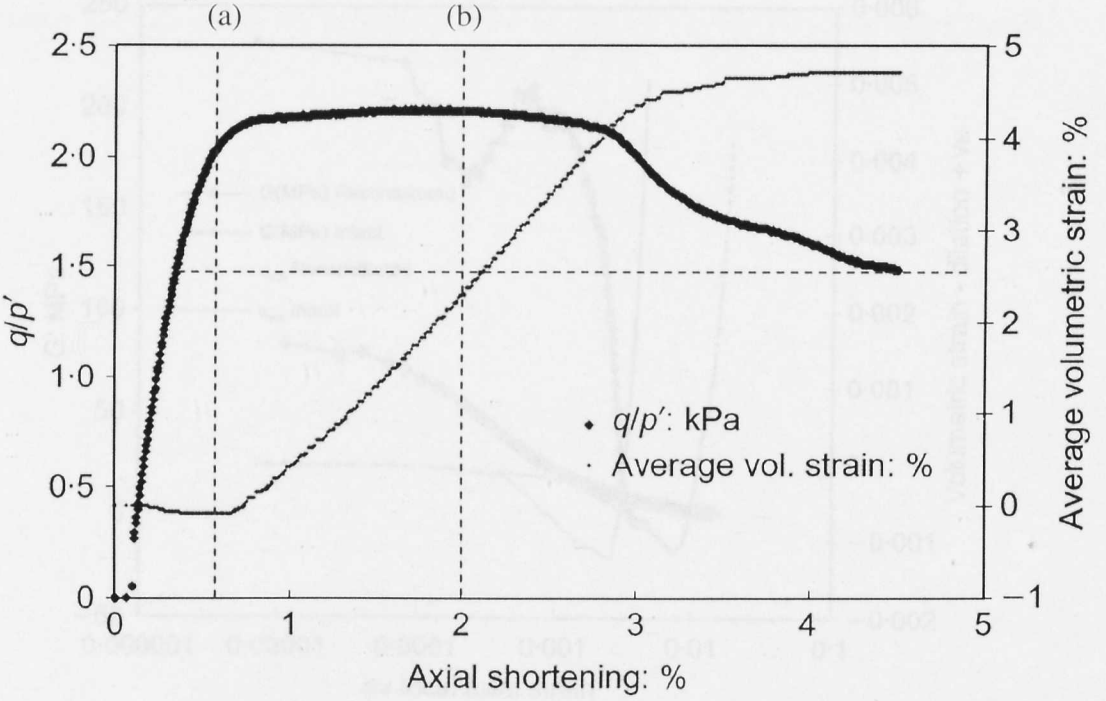


***Figure 2-37*** *Typical stress: strain data for an intact sample of Reigate silver sand at an effective cell pressure of 200kPa (after Cresswell & Powrie, 2004)*

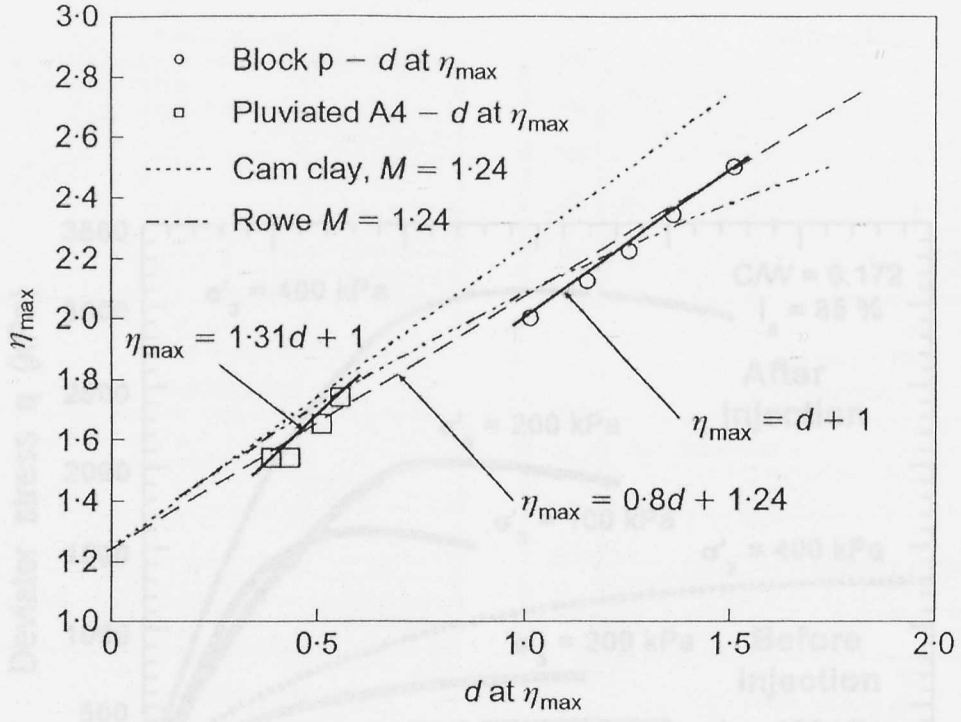


***Figure 2-38*** *Rate of dilation d, at the maximum stress ratio, $\eta_{max}$, for tests on both intact and pluviated A4 sand at different cell pressures (after Cresswell & Powrie, 2004)*

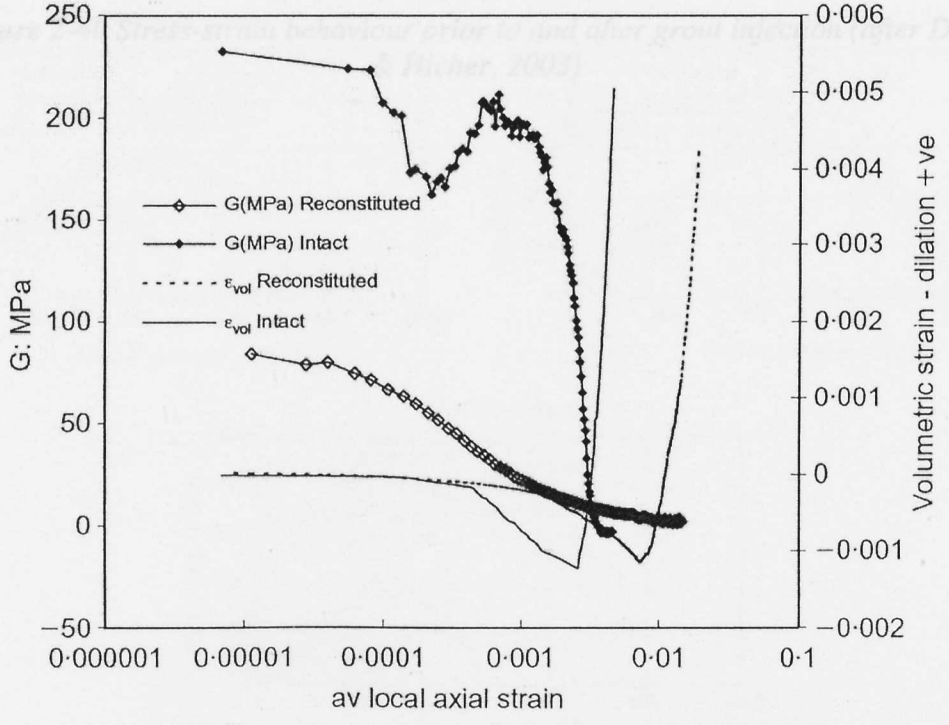


***Figure 2-39*** *Shear modulus G and volumetric strain $\varepsilon_{vol}$ plotted against average local axial strain for intact and pluviated samples of A4 sand (effective cell pressure 100kPa) (after Cresswell & Powrie, 2004)*

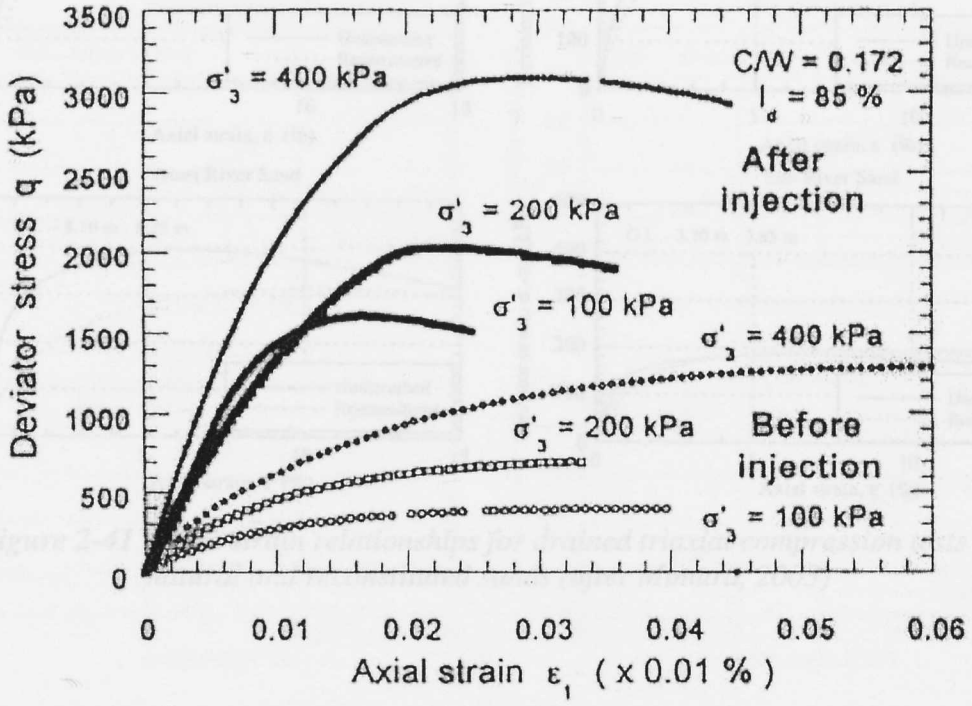


***Figure 2-40*** *Stress-strain behaviour prior to and after grout injection (after Dano & Hicher, 2003)*

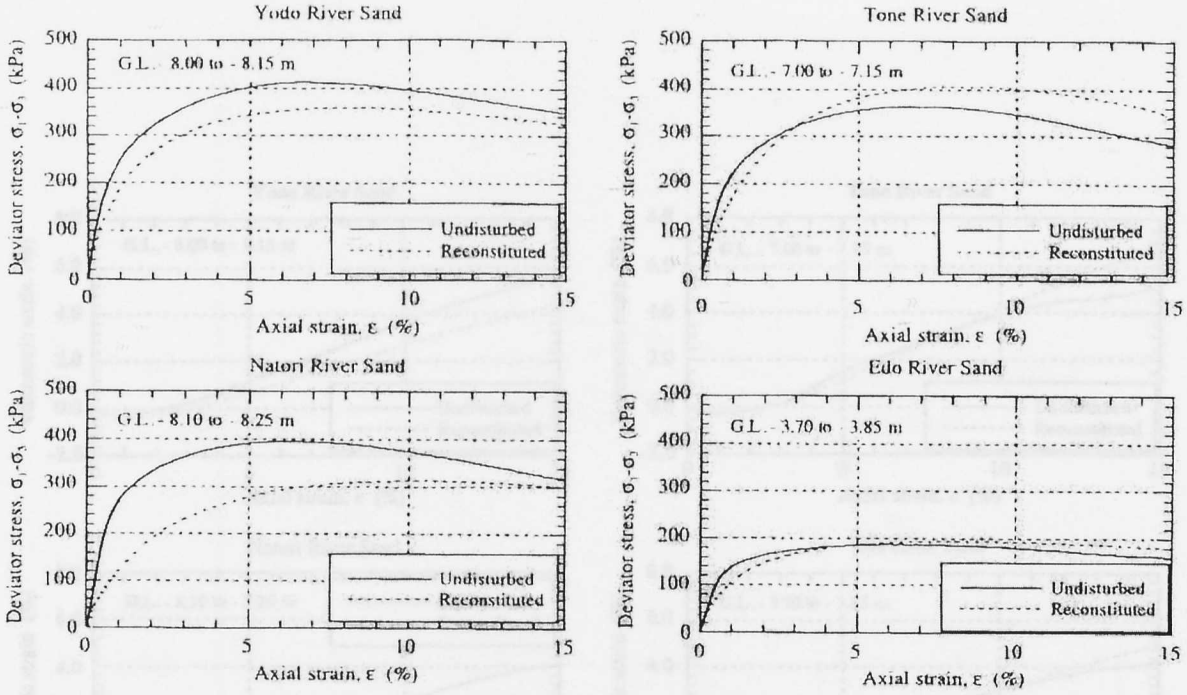


***Figure 2-41*** *Stress-strain relationships for drained triaxial compression tests of natural and reconstituted sands (after Mimura, 2003)*

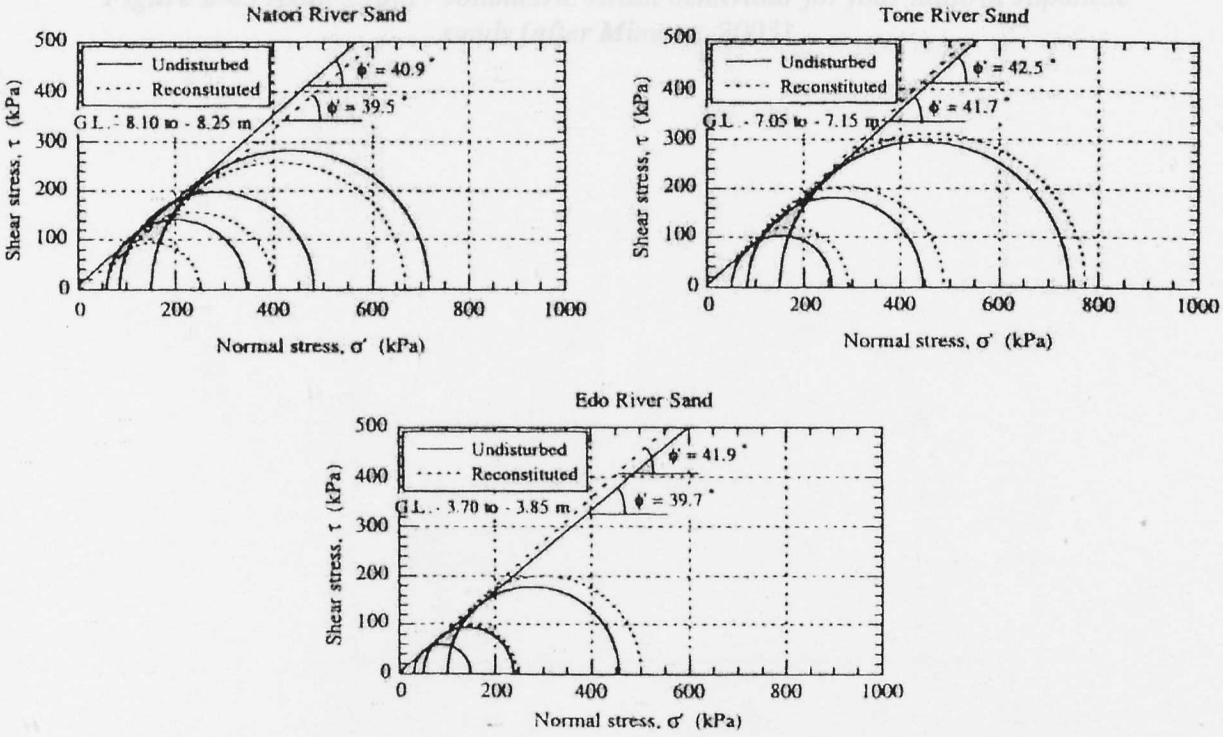


***Figure 2-42*** *Angles of shearing resistance for three sands (after Mimura, 2003)*

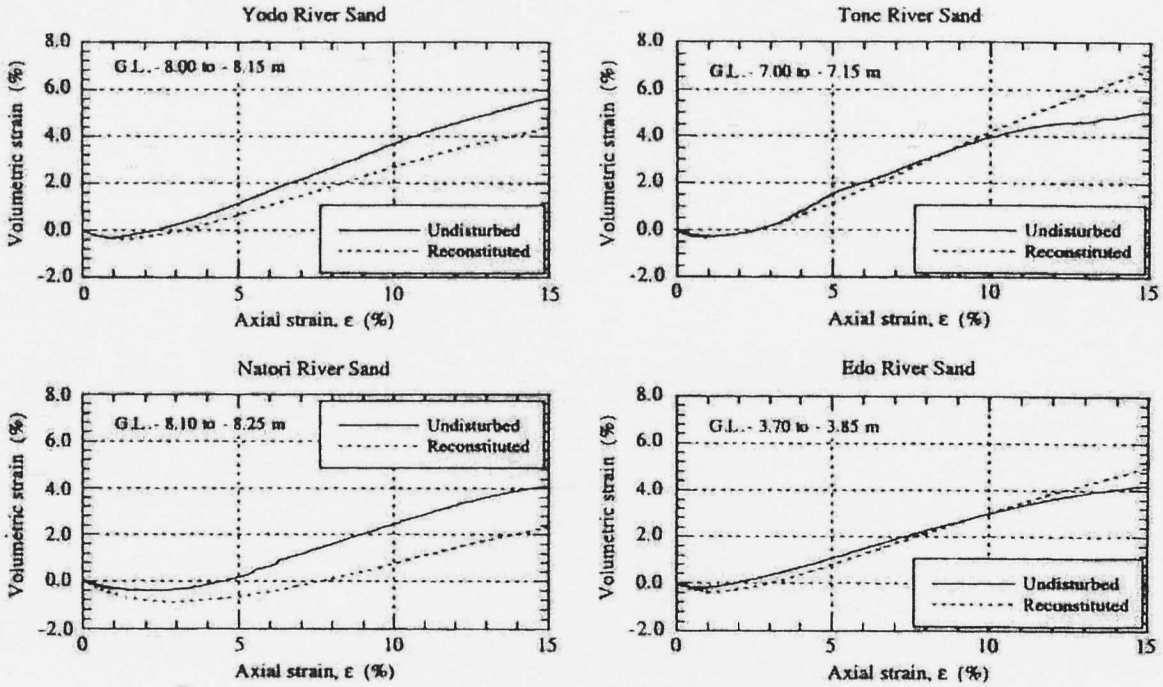


***Figure 2-43*** *Axial strain - volumetric strain behaviour for four natural Japanese sands (after Mimura, 2003)*

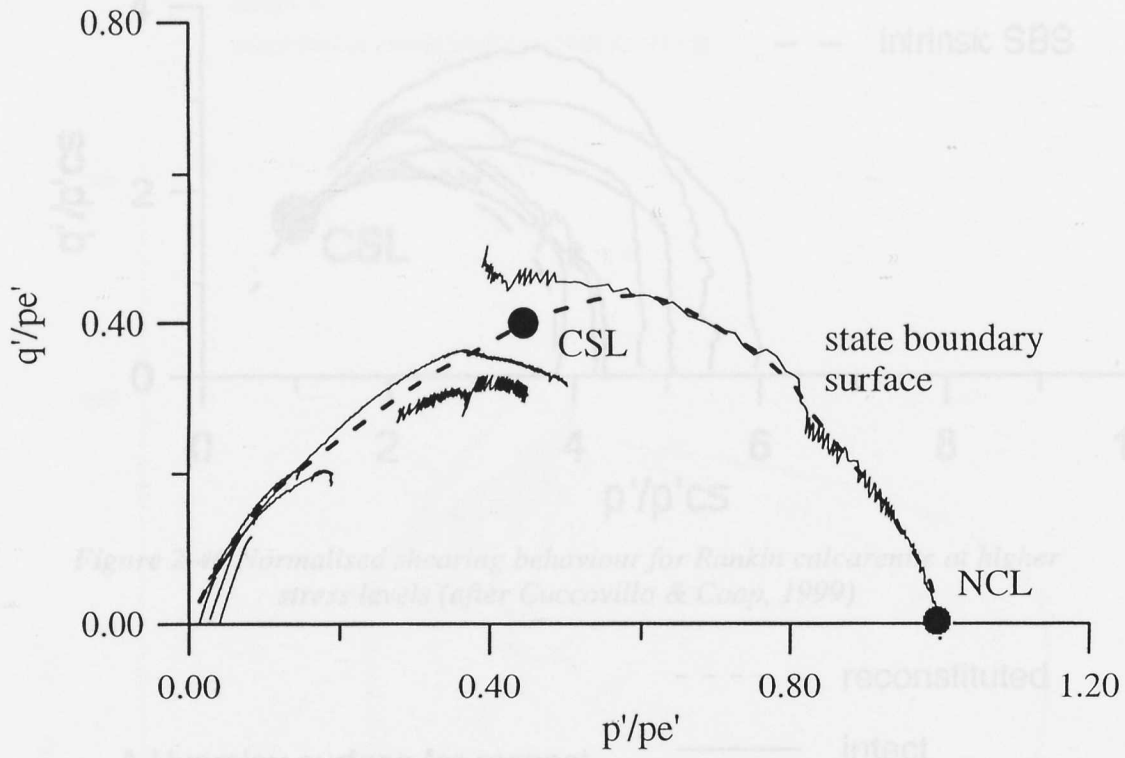


***Figure 2-44*** *Normalised shearing data for a reservoir sand (after Coop & Wilson, 2003)*

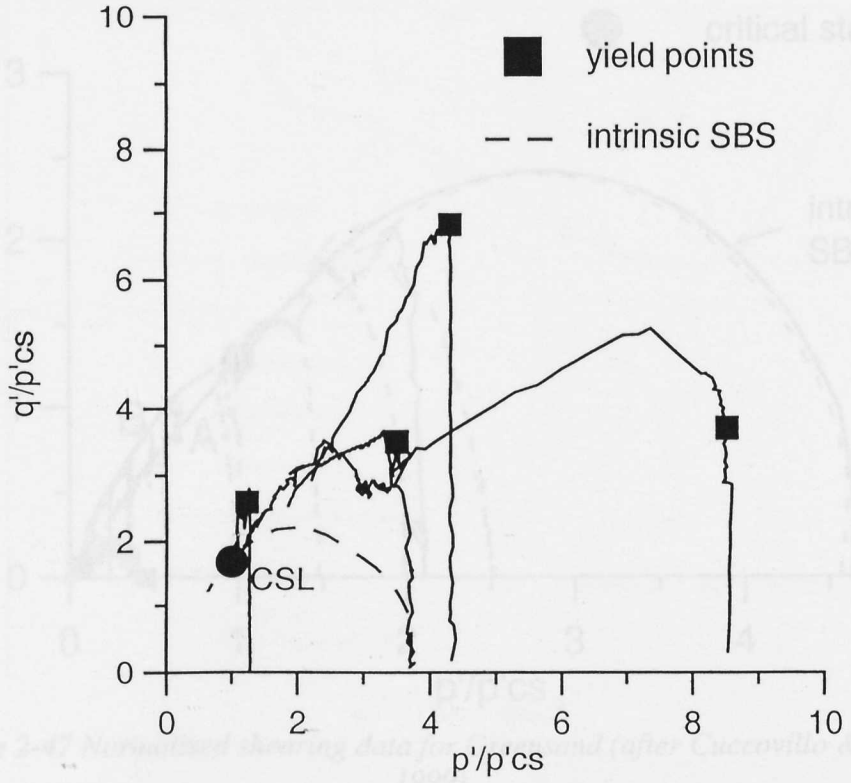


***Figure 2-45*** *Normalised shearing behaviour for Rankin calcarenite at lower stress levels (after Cuccovillo & Coop, 1999)*

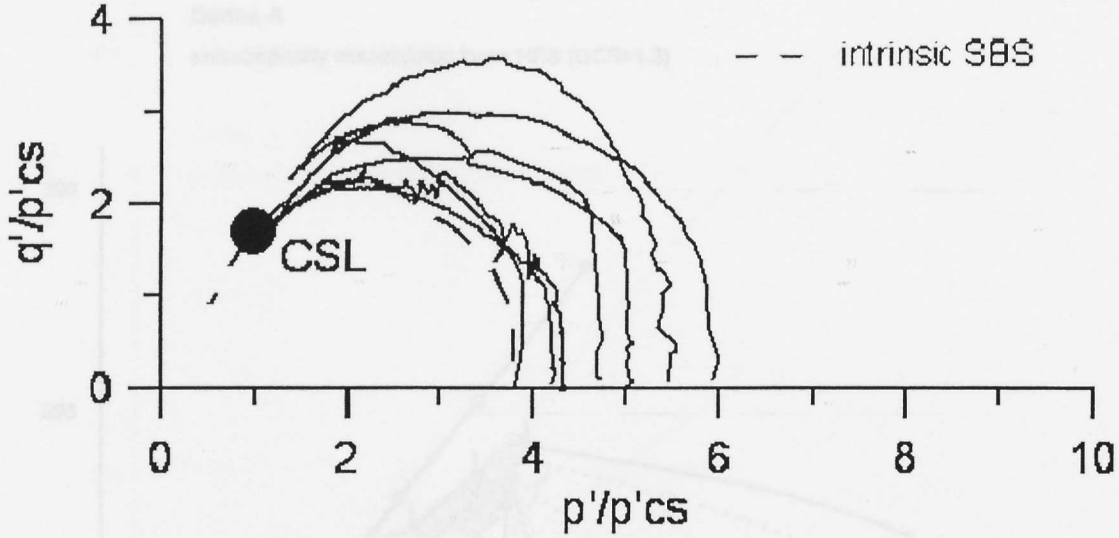


*Figure 2-46 Normalised shearing behaviour for Rankin calcarenite at higher stress levels (after Cuccovillo & Coop, 1999)*

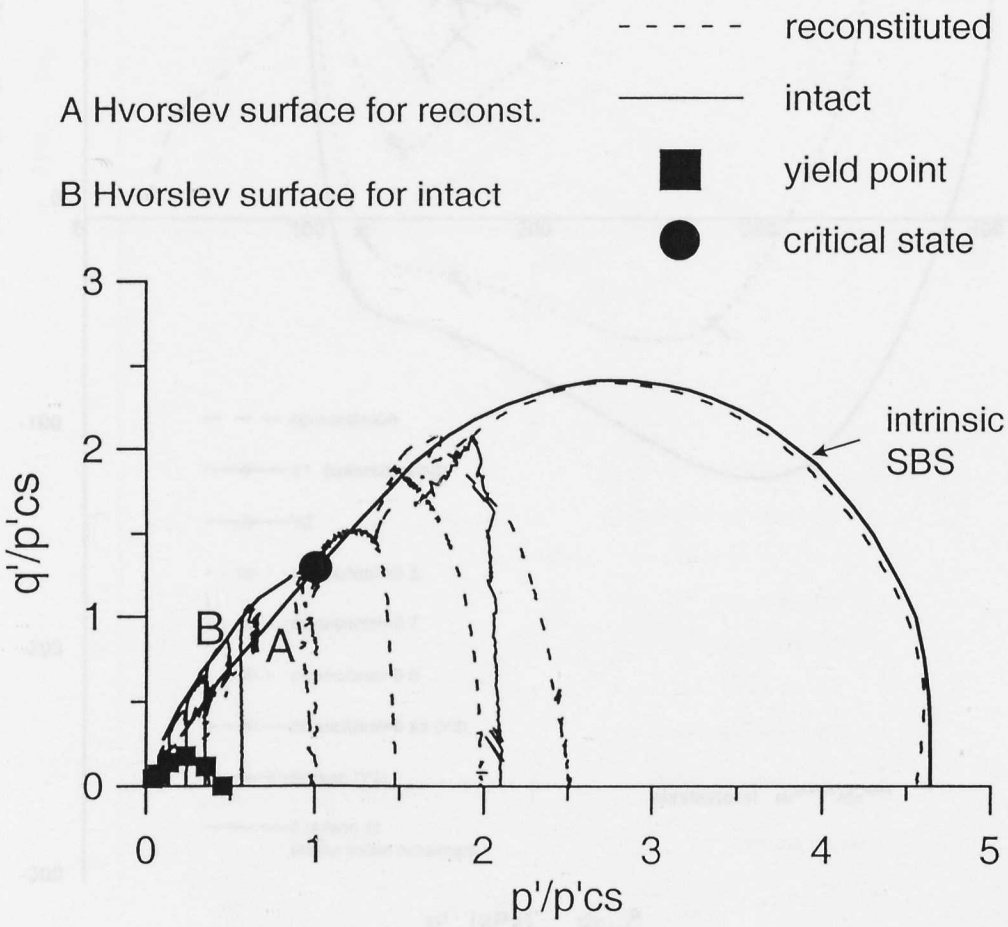


*Figure 2-47 Normalised shearing data for Greensand (after Cuccovillo & Coop, 1999)*

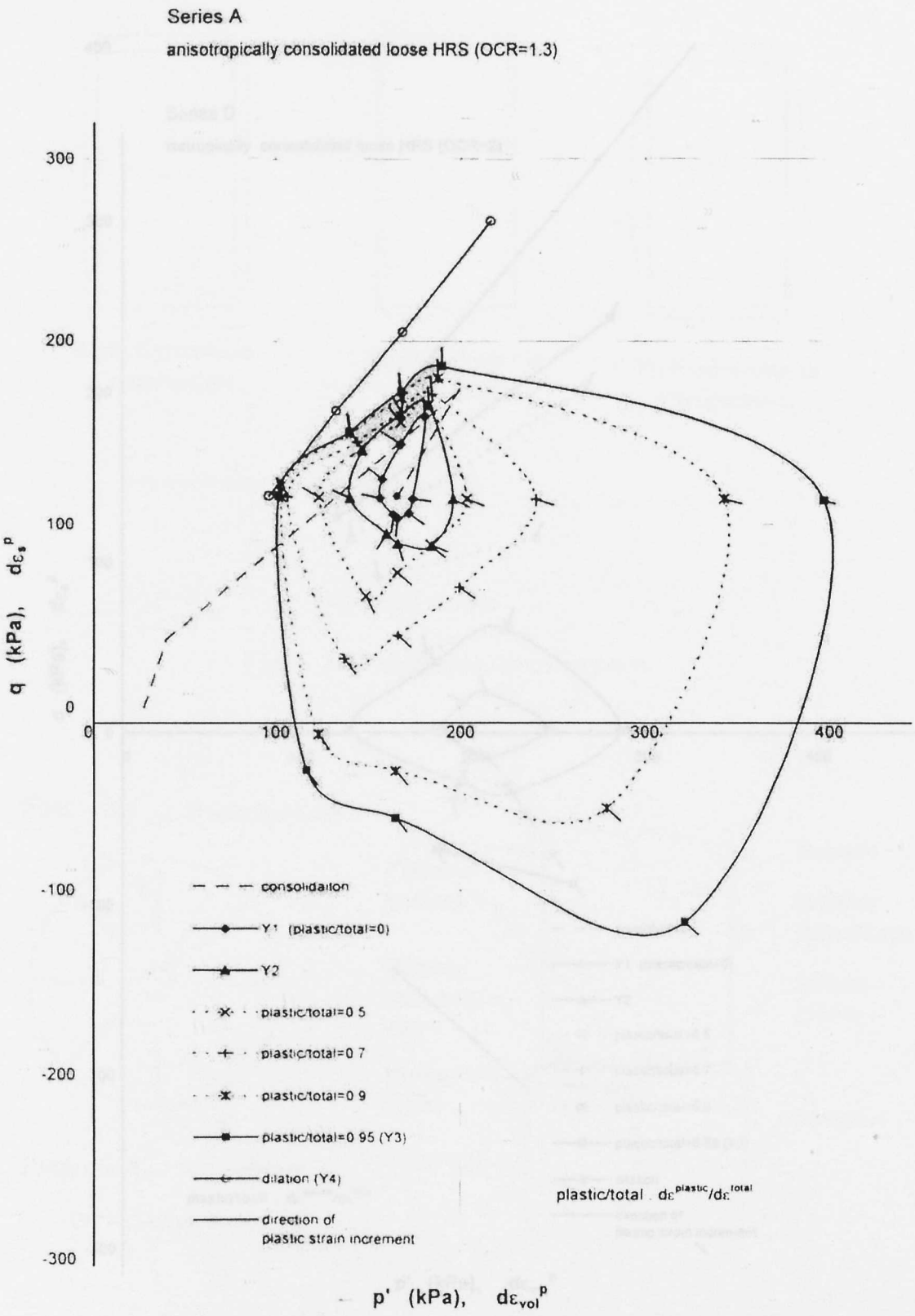


*Figure 2-48 Multiple sub-yield surfaces and plastic strain increment vectors for anisotropically consolidated loose HRS (OCR=1.3) (after Kuwano, 1999)*

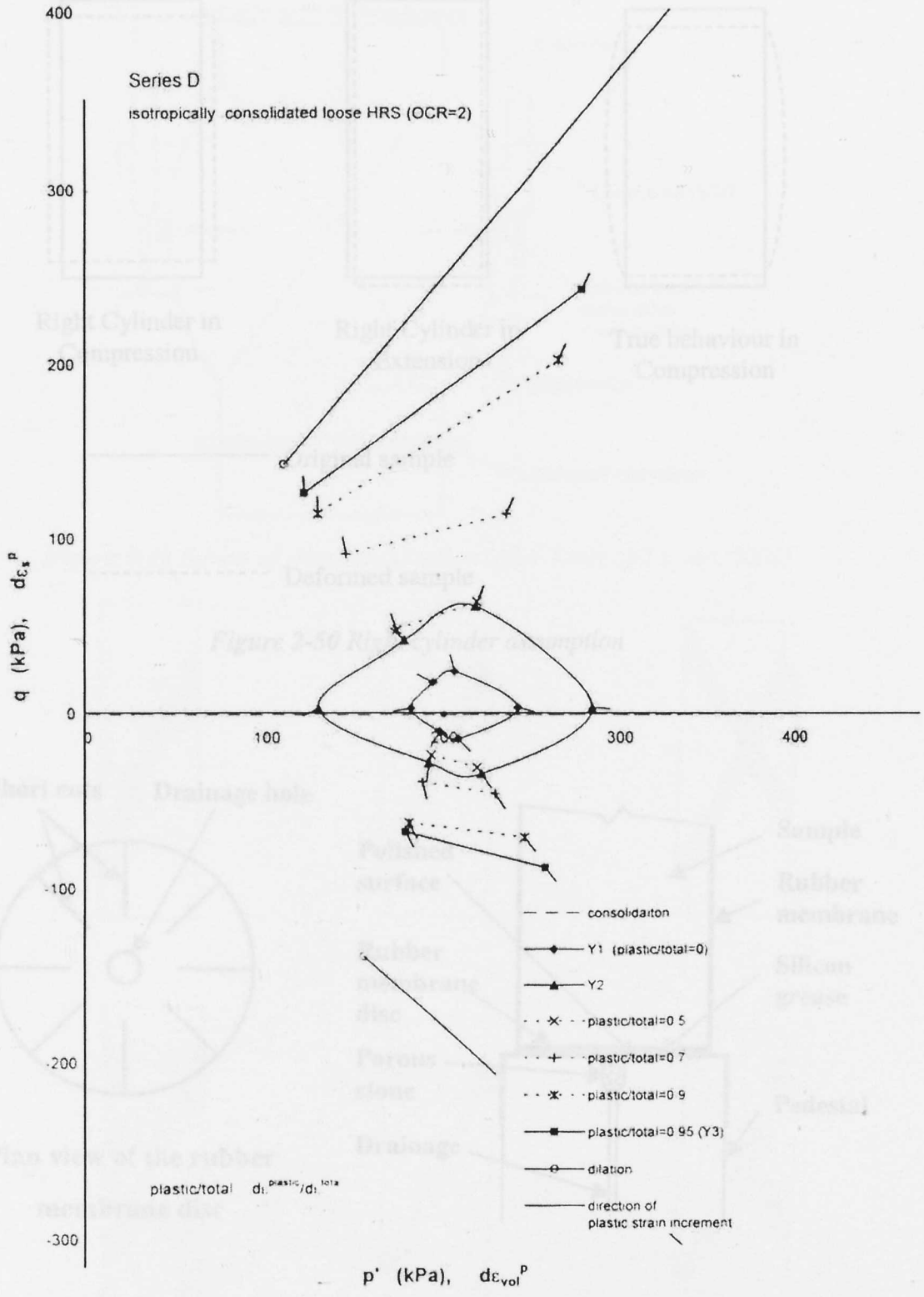


***Figure 2-49*** *Multiple sub-yield surfaces and plastic strain increment vectors for isotropically consolidated loose HRS (OCR=2) (after Kuwano, 1999)*

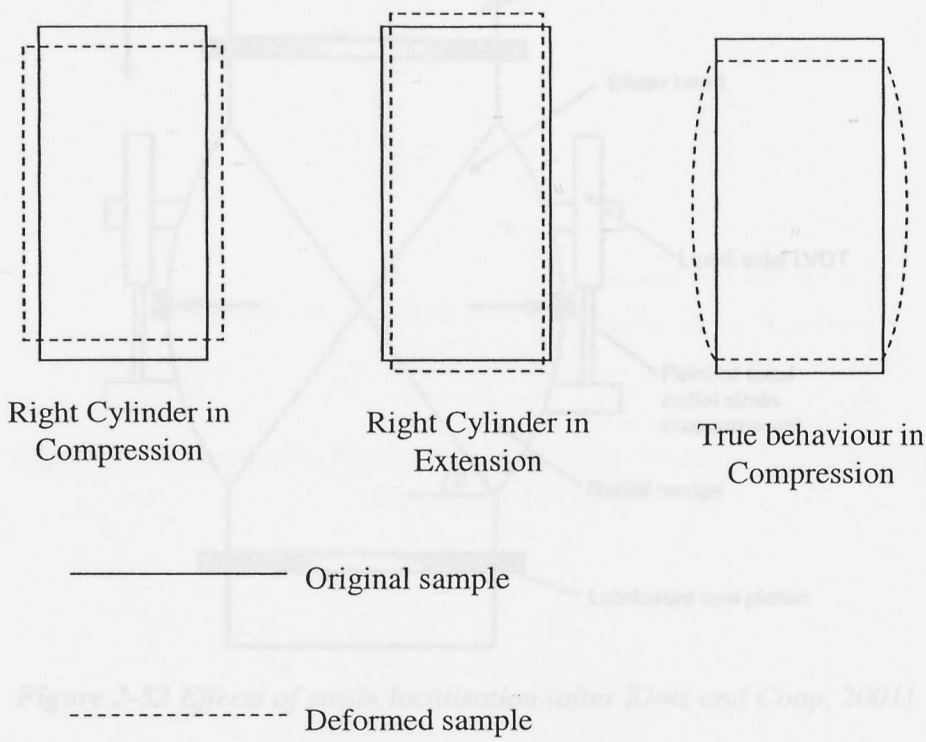


*Figure 2-50 Right cylinder assumption*

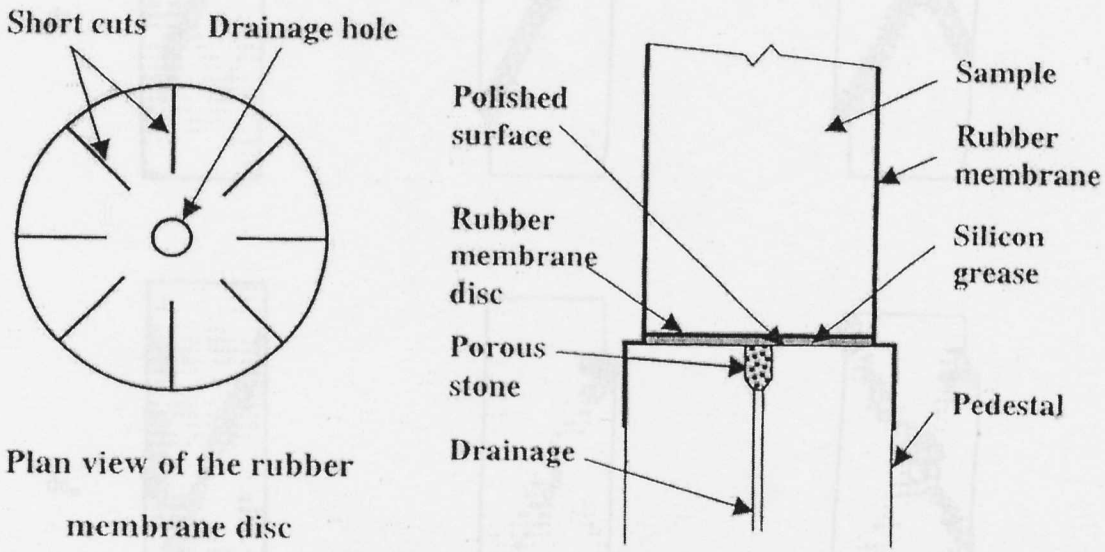


*Figure 2-51 Details of the lubricated end platens (adapted from Head (1985), by Klotz (2000) and Qadimi (2004))*

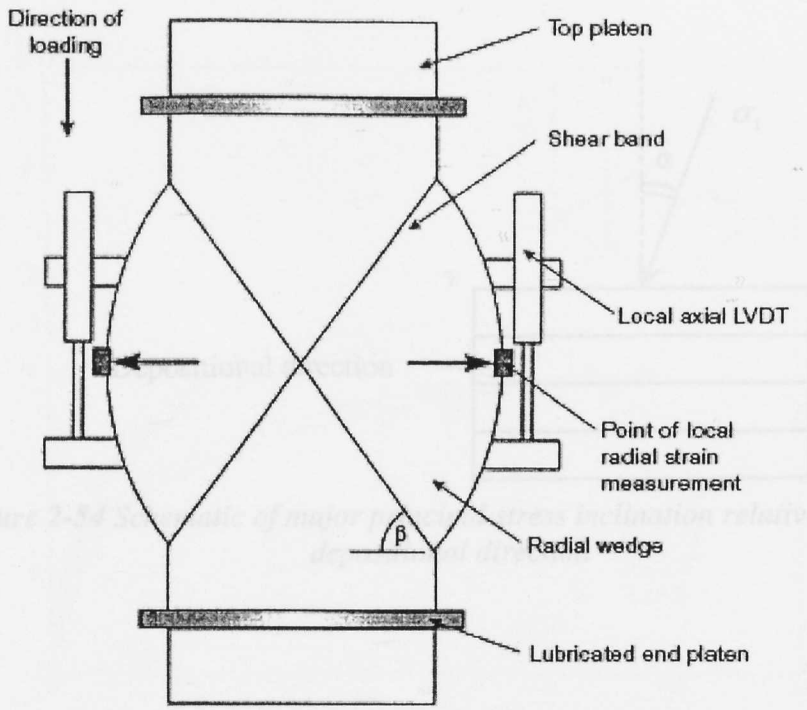


***Figure 2-52*** *Effects of strain localisation (after Klotz and Coop, 2001)*

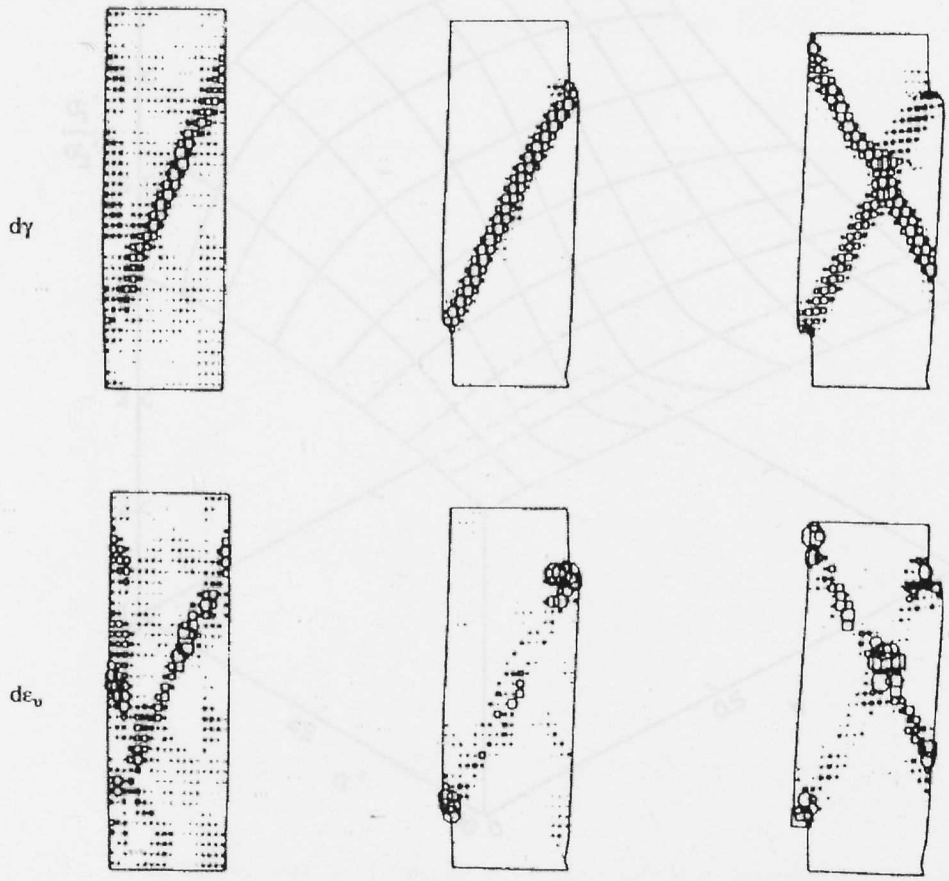


***Figure 2-53*** *Dilatancy in recent and old shear bands: towards a limiting void ratio (after Desrues et al., 1991)*

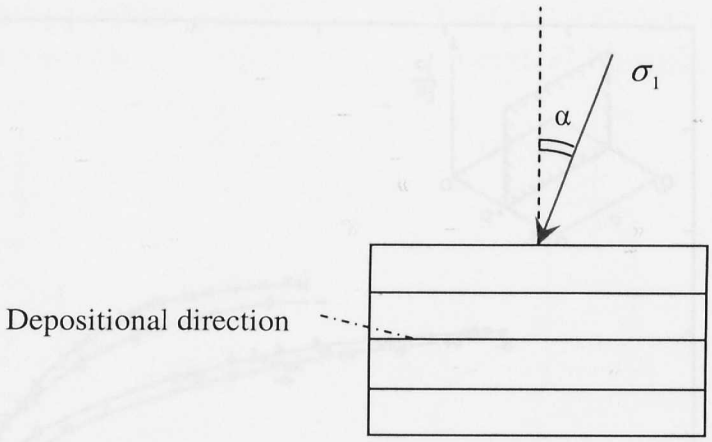


***Figure 2-54*** *Schematic of major principal stress inclination relative to the soil depositional direction*

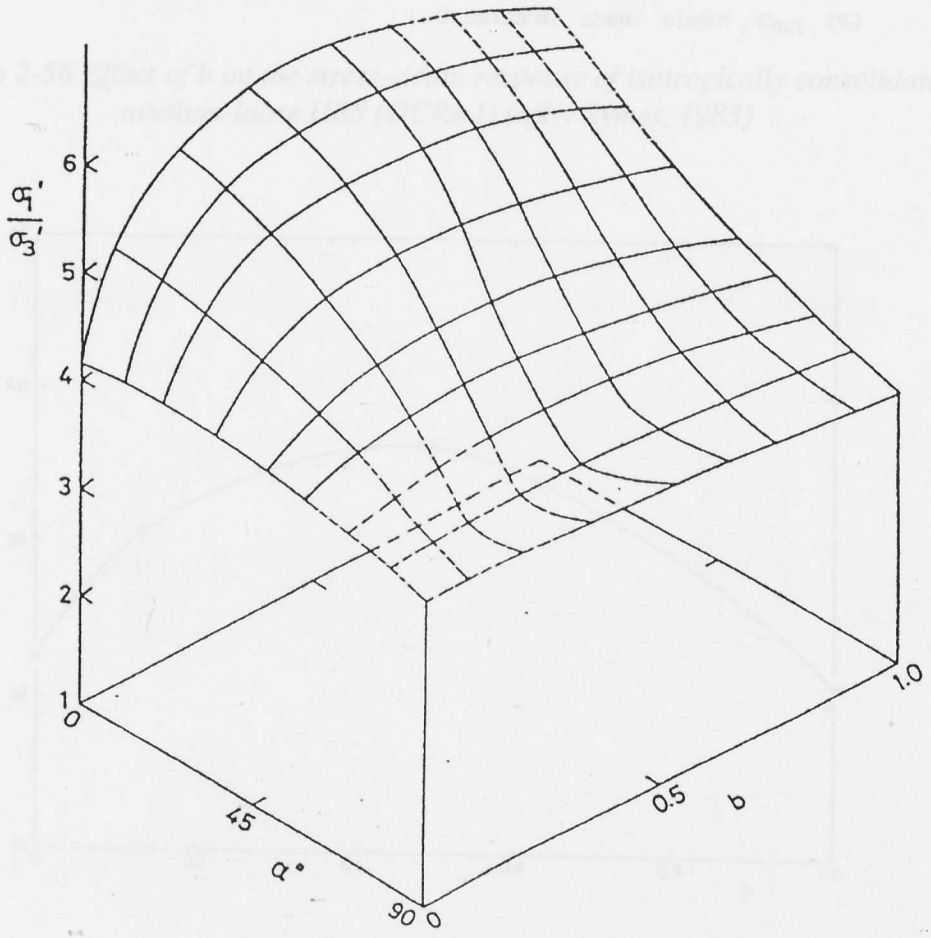


***Figure 2-55*** *Dependency of stress ratio at failure on α and b in isotropically consolidated HRS (OCR=1) (after Symes, 1983)*

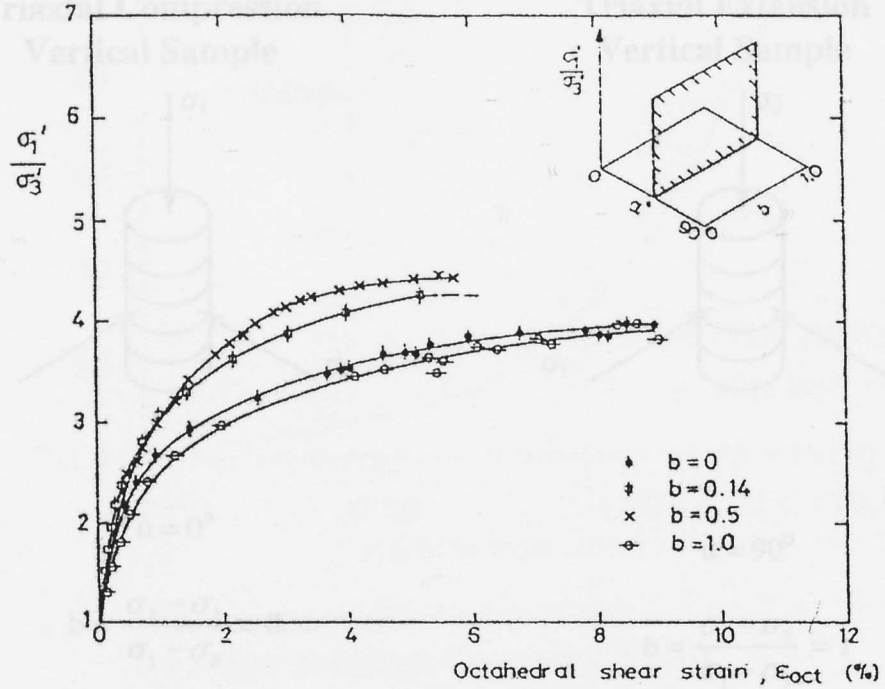


***Figure 2-56*** *Effect of b on the stress-strain response of isotropically consolidated medium-loose HRS (OCR=1) (after Symes, 1983)*

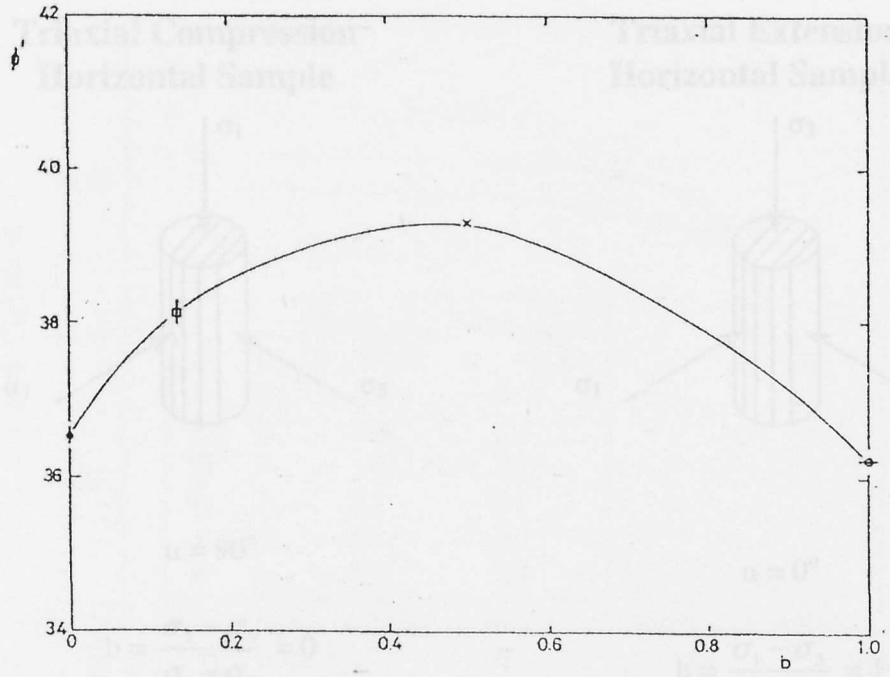


***Figure 2-57*** *Effect of b on the ultimate φ' of isotropically consolidated medium-loose HRS (OCR=1) (α = 45$^0$) (after Symes, 1983)*

**Triaxial Compression**
**Vertical Sample**

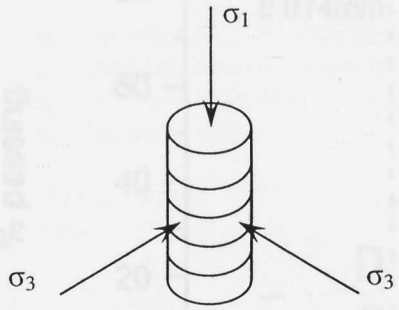


$\alpha = 0^{o}$

$$b = \frac{\sigma_2 - \sigma_3}{\sigma_1 - \sigma_3} = 0$$

$(\sigma_2 = \sigma_3)$

**Triaxial Extension**
**Vertical Sample**

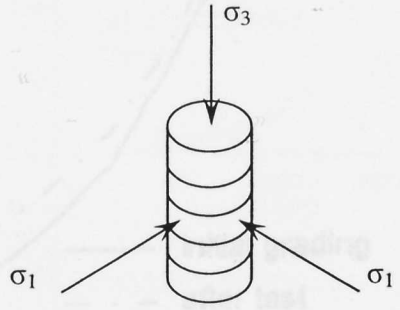


$\alpha = 90^{o}$

$$b = \frac{\sigma_1 - \sigma_3}{\sigma_1 - \sigma_3} = 1$$

**Triaxial Compression**
**Horizontal Sample**

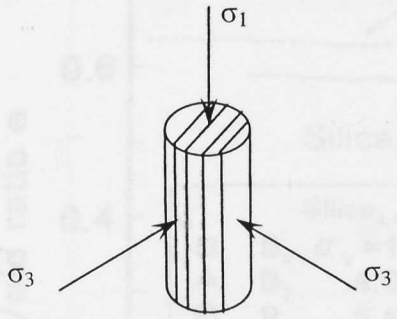


$\alpha = 90^{o}$

$$b = \frac{\sigma_2 - \sigma_3}{\sigma_1 - \sigma_3} = 0$$

$(\sigma_2 = \sigma_3)$

**Triaxial Extension**
**Horizontal Sample**

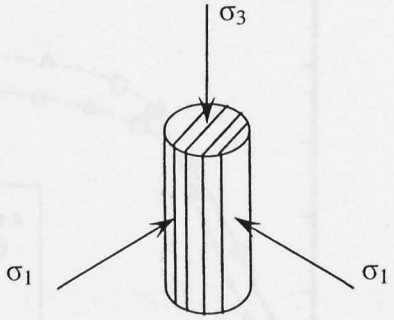


$\alpha = 0^{o}$

$$b = \frac{\sigma_1 - \sigma_3}{\sigma_1 - \sigma_3} = 1$$

*Figure 2-58 Influence of shearing mode and sample orientation on α and b.*

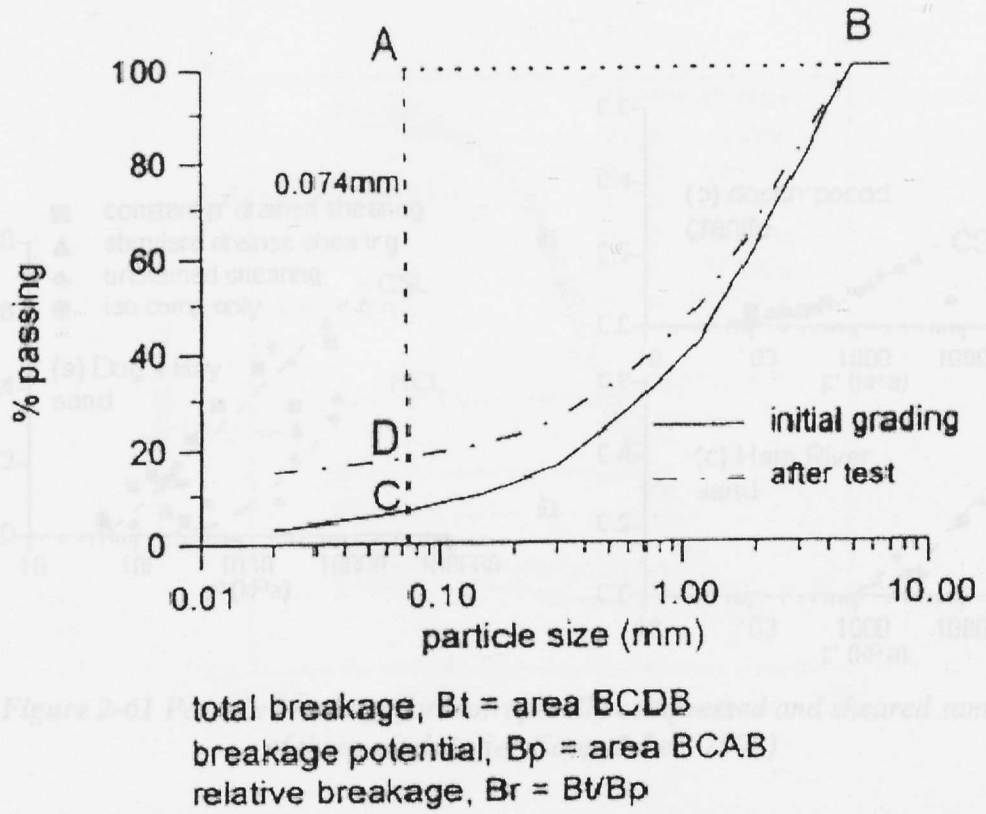


*Figure 2-59 Definition of relative breakage, Br (Hardin, 1985)*

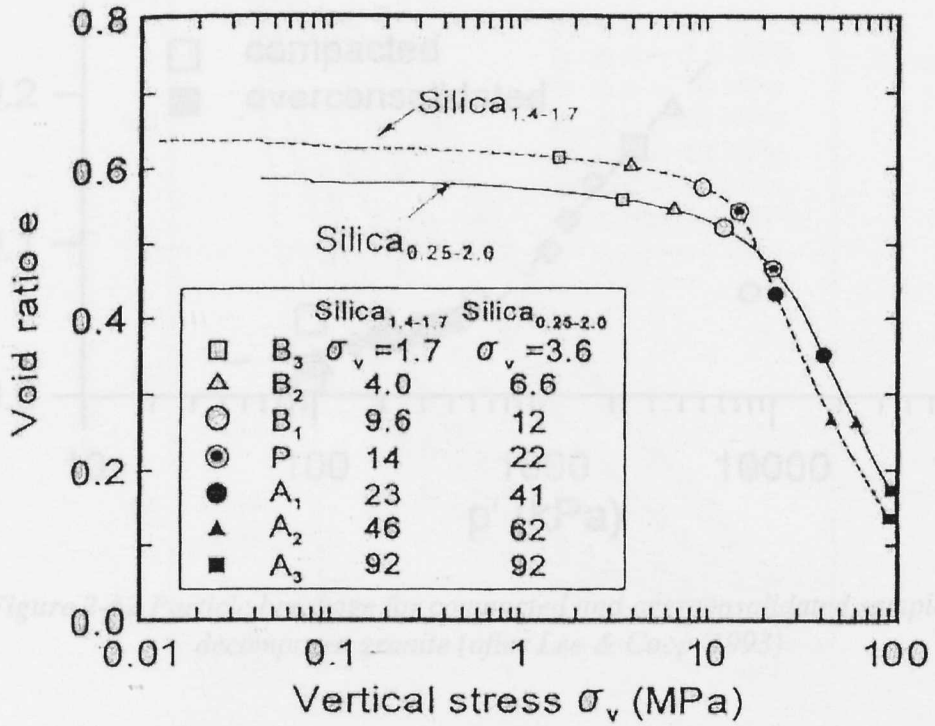


*Figure 2-60 One-dimensional compression curves for uniformly and well graded sands (after Nakata et al., 2001)*

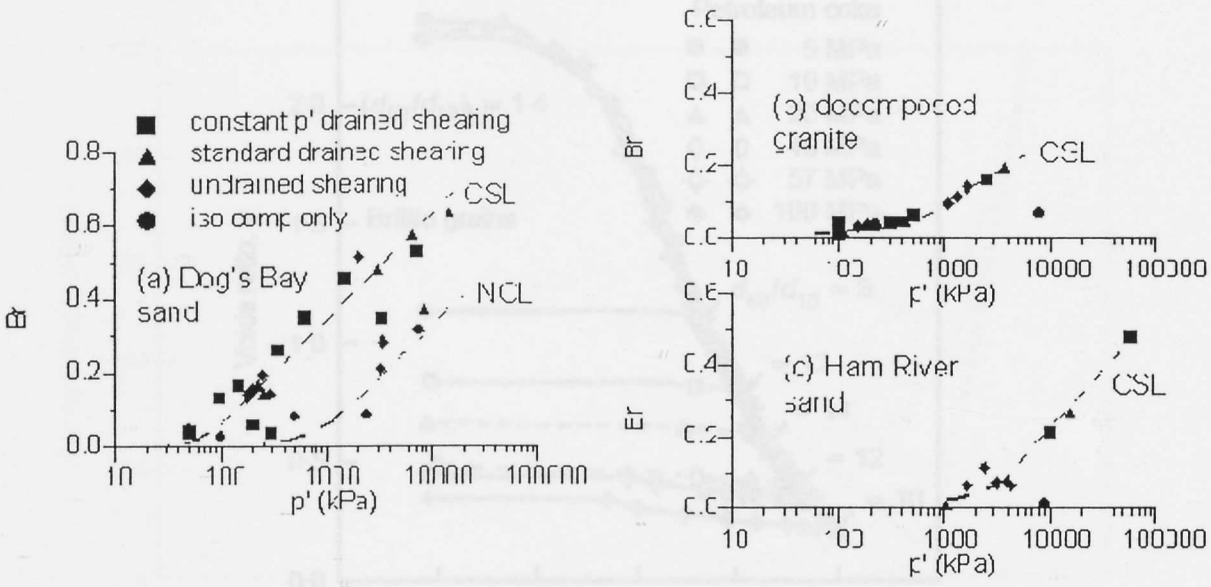


***Figure 2-61*** *Particle breakage for isotropically compressed and sheared samples of three sands (after Coop & Lee, 1993)*

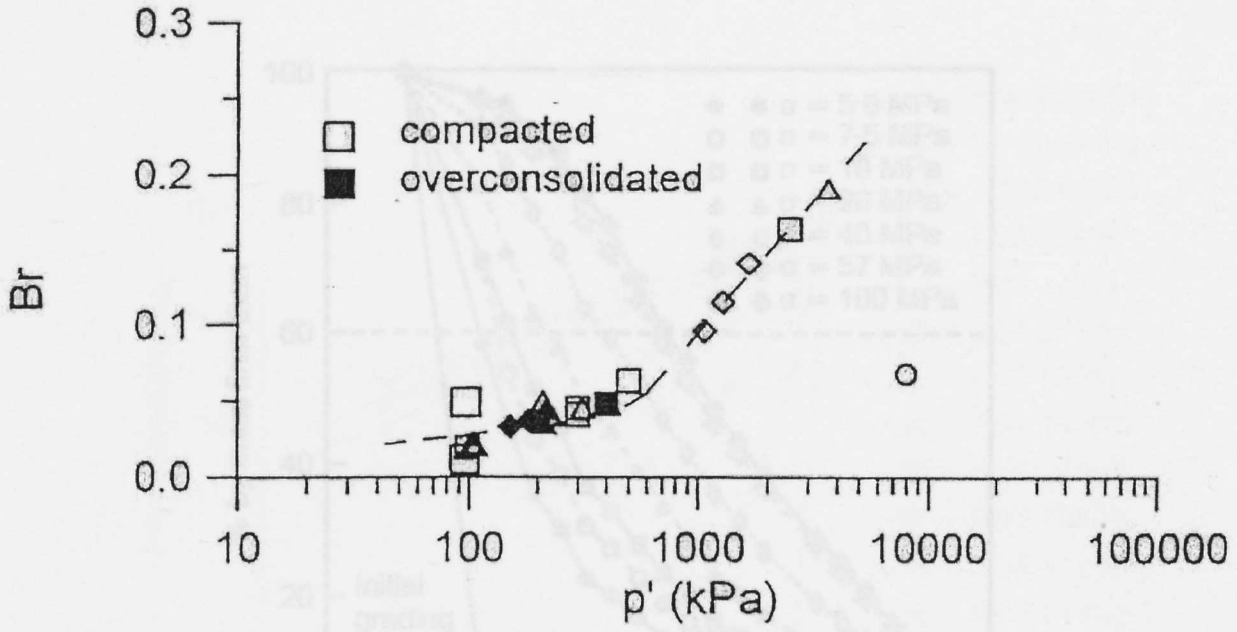


***Figure 2-62*** *Particle breakage for compacted and overconsolidated samples of decomposed granite (after Lee & Coop, 1993)*

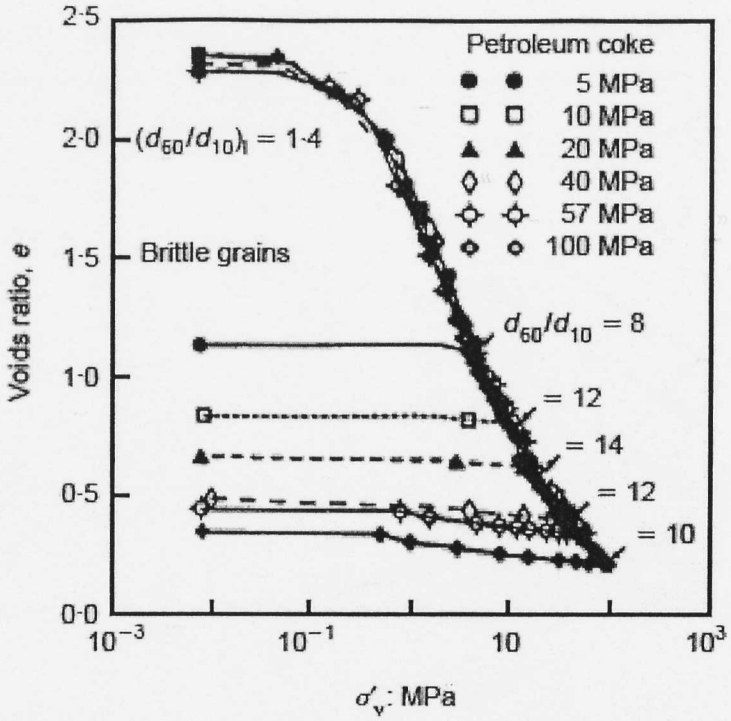


***Figure 2-63*** *Compression curves for petroleum coke (after McDowell & Bolton, 1998)*

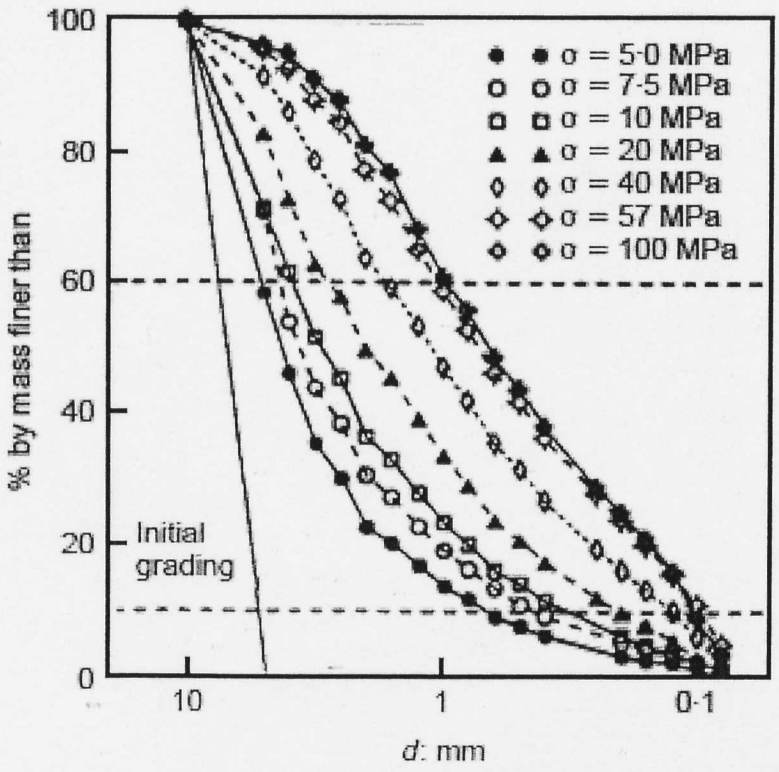


***Figure 2-64*** *Evolving particle breakage for petroleum coke (after McDowell & Bolton, 1998)*

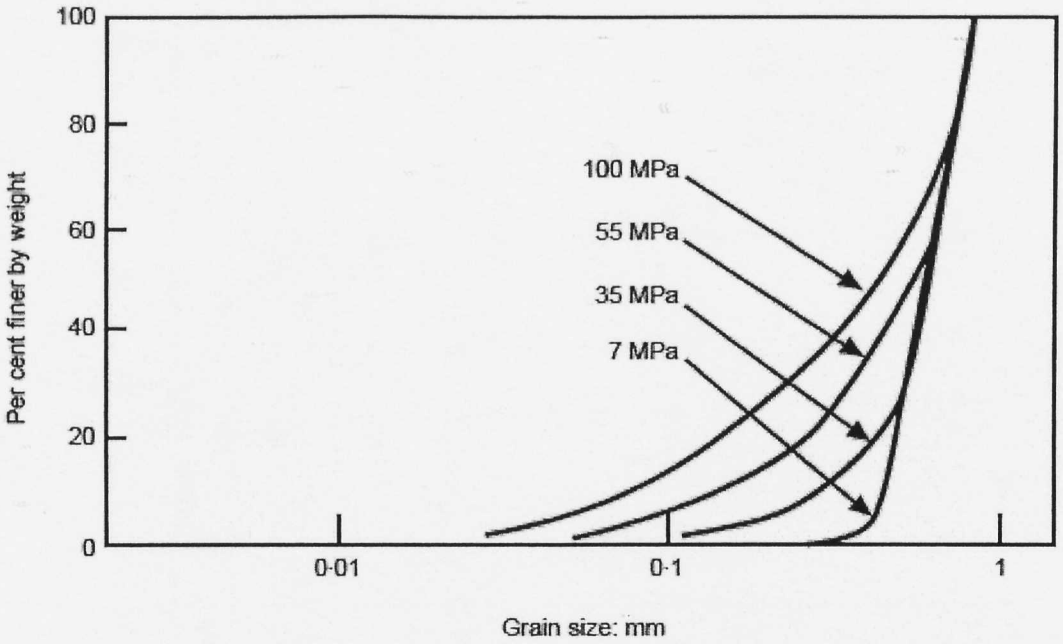


***Figure 2-65*** *Evolving particle size distribution curves for one-dimensionally compressed Ottawa sand (after Fukumoto, 1992)*

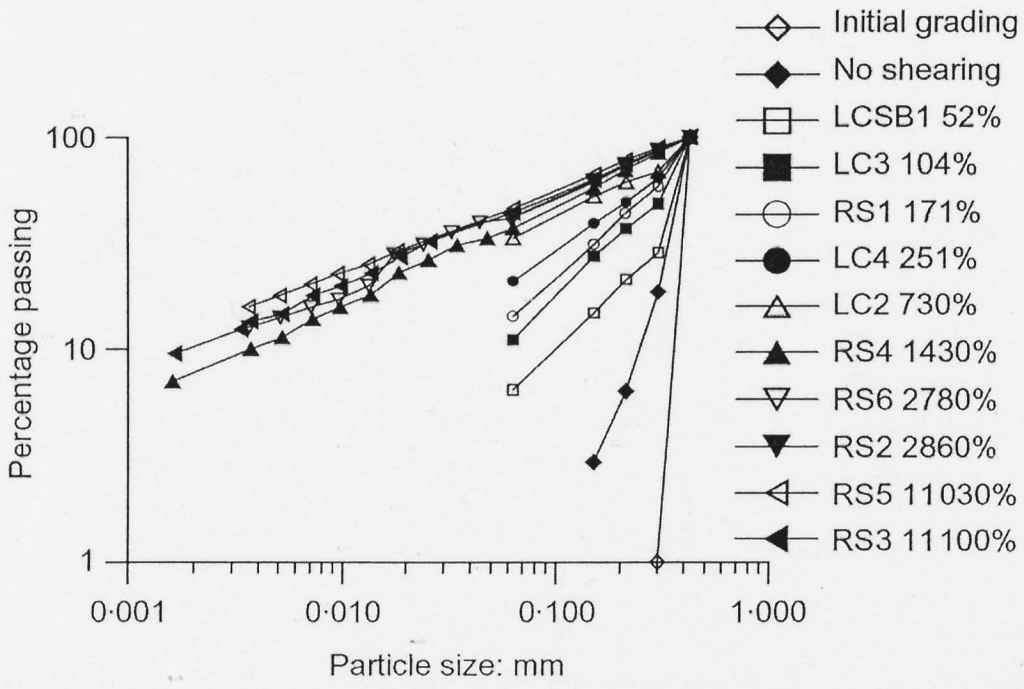


***Figure 2-66*** *Evolving particle size distributions for ring shear tests on Dogs Bay sand with $\sigma_v$ in range 650-930 kPa (after Coop et al., 2004)*

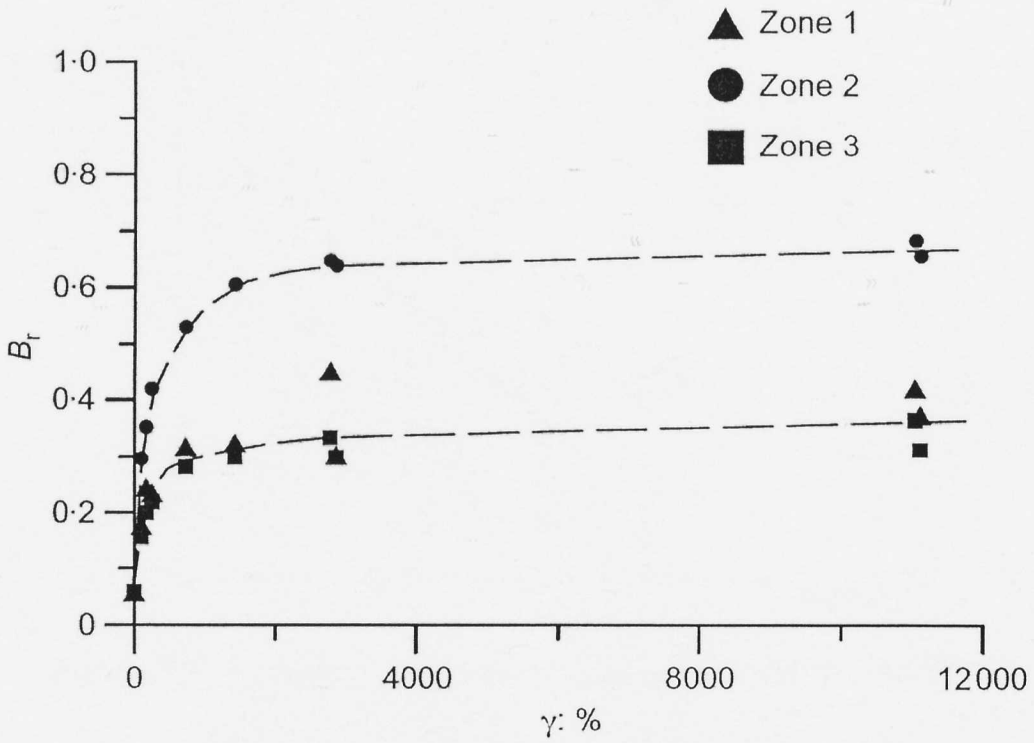


***Figure 2-67*** *Particle breakage for ring shear tests on Dogs Bay sand in stress range 650-930 kPa (after Coop et al., 2004)*

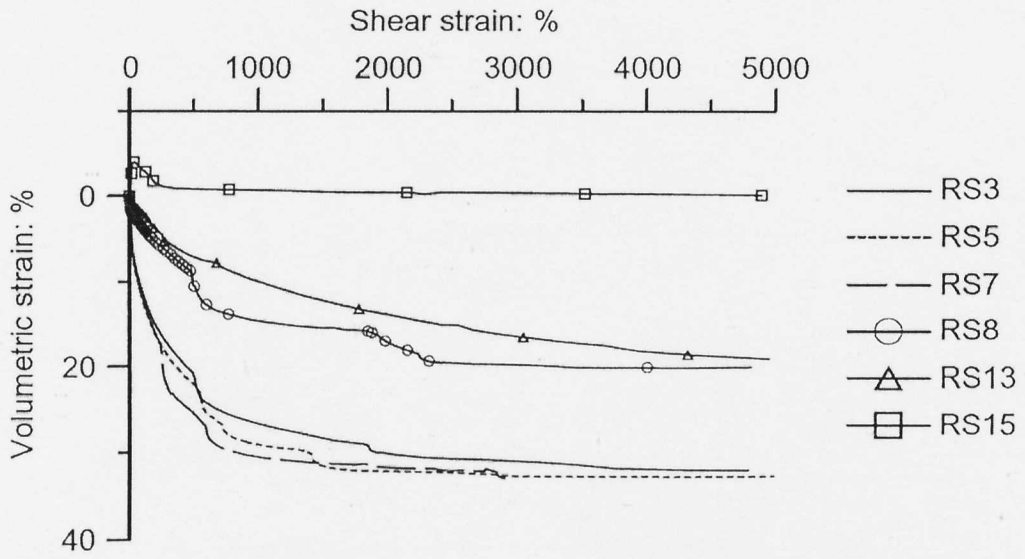


***Figure 2-68*** *Volumetric strain behaviour with increasing levels of shear strain for ring shear tests on Dogs Bay sand (after Coop et al., 2004)*

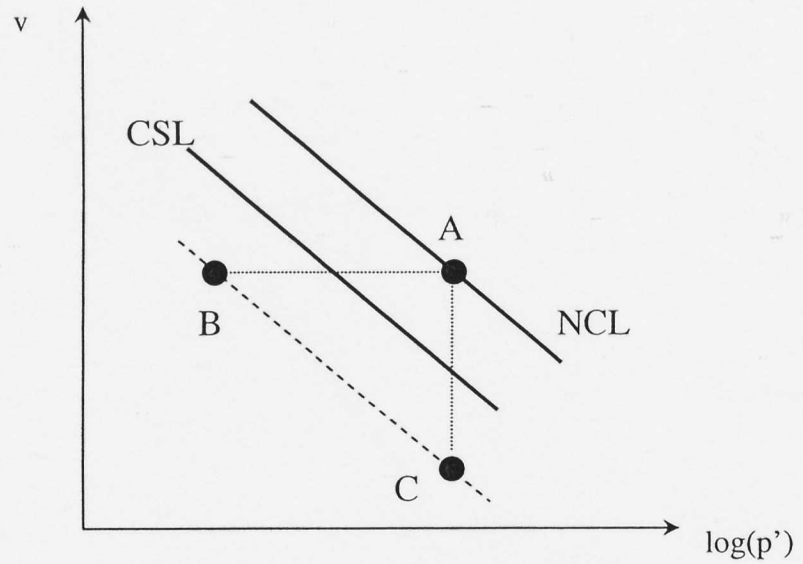


***Figure 2-69*** *Schematic showing the influence of state (after Qadimi, 2005)*

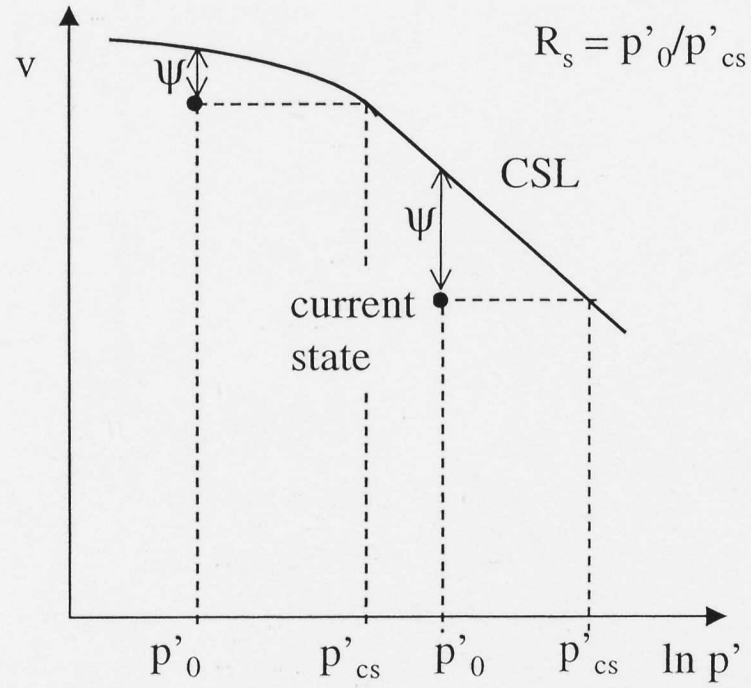


***Figure 2-70*** *Definition of State parameters (after Klotz & Coop, 2001)*

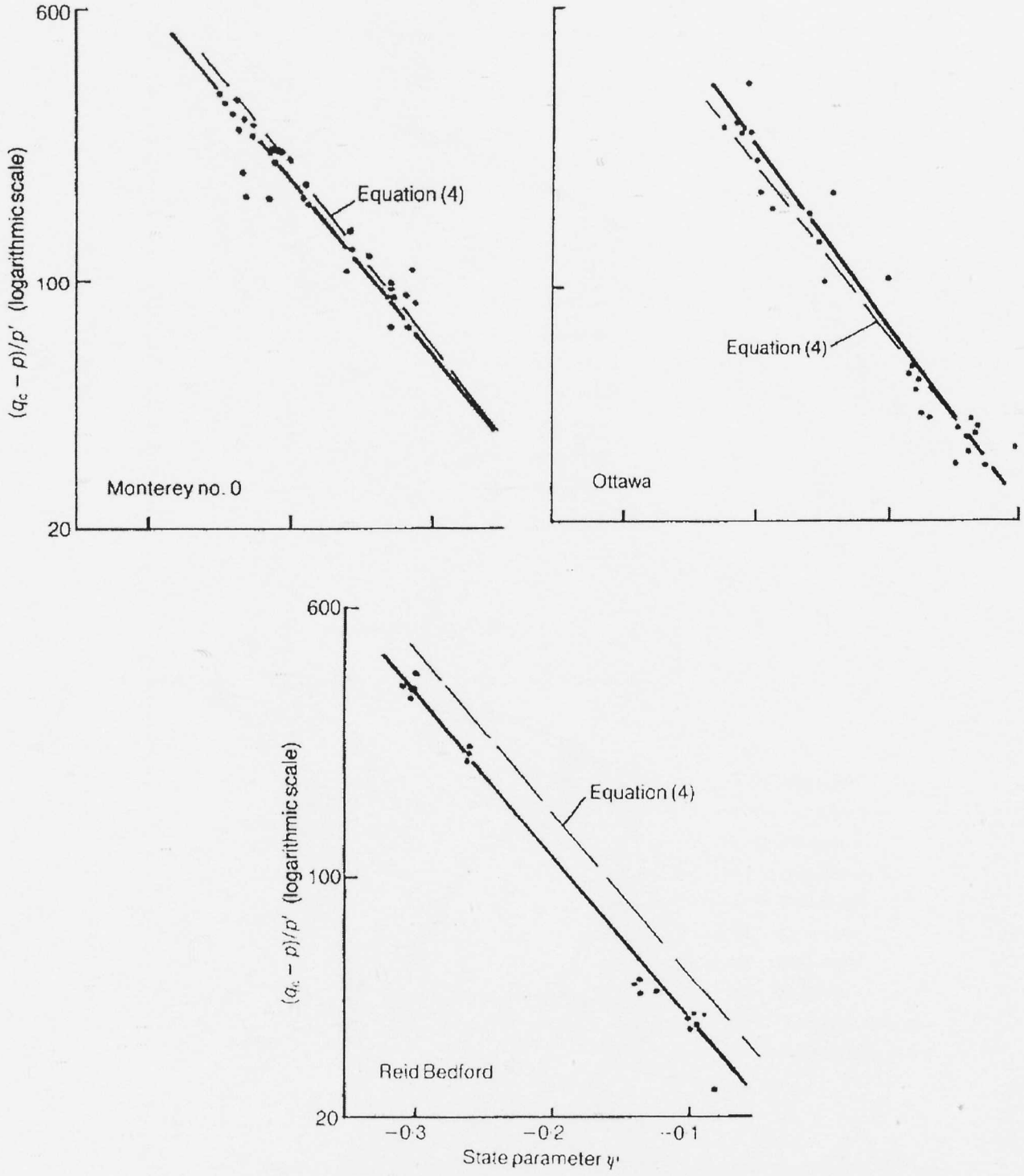


***Figure 2-71*** *Normalised CPT data for three different sands (after Been et al., 2001)*

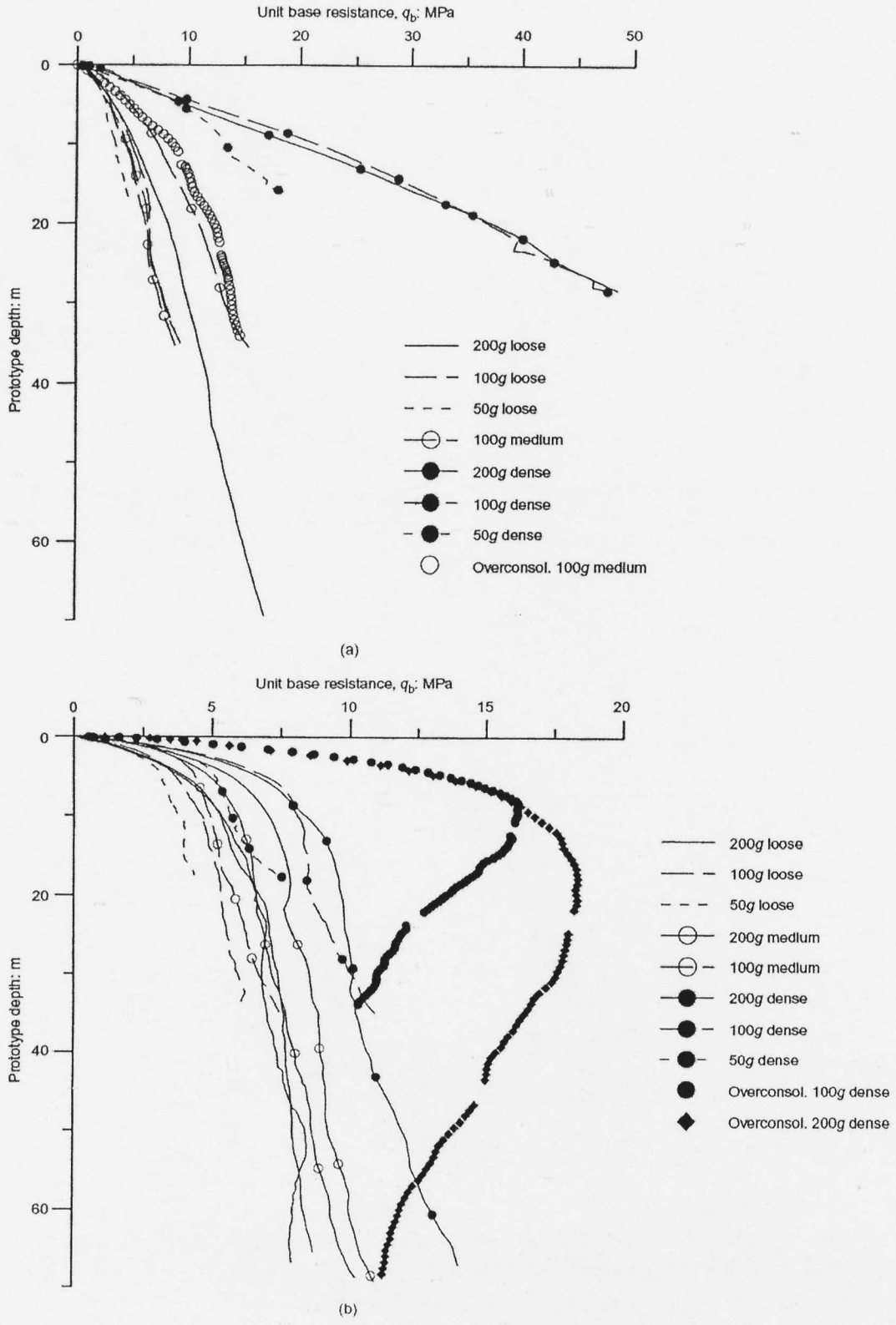


***Figure 2-72*** *Unit base resistance during pile installation (a) Leighton Buzzard sand, (b)Dogs Bay sand (after Klotz & Coop, 2001)*

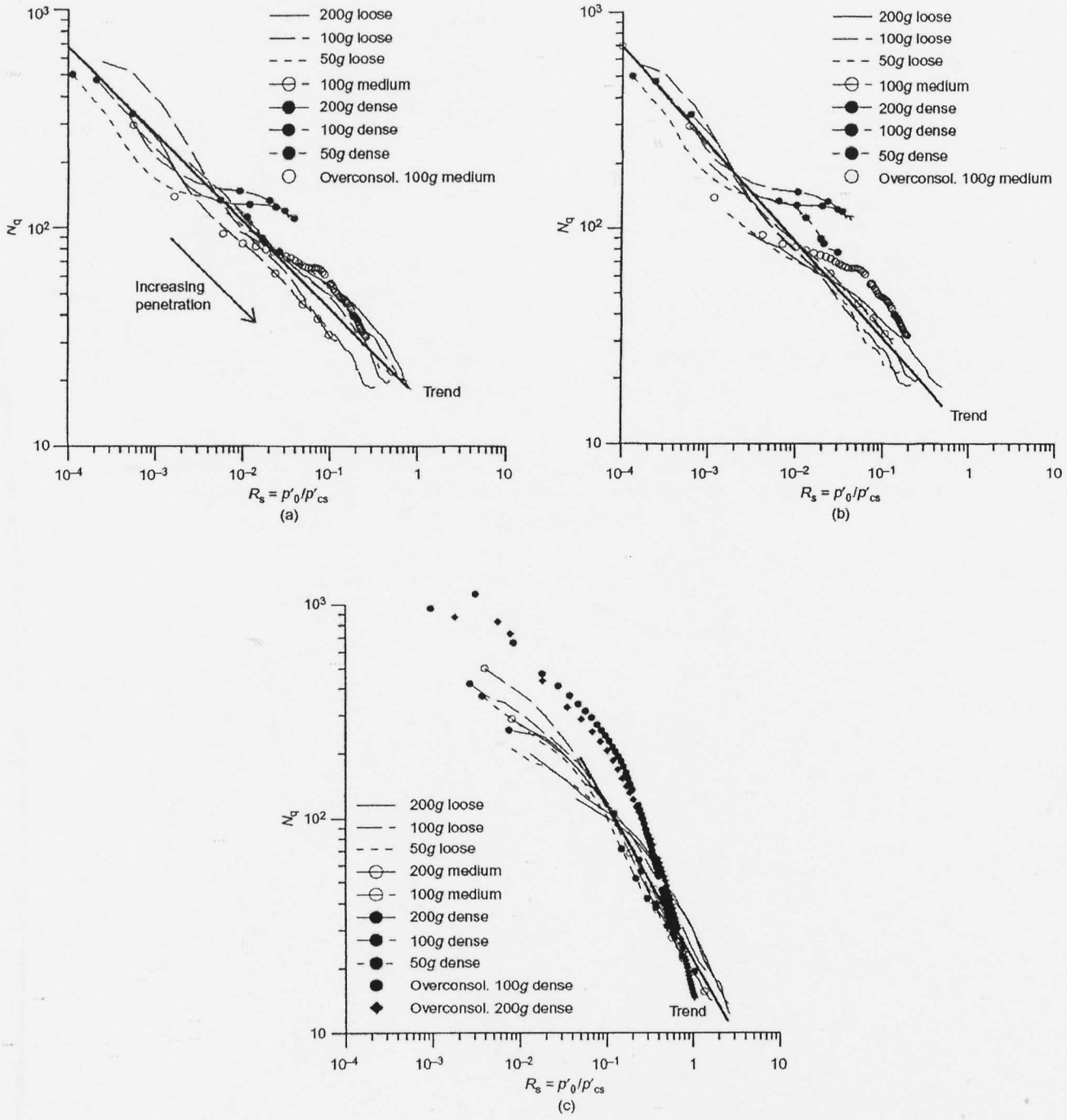


***Figure 2-73*** *Normalised base resistance for (a) Leighton Buzzard sand using a non-linear CSL, (b) Leighton Buzzard sand using a linear CSL, (c)Dogs Bay sand (after Klotz & Coop, 2001)*

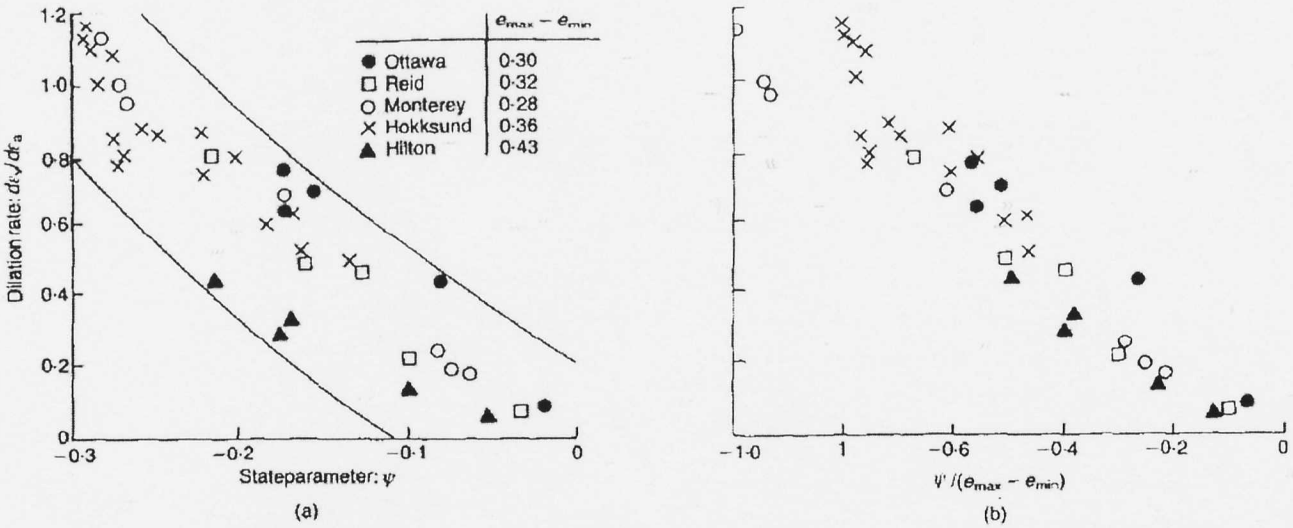


*Figure 2-74 Peak dilation rate as a function of: (a) state parameter; (after Been & Jefferies, 1986) (b) Normalised state parameter for several sands (after Konrad, 1988)*

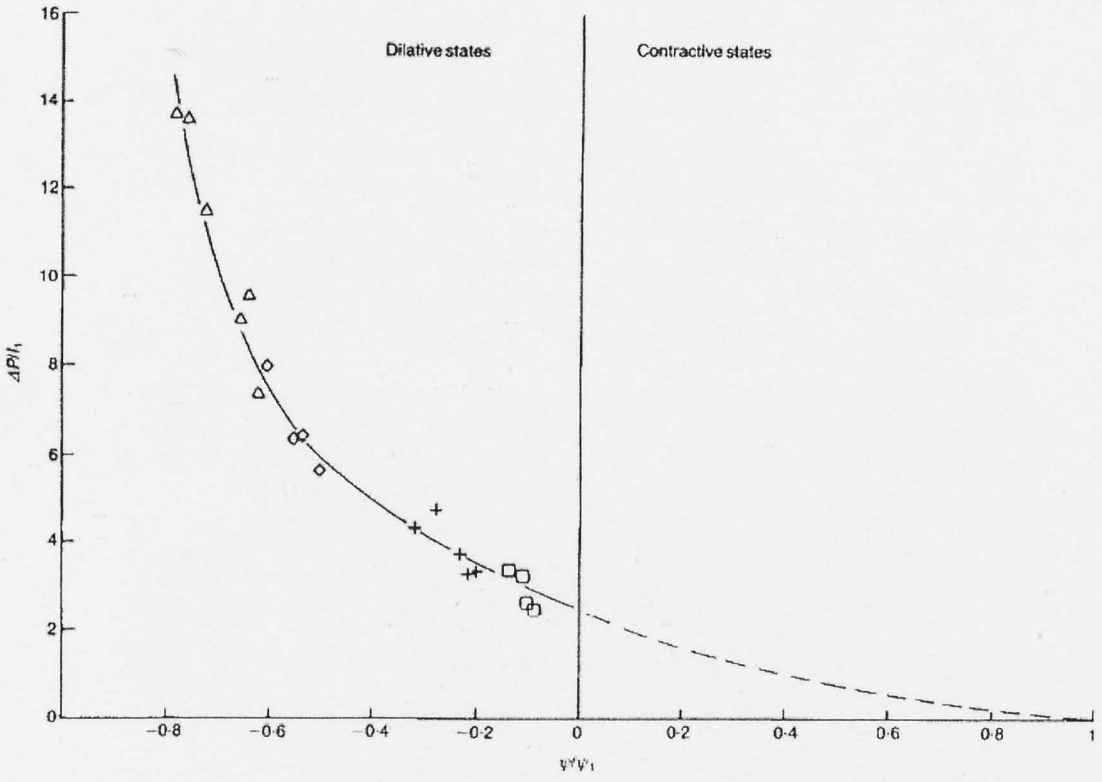


*Figure 2-75 DMT test results on Ottawa sand in terms of normalised state parameter (after Konrad, 1988)*

3 APPARATUS DESCRIPTION & PROCEDURES.....67

3.1 Bishop & Wesley Triaxial Cell And Instrumentation.....67

3.1.1 General structure ..... 67
3.1.2 Measuring stresses ..... 68
3.1.3 Measuring strains ..... 69
3.1.4 Modifications to the apparatus ..... 69

3.2 High Pressure Triaxial Cell And Instrumentation.....70

3.2.1 General structure ..... 70
3.2.2 Measuring stresses ..... 71
3.2.3 Measuring strains ..... 72
3.2.4 Bender elements ..... 72

3.3 100mm Triaxial Cell And Instrumentation .....73

3.3.1 General structure ..... 73
3.3.2 Measuring stresses ..... 75
3.3.3 Measuring strains ..... 75
3.3.4 Bender elements ..... 76

3.4 Test Procedures .....76

3.4.1 Sample preparation – Intact cored samples..... 76
3.4.2 Sample preparation – Intact block samples..... 78
a) Block sample extraction in CTRL tunnel at Stratford ..... 78
b) Laboratory triaxial sample preparation ..... 79
3.4.3 Reconstituted samples..... 79

3.5 Test Phase Description.....81

3.5.1 Saturation ..... 81
3.5.2 Isotropic compression ..... 82
3.5.3 Shearing..... 83
a) Shearing in compression ..... 83
b) Shearing in extension ..... 83
3.5.4 Y1 and Y2 probing..... 84

3.6 Formulae Used For The Data Analysis.....85

3.7 Right Cylinder Assumption & Strain Localisation .....91

# 3 APPARATUS DESCRIPTION & PROCEDURES

## 3.1 Bishop & Wesley Triaxial Cell And Instrumentation

### 3.1.1 General structure

The medium pressure tests were conducted using a computer controlled hydraulic stress path apparatus, similar to the one Bishop & Wesley have described (1975). A schematic of this apparatus is presented in Figure 3-1. The specimens tested in this apparatus were 38mm in diameter and 76mm in height keeping a 2 to1 ratio.

This equipment was installed in the main laboratory where the room temperature is, ideally, controlled with the use of a central air-conditioning unit. This minimizes the thermal expansion & contraction effects that could in turn introduce changes in strain readings or pore pressures. Considering also that the stability of signals in electronic equipment are susceptible to temperature changes as small as $\pm 1^{o}C$, keeping the temperature at a fixed level (room temperature variation less than $\pm 0.3^{o}C$) helps reduce inaccuracies.

In order to regulate the pressure, the triaxial cell is equipped with three pressure controllers; one to control the cell pressure, one for the back pressure and finally one to control the axial ram pressure. Air under a maximum pressure of 800kPa is supplied by an air compressor and is passed through three stepper motor driven pressure regulators which are linked to the controlling computer. These regulators can apply pressure increments as low as 0.07kPa. The controlling computer, in turn, adjusts the air pressure to meet the needs of the experiment.

The air pressure that is adjusted and controlled as described above is converted into water pressure that is finally used in the apparatus. This is achieved with the use of air/water interfaces. In the case of the back pressure the $50cm^3$ IC volume

gauge, besides being an air/water interface, is a device that can measure the amount of water that moves into or out of the sample.

For the strain controlled tests (i.e. shearing stages) a constant rate of strain pump (CRSP) with a stepper motor is used to control the axial displacements. This pump supplies water at a rate defined by the controlling computer.

### *3.1.2 Measuring stresses*

To measure the deviatoric force, a submersible load cell of a maximum capacity of 4.5kN was used (Figure 3-2). By using a load cell within the triaxial cell, it is possible to measure the true deviatoric force, without the effects of the friction between the triaxial cell and the axial loading ram. The load cell was connected to the sample with the use of a suction cap that eliminates alignment errors (Figure 3-3).

In order for the cell and the back pressure to be measured, two separate pressure transducers were used, one connected to the back pressure line and one to the cell pressure line.

At the preparation stage of every experiment, all three transducers were reset to zero by filling the triaxial cell with water to the top while having an open connection to the atmosphere. This ensures that no cumulative error in the pressure readings will be present at the beginning of each test. At the end of every experiment, the stresses were once again reset to zero. The offset readings were noted and incorporated into the data analysis. In most cases these readings resulted in offsets less than 1kPa and were caused by instrument drift with time.

### *3.1.3 Measuring strains*

The external axial displacement and therefore the external axial strain was measured with a resistive type transducer. Additionally, internal strain electrolevel inclinometers (Figure 3-4) were attached directly on the sample in diametrically opposite positions, in order to measure the axial displacement on the sample. Without having the inclinometers attached, to correct external strains for system compliance and seating errors after each test, a rigid dummy sample could have been tested using the same stress path. Then, the two sets of results should have been superimposed for the actual soil sample behaviour to be obtained, removing the system compliance effect (Figure 3-3). However, bedding errors cannot be accounted for in this way.

The volumetric strain of the sample was measured with a resistive type transducer on the volume gauge. By knowing the amount of water that goes into or comes out of the sample, as well as the initial sample dimensions, the volumetric strain can in turn be calculated.

An overview of the accuracies of the instrumentation that was used is presented in Table 3-1.

### *3.1.4 Modifications to the apparatus*

In order to be able to run tests up to an effective confinement of 1MPa, pressure multipliers were placed in both the axial pressure line as well as the cell pressure line. These tests were performed at up to 1,200kPa cell pressure, without placing any reinforcement on the cell body.

The multipliers were unequal air-water piston interfaces, similar in principle to the volume gauge (Figure 3-5). Air pressure was applied to the bottom and was converted into water pressure at the top. The ratio of the lower piston area (air) to

the upper piston area (water) of the multipliers was 2.5:1, giving a 2.5 times pressure increase.

## 3.2 *High Pressure Triaxial Cell And Instrumentation*

### *3.2.1 General structure*

The high pressure tests were conducted using a computer controlled high pressure hydraulic stress path apparatus with a cell pressure capacity of 5MPa (Figure 3-6 & Figure 3-7).

This equipment is installed in the Bishop laboratory where the room temperature is, ideally, controlled with the use of a central air-conditioning unit. Just as with the low pressure system, this minimizes errors. The high pressure triaxial cell uses oil instead of water in the cell chamber since the maximum cell pressure used exceeds the crushing limit of all internal instrumentation using a sealed chamber to protect the electronics and wiring and therefore unsealed instrumentation is used. If, however, any wiring were to come in contact with the water being contained within the cell, then short-circuiting of the local instrumentation would take place and it is therefore important to avoid contaminating the cell oil with water.

In comparison with the medium pressure apparatus, the high pressure triaxial apparatus is equipped with two controlling systems; a "conventional" medium pressure system like that previously described for the Bishop & Wesley triaxial cell which uses, in this case, air/oil interfaces to transfer pressure from the main air compressor to the triaxial cell, and a high pressure system that the test is switched to, once the maximum pressure from the low pressure system has been reached (Figure 3-6). The high pressure system consists of two high pressure motorised hydraulic pumps (Figure 3-8) that can provide pressurized oil into the axial hydraulic cylinder (that in turn provides the axial load on the sample) and to

the triaxial cell chamber respectively. A schematic of the pumps is presented in Figure 3-9. For the axial load, it is also possible to use the low pressure system combined with a 1:2.5 multiplier as an alternative. The limitations in this case are firstly the maximum possible pressure that can be applied to the sample by using the multiplier and secondly the limitation of axial movement the multiplier is subjected to due to its geometry. The back-pressure is applied through an IC volume gauge that also acts as an air/water interface, just as was previously described for the medium pressure triaxial cell.

The stress controlled tests on the high pressure triaxial apparatus were performed by using a combination of the air/liquid interfaces and the high pressure motorised hydraulic pumps. The strain controlled tests were performed with the use of a motorized 5 tonne loading frame. The use of the high pressure axial motorised hydraulic pump to perform the strain controlled tests was also possible, although it was avoided since it was considered to be more a complex operation.

### *3.2.2 Measuring stresses*

Higher capacity pressure transducers (6MPa) were used to measure the cell and back pressures. The deviatoric force was measured with a submersible load cell that again had a higher load capacity (25kN). As in the previous case, the load cell measured the true deviatoric force, without the effects of the friction between the cell and the axial loading ram. The load cell was again connected to the sample with the use of a suction cap eliminating alignment errors.

The difficulty in using a suction cap in the high pressure triaxial cell is connecting the sample to the loading ram without having direct visual contact. In order to ensure that the disturbance of the sample during suction cap connection was kept to the absolute minimum, a higher effective stress was applied to the sample, typically of about 150kPa, before connection commenced.

### *3.2.3 Measuring strains*

The external axial displacement was measured with the use of an LVDT. The internal axial strain readings were taken by a set of small LVDTs attached directly on the sample in diametrically opposite positions. The LVDTs were designed to function submerged in oil (Figure 3-10). The radial strain readings were taken with the use of a radial belt that was attached horizontally at the mid-height of the sample. The radial belt was also equipped with the same LVDT as those used to measure local axial displacements on the sample (Figure 3-11). Finally, as with the standard pressure apparatus, the volumetric strain of the soil sample was measured using an LVDT on an IC volume gauge.

An overview of the accuracies of the instrumentation that was used is presented in Table 3-1.

### *3.2.4 Bender elements*

An additional feature of the high pressure triaxial cell is the set of bender elements that it is equipped with. In principle, two bender elements are installed at the top and the bottom of the sample (Figure 3-12), one being the transmitter and one being the receiver. A schematic of their specific characteristics is presented in Figure 3-13. It was ensured that the top element was aligned with the bottom element during setup of the sample.

A shear wave is generated by applying a voltage to the transmitter using the function generator. Typically a single shot sinusoidal wave followed by a pause was used. This shear wave travels through the solid phase of the sample and reaches the end when it is picked up by the receiver. The signal is then passed through a filter and an amplifier and is finally displayed on the oscilloscope. On the screen of the oscilloscope both the transmitted and received waves are plotted.

The time difference "T" between the two waves was determined based on the first arrival method, as shown in Figure 3-14. This time difference "T" indicates the time needed for the wave to cross the distance between the transmitter and the receiver. This distance is equal to the height of the sample minus the amount the two bender elements are embedded into it. If this distance is considered to be "L" then the shear wave velocity can be calculated as follows:

$$V_s = \frac{L}{T} \qquad (3\text{-}1)$$

By knowing the shear wave velocity, the elastic shear modulus $G_0$ can in turn be calculated as follows:

$$G_0 = \rho V_s^2 \qquad (3\text{-}2)$$

where $\rho$ is the total mass density of the sample.

What is denoted here as $G_0$ is in fact the $G_{VH}$ reading, or in other words the vertically transmitted wave under horizontal polarisation. The term $G_{VH}$ is not used as, for the bulk of the tests, $G_{HV}$ will be the only bender element reading taken and therefore, no direct need for a distinction to be made.

## 3.3 100mm Triaxial Cell And Instrumentation

### 3.3.1 General structure

The last experiment undertaking Y1 and Y2 probes was conducted in a computer controlled 100mm hydraulic stress path apparatus. The specific cell was designed at Imperial College and is typically used for research on natural soils as well as small strain probing. A picture of the apparatus is presented in Figure 3-15. The

specimens tested in this apparatus are 100mm in diameter and 200mm in height keeping, just as in the previous two cases, a 2 to1 ratio.

This equipment is installed in the Bishop laboratory where the room temperature is, ideally, controlled with the use of a central air-conditioning unit. This minimizes the thermal expansion and contraction effects that could in turn introduce changes to the strain readings and pore pressures.

Just as in the case of the 38mm triaxial cell, in order to regulate the pressure, the triaxial cell is equipped with three pressure controllers; one to control the cell pressure, one for the back pressure and finally one to control the axial ram pressure. Air under a maximum pressure of 800kPa is supplied by an air compressor and is passed through three stepper motor driven pressure regulators which are linked to the controlling computer. These regulators again can apply pressure increments as low as 0.07kPa. The controlling computer, in turn, adjusts the air pressure to meet the needs of the experiment.

The air pressure that is adjusted and controlled as described above is converted into either water or oil pressure that is finally used in the apparatus. Oil was only used for the ram interface whereas water was used for cell and back pressure systems. This is achieved with the use of air/water or air/oil interfaces. For the back pressure, the $100cm^3$ IC volume gauge, besides being an air/water interface, is a device that can measure the amount of water that moves into or out of the sample.

For the strain controlled tests (i.e. shearing stages) a constant rate of strain pump (CRSP) with a stepper motor is used to control the axial displacements. This pump supplies water at a rate defined by the controlling computer. Since the CRSP gave an accuracy of control better than the ram pressure interface, the CRSP was used to control directly the axial stress as well as strains in preference to the more standard approach of using the pressure controlled interface for pressures and CRSP for strains.

### *3.3.2 Measuring stresses*

To measure the deviatoric force, a submersible load cell of maximum capacity of 4 kN was used. The load cell was in this case connected to the sample with the use of a combination of a suction cap and a half ball. This minimised distortions caused to the sample due to the connection process.

In order for the cell and the back pressures to be measured, two separate pressure transducers were used, one connected to the back pressure line and one to the cell pressure line. In addition to the standard pressure transducers that were seen in the 38mm triaxial sample, the 100mm triaxial cell was also equipped with a mid-height pore pressure probe. This provided a means to verify that there was no pore pressure differential across the sample. A schematic of the pore pressure probe is presented in Figure 3-16

### *3.3.3 Measuring strains*

The external axial displacement was measured with the use of an LVDT. The internal axial strain readings were taken by a set of small LVDTs attached directly on the sample in diametrically opposite positions. The LVDTs were designed to function submerged in water (Figure 3-17). The radial strain readings were taken with the use of a radial belt that was attached horizontally at the mid-height of the sample. The radial belt was also equipped with the same LVDT as those used to measure local axial displacements on the sample. Finally, as with the 38mm triaxial cell, the volumetric strain of the sample was measured using an LVDT on an IC volume gauge.

### *3.3.4 Bender elements*

The 100mm triaxial cell was equipped with horizontal bender elements, as shown in Figure 3-18. These bender elements allowed the measurement of both $G_{HH}$ (shear modulus for horizontal wave propagation and horizontal wave polarisation) and $G_{HV}$ (shear modulus for horizontal wave propagation and vertical wave polarisation) and were therefore used for a direct assessment of material anisotropy, as shall be discussed in Section 6.3.5. Additionally, the use of the bender elements allowed to verify that the sample had not been permanently strained while being subjected to various probes (see Section 3.5.4).

## *3.4 Test Procedures*

### *3.4.1 Sample preparation – Intact cored samples*

Initially, the soil that was available for testing had been extracted using the rotary coring technique. For the intact vertical samples that were required to be formed for testing, the material had to be extracted from the plastic protective cored tubes and then carefully cut to the approximate dimensions required with the use of a knife or a large wire saw. For the final exact dimensions to be achieved, trimming with the use of a thin wire saw was required. This trimming process involved mounting the sample onto a hand lathe and then gently repeatedly cutting thin slices of sand from the perimeter of the sample, until the required dimensions were achieved. Once the correct diameter was formed, the sample was placed into a cradle where the ends were carefully trimmed and the final geometry of the sample for testing was reached. The conventional triaxial apparatus required 76mm by 38mm samples whereas the high pressure triaxial apparatus required 100mm by 50mm samples. The material that remained was weighed in tins and used for water content determination.

Samples that were not intended to be tested immediately after the trimming process were usually trimmed to a larger diameter and length than what would be appropriate for testing. These samples were then wrapped in cling-film and waxed to prevent any moisture loss. This was done deliberately so that if the samples were slightly damaged during storage time the excess material that was left on would suffer most of these effects, keeping the inner core protected and undisturbed. When one of these samples was to be tested, it was again placed on the hand lathe and cut to the correct dimensions as before.

In the case of the high pressure apparatus, the top and bottom ends of the sample had to accommodate the bender element source and receiver respectively. Because the sand samples had quite a high initial density, a small excavation had to be made to allow sufficient space for the bender elements to be tightly placed within the sample without cracking it.

The standard pressure tests were set-up using a single 0.3mm thick latex membrane on the samples. For the high pressure tests, a minimum of two membranes had to be used as the sand particles tended to puncture the membrane at higher pressures. Also, the outer membrane had to be a 0.7mm neoprene membrane, as latex could not be used in direct contact with the oil in the cell chamber. The inner membrane was either another 0.7mm neoprene membrane or a 0.3mm latex membrane.

To calculate the sample unit weight, the samples were weighed at their initial state (natural moisture content) prior to being placed on the triaxial apparatus. The exact sample diameter was measured once the sample was placed on the triaxial apparatus with the membrane(s) that would be used for testing. Typically, between six and nine diameter readings were taken; they were equally distributed along the bottom, middle and top of the sample. As the thickness of the membrane(s) was known, the soil diameter could be calculated. An average of all readings was then taken and considered to be the actual sample diameter at the beginning of the test. The height of the sample was measured once the sample was placed and prepared in the triaxial apparatus. At least three readings were taken

and then the average height calculated was compared to the cutting mould intending sample height.

Once a sample was set-up, saturation would commence under back pressure prior to moving on to the main testing phase, until a B-value of 95% or higher was reached for the drained tests and 98% or higher for the undrained tests.

### *3.4.2 Sample preparation – Intact block samples*

#### *a) Block sample extraction in CTRL tunnel at Stratford*

Three block samples were extracted from the Channel Tunnel Rail Link (CTRL) tunnel at Stratford. The sand was sampled from the bottom of a service tunnel connecting the two main train tunnels marked as Cross-passage C4 (Figure 3-19). The sampling location was approximately 10m from the outer perimeter of the main tunnels. The entire area had been de-watered, which enabled access to Thanet sand that lay only a few metres above the chalk. The log of the closest borehole to the location of the sample extraction (SA8830A) has been highlighted and is presented in Figure 3-19 to Figure 3-24.

Initially, a layer of Thanet sand of about a metre in thickness was removed from the top, as it was considered potentially to have been disturbed by the various construction activities. Once a desired safe depth had been reached, then the three areas that would form the block samples were marked. The soil around these areas was gradually extracted without the use of any heavy equipment that could again potentially disturb the soil. Once the approximate block dimensions had been reached, the samples were trimmed with the use of a large wire saw (Figure 3-25). After the soil had been cut down to the required dimensions (Figure 3-26), it was covered with two of layers of cling-film and melted wax, in order to create an effective barrier against moisture loss (Figure 3-27). In order to transport the samples, they had to be placed in wooden boxes for protection. The void between the soil sample and the box was filled with expansive foam (Figure 3-28), which

provided a confinement, minimizing the disturbance of the samples due to vibrations and movements during transportation. Initially the four sides were filled with foam and then the top of the box was fixed in place (Figure 3-29). The samples were then left overnight for the foam to set, prior to their base being cut (Figure 3-30). Once the base of the sand was cut and the sample gently turned over, the base too was sealed with layers of cling-film and wax. Finally, expansive foam was placed on the base prior to the attachment of the base plate of the box. The three samples were finally transported out of the tunnel and brought back to the soil mechanics laboratory.

*b) Laboratory triaxial sample preparation*

The intact block samples that were retrieved from Stratford were opened in the lab and cut into smaller blocks of soil using a band saw. These smaller blocks were covered with cling-film and wax to prevent any moisture loss and then temporarily stored in plastic boxes, wrapped in bubble wrap for protection. As intact samples had to be formed for testing, the soil blocks were progressively opened. For the 38mm, 50mm and 100mm diameter samples, the rest of the trimming and preparation procedure was the same as in the case of the intact rotary cored samples, as described in Section 3.4.1.

One of the advantages of having block samples instead of rotary cored samples was that not only vertical samples could be formed. This allowed three sets of samples to be cut, a vertical set, and two horizontal sets, each at $90^0$ to each other (Figure 3-31). These samples were used to examine the anisotropy of the soil and the influence of the intermediate principal stress, as will be discussed in detail later.

### *3.4.3 Reconstituted samples*

The reconstituted samples were formed from the unused trimmings of the either the rotary drilled cores or the block samples. These trimmings were completely

dried so as to allow the initial water content of the sample being setup to be calculated.

For a reconstituted sample to be set up, a mould with a venturi system to provide suction was used. Thanet sand has a rather high fines content which prevents pluviation through water due to particle segregation. As a result, a dry set-up method had to be adopted. During the dry set-up, the soil was placed within the membrane, while the membrane was supported by the mould and the suction system. It was compacted to the required dry density by vibrating the mould. No direct vibration and tamping on the sample was used to avoid any sand particle breakage. Once the sample had been formed, water was gently pushed through it from the volume gauge, while a gap was left open at the top end of the sample between the membrane and the top platen to act as an escape route for the air being displaced upwards. Once water had filled the sample, the gap between the membrane and top platen was sealed and the suction was directly applied to the sample through the use of the venturi system and an air/water interface.

Samples were set-up using, just as before, a 0.3mm thick latex membrane in the case of the standard pressure tests and a combination of a 0.3mm latex and a 0.7mm thick neoprene membrane in the case of the high pressure tests. This alteration for the high pressure tests is due to the fact that the 0.7mm membrane is too thick to be used with the mould and the suction system. However, by using a thinner inner membrane, the sample is more susceptible to its membranes being punctured by sand grains at high pressures.

It was sometimes intended, though not always achieved, that the reconstituted samples should be set-up at approximately the same void ratio as the intact samples that had been tested before them, allowing a more direct assessment of the influence of structure on the engineering behaviour of Thanet sand.

## 3.5 Test Phase Description

### 3.5.1 Saturation

At the beginning of every triaxial test, it was necessary to examine the saturation level of the sample. The intact samples, both rotary cored as well as the block samples, were initially poorly saturated. Additionally, the reconstituted samples were initially completely dry upon set-up, as described in Section 3.4.3. It was therefore necessary to go through a saturation process, to ensure that the samples were sufficiently saturated.

Saturation commenced by applying a small positive effective stress of about 30kPa on the sample and then raising simultaneously both the cell as well as the back pressure, keeping the initially applied 30kPa effective stress constant. The pressures were increased until typical maximum back pressures of 350kPa on the standard pressure system and 650kPa on the high pressure system were reached. Then the pressures were kept constant and the sample was allowed to saturate under constant pressure for at least 48 hours. Once the first 48 hours had passed, a B-test was performed. Raising the cell pressure by 50kPa while having the drainage valve closed and allowing the sample to reach equilibrium, the pore pressure increase was measured. The ratio of the pore pressure increase over the cell pressure increase is the B-factor.

$$B = \frac{\text{pore pressure increase}}{\text{cell pressure increase}} \times 100\% \quad \textit{(3-3)}$$

A sample was considered to be sufficiently saturated if a B-value of 95% or higher was achieved if the sample was intended for a drained test and a B-value of 98% or higher was achieved if the sample was intended for an undrained test. If the B-value was less than what was desired, which was usually the case then the

sample was kept under constant pressure for another 24 hours at the end of which the B-value was checked again. In some cases, prolonging the constant stress stage did not appear to improve the B-value of the sample; to overcome this, the total stresses were further increased by 100kPa under a constant effective stress and then the sample was left to saturate for another 24 hour period at the end of which a B-test was again performed. Once an acceptable B-value had been achieved then the testing process could commence.

### *3.5.2 Isotropic compression*

Before the final shearing stage, the sand sample had to be gradually taken to the required effective stress condition. This varied from 125kPa to 1.0MPa for the standard pressure tests and from 2.0MPa to 4.0MPa for the high pressure tests. This was done by first connecting the suction cap and then isotropically compressing the sample, while keeping the back pressure of the system constant. The isotropic compression stage was fully automated with the entire triaxial apparatus being directly regulated by the controlling computer. The high permeability of the sand allowed excess pore water pressures to dissipate rapidly. The isotropic compression rates that were used for the high pressure test were about 150kPa per hour, whereas 50kPa per hour was used for the standard pressure triaxial tests. It was necessary to use such different loading rates for the two experiments considering time constraints and the large effective stresses that had to be reached in order for the high pressure tests to be performed. In the case of the high pressure tests, during the progress of the isotropic compression stage, bender element readings were taken approximately at every 200kPa effective stress increase. These gave the variation of the dynamic shear modulus (i.e. $G_0$) of the soil sample with confining pressure. The detailed results are presented in Chapeter 6.

### *3.5.3 Shearing*

*a) Shearing in compression*

Once the required effective stress condition had been achieved then the final stage of the experiment would begin; the axial shearing. Typically, the shearing rates were initially small at about 0.1% axial strain per hour. This allowed a better observation of the small strain behaviour of the soil. Once the sample had been sheared past its small strain region which is considered to extend up to 1% shear strain, the shearing rates could be gradually increased from 0.1% per hour to a maximum of 0.4% per hour. This was done due to practical constraints on the overall time required for completion of an experiment. To verify that the gradual shearing rate increase had no effect on the results produced, a series of tests was performed that were sheared until the end without an increase of the shearing rate. The results did not show any evidence that the gradual increase of shearing rate affects the behaviour of the material. The Thanet sand samples tested in compression were sheared to a minimum of a 20% axial strain and some tests were sheared to 30% axial strain or more.

Once the test was completed, the sample was extracted for a final water content measurement to be taken. This measurement was used to calculate the initial void ratio using the volume strain readings that were taken during the experiment.

*b) Shearing in extension*

Two intact samples derived from a block, one vertical and one horizontal, were tested in extension at an effective confinement of 1,000kPa. The only difference, apart of the mode of failure that will be discussed later, is the maximum axial strain that was achieved during shearing. Unlike the compression tests that could

easily reach a 20% axial strain, these samples had formed clear failure planes at axial strains no more than 8%.

### *3.5.4 Y1 and Y2 probing*

One of the last objectives of this project was to obtain the elastic parameters and define the limits of the elastic surface for Thanet sand. This was achieved by performing a combination of both drained and undrained probes that showed the location of the Y1 and the Y2 yield envelopes.

Initially, a large intact sample was cut from the block and trimmed to form a cylinder measuring 100mm in diameter and 200mm in height. The sample was then inserted into the large diameter triaxial cell and allowed to saturate for approximately seven days. Upon saturation, it was taken to its in-situ pre-selected stresses. As the Y1 and Y2 envelopes may be stress state and stress history dependent, it was decided to select stress conditions and an approach path representative of typical in-situ stresses in the ground as well as the recent stress history of Thanet sand within the greater London area rather than consider the specific in-situ stresses and stress history at the sampling location. After communication with the geotechnical division at Ove Arup, a typical stratographic profile of the area around Canary Wharf was obtained. Additionally, from site investigations performed in the past they were able to provide unit weights for the materials in question, the depth at which the water table was typically found at as well as $K_0$ estimates for Thanet sand. This allowed the selected in-situ stresses to be calculated (see Figure 3-32). A representative depth of 39m was assumed for the calculation of the stresses with a $K_0$ of 1.03. This gave an in-situ p' of 480kPa and q of -15kPa. Finally, to simulate the erosion and therefore unloading that took place last within the soil, the sample was initially compressed to a higher stress, allowed to stabilise and then swelled to its in-situ state ($K_0$ unloading).

Once at the selected in-situ conditions, the Y1 and Y2 probes were performed. The probes were chosen in order to allow the measurement of the elastic

parameters of Thanet sand. A schematic of the probes is shown in Figure 3-33. During the probes, the maximum rate that stress was applied to the soil did not exceed 5kPa per hour. This ensured that whatever excess pore pressures developed in the sample would be allowed to dissipate. Finally, once a probe was complete, sufficient time for creep was allowed prior to commencing another probe. Typically, after a Y1 probe, a minimum of four hours was allowed whereas after a Y2 probe a minimum of a day was allowed. Additionally, once the sample was thought to have stabilised, a series of bender element readings were taken. These readings were compared with the readings taken before the probe and hence verified that the sample had not been irreversibly strained during the last probe undertaken. In all cases checked, the $G_{HV}$ and $G_{HH}$ readings for the 100mm sample remained unchanged prior to and after probing.

## 3.6 *Formulae Used For The Data Analysis*

In order for the results that shall be presented to be clearly understood, all the main formulae that were used in the analysis must be explained.

The Axial Strain "$\varepsilon_a$" was calculated based on the change of axial length $\Delta l$ over the initial sample length $l_0$ for both internal and external axial displacements.

$$\varepsilon_a = \frac{\Delta l}{l_0} \qquad (3\text{-}4)$$

The Volumetric Strain "$\varepsilon_v$" was in turn calculated by taking the ratio of the change in volume gauge reading $\Delta V$ (and therefore the change in volume) over the initially calculated volume of the sample $V_0$.

$$\varepsilon_v = \frac{\Delta V}{V_0} \qquad (3\text{-}5)$$

The triaxial Shear Strain of the sample "$\varepsilon_s$" (that is equal to $^2/_3\gamma$, where $\gamma$ is the engineering shear strain) was calculated based on a combination of the axial strain (internal and/or external) and the volumetric strain.

$$\varepsilon_s = \varepsilon_a - \frac{\varepsilon_v}{3} \qquad (3\text{-}6)$$

It must be noted that this equation is valid only for small strains. However, as shear strain calculations were used only for shear moduli comparisons, whose range typically ends before $\varepsilon_s$=1%, it was considered sufficient to only use the simplified small strain version as shown above.

The deviatoric stress on the sample "q" was calculated based on the deviatoric force "F" and current sample area "$A_{current}$", assuming a right cylinder area correction.

$$q = {}^F/_{A_{Current}} \qquad (3\text{-}7)$$

The initial sample void ratio "$e_o$" can be calculated with up to four different approaches. Typically not all four methods give similar values of void ratio; an average was then taken with any extreme values neglected from the calculation. A typical accuracy of void ratio calculation is about ±0.02.

*void ratio calculation based on the water content from the preparation trimmings of the sample "$w_0$"*

$$e_0^a = Gs \times w_0 \qquad (3\text{-}8)$$

*void ratio calculation based on the initial bulk unit weight of the sample "$\gamma_b$"*

$$e_0^b = \frac{Gs - 1}{\frac{\gamma_b}{g} - 1} \qquad (3\text{-}9)$$

*void ratio calculation based on the initial dry unit weight of the sample "$\gamma_d$"*

$$e_0^c = \frac{Gs \times \gamma_w}{\gamma_d} - 1 \qquad (3\text{-}10)$$

*void ratio calculation based on the final water content of the sample "$w^{Final}$" & the volumetric strains during the experiment*

$$e_0^d = \frac{\left(Gs \times w^{Final} + 1\right)}{\left(1 - \varepsilon_v^{Compression}\right)\left(1 - \varepsilon_v^{Shearing}\right)} - 1 \qquad (3\text{-}11)$$

It should be noted that for the initial void ratio calculation of an intact sample it is possible for all four equations to be used whereas, for reconstituted samples, equation 3-8 cannot be used.

As mentioned in Section 2, to normalize the shearing data, $p'_{cs}$ was used (Figure *2-21*). It is calculate based on the following formula:

$$p'_{cs} = e^{\left[\frac{\Gamma - v}{\lambda}\right]} \qquad (3\text{-}12)$$

The rate of dilation $d\varepsilon_v / d\varepsilon_s$ was calculated by a simple 30 point linear regression through volumetric strain and shear strain data at higher stress ratios and by linear regressions that reached up to 250 points at low stress ratios, in order to account for the increased number data points taken at small strains and to eliminate the scatter produced with a smaller regression interval.

For the monotonic equivalent tangent shear moduli, the formula used is as follows:

$$G_{eq} = \delta q / 3\delta\varepsilon_s \qquad (3\text{-}13)$$

The equivalent tangent shear moduli for both internal and/or external data were also based on a linear regression to reduce scatter. For this regression, to give better results, the data were filtered for any extreme readings due to elevated noise. Additionally, the number of the data points used in every part of the regression varied. They were chosen in such a way that the range of the regression was limited to about 20% of the current sample shear strain. A longer regression range would alter the shape of the stiffness - log strain curve.

Finally, the critical state angles of shearing resistance of the soil both for compression as well as extension were calculated based on Equations 3-14 and 3-15 respectively.

$$\sin\varphi' = \frac{3M}{6+M} \qquad \textit{(3-14)}$$

$$\sin\varphi' = \frac{3M}{6-M} \qquad \textit{(3-15)}$$

where $M = {}^{q}/_{p'}$, at the critical state

The constitutive equations for the elastic parameters are as follows:

$$\delta\varepsilon_v = \frac{1}{E_v}\delta\sigma_v' - \frac{2\nu_{vh}}{E_v}\delta\sigma_h' \qquad \textit{(3-16)}$$

$$\delta\varepsilon_h = -\frac{\nu_{vh}}{E_v}\delta\sigma_v' + \frac{1-\nu_{hh}}{E_h}\delta\sigma_h' \qquad \textit{(3-17)}$$

where, $E_v$ and $E_h$ are the vertical and horizontal Young's moduli respectively and $\nu_{vh}$ and $\nu_{hh}$ are the vertical and horizontal Poisson's ratios respectively

For axial compression or extension ($\delta\sigma_h' = 0$) Equations 3-16 and 3-17 simplify as follows:

$$\delta\varepsilon_v = \frac{1}{E_v}\delta\sigma_v' \qquad (3\text{-}18)$$

$$\delta\varepsilon_h = -\frac{\nu_{vh}}{E_v}\delta\sigma_v' \qquad (3\text{-}19)$$

In turn, Equations 3-18 and 3-19 can be rearranged, giving the vertical Young's modulus $E_v$ and Poisson's ratio $\nu_{vh}$ as shown below:

$$E_v = \left(\frac{\delta\sigma_v'}{\delta\varepsilon_v}\right)_{\delta\sigma_h'=0} \qquad (3\text{-}20)$$

$$\nu_{vh} = \left(\frac{\delta\varepsilon_h}{\delta\varepsilon_v}\right)_{\delta\sigma_h'=0} \qquad (3\text{-}21)$$

For radial compression or extension ($\delta\sigma_v' = 0$) Equations 3-16 and 3-17 simplify as follows:

$$\delta\varepsilon_v = -\frac{2\nu_{vh}}{E_v}\delta\sigma_h' \qquad (3\text{-}22)$$

$$\delta\varepsilon_h = \frac{1-\nu_{hh}}{E_h}\delta\sigma_h' \qquad (3\text{-}23)$$

The parameter F can be directly measured from the probes as follows:

$$F_h = \frac{E_h}{1-\nu_{hh}} \qquad (3\text{-}24)$$

Hence, by combining what has been previously calculated, $E_h$ can be derived:

$$E_h = \frac{4F_h G_{hh}}{F_h + 2G_{hh}} \qquad (3\text{-}25)$$

where $G_{hh}$ is measured with the horizontally mounted bender elements

The Poisson's ratio $\nu_{hh}$ can be calculated by combining Equations 2-24 and 2-25.

$\nu_{hv}$ is in turn calculated based on the following equations:

$$\nu_{hv} = -\frac{\delta\varepsilon_v}{\delta\varepsilon_h}\frac{(1-\nu_{hh})}{2} \qquad (3\text{-}26)$$

$$\nu_{hv} = -\frac{E_h}{2}\frac{\delta\varepsilon_v}{\delta\sigma_h} \qquad (3\text{-}27)$$

Probes at constant p' and constant q allow the measurement of the bulk modulus K', the equivalent shear modulus $G_{eq}$ and the coupling moduli $J_{pq}$ and $J_{qp}$. The constitutive equations are as follows:

$$\delta\varepsilon_p = \frac{\delta p'}{K'} + \frac{\delta q}{J_{pq}} \qquad (3\text{-}28)$$

$$\delta\varepsilon_q = \frac{\delta p'}{J_{qp}} + \frac{\delta q}{3G_{eq}} \qquad (3\text{-}29)$$

where $\varepsilon_p$ and $\varepsilon_q$ are the volumetric and shear strains respectively. For an elastic material, $J'_{pq} = J'_{qp} = J'$. Finally, by rearranging Equations 3-28 and 3-29 we can obtain:

$$G_{eq} = \frac{3}{4\left[\frac{(1+2\nu_{vh})}{E_v} + \frac{(1-\nu_{hh})}{2E_h}\right]} \qquad (3\text{-}30)$$

$$K' = \frac{1}{\left[\frac{(1-4\nu_{vh})}{E_v} + \frac{2(1-\nu_{hh})}{E_h}\right]} \qquad (3\text{-}31)$$

$$J' = \frac{3}{2\left[\frac{(1-\nu_{vh})}{E_v} - \frac{(1-\nu_{hh})}{E_h}\right]} \qquad (3\text{-}32)$$

## 3.7 Right Cylinder Assumption & Strain Localisation

In order for the cross-sectional area of a sample tested to be calculated, the standard right cylinder assumption was adopted. As mentioned in Section 2.3.4, as large strains accumulate in the sample, they cause strain localisation and its behaviour deviates from this idealised adopted geometry. The sample may also barrel (Figure 2-50). Barrelling and localisation both have a direct impact on volumetric strain calculations. As internal volumetric strains based on internal axial and radial measurements indicate completely different soil behaviour to the measurements derived from the volume gauge which considers the overall sample behaviour, the internal strain readings have been considered only up to a maximum of 5% axial strain. Past that point, the sample does not truly follow the right cylinder deformation pattern and the volumetric strains calculated based on the combined readings of the internal axial and radial instrumentation deviate from the global volumetric strains measured by the volume gauge. Again, as mentioned in Section 2.3.4, a partial solution for the sample barrelling would be to adopt the use of lubricated end platens. Even though modifying the Bishop & Wesley triaxial cell for the use of lubricated end platens would have been possible, the modification of the 50mm high pressure triaxial cell would not. The apparatus was built in such a way that could not accommodate a straightforward alteration. Top & base bender elements, along with the one way drainage of the system and the high back pressure used to accelerate the sample saturation would have led to a series of problems (such as continuous clogging of the base porous

stone by the grease applied) that eliminated any possibility for modifying the apparatus. Therefore, as being consistent in terms of testing procedures was necessary to allow direct comparison of the results obtained from both apparatuses and both triaxial cells could not have been modified to accommodate lubricated end platens, standard frictional surfaces (i.e. a standard porous stone on the base and a metal/plastic surface on top) were used in all tests.

| | *Standard Triaxial Apparatus* | *High Pressure Triaxial Apparatus* | *Accuracies* |
|---|---|---|---|
| *Pressure Transducers – Cell Pressure* | ±0.5kPa | ±2kPa | |
| *Pressure Transducers – Back Pressure* | ±0.5kPa | ±2kPa | |
| *Load Cell* | ±1N | ±5N | |
| *Resistive Type Transducers for External Axial & Volumetric Strains – Small Strain Region* | ±0.001% - absolute | n/a | |
| *Resistive Type Transducers for External Axial & Volumetric Strains – Large Strain Region* | ±0. 5% of current strain level | n/a | |
| *LVDT for External Axial & Volumetric Strains Small Strain Region* | n/a | ±0.001% - absolute | |
| *LVDT for External Axial & Volumetric Strains Large Strain Region* | n/a | ±0.5% of current strain level | |
| *Internal LVDTs – Small Strain Region* | n/a | ±0.0001%- absolute | |
| *Internal LVDTs – Large Strain Region* | n/a | ±0.5% of current strain level | |
| *Inclinometers – Small Strain Region* | ±0.001% - absolute | n/a | |
| *Inclinometers – Large Strain Region* | ±0.5% of current strain level | n/a | |

***Table 3-1*** *Summarizing table of approximate instrumentation accuracies*

| | *Type of measurements* | *Capacity* | *Resolution* |
|---|---|---|---|
| ***Pressure transducer*** | Cell and pore pressures | 1MPa | 0.03 kPa |
| ***Mid-Height Probe*** | Pore Pressure | 1MPa | 0.01 kPa |
| ***IC Load Cell*** | Deviatoric Force | 4kN | 0.2 N |
| ***IC Volume Gauge*** | Volume strain | 50cc<br>100cc | 0.001 cc |
| ***Displacement transducer*** | Axial strains | 25mm | 5μm |
| ***External LVDT*** | Axial strains | 34mm | 0.2μm |
| ***Electrolevels*** | Local axial strain | 5mm | 0.1μm |
| ***Internal LVDT*** | Local axial and radial strains | ±5mm | $2 \times 10^{-5}$μm |

***Table 3-2*** *Summarizing table of approximate instrumentation resolution – 100mm apparatus (after Gasparre, 2005)*

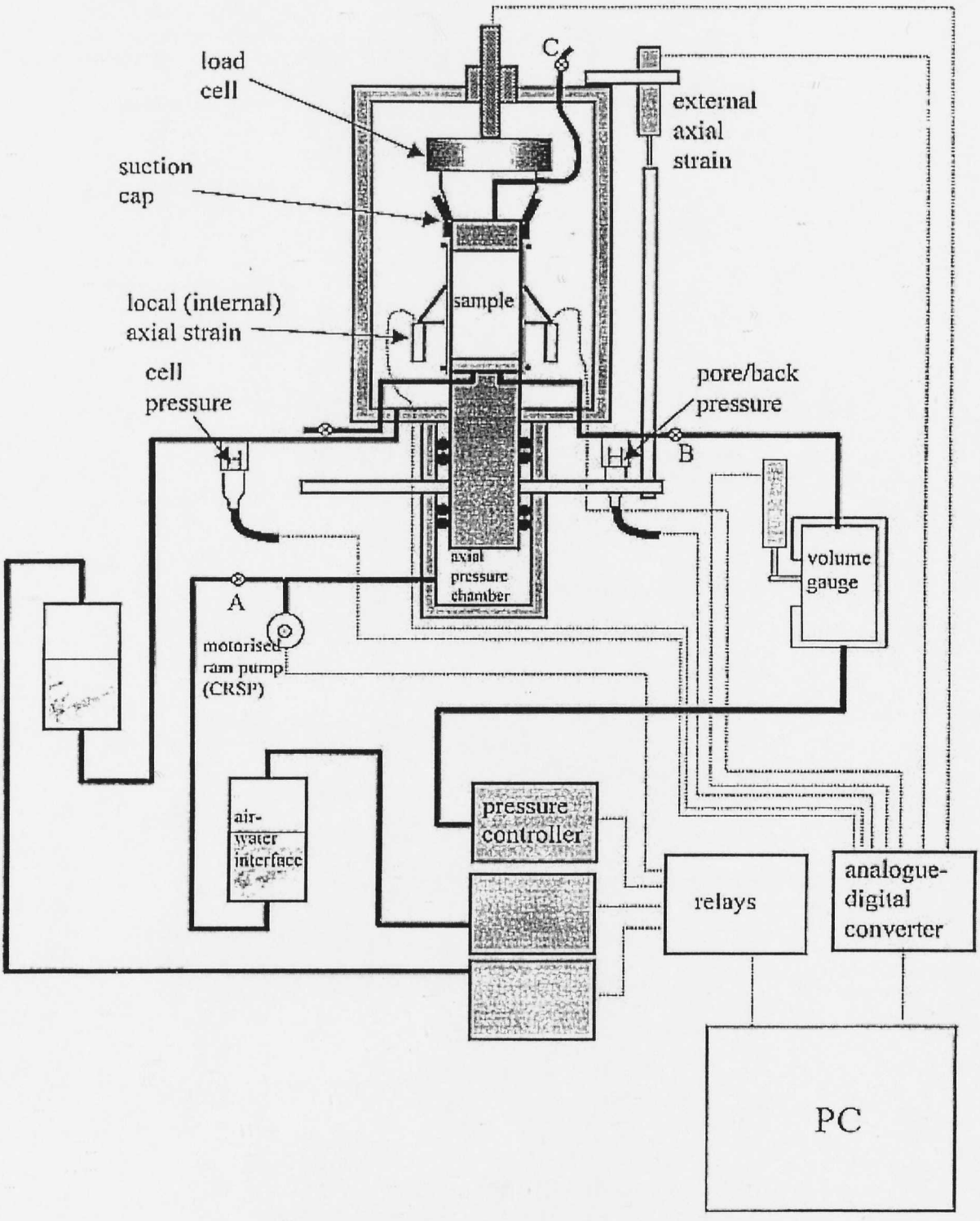


***Figure 3-1*** *Schematic diagram of the Bishop & Wesley (1975) triaxial cell (after Qadimi, 2005)*

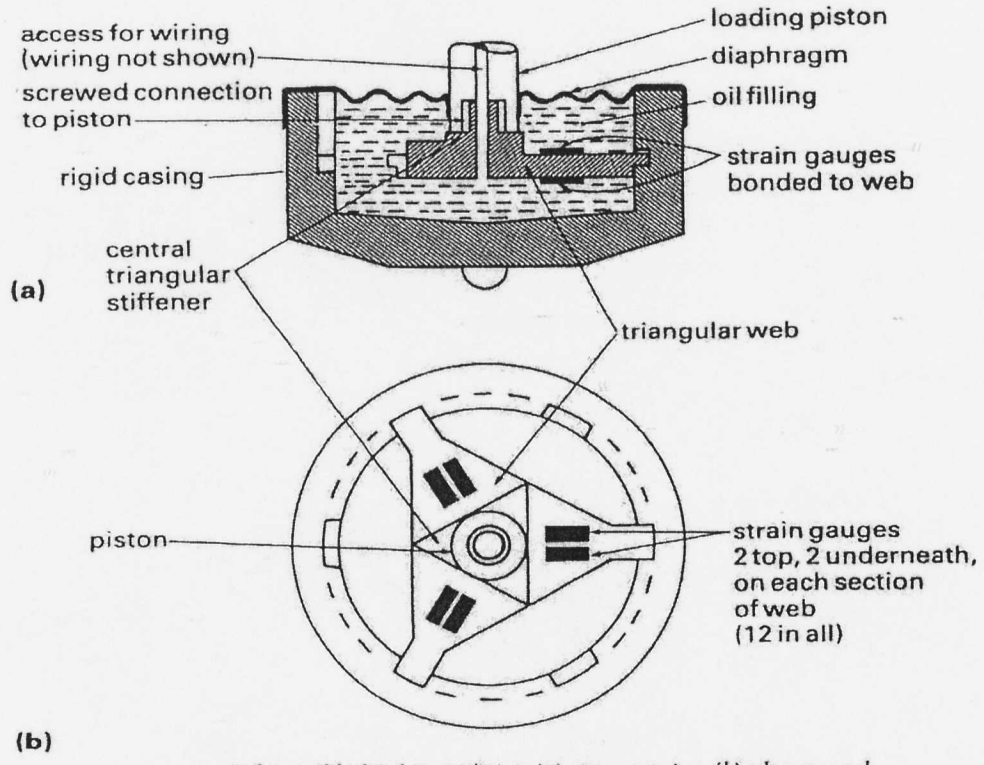


*Figure 3-2 Submersible load cell (after Head, 1985)*

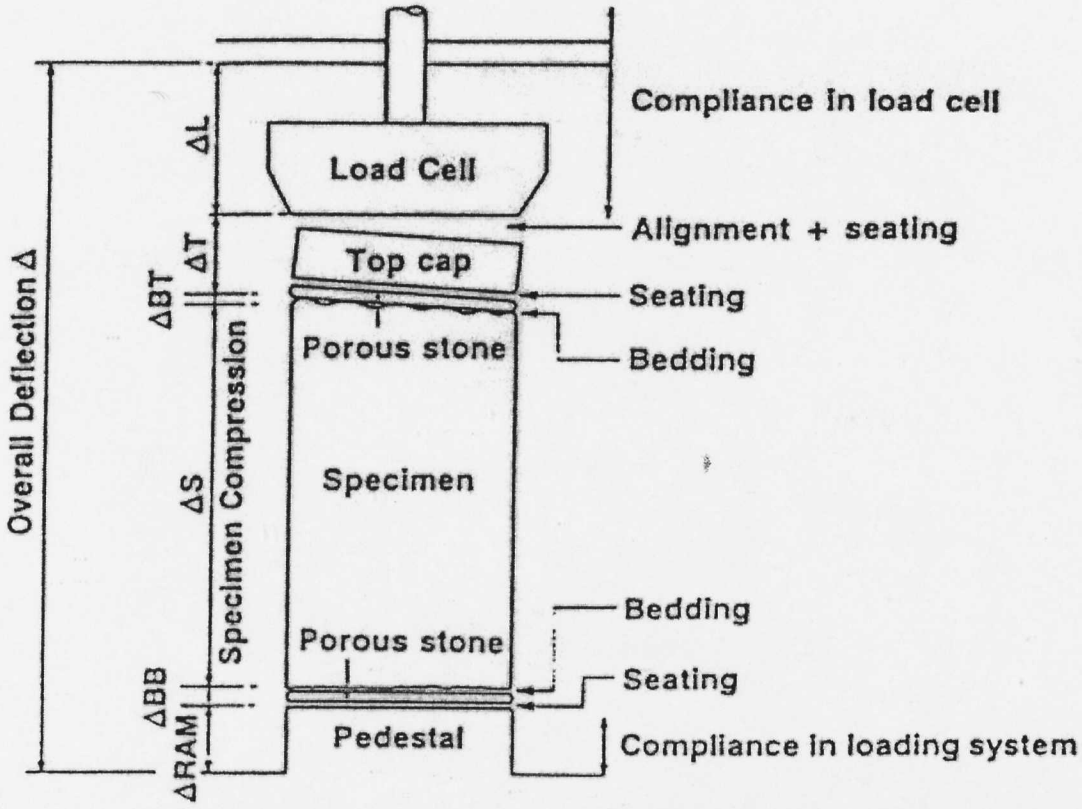


*Figure 3-3 Sources of error in external axial deformation measurements (after Burland et al., 1984)*

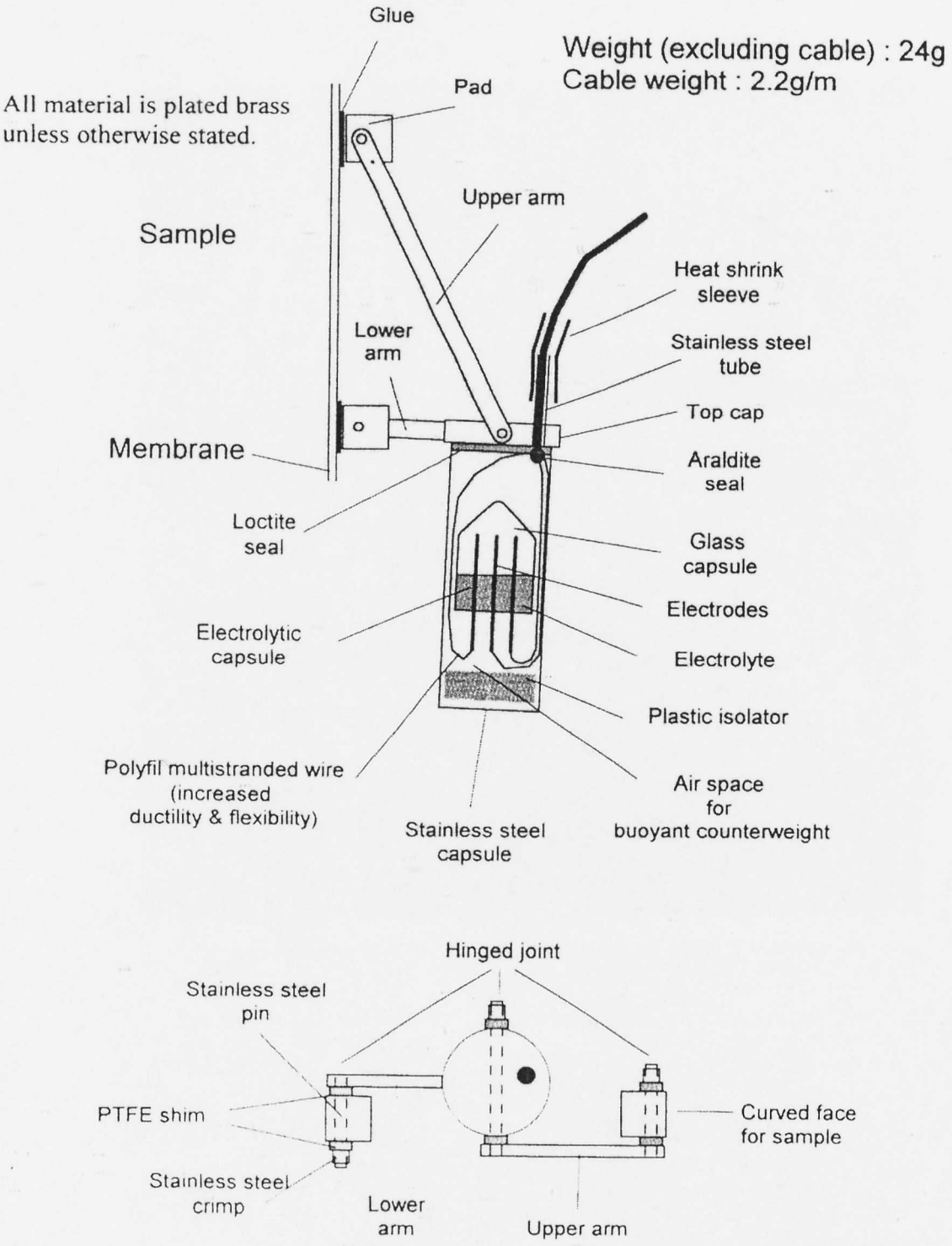


***Figure 3-4** of electrolevel inclinometer (after Kuwano, 1999)*

***Figure 3-5** Multiplier used on the Bishop & Wesley triaxial cell*

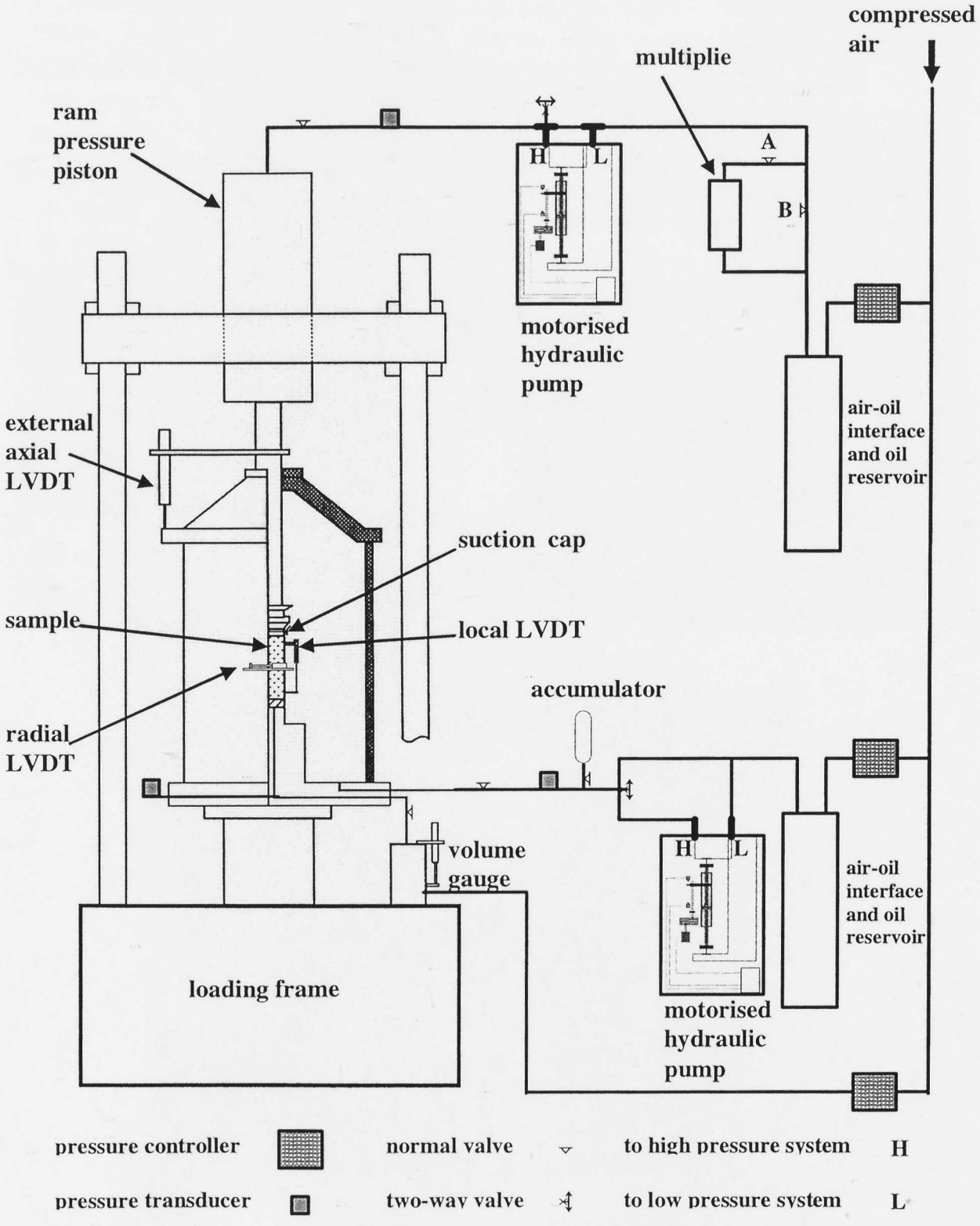


*Figure 3-6 Schematic diagram of the high pressure apparatus (after Qadimi, 2005)*

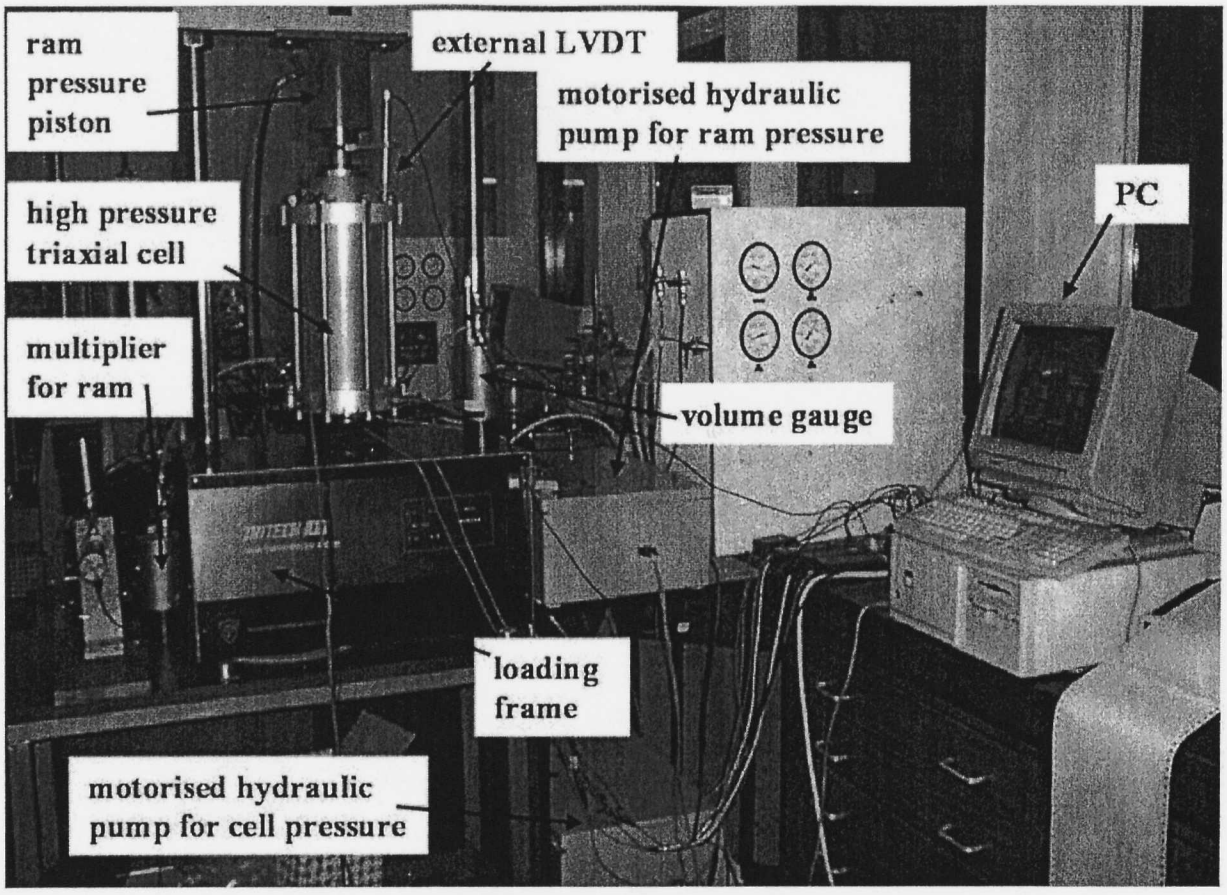


*Figure 3-7 The high pressure apparatus*

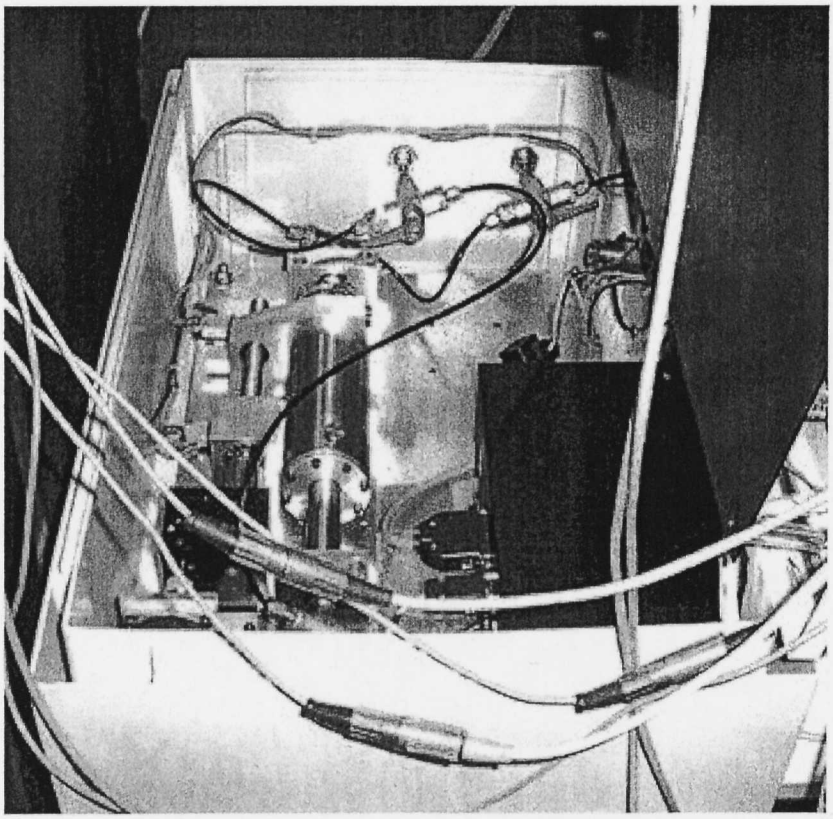

*Figure 3-8 Motorised hydraulic pump*

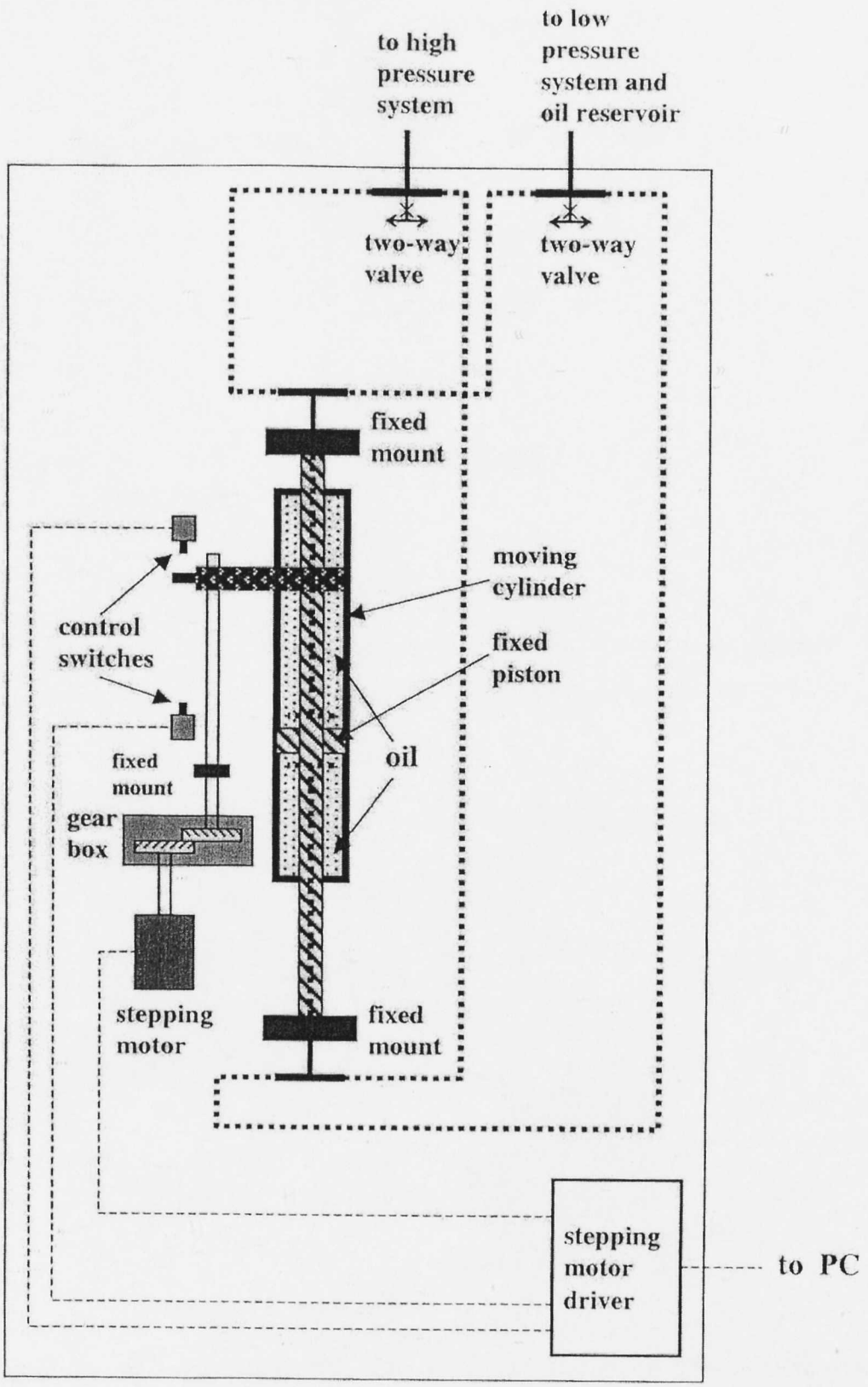


***Figure 3-9*** *Schematic diagram of the motorised hydraulic pump (after Qadimi, 2005)*

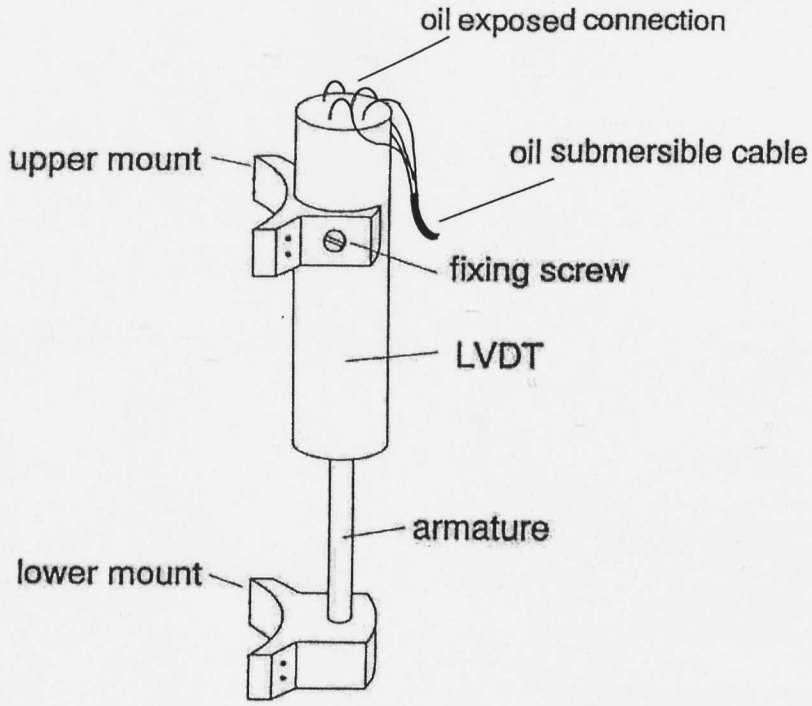


***Figure 3-10*** *Oil submersible LVDT for measuring internal axial strains on the high pressure triaxial apparatus (after Cuccovillo & Coop, 1997)*

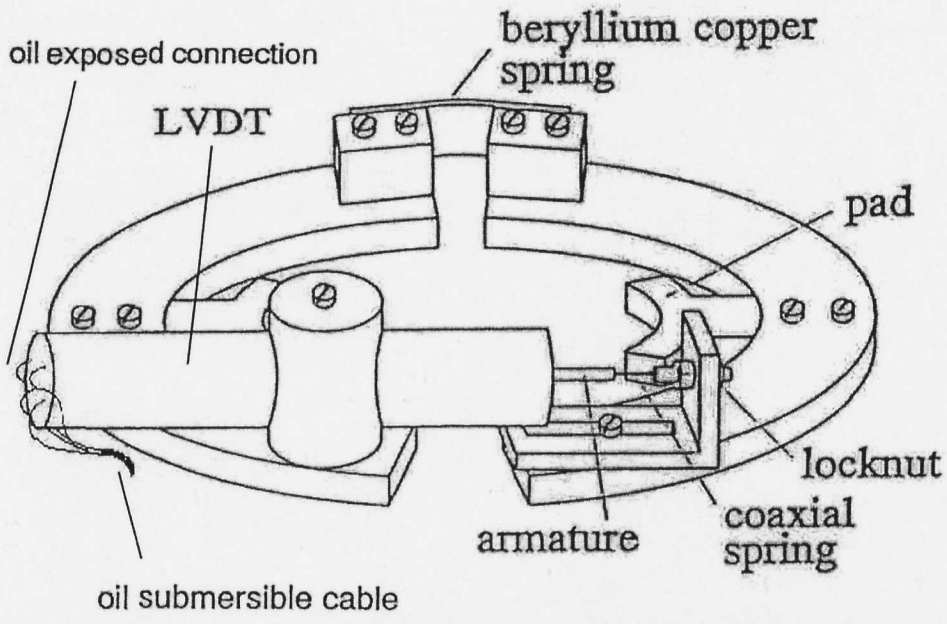


***Figure 3-11*** *Oil submersible LVDT for directly measuring internal radial strains on the high pressure triaxial apparatus (after Qadimi, 2005)*

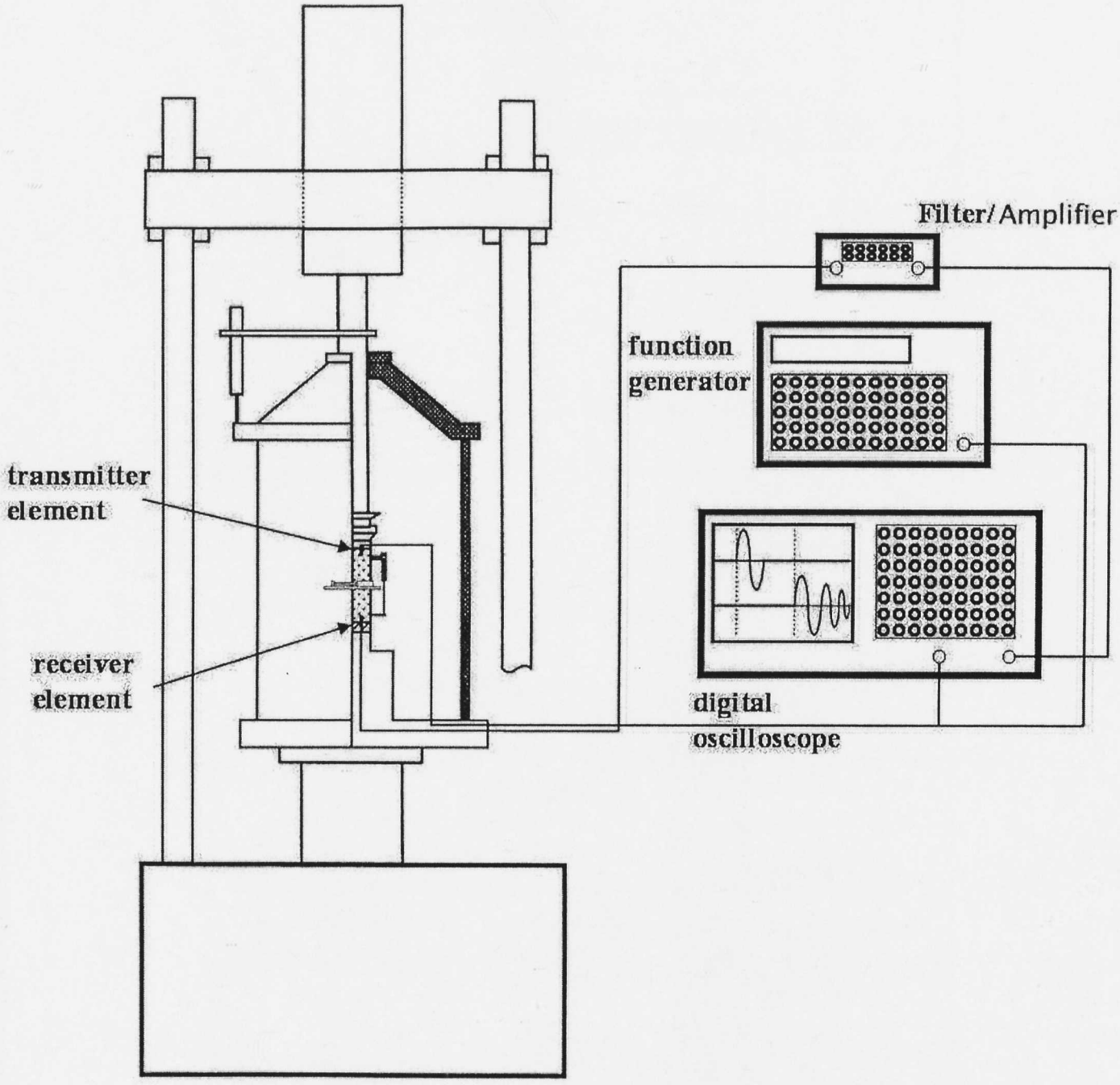


*Figure 3-12 Bender element equipment setup on the high pressure system (after Qadimi, 2005)*

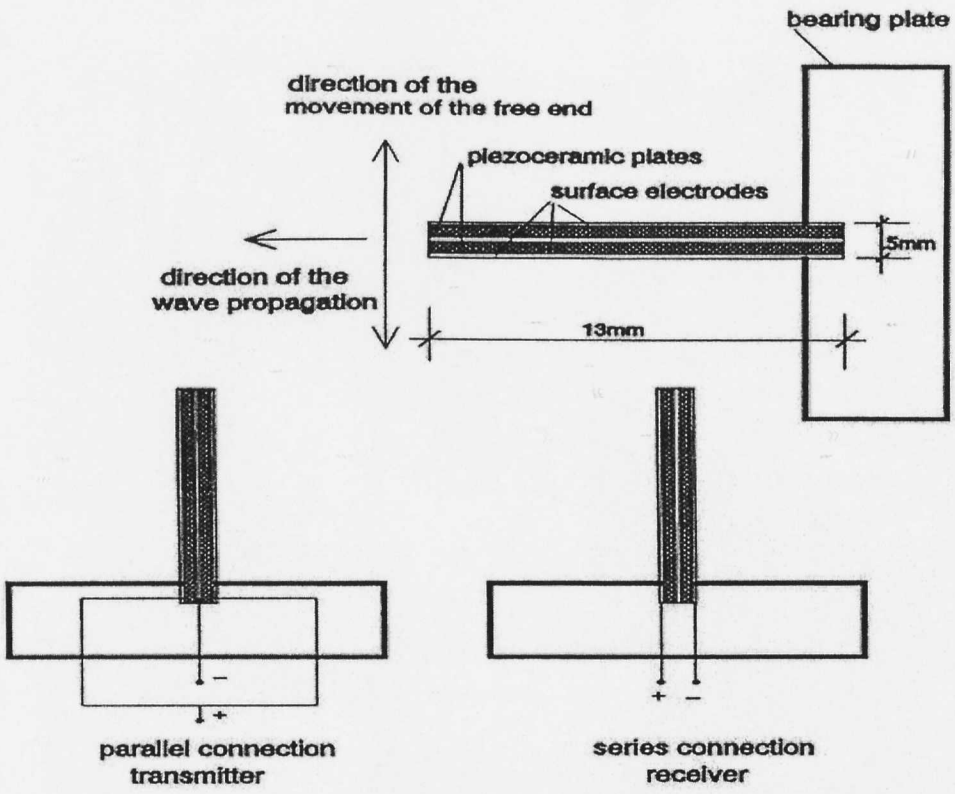


*Figure 3-13 Schematic diagram of the bender elements (after Jovicic, 1997)*

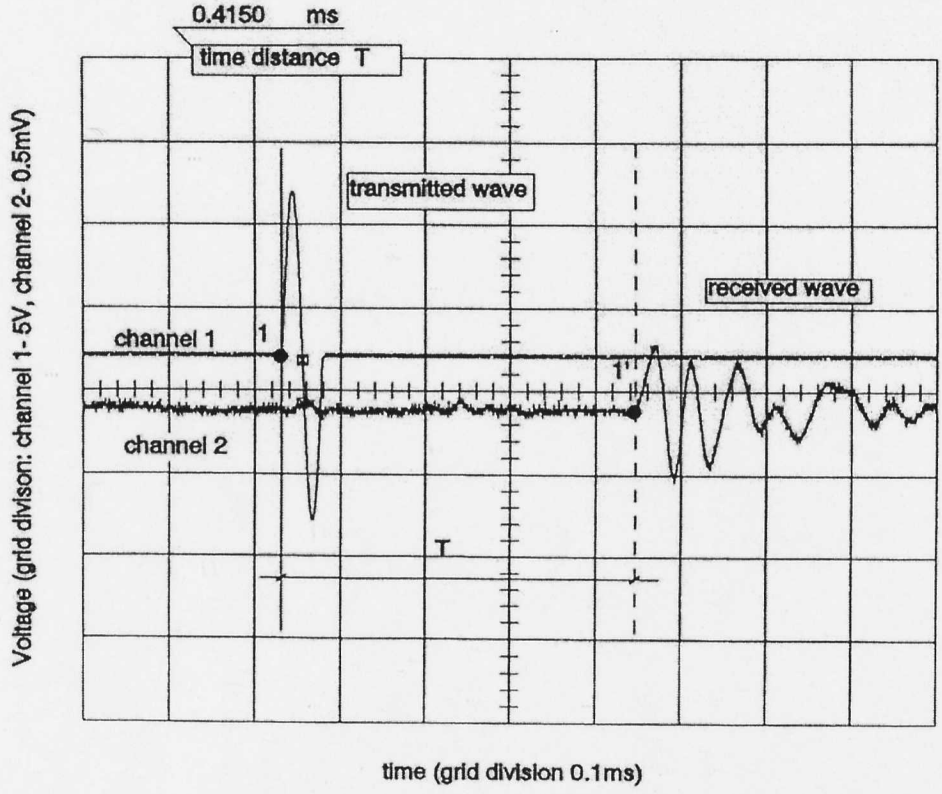


*Figure 3-14 Measurement of the arrival time from the screen of the oscilloscope (after Jovicic, 1997)*

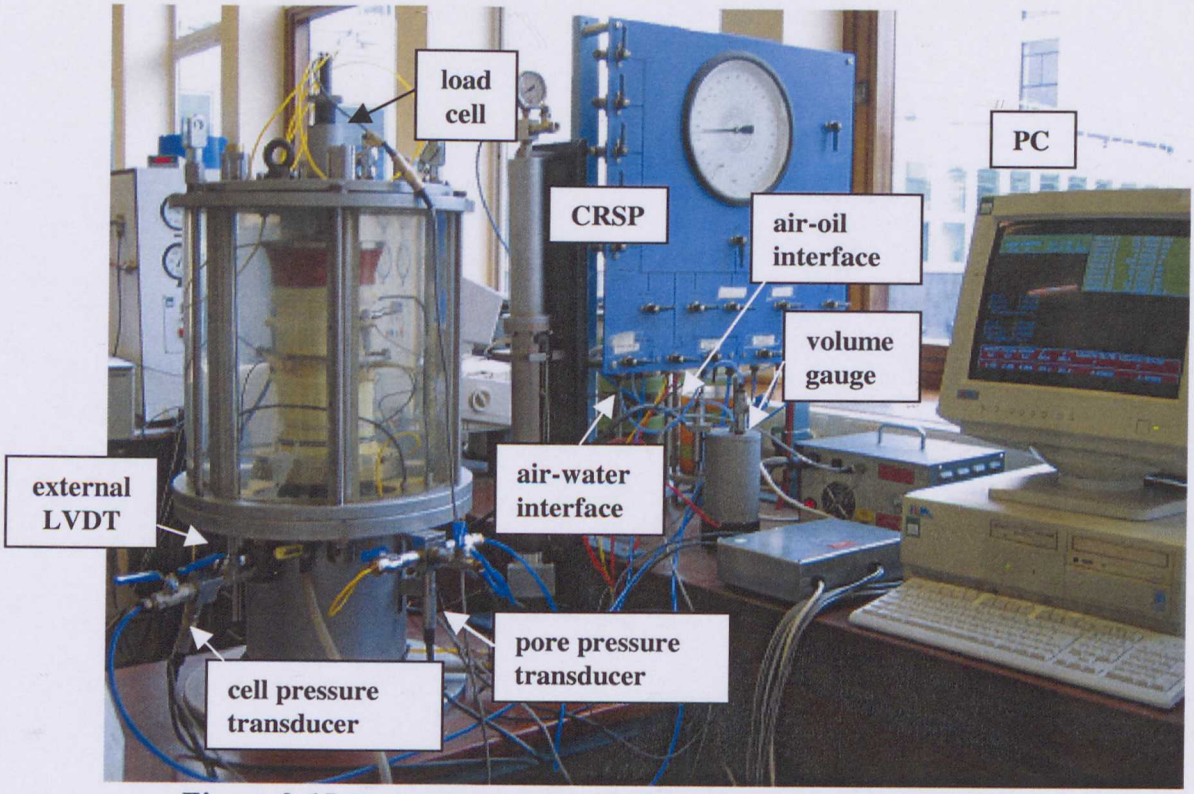


***Figure 3-15*** *Hydraulic triaxial cell for 100mm diameter samples*

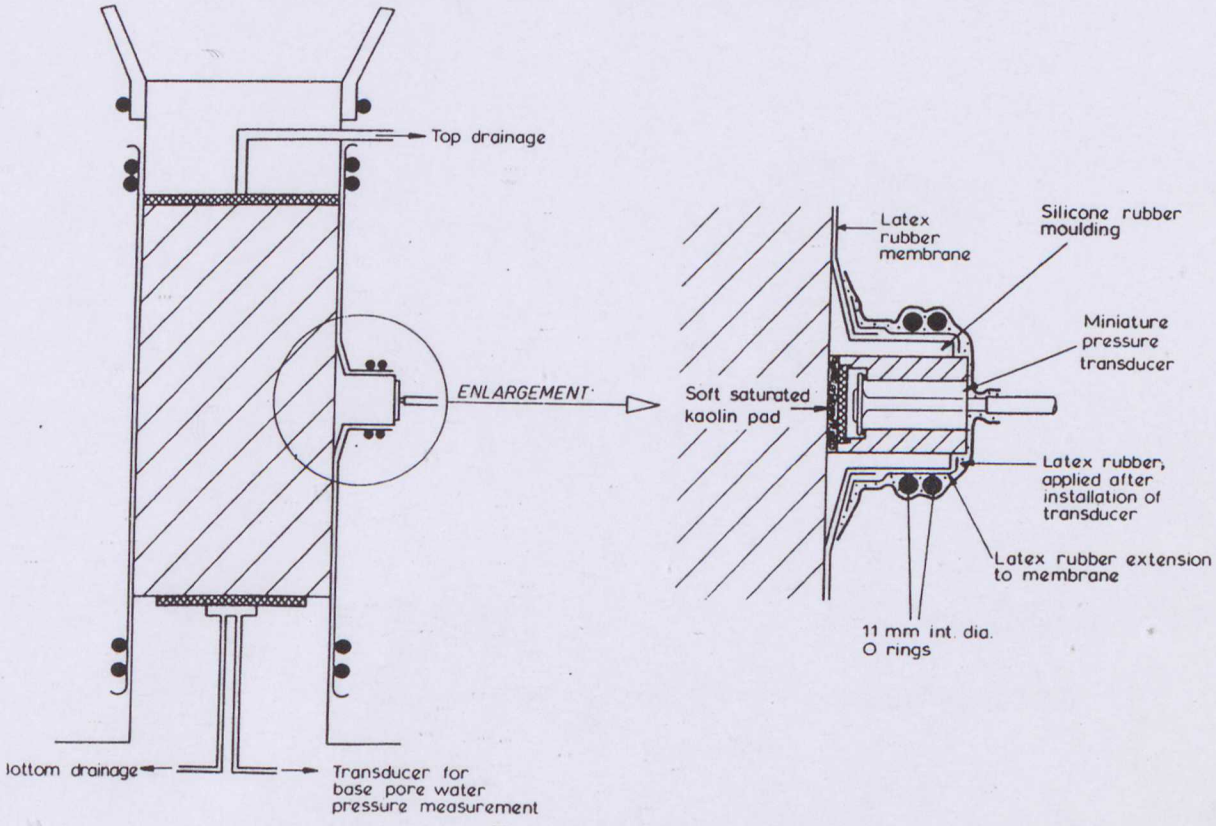


***Figure 3-16*** *Mid-height pore pressure probe (after Hight, 1983)*

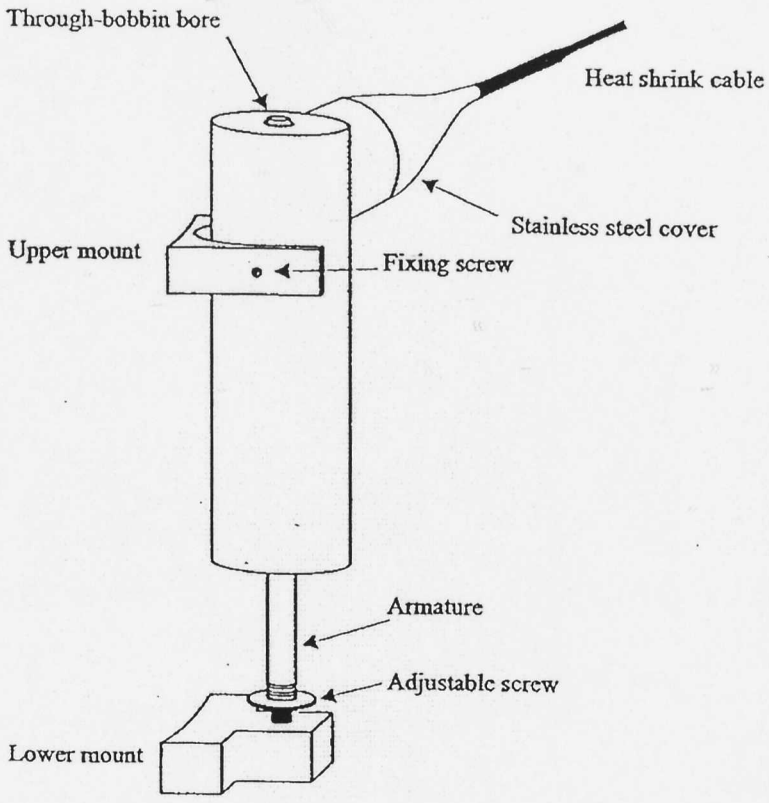


***Figure 3-17*** *Axial LVDT with adjustable screw (after Rolo, 2003)*

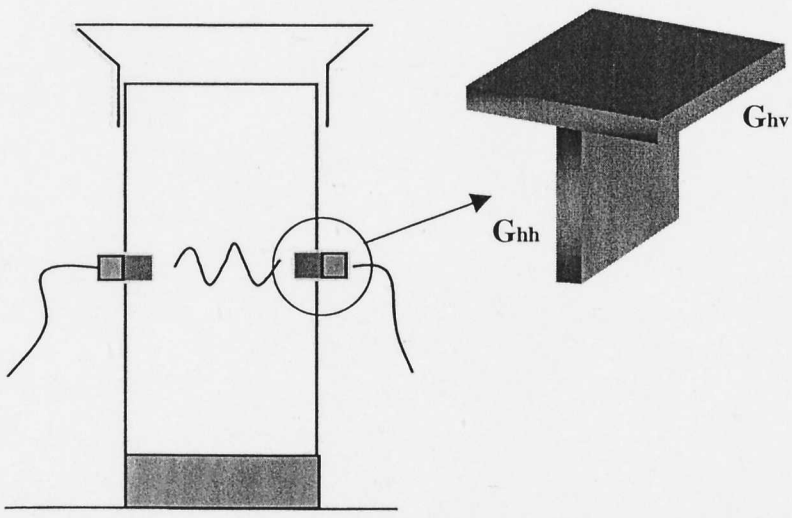


***Figure 3-18*** *Schematic diagram of the lateral bender elements (after Gasparre, 2005)*

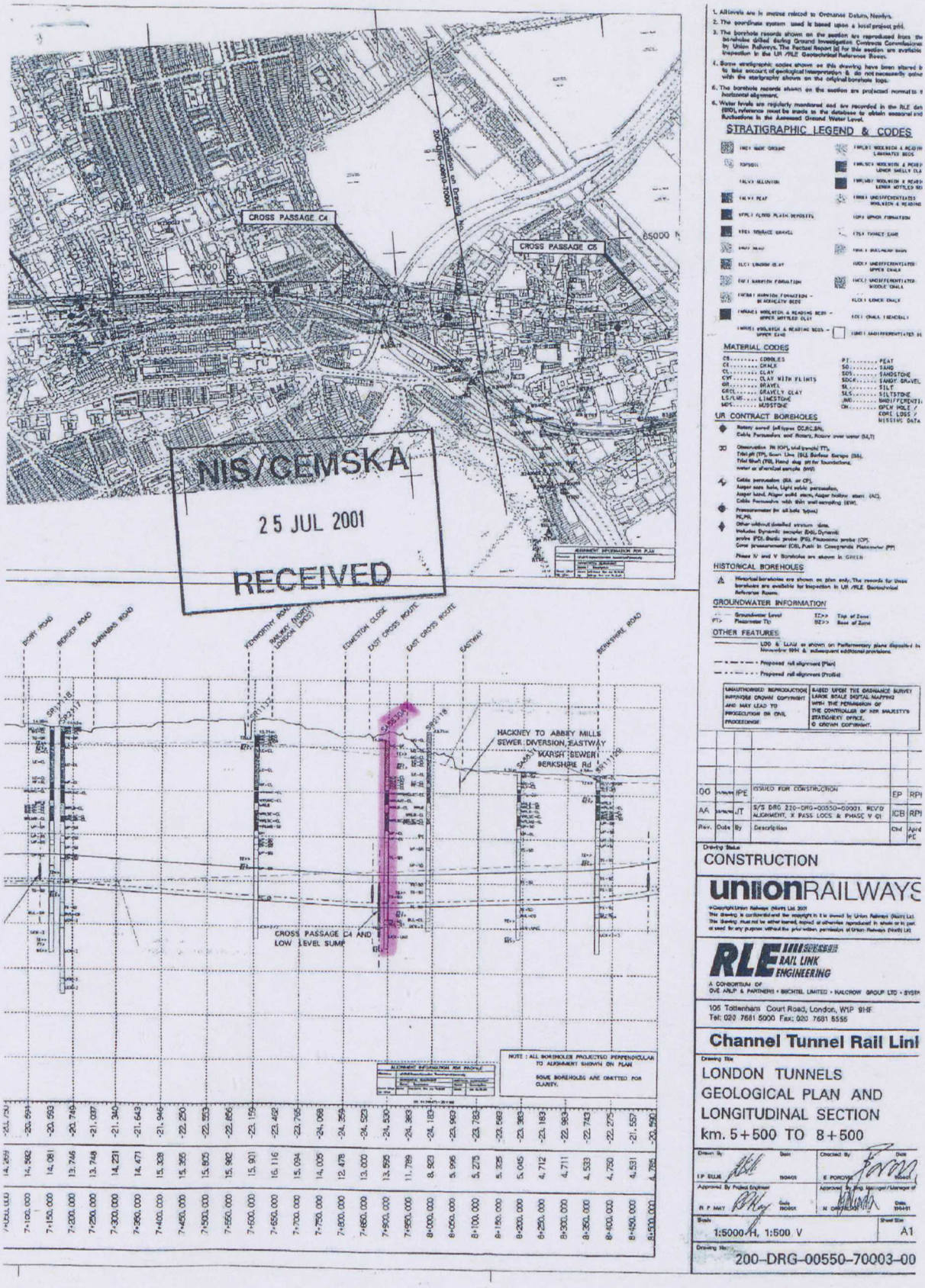


***Figure 3-19*** *Borehole log - map of area & list of boreholes (after Soil Mechanics, 2003)*

Soil Mechanics

**BOREHOLE No. SA8830A**

Sheet 1 of 7

Equipment & Methods
Hand dug inspection pit to 1.20m. Cable tool boring, 300mm dia to 13.00m. then 200mm dia to 20.00m. then 150mm dia to 46.50m.

Location No. 8109
Location CONTRACT 2 FOR PHASE 4 (1997) GROUND INVESTIGATIONS IN PROJECT AREA 200 (TROWBRIDGE)

Carried out for
Union Railways Limited

Ground Level
11.56 m AOD

Coordinates
536522.84 mE
184916.73 mN

Date
03/09/97 to 12/09/97

| Description | Reduced Level | Legend | Depth (Thick) | Samples/Tests: Depth | Sample Type | Sample No. | Test | Field Records |
|---|---|---|---|---|---|---|---|---|
| | 11.56 | | | 0.00 | | | | |
| 0.00-1.50m, with many cobbles of brick and concrete | | | | 0.00 - 1.50 | B | 1 | | |
| | | | | 1.50 - 1.95 | | | C N=14 | 2,3/4,3,3,4 |
| | | | | 1.50 - 3.00 | D | 2 | | |
| Medium dense black and brown, locally clayey, sandy angular to rounded fine to coarse GRAVEL of brick, concrete, ash, flint, slate and wood. Locally varying to sandy CLAY with some gravel. (MADE GROUND - GRAVEL) | | | | 3.00 - 3.45 | | | C N=10 | 2,3/3,2,3,2 |
| | | | | 3.00 - 4.50 | B | 3 | | |
| | | | (8.00) | | | | | |
| | | | | 4.50 - 4.95 | | | C N=12 | 2,3/3,3,3,3 |
| | | | | 4.50 - 6.00 | D | 4 | | |
| | | | | 6.00 - 6.45 | | | C N=8 | 1,2/1,2,2,3 |
| | | | | 6.00 - 7.50 | B | 5 | | |
| Black, brown and grey CLAY with a little subrounded fine to medium gravel of flint. Locally with a little black fibrous peat. (ALLUVIUM - CLAY) | | | | 7.50 - 7.95 | | | C N=13 | 2,3/2,3,4,4 |
| Grey fine to coarse SAND with some rounded to subrounded fine to coarse gravel of flint. (Foreman records as clayey) (ALLUVIUM - SAND) | 3.56 | | 8.00 | | | | | |
| | | | (0.60) | 8.00 - 8.60 | B | 6 | | |
| Firm dark grey and brown mottled CLAY (Foreman records as peaty) (ALLUVIUM - CLAY) | 2.96 | | 8.60 | | | | | |
| | | | (0.40) | 8.60 - 9.00 | D | 7 | | |
| | 2.56 | | 9.00 | | | | | |
| | | | | 9.00 - 9.45 | D | 8 | S N=11 | 1,2/3,2,3,3 |
| CLAY (As sheet 2) (ALLUVIUM - CLAY) | | | (0.80) | 9.00 - 9.80 | B | 9 | | |
| | 1.76 | | 9.80 | | | | | |

Remarks
1. Aquifer protection installed at 11.65m.
2. Slotted standpipe installed on completion, see sheet 7.

Logged by TDW
Scale 1:50

Notes:
Materials are described in accordance with Appendices. For explanation of symbols and abbreviations see Fig. 1.

(c) Soil Mechanics (Ver 5.5) 16/12/97 15:35:55

Fig. 3

*Figure 3-20 Borehole log - 0.00 to 9.80m (after Soil Mechanics, 2003)*

Soil Mechanics

**BOREHOLE No. SA8830A**

Sheet 2 of 7

Equipment & Methods: As sheet 1

Location No. 8109

Location: CONTRACT 2 FOR PHASE 4 (1997) GROUND INVESTIGATIONS IN PROJECT AREA 200 (TROWBRIDGE)

Carried out for: Union Railways Limited

Ground Level: As sheet 1 | Coordinates: As sheet 1 | Date: As sheet 1

| Description | Reduced Level | Legend | Depth (Thick) | Samples/Tests: Depth | Sample Type | Sample No. | Test | Field Records |
|---|---|---|---|---|---|---|---|---|
| Firm grey CLAY with a little to some subrounded fine to coarse gravel of flint. (ALLUVIUM - CLAY) | | | | 10.00 - 10.45 | D | 10 | S N=12 | 3,4/5,3,2,2 |
| | | | (1.20) | 10.00 - 11.00 | B | 11 | | |
| | 0.56 | | 11.00 | | | | | |
| | | | | 11.00 - 11.45 | U | 12 | | 43 blows |
| Stiff bluish grey to silverish grey very silty CLAY with some greenish brown slightly silty to medium sand. (WOOLWICH AND READING BEDS - UPPER MOTTLED CLAY) | | | | 11.45 - 11.65 | D | 13 | | |
| | | | (2.00) | | | | | |
| | | | | 11.65 - 13.00 | B | 14 | | |
| | -1.44 | | 13.00 | | | | | |
| | | | | 13.00 - 13.45 | U | 15 | | 56 blows |
| Stiff brown, reddish brown and bluish grey mottled CLAY. (WOOLWICH AND READING BEDS - UPPER MOTTLED CLAY) | | | | 13.45 - 13.65 | D | 16 | | |
| | | | (1.20) | 13.65 - 14.10 | D | 17 | S N=21 | 3,4/4,5,6,6 |
| | | | | 13.65 - 14.20 | B | 18 | | |
| | -2.64 | | 14.20 | | | | | |
| Stiff grey thinly laminated very silty CLAY with occasional lenses and pockets (<50mm thick) of fine to medium sand. (WOOLWICH AND READING BEDS - LAMINATED BEDS) | | | | 14.50 - 14.95 | D | 19 | S N=16 | 2,4/3,4,5,4 |
| | | | (1.80) | | | | | |
| | | | | 15.00 - 16.00 | D | 20 | | |
| | -4.44 | | 16.00 | | | | | |
| | | | | 16.00 - 16.45 | U | 21 | | |
| | | | | 16.45 - 16.50 | D | 22 | | |
| | | | | 16.50 - 16.95 | D | 23 | S N=38 | 5,7/8,8,9,13 |
| | | | | 16.50 - 17.20 | D | 24 | | |
| Very stiff grey and brown, locally thinly laminated, CLAY with occasional pockets (<100mm across) of grey silt. Occasional fine to coarse gravel size shell fragments. (WOOLWICH AND READING BEDS - LOWER SHELLY CLAY) | | | | 17.20 - 17.65 | U | NR | | 91 blows |
| | | | | 17.70 - 18.15 | D | 25 | S N=48 | 9,10/11,12,12,13 |
| | | | (4.00) | 17.70 - 18.50 | D | 26 | | |
| 18.50-18.50m, grey and brown slightly clayey fine to medium SAND with some gravel size shell fragments | | | | 18.50 - 18.95 | U | 27 | | 73 blows |
| | | | | 18.95 - 19.00 | D | 28 | | |
| | | | | 19.00 - 19.30 | | | C 54 | 11,13/26,28 |
| 19.80-20.00m, grey LIMESTONE, strong | | | | 19.80 - 20.00 | D | 29 | | |
| | -8.44 | | 20.00 | | | | | |

Remarks

Logged by: TDW

Scale: 1:50

Notes:

Materials are described in accordance with Appendices. For explanation of symbols and abbreviations see Fig. 1. 16/12/97 14:45:27

(c) Soil Mechanics (Ver 5.5)

Fig. 3

*Figure 3-21 Borehole log - 10.00 to 20.00m (after Soil Mechanics, 2003)*

Soil Mechanics

BOREHOLE No. SA8830A

Sheet 3 of 7

Equipment & Methods: As sheet 1

Location No. 8109

Location: CONTRACT 2 FOR PHASE 4 (1997) GROUND INVESTIGATIONS IN PROJECT AREA 200 (TROWBRIDGE)

Carried out for: Union Railways Limited

Ground Level: As sheet 1

Coordinates: As sheet 1

Date: As sheet 1

| Description | Reduced Level | Legend | Depth (Thick) | Samples/Tests: Depth | Sample Type | Sample No. | Test | Field Records |
|---|---|---|---|---|---|---|---|---|
| | | | | 20.00 - 20.21 | | | C 50 | 25 for 70mm,/29.21 for 65mm |
| | | | | 20.00 - 21.00 | B | 30 | | |
| Green and brown slightly sandy CLAY with some rounded fine to coarse gravel of flint. (UPNOR FORMATION - CLAY) | | | (1.60) | | | | | |
| | | | | 21.00 - 21.20 | | | C 50 | 19,6 for 20mm/31,19 for 30mm |
| | -10.04 | | 21.60 | | | | | |
| Green, dark green and brown very silty CLAY occasional pockets (<50mm) of fine to ium sand. NOR FORMATION - CLAY) | | | (0.90) | 21.60 - 22.50 | D | 31 | | |
| | -10.94 | | 22.50 | 22.50 - 22.80 | D | 32 | S 50 | 11,13/20,26.4 for 0mm |
| | | | | 22.50 - 24.00 | D | 33 | | |
| | | | | 24.00 - 24.14 | | | C 50 | 25 for 70mm,/50 for 70mm |
| | | | | 24.00 - 25.50 | D | 34 | | |
| | | | | 25.50 - 25.95 | | | C N=47 | 9,10/11,11,13,12 |
| y dense grey silty fine to medium SAND. IANET SAND) | | | (18.50) | 25.50 - 27.00 | D | 35 | | |
| | | | | 27.00 - 27.45 | | | C N=46 | 7,9/10,10,13,13 |
| | | | | 27.00 - 28.50 | D | 36 | | |
| | | | | 27.00 - 28.50 | D | 36 | | |
| | | | | 28.50 - 28.95 | | | C N=74 | 10,12/14,15,19,26 |
| | | | | 28.50 - 30.00 | B | 37 | | |

Remarks

Logged by: TDW

Scale: 1:50

Notes: (c) Soil Mechanics (Ver 5.5)

Materials are described in accordance with Appendices. For explanation of symbols and abbreviations see Fig. 1. 16/12/97 14:45:43

Fig. 3

*Figure 3-22 Borehole log - 20.00 to 30.00m (after Soil Mechanics, 2003)*

**Soil Mechanics**

**BOREHOLE No.SA8830A**

Sheet 4 of 7

Equipment & Methods: As sheet 1

Location No. 8109

Location: CONTRACT 2 FOR PHASE 4 (1997) GROUND INVESTIGATIONS IN PROJECT AREA 200 (TROWBRIDGE)

Carried out for: Union Railways Limited

Ground Level: As sheet 1 | Coordinates: As sheet 1 | Date: As sheet 1

| Description | Reduced Level | Legend | Depth (Thick) | Samples/Tests: Depth | Sample Type | Sample No. | Test | Field Records |
|---|---|---|---|---|---|---|---|---|
| | | | | 30.00 - 30.20 | | | C 50 | 10,15 for 10mm/28,22 for 40mm |
| | | | | 30.00 - 31.50 | D | 38 | | |
| | | | | 31.50 - 31.95 | | | C N=50 | 9,10/11,11,13,15 |
| | | | | 31.50 - 33.00 | D | 39 | | |
| | | | | 33.00 - 33.30 | | | C 52 | 11,14/21,31 |
| | | | | 33.00 - 34.50 | D | 40 | | |
| | | | | 34.50 - 34.95 | | | C N=61 | 9,10/12,15,15,19 |
| SAND. (As sheet 3) (THANET SAND) | | | (18.50) | 34.50 - 36.00 | D | 41 | | |
| | | | | 36.00 - 36.35 | | | C 50 | 12,12/14,17,19 for 50mm |
| | | | | 36.00 - 37.50 | D | 42 | | |
| | | | | 37.50 - 37.70 | | | C 50 | 18,7 for 15mm/28,22 for 35mm |
| | | | | 37.50 - 39.00 | D | 43 | | |
| | | | | 39.00 - 39.30 | | | C 49 | 11,13/20,29 |
| | | | | 39.00 - 40.50 | D | 44 | | |

Remarks

Logged by: TDW

Scale: 1:50

Notes:

Materials are described in accordance with Appendices. For explanation of symbols and abbreviations see Fig. 1.

(c) Soil Mechanics (Ver 5.5) 16/12/97 14:46:00

Fig. 3

***Figure 3-23** Borehole log - 30.00 to 40.50m (after Soil Mechanics, 2003)*

**Soil Mechanics**

**BOREHOLE No. SA8830A**

Sheet 5 of 7

Equipment & Methods: As sheet 1

Location No. 8109

Location: CONTRACT 2 FOR PHASE 4 (1997) GROUND INVESTIGATIONS IN PROJECT AREA 200 (TROWBRIDGE)

Carried out for: Union Railways Limited

Ground Level: As sheet 1 | Coordinates: As sheet 1 | Date: As sheet 1

| Description | Reduced Level | Legend | Depth (Thick) | Samples/Tests: Depth | Sample Type | Sample No. | Test | Field Records |
|---|---|---|---|---|---|---|---|---|
| SAND. (As sheet 3) (THANET SAND) | | | (18.50) | 40.50 - 40.95 | | | C N=49 | 11,12/9,12,13,15 |
| | -29.44 | | 41.00 | | | | | |
| Black sandy angular fine to coarse GRAVEL of flint with many cobbles. (BULLHEAD BED - GRAVEL AND COBBLES) | | | (0.50) | 41.00 - 41.50 | B | 45 | | |
| 41.50-42.80m, recovered as gravel to cobble size fragments of chalk and flint. | -29.94 | | 41.50 | 41.50 - 42.00 | B | 46 | | |
| | | | | 42.00 - 42.45 | U | NR | | 120 blows |
| | | | | 42.00 - 43.00 | B | 47 | | |
| | | | | 43.00 - 43.45 | U | NR | C N=84 | 176 blows |
| | | | | 43.50 - 43.95 | | | | 12,13/15,19,21,29 |
| | | | | 43.00 - 44.00 | B | 48 | | |
| White CHALK. Recovered as a slurry with some angular to subangular gravel to cobble size fragments of flint. (UPPER CHALK) | | | (5.00 pen) | 44.00 - 44.45 | U | NR | | 186 blows |
| | | | | 44.50 - 44.62 | | | C 50 | 25 for 70mm,/50 for 50mm |
| | | | | 44.50 - 45.50 | B | 49 | | |
| | | | | 45.50 - 45.95 | U | NR | | 190 blows |
| | | | | 46.00 - 46.18 | | | C 50 | 17,8 for 20mm/36,14 for 10mm |
| | | | | 45.50 - 46.50 | B | 50 | | |
| BOREHOLE ENDS AT 46.50 m. | -34.94 | | 46.50 | | | | | |

Remarks

Logged by: TDW

Scale: 1:50

Notes: Materials are described in accordance with Appendices. For explanation of symbols and abbreviations see Fig. 1.

(c) Soil Mechanics (Ver 5.5) 16/12/97 15:36:08

Fig. 3

*Figure 3-24 Borehole log - 40.50 to 46.50m (after Soil Mechanics, 2003)*

***Figure 3-25*** *Block sample being trimmed*

***Figure 3-26*** *Sample cut to correct dimensions*

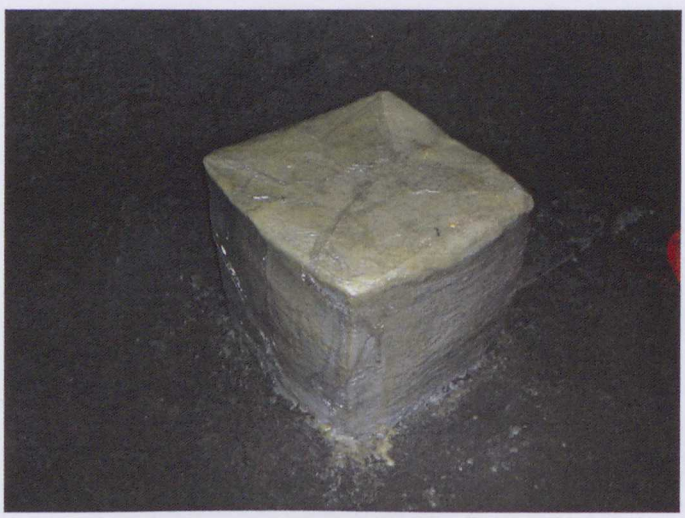

***Figure 3-27*** *Block sample wrapped in cling film & wax*

***Figure 3-28*** *Voids between sample and box filled with expansive foam*

***Figure 3-29*** *Top of box end sealed*

***Figure 3-30*** *Block samples left for foam to set*

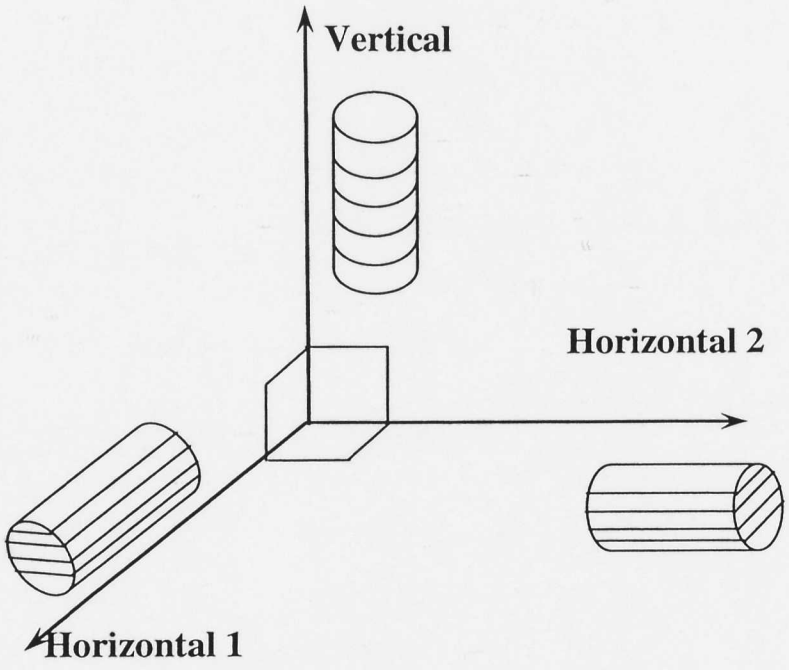


***Figure 3-31*** *Directions of samples extracted from sand blocks*

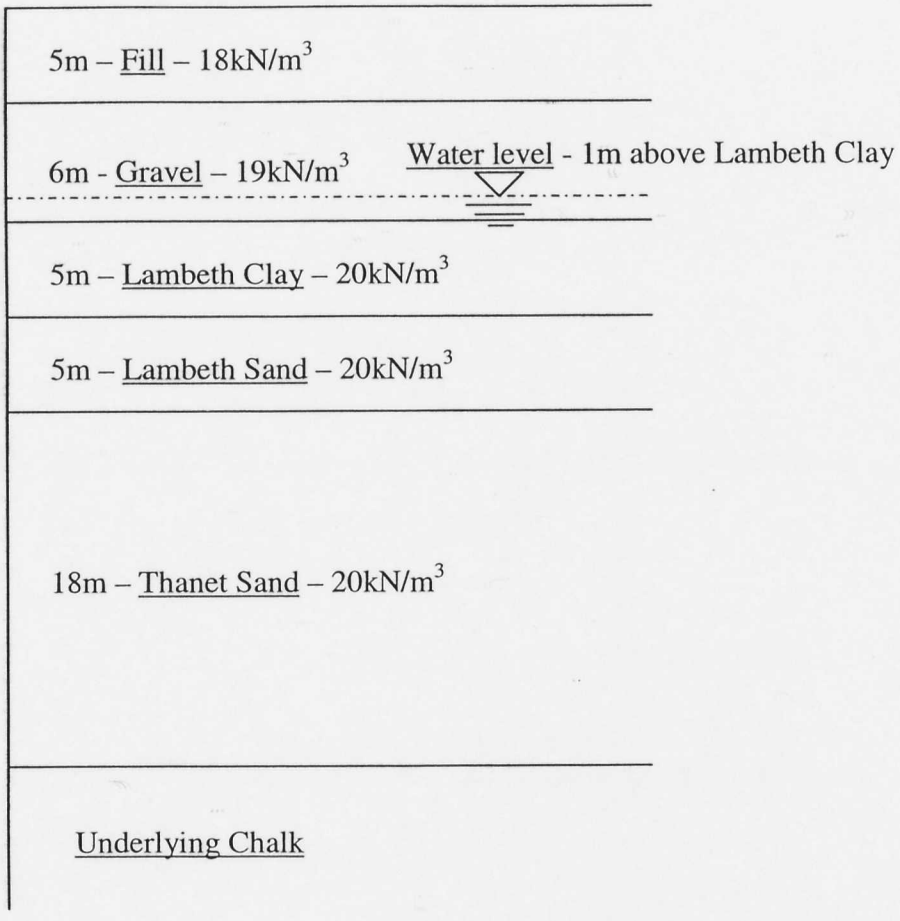


***Figure 3-32*** *Typical Thanet sand in-situ conditions*

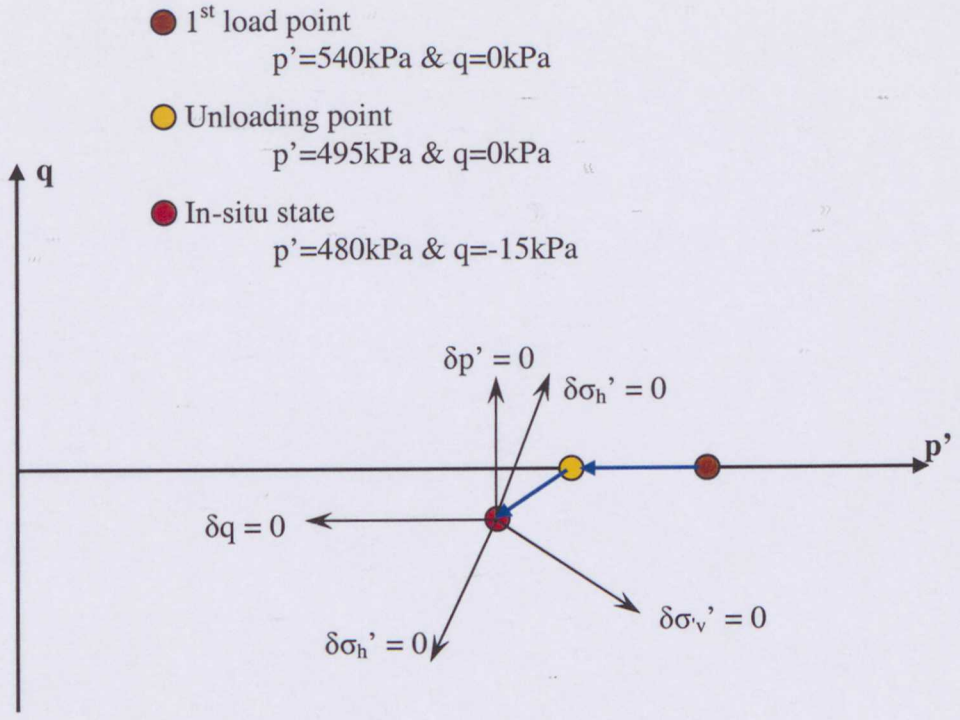


***Figure 3-33*** *Y1 and Y2 selected probe directions*

4 THANET SAND DESCRIPTION & EXPERIMENTS PERFORMED ..... 117

4.1 Thanet Sand Description & Existing Field Data ..... 117

4.2 Testing Programme And Description Of The Sand ..... 119

# 4 THANET SAND DESCRIPTION & EXPERIMENTS PERFORMED

## 4.1 Thanet Sand Description & Existing Field Data

Thanet sand is generally described as very dense, grey, silty, quartzitic, fine sand with sporadic aggregate sized rock particles. Typically, the Thanet sand is about 15m thick. It was deposited in a shallow sea environment adjacent to a low arid upland of Chalk. The sediment supply was very slow, especially at the beginning of the depositional process.

Interest in the characteristics of Thanet sand was initially scarce compared to the other strata in London, as it lies deep enough not to be reached by most foundation works. The poor understanding of the Thanet sand stratum became apparent when a series of pile tests at Canary Warf did not meet either the load displacement criterion or their ultimate end bearing capacity criterion, despite having been designed according to current codes. Nicholson et al. (2002) highlighted the unusual behaviour of Thanet sand at Canary Warf. Figure 4-1 shows the back-calculated end bearing capacity factors "$N_q$*" from pile load tests. "Nq*" is the ultimate pile base stress ($q_{b\ ult}$) that was extrapolated using a method proposed by Fleming (1992), normalised by the mean effective stress at the pile toe level for the ground levels and water pressures appropriate at the time of the test. The values for Thanet sand show a decrease of bearing capacity with depth.

A series of SPT tests was performed in an attempt to explain the anomalous pile bearing capacity behaviour within the Thanet sand layer. The results of the corrected SPT "N" values versus depth within the Thanet sand layer are presented in Figure 4-2. Typically, the deeper into a sand layer, the higher the resistance and hence the "N" value should be. Taking a trend in Figure 4-2, an approximately constant "N" value with depth is observed, with an expected amount of scatter.

This is highly atypical for a sand as, instead of an increase in resistance with depth, a rather constant behaviour is clearly observed.

From trial pile tests that have been performed at Canary Warf and more precisely at Heron Quays, the pile base capacity within the top 6m of the Thanet sand could measure as much as twice the pile base capacity within the bottom 9m of the stratum. This can be clearly seen in Figure 4-3 where the back calculated end bearing factors "Nq*" from the trial pile tests performed at Heron Quays are presented. These results suggested a diverse behaviour of Thanet sand, depending on the depth within the material. This idea was supported by pressuremeter and geophysical tests that were available.

In Figure 4-4 pressuremeter results from the Thanet sand are shown. It could be argued that for the first five to seven metres from the top of the sand, the pressuremeter gives high but constantly decreasing results. Below the seven metre threshold, a minimum value is reached and maintained with increasing depth.

Also in, Figure 4-5, Figure 4-6 and Figure 4-7 resistivity and conductivity results from different sites are respectively shown. These are inverse physical properties; when high resistivity is observed, low conductivity should be expected and vice-versa. In Figure 4-6 from the top of the Thanet sand layer until about seven metres down, the resistivity is high with an almost constant value versus depth. At about seven metres into the Thanet sand layer, the value of resistivity suffers a sudden drop and from then on it follows a constant value with depth. In Figure 4-7 the conductivity is low for the top seven metres of the Thanet sand. Again, a sudden change takes place and the value of conductivity, as expected, increases. In this case though, the value is not completely constant with depth, as a drop and a subsequent rise take place at a depth of about twelve metres into the Thanet sand.

In Figure 4-8 the uncorrected SPT blow-count ("N") and soil resistivity for Heron Quays have been combined in one plot. It can be clearly seen that the two testing methods clearly correlate as the drop of resistivity coincides with a reduced SPT blow-count. Additionally, conductivity data have been combined with a Gamma ray depth profile, as shown in Figure 4-9, and again show a good correlation

between the different testing techniques. Figure 4-10 shows conductivity data retrieved from different boreholes within the Heron Quays site at Canary Warf, showing good repeatability within the specific site.

The pile, pressuremeter and geophysical tests suggest that within Thanet sand, two distinct soil strata exist, as suggested by Nicholson et al. (2002). Based on experiments and measurements taken in the lab that are presented in the early parts of Section 5 it was established that these two strata not only are physically defined by the amount of silt contained within the sand, but this difference in silt dominates many of the behavioural characteristics of the soil. The upper part has a low silt content (5%-10%) whereas the lower sand layer has higher silt content (15%-30%). As was mentioned earlier, this sub-strata distinction was also hinted at by the on-site data that were available at the time, even though a clear relationship between the supposed silt content difference and material behavior had never been established. In Figure 4-11 the fines content and conductivity have been plotted with depth. Just as in the case of the SPT "N" value and resistivity, this cross-comparison shows a good agreement, within an expected amount of scatter.

## 4.2 *Testing Programme And Description Of The Sand*

Table 4-1 summarises all the experiments this Thesis is based on. The experiments have either been performed by the author within the Imperial College laboratory, or by various other people at Imperial College and City University whose data were then retrieved and re-analysed. All experiments not performed by the author have been highlighted in light orange and have been included on the first page of the table.

Soil samples from four different sites have been used; Millennium Tower and Moore House in the City, River Side on the Isle of Dogs and finally the CTRL tunnel at Stratford. A map with the locations of the different sites is presented in

Figure 4-12. A direct comparison between them is presented in an attempt to distinguish whether the sand from different sites had different behaviour.

Samples from both the upper and lower layers of the Thanet sand have also been tested. The results from samples with either low or high silt contents respectively are compared, in an attempt to explain the differences in engineering behaviour that the amount of silt introduces. The average void ratio for the high silt content Thanet sand was 0.754 whereas for the low silt content Thanet sand it was 0.656, as can be calculated from Table 4-1. In Figure 4-13 a series of particle size distribution curves, one from each sub-layer and for different sites are presented.

Triaxial tests on both intact as well as reconstituted Thanet sand samples have been performed. The difference in behaviour between intact and reconstituted samples quantifies the influence that structure has on the overall engineering behaviour of Thanet sand.

It must be noted that two distinct sources of intact samples were available; rotary cored samples from River Side, Moore House and Millennium Tower as well as block samples from the CTRL tunnel at Stratford. The rotary cored samples were taken using a triple barrelled cover and a polymer flush. A comparison between these samples allows the effect of sampling method also to be examined and in a sense to assess to what extent rotary coring and block sampling produce truly undisturbed samples.

More importantly though, having intact Thanet sand intact samples cut in different directions (refer to Figure 3-31) allows the anisotropy of the soil to be examined (see Section 5.6). In Figure 2-58, the possible variations of the intermediate stress factor "b" as well as the angle of major principal stress to the bedding plane "α" are shown.

The possibility of the Glauconite having an effect on the engineering behaviour of Thanet sand was also investigated. As glauconite can only be found in the coarser part (>63microns) of the high silt content Thanet sand, a sample of approximately 500g of the high silt content sand (lower stratum) was put through a magnetic

separation process at University College London. This allowed the glauconitic particles that have magnetic properties to be extracted from the rest of the material (Figure 4-14). Once the glauconite had been removed, the particle size distribution curve for sizes larger than 63microns was adjusted to compensate for the loss of the glauconitic material. This was done in an attempt to keep the ratio between the particles larger than as well as smaller than 63 microns constant. Once that process had been completed, two triaxial tests were performed using the Glauconite-free material (RS10 & RS11, see Table 4-1).

Intact samples of untested Thanet sand were impregnated with resin and in turn left for enough time to solidify, in order to allow thin sections to be taken. The pictures of Thanet sand vertically cut thin sections under plain transmitted light and cross-polarised light are presented in Figure 4-15 and Figure 4-16 respectively. They can be compared with Figure 2-29 and Figure 2-30 presented in Section 2 to show the relative particle arrangement and packing between the three corresponding sands presented in the Figures. Thanet sand neither appears to have a locked fabric nor any large traces of cement visible, as can be seen in Figure 4-15 and Figure 4-16. This is in agreement with the observation from Figure 2-28 that Thanet sand has relatively high void ratio for its age.

The raw data from the experiments that was used and analysed for this thesis have been presented at the end of this chapter. From Figure 4-17 to Figure 4-29 the isotropic compression data are presented for all the available tests. Figure 4-30 to Figure 4-51 show the stress ratio versus external axial strain plots coupled with volumetric strain versus external axial strain plots for all the drained compression tests. On Figure 4-52 and Figure 4-53, the stress ratio versus external axial strain plot has been coupled with pore pressure versus external axial strain plot for the undrained experiments sheared in compression. The remaining two plots, Figure 4-54 and Figure 4-55, contain the raw data for the two tests performed in extension.

As discussed in Section 3.5.4, in order to assess the elastic parameters of Thanet sand, a 100mm diameter intact sample was tested. On this sample, a series of Y1

and Y2 probes was performed that allowed the Y1 and Y2 loci to be derived, as discussed in further detail in Section 6.5.

Finally, for an easier understanding of the data gathered from the triaxial tests, the analyses and discussions have been grouped into two main categories; the large strain behaviour and the small strain behaviour (Chapter 5 and Chapter 6 respectively).

| *Test Name & Number* | *Test Name* | *Test Date* | *Sample Depth (m)* | *Silt Content* | *v @ beginning of test* | *Sample Direction* | *Sample State* | *Test Type* | *Sample Diameter* |
|---|---|---|---|---|---|---|---|---|---|
| Millennium Tower - mtu | mtu | | 62.9-63.25 | Low | 1.633 | Vertical | Intact-Cored | DC @ 12MPa | 50mm |
| Millennium Tower - mtv | mtv | | 62.9-63.25 | Low | 1.634 | Vertical | Intact-Cored | DC @ 6MPa | 50mm |
| Millennium Tower - mtw | mtw | | 58.46-58.78 | Low | 1.606 | Vertical | Intact-Cored | DC @ 20MPa | 50mm |
| Millennium Tower - mty | mty | | 64.3-64.7 | Low | 1.700 | Vertical | Intact-Cored | DC @ 3MPa | 50mm |
| Moore House – mh1 | MH1 | 02/05/2001 | 63.9-64.4 | High | 1.749 | Vertical | Intact-Cored | DC @ 1.8MPa | 50mm |
| Moore House – mh2 | MH2 | 01/06/2001 | 62.85-63.25 | High | 1.734 | Vertical | Intact-Cored | DC @ 2MPa | 50 mm |
| Moore House – mh3 | MH3 | 02/07/2001 | 62.85-63.25 | High | 1.740 | Vertical | Intact-Cored | DC @ 4.4MPa | 50mm |
| Moore House – mh5 | MH5 | 06/08/2001 | 63.9-64.4 | High | 1.763 | Vertical | Intact-Cored | DC @ 4.5MPa | 50mm |
| Moor House - #1 | MH6 | 14/06/2002 | 62.85-64.24 | High | 1.747 | Vertical | Intact-Cored | DC @ 0.55MPa | 38mm |
| Moor House - #2 | MH7 | 14/07/2002 | 62.85-64.24 | High | 2.023 | | Reconstituted | DC @ 0.55MPa | 38mm |
| Moor House - #7 | MH8 | 13/03/2003 | 62.85-64.24 | High | 1.729 | Vertical | Intact-Cored | DC @ 0.55MPa | 38mm |
| River Side - #3 | RS1 | 14/10/2002 | 26.4 | Low | 1.714 | Vertical | Intact-Cored | DC @ 4MPa | 50mm |
| River Side - #4 | RS2 | 05/11/2002 | 26.4 | Low | 1.704 | | Reconstituted | DC @ 4MPa | 50mm |
| River Side - #5 | RS3 | 03/02/2003 | 34.60-35.20 | High | 1.968 | | Reconstituted | DC @ 0.55MPa | 38mm |
| River Side - #6 | RS4 | 27/02/2003 | 34.60-35-20 | High | 1.965 | | Reconstituted | UDC @ 0.5MPa | 38mm |
| River Side - #8 | RS5 | 19/03/2003 | 33.59-34.40 | High | 1.681 | Vertical | Intact-Cored | DC @ 4MPa | 50mm |
| River Side - TS2 - #9 | RS6 | | 33.59 - 34.40 | High | 1.712 | | Reconstituted | DC @ 0.5MPa | 38mm |
| River Side - TS3 - #10 | RS7 | 05/11/2002 | 25.90 - 26.40 | Low | 1.760 | Vertical | Intact-Cored | DC @ 0.5MPa | 38mm |
| River Side - TS4 - #11 | RS8 | | 25.90 - 26.40 | Low | 1.659 | | Reconstituted | DC @ 0.5MPa | 38mm |

| *Test Name & Number* | *Test Name* | *Test Date* | *Sample Depth (m)* | *Silt Content* | *v @ beginning of test* | *Sample Direction* | *Sample State* | *Test Type* | *Sample Diameter* |
|---|---|---|---|---|---|---|---|---|---|
| River Side - #12 | RS9 | 25/08/2003 | 33.59 - 34.40 | High | 1.831 | | Reconstituted | DC @ 4MPa | 50mm |
| River Side - NO GLAUCONITE - #13 | RS10 | 10/11/2003 | 33.59 - 34.40 | High | 1.747 | | Reconstituted | DC @ 4MPa | 50mm |
| River Side - NO GLAUCONITE - #14 | RS11 | 30/01/2004 | 33.59 - 34.40 | High | 1.836 | | Reconstituted | DC @ 2MPa | 50mm |
| River Side - #15 | RS12 | 15/03/2004 | 25.60-26.50 | Low | 1.773 | | Reconstituted | DC @ 3MPa | 50mm |
| River Side - #16 | RS13 | 02/04/2004 | 33.59 - 34.40 | High | 1.861 | | Reconstituted | DC @ 2MPa | 50mm |
| River Side - #17 | RS14 | 02/04/2004 | 25.60 - 26.50 | Low | 1.756 | | Reconstituted | DC @ 1MPa | 38mm |
| River Side - #18 | RS15 | 11/05/2004 | 25.60 - 26.50 | Low | 1.763 | | Reconstituted | DC @ 2MPa | 50mm |
| River Side - #19 | RS16 | 11/05/2004 | 34.60-35-20 | High | 1.907 | | Reconstituted | DC @ 1MPa | 38mm |
| River Side - #22 | RS17 | 20/06/2004 | 25.60 - 26.50 | Low | 1.761 | | Reconstituted | DC @ 0.55MPa | 38mm |
| River Side - #30 | RS18 | 24/08/2004 | 25.60 - 26.50 | Low | 1.808 | | Reconstituted | DC @ 0.25MPa | 38mm |
| River Side - #31 | RS19 | 02/09/2004 | 25.60 - 26.50 | Low | 1.802 | | Reconstituted | DC @ 0.125MPa | 38mm |
| CTRL Stratford - #20 | CTRL1 | 11/06/2004 | approx 39 | High | 1.877 | | Reconstituted | DC @ 4MPa | 50mm |
| CTRL Stratford - #21 | CTRL2 | 04/06/2004 | approx 39 | High | 1.906 | | Reconstituted | DC @ 1MPa | 38mm |
| CTRL Stratford - #23 | CTRL3 | 07/07/2004 | approx 39 | High | 1.859 | | Reconstituted | DC @ 0.55MPa | 38mm |
| CTRL Stratford - #24 | CTRL4 | 16/07/2004 | approx 39 | High | 1.807 | Vertical | Intact-Block | DC @ 0.55MPa | 38mm |
| CTRL Stratford - #25 | CTRL5 | 01/08/2004 | approx 39 | High | 1.787 | Horizontal 1 | Intact-Block | DC @ 0.55MPa | 38mm |
| CTRL Stratford - #26 | CTRL6 | 14/08/2004 | approx 39 | High | 1.800 | Horizontal 2 | Intact-Block | DC @ 0.55MPa | 38mm |
| CTRL Stratford - #27 | CTRL7 | 24/08/2004 | approx 39 | High | 1.937 | | Reconstituted | DC @ 0.55MPa | 38mm |

| *Test Name & Number* | *Test Name* | *Test Date* | *Sample Depth (m)* | *Silt Content* | *v @ beginning of test* | *Sample Direction* | *Sample State* | *Test Type* | *Sample Diameter* |
|---|---|---|---|---|---|---|---|---|---|
| CTRL Stratford - #28 | CTRL8 | 15/08/2004 | approx 39 | High | 1.935 | | Reconstituted | DC @ 0.25MPa | 38mm |
| CTRL Stratford - #29 | CTRL9 | 21/08/2004 | approx 39 | High | 1.940 | | Reconstituted | DC @ 0.125MPa | 38mm |
| CTRL Stratford - #32 | CTRL10 | 17/09/2004 | approx 39 | High | 1.829 | Vertical | Intact-Block | DEX @ 1MPa | 38mm |
| CTRL Stratford - #33 | CTRL11 | 25/09/2004 | approx 39 | High | 1.794 | Horizontal 2 | Intact-Block | DEX @ 1MPa | 38mm |
| CTRL Stratford - #34 | CTRL12 | 05/10/2004 | approx 39 | High | 1.789 | Vertical | Intact-Block | UDC @ 0.4MPa | 38mm |
| CTRL Stratford - #35 | CTRL13 | 12/10/2004 | approx 39 | High | 1.985 | | Reconstituted | UDC @ 0.4MPa | 38mm |
| CTRL Stratford - #36 | CTRL14 | 19/10/2004 | approx 39 | High | 1.758 | Horizontal 1 | Intact-Block | UDC @ 0.4MPa | 38mm |
| CTRL Stratford - #37 | CTRL15 | 29/10/2004 | approx 39 | High | 1.780 | Horizontal 2 | Intact-Block | UDC @ 0.4MPa | 38mm |
| CTRL Stratford - #38 | CTRL16 | 14/10/2004 | approx 39 | High | 1.939 | | Reconstituted | DC @ 3MPa | 50mm |
| CTRL Stratford - #39 | CTRL17 | 30/10/2004 | approx 39 | High | 1.744 | Vertical | Intact-Block | DC @ 3MPa | 50mm |
| CTRL Stratford - #40 | CTRL18 | 23/11/2004 | approx 39 | High | 1.750 | Vertical | Intact-Block | DC @ 3MPa | 50mm |
| CTRL Stratford - #41 | CTRL19 | 28/01/2005 | approx 39 | High | 0.832 | Vertical | Intact-Block | Y1/Y2 probes | 100mm |

***Table 4-1*** *Summary table of experiments*

**DC**: Drained shearing in Compression
**UDC**: Undrained shearing in Compression
**DEX**: Drained shearing in Extension

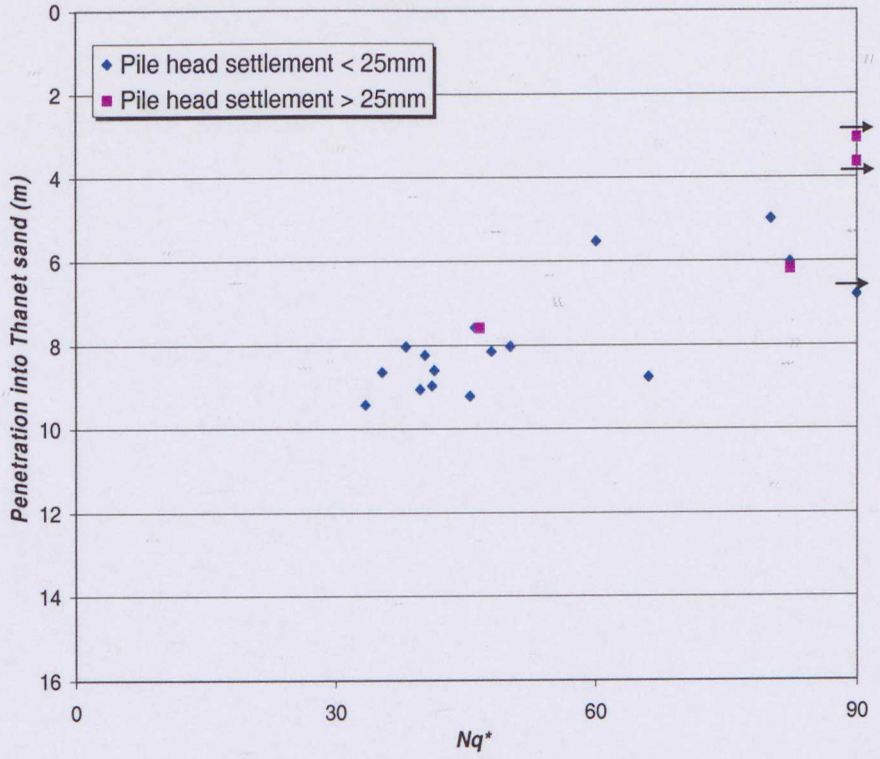


***Figure 4-1*** *Back analysed Nq* against pile base penetration into Thanet sand (after Nicholson et al., 2002)*

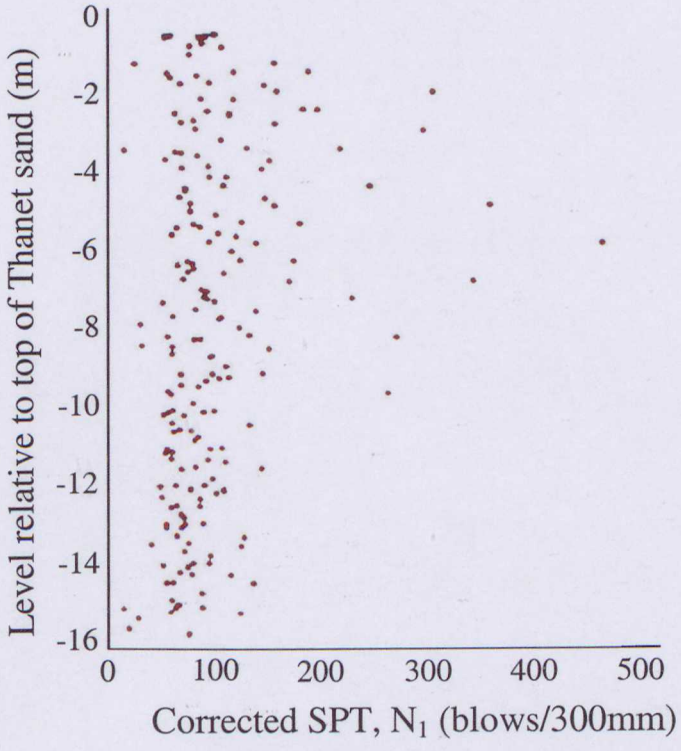


***Figure 4-2*** *Corrected SPT "N" values (after Nicholson et al., 2002)*

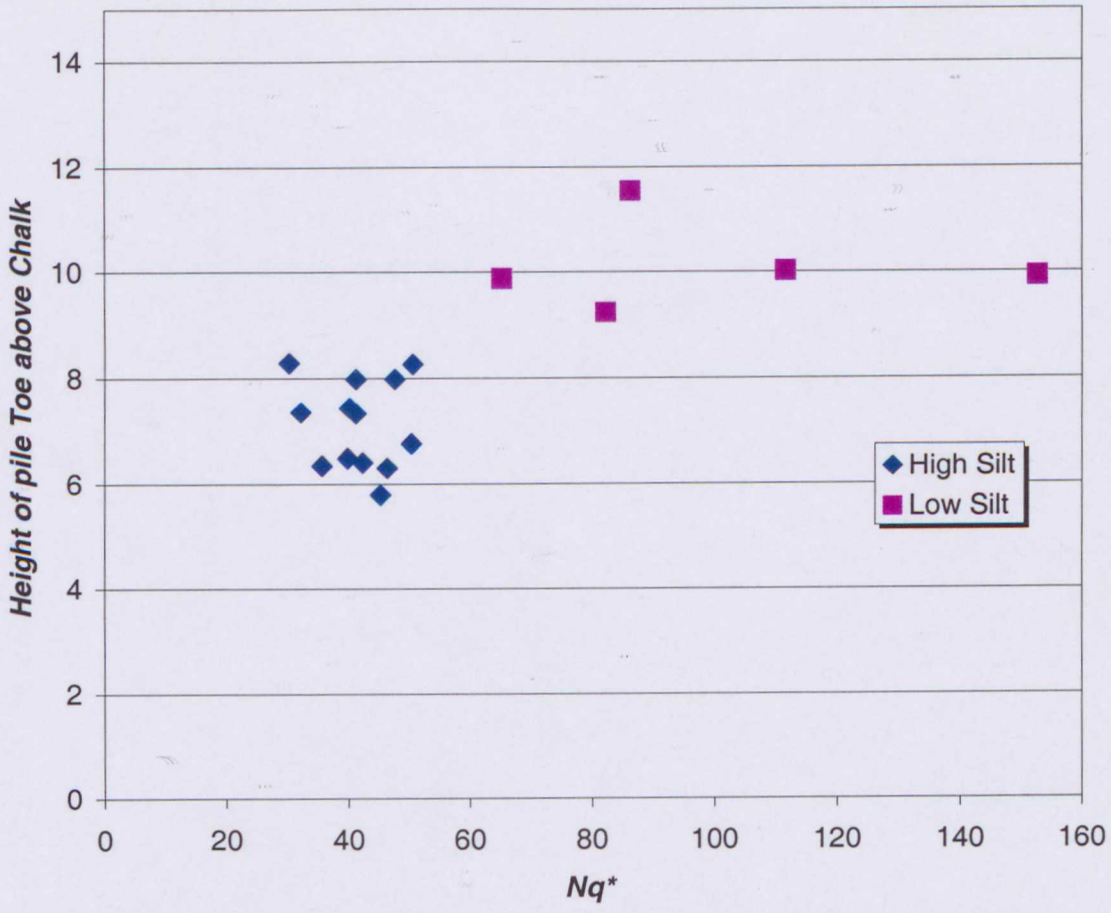


***Figure 4-3*** *Calculated Nq* versus height above Chalk at Heron Quays (after ARUP Geotechnics)*

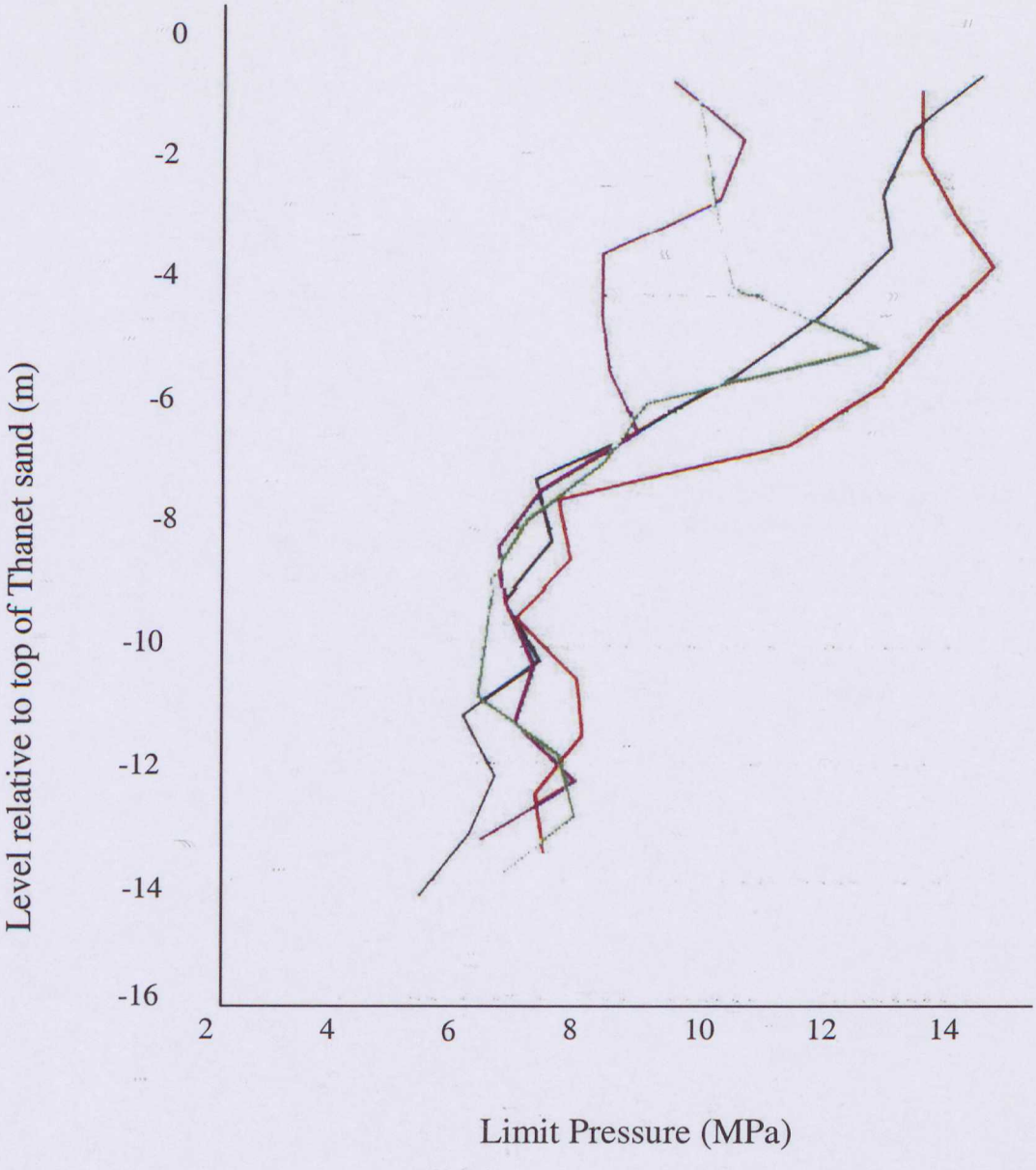


***Figure 4-4*** *Pressuremeter results for Thanet sand (after Nicholson et al., 2002)*

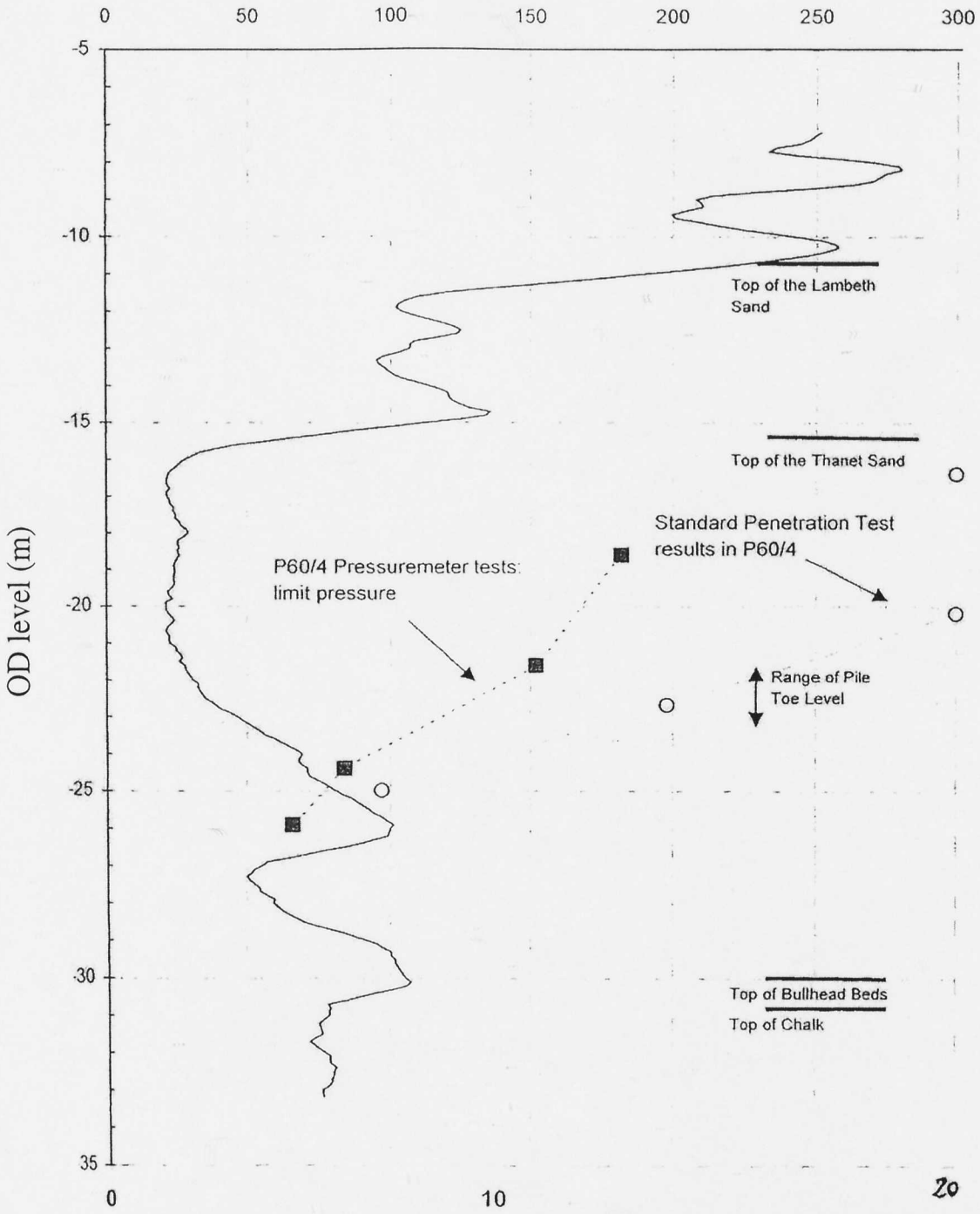


***Figure 4-5*** *Conductivity versus depth from top of Thanet sand at Heron Quays (after ARUP Geotechnics)*

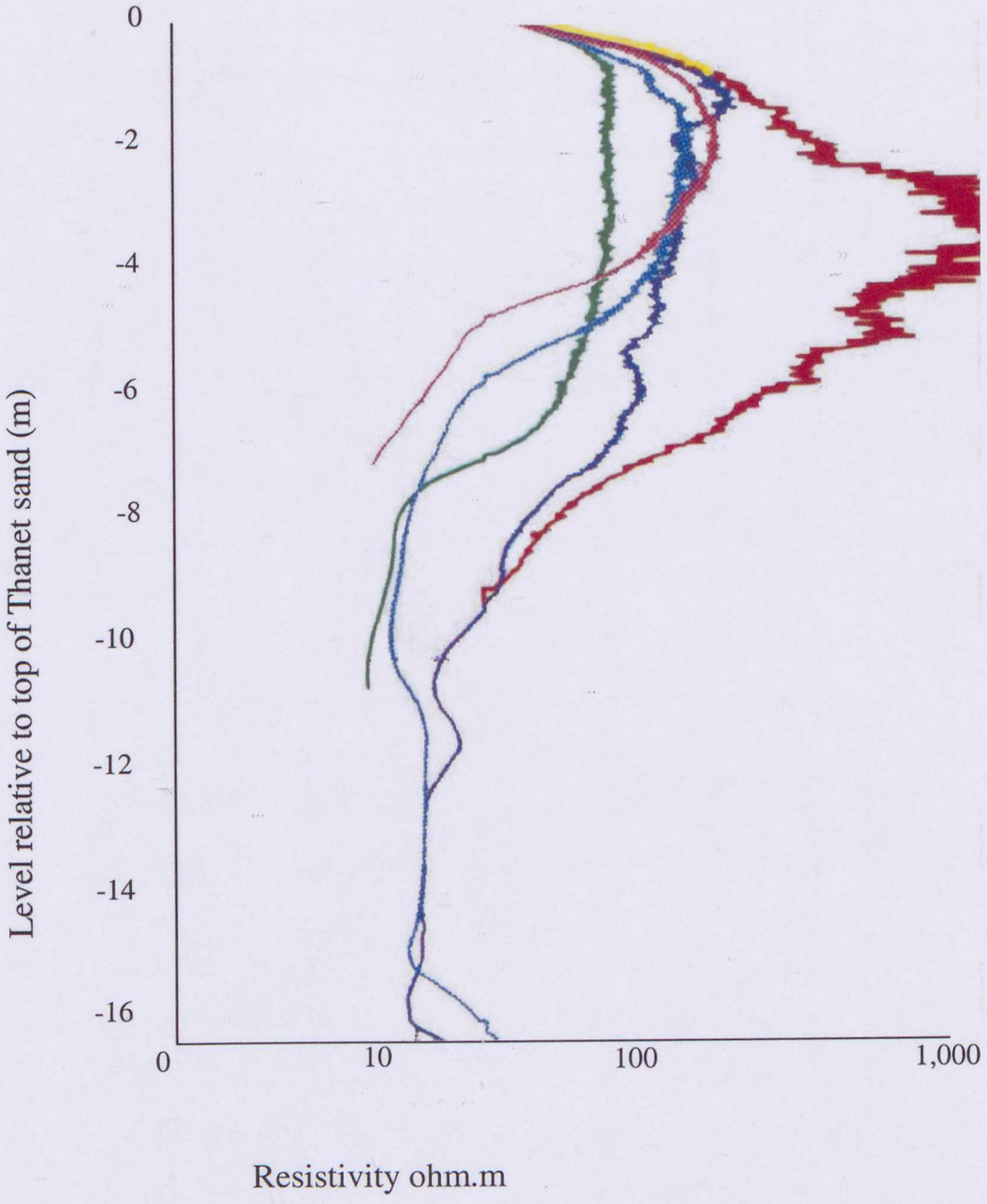


***Figure 4-6*** *Resistivity versus depth at North Quay (after after Nicholson et al., 2002)*

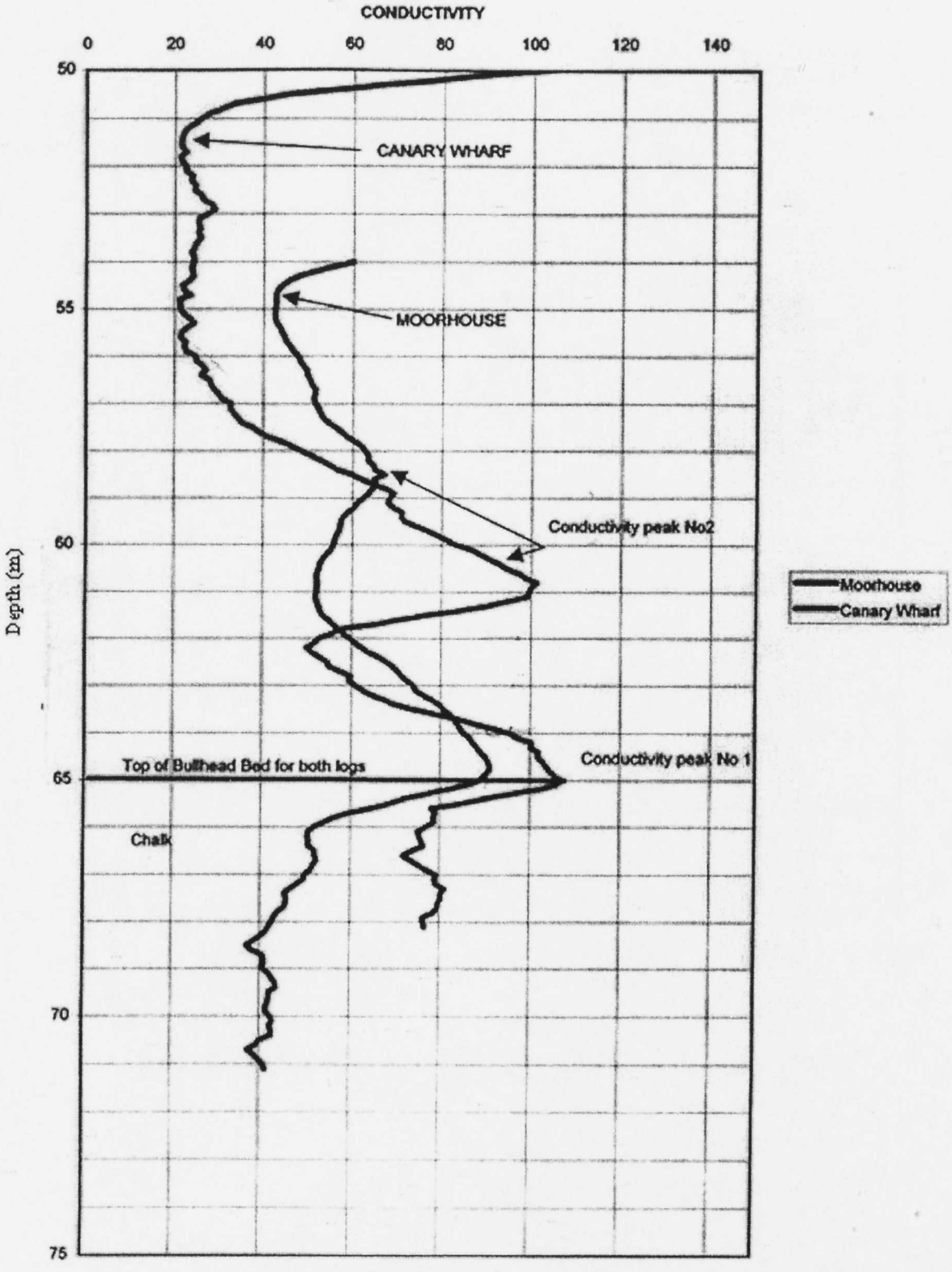


***Figure 4-7*** *Conductivity data for Thanet sand (after Pascal, 2002 – personal communication)*

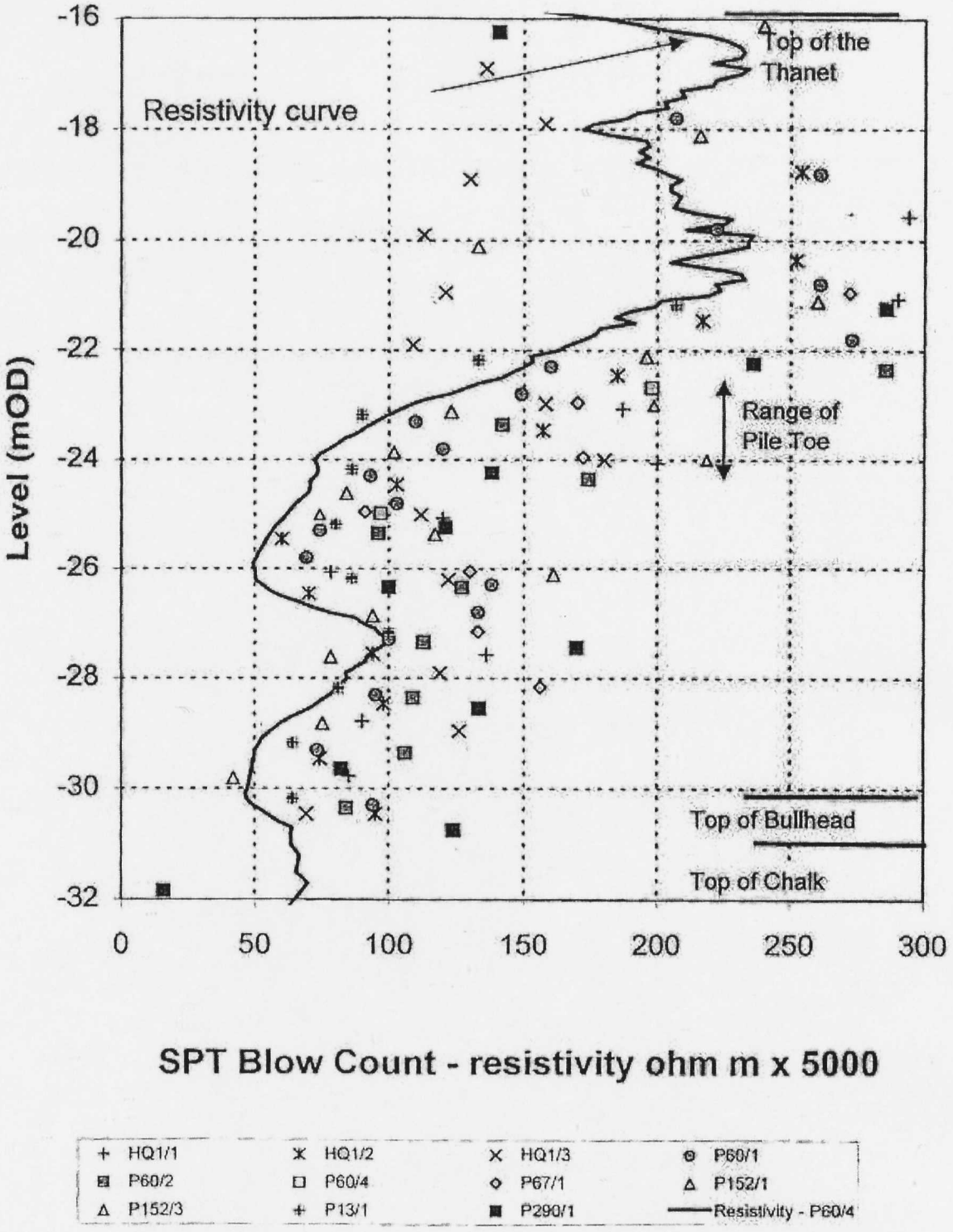


*Figure 4-8 Comparison of resistivity and SPT N at Heron Quays (after ARUP Geotechnics)*

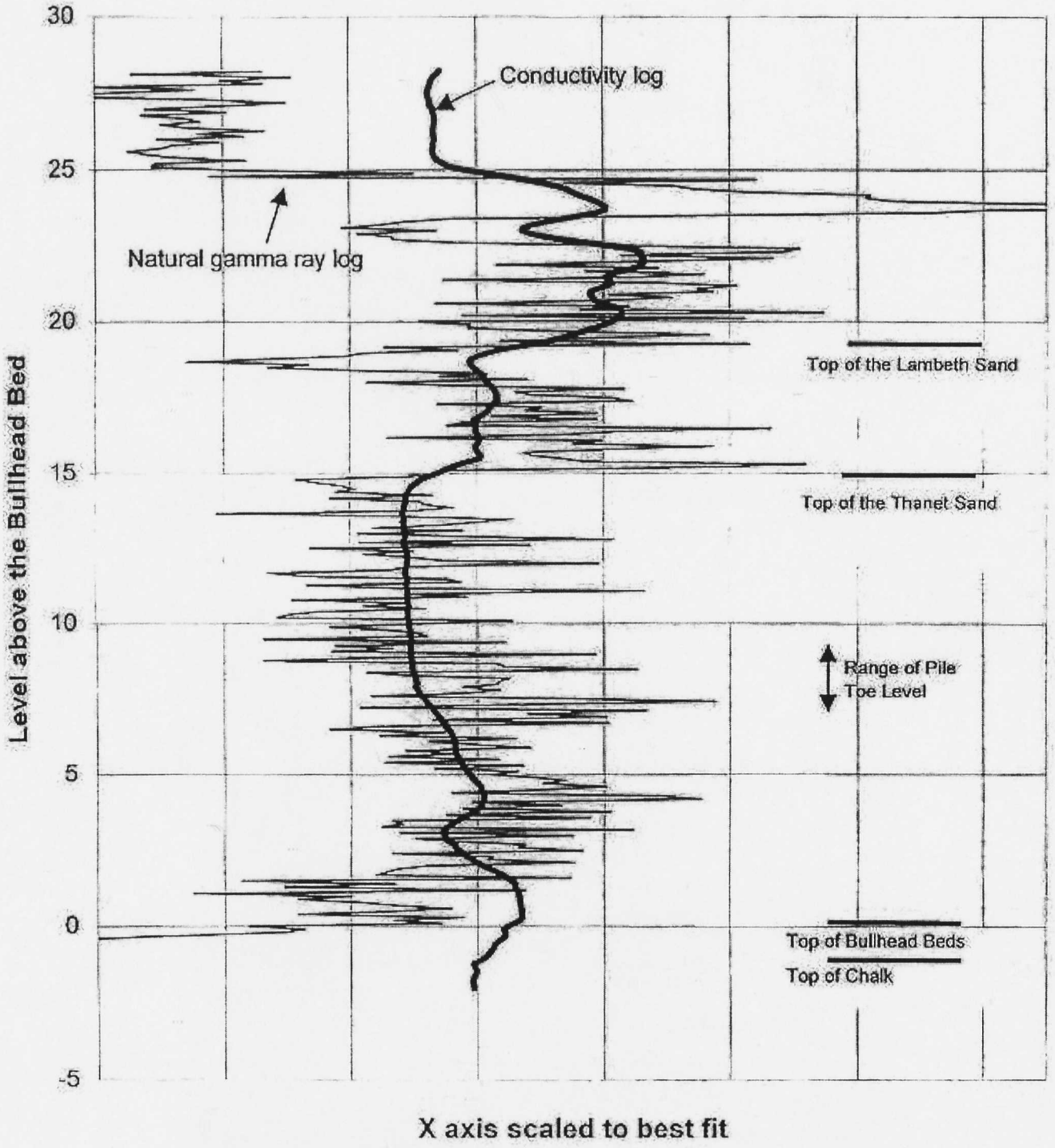


*Figure 4-9* *Comparison of Gamma ray and conductivity logs at Heron Quays (after ARUP Geotechnics)*

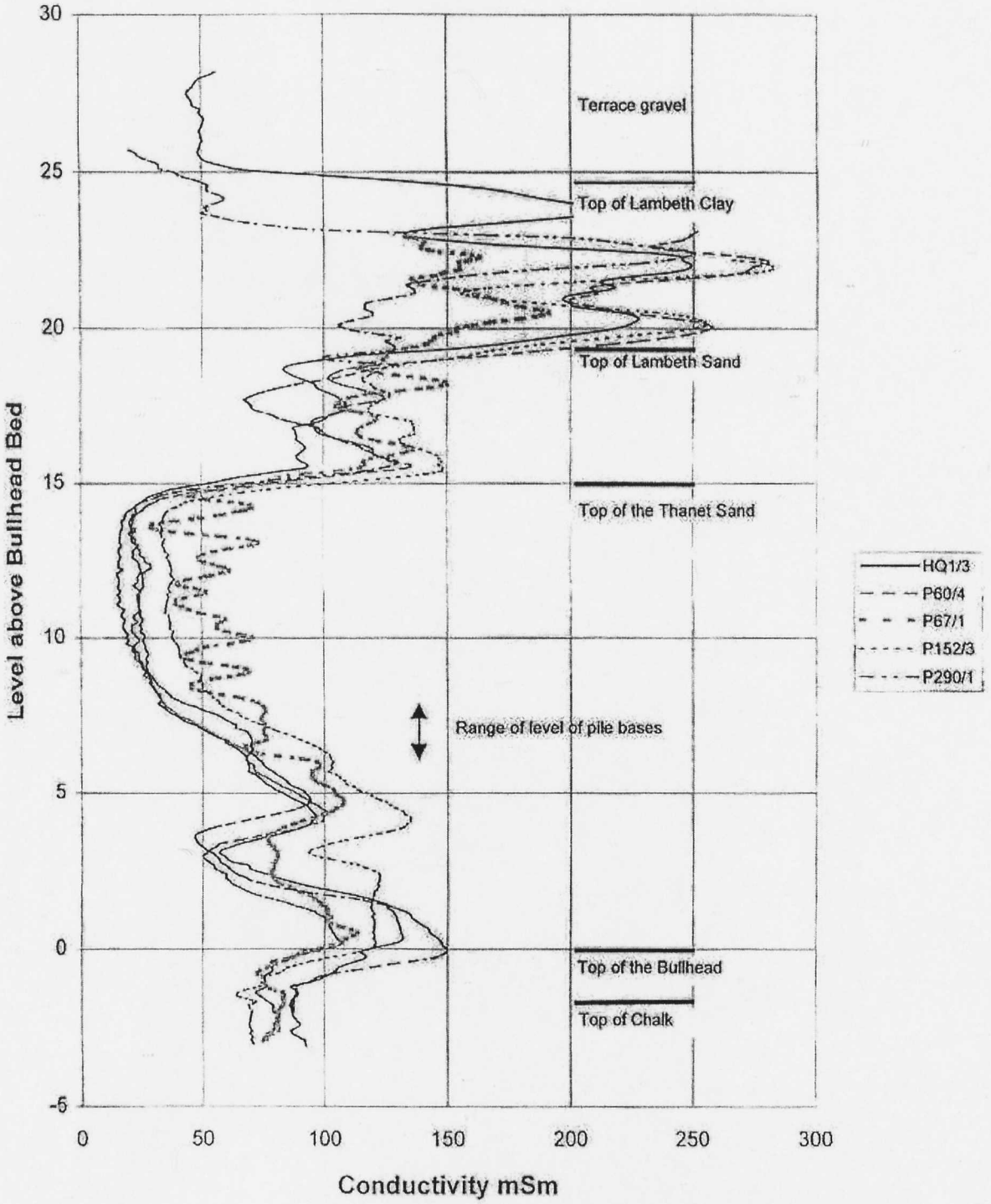


***Figure 4-10*** *Wireline conductivity measurements at Heron Quays. (after ARUP Geotechnics)*

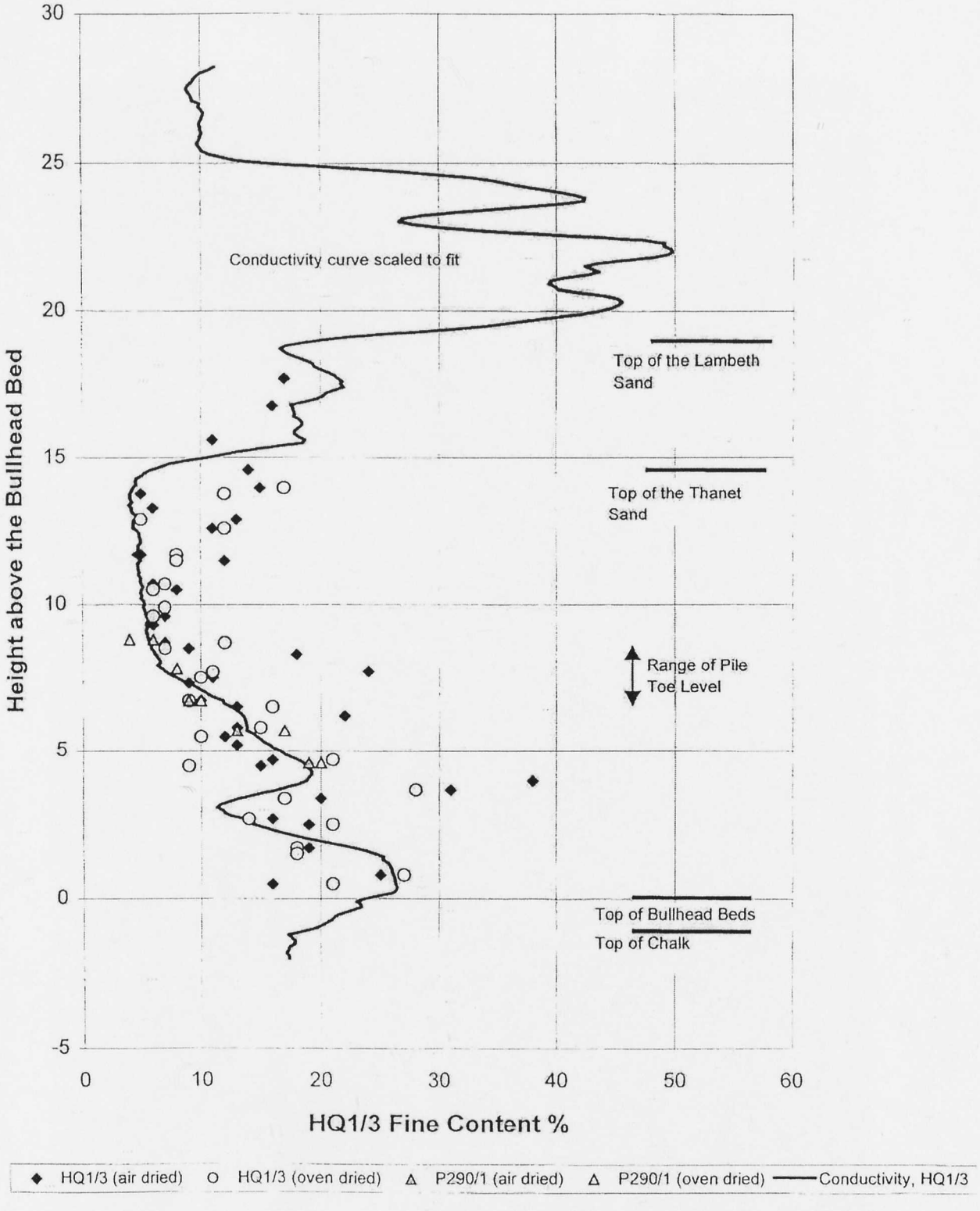


*Figure 4-11 Comparison of fines content with conductivity at Heron Quays (after ARUP Geotechnics)*

***Figure 4-12*** *Map of the four sites within London*

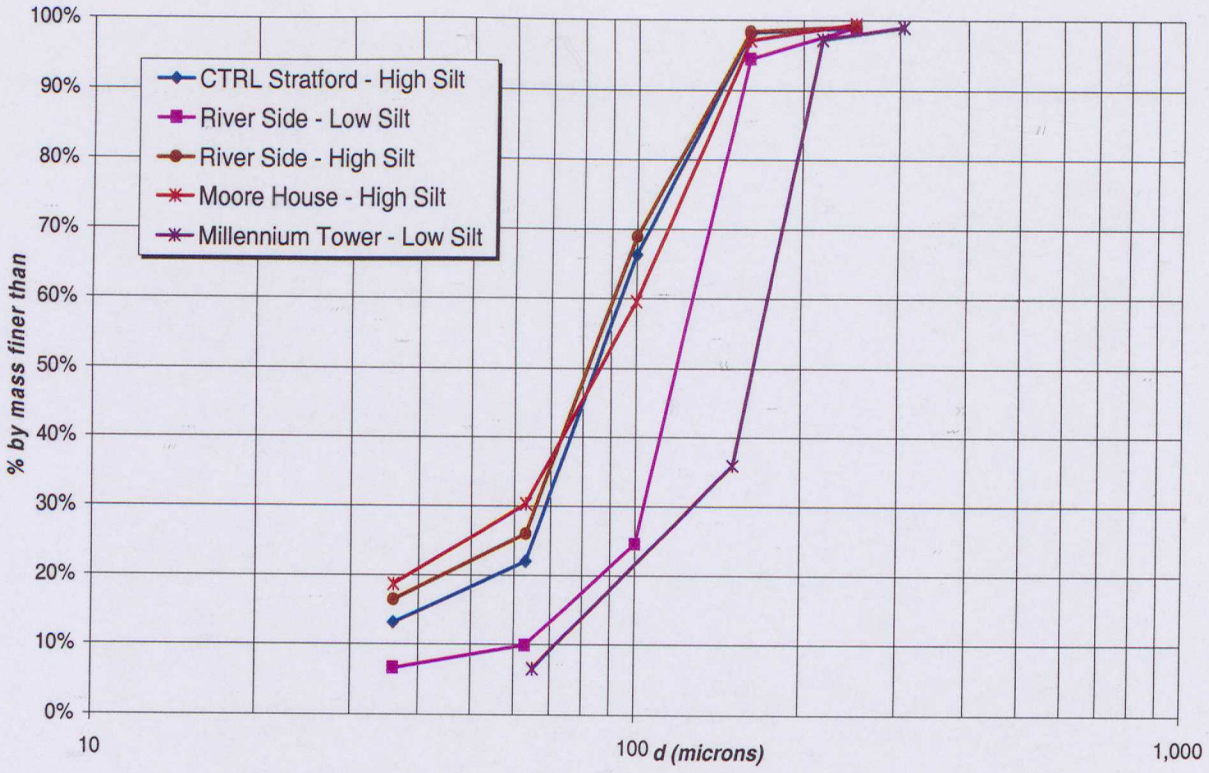


***Figure 4-13*** *Particle size distribution curves for all available sites*

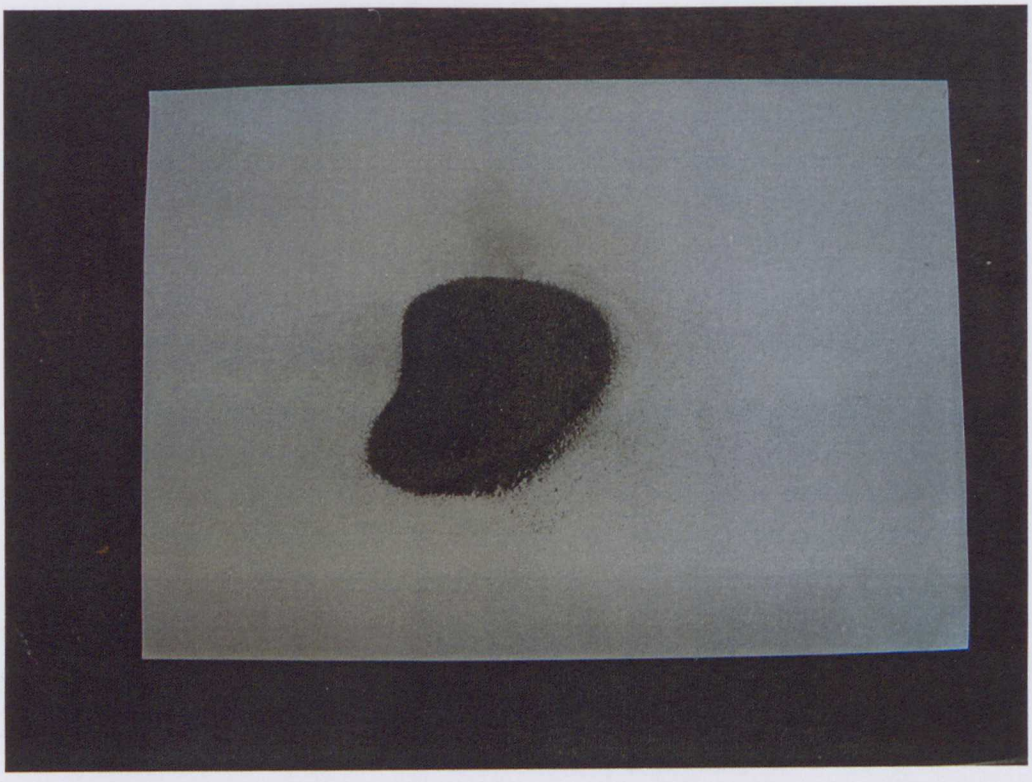

***Figure 4-14*** *Glauconite extracted from high silt content Thanet sand*

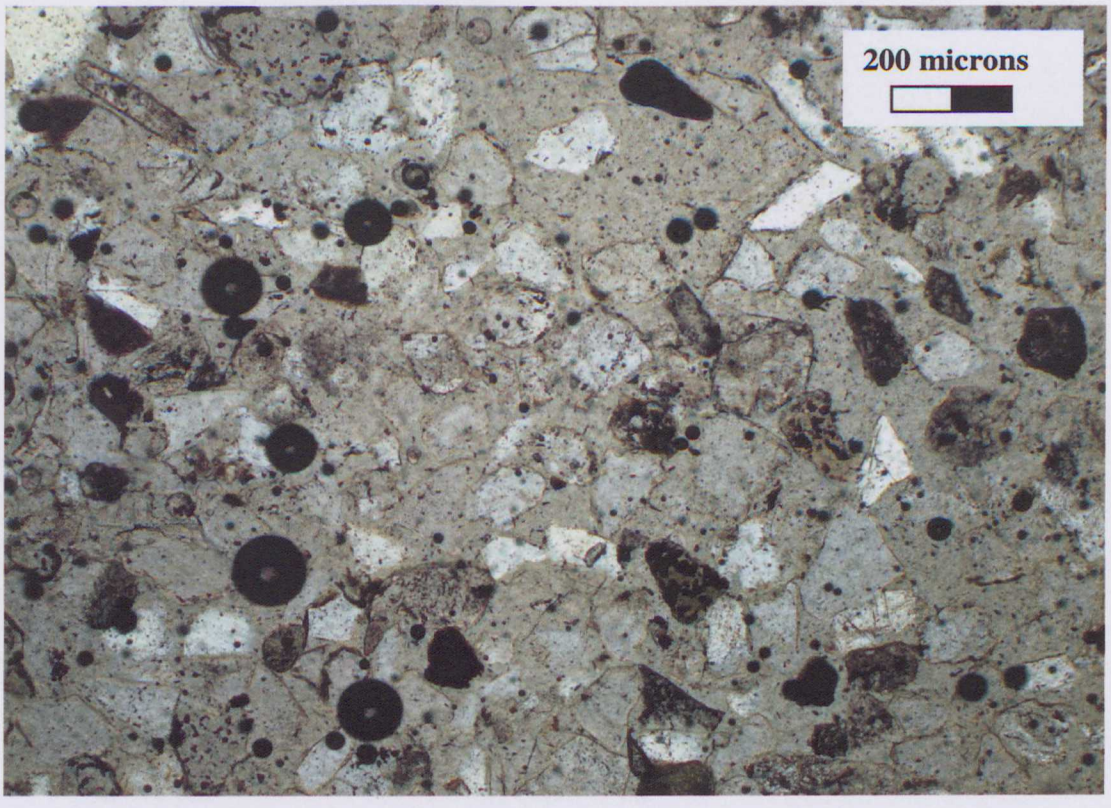


***Figure 4-15*** *Thin section of intact Thanet sand under plain transmitted light*

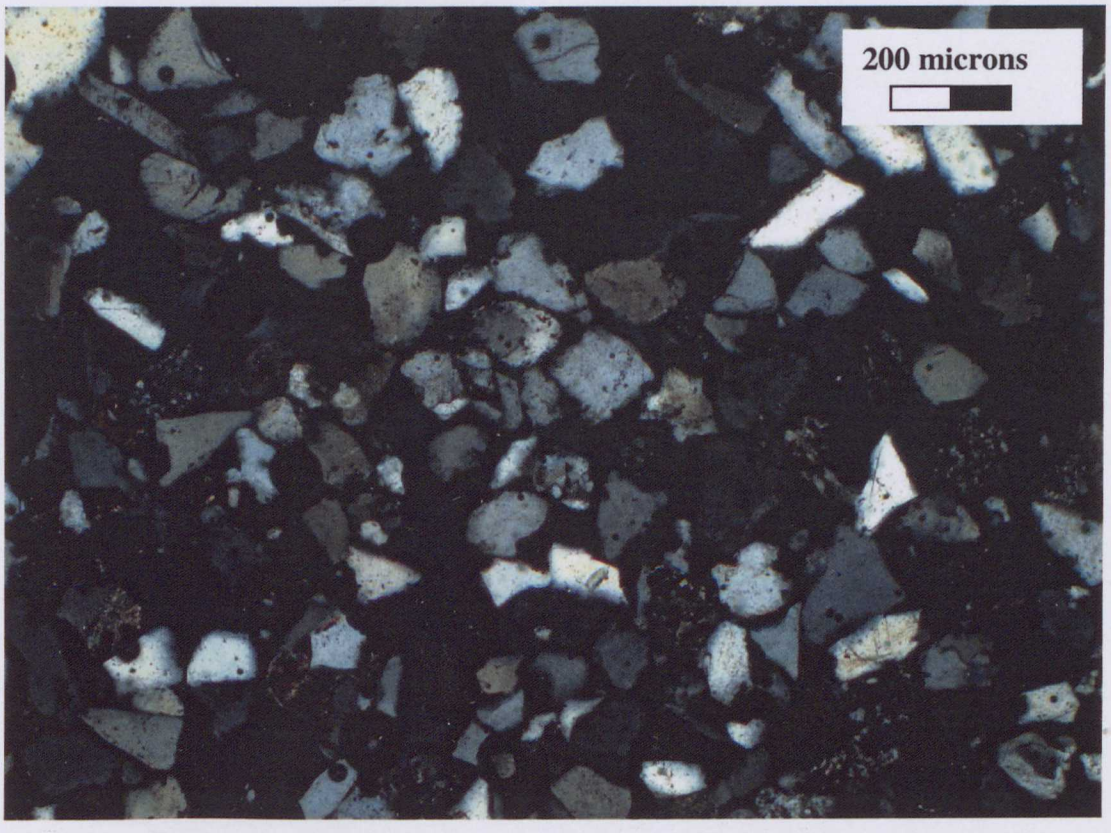


***Figure 4-16*** *Thin section of intact Thanet sand under cross-polarised light*

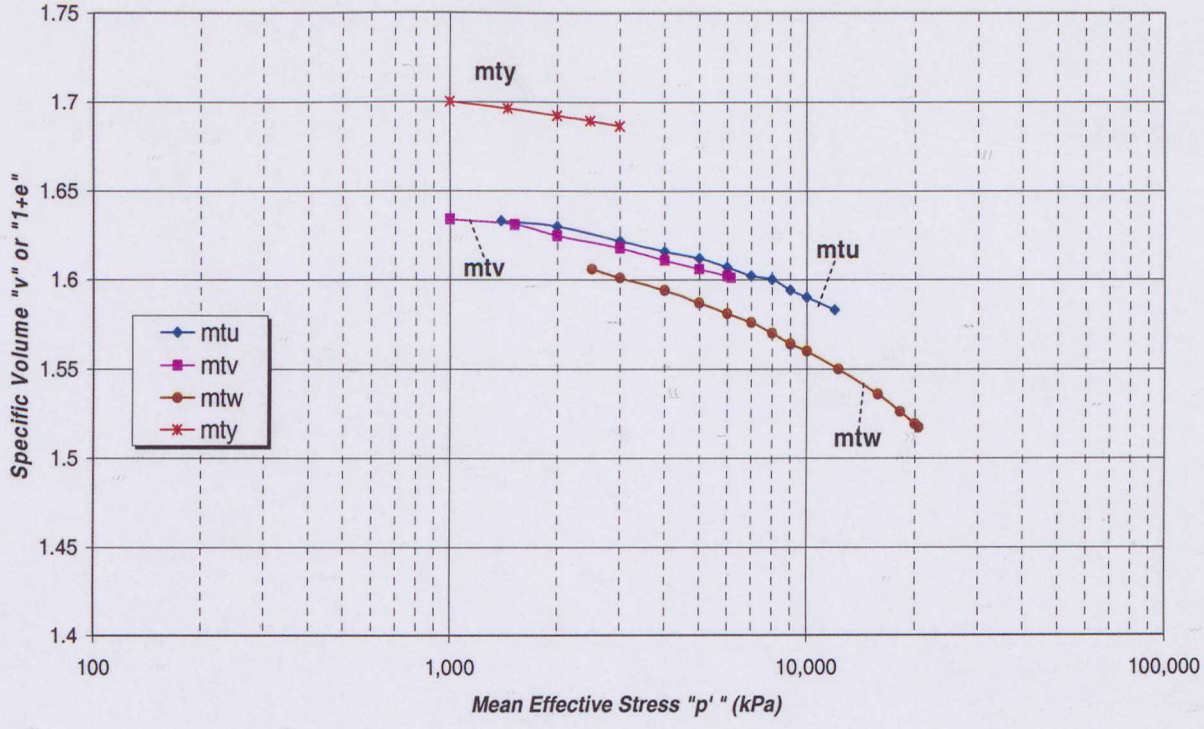


***Figure 4-17*** *Isotropic Compression data for Millennium Tower*

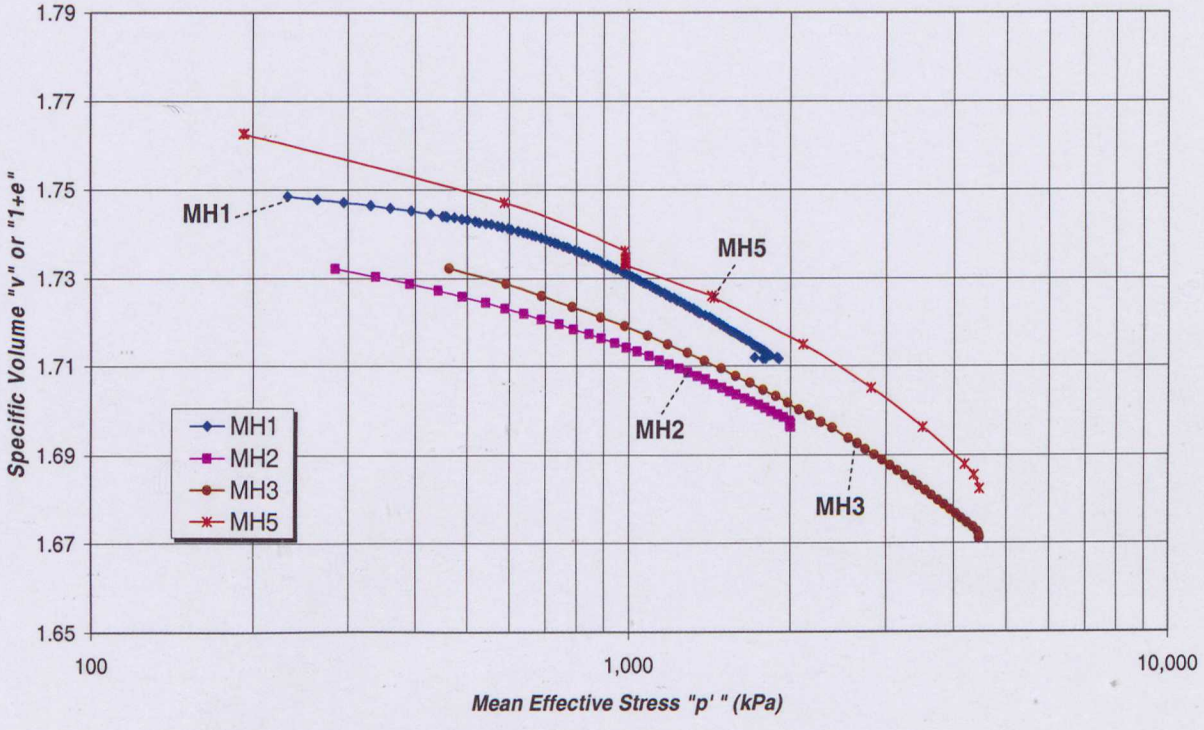


***Figure 4-18*** *Isotropic Compression data for Moore House*

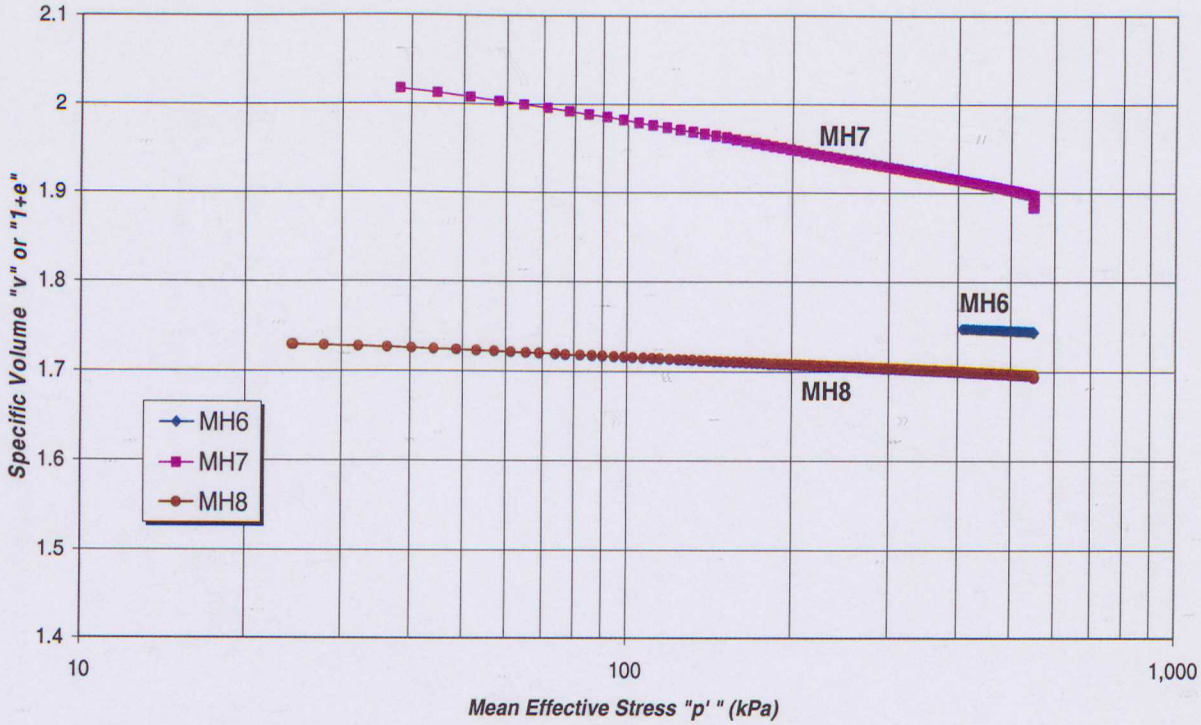


***Figure 4-19*** *Isotropic Compression data for Moore House*

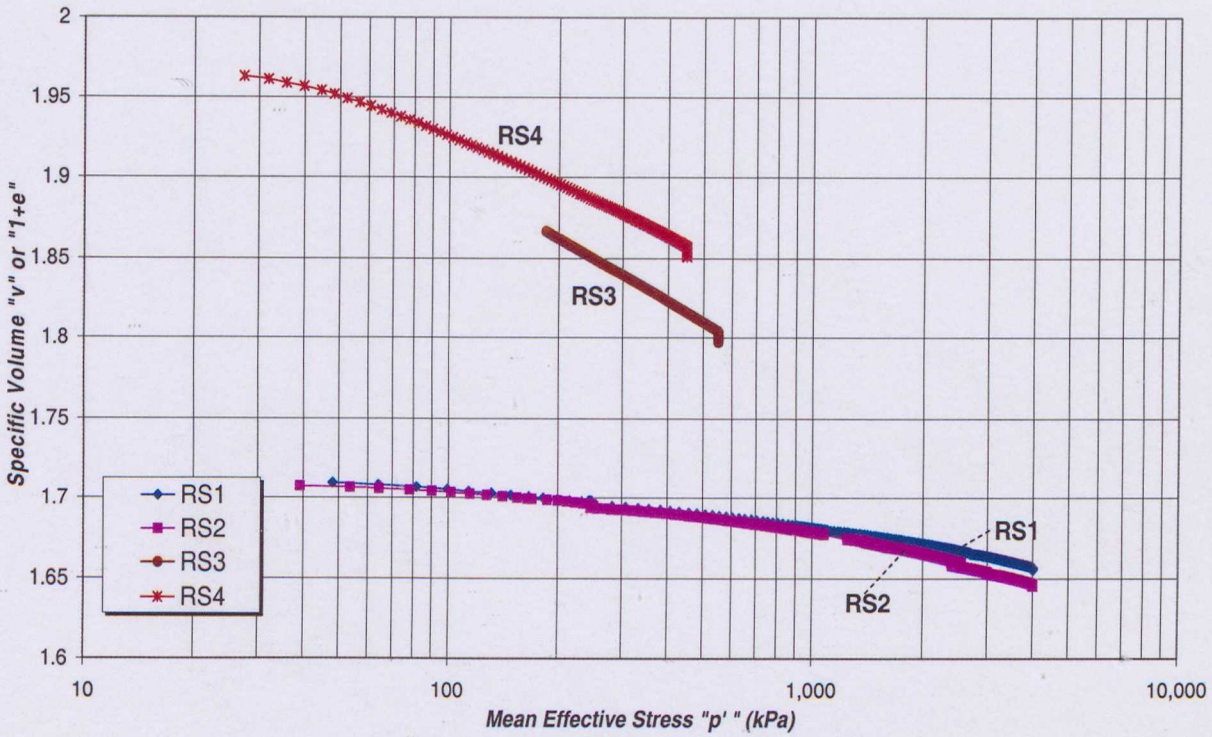


***Figure 4-20*** *Isotropic Compression data for River Side*

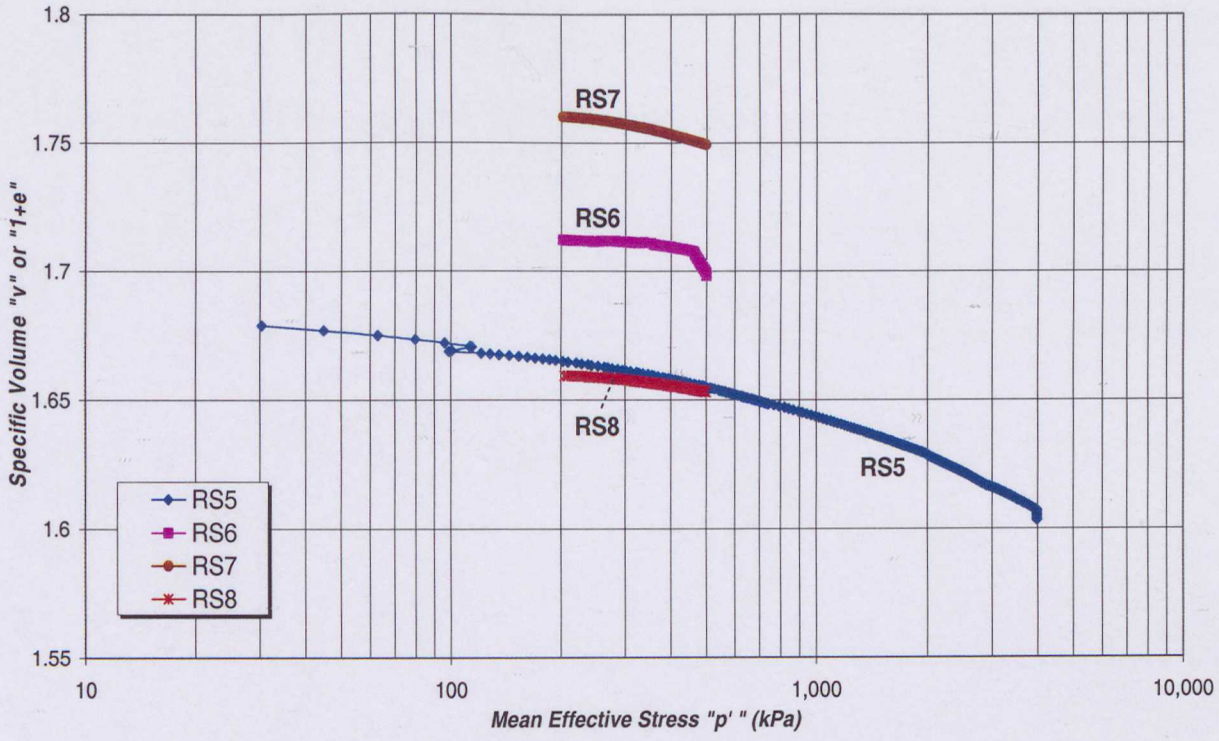


*Figure 4-21* Isotropic Compression data for River Side

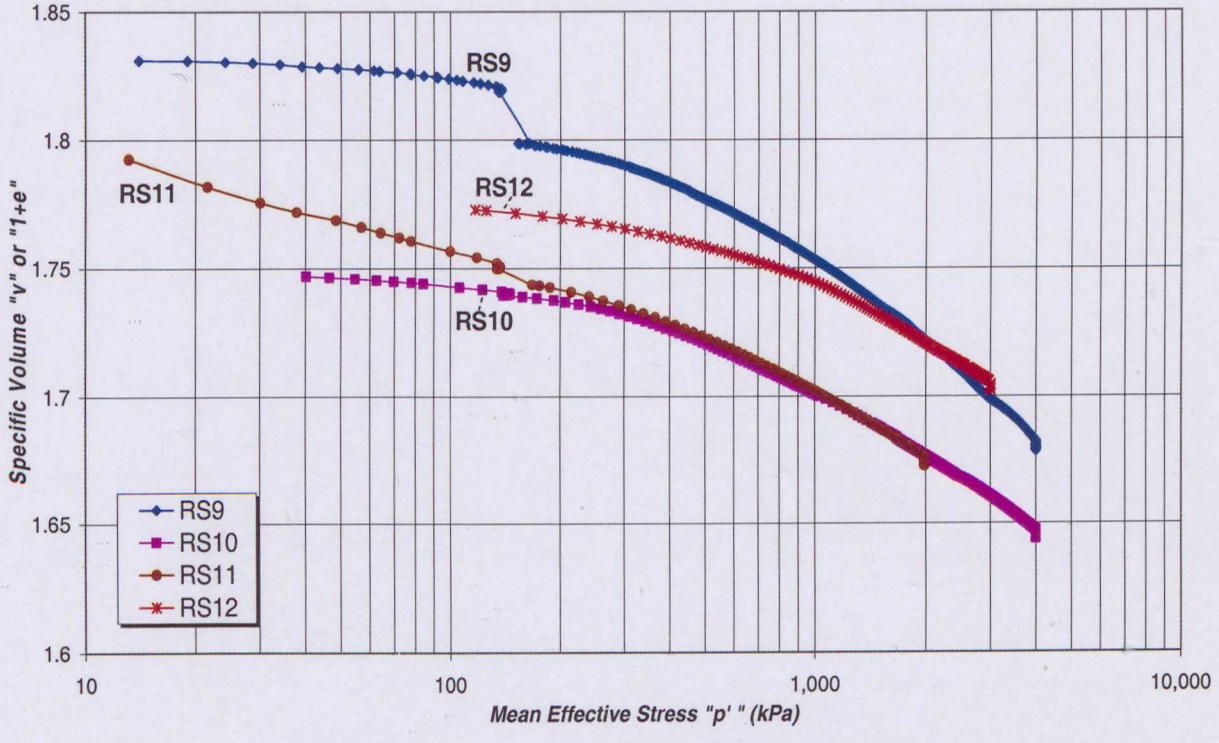


*Figure 4-22* Isotropic Compression data for River Side

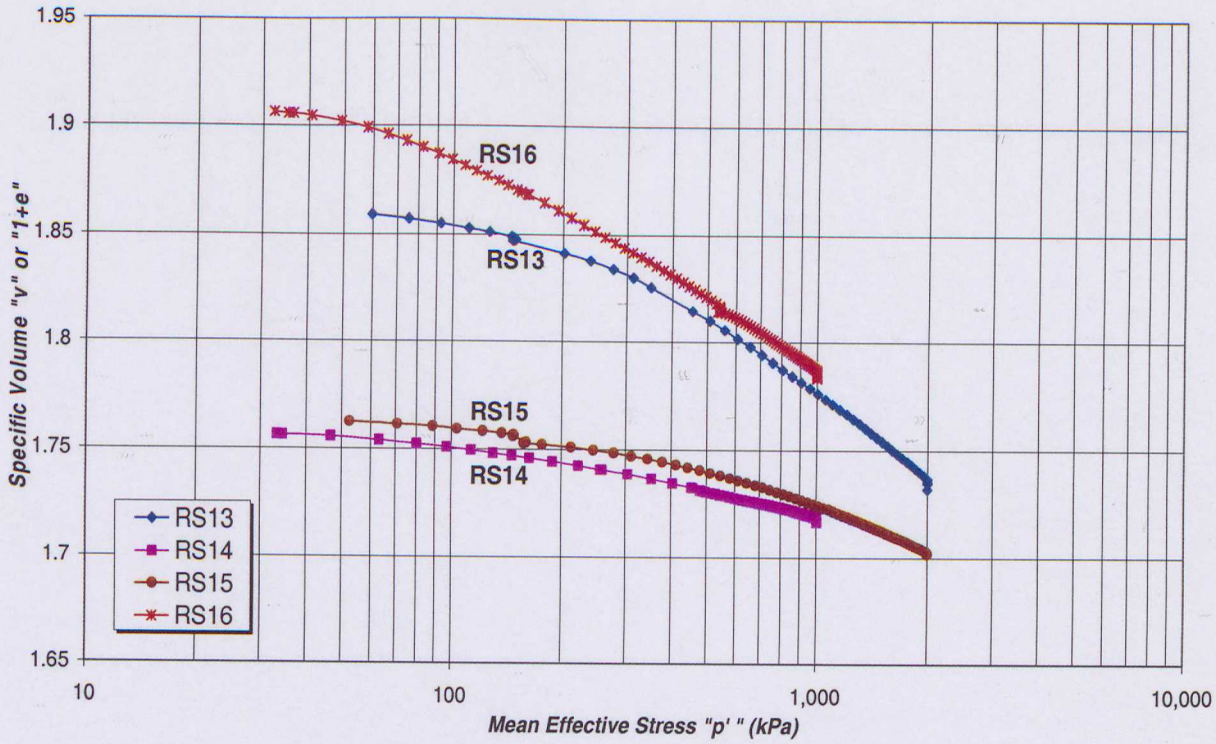


*Figure 4-23* Isotropic Compression data for River Side

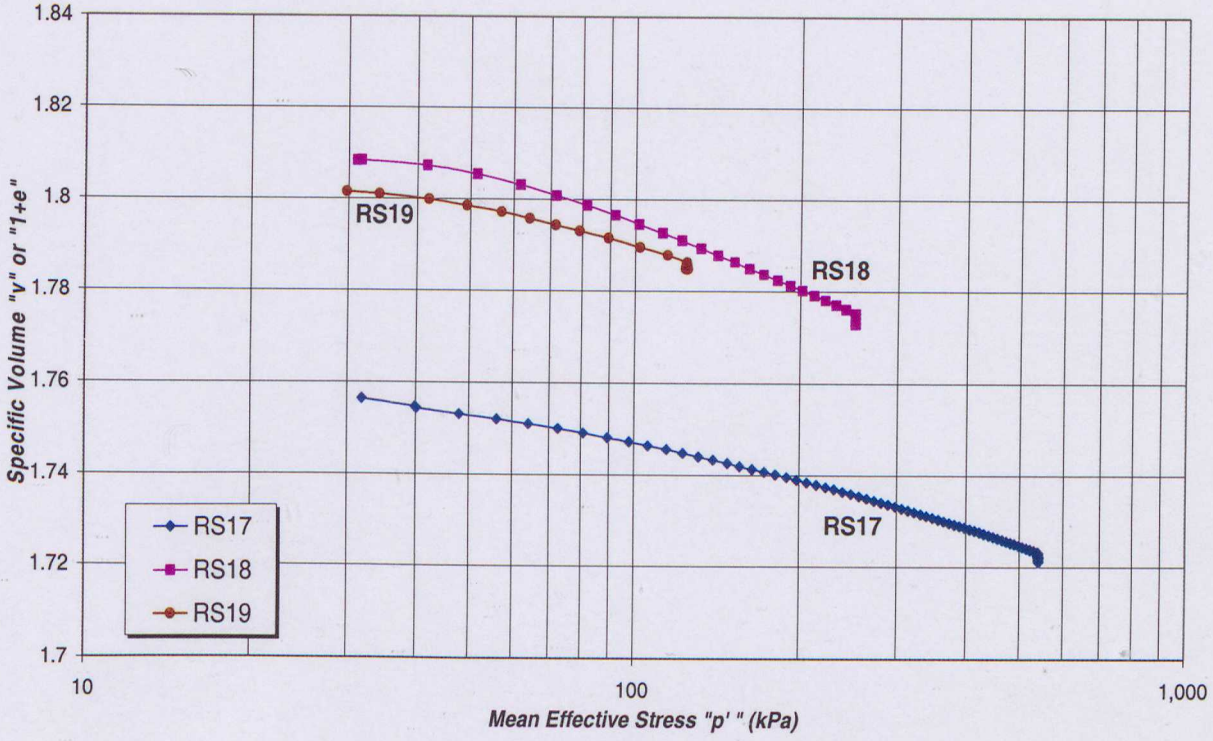


*Figure 4-24* Isotropic Compression data for River Side

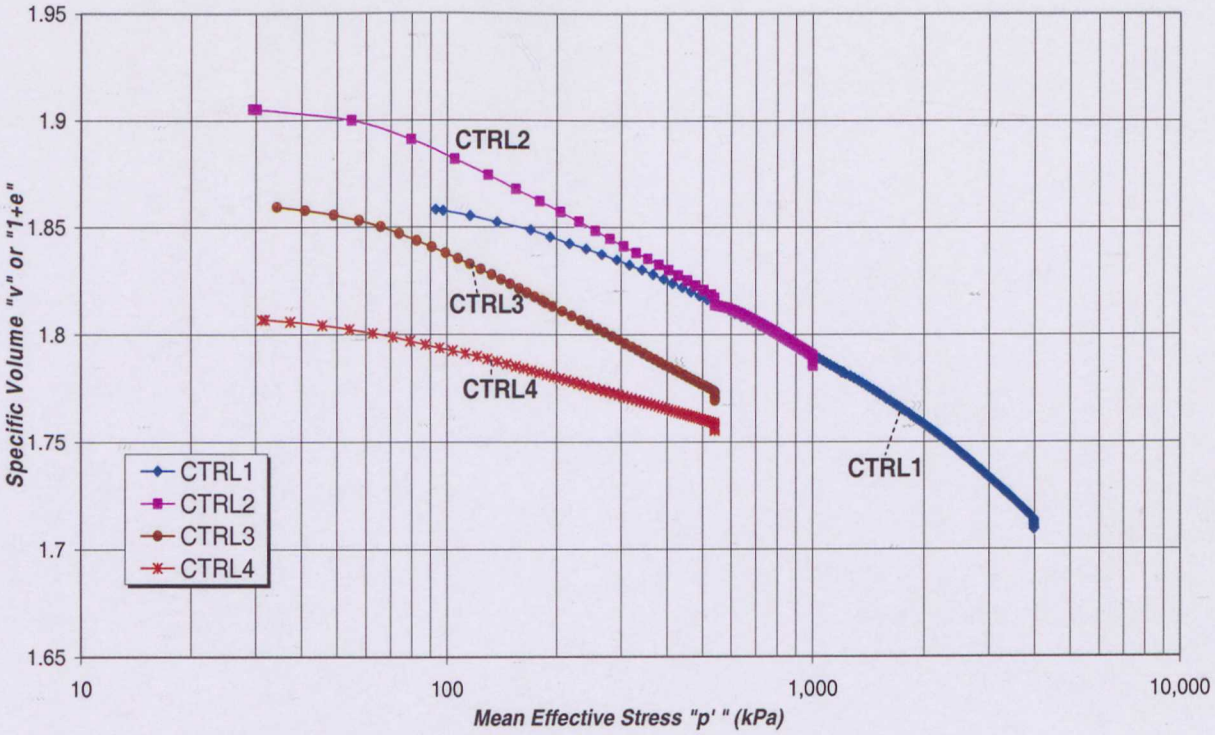


***Figure 4-25*** *Isotropic Compression data for CTRL Stratford*

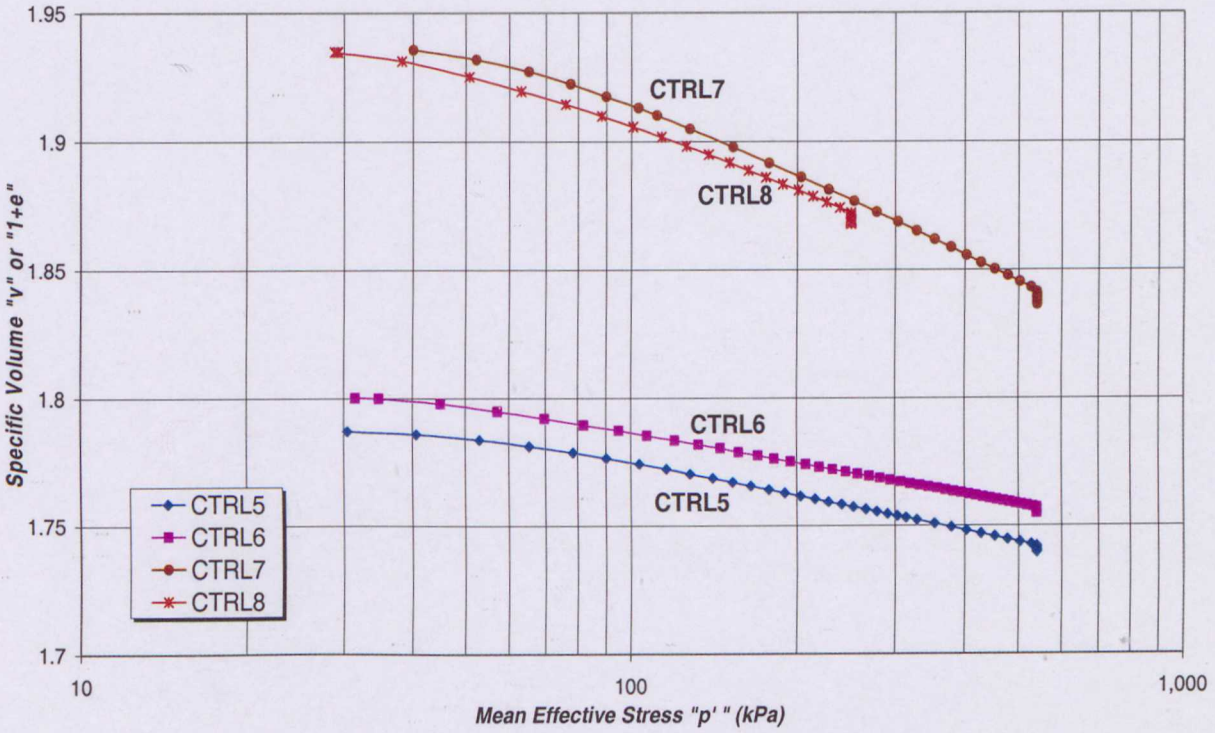


***Figure 4-26*** *Isotropic Compression data for CTRL Stratford*

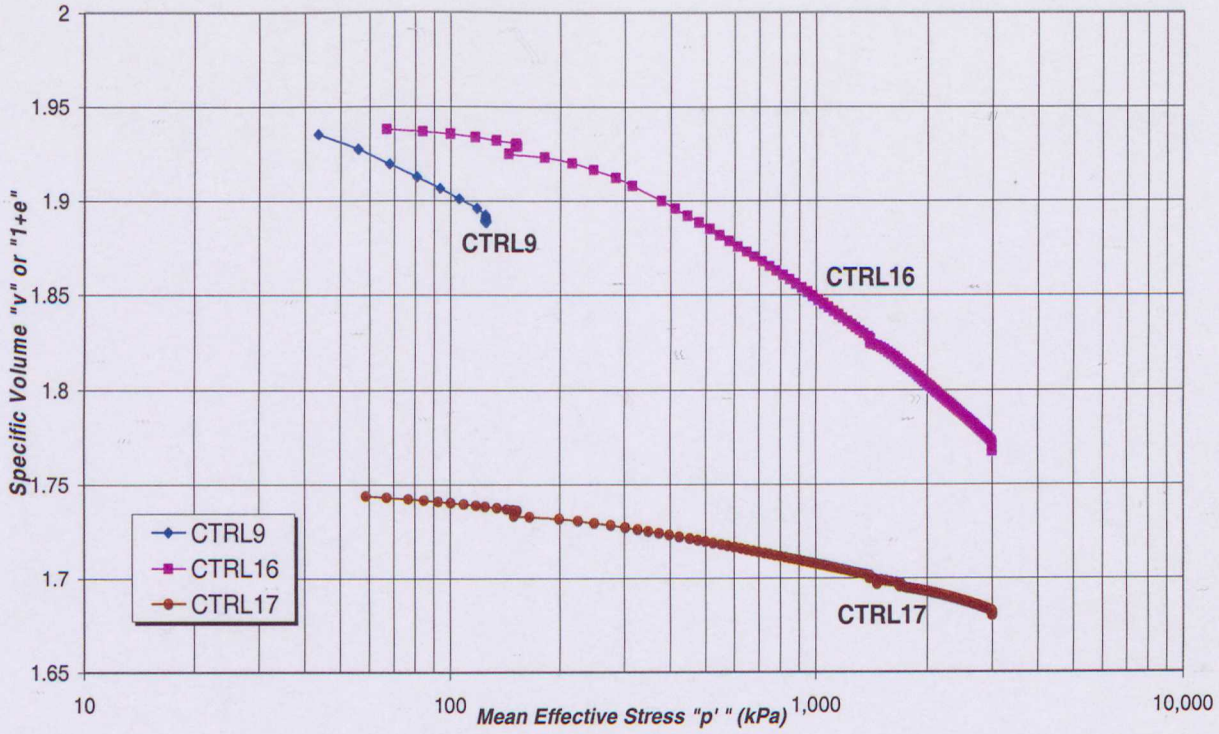


***Figure 4-27*** *Isotropic Compression data for CTRL Stratford*

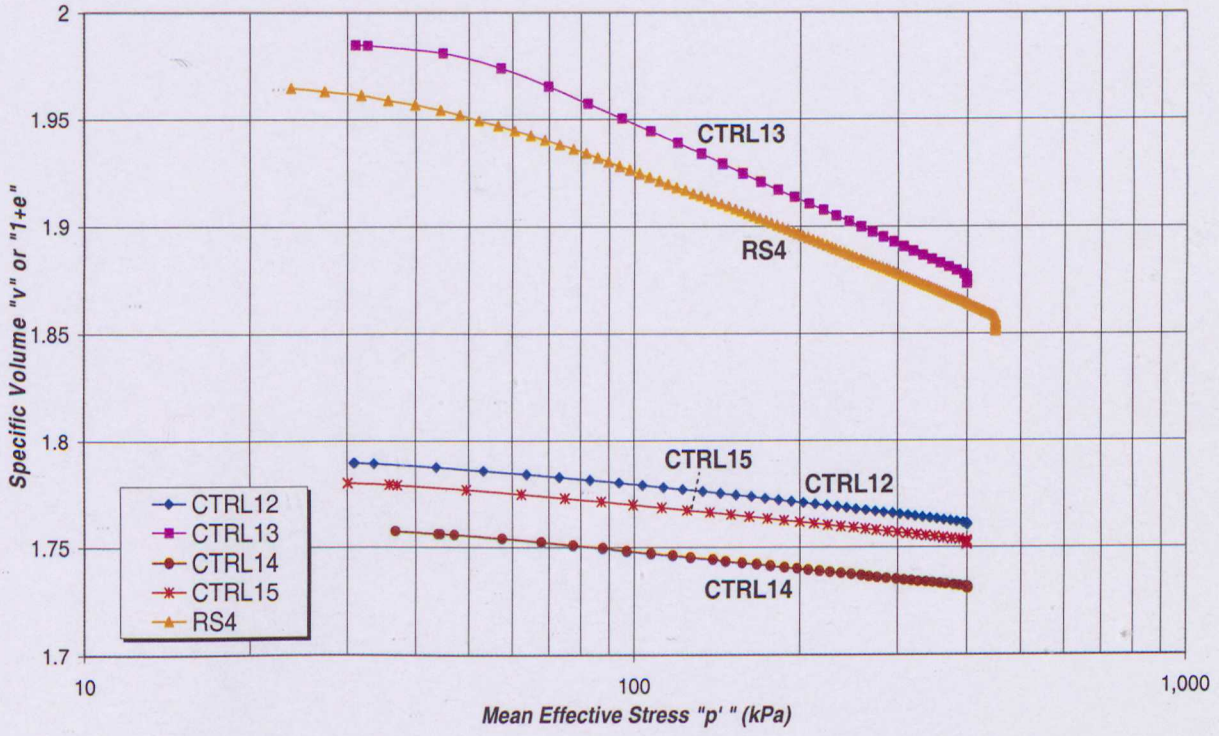


***Figure 4-28*** *Isotropic Compression data for undrained experiments*

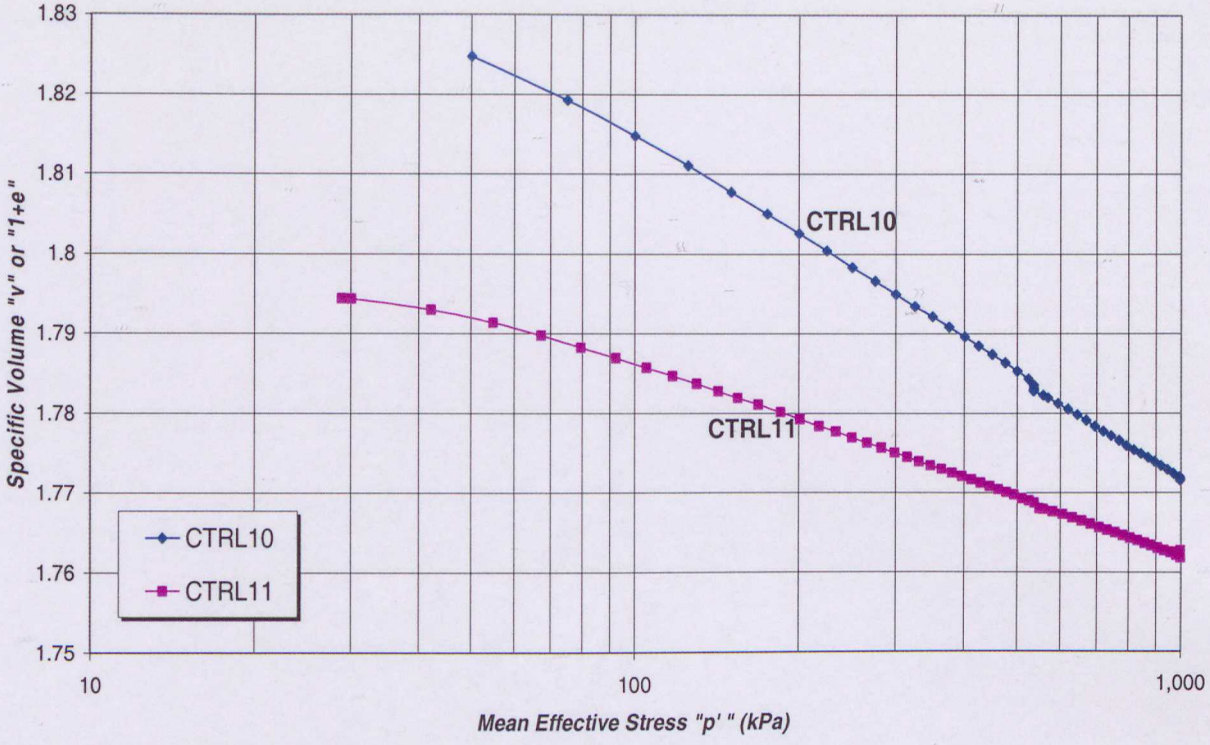


***Figure 4-29*** *Isotropic Compression data for extension tests*

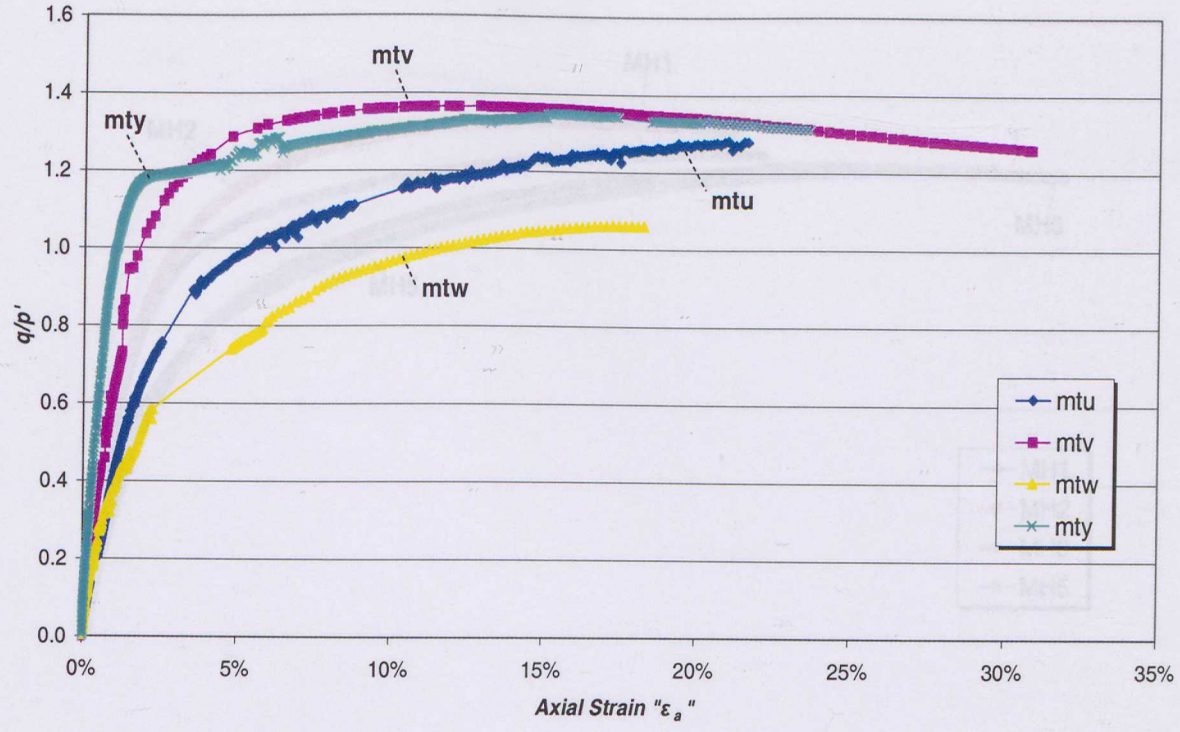


*Figure 4-30* Stress-strain data for Millennium Tower

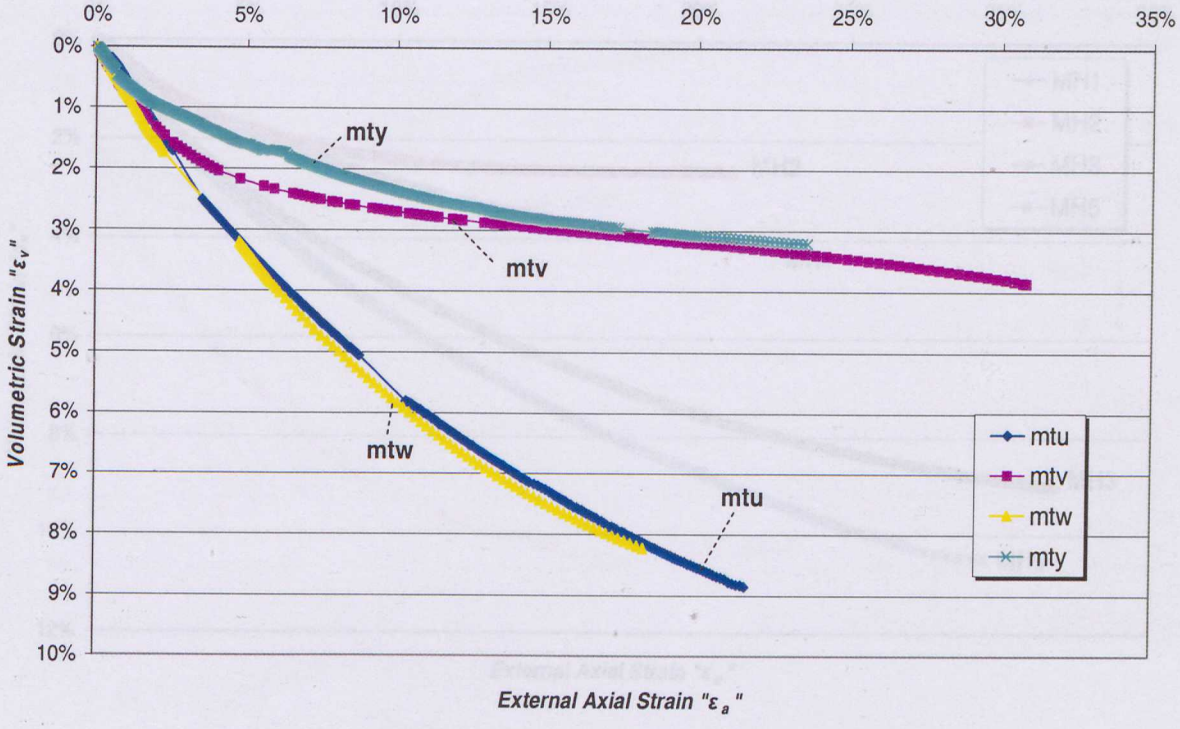


*Figure 4-31* Volumetric strain Data for Millennium Tower

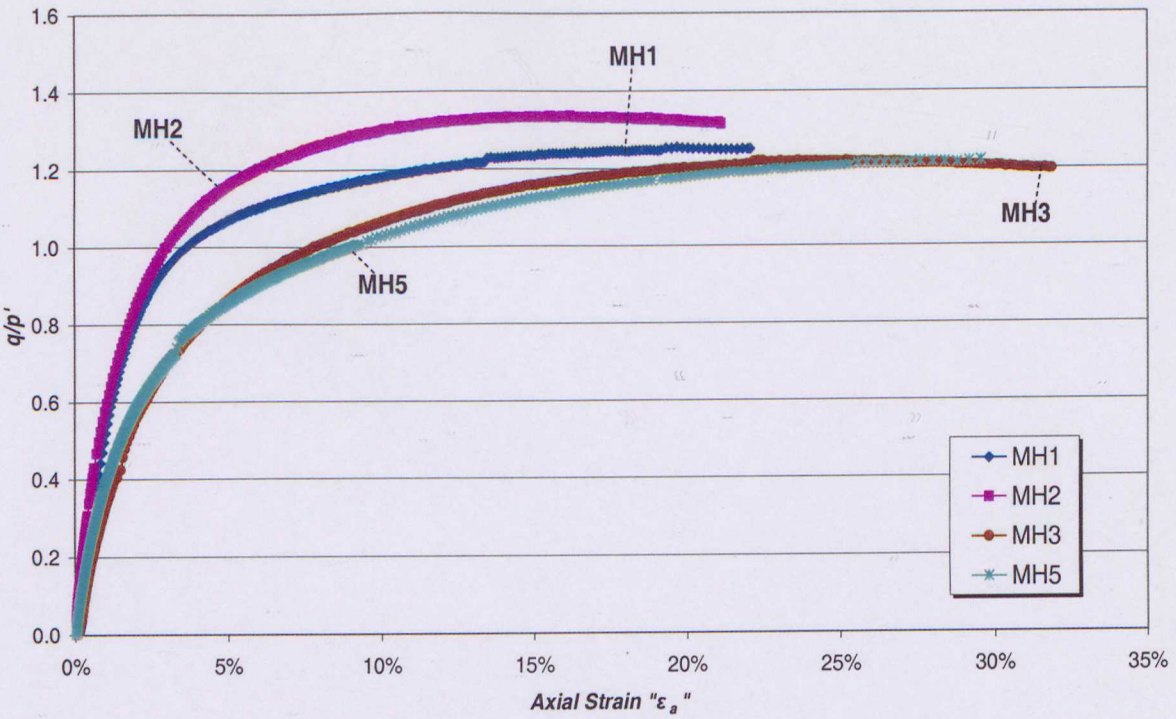


*Figure 4-32* Stress-strain data for Moore House

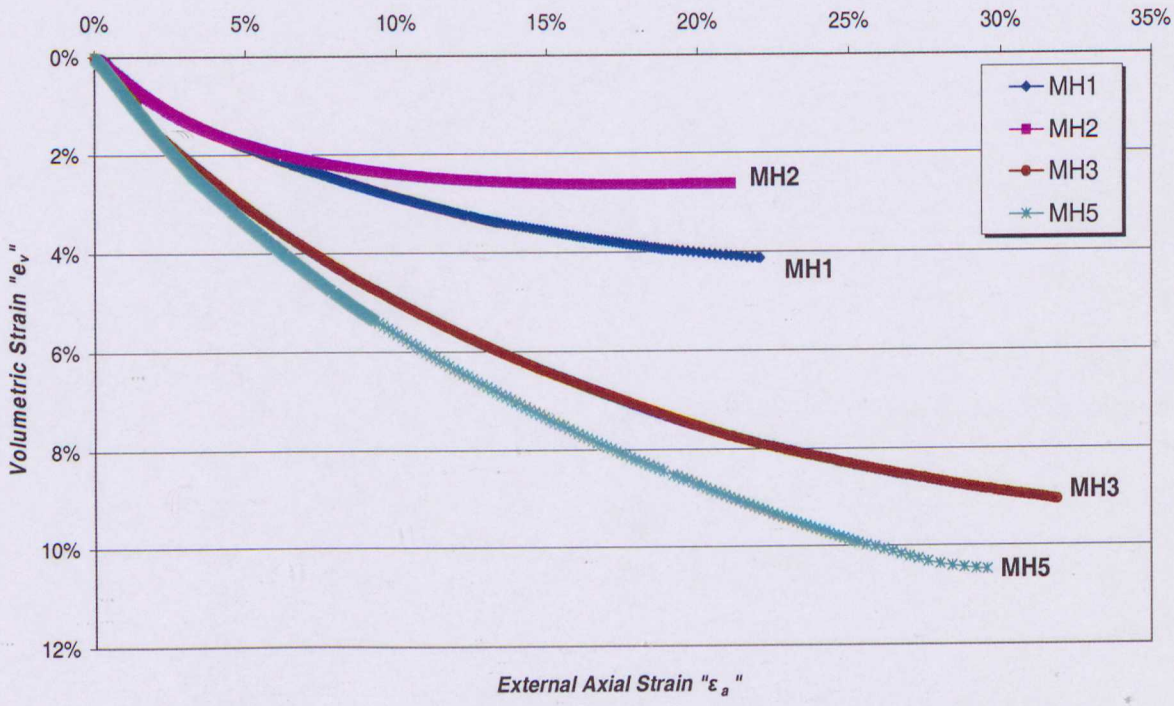


*Figure 4-33* Volumetric strain data for Moore House

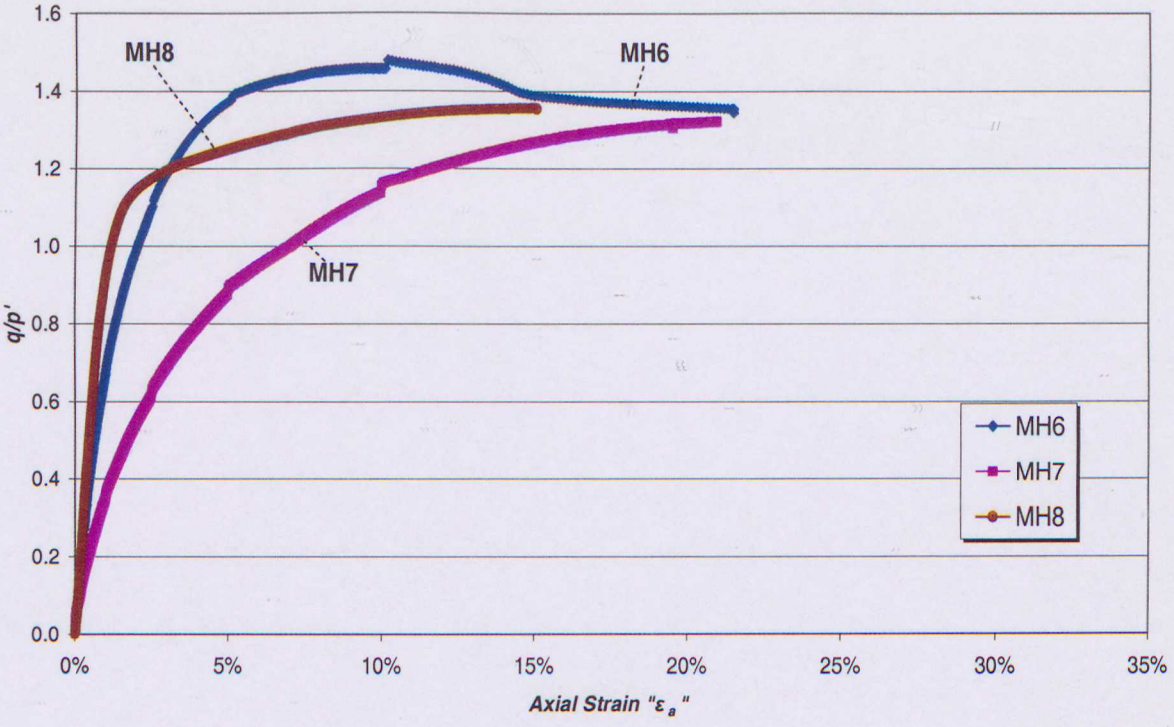


***Figure 4-34*** *Stress-strain data for Moore House*

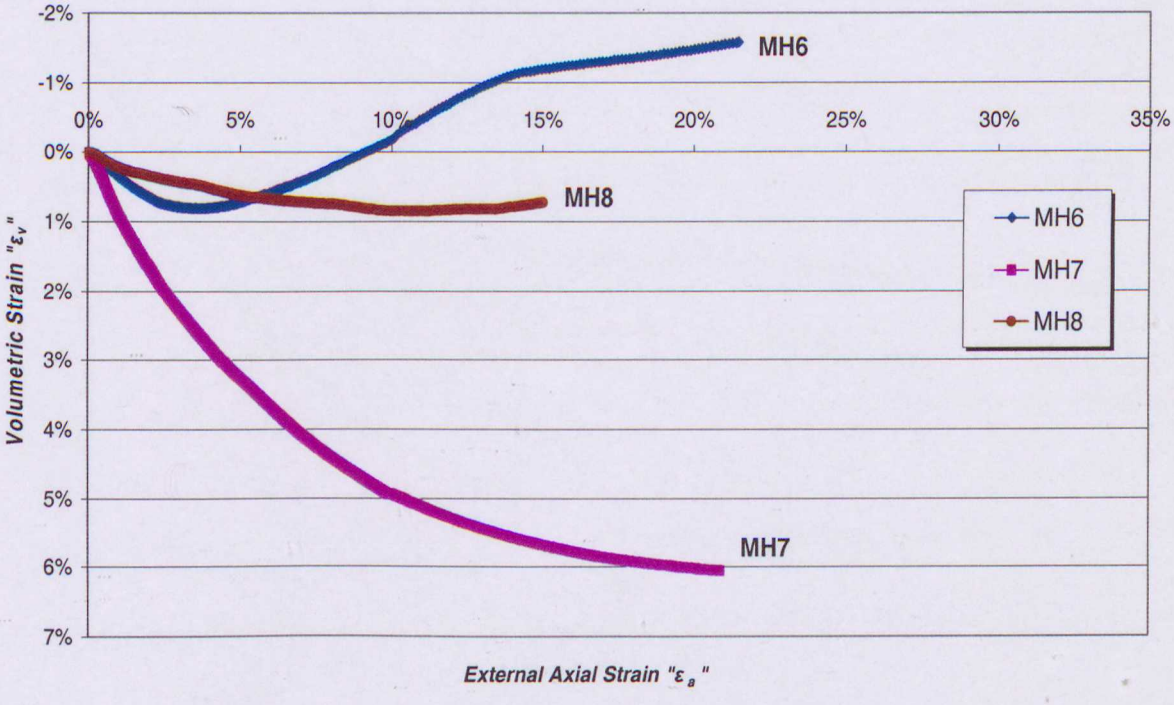


***Figure 4-35*** *Volumetric strain data for Moore House*

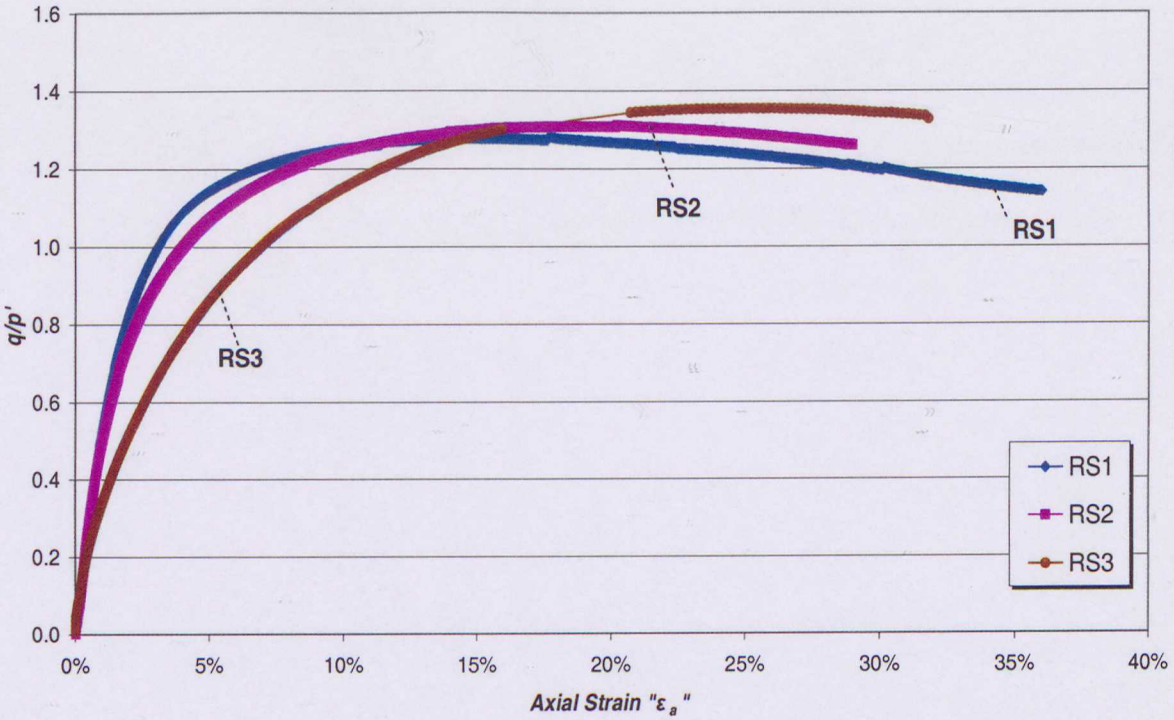


***Figure 4-36*** *Stress-strain data for Rive Side*

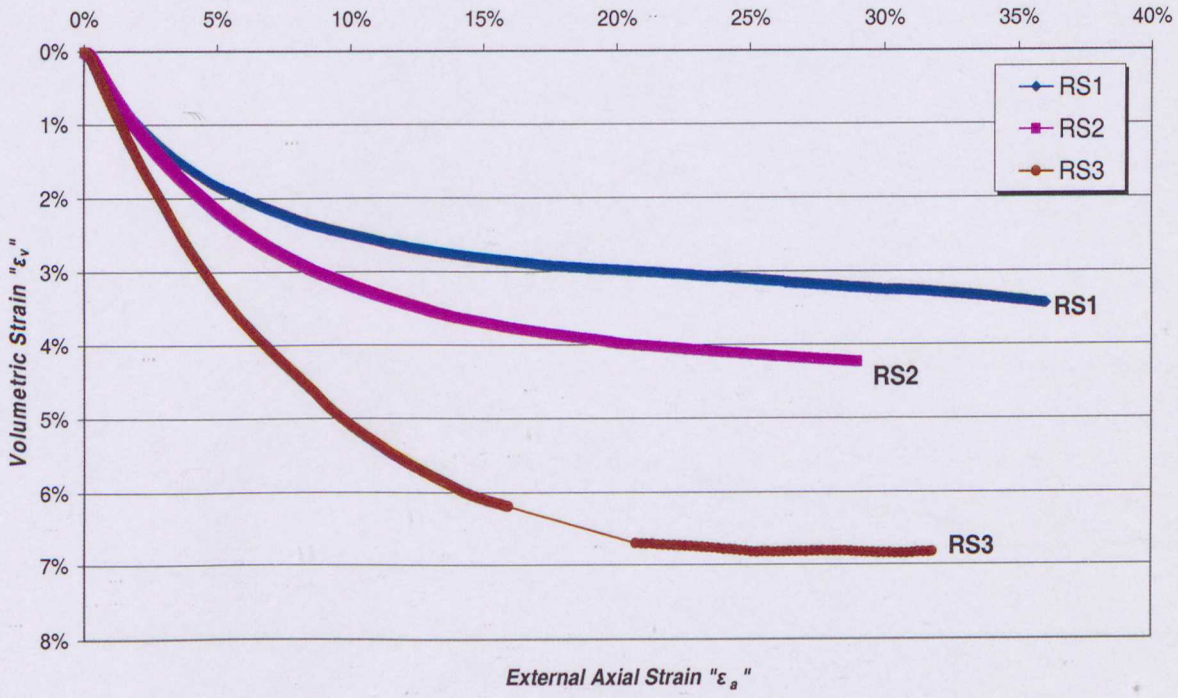


***Figure 4-37*** *Volumetric strain data for River Side*

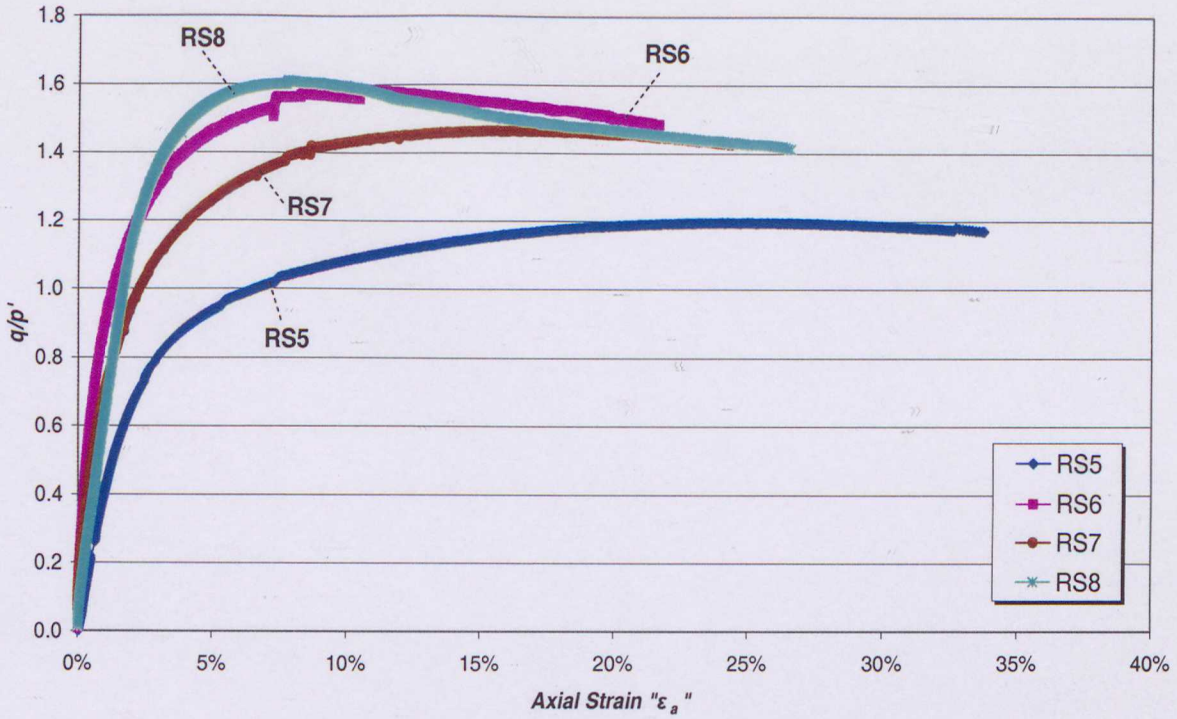


*Figure 4-38 Stress-strain data for River Side*

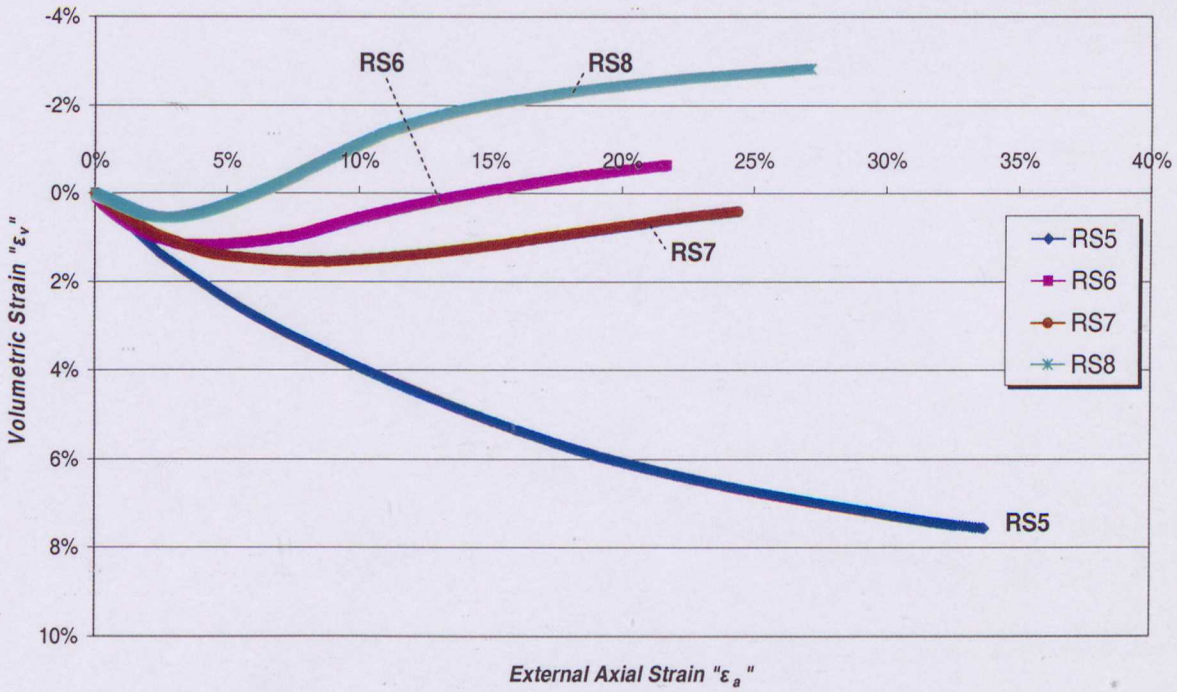


*Figure 4-39 Volumetric strain data for River Side*

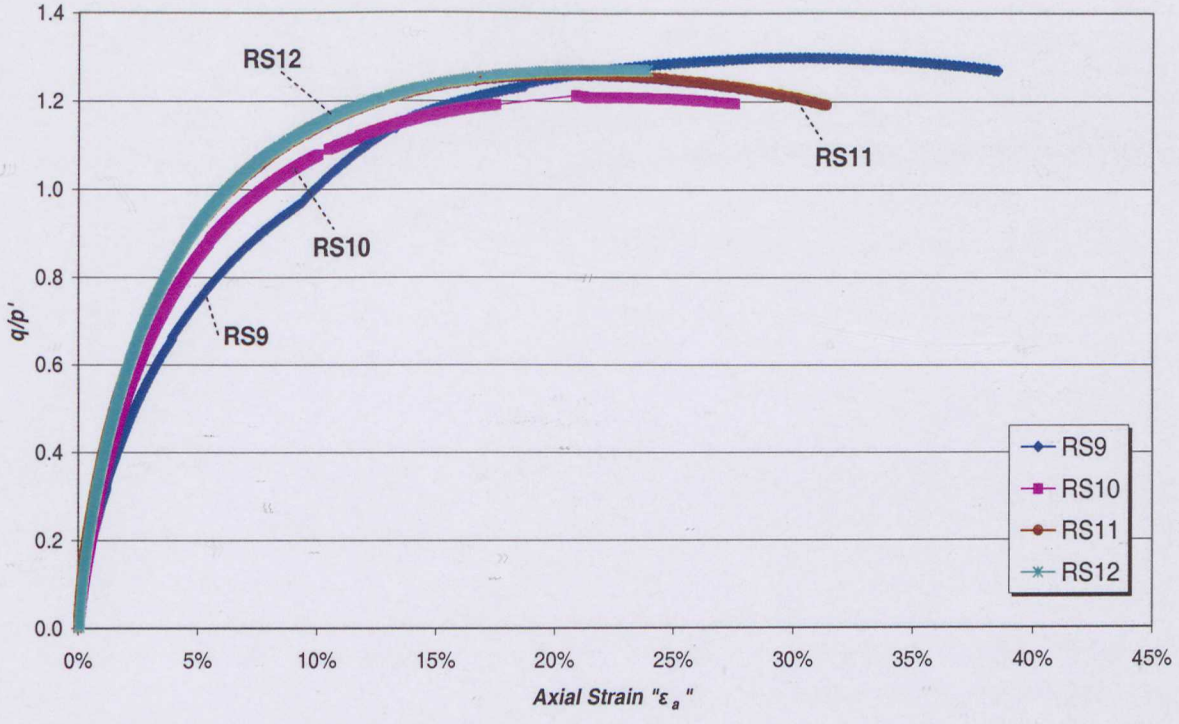


*Figure 4-40* Stress-strain data for River Side

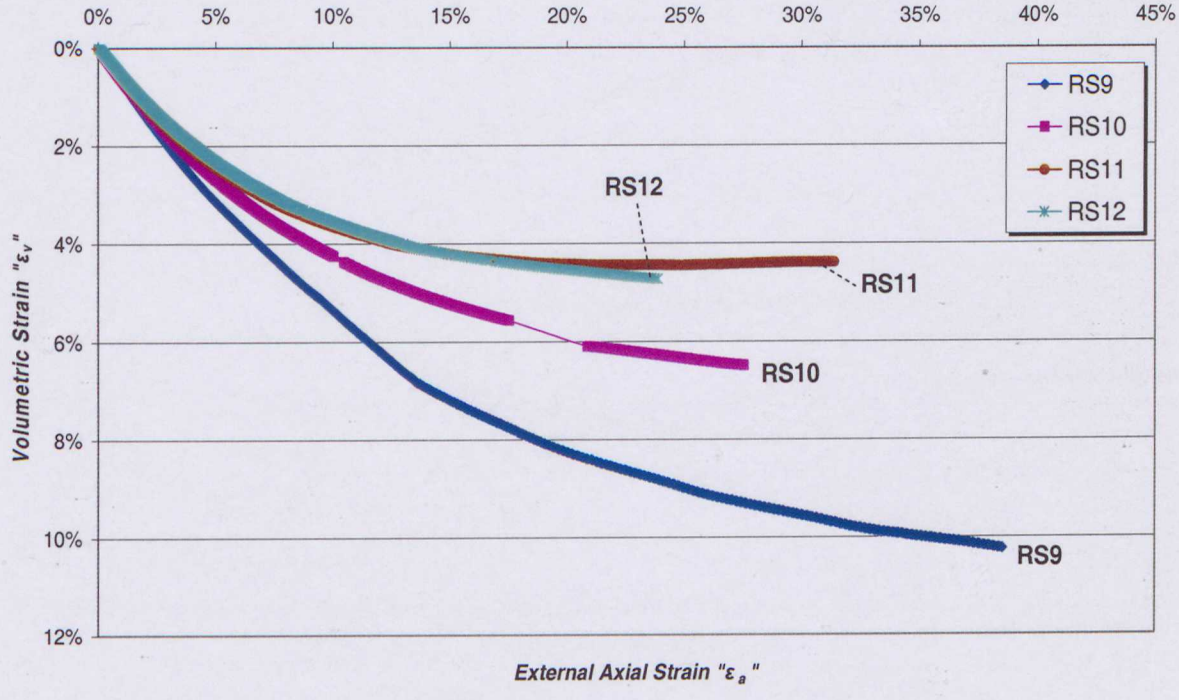


*Figure 4-41* Volumetric strain data for River Side

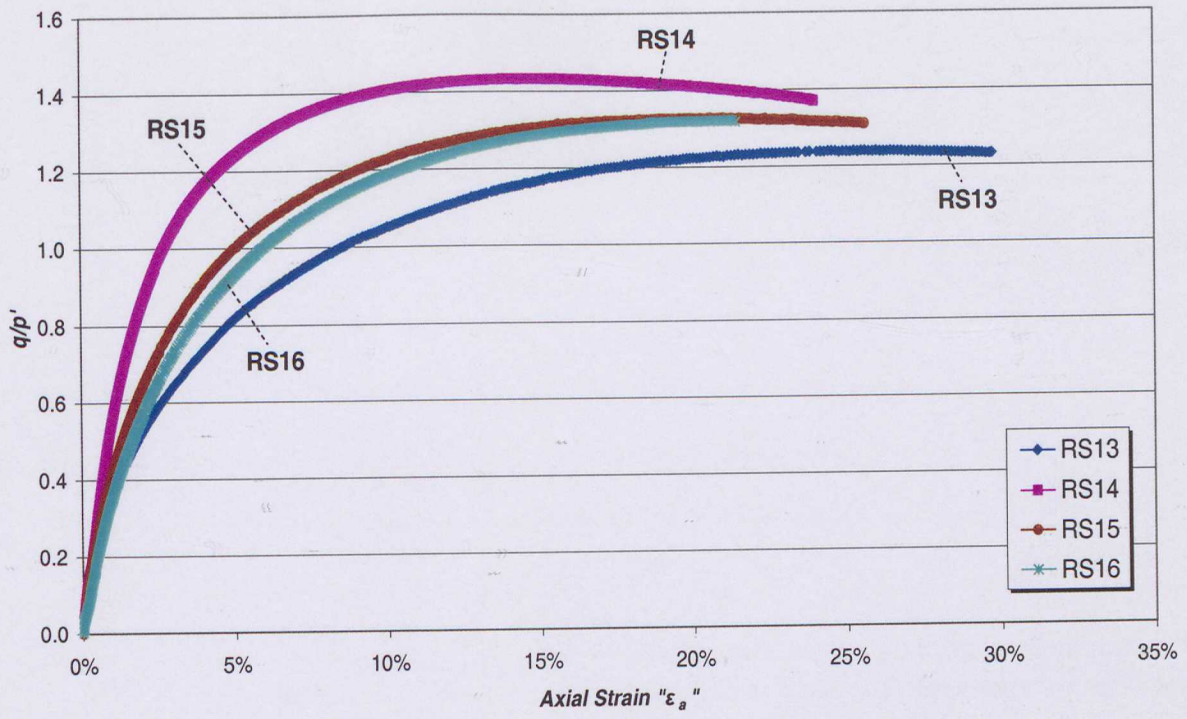


*Figure 4-42* Stress-strain data for River Side

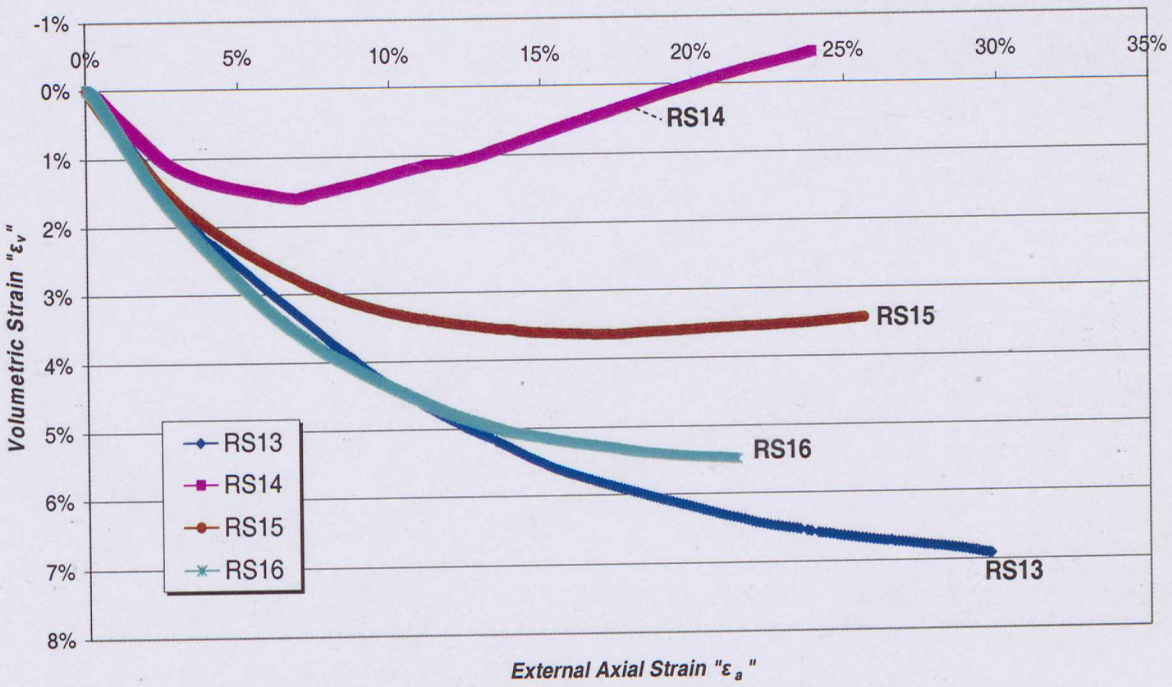


*Figure 4-43* Volumetric strain data for River Side

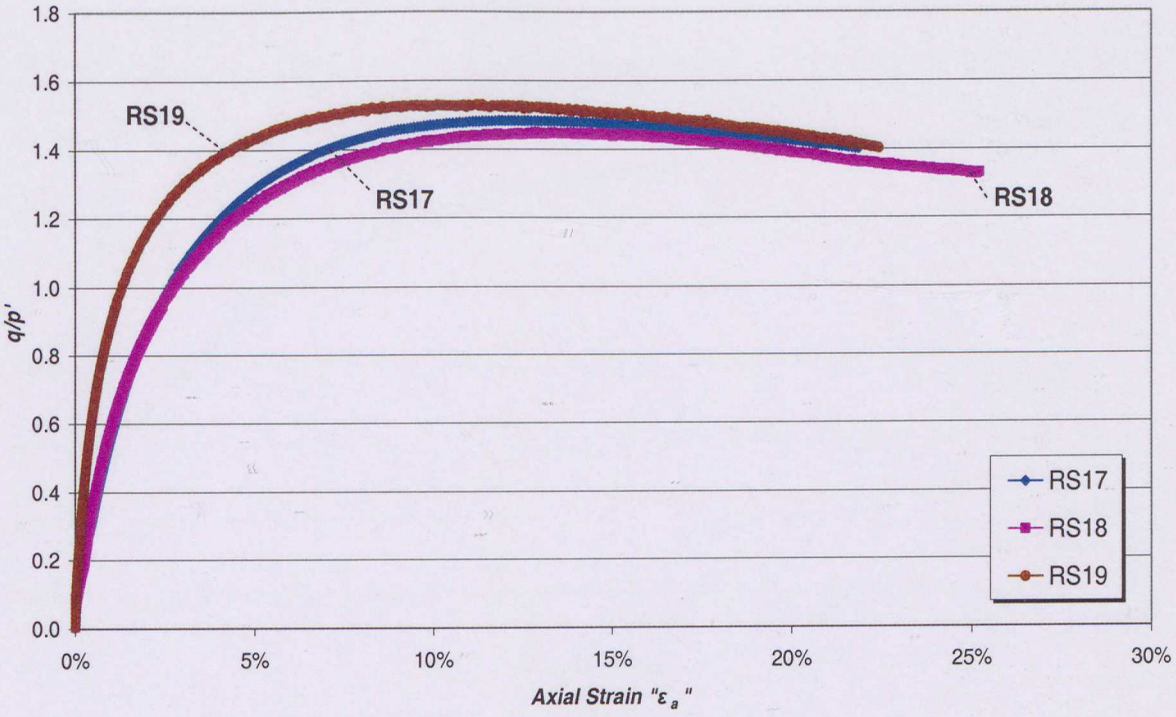


***Figure 4-44*** *Stress-strain data for River Side*

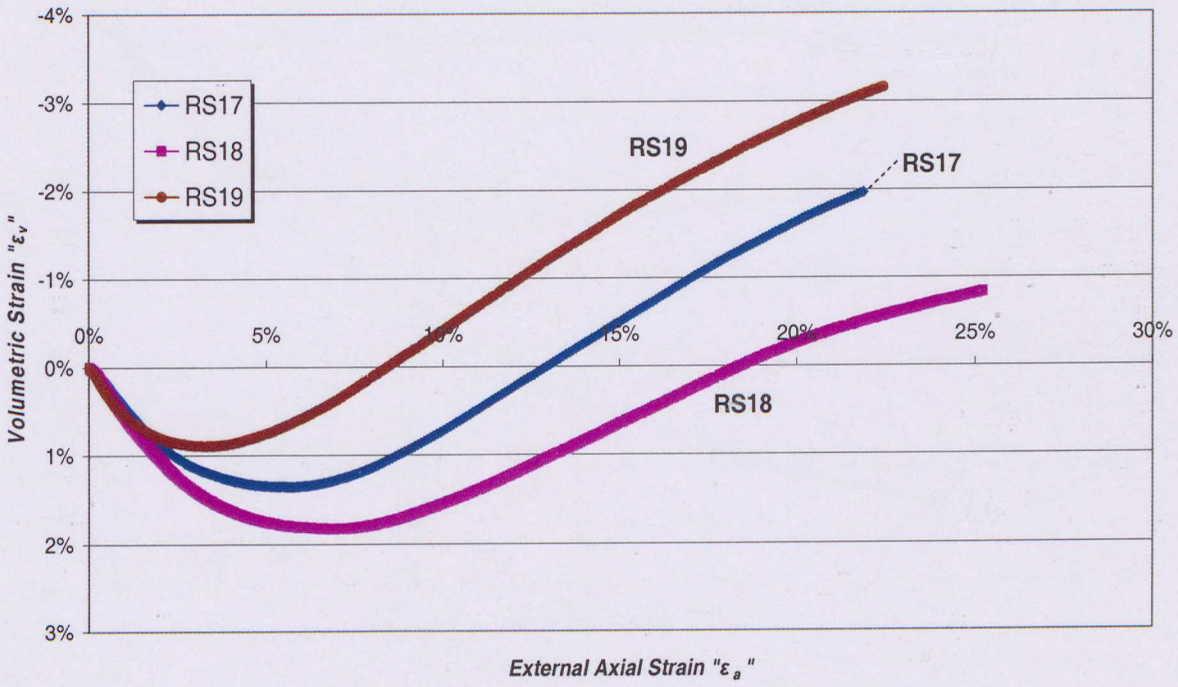


***Figure 4-45*** *Volumetric strain data for River Side*

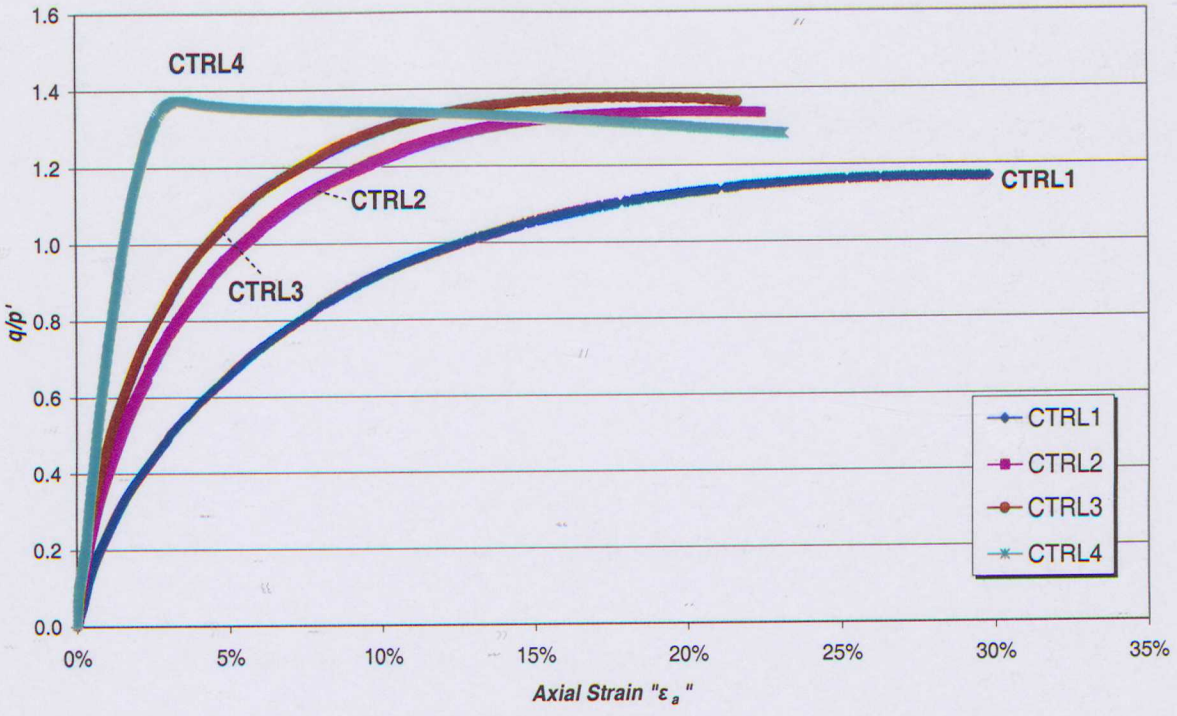


*Figure 4-46* Stress-strain data for CTRL Stratford

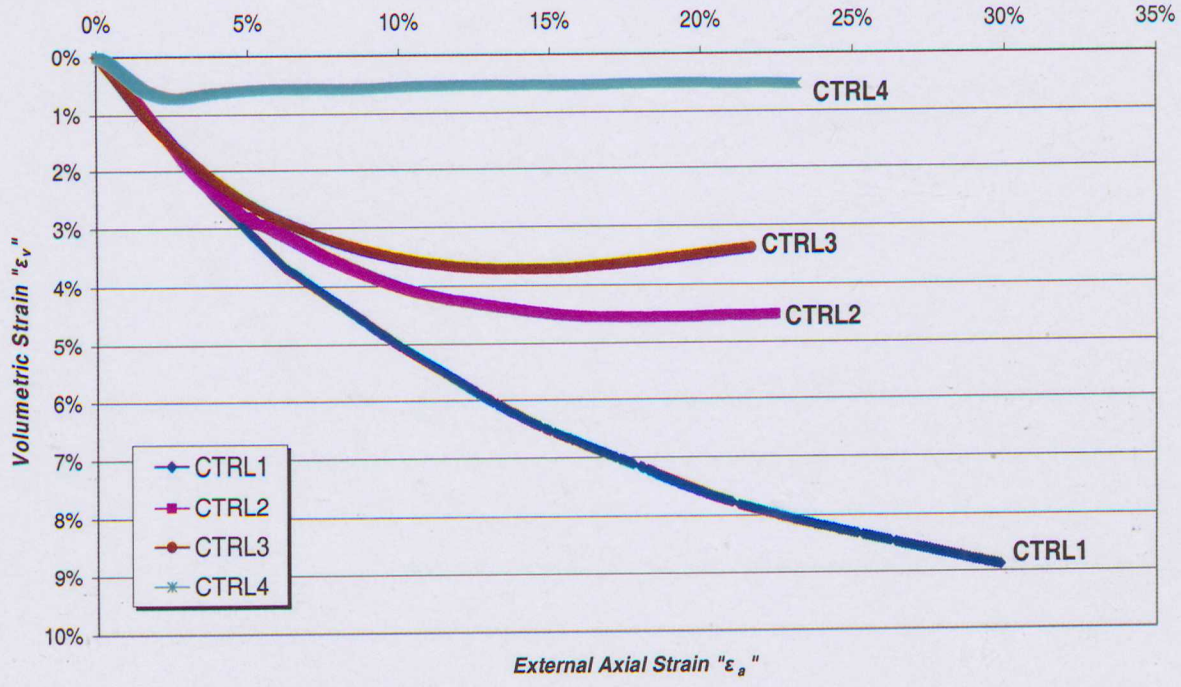


*Figure 4-47* Volumetric strain data for CTRL Stratford

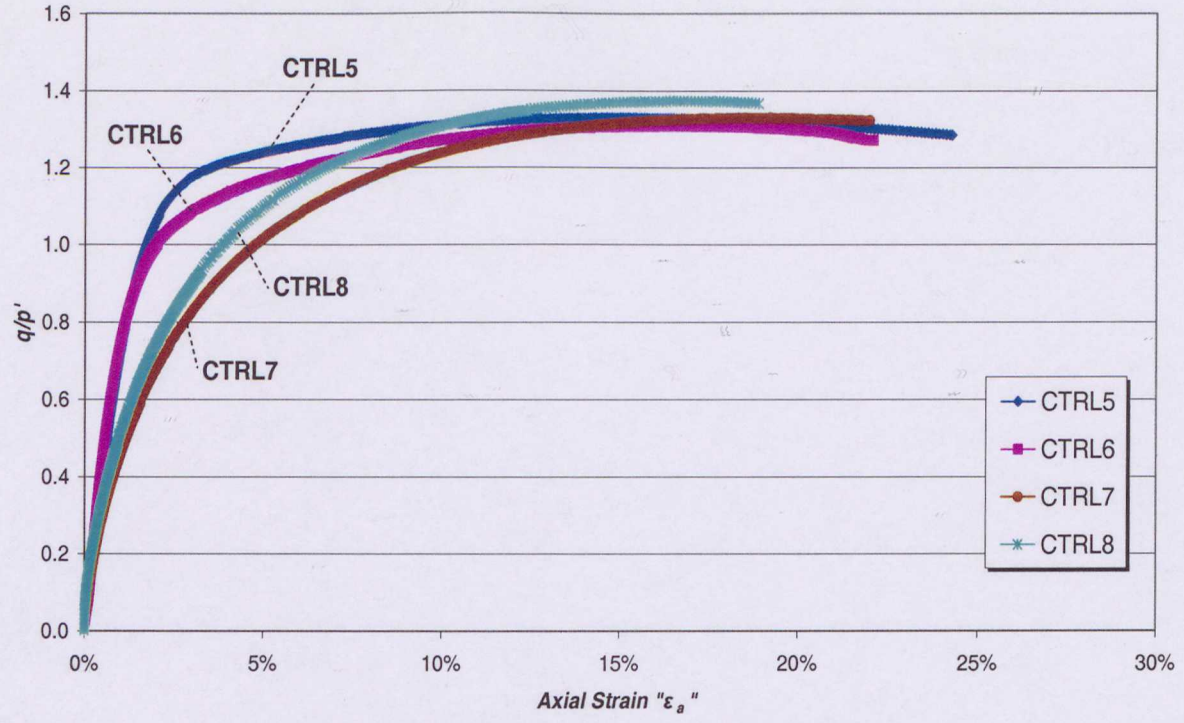


***Figure 4-48*** *Stress-strain data for CTRL Stratford*

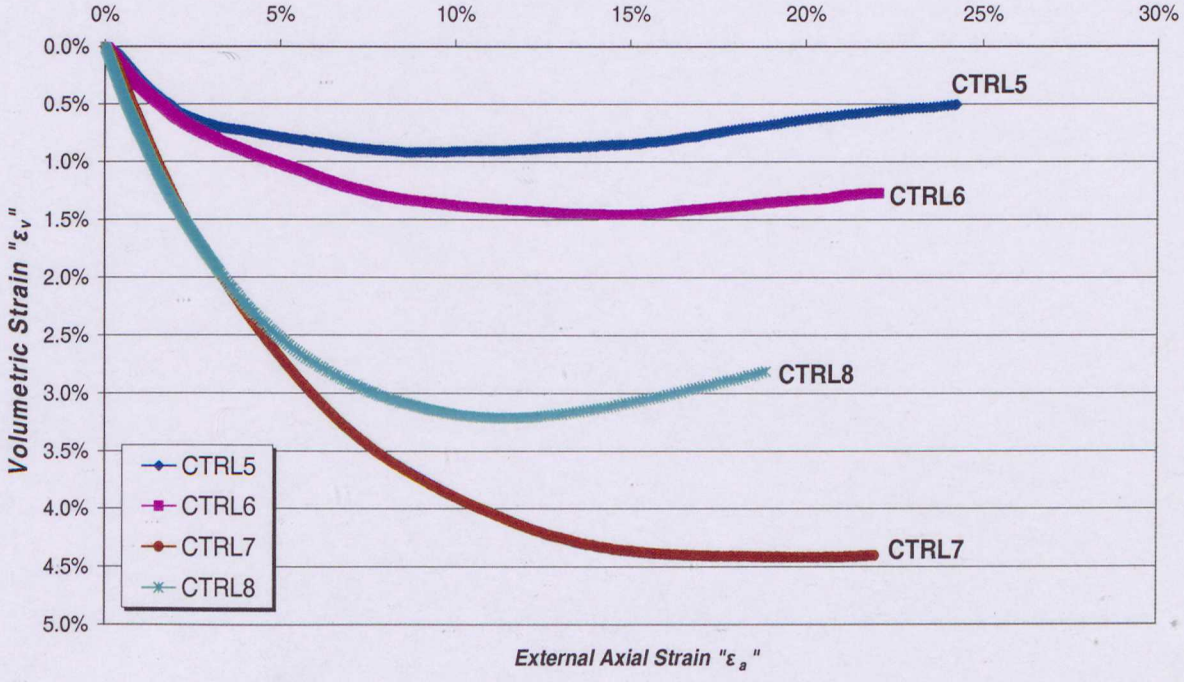


***Figure 4-49*** *Volumetric strain data for CTRL Stratford*

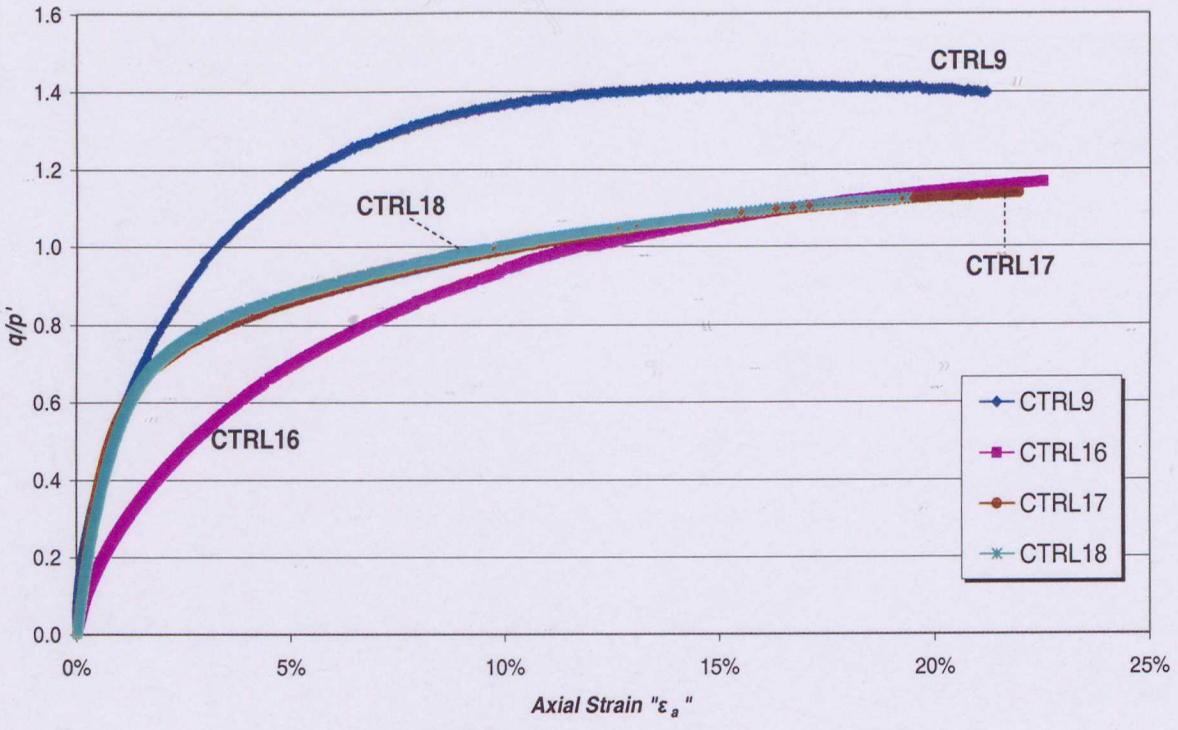


***Figure 4-50*** *Stress-strain data for CTRL Stratford*

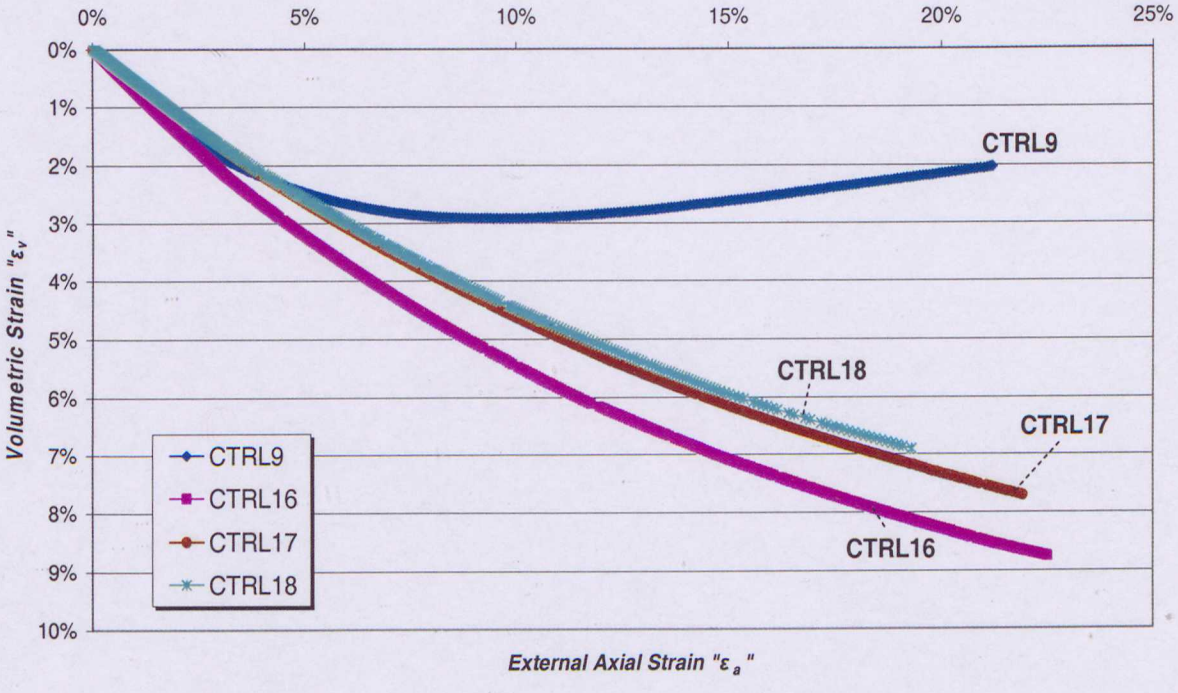


***Figure 4-51*** *Volumetric strain data for CTRL Stratford*

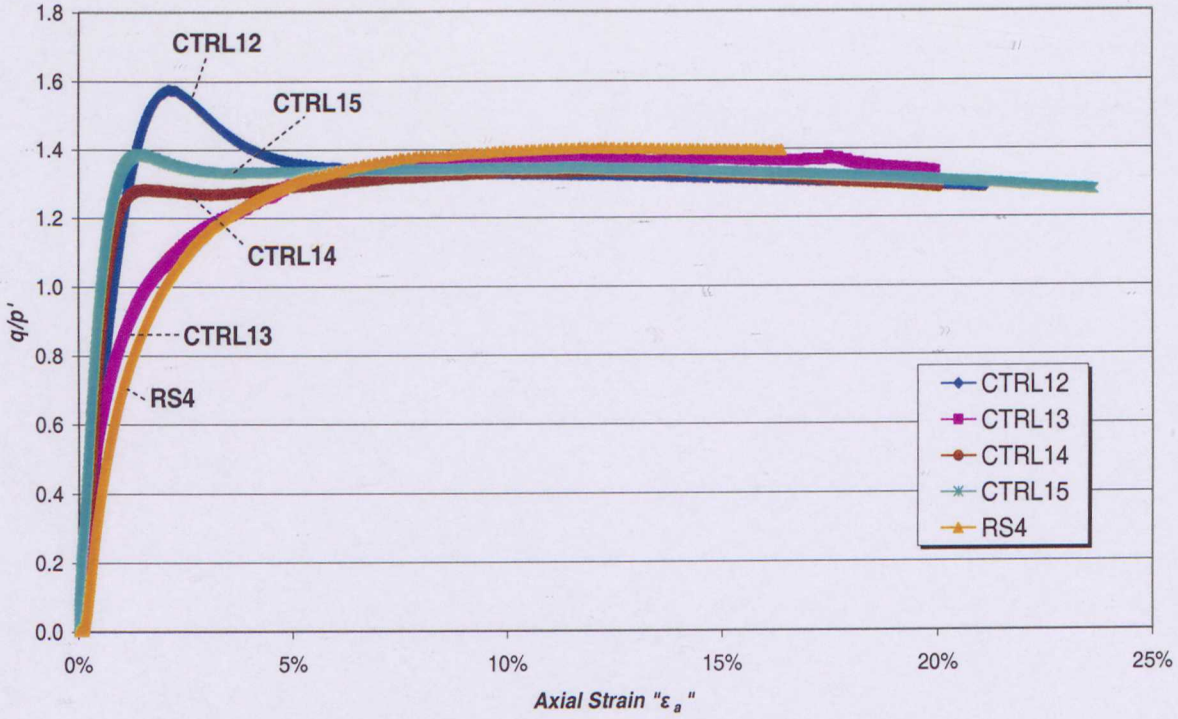


*Figure 4-52* Stress-strain data for all undrained tests

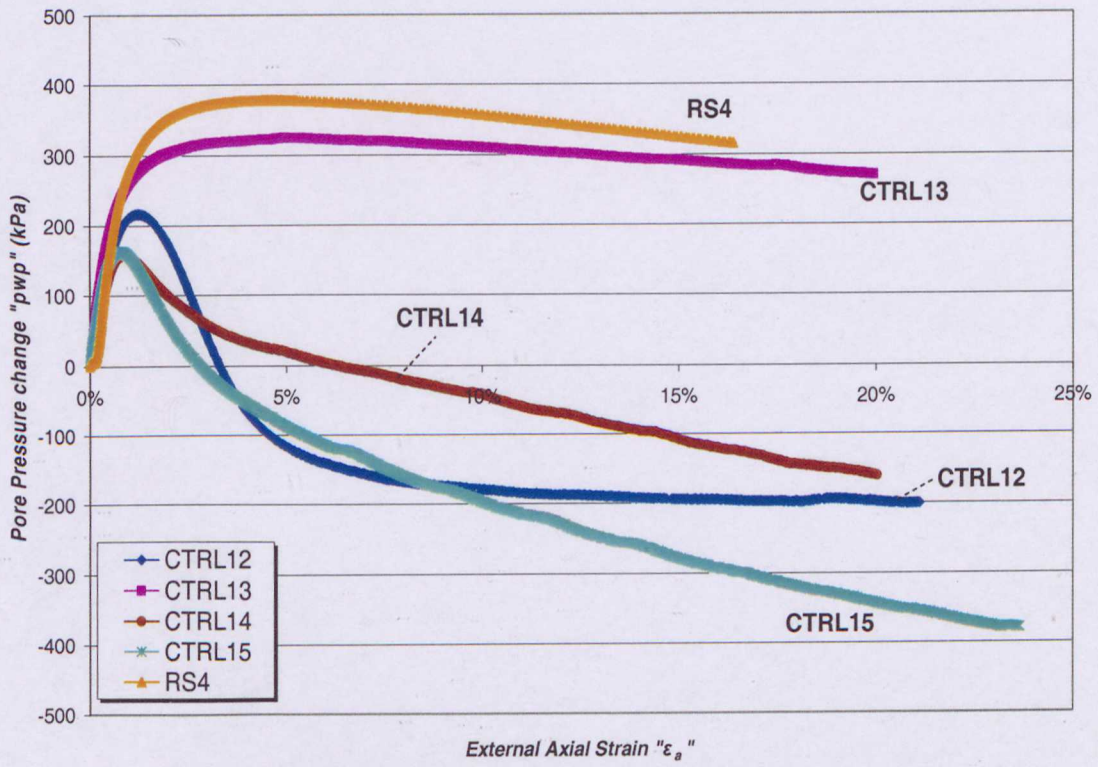


*Figure 4-53* Pore pressure response for all undrained tests

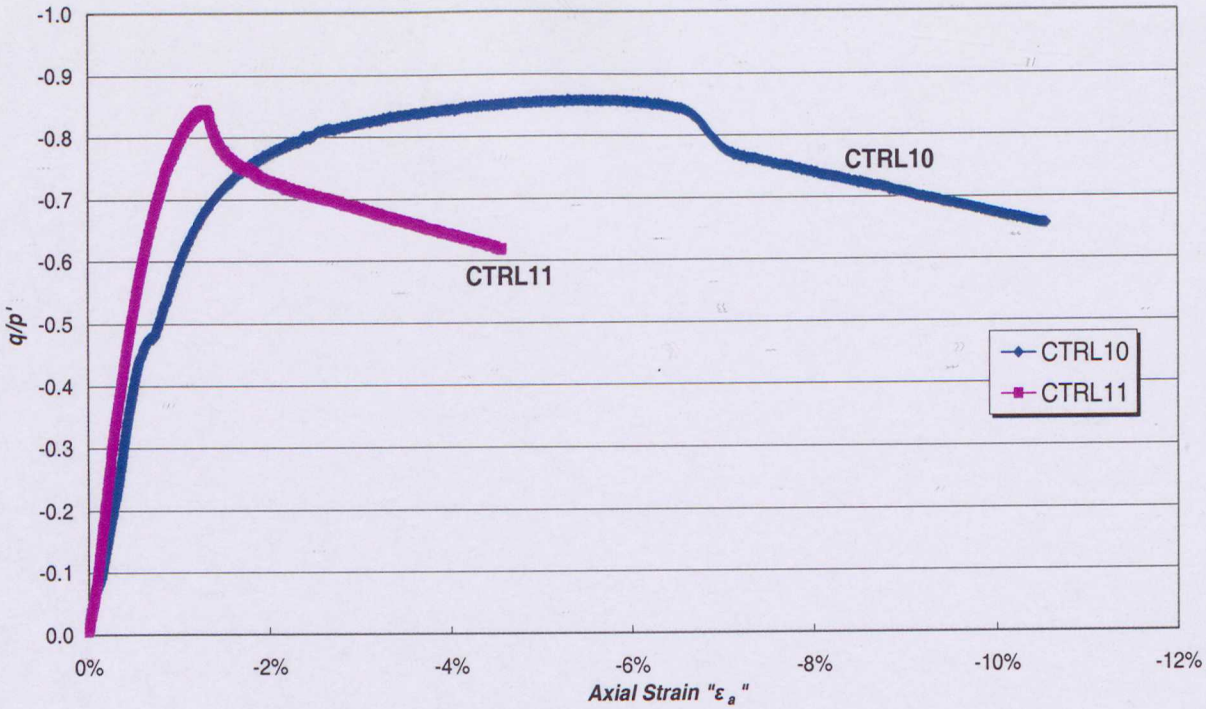


*Figure 4-54 Stress-strain data for both extension tests*

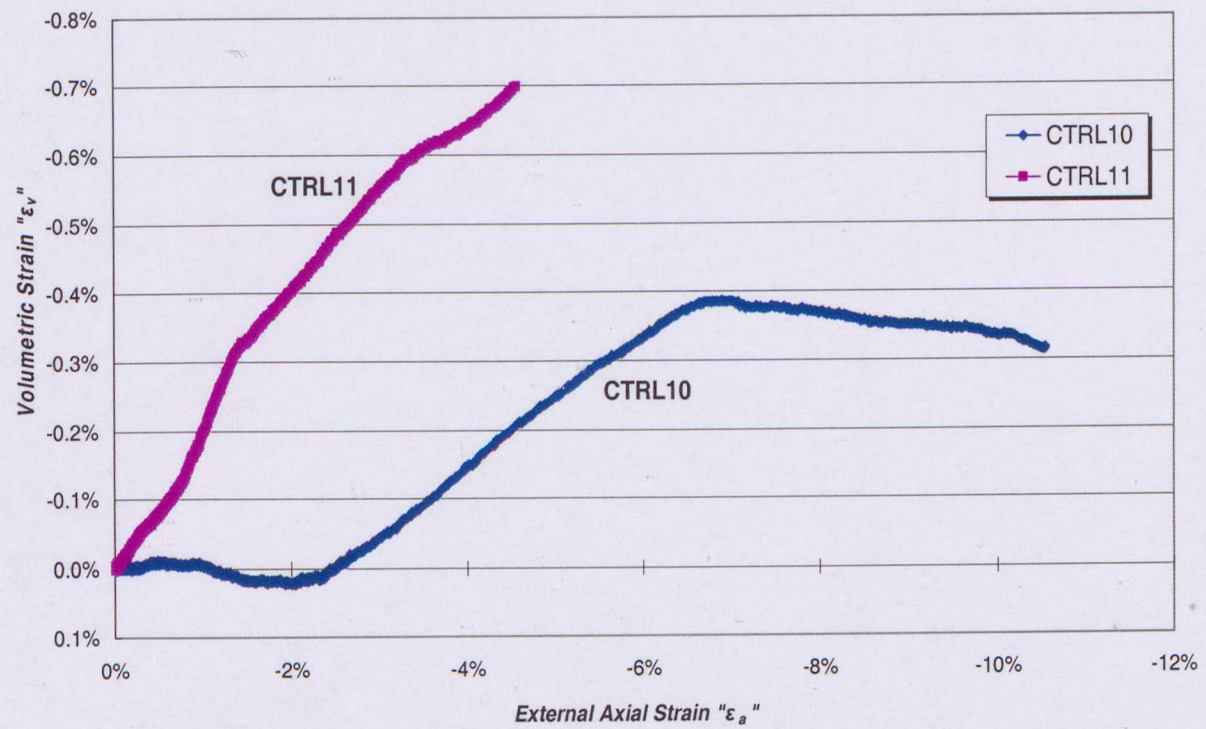


*Figure 4-55 Volumetric strain data for both extension tests*

5 LARGE STRAIN BEHAVIOUR ..... 160

5.1 Introduction ..... 160

5.2 Isotropic Compression Behaviour ..... 160

5.3 Critical States Of Thanet Sand ..... 162

5.4 Stress – Strain Behaviour ..... 166

5.4.1 Silt content effect ..... 166
5.4.2 Intact – reconstituted effect ..... 168
5.4.3 Glauconite effect ..... 171
5.4.4 Influence of effective confining stress ..... 171
5.4.5 Influence of site location ..... 173

5.5 Normalised Stress Paths ..... 173

5.6 Influence Of Anisotropy ..... 175

5.6.1 Drained compression tests ..... 175
5.6.2 Undrained compression tests ..... 176
5.6.3 Drained extension tests ..... 177
5.6.4 Overview ..... 177

5.7 Particle Breakage ..... 179

5.8 Pile And Pressuremeter Test Data ..... 180

# 5 LARGE STRAIN BEHAVIOUR

## 5.1 Introduction

This chapter is dedicated to presenting, discussing and assessing the behaviour of Thanet sand at large strains based on all the triaxial test data that were available for analysis. By means of a series of cross-comparisons, the factors influencing the material's behaviour will be distinguished and identified. The main factors investigated were: the silt content of the sand, whether the soil tested was intact or reconstituted, the site the specific sample tested came from as well as the sampling method used. Finally, the question of anisotropy of the soil has also been addressed.

## 5.2 Isotropic Compression Behaviour

Being a predominantly quartzitic soil, Thanet sand has a yield point that lies around the 10MPa region, as was found from high pressure oedometer experiments (see Section 7.2). The 4MPa cell pressure limitation of the high pressure triaxial apparatus that was available, only takes the soil through the initial flatter pre-yield part of the compression curve. Therefore, all comparisons made here are restricted to this region. Additionally, as the void ratio calculation has a far greater impact on a soil's compression behaviour in the v:lnp' plane than the calculation of the sample's current stress state, it should be remembered that the current void ratio is based on the initial void ratio that is calculated on the basis of four distinct methods, giving a accuracy of about ±0.02 (see Section 3.6) together with the global volumetric strains derived from the volume gauge (see Section 3.7).

Figure 5-1 and Figure 5-2 show data from four different tests for samples from the River Side site grouped according to the initial condition of the soil, with the intact material in Figure 5-1 and reconstituted material in Figure 5-2. This allows the effect of the silt content of the material to be examined, as all other parameters remain the same. In both figures the low silt content samples (RS1 and RS2 respectively) appear to have flatter compression curves than their high silt counterparts (RS5 and RS9 respectively), giving smaller reductions in void ratio. Clearly, the initial void ratio would have an effect on the compression behaviour of the soil. As can be seen though in Figure 5-1, the low silt content sample (RS1) is looser than the high silt content sample (RS5) whereas in Figure 5-2 we have the reverse case with the low silt content sample (RS2) being initially denser than the high silt content sample RS9. Therefore, even though the pairs of samples examined show no pattern in terms of density relative to each other, in both cases, the low silt content material compresses less than the high silt material. It should be noted that the jumps that are seen in the data at around 150kPa to 250kPa, especially for RS9, are due to the suction cap connection in the apparatus. The large isotropic compression that follows should eliminate this disturbance of the sample for the subsequent shearing behaviour.

Figure 5-3 to Figure 5-5 have been drawn to examine the effect that the initial condition of the sample has on the compression behaviour of the soil. In these plots, data for intact samples are directly compared with data for reconstituted samples that were formed from exactly the same material as the intact samples. In Figure 5-3 and Figure 5-4 data for the high silt content material are presented that came from two different sites in London, River Side and CTRL at Stratford. Figure 5-5 shows data from low silt material that was again taken from River Side. In all three plots, the intact samples seem to compress far less than their reconstituted counterparts. It could be argued that this is due to the higher initial void ratios that the reconstituted samples had, but by examining Figure 5-5 it can be seen that even though RS1 and RS2 had been setup at almost exactly the same initial specific volume, the reconstituted sample RS2 appears to be more compressive than RS1, ruling out the effect of the initial void ratio and verifying that Thanet sand compresses less when intact than when reconstituted.

In Figure 5-6 two tests on intact material are presented, both from high silt content soil. Their major difference is the way the sample was extracted from the ground, as RS5 was cored and CTRL17 was taken as a block (see Section 3.4.2a). As will be shown later in this chapter, the specific site that Thanet sand samples originate from has no major influence on behaviour, leaving the sampling method as the only other difference between the samples. As can be seen, both curves seem to be very similar, suggesting that sampling method has no major impact in terms of the behaviour in compression.

## 5.3 *Critical States Of Thanet Sand*

A triaxial sample is considered to have reached a critical state when both the deviator stress and volumetric strain or deviator stress and pore pressure, depending on whether the soil was tested drained or undrained, have reached a plateau. In some cases though, as can be seen from the raw data plots in Section 4.2, samples had not yet reached a plateau at the end of the test. In these cases, the test end-point, both in terms of stress ratio as well as in terms of void ratio, were extrapolated to a plateau. An example of data that were extrapolated is experiment CTRL1 that had almost converged in terms of axial strain - volumetric strain (Figure 4-47) at the end of the experiment. The extrapolation was made by eye and was only applied for tests which were close to reaching a critical state. The extrapolation used for test CTRL1 is shown in Figure 5-7. An example of an experiment that was not possible to extrapolate is experiment RS19, where the axial strain - volumetric strain behaviour does not show any indication of curving around towards a plateau (Figure 4-45) even at large axial stresses, and so any extrapolation would be too subjective. In such cases, the incomplete nature of the test is indicated on stress and state paths with an arrow.

In order to examine the effect of the silt content, on the critical states, Figure 5-8 has been drawn. Here, the critical states and the end of test states from all compressive shearing tests, both drained as well as undrained, have been plotted. As shown in the legend, empty triangles indicate a high silt content test whereas

an empty square indicates low silt content. The two full triangles represent the two high silt content tests on samples that had their Glauconite removed (see Section 4.2 and Figure 4-14). On the right side of the plot, where the stresses are higher, all the test end-points appear to converge to two straight parallel lines, one for each stratum, with the low silt content critical state line lying higher than the high silt content line. In the central part of the plot, especially at stresses of about 1MPa, the amount of scatter is increased, probably because the number of tests available in that region was distinctly higher. On the left side of the plot, the two low silt content end-points at approximately 450kPa and 250kPa represent tests RS18 and RS19 respectively. As can be seen from Figure 4-44 and Figure 4-45, neither of these two tests had reached a plateau. In fact, they were both still dilating when the tests were terminated and hence a further increase in specific volume would have been expected, if the test had not been stopped. To account for this, two arrows have been positioned next to these tests on Figure 5-8, showing that their true critical state position should be higher than their end of test points on the plot.

Figure 5-9 shows the same plot as Figure 5-8 with the addition of the two selected Critical State Lines, based on the amount of silt contained in the soil. These lines are trends for the behaviour of the soil at strains reaching critical state and shall be used for the data normalisation based on Equation 3-12 in Section 5.5. It should also be noted that a factor introducing scatter into this plot and hence an uncertainty to the exact location of the selected CSL is the potential error in the specific volume calculation. As was mentioned in Section 3.6, the accuracy of the initial specific volumes calculated is about ±0.02. Additionally, partial incompleteness of the tests as well as possible strain localisations could also be adding to the scatter seen on the diagram. Finally, the variability of the soil within each stratum is also contributing to the scatter seen in Figure 5-9, as that was seen in Figure 4-11 through the fines content variation with depth.

One could argue that at lower stresses, where the two CSLs have been presented with dotted lines, the two lines are not straight and are in fact curving towards the horizontal. Similar examples have been presented in Chapter 2 and can be found

in the literature. Typically, though, critical state lines for quartzitic sands have been shown to be non-linear at stress levels below about 100kPa (Verdugo & Ishihara, 1996) and in this case, the effective stresses are rather higher. It is possible that the two CSLs shown in Figure 5-9 are curving due to incomplete testing and strain localisations, as was suggested by Klotz & Coop (2002). As was discussed above, tests RS18 and RS19 were certainly still dilating when the experiments were discontinued. Since no concrete proof for a curved set of critical state lines can be found in the case of Thanet sand, either for the high silt content or low silt content, they will be considered to be straight. To indicate the uncertainty, a question mark has been placed next to the CSLs for stresses lower than 1,000kPa in Figure 5-9. For the high stress region, the straightness of both CSLs is in agreement with what was seen in Figure 2-2. The maximum pressures that have been used in testing Thanet sand throughout this project are too low to reach the high pressure curving zone of the CSL, as shown in Figure 2-11. Additionally it must be noted that, between the two Thanet sand subdivisions based on silt, the more well-graded soil gives a lower CSL (Figure 5-9). This is in agreement with what would be expected based on what was seen in the literature (Section 2.3.1) (Coop & Atkinson, 1993).

As it has been established that the silt content within the soil has an effect on the behaviour, the comparison for the effect of the specific site of origin of the soil tested will be split into two plots; one for the high silt content material (Figure 5-10) and one for the low silt content (Figure 5-11). In these two figures the test end-points have been grouped based on their site location, as shown in the legend. Unlike the silt content comparison, here no distinct pattern arises, so that the specific site a sample comes from has no clear impact on its Critical State Line. This implies that the two Thanet sand strata are, in relative terms, uniform within the area covered by the various sites. Alternatively, the available data could simply not be sufficient, in either quality or quantity for a distinction to be made.

Finally, the last two plots of test end-points in v-lnp' space are shown in Figure 5-12 and Figure 5-13. Here, the data have been grouped based on the initial condition of the soil sample at the beginning of the test, being either intact or reconstituted. Also, a distinction has been made for the intact samples based on

their sampling method as discussed in Section 5.1. Diamonds indicate intact samples extracted via rotary coring, squares block samples and stars reconstituted samples. Figure 5-12 shows the high silt content tests and Figure 5-13 the low silt content tests. Neither of these two figures indicates any effect of any possible soil structure on its critical state. As will be shown in Sections 5.4.2 and 5.6, whatever differences in structure and in sampling method might initially exist, a sample having undergone shearing to large strains would have been so disturbed that having been initially intact or reconstituted would be unlikely to have an effect on the final critical state behaviour. However, for a cemented quartz sandstone, Cuccovillo & Coop (1999) found that the Critical State Lines of the intact and reconstituted samples were distinctly different, as discussed in Section 2.3.2.

Another means of examining the data is to move from the v-lnp' plane into logq-logp' space. Having both x and y axes on a log scale allows the results of all the triaxial compression tests to be compiled into the same plot, regardless of the initial effective confining pressure of the test. This means that by choosing log scales for both axes, a 125kPa test can be presented on the same graph as a 12MPa test.

In Figure 5-14 all the test end-points have been grouped based on the silt content of the samples tested. A well defined linear band can be seen for all tests. In contrast to v-logp' space, the amount of silt does not appear to have an effect on the Critical State Line of Thanet sand in q-p' space. The Glauconite also appears to have no effect. Figure 5-15 shows the same plot, but in this case the data have been grouped based on the site each sample came from. Again, the same linear band can be observed without a particular pattern arising. Finally, Figure 5-16 shows the data grouped based on the type of sample tested. Again, the end-points lie on the same line regardless of sample type or sampling method.

Figure 5-17 shows the same set of data as before with the addition of the CSL from all tests based on an average value of M=1.3, which corresponds to a $\phi'_{cs}$. of $32.3^0$

## 5.4 *Stress – Strain Behaviour*

In order to assess the influence of each of the factors on the shearing behaviour of the soil, the three main plots of stress-ratio versus external axial strain, volumetric strain versus external axial strain and stress-dilatancy are presented for each comparison. When a pair of tests is compared one must remember that both tests were performed under the same initial effective cell pressure. In some volumetric strain-axial strain diagrams, a 1 to 1 Cartesian system has not been used and the volumetric scale has been exaggerated for the purposes of clarity.

### 5.4.1 *Silt content effect*

To examine the effect that silt content has on the shearing behaviour of Thanet sand, two pairs of tests are presented; one pair of high and low silt content samples that are initially intact and one pair of reconstituted samples.

Figure 5-18 and Figure 5-19 show the stress-strain and volumetric strain plots for the intact pair sheared in drained compression at an initial mean effective stress of 4MPa. The low silt content sample reaches a higher stress ratio than the high silt content sample at the beginning and middle of the test, giving though a similar ratio at the end of shearing. Additionally, it is evident that RS1 (low silt content) compresses far less during shearing than RS5 (high silt content) even if RS1 has a slightly higher initial voids ratio (Table 4-1). In their comparison of stress-dilatancy, Figure 5-20 shows both tests have a large scatter of data points at lower stress ratios as expected, but as the stresses become higher, both tests form two coinciding lines with a projected intercept at q/p' again of 1.3. It must be noted that it is not known why RS1 had a reducing stress-ratio towards the end of the test as it does not correspond to a reduction of dilation rate, as seen in Figure 5-20.

Figure 5-21 and Figure 5-22 show the stress-strain and volumetric strain data for the two reconstituted samples used for this comparison sheared in drained

compression at initial mean effective stress of 4MPa. The specific volumes of experiments RS2 and RS9 presented here prior to shearing were almost identical (1.645 and 1.679 respectively), excluding any possible effect a difference in specific volumes might introduce. Just as before, the low silt content sample appears initially to reach a higher stress ratio than the high silt content sample, while giving the same stress ratio at the end of the test. The low silt content test again gives less than half the compressive volumetric strain of the high silt content test. This is because the CSL for the high silt content sand is lower in the v:lnp' plane and therefore the soil has to compress more to reach it. In terms of stress-dilatancy, Figure 5-23 shows both high and low silt samples again form the same line at higher stress-ratios with an intercept of about 1.30. As explained in Section 3.6, the rate of dilation $d\varepsilon_v / d\varepsilon_s$ was calculated by a simple 30 point linear regression through volumetric strain and shear strain data at higher stress ratios and by linear regressions that reached up to 250 points at low stress ratios, in order to avoid excessive scatter because of the very large number of data points taken at small strains.

By combining both pairs, one can see that, in terms of stresses, in both cases high and low silt content samples appear to reach the same stress ratio at the end of shearing, with the high silt content samples giving significantly higher compressive volumetric strains than the low silt content. This agrees with the conclusion of Section 5.3, where in v-logp' space, the silt content had a distinguishable effect on the location of the CSL, whereas in q-p' space it was not possible to observe any difference between high silt and low silt content tests. The more compressive behaviour of the high silt content Thanet sand may be caused by the lower location of the its CSL. To distinguish the effects though, samples with the same initial state parameters should be compared. Unfortunately though, this was not possible as not sufficient high and low silt content experiments existed at the same initial state parameters to form a full comparison group.

### 5.4.2 *Intact – reconstituted effect*

By comparing tests from two samples, one intact and the other reconstituted, it is possible to quantify the effect of structure, if any, on the large strain behaviour of Thanet sand. To make a valid comparison, three pairs of tests are presented; one from a rotary cored high silt content material, one rotary cored low silt content material, as well as a pair from the high silt content soil extracted as a block sample. It has been attempted, not always with complete success, not to vary any other parameters of the two samples being compared, such as the stress-path, stress level or the initial void ratio, so that whatever differences in behaviour that can be observed from the plots presented are solely due to the structure of the material.

Stress-strain and volumetric strain data for experiments RS5 and RS9 are presented in Figure 5-24 and Figure 5-25. This is a pair of high silt content rotary cored and reconstituted samples sheared drained at the same initial effective confining stress of 4MPa. As can be seen from the plots, the intact sample seems to gain in strength faster than the reconstituted sample, while the latter reaches a slightly higher stress ratio at the end of the test although, as will be shown in Figure 5-29 and in Figure 5-32 there is no consistent difference between M for the intact and reconstituted samples. Additionally, the intact sample seems to be compressing less during shearing than the reconstituted. This must be due to the higher initial void ratio of the reconstituted sample RS9 of 0.83 upon setup compared to 0.68 for the intact sample RS5 because it was shown in Figure 5-12 that there is no difference in the v-lnp' plane in the location of the CSL of the intact & reconstituted samples. The stress-dilatancy comparison for the two tests is presented in Figure 5-26. Both intact and reconstituted samples form similar lines at higher stress ratios that give intercepts of 1.3 and 1.4 respectively, although as discussed above, this is not a consistent difference between intact and reconstituted samples. Since the stress-dilatancy data for the intact and reconstituted are similar, the higher mobilised stress ratio at the start of the test for

the intact sample may simply correspond to the lower rate of compression and hence to the lower initial void ratio.

Moving from high silt content cored samples to high silt content block samples, experiments CTRL17 and CTRL16 are a pair of intact and reconstituted tests, sheared drained at an initial effective confining stress of 3MPa. The shearing data are presented in Figure 5-27 and Figure 5-28. Here, the intact sample CTRL17 again develops a higher stress ratio and is stiffer compared to the reconstituted sample CTRL16 until about 15% axial strain. From that point onwards, both tests appear to coincide, until the end of shearing. From the volumetric strain behaviour, the reconstituted sample compresses slightly more than the intact sample but again, this is due to its higher initial void ratio upon setup which was 0.94 compared to 0.74 for the intact sample. In Figure 5-29, the stress-dilatancy data for both tests form the same line at higher stress-ratios which, if extended, again gives an intercept of about 1.3. This indicates that the stiffer initial behaviour of the intact sample may simply again be the result of the fact that it is denser. When looking at the stress-dilatancy data in Figure 5-29 the delayed dilation seen in CTRL17 can at first suggest the presence of structure, as discussed in Section 2.3.2. This though will be shown at a later stage of the Thesis not to be repeated in any of the other experiments performed on intact block samples of Thanet sand (Figure 5-60) and is therefore probably attributed to a disturbance during the shearing of the sample and not on the effect of structure.

The final pair of tests compared to determine the effect of structure consists of experiments RS1 and RS2, a low silt content cored sample and the corresponding reconstituted sample respectively. These were sheared in drained compression at an initial mean effective confinement of 4MPa. In Figure 5-30, the stress ratio versus strain plots are presented. The intact and reconstituted samples seem to have little difference in behaviour. RS1 seems again initially to be marginally stiffer than RS2, but as the shearing continues, RS2 gains more strength and the situation is reversed with the reconstituted sample giving a slightly higher stress ratio at the end of shearing. Figure 5-31 shows the volumetric strain plots for these two experiments. Here, just as in the two previous cases, the intact sample compresses less during shearing than its reconstituted counterpart. In this case

though, the reconstituted sample (e=0.70) was setup with almost exactly the same initial void ratio as the intact sample (e=0.71). Therefore, the larger volumetric strains the reconstituted sample developed during shearing cannot be attributed to an initial void ratio difference, although it was shown earlier (Figure 5-13) that there is no consistent difference in the CSL location for the low silt content soil detween intact and reconstituted samples. Finally, Figure 5-32 shows the stress-dilatancy relationships for the two experiments. Both RS1 and RS2 form straight lines at higher stress-ratios that almost coincide, giving intercepts again of approximately 1.30.

Bringing the results of all three pairs of tests together, it can be seen that the higher volumetric strains developed by the reconstituted samples tested are partially governed by their higher initial void ratios upon setup, with the exception of the last pair that was examined (RS1 & RS2). As for stress-dilatancy behaviour of the soil, all test pairs gave similar lines with y-axis intercepts of approximately 1.3, so that the higher initial stiffnesses of the intact samples is perhaps to some extent the result of their being denser although the comparison of RS1 and RS2 at the same initial e does suggest that structure increases the stiffness. When comparing the stress-dilatancy behaviour seen here to what was presented in Section 2.3.2 by Cuccovillo & Coop (1999) and Cresswell and Powrie (2004) (Figure 2-34, Figure 2-36 & Figure 2-37) the behaviour of Thanet sand does not resemble the behaviour observed by either the cemented or the locked sands. Instead, in terms of stress-dilatancy, Thanet sand appears to behave more like a reconstituted soil, as the intact samples presented in this chapter do not show any delayed dilation effects, with the exception of experiment CTRL17 discussed previously. Therefore, it can be concluded that, Thanet sand does not have a locked fabric, which was expected from the analysis of the thin sections in Section 4.2 (Figure 4-15 & Figure 4-16) and from the fact that Thanet sand has a relatively high void ratio for its age, as discussed in Section 2.3.2 (Figure 2-28). However, the slightly stiffer stress:strain behaviour may be an indication of some effect of structure.

### 5.4.3 *Glauconite effect*

As mentioned in Section 4.2, Glauconite-free material was tested in order to allow the effect of Glauconite, if any, to be quantified. Figure 5-33 shows the stress-strain results from two high silt content reconstituted samples, both sheared at an initial effective confining stress of 4MPa. RS9 was a normal high silt content reconstituted sample whereas RS10 is one of the two samples that were created from Glauconite-free high silt content Thanet sand. The Glauconite-free soil appears to be slightly stiffer at first, giving though a marginally lower stress ratio at strains greater than 15%. For the volumetric strain behaviour, it can be seen in Figure 5-34 that RS10, the sample formed without Glauconite compresses less than RS9. Finally, Figure 5-35 shows the stress-dilatancy plot for the two experiments in question. At higher stress-ratios, both RS9 and RS10 tend to define a similar line, whose intercept is again in the region of 1.30, with RS9 being slightly higher than RS10, although within the scatter of the data the difference does not appear significant. Neither of these differences are believed to be caused by the lack of Glauconite. Test RS9, the normal high silt content sample, had a larger specific volume than RS10 by about 0.1. This difference in initial specific volume is probably the reason for the slightly reduced compression of RS10 and its slightly stiffer behaviour. This is supported by Figure 5-10 and Figure 5-14 where it was shown that Glauconite neither affects the location of the CSL in v-lnp' plane, nor the critical state stress ratio M.

### 5.4.4 *Influence of effective confining stress*

The higher the initial effective confining stress on a tested sample, the more the sample will tend to compress during shearing. Peaks are expected to be seen at lower confining stresses, as increased pressure has a restraining effect on dilation. Figure 5-38 and Figure 5-39 show both the stress-ratio as well as volumetric strain plots for seven different experiments performed at a range of initial confining pressures. In general, the behaviour seen is as expected. For example, test RS2 at

4MPa compresses more and develops lower stress ratios than RS19 at 125kPa. The fact though that not all samples were set up at exactly the same initial specific volume adds some scatter when comparing tests at similar confining pressures. For example, RS17 at 550kPa and RS18 at 250kPa do not behave as expected. The lower confining pressure test, RS18 would have been expected to dilate more than RS17 and to show a higher stress-ratio peak than RS17, but the initial void ratio of RS18 was 0.81 and that of RS17 was 0.76. However, no matter what the initial effective confining stress is, all samples give approximately the same stress ratio of about 1.30 at the end of shearing. This can also be verified in the stress-dilatancy plot of Figure 5-40 where all experiments lie on a similar trend with an intercept of approximately 1.30. This is in agreement with what was presented in Section 5.3, where all test end-points lay on a single line in logq-logp' space with a gradient M of 1.30 (Figure 5-14 to Figure 5-16). Additionally, as mentioned in Section 2.3.1, there are some stress-dilatancy models such as that suggested by Yang and Li (2004) that consider a state dependant behaviour (Figure 2-24 & Figure 2-25). This is clearly not true for the case of Thanet sand as all experiments presented in Figure 5-40, Figure 5-43 and Figure 5-46 lie on a similar linear trend at higher stress ratios, and although there is some scatter, there is no correlation between the location of the relationship and stress level, initial void ratio at the start of shearing ($e_s$), nor state parameter ($\psi$).

When comparing pairs of intact and reconstituted samples in Section 5.4.2, it was difficult to understand to what extent the slightly stiffer behaviour of the intact samples was the result of small differences in initial specific volume and to what extent it was an effect of structure. Through more general comparisons for all the stress:strain data of intact and reconstituted samples for the high and low silt content at all stress levels (Figure 5-36 to Figure 5-46), it is evident that the intact samples tend to be slightly stiffer. This can be translated as an indication of an effect of structure.

### 5.4.5 *Influence of site location*

When the effect of the specific site a tested sample came from was examined in Section 5.3, it was not possible to distinguish any clear effect. The same is attempted here with the use of four intact sample tests, each one from a different site of origin. Two of the tests are of high silt content material whereas the other two are of low silt content material. Figure 5-47, Figure 5-48 and Figure 5-49 contain all the combined data for these tests. Unfortunately, because of other factors apart from the site location, such as silt content, effective confining stress and initial void ratio, it is not possible for clear conclusions to be made. What is clear though is that the two low silt content samples and the two high silt content samples have similar volumetric compression characteristics, as mentioned in Section 5.4.1. Also, all four tests tend towards the same stress-ratio at the end of shearing as can be seen in both Figure 5-47 and Figure 5-49.

## 5.5 *Normalised Stress Paths*

In order to normalise the stress path data, it is essential to know the location of either the Critical State Line or the Normal Compression Line, as shown in Figure 2-21. Considering that in order to obtain the location of the NCL a very high pressure isotropic compression beyond the pressure capacity of the apparatus available (see Section 3.2.1) would be necessary, the only alternative is to normalise based on the location of the CSL using Equation 3-12. The distinct Critical State Lines for both high and low silt content materials were derived as shown in Figure 5-9. All normalisations have been based on the selection of these two CSLs, assuming them to be straight over the range of stresses and void ratios investigated. The normalised data have been grouped according to the specific influence factor that is being examined. Based on Critical State theory, all experiments should converge on a point with coordinates (1,M), where M is the

stress-ratio at the critical state. Most experiments have been shown to converge to a stress ratio of around 1.3.

In Figure 5-50, the high silt content tests have been grouped based on whether the sample was initially intact or was setup reconstituted. Also, as shown on the legend, a distinction has been made between intact cored and block samples. All the paths do tend towards the point (1,1.3), but many of them do not actually reach that point. This corresponds to the scatter of data that was seen in Figure 5-8 and some results from incomplete testing and errors in the initial void ratio calculation. The paths for intact samples are steeper and form sharper corners as $p'/p'_{cs}$ reduces compared to the paths for reconstituted samples, again perhaps an indication of some influence of structure.

In Figure 5-51, only the high silt content intact samples are presented. It is not possible to see any consistent difference between the block and rotary cored samples.

Figure 5-52 presents a comparison of the low silt content intact and reconstituted samples. Just as in the case of the high silt content tests, all stress-paths converge towards the vicinity of (1,1.3), with the paths for intact samples being again steeper and forming sharper corners compared to the paths for reconstituted samples, again an indication of an effect of structure.

Figure 5-53 presents all the high silt content experiments in normalised stress space, with the two Glauconite-free tests highlighted. The lack of Glauconite of these samples again does not give rise to a different behaviour.

All high silt content and all low silt content experiments are grouped by site in Figure 5-54 and Figure 5-55 respectively. Apart from the effect of sample type highlighted above, no distinguishable pattern can be observed from these two plots. Combining what can be seen here with the discussion in Sections 5.3 and 5.4.5, it can be said that the specific site a sample came from has no effect on the behaviour. In other words, Thanet sand can be considered to be relatively uniform, within the area marked by the four sites the samples were extracted

from, although there may well be significant variation within the two sub-strata identified.

Finally, Figure 5-56 contains all experiments, grouped based on the silt content of the samples. The high silt content tests extend more towards the right hand side of the plot up to values of $p'/p'_{cs}$ of 3.5, whereas the low silt content tests appear to be more closely concentrated around the central part of the plot. This results from the fact that the high silt content CSL lies lower in the v:lnp' plane giving higher $p'/p'_{cs}$ values within the pressure capacity of the apparatus used. Within this capacity, it is not possible to reach the NCL for either soil. Otherwise, there is little difference in the normalised stress paths or the shape of the state boundary surface for high and low silt content strata. The state boundary surface has been highlighted on Figure 5-57. The CSL is not located at the apex of the plot. A similar pattern was previously seen by Coop & Lee (1993) for various different reconstituted sands (Figure 2-22), although for Thanet sand the tendency for the CSL not to lie at the apex of the state boundary surface is perhaps more pronounced than for other sands.

## 5.6 *Influence Of Anisotropy*

In order to assess the anisotropy of Thanet sand, a block sample was used to cut samples in all three principal directions, as shown in Figure 3-31. Groups of samples were in turn tested in drained and undrained compression as well as drained extension for the anisotropy of the material to be examined.

### 5.6.1 *Drained compression tests*

Results from the four samples that were tested in drained compression at an initial effective confining stress of 550kPa are presented in Figure 5-58, Figure 5-59 and Figure 5-60. As indicated on the legend, there are three intact samples, one vertical and two horizontal as well as a reconstituted sample. All the intact

samples were from the same block, having almost identical initial void ratios of about 0.80 (see Table 4-1). The reconstituted sample was set-up at a higher void ratio of 0.94, hence resulting in larger volumetric strains during shearing, as well as a softer stress:strain curve. The two intact horizontal samples seem to have a very similar behaviour. On the other hand, there is a significant difference between the vertical and the two horizontal samples, both in terms of stress:strain behaviour as well as volumetric strains. The vertical sample shows a peak in terms of stress-ratio, but as the shearing continues, it converges with the other samples to the same stress ratio at the end of shearing. This can also be seen on the stress-dilatancy plot where all four tests form a straight line that crosses the q/p' axis again at approximately 1.3.

### *5.6.2 Undrained compression tests*

To complement the drained experiments that were performed, a set of four undrained tests was also conducted at an initial effective confining stress of 400kPa; one for each sample direction as well as one reconstituted sample. The results are presented in Figure 5-61 and Figure 5-62. Just as before, the reconstituted sample has a higher $e_o$ (0.985) and is therefore less stiff than the three intact samples, giving though the same final stress ratio, while being the only experiment generating positive changes in pore pressure. The vertical sample, when compared with the two horizontal samples, again develops a higher peak stress-ratio. Looking more closely at Figure 5-62, it is clear that the two horizontal samples behave in a similar fashion, changing from compression into dilation at exactly the same phase transformation point. This can be seen more clearly in Figure 5-63 where the effective stress-paths have been plotted for all these tests for compression, both drained as well as undrained. It is clear that the two undrained horizontal tests (CTRL14 and CTRL15) have the same phase transformation point, whereas the phase transformation point of the vertical sample (CTRL12) lies at lower p' values. The difference between the vertical and horizontal stress-paths suggests a higher horizontal stiffness. This is indeed the case and shall be discussed in greater detail in Section 6.3.5.

### 5.6.3 *Drained extension tests*

So that the assessment of Thanet sand anisotropy was complete, two intact samples were sheared in extension; one vertical and one horizontal. The stress ratio versus external axial strain data for the two tests are shown in Figure 5-64 and Figure 5-65 shows the same plot based on the internal strain readings. In contrast to the compression tests, both vertical and horizontal samples seem to have the same peak stress ratios of about 0.85. The principle difference between the two is that the horizontal sample CTRL11 is much stiffer. Figure 5-66 shows the volumetric strain data for the two experiments. Finally, the mobilised angle of shearing resistance for both experiments is shown in Figure 5-67 where, as expected from the stress-ratio plot, both horizontal and vertical samples give approximately the same a peak angle of about $29^0$ - $30^0$.

### 5.6.4 *Overview*

From what can be seen from the two sets of compression tests, the behaviour of the two horizontal samples seems to be very similar. On the other hand, the vertical and horizontal samples do show differences in peak stress-ratio, and phase transformation points (effects of α, Figure 2-58). This is indicating a cross-anisotropic soil behaviour. In terms of critical state stress ratios though, all compression tests define a unique stress ratio of approximately 1.3. This corresponds to an angle of shearing resistance at critical state ($\phi'_{cs}$) of about $32.3^0$ (Equation 3-14). The extension tests on the other hand gave a final stress-ratio prior to necking of approximately 0.85 that based on Equation 3-15 and corresponds to a peak angle of shearing resistance of $29.9^0$. The critical state φ' could not be measured in extension due to necking.

If a vertical sample sheared in triaxial compression (α=0 & b=0) is compared with a horizontal sample sheared in triaxial extension (α=0 & b=1), the effect of the

intermediate stress factor "b" can be assessed, as shown in Figure 2-58. The two experiments give different values of q/p' at both the peaks and the end of the tests, which in turn correspond to different angles of shearing resistance, with the sample sheared in compression giving higher values. In other words, b = 0 gives a higher $\phi'$ than b = 1. A comparison between the horizontal samples sheared in compression ($\alpha = 90^0$, b=0) with the vertical sample in extension ($\alpha = 90^0$, b=1) also shows that $\phi'$ is reduced for b=1. The horizontal samples had no peak $\phi'$ but $\phi'_{cs}$ was greater than $\phi'_{peak}$ in extension for the vertical sample.

In contrast, "α" has an effect on the peak angle of shearing resistance as shown by the drained compression tests on vertical and horizontal samples and also by the corresponding undrained tests with α=0 giving higher values of $\phi'_{peak}$ compared to $\alpha=90^0$. However, α has no effect on the $\phi'_{cs}$ as can be seen for both drained and undrained tests. It might be expected that α would only affect the peak strength as anisotropy would be less likely to influence the critical state because of the large strains involved. In contrast, the effect of b is not dependant on strain.

Another major factor that influences $\phi'_{peak}$ apart from anisotropy is the state parameter "ψ". However, all tests used in these comparisons had the same initial void ratio as well as similar p' values at failure, so the state parameters should be similar.

For better understanding, all the tests presented in Section 5.6 have summarised in Table 5-1. Finally, the effective stress-paths for all anisotropy experiments, both in compression as well as in extension, have been plotted in Figure 5-68 where the Critical State Line for compression can again be seen.

## 5.7 *Particle Breakage*

The particle breakage of the soil was not considered to be a dominant factor of its behaviour, considering that the pressures the samples were subjected to were far below its gross-yielding point in compression. Nevertheless, the Relative Breakage factors "Br" for two experiments (RS1 and RS5), isotropically compressed and sheared at an initial effective confining pressure of 4MPa, have been calculated. The definition of "Br" as given by Hardin was presented in Figure 2-59.

Figure 5-69 shows the two particle size distribution curves of the high silt content Thanet sand obtained from River Side. The initial curve corresponds to that of the natural high silt content soil and was taken from trimmings of the soil sample during sample preparation whereas the second curve is for test RS5 after shearing. The Relative Breakage factor "Br" as defined by Hardin obtained from the difference of these two plots is approximately 0.17.

Figure 5-70 presents two particle distribution curves of low silt content Thanet sand again obtained from River Side. Again, one curve corresponds to the natural low silt content soil taken from trimmings, whereas the second curve corresponds to sample RS1 after shearing to failure. In this case, the Relative Breakage factor "Br" obtained from these two plots is approximately 0.10.

From Figure 2-61 the Br of Ham River sand at the final p' of these tests, which was about 7MPa, is approximately 0.2. When comparing Br factors obtained for Thanet sand with Ham River sand which is again a quartzitic sand, there is a closer agreement of breakage factors with the high silt content material than the low silt content Thanet sand. It is perhaps unusual that the high silt content Thanet sand produces a higher Relative Particle Breakage factor compared to the low silt content Thanet sand. What might have been expected is in fact the reverse, with the high silt content producing lower levels of breakage due to the fact that the

presence of finer particles should lead to lower inter-particle stresses and hence lower breakage within the soil.

## 5.8 *Pile And Pressuremeter Test Data*

Apart from the laboratory experiments that were performed, a limited but yet important set of in-situ test data was available for analysis. This includes a set of trial-pile test data, as shown in Figure 4-3 as well as a few pressuremeter limit pressure results, as shown in Figure 4-5. This information was obtained from existing reports and the data have been analysed using a state parameter approach similar to Klotz and Coop (2001).

Figure 5-71 shows the pile end bearing capacities for the in-situ tests in Thanet sand, along with the capacity relationships of two other sands determined from centrifuge tests for Klotz and Coop. For the end bearing capacities shown in Figure 4-3 to be analysed, apart from the in-situ stress-states at the pile base, the normalising stress $p'_{cs}$ was also needed. As $p'_{cs}$ is not only void ratio but critical state line dependent as well, Thanet sand was devied into two sub-strata based on silt content. Additionally, as the exact specific volume of Thanet sand at the pile base was also not known, two average void ratios were used; one based on the intact high silt content samples tested in this project and one based on the intact low silt content samples tested. This assumption, along with unit weights and $K_0$ factor that were given by ARUP (Figure 3-32) allowed the pile end bearing capacities to be plotted in terms of $p'/p'_{cs}$, where p' is the in-situ effective stress at the pile tip. In Figure 5-71 the data for the in-situ tests in Thanet sand have been compared with the trends proposed by Klotz & Coop (2001) for their centrifuge tests. This relationship shows that different end bearing capacities of the two strata are primarily related to their different state parameters. The Thanet sand data look similar to Dogs Bay sand trend. This is coincidence as the Thanet sand data were for full scale bored pile tests whereas the Dogs Bay sand data were for

small scale centrifuge model piles that were driven instead of being bored. Additionally, one must also take into account that Ham River sand is a carbonate sand whereas Thanet sand is a quartzitic sand. However, the trend of decreasing normalised capacity with increasing $p'/p'_{cs}$ is similar.

Figure 5-72 shows the relationship between self boaring pressuremeter limit pressures normalised by the vertical effective stress and $p'/p'_{cs}$. Once again, the Thanet sand behaviour appears to be directly influenced by the amount of fines contained, with the four limit pressures tending towards the creation of two distinct groups, one for high silt content and one for low silt content sand but again indicating that it is the different states of the two soils relative to their different CSLs that gives the different limit pressures. The normalised limit pressure also decreases with increasing $p'/p'_{cs}$ similar to the pile end bearing capacity.

| *Test* | *Sample Type* | *Test Type* | $\alpha$ | $b$ | $\left(q/p'\right)_{Peak}$ | $M$ | $\varphi'_p$ | $\varphi'_{CS}$ |
|---|---|---|---|---|---|---|---|---|
| CTRL4 | Intact | Vertical - DC | 0 | 0 | 1.38 | 1.3 | $34.1^0$ | $32.3^0$ |
| CTRL5 | Intact | Horizontal - DC | $90^0$ | 0 | - | 1.3 | - | $32.3^0$ |
| CTRL6 | Intact | Horizontal - DC | $90^0$ | 0 | - | 1.3 | - | $32.3^0$ |
| CTRL7 | Reconstituted | DC | n/a | 0 | - | 1.3 | - | $32.3^0$ |
| CTRL12 | Intact | Vertical - UDC | 0 | 0 | 1.58 | 1.3 | $38.7^0$ | $32.3^0$ |
| CTRL13 | Reconstituted | UDC | n/a | 0 | - | 1.3 | - | $32.3^0$ |
| CTRL14 | Intact | Horizontal - UDC | $90^0$ | 0 | - | 1.3 | - | $32.3^0$ |
| CTRL15 | Intact | Horizontal - UDC | $90^0$ | 0 | 1.39 | 1.3 | - | $32.3^0$ |
| CTRL10 | Intact | Vertical - DEX | $90^0$ | 1 | -0.85 | ? | $29.9^0$ | ? |
| CTRL11 | Intact | Horizontal - DEX | 0 | 1 | -0.85 | ? | $29.9^0$ | ? |

***Table 5-1*** *Summary table of anisotropy influence*

**DC**: Drained shearing in Compression
**UDC**: Undrained shearing in Compression
**DEX**: Drained shearing in Extension

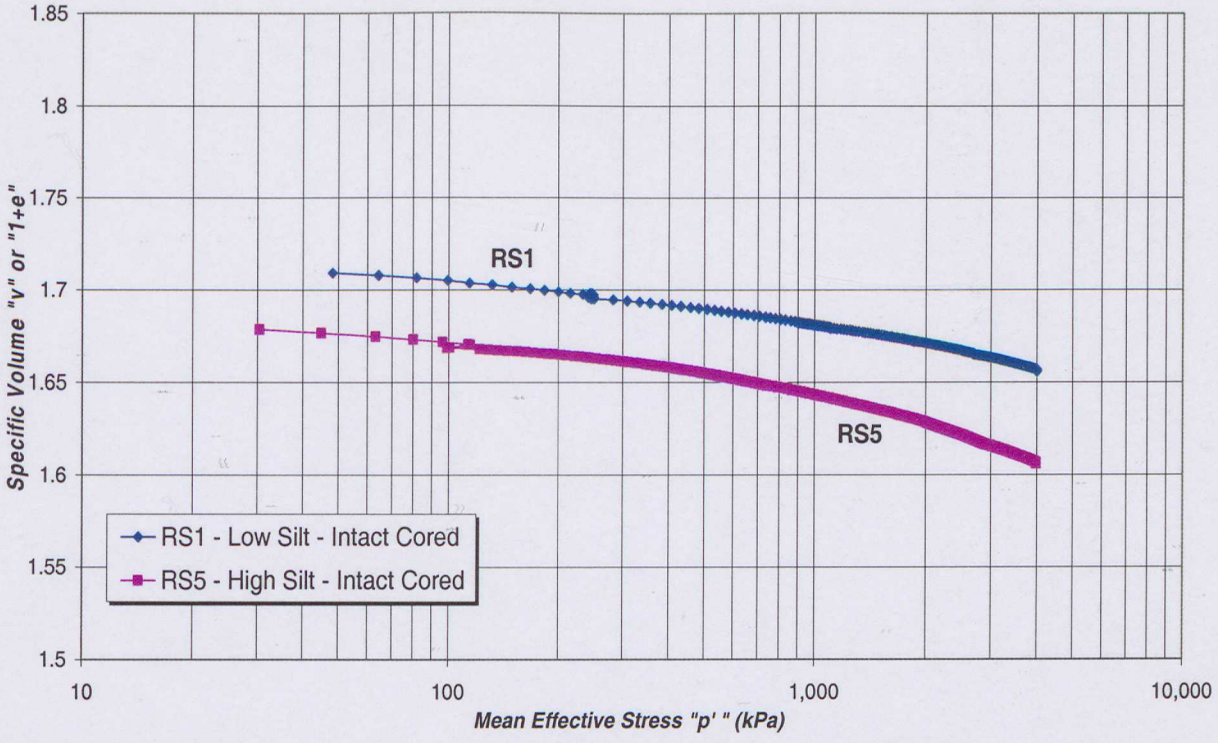


***Figure 5-1*** *High/low silt content comparison for isotropic compression of the intact material*

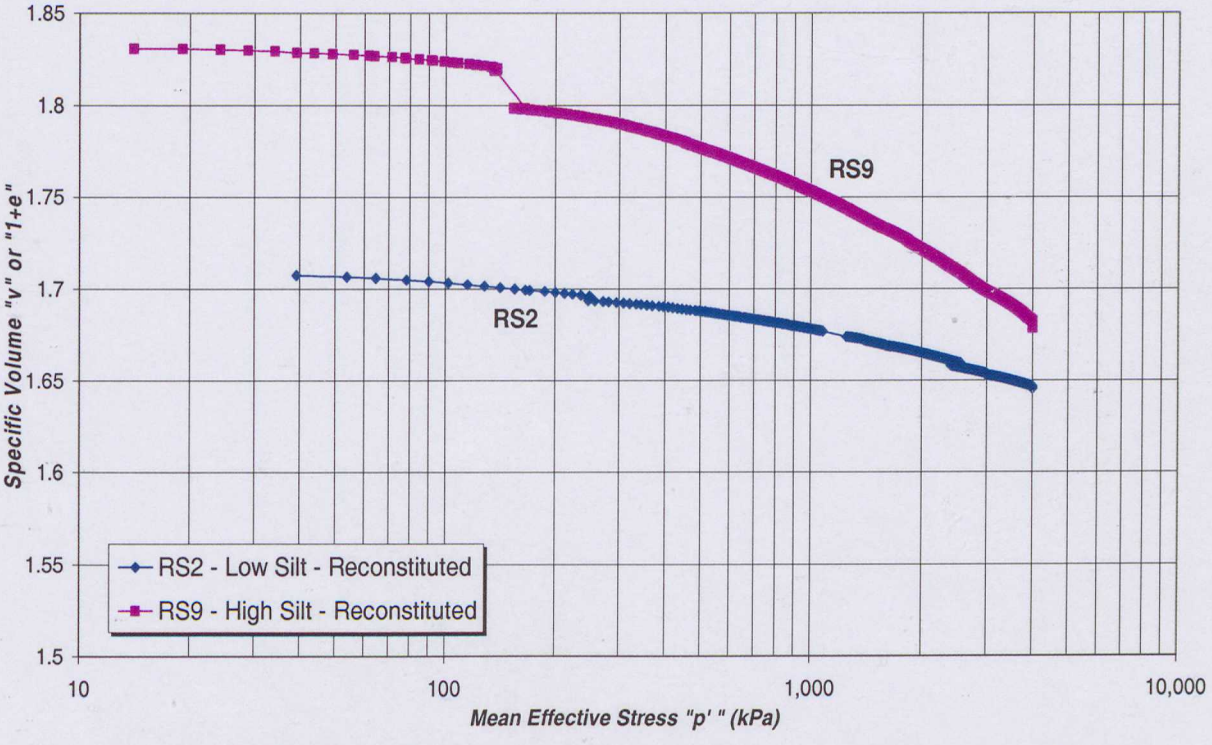


***Figure 5-2*** *High/low silt content comparison for isotropic compression of the reconstituted material*

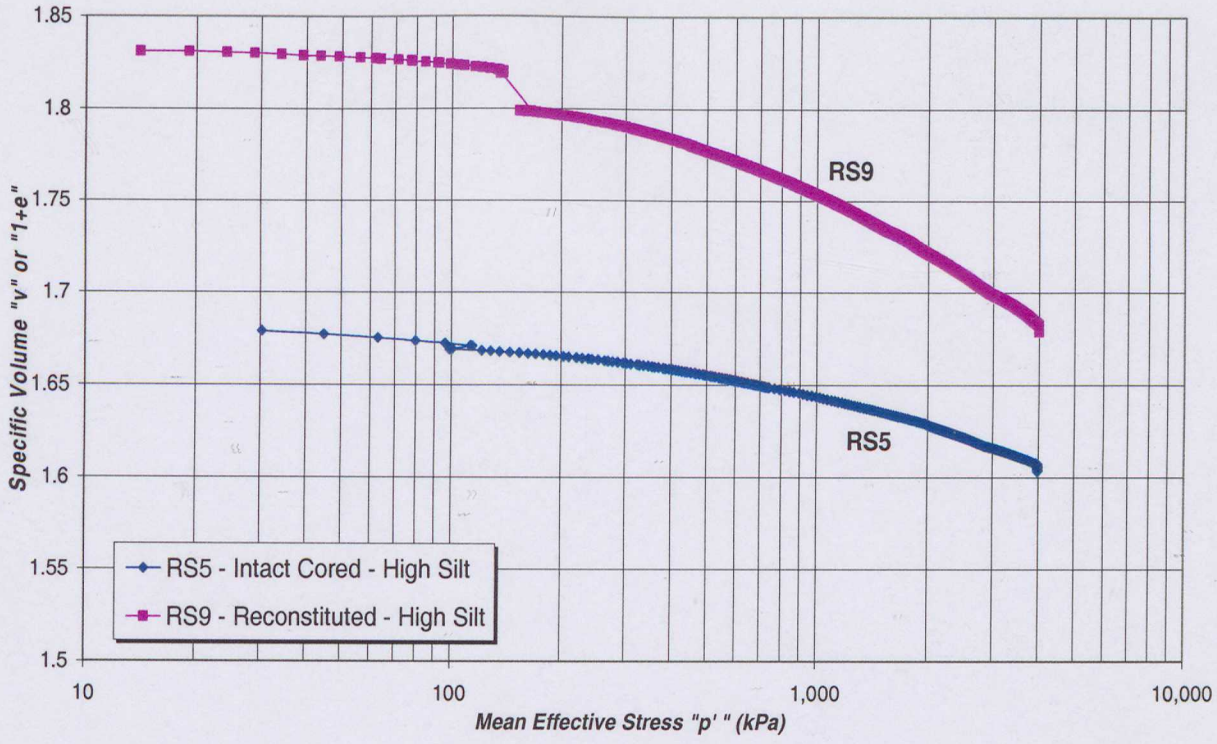


***Figure 5-3*** *Sample type comparison for isotropic compression of high silt content material (rotary cored sample from River Side)*

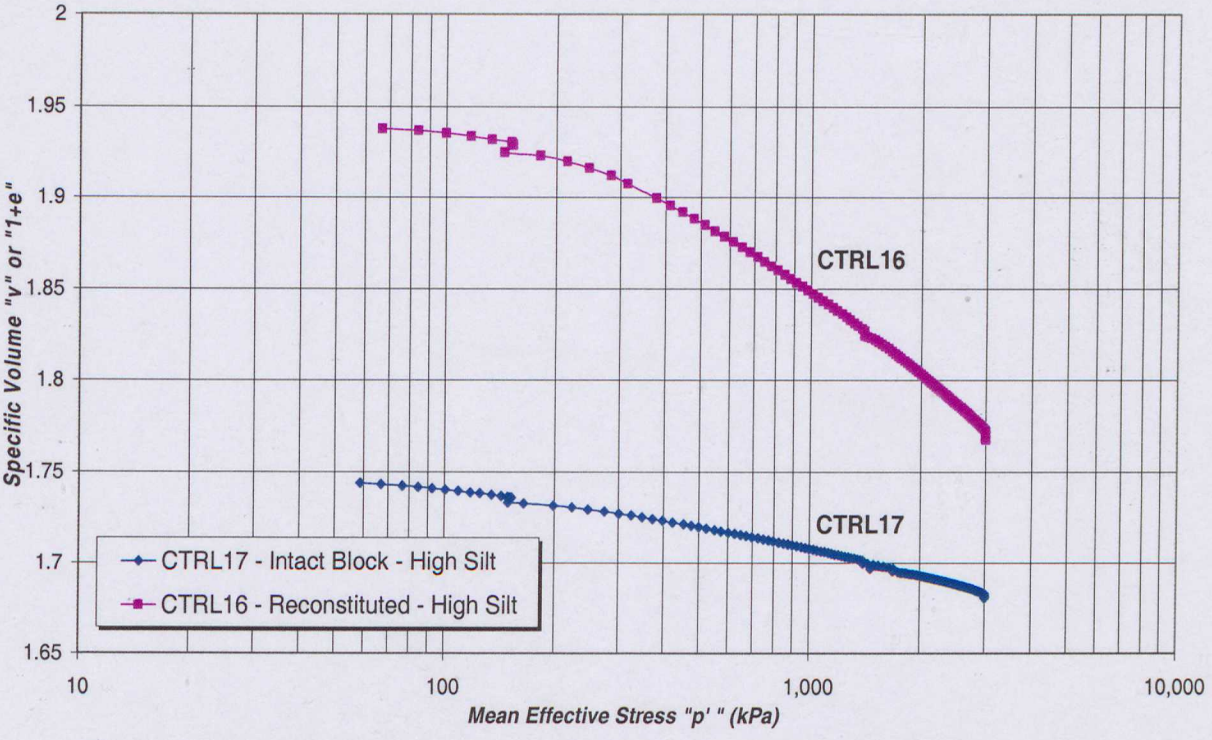


***Figure 5-4*** *Sample type comparison for isotropic compression of high silt content material (block sample from CTRL Stratford)*

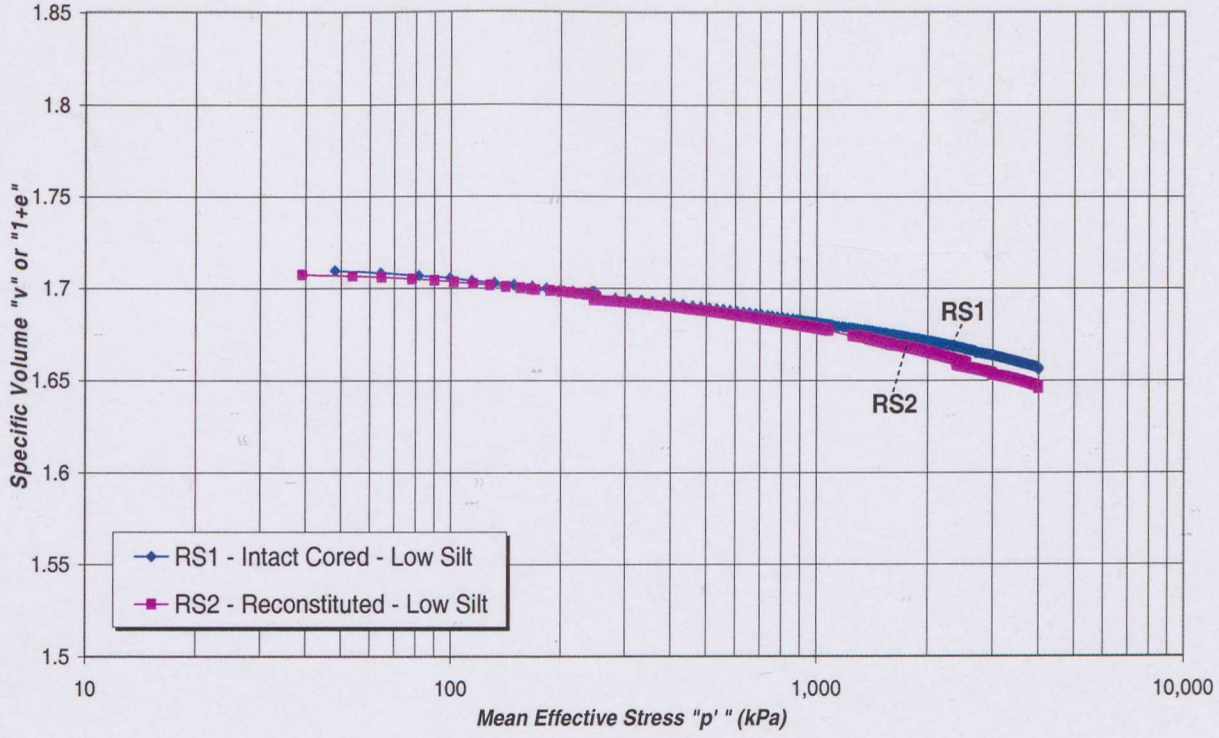


***Figure 5-5*** *Sample type comparison for isotropic compression of low silt content material (rotary cored sample from River Side)*

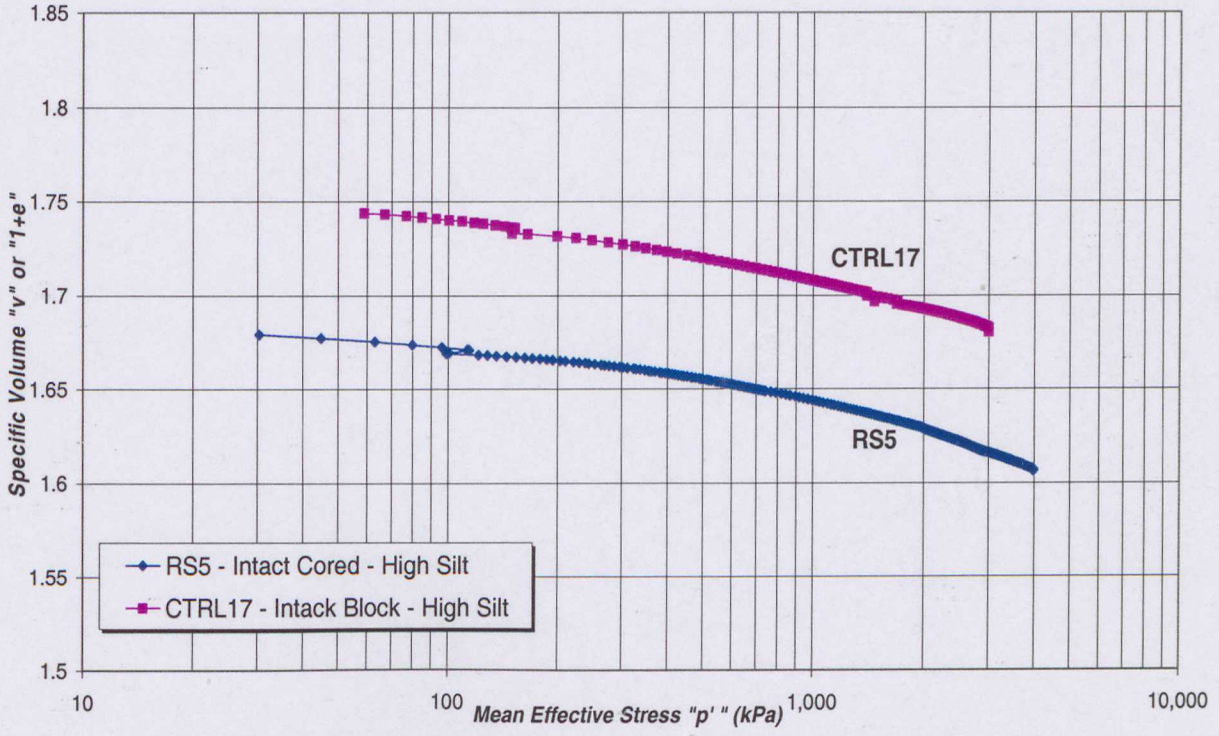


***Figure 5-6*** *Effect of sampling method on isotropic compression of high silt content material*

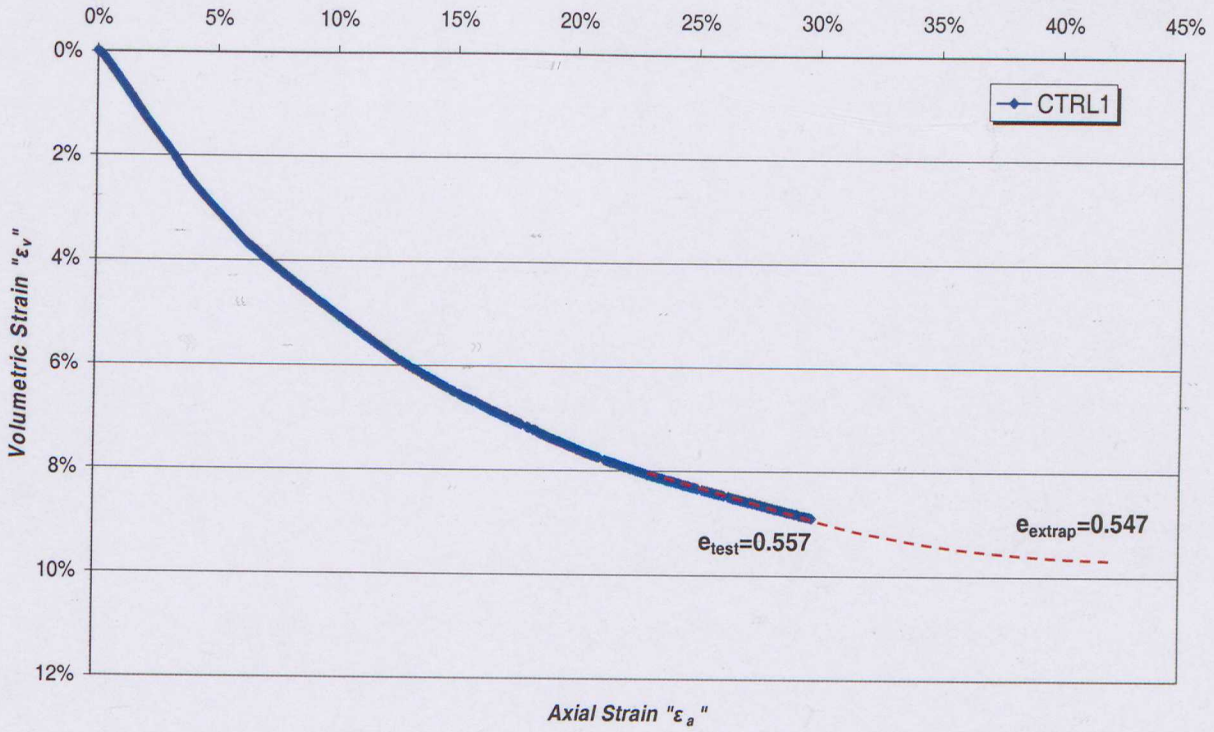


***Figure 5-7*** *Extrapolation of volumetric strains to a Critical State for test CTRL1*

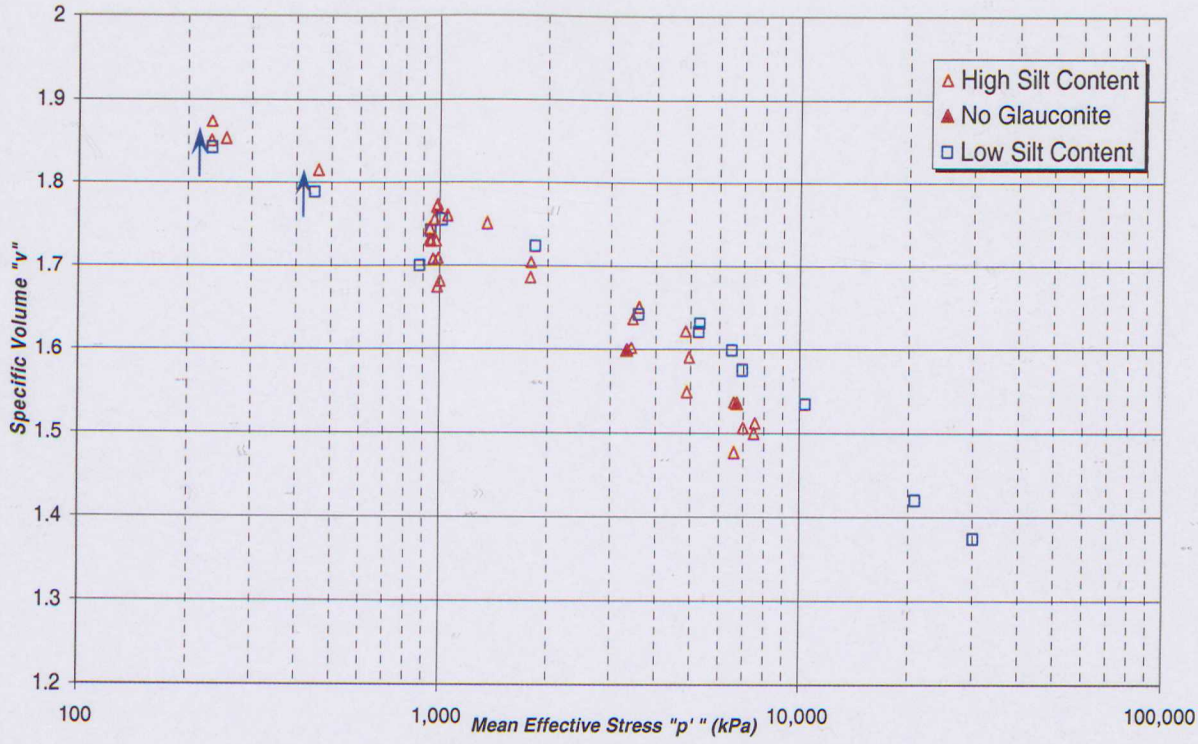


*Figure 5-8 Critical States – high/low silt content comparison*

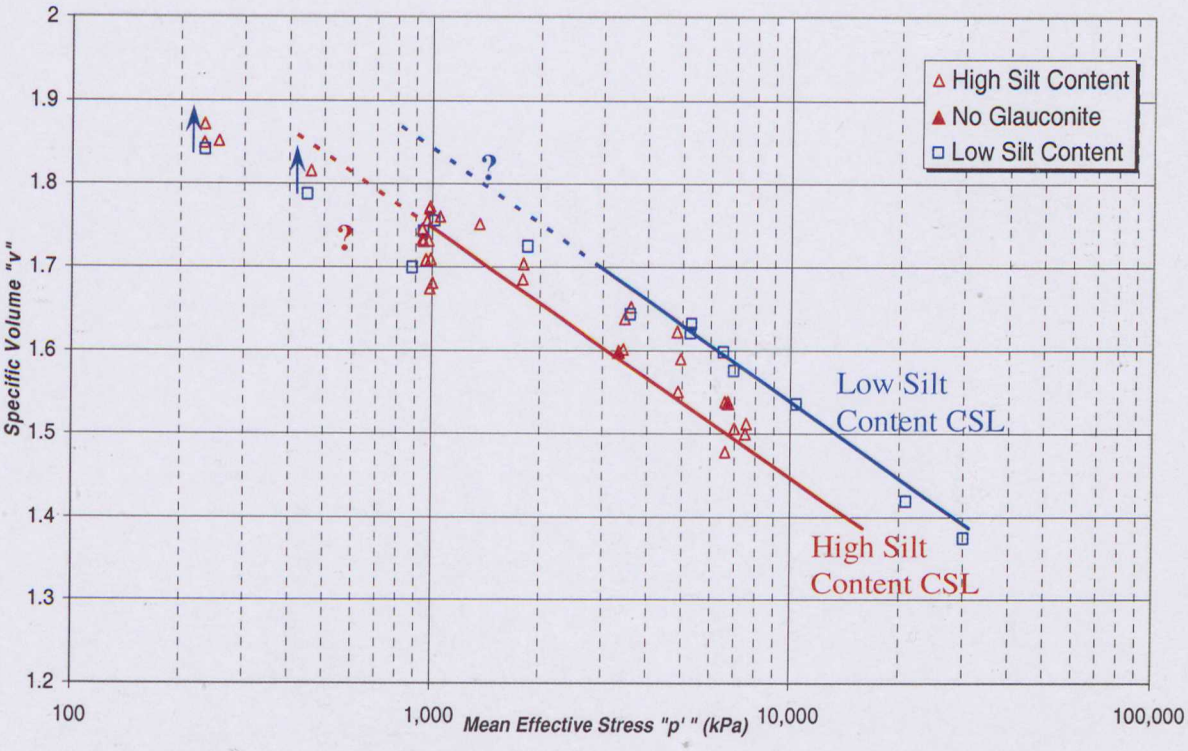


*Figure 5-9 Identification of critical state lines for high and low silt content material*

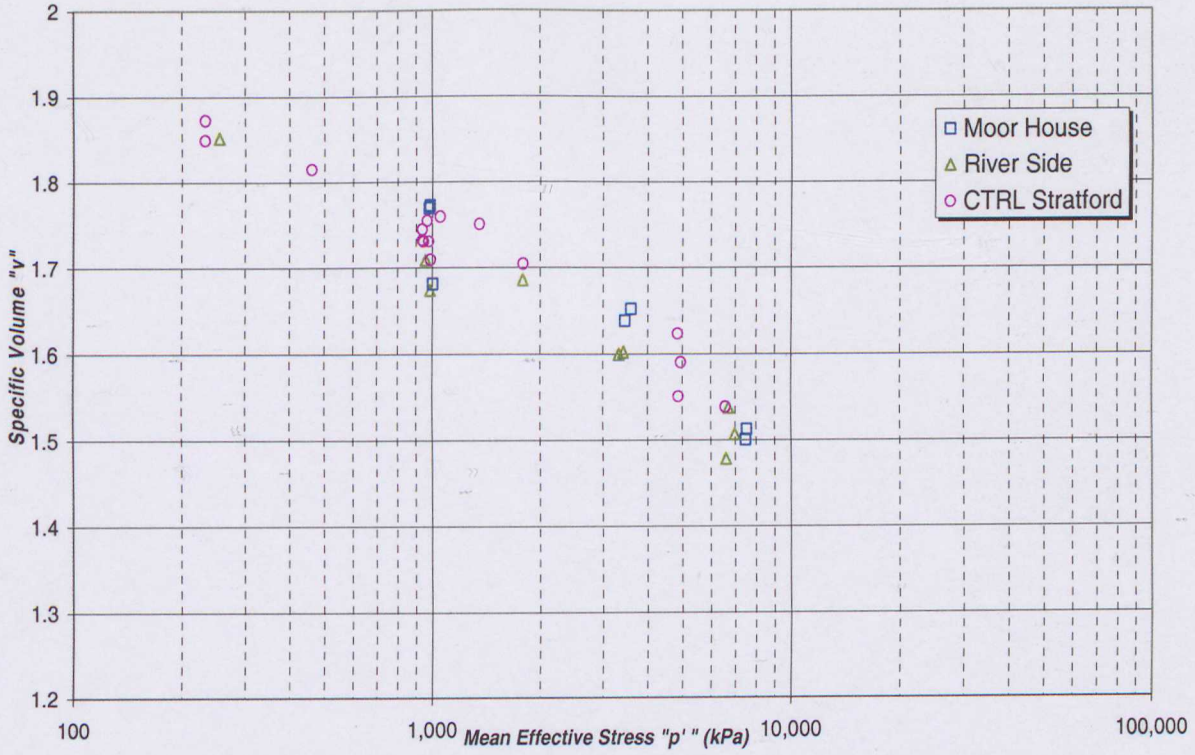


***Figure 5-10*** *Site comparison for high silt content material*

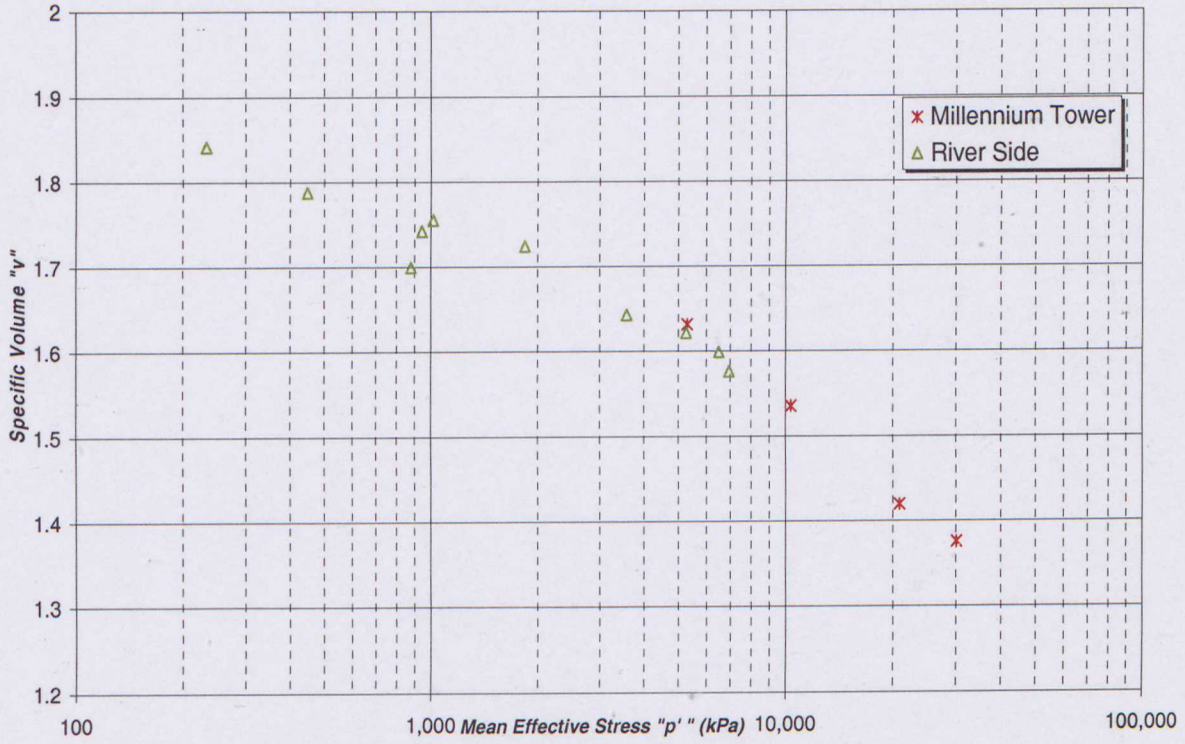


***Figure 5-11*** *Site comparison for low silt content material*

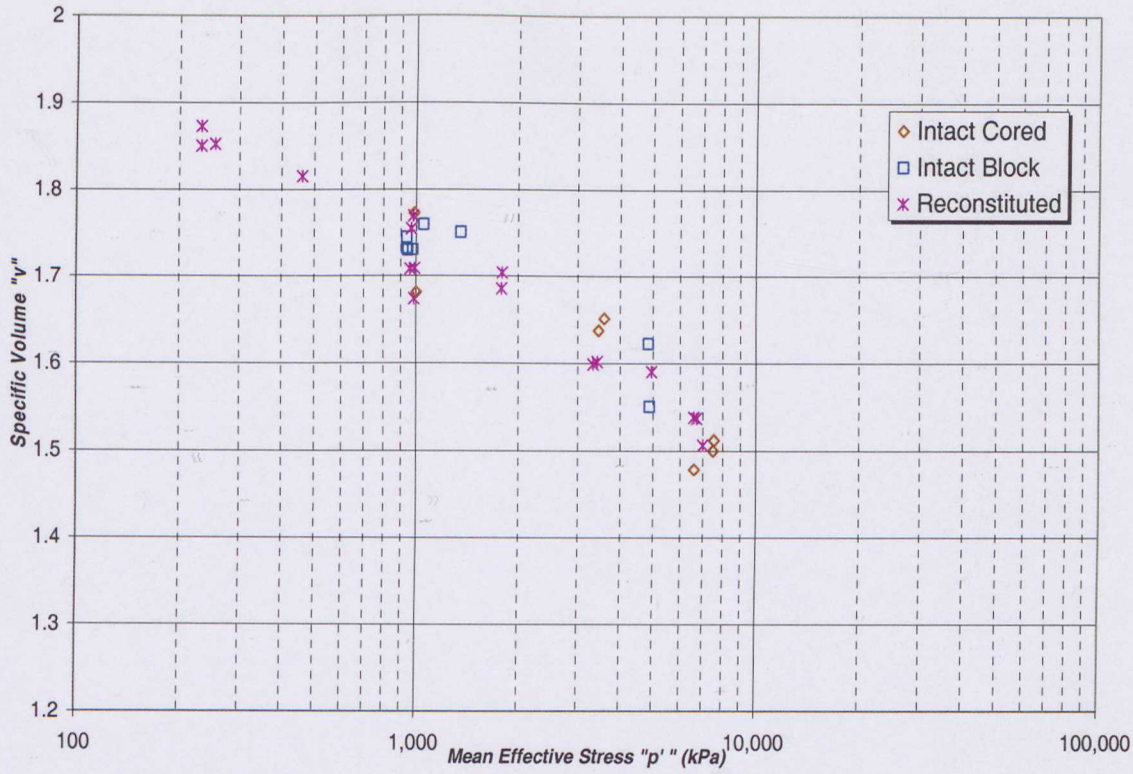


***Figure 5-12*** *Sample type comparison for critical states of high silt material*

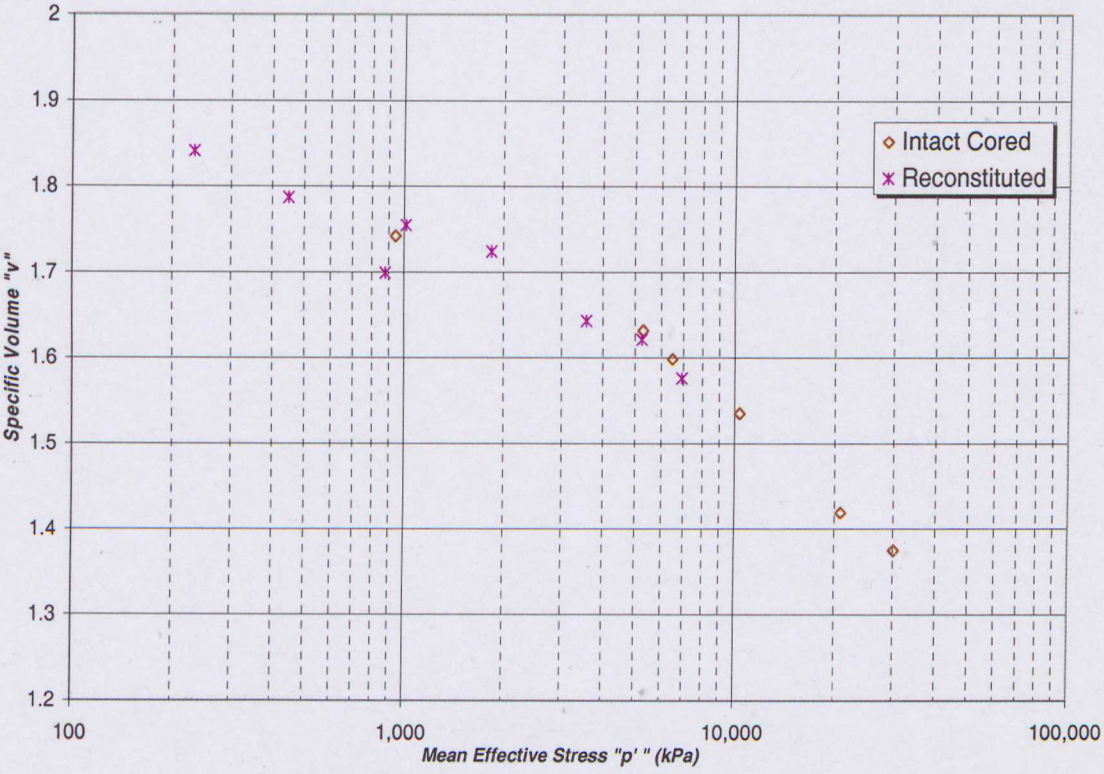


***Figure 5-13*** *Sample type comparison for critical states of low silt content*

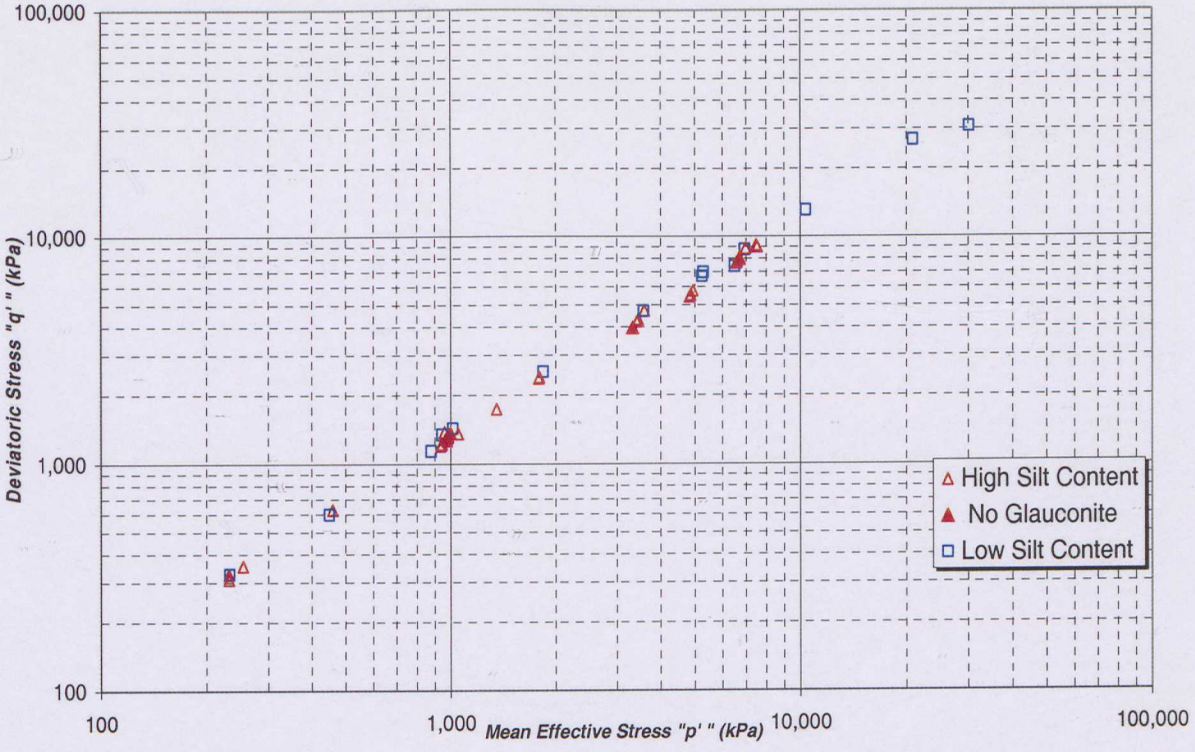


***Figure 5-14*** *High/low silt content comparison for critical states in the q-p' plane*

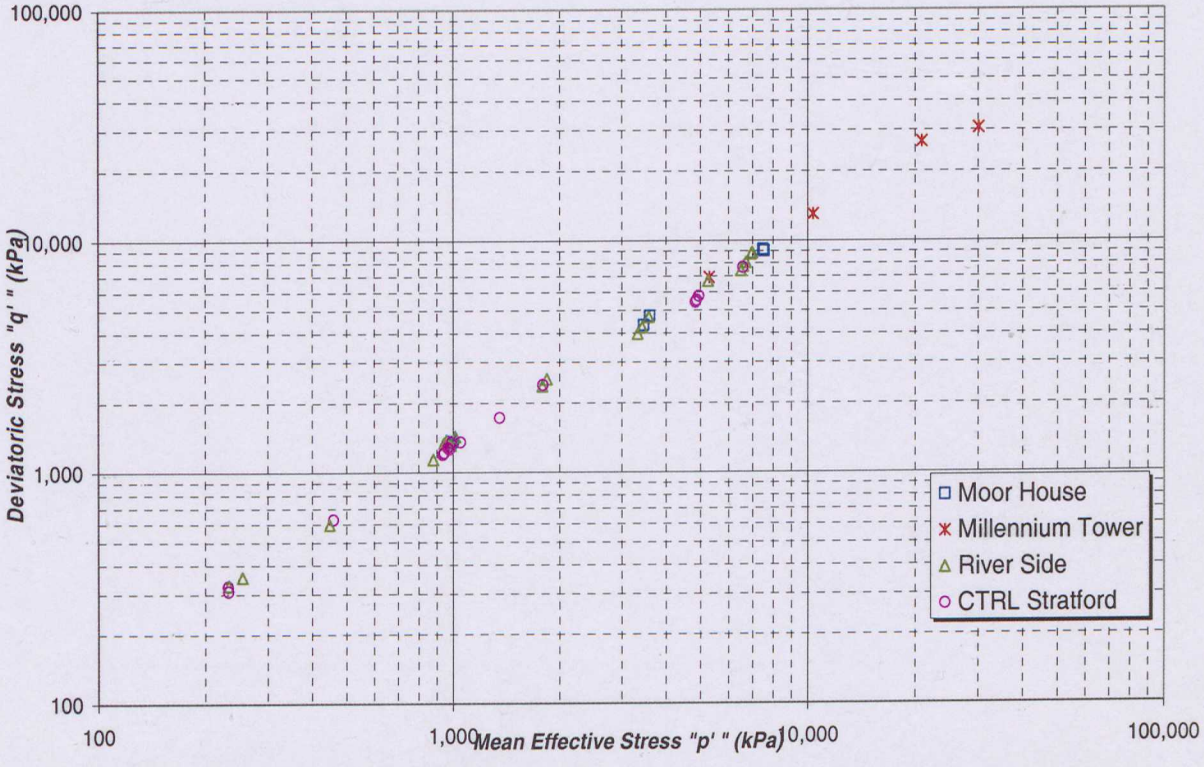


***Figure 5-15*** *Site comparison for critical states in the q-p' plane*

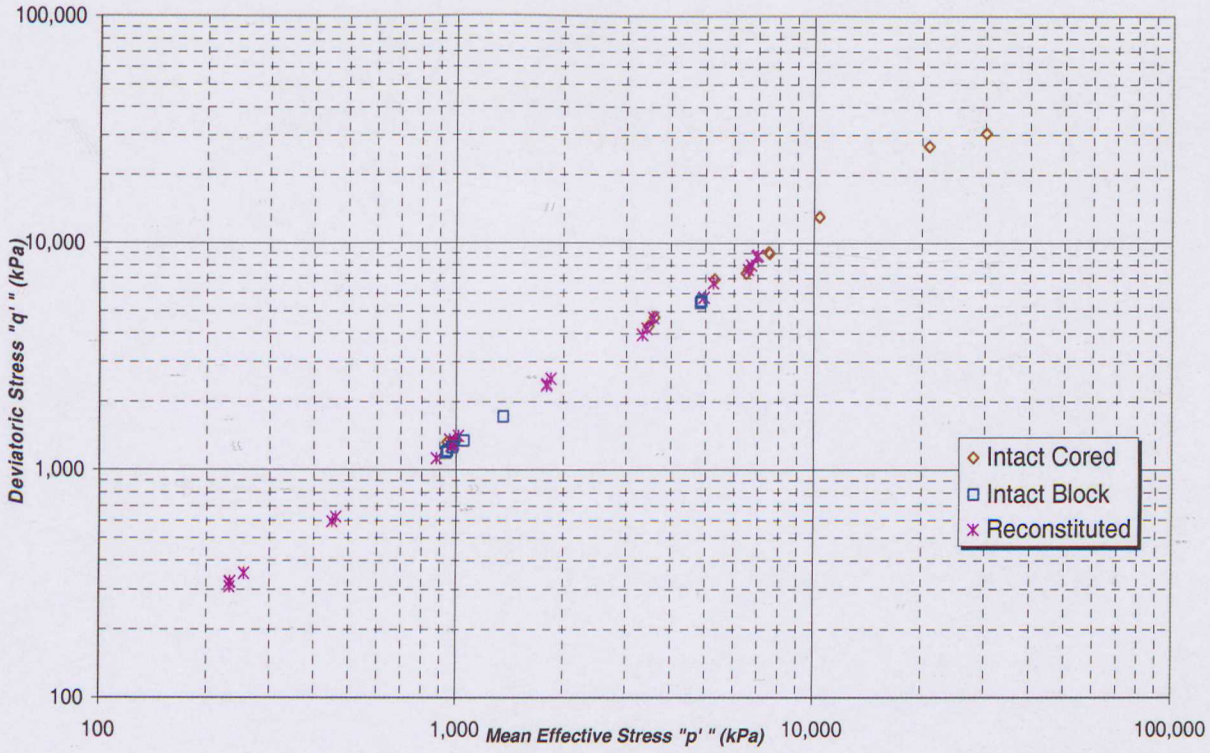


***Figure 5-16*** *Sample type comparison for critical states in the q-p' plane*

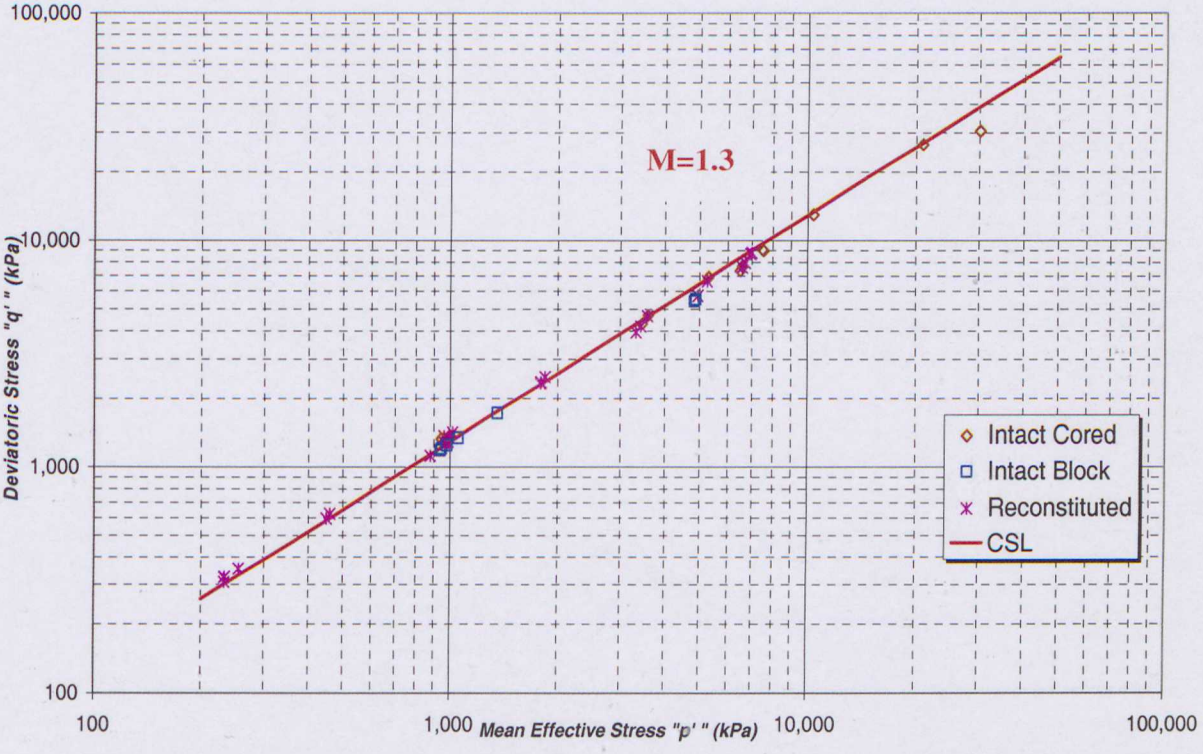


***Figure 5-17*** *Sample type comparison for critical states in the q-p' plane including the chosen CSL*

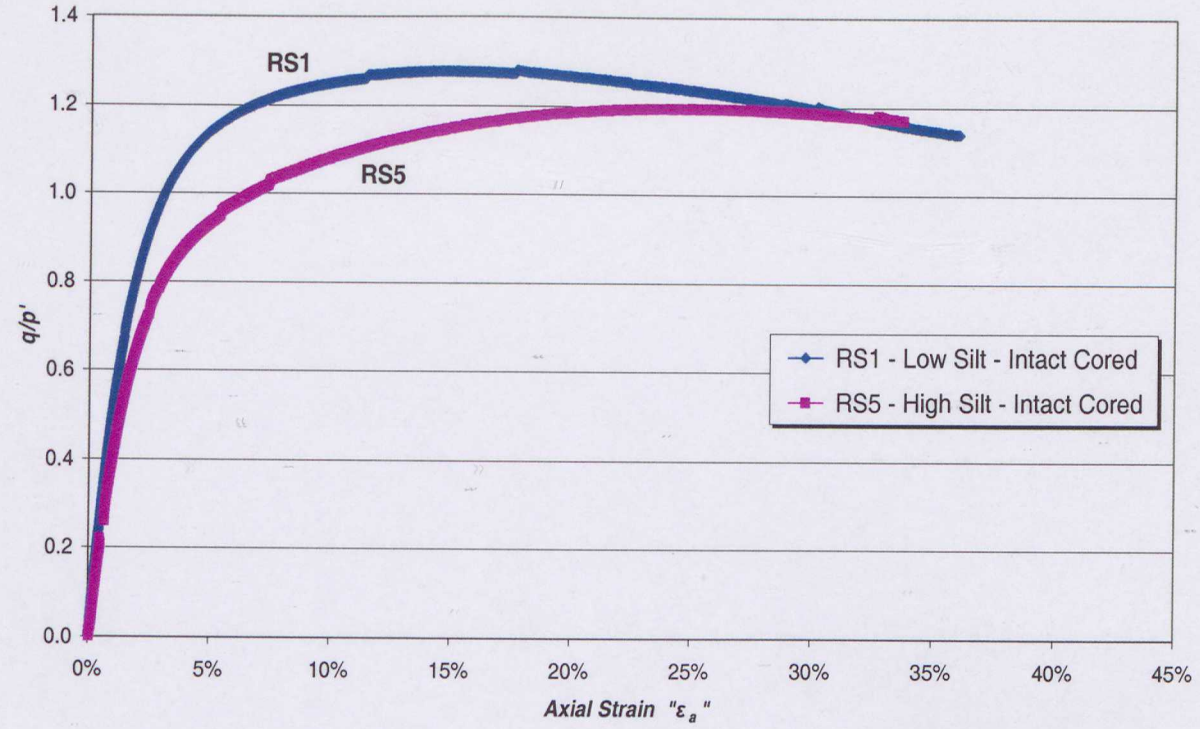


***Figure 5-18*** *High/low silt content comparison for stress:strain behaviour of intact material*

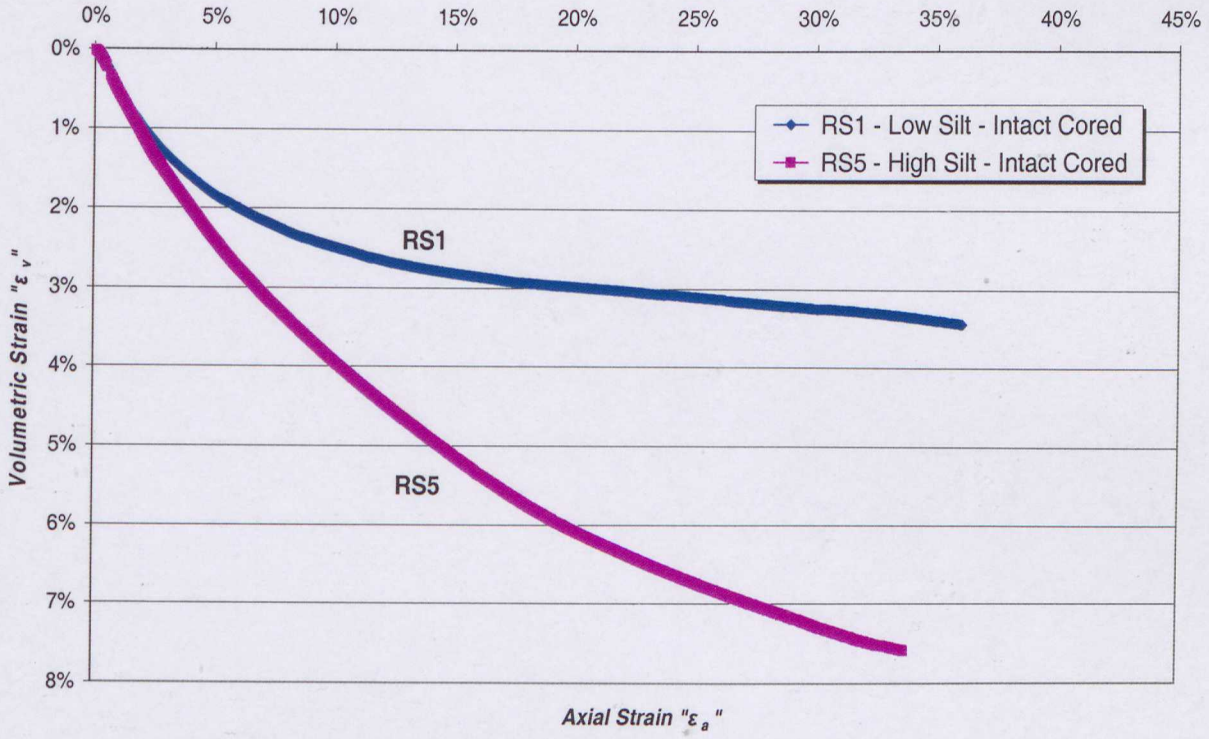


***Figure 5-19*** *High/low silt content comparison for volumetric strain behaviour of intact material*

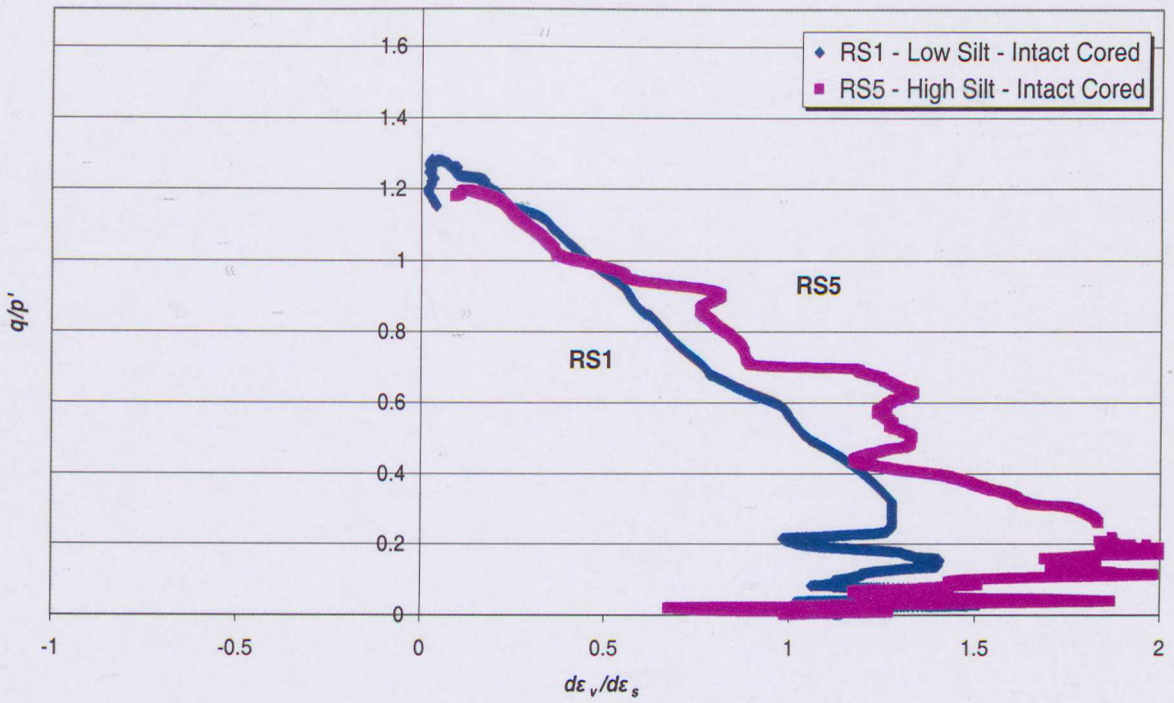


***Figure 5-20*** *High/low silt comparison for stress:dilatancy of intact material*

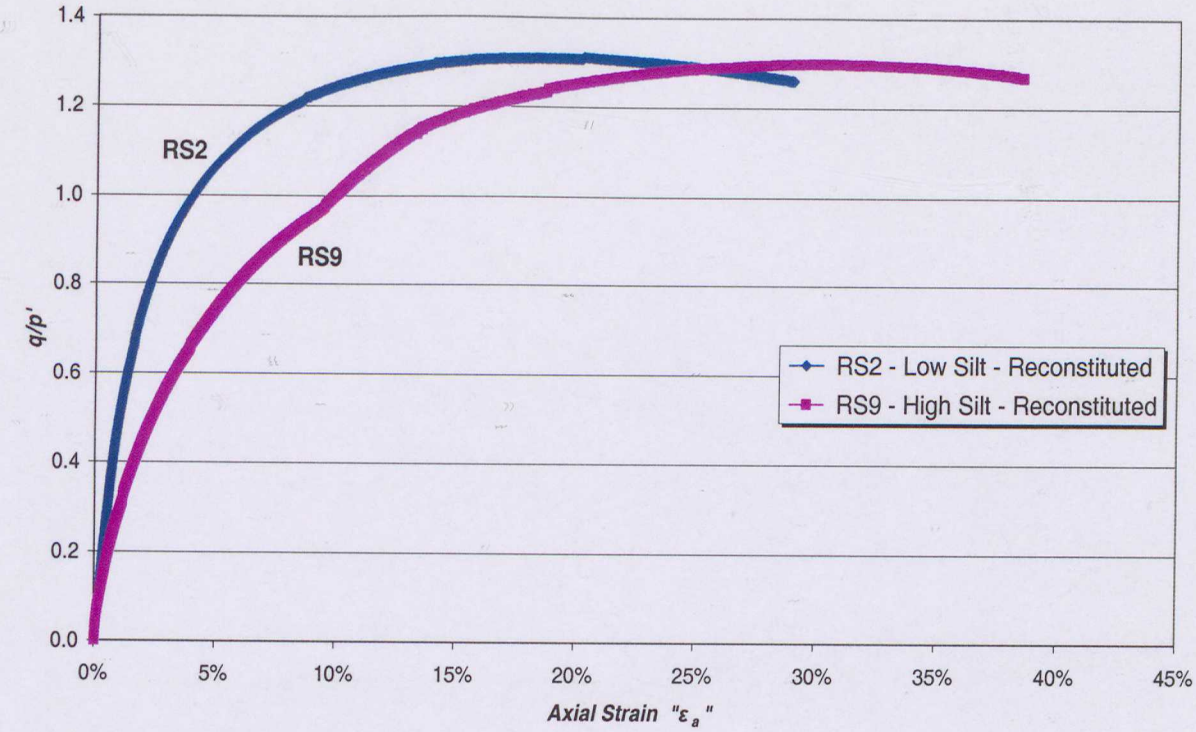


***Figure 5-21*** *High/low silt comparison for stress:strain behaviour of reconstituted material*

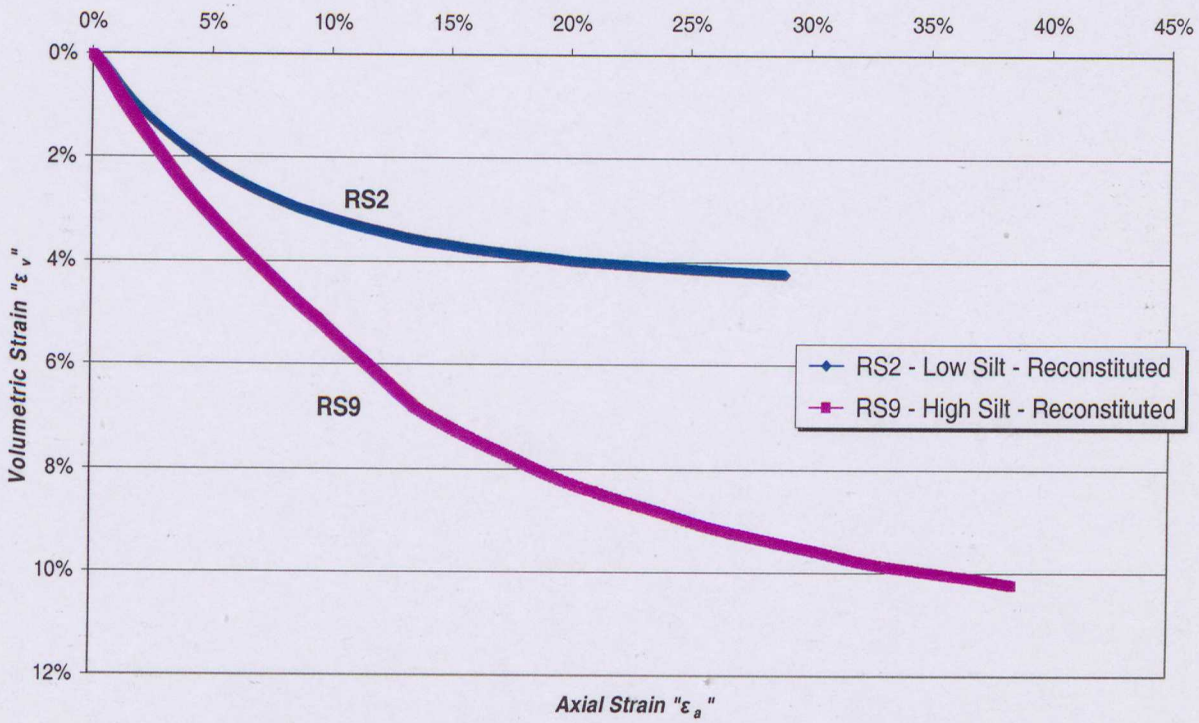


***Figure 5-22*** *High/low silt content comparison for volumetric strain behaviour of reconstituted material*

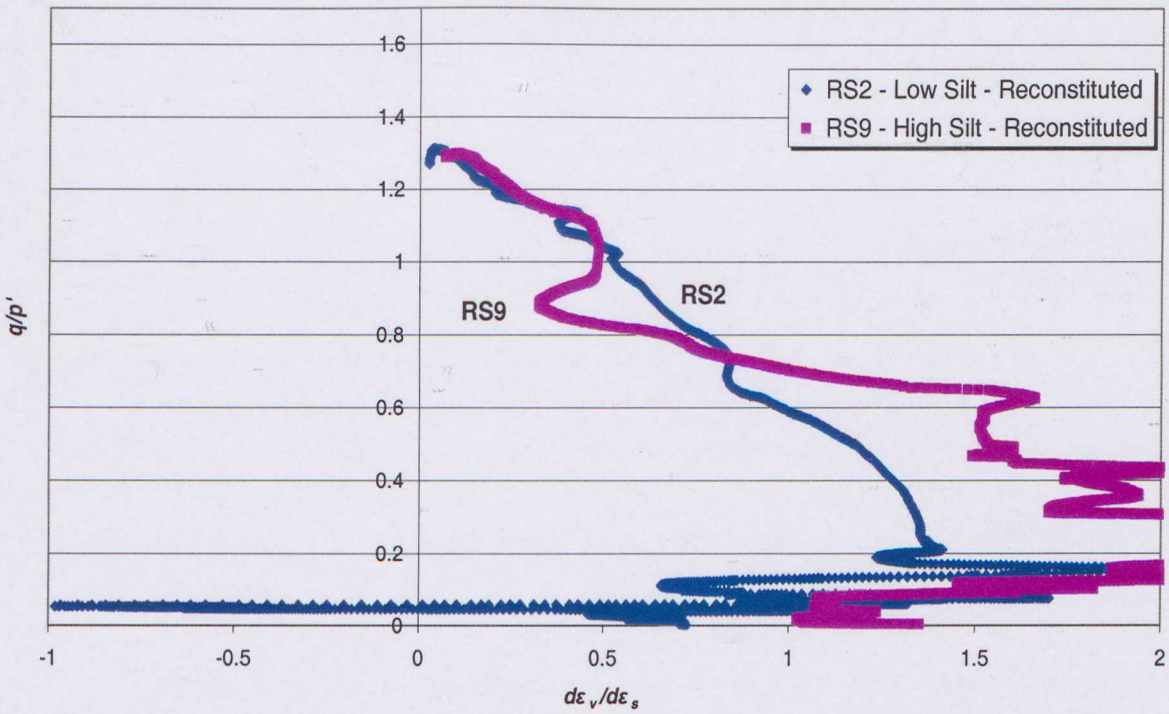


***Figure 5-23*** *High/low silt comparison for stress:dilatancy of reconstituted material*

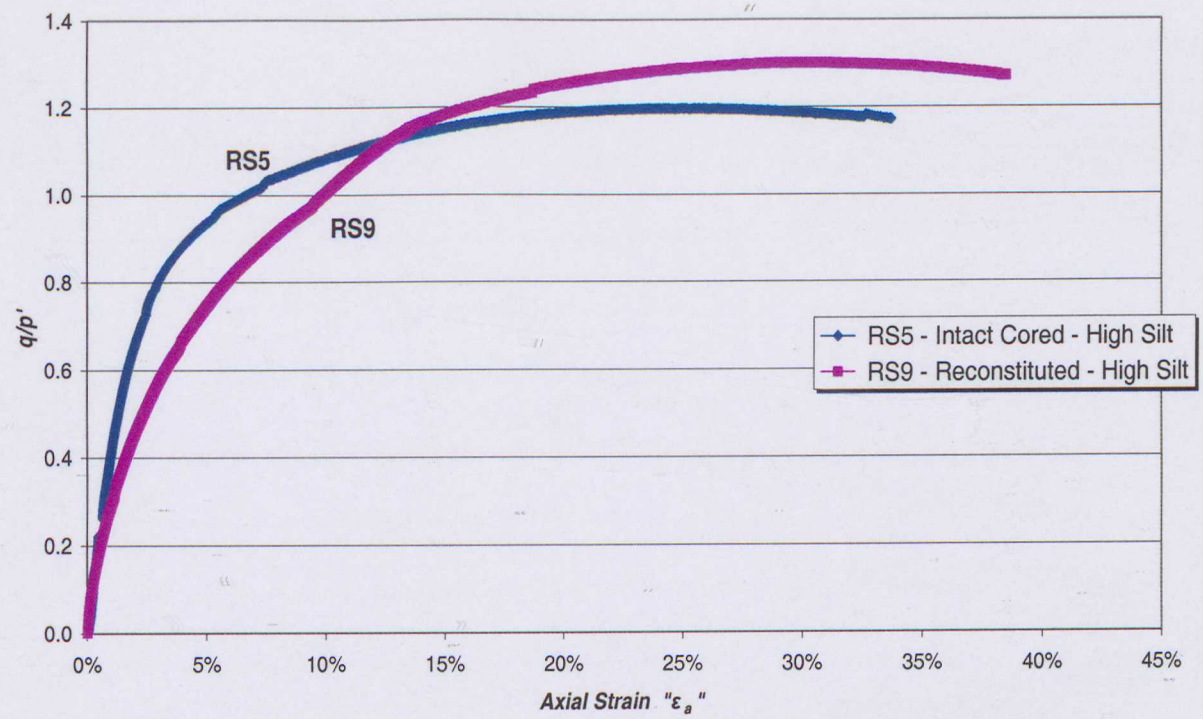


***Figure 5-24*** *Sample type comparison for stress:strain behaviour of high silt content material*

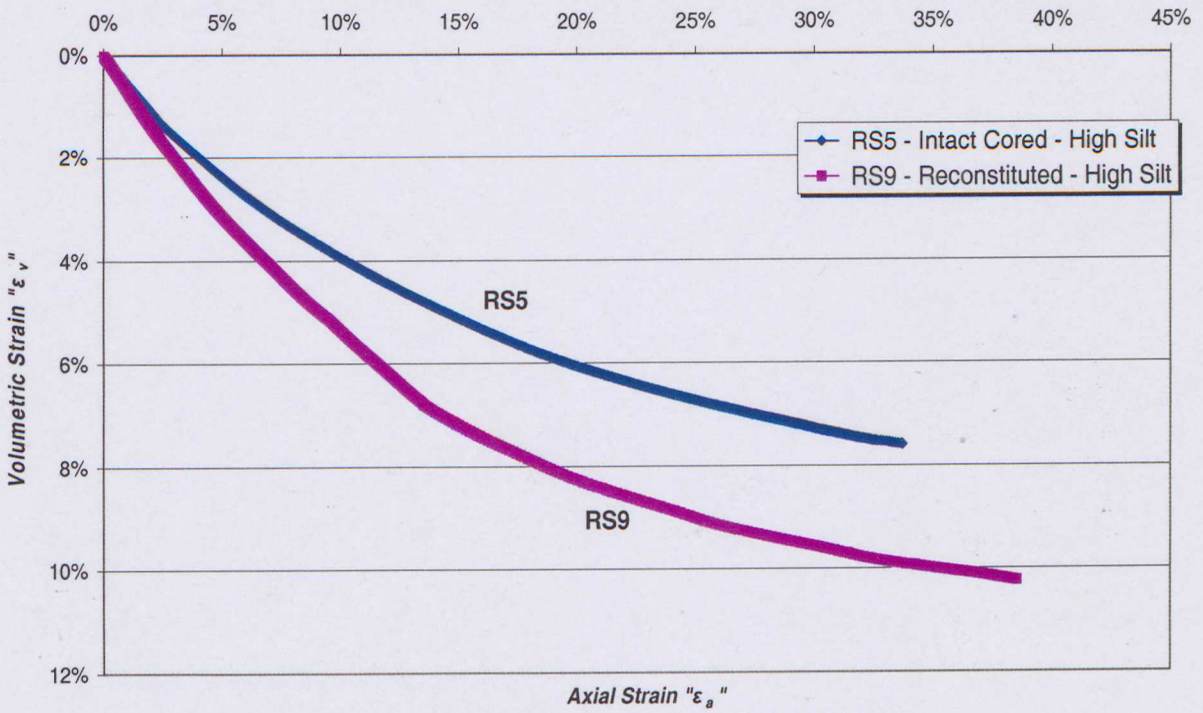


***Figure 5-25*** *Sample type comparison for volumetric strain behaviour of high silt content material*

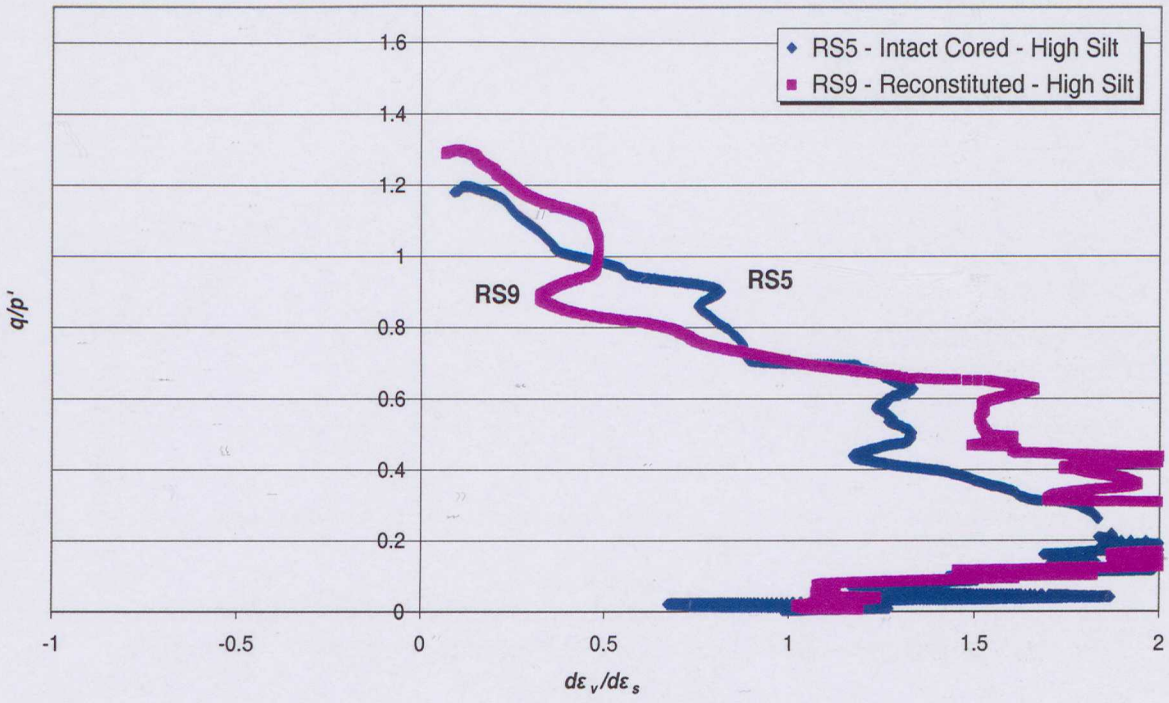


***Figure 5-26*** *Sample type comparison for stress:dilatancy of high silt content material*

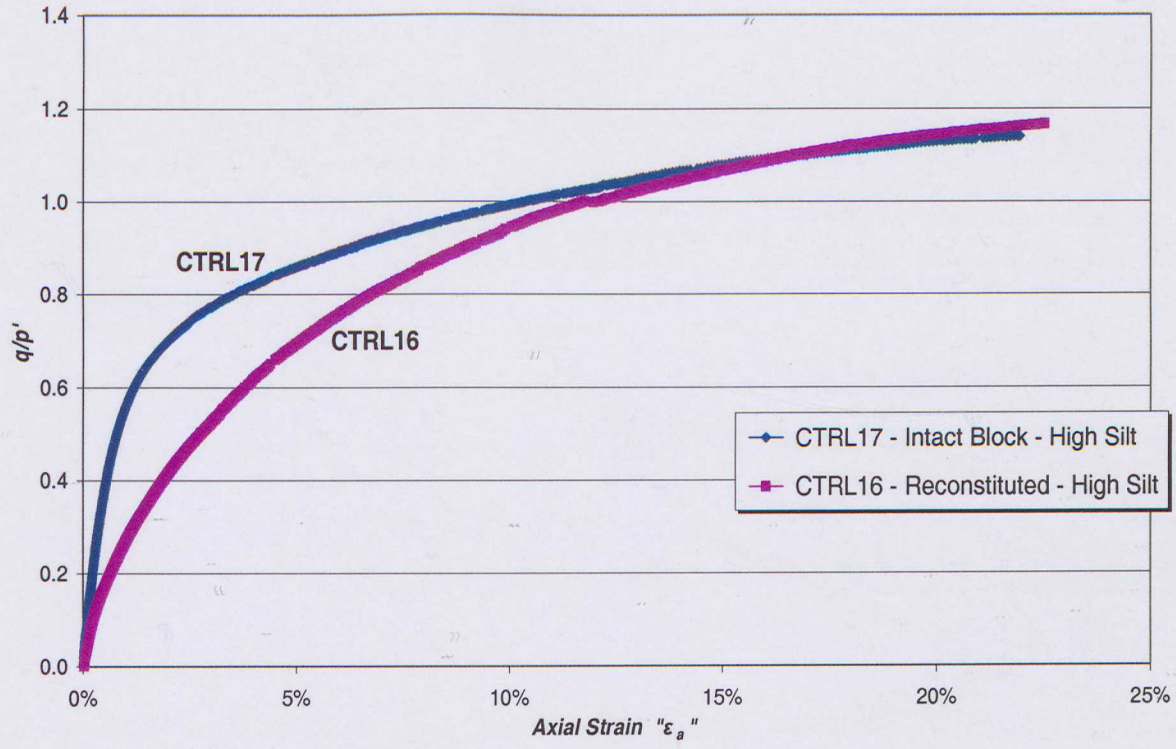


***Figure 5-27*** *Sample type comparison for stress:strain behaviour of high silt content material*

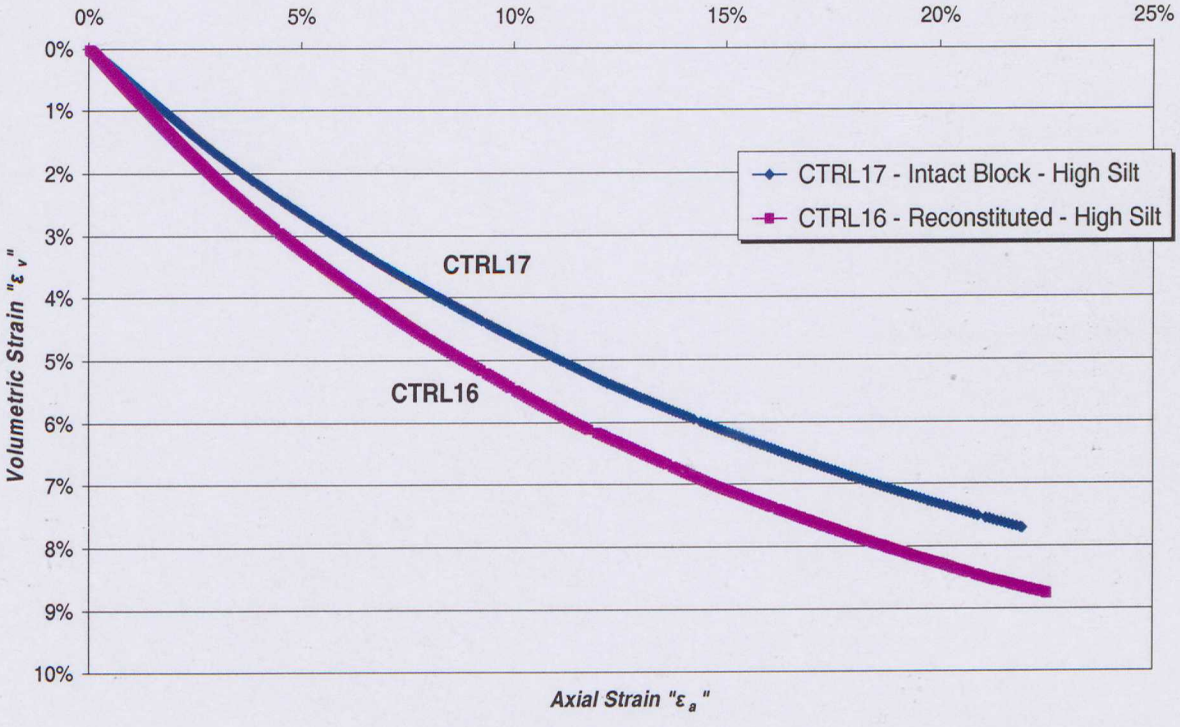


***Figure 5-28*** *Sample type comparison for volumetric strain behaviour of high silt content material*

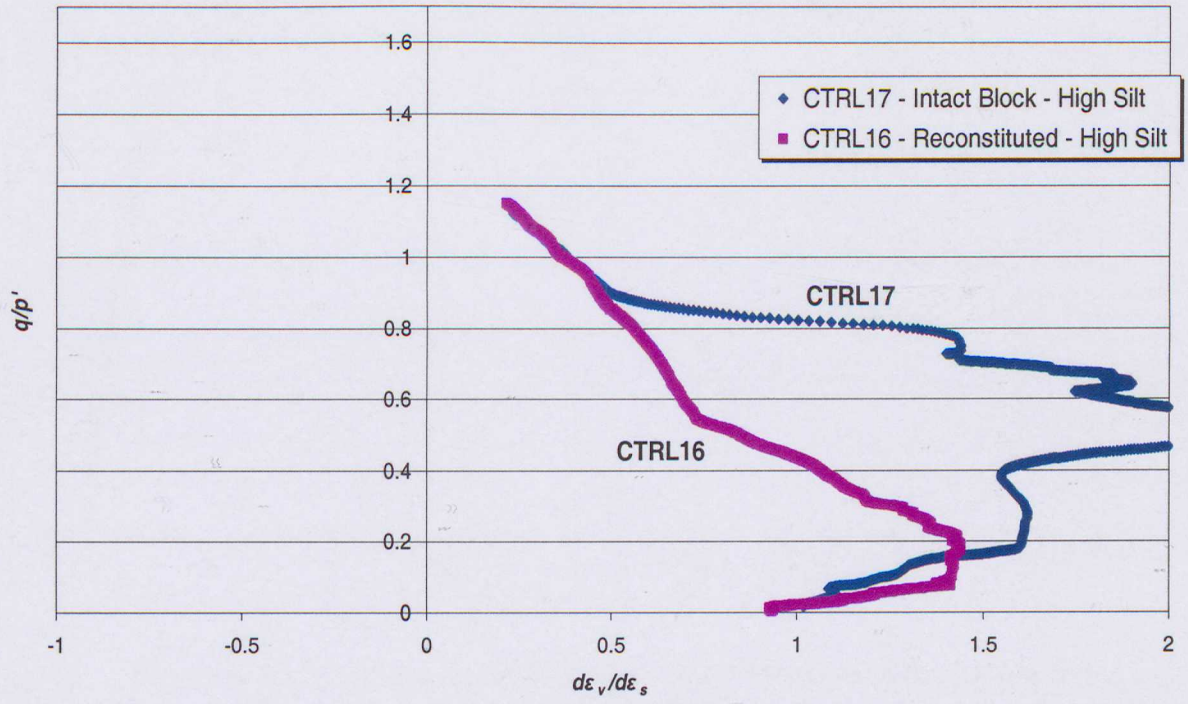


***Figure 5-29*** *Sample type comparison for stress:dilatancy of high silt content material*

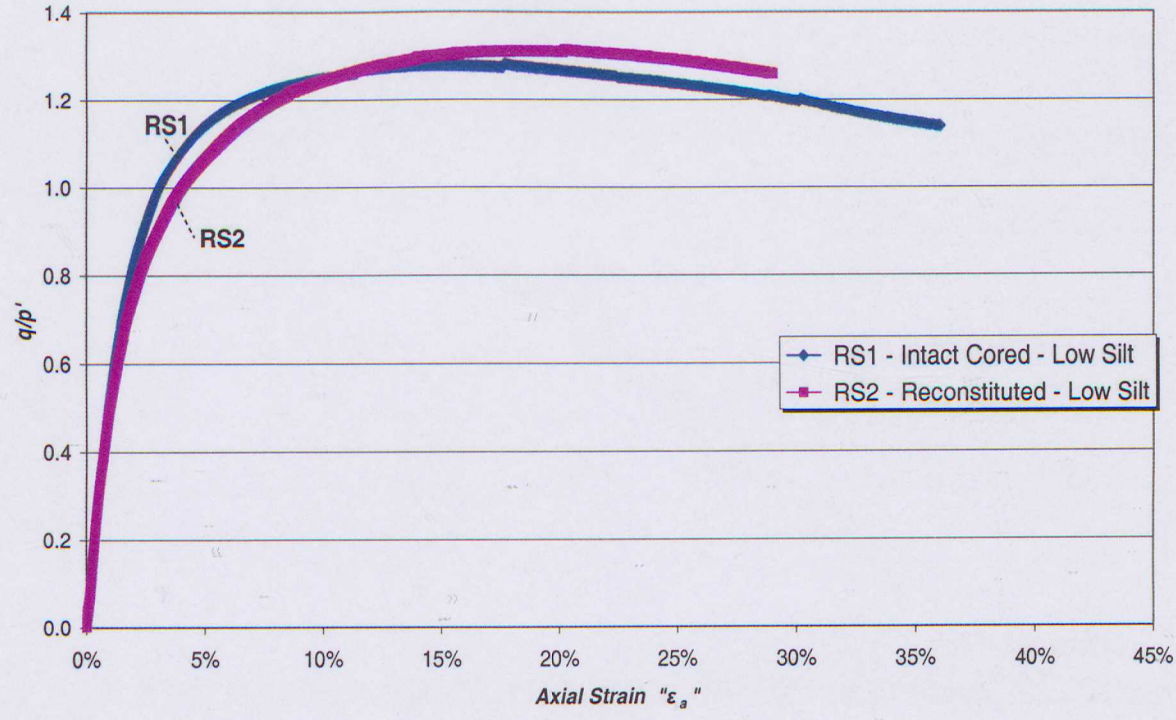


***Figure 5-30*** *Sample type comparison for stress:strain behaviour of low silt content material*

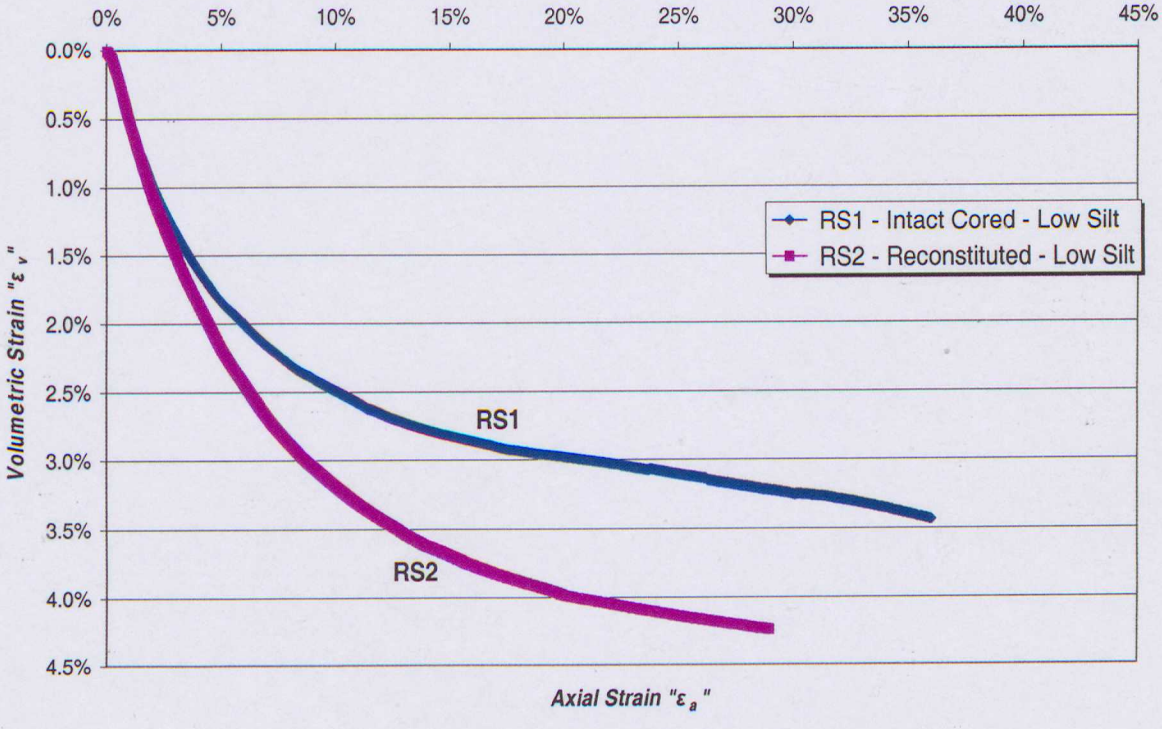


***Figure 5-31*** *Sample type comparison for volumetric strain behaviour of low silt content material*

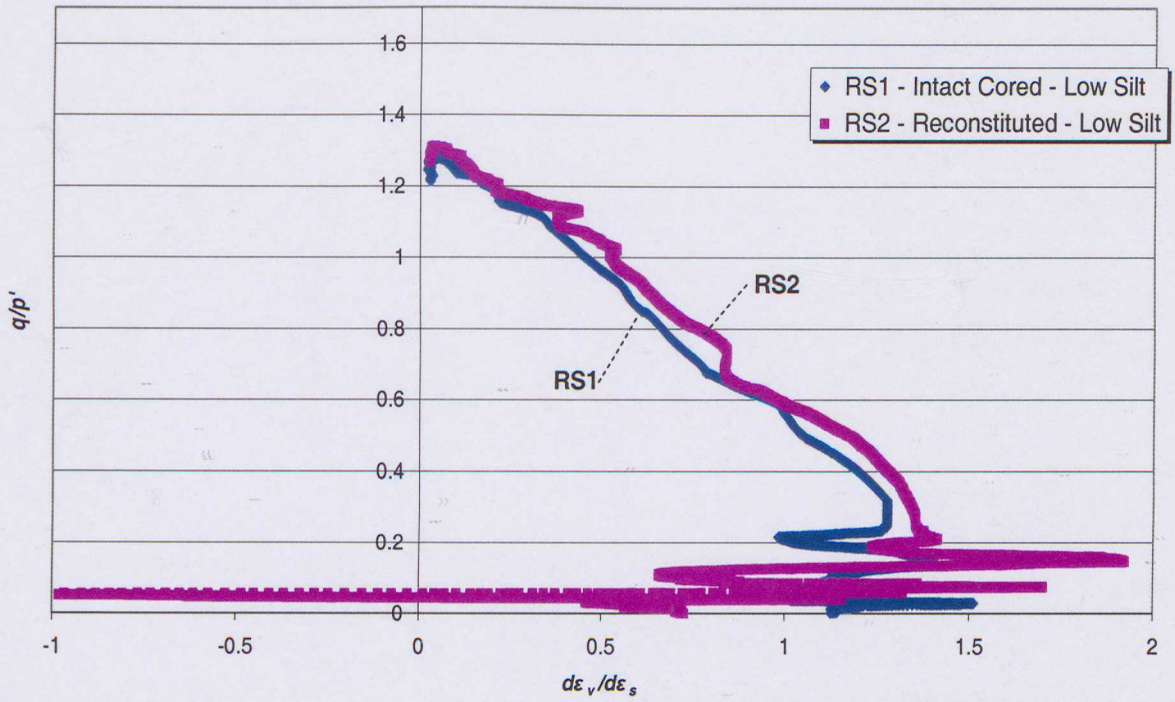


***Figure 5-32*** *Sample type comparison for stress:dilatancy of low silt content material*

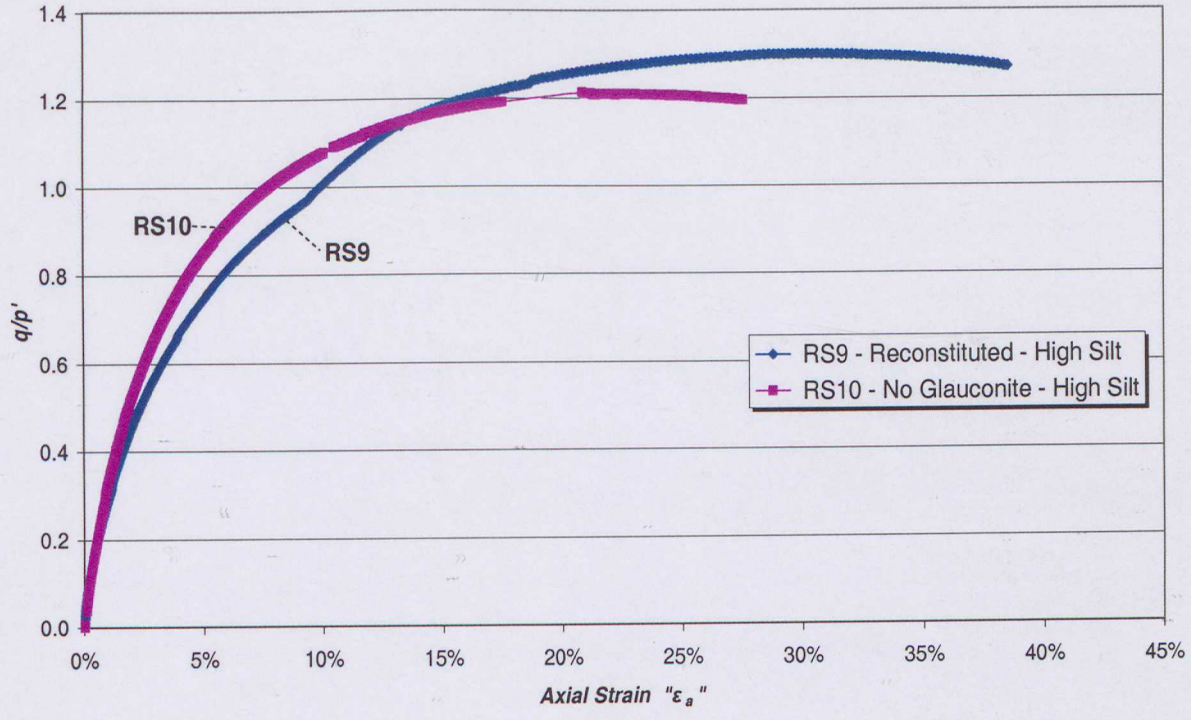


***Figure 5-33*** *Glauconite effect for stress:strain behaviour of high silt content material*

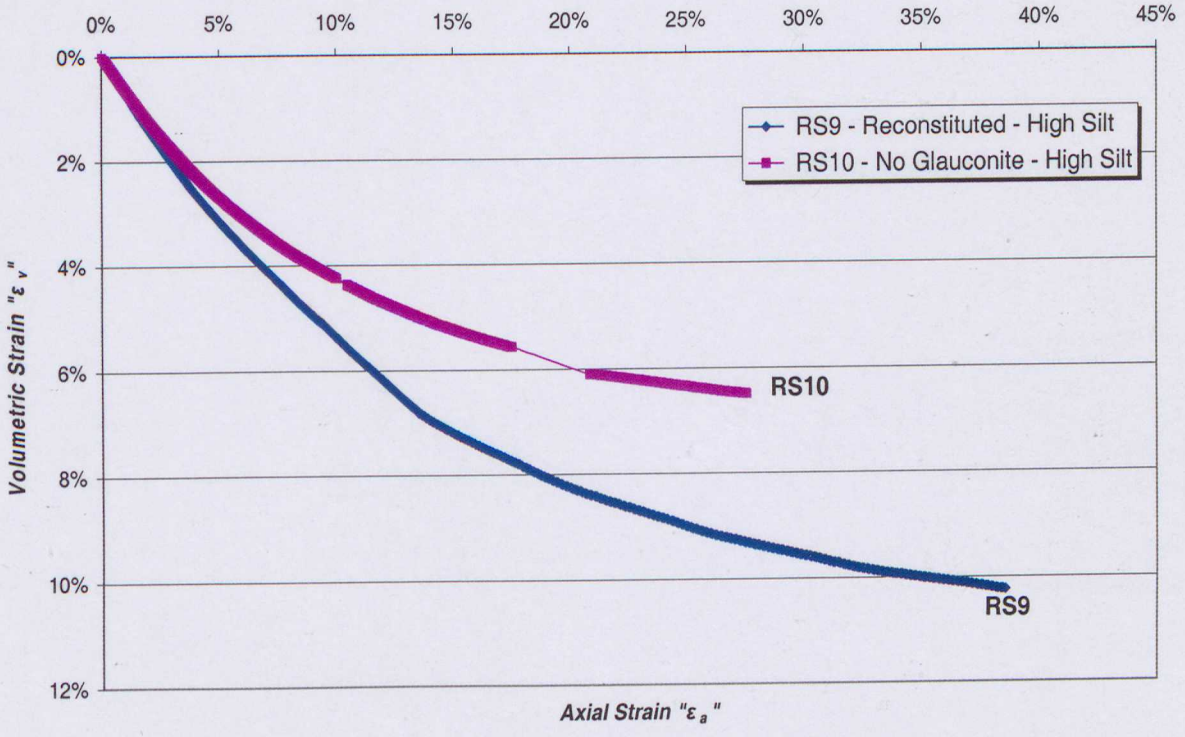


***Figure 5-34*** *Glauconite effect for volumetric strain behaviour of high silt content material*

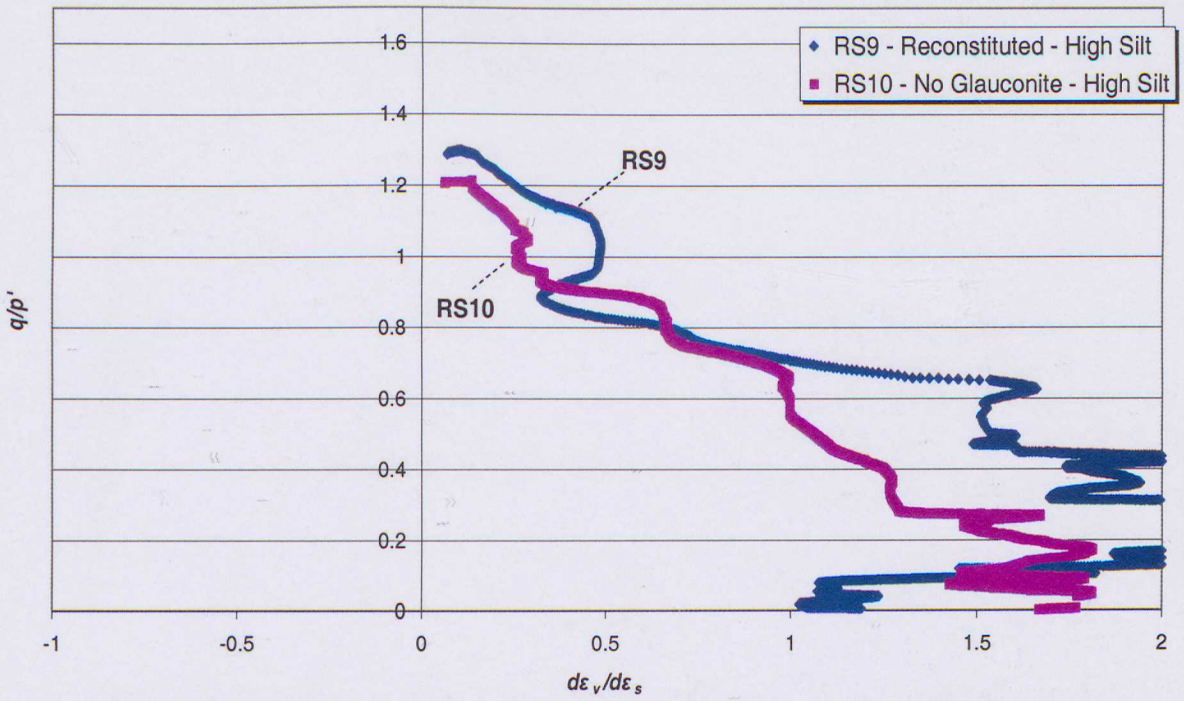


***Figure 5-35*** *Glauconite effect for stress:dilatancy behaviour of high silt content material*

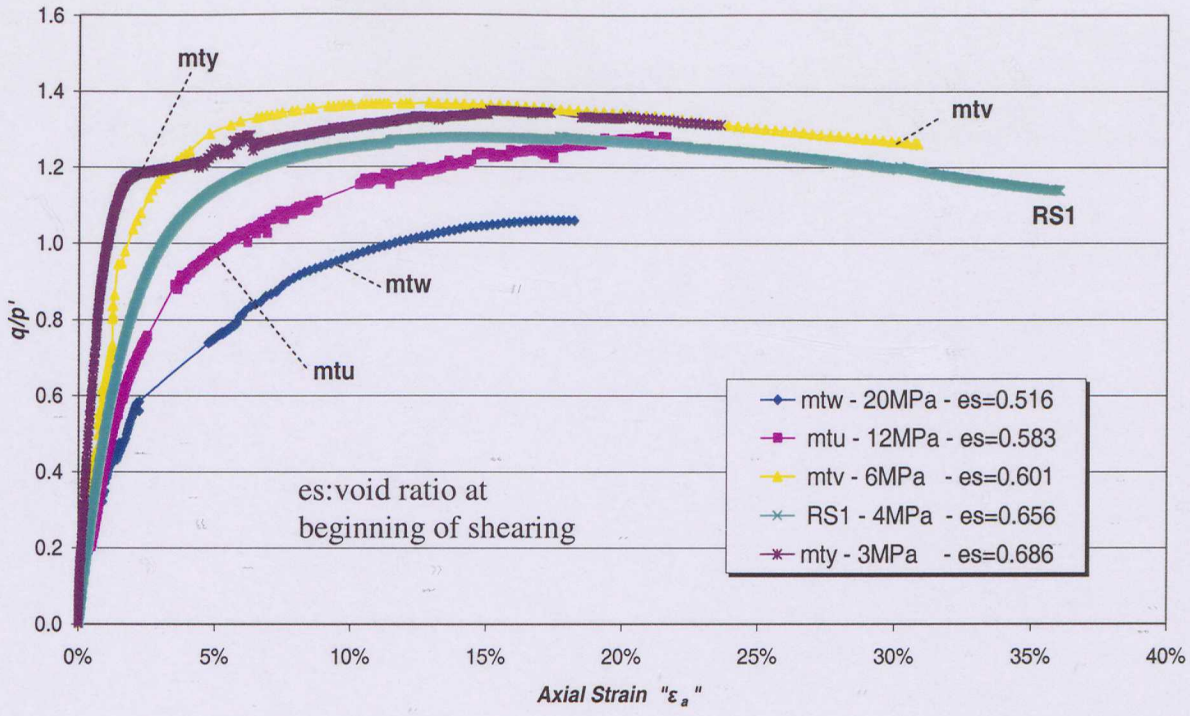


***Figure 5-36*** *Influence of effective confining stress on stress:strain behaviour – intact low silt content samples*

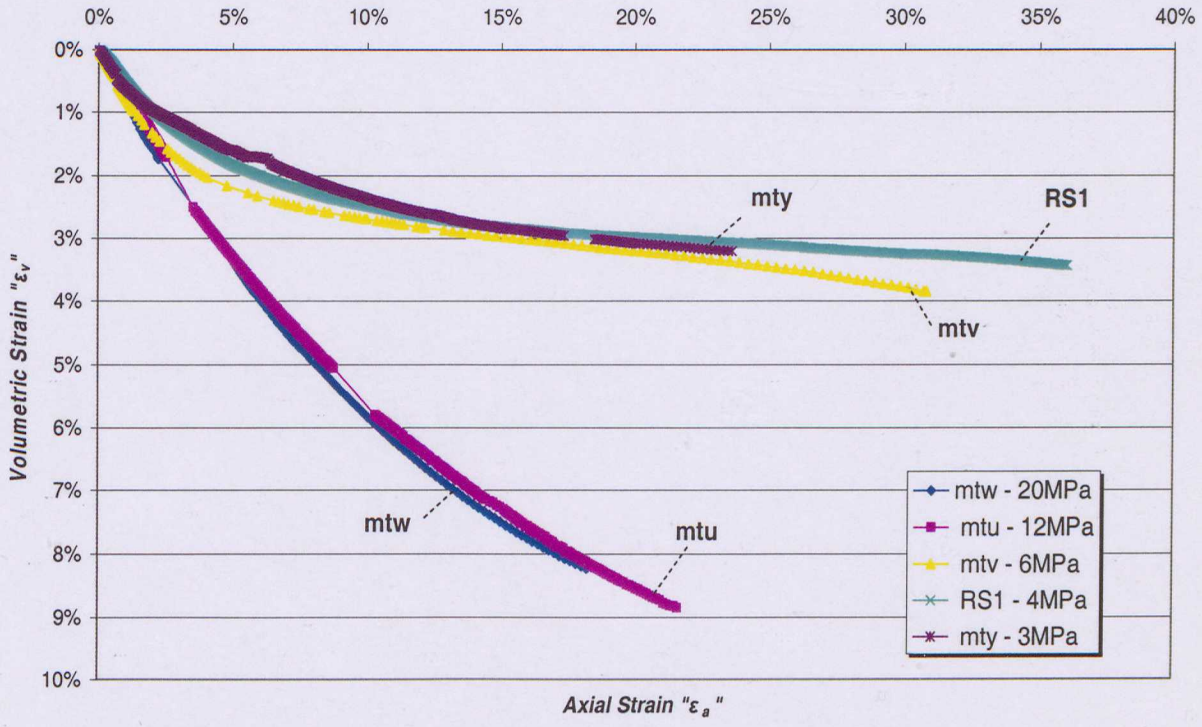


***Figure 5-37*** *Influence of effective confining stress on volumetric strain behaviour – intact low silt content samples*

| *Test name* | *Soil State Parameter "ψ" prior to shearing* |
|---|---|
| mtw | -0.070 |
| mtu | -0.069 |
| mtv | 0.004 |
| RS1 | 0.003 |
| mty | 0.011 |

*Table of soil state parameters "ψ" prior to shearing for low silt content reconstituted samples*

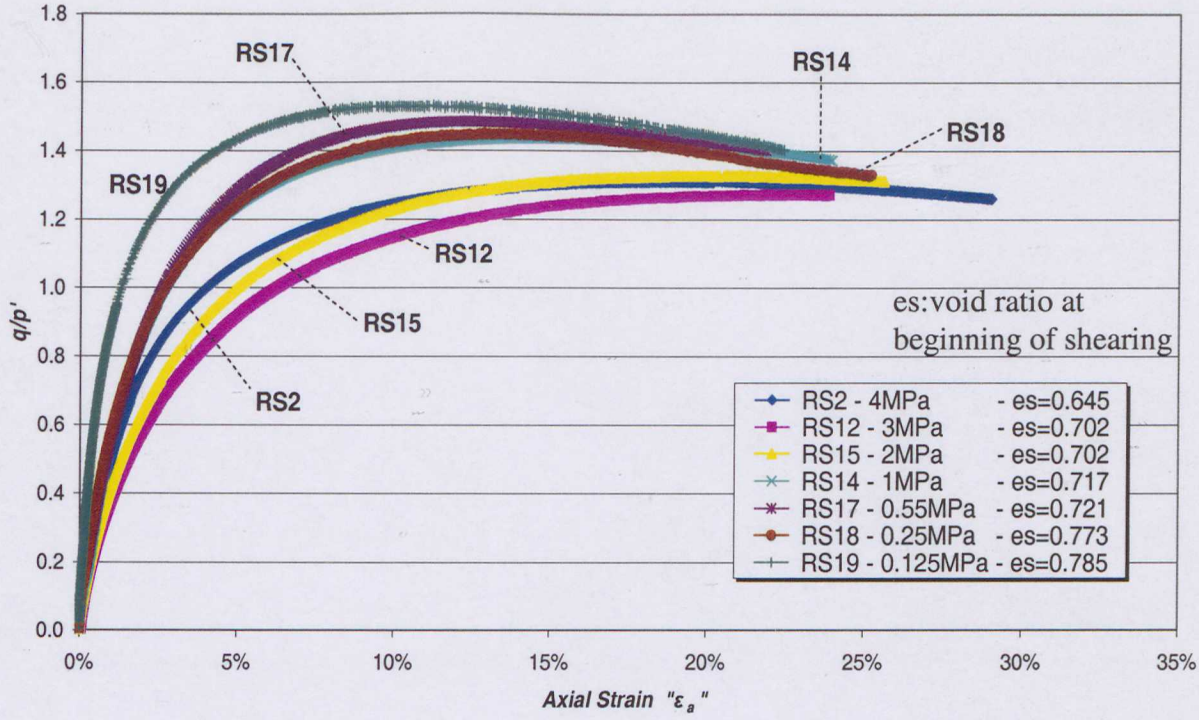


***Figure 5-38*** *Influence of effective confining stress on stress:strain behaviour – reconstituted low silt content samples*

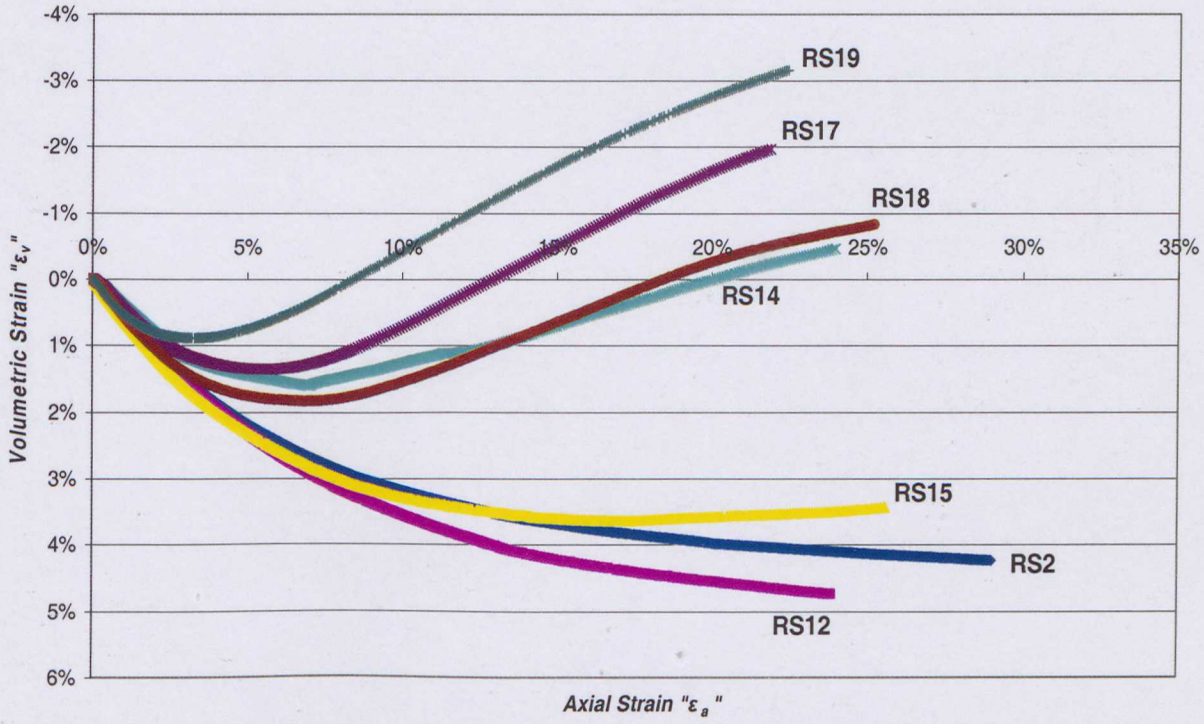


***Figure 5-39*** *Influence of effective confining stress on volumetric strain behaviour – reconstituted low silt content samples*

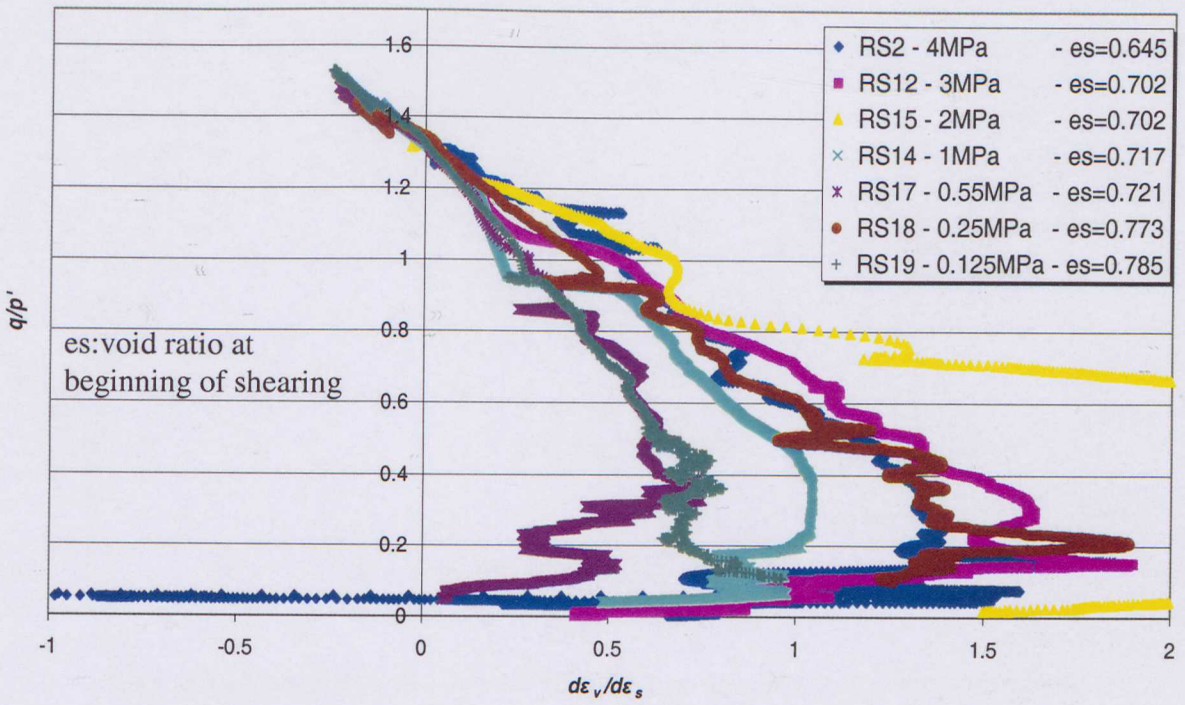


***Figure 5-40*** *Influence of effective confining stress on stress:dilatancy relationship for reconstituted low silt content samples*

| *Test name* | *Soil State Parameter "ψ" prior to shearing* |
|---|---|
| RS2 | 0.014 |
| RS12 | -0.005 |
| RS15 | 0.049 |
| RS14 | 0.126 |
| RS17 | 0.201 |
| RS18 | 0.253 |
| RS19 | 0.333 |

*Table of soil state parameters "ψ" prior to shearing for low silt content reconstituted samples*

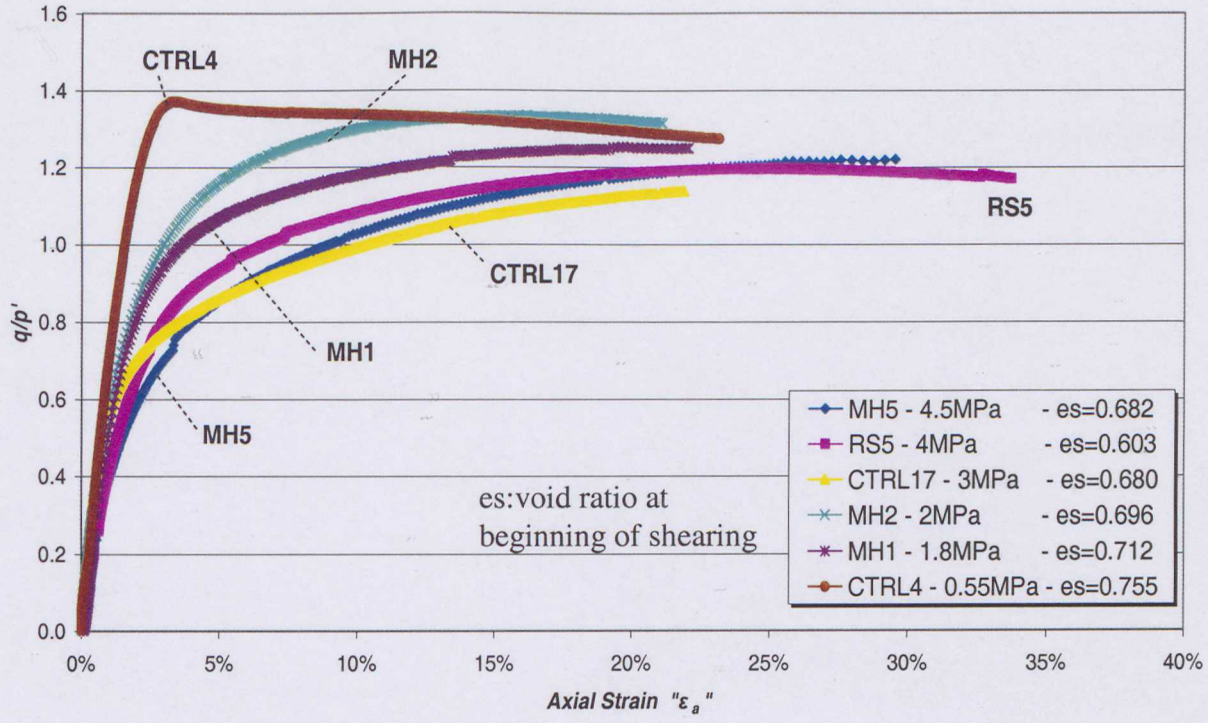


***Figure 5-41*** *Influence of effective confining stress on stress:strain behaviour – intact high silt content samples*

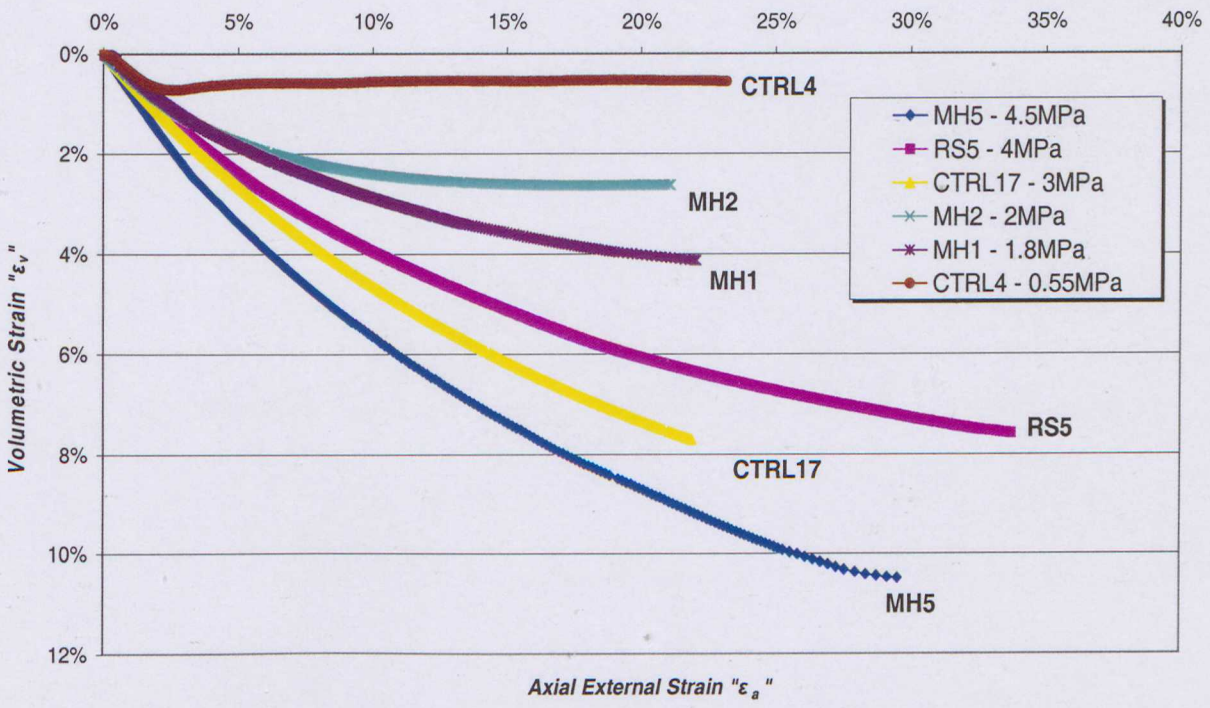


***Figure 5-42*** *Influence of effective confining stress on volumetric strain behaviour – intact high silt content samples*

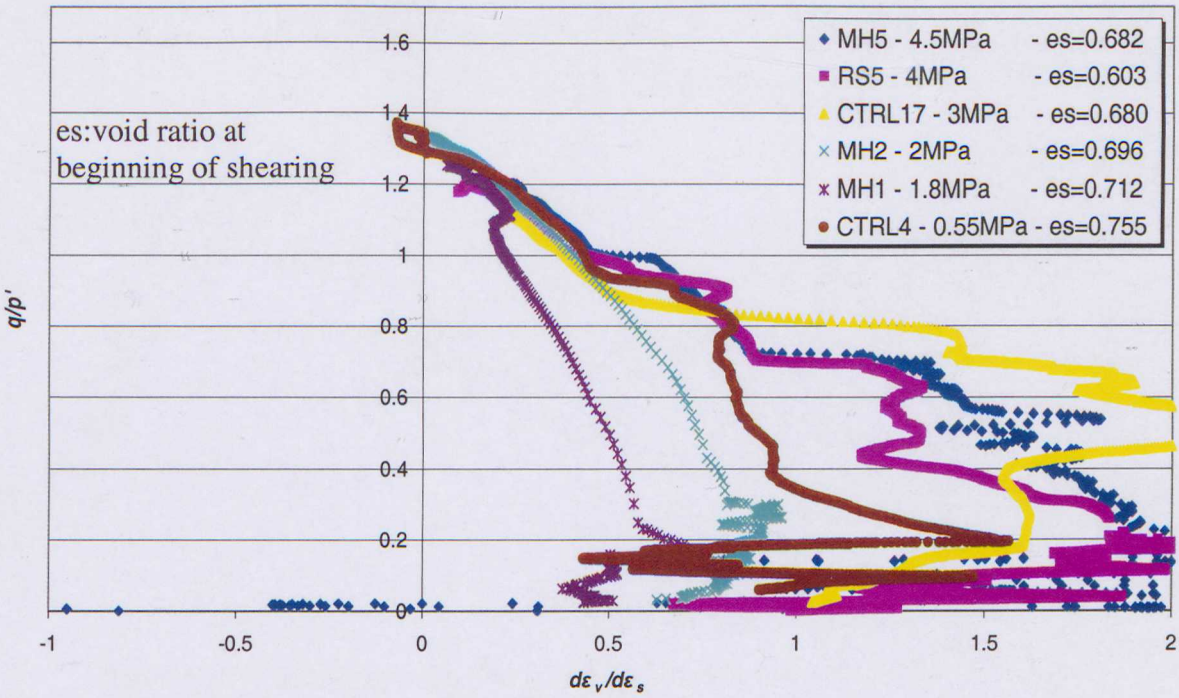


***Figure 5-43*** *Influence of effective confining stress on stress:dilatancy relationship for intact high silt content samples*

| *Test name* | *Soil State Parameter "ψ" prior to shearing* |
|---|---|
| MH5 | -0.131 |
| RS5 | -0.037 |
| CTRL17 | -0.076 |
| MH2 | -0.040 |
| MH1 | -0.042 |
| CTRL4 | 0.070 |

*Table of soil state parameters "ψ" prior to shearing for high silt content intact samples*

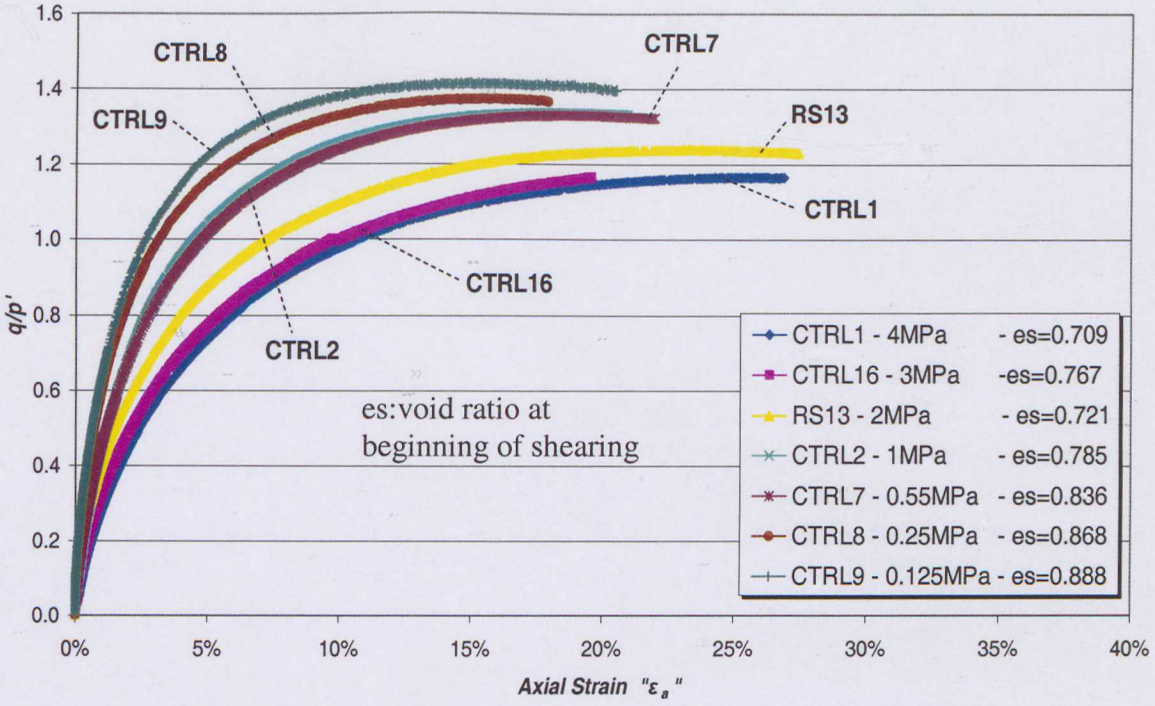


***Figure 5-44*** *Influence of effective confining stress on stress:strain behaviour – reconstituted high silt content samples*

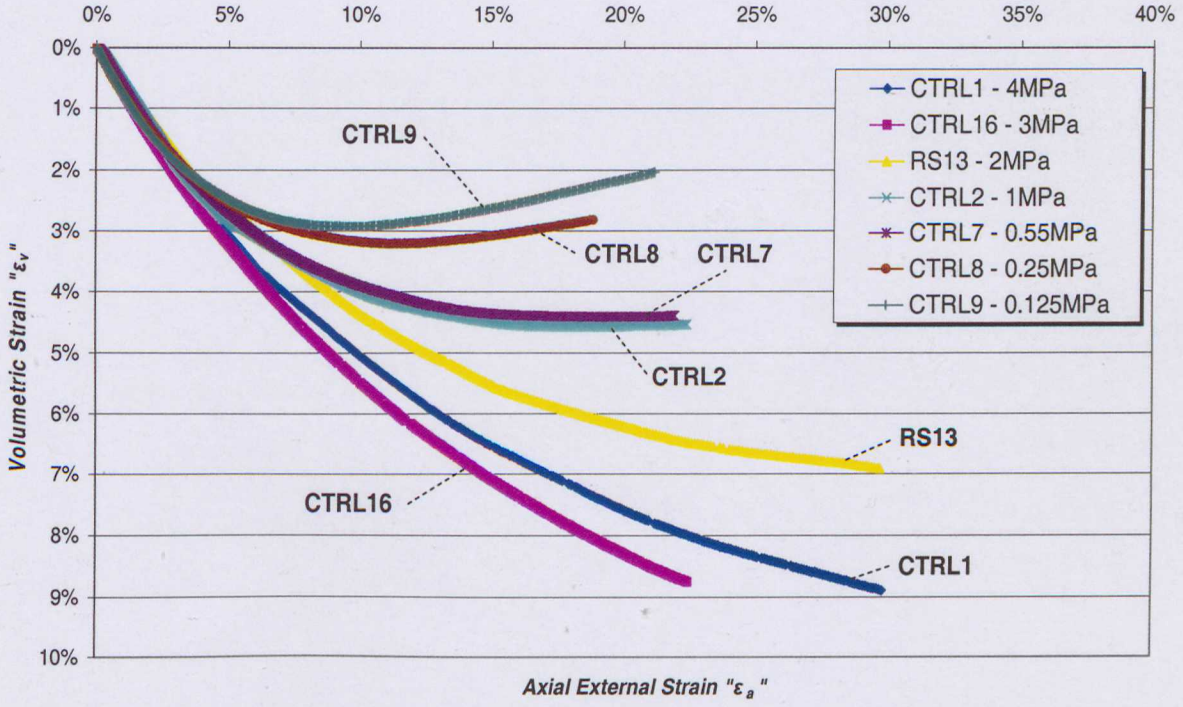


***Figure 5-45*** *Influence of effective confining stress on volumetric strain behaviour – reconstituted high silt content samples*

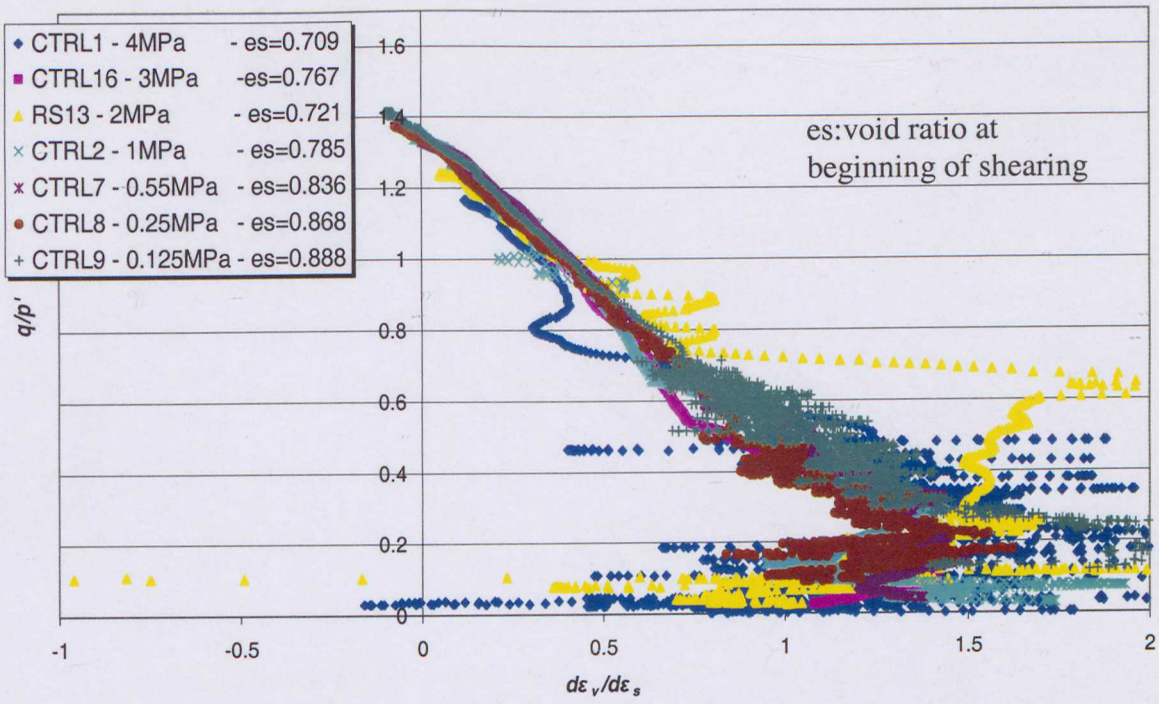


***Figure 5-46*** *Influence of effective confining stress on stress:dilatancy relationship for reconstituted high silt content samples*

| *Test name* | *Soil State Parameter "ψ" prior to shearing* |
|---|---|
| CTRL1 | -0.143 |
| CTRL16 | -0.163 |
| RS13 | -0.065 |
| CTRL7 | -0.038 |
| CTRL8 | -0.011 |
| CTRL9 | 0.059 |

*Table of soil state parameters "ψ" prior to shearing for high silt content intact samples*

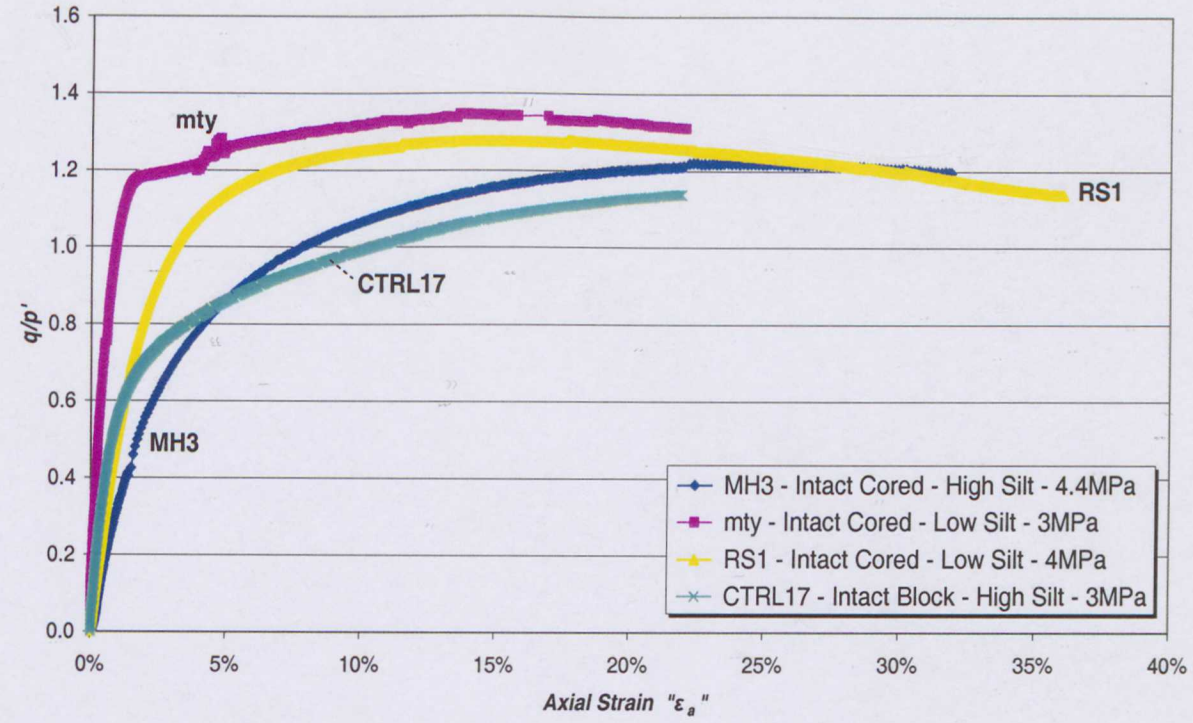


***Figure 5-47*** *Effect of site location on stress:strain behaviour*

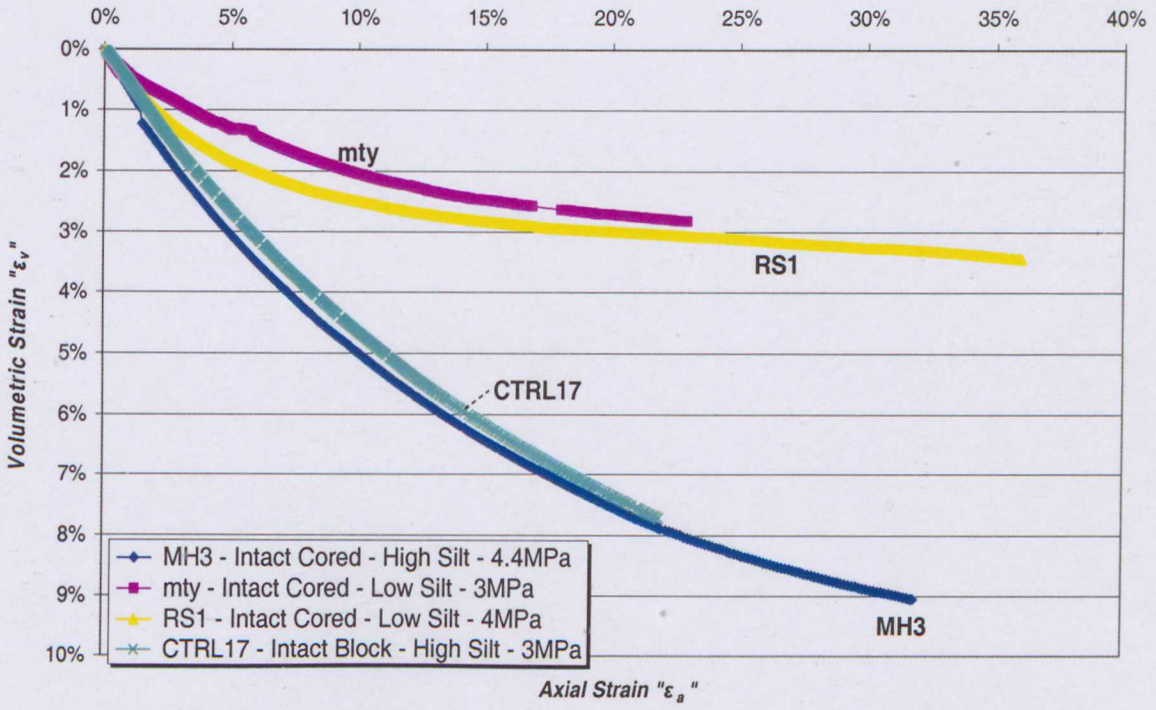


***Figure 5-48*** *Effect of site location on volumetric strain behaviour*

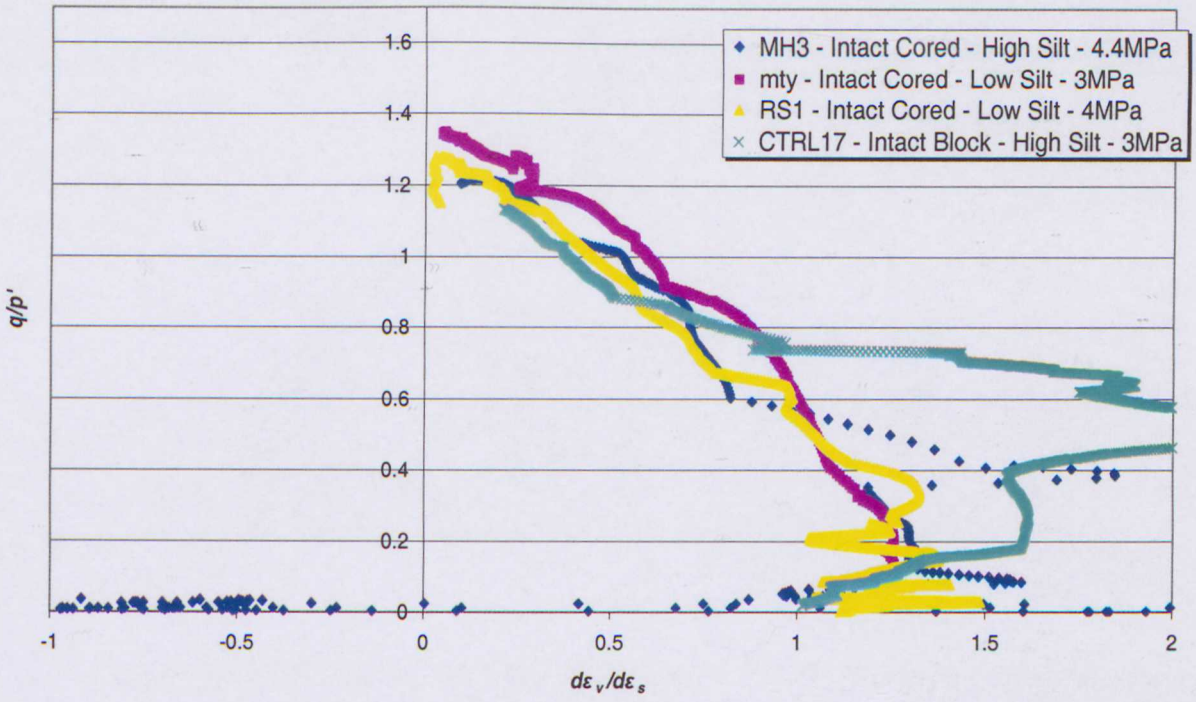


***Figure 5-49*** *Effect of site location on stress:dilation behaviour*

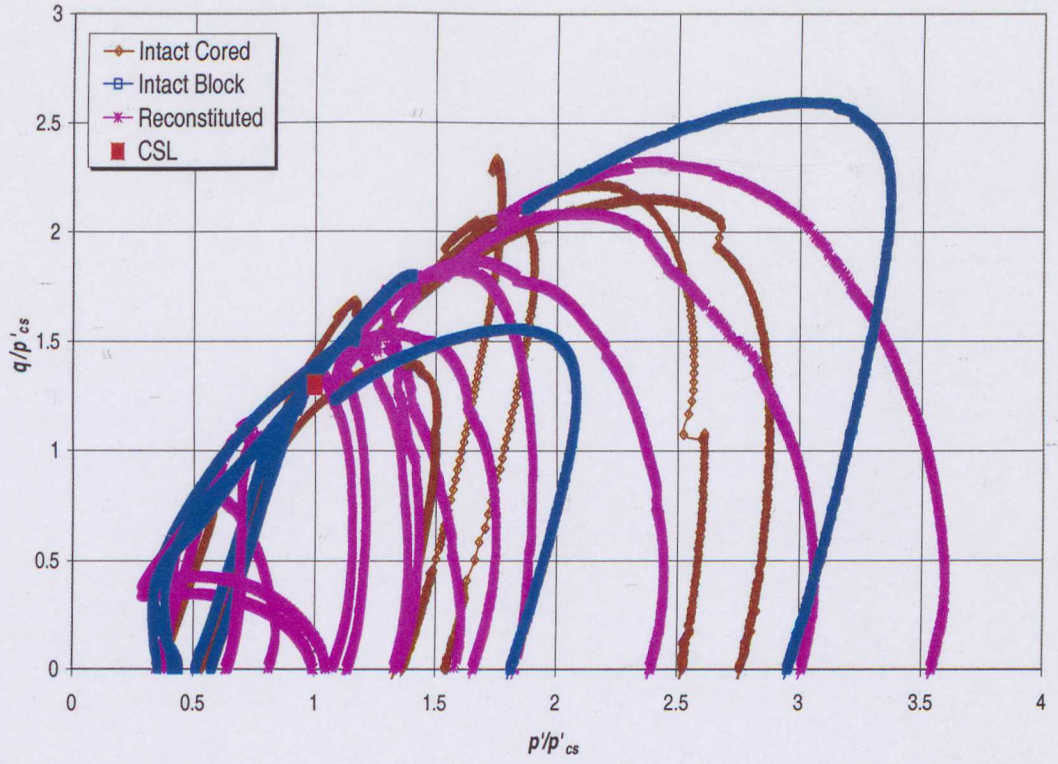


***Figure 5-50*** *Effect of sample type on normalised stress paths for high silt content material*

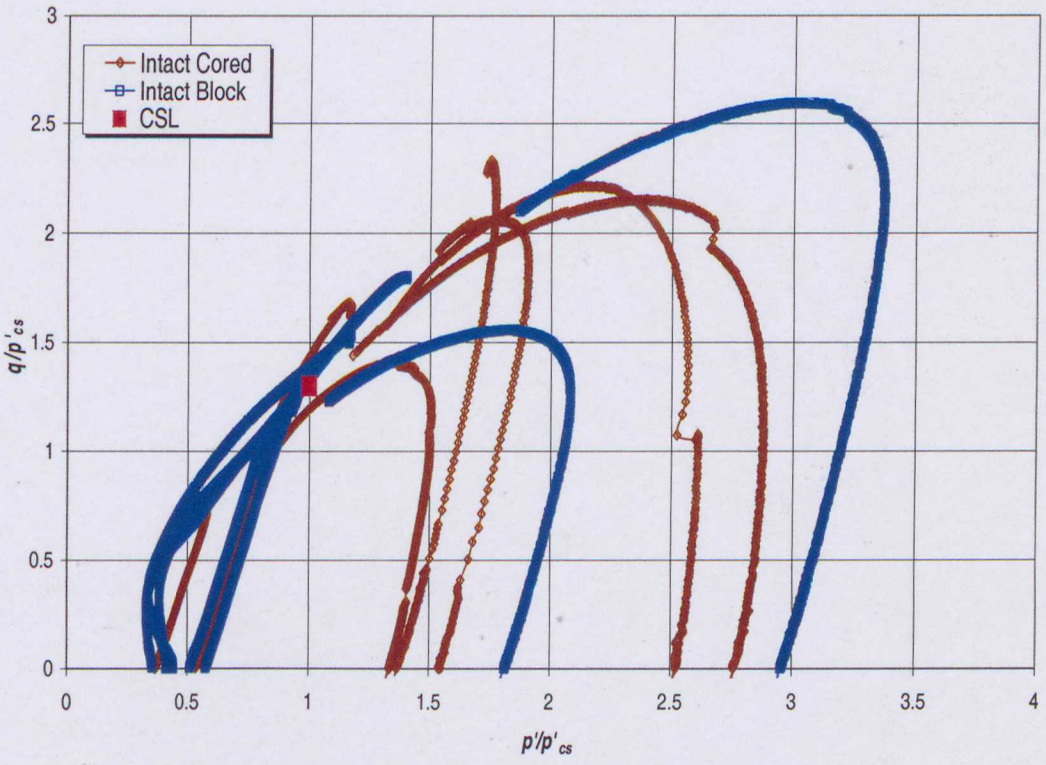


***Figure 5-51*** *Effect of sampling method on normalised stress paths for high silt content material*

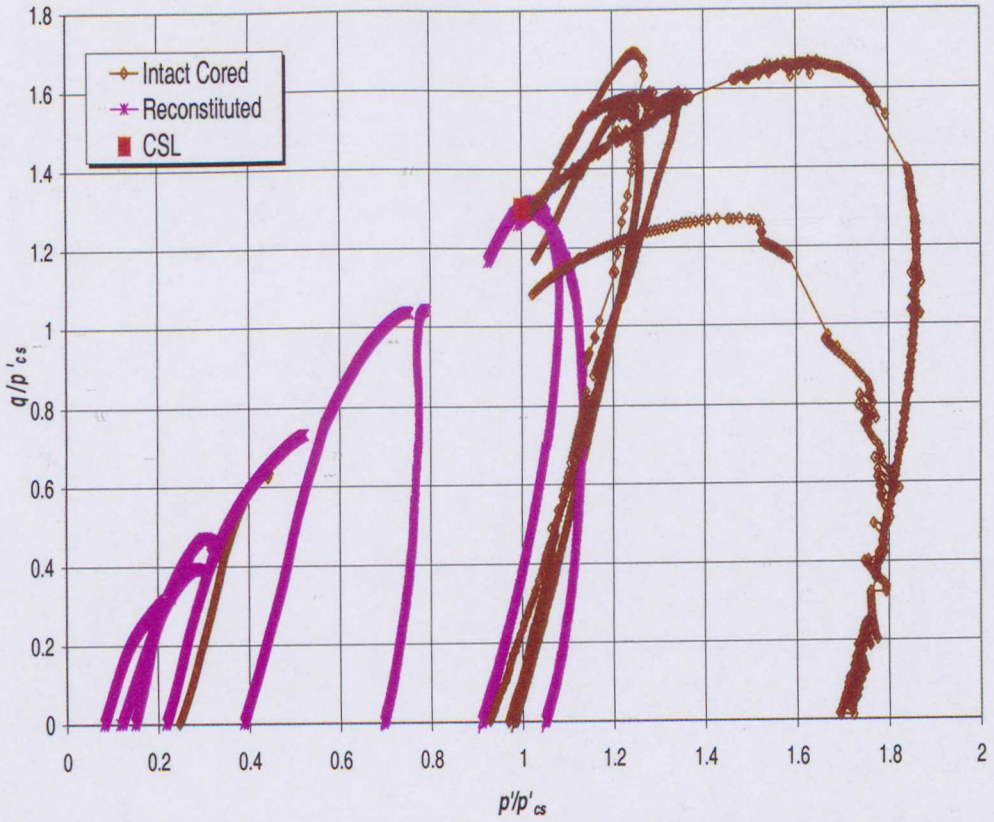


***Figure 5-52*** *Effect of sample type on normalised stress paths for low silt content material*

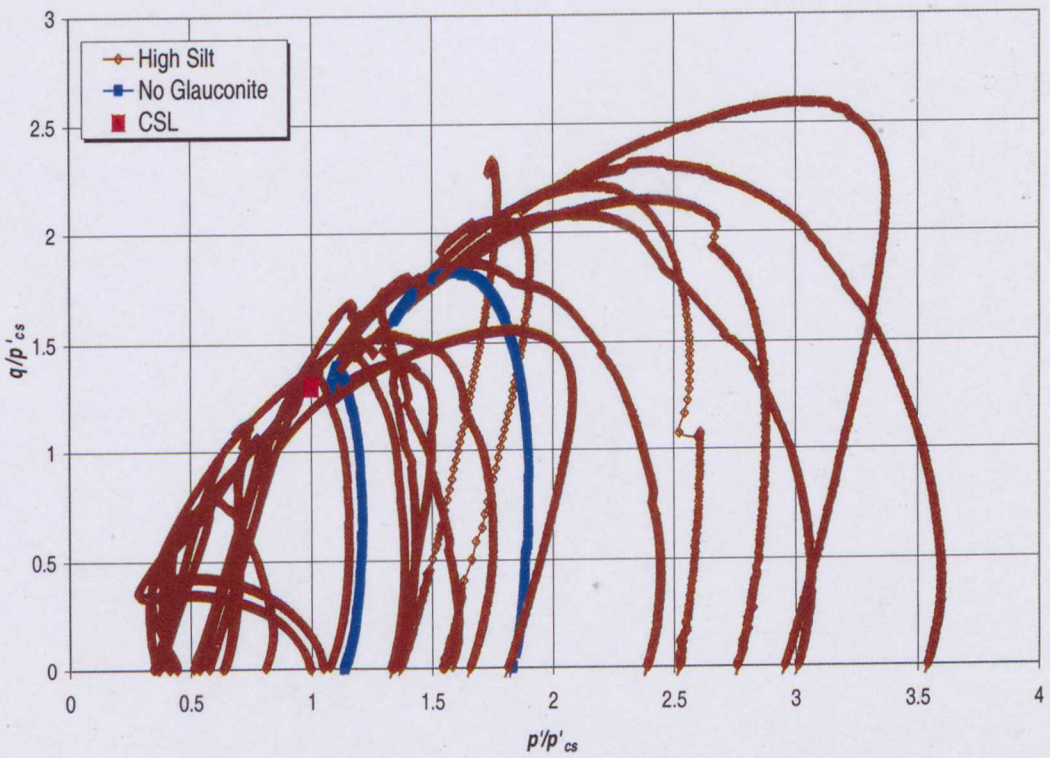


***Figure 5-53*** *Effect of glauconite on normalised stress paths for high silt content material*

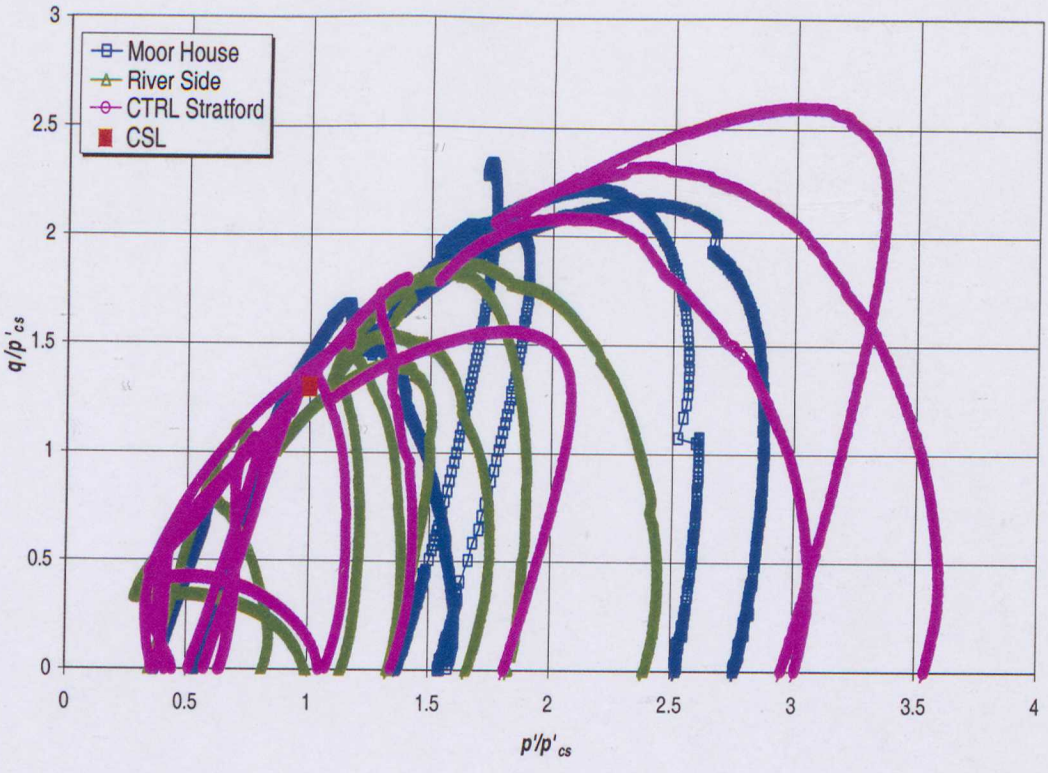


***Figure 5-54*** *Effect of site location on normalised stress paths for high silt content material*

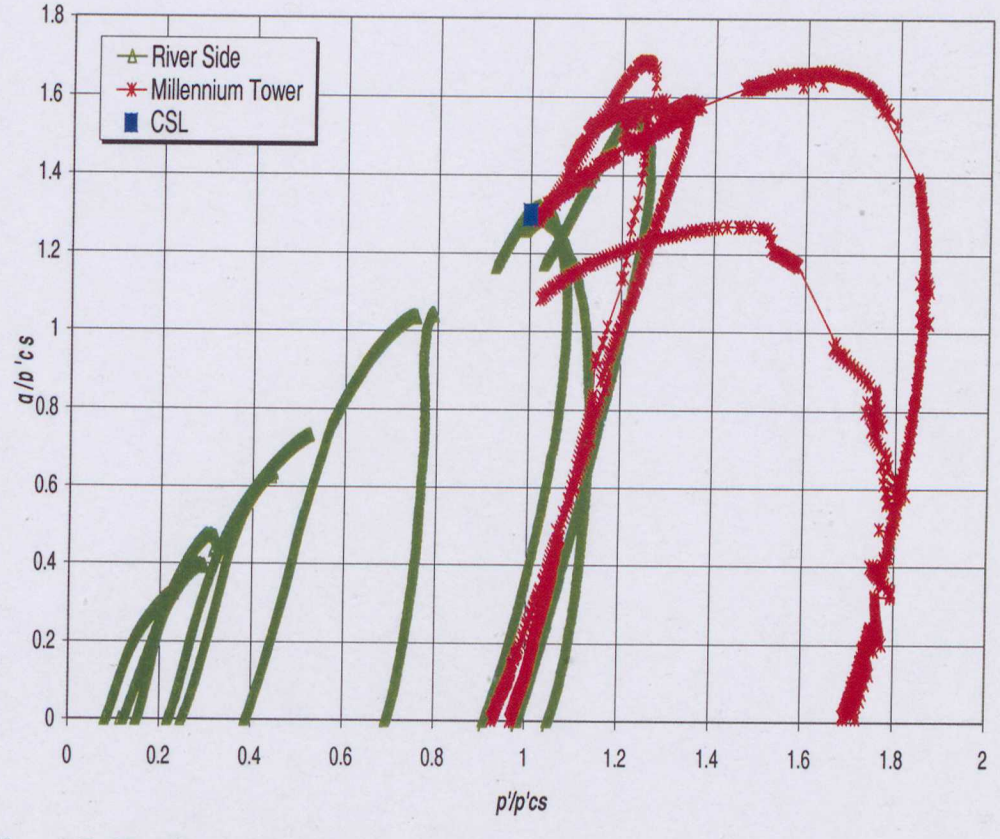


***Figure 5-55*** *Effect of site location on normalised stress paths for low silt content material*

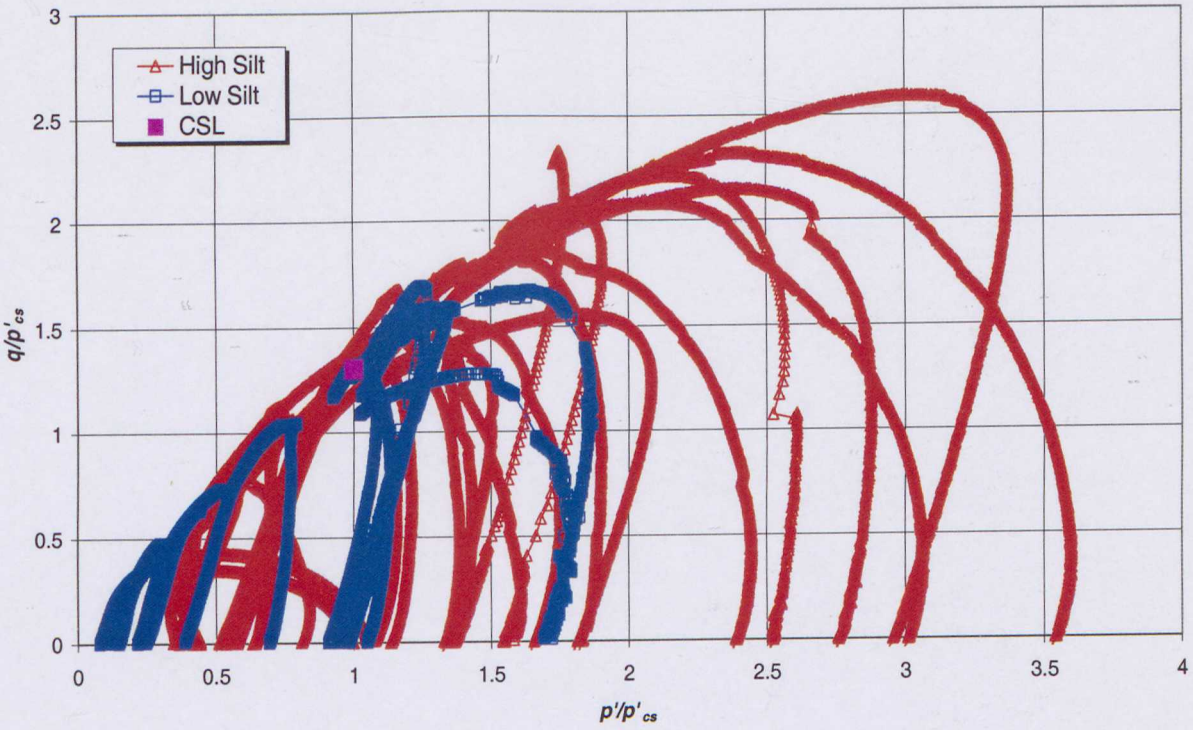


***Figure 5-56*** *Effect of silt content on normalised stress paths*

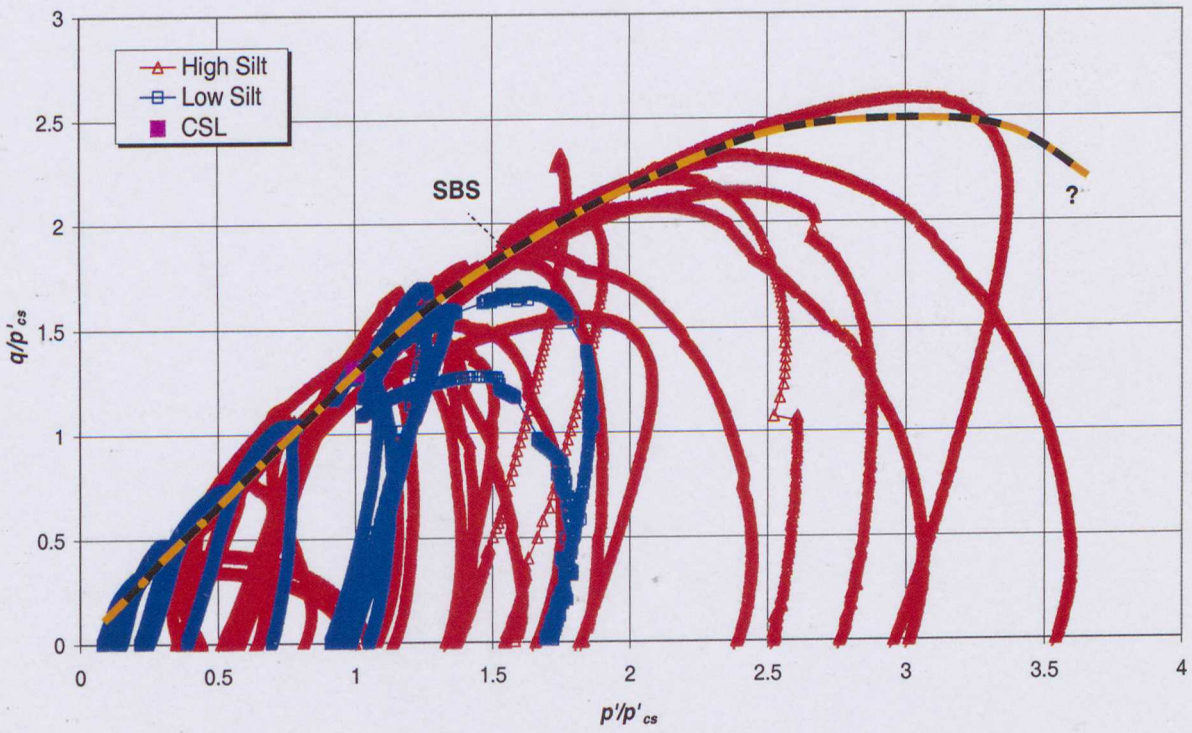


***Figure 5-57*** *Effect of silt content on normalised stress path space – State Boundary Surface*

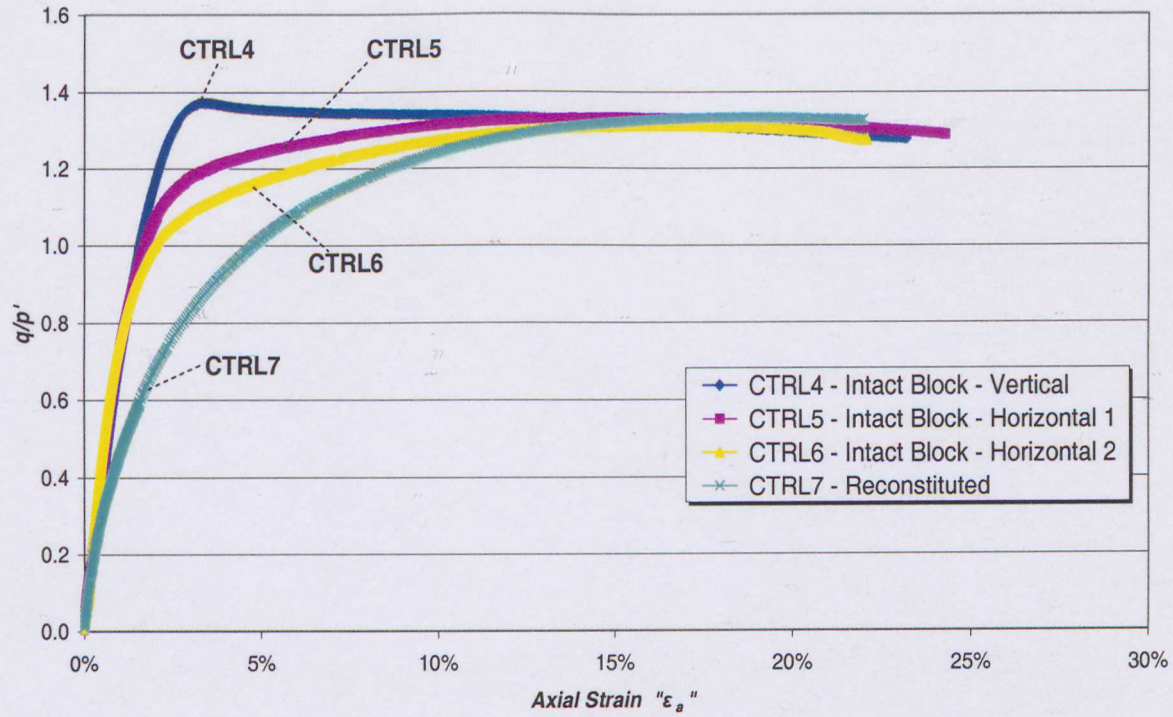


***Figure 5-58*** *Influence of anisotropy on stress:strain behaviour of drained tests*

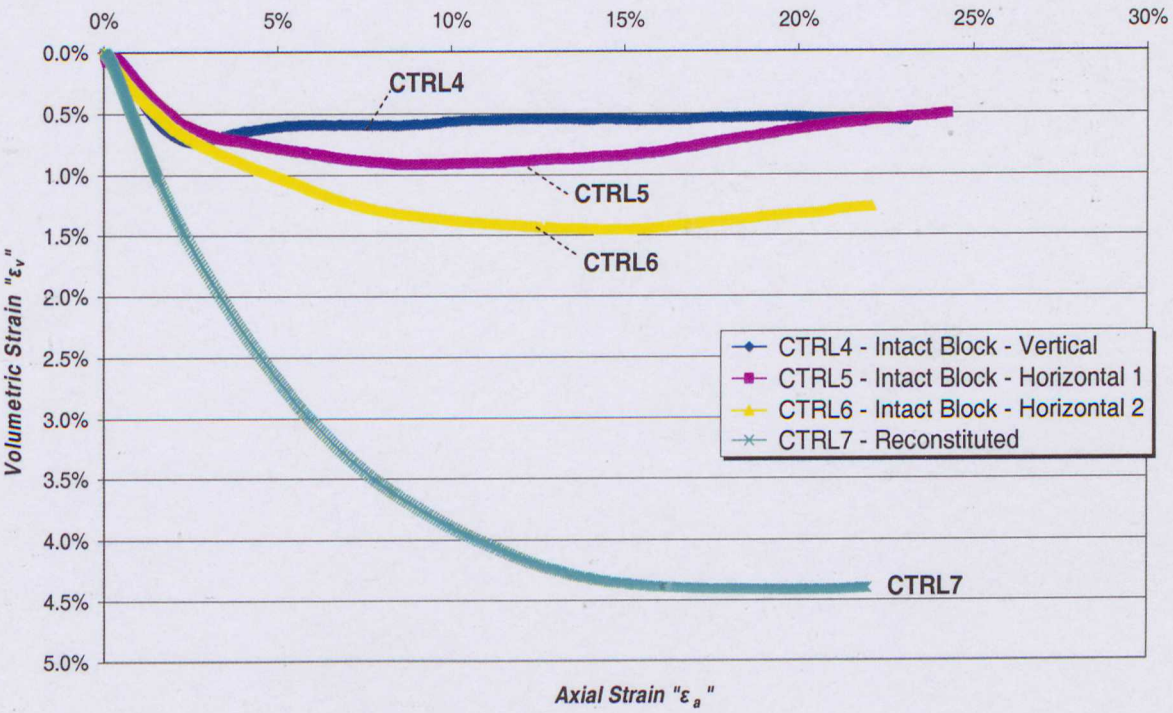


***Figure 5-59*** *Influence of anisotropy on volumetric strain behaviour*

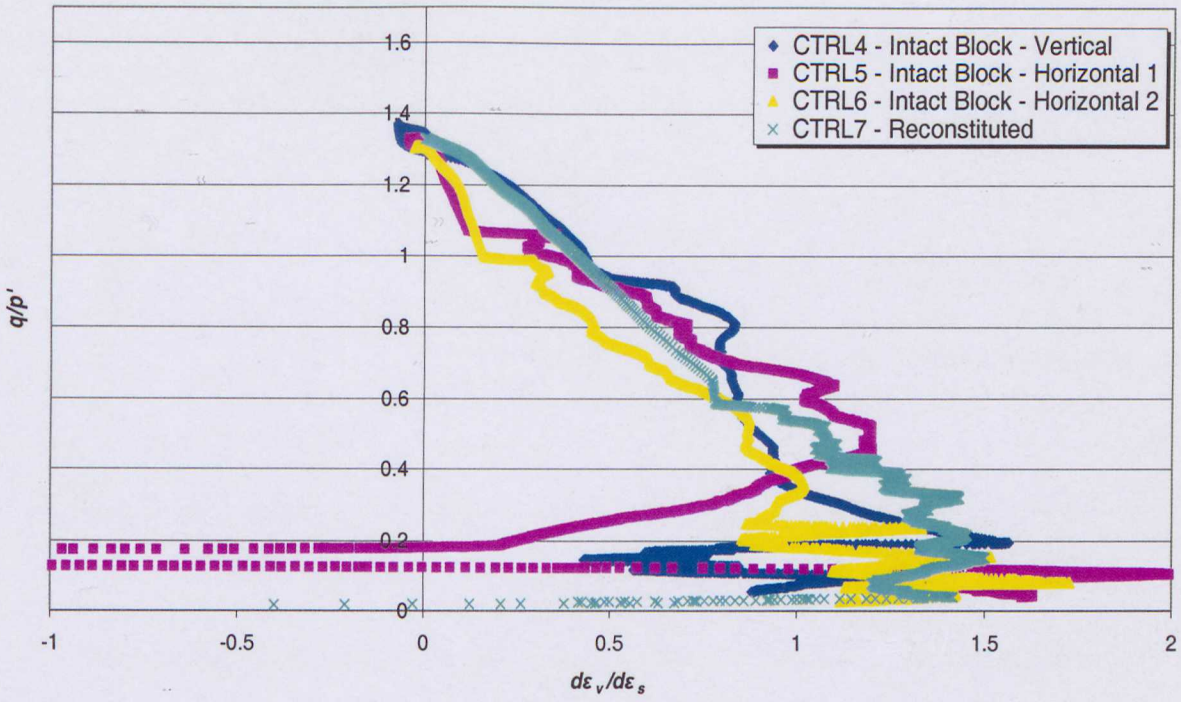


***Figure 5-60*** *Effect of anisotropy on stress:dilatancy behaviour*

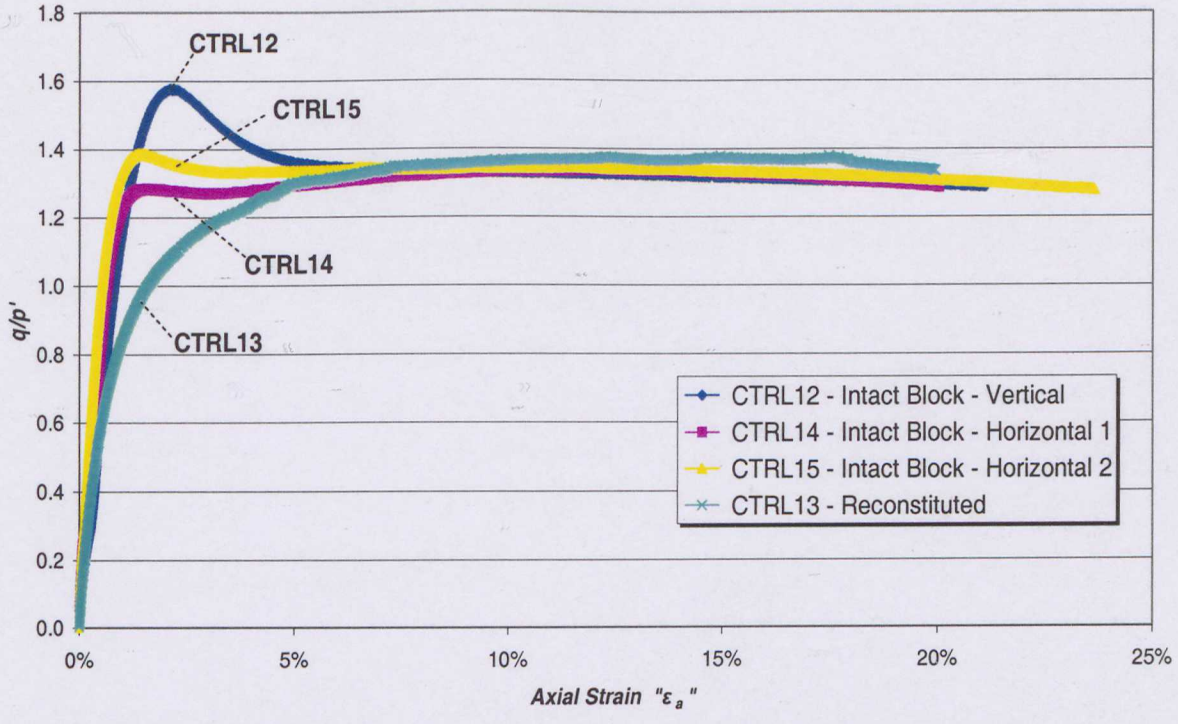


***Figure 5-61*** *Influence of anisotropy on stress:strain behaviour of undrained tests*

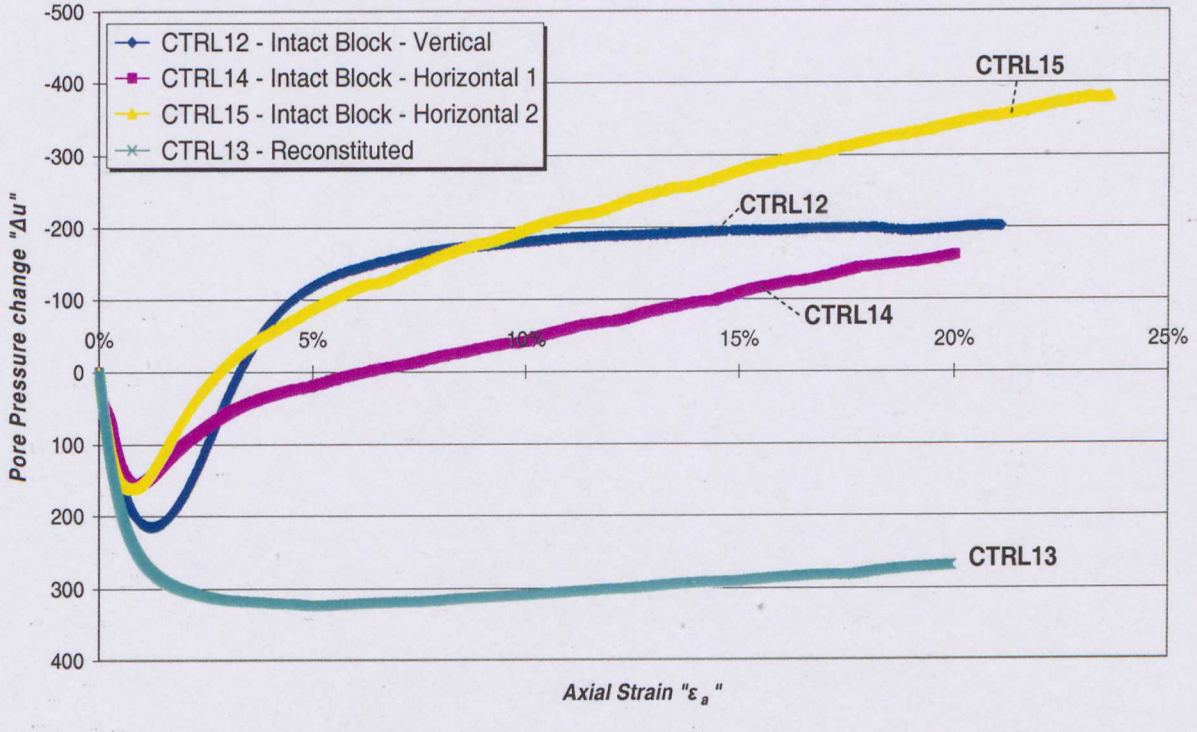


***Figure 5-62*** *Influence of anisotropy on generated pore pressure behaviour*

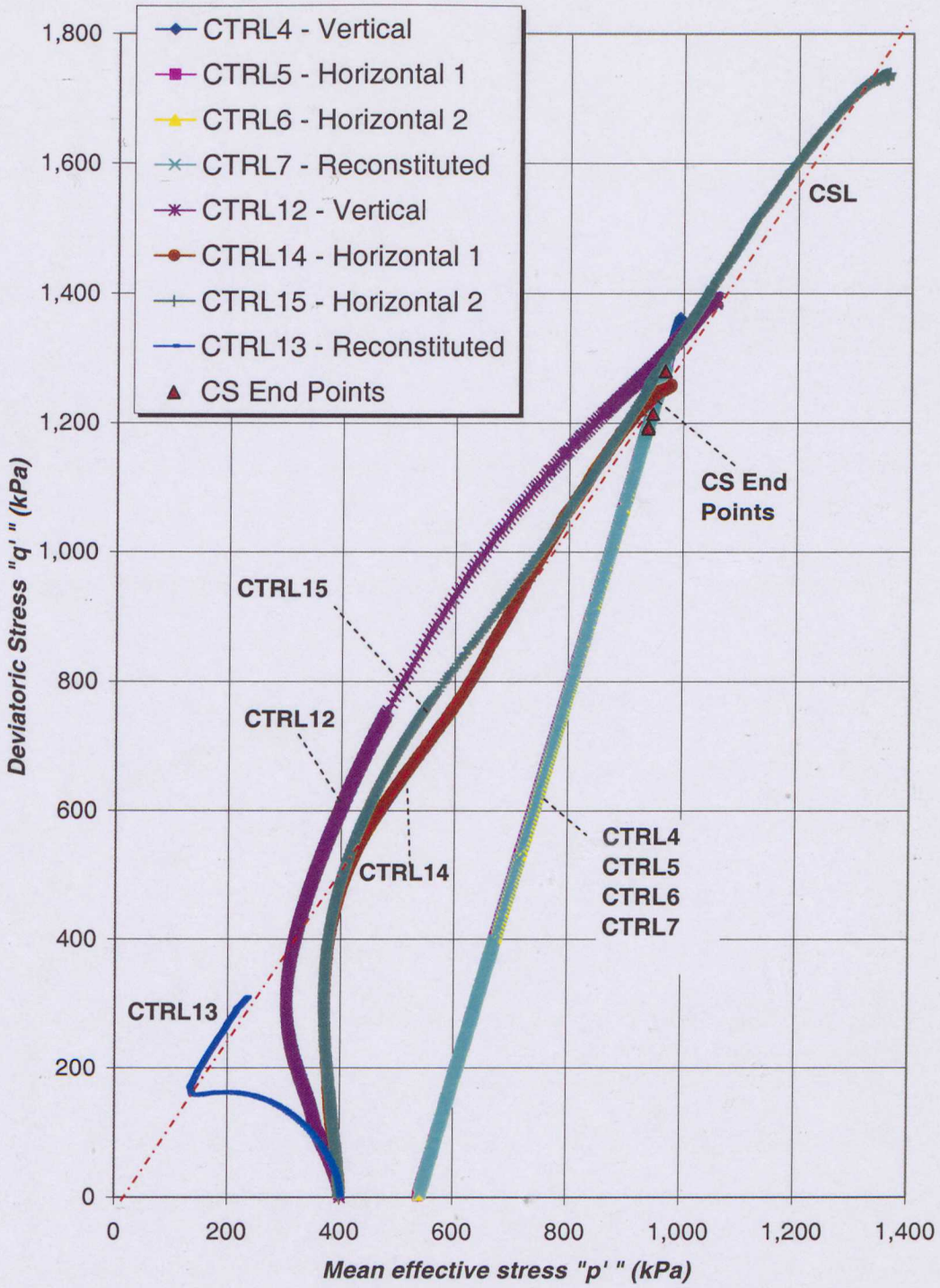


*Figure 5-63 Effect of anisotropy – all compression tests*

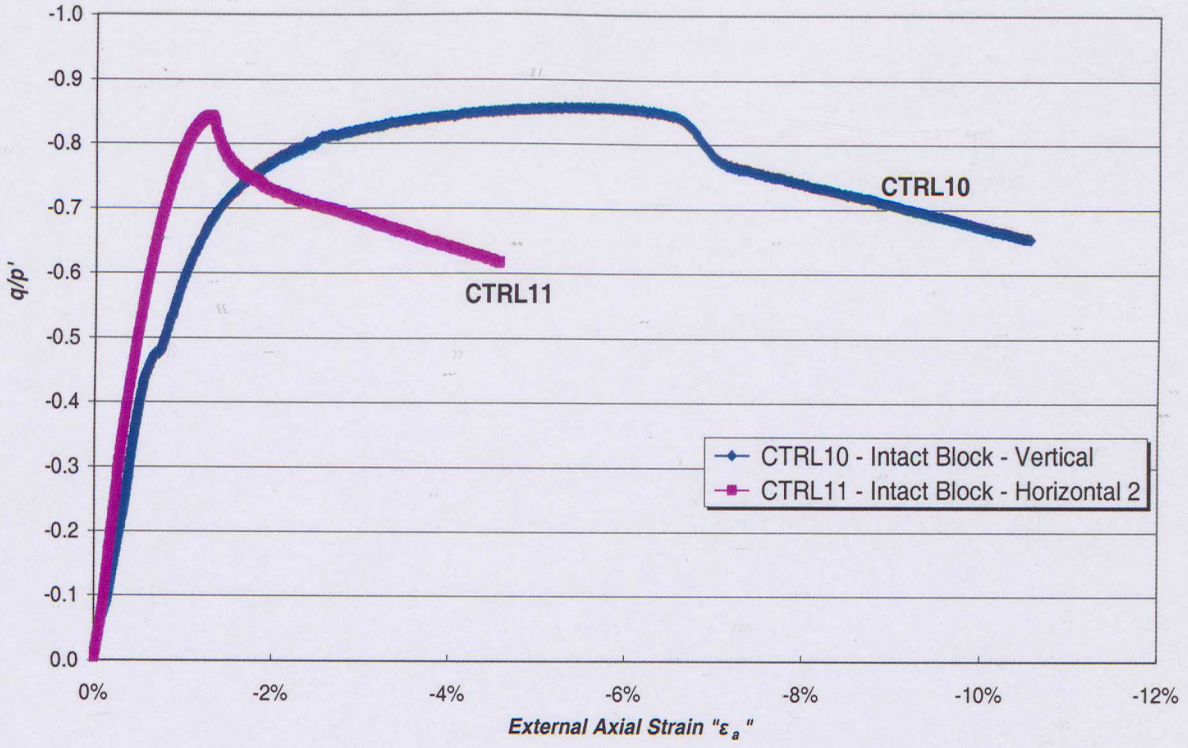


***Figure 5-64*** *Influence of anisotropy –extension tests plotted with external strains*

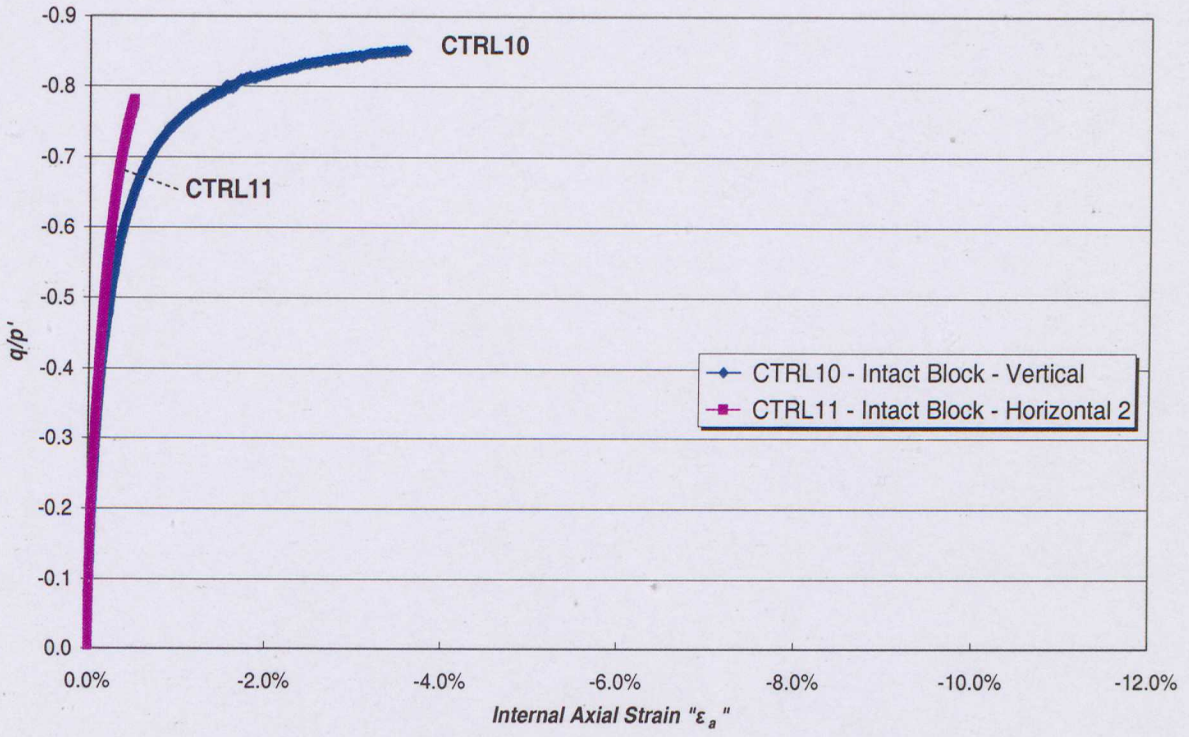


***Figure 5-65*** *Influence of anisotropy –extension tests plotted with internal strains*

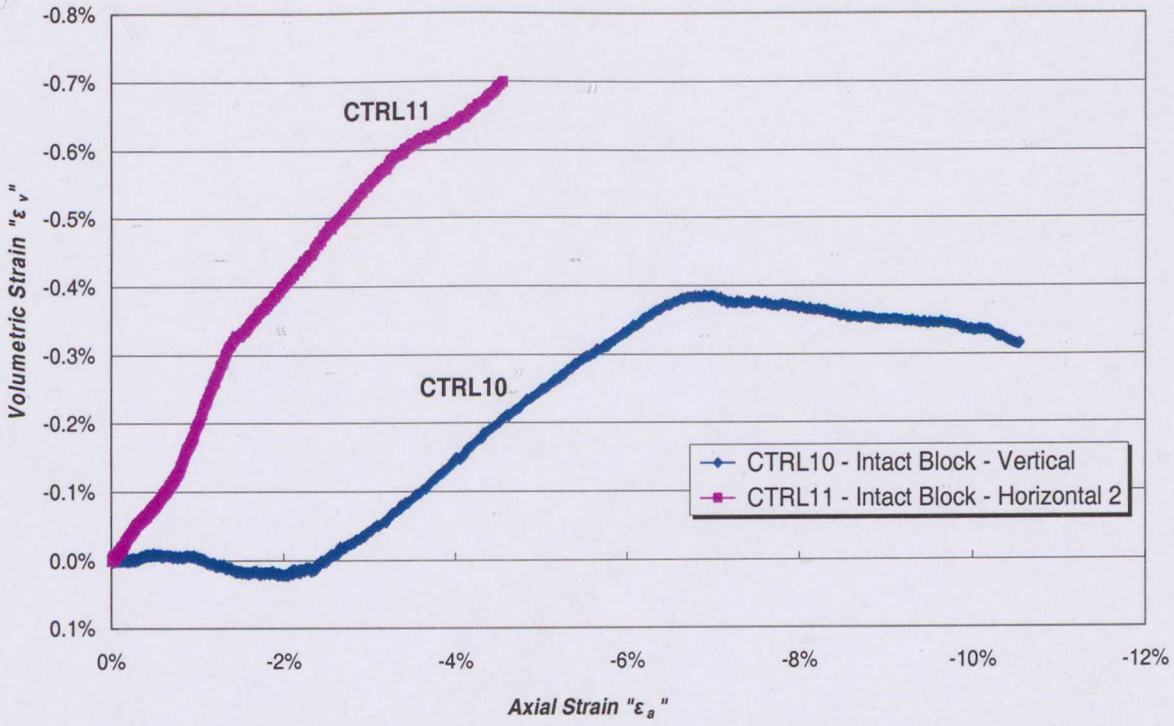


***Figure 5-66*** *Influence of anisotropy –extension tests plotted with external strains*

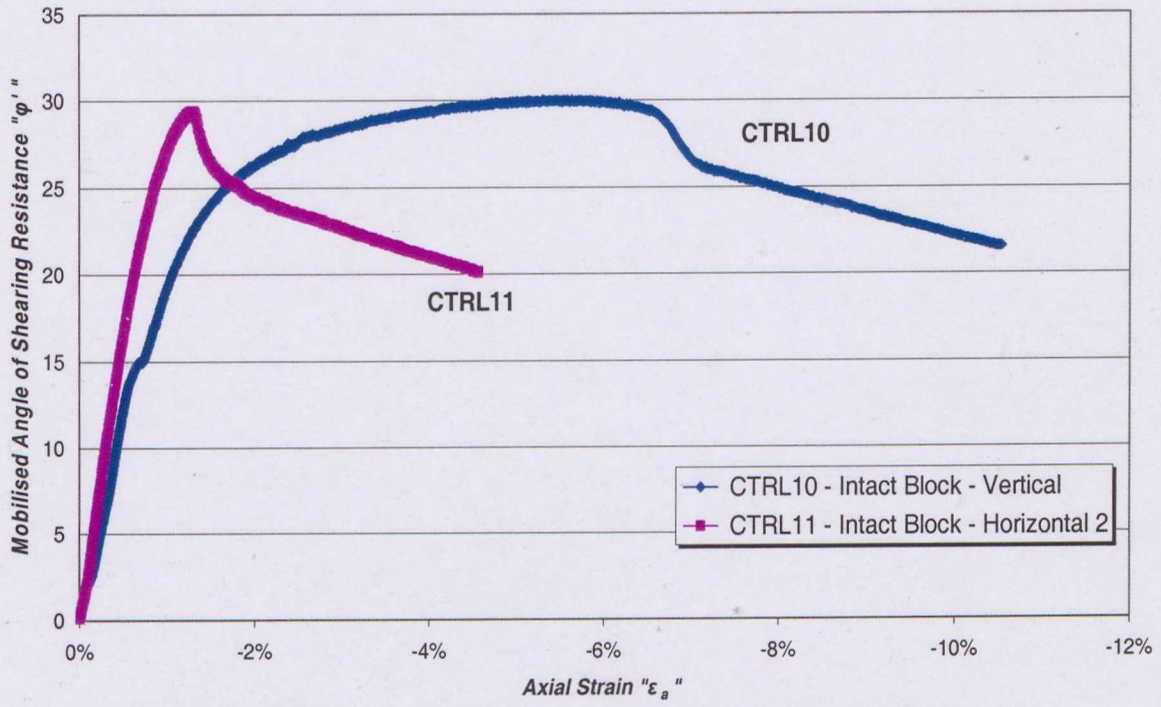


***Figure 5-67*** *Influence of anisotropy –extension tests plotted with external strains*

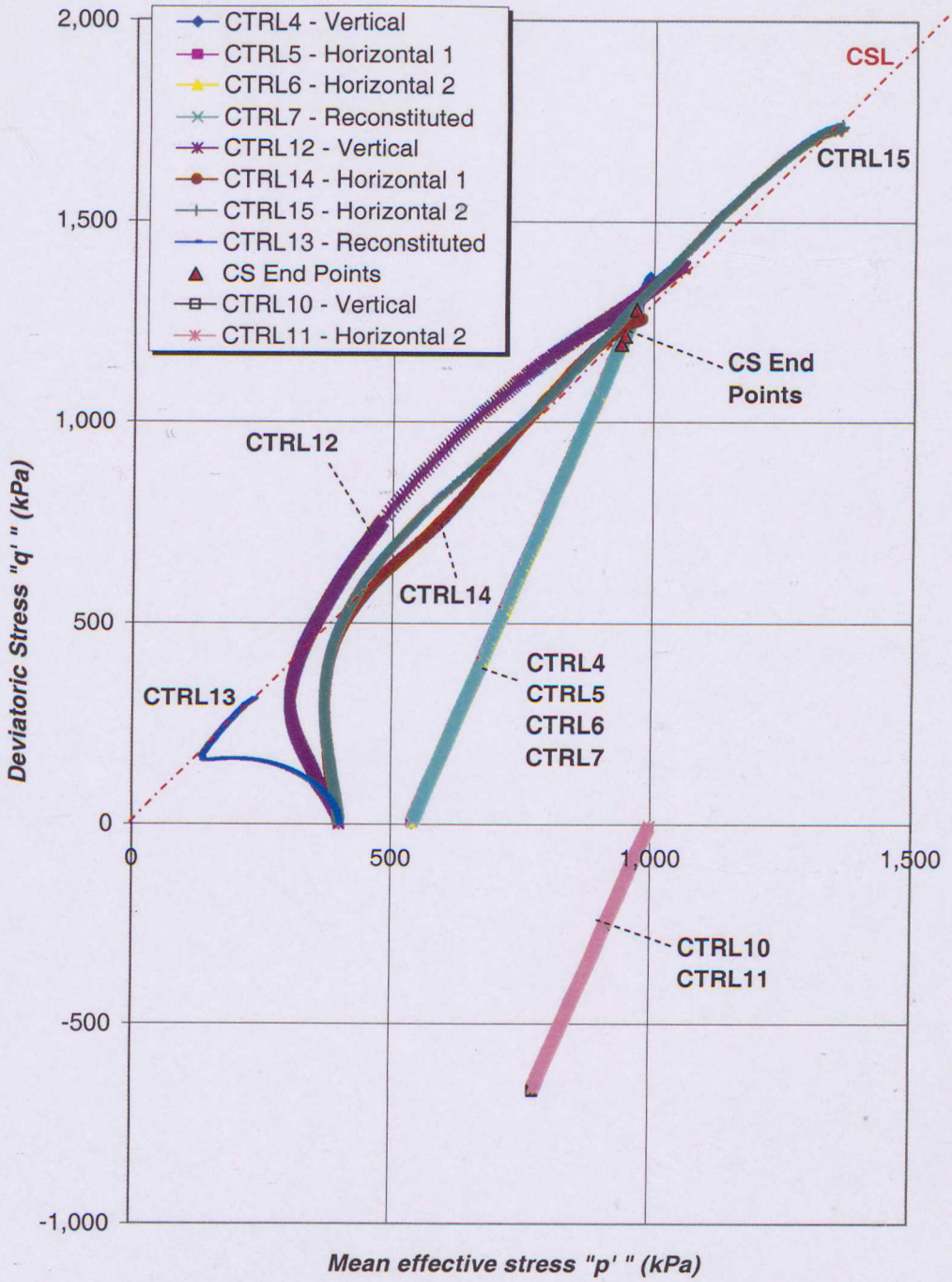


*Figure 5-68 Material anisotropy comparison – all tests*

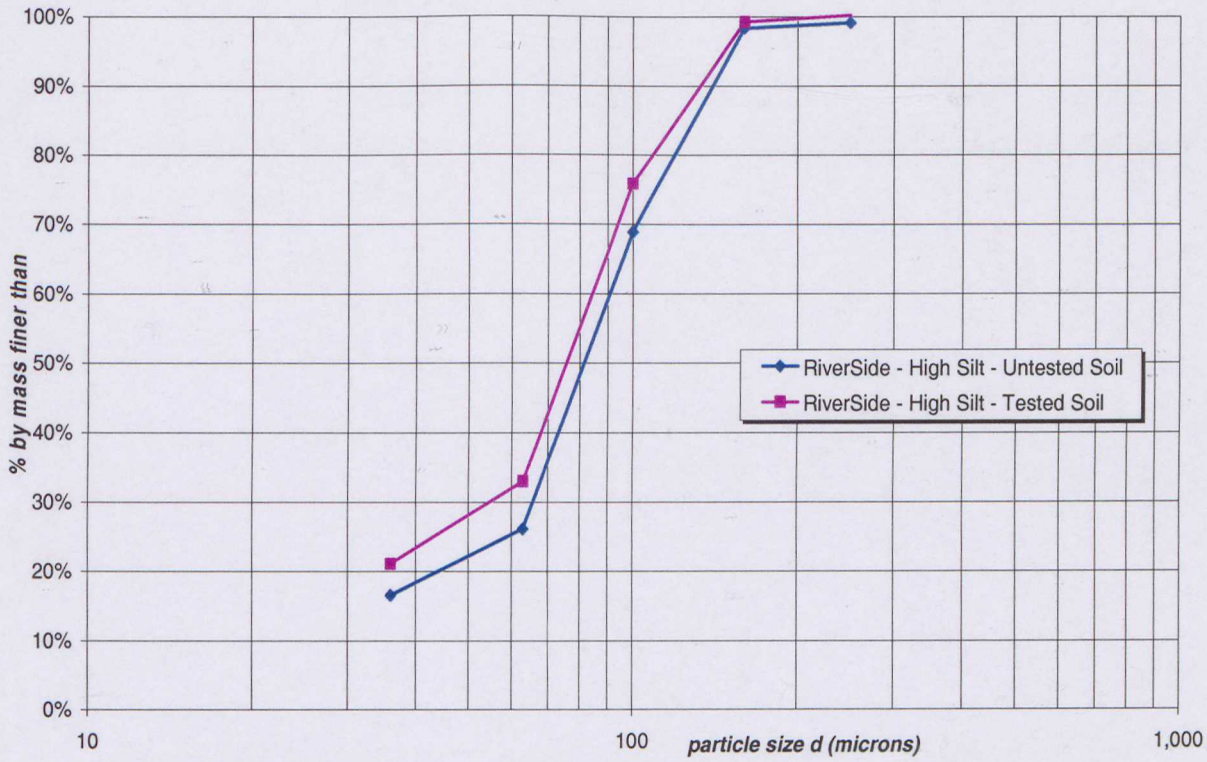


***Figure 5-69*** *Particle breakage – high silt content soil (experiment RS5)*

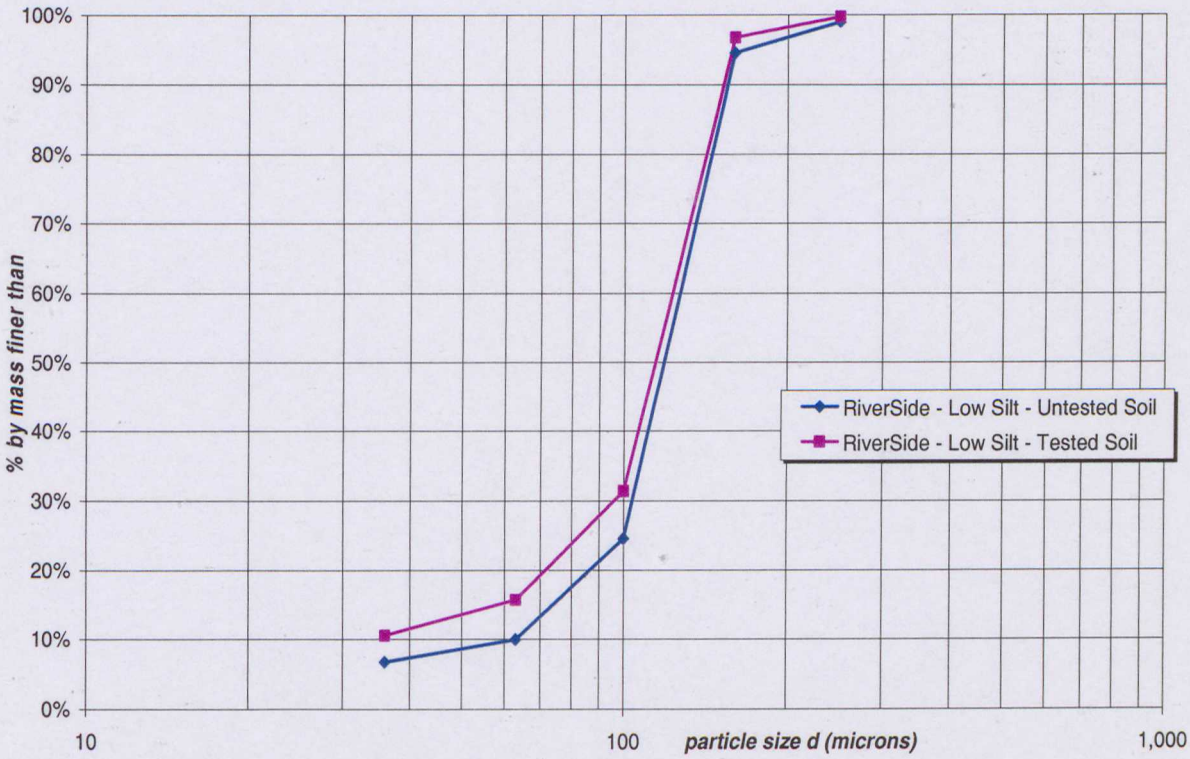


***Figure 5-70*** *Particle breakage – low silt content soil (Experiment RS1)*

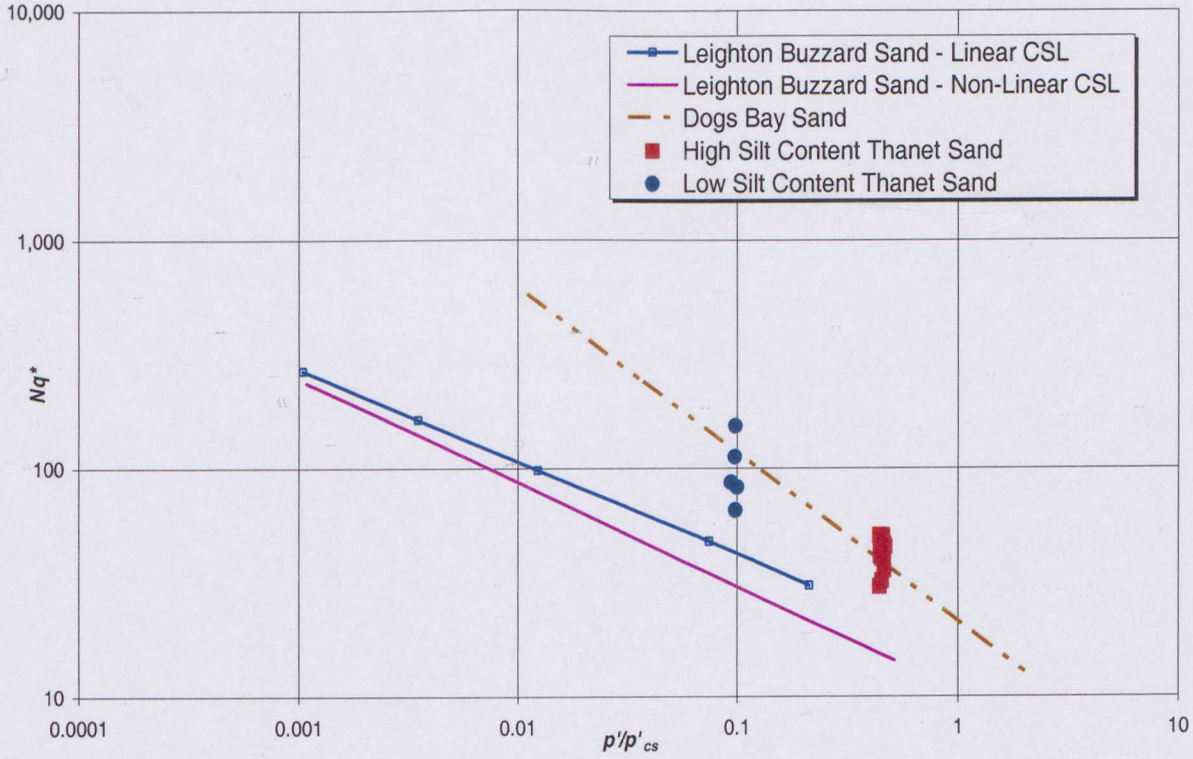


***Figure 5-71*** *Comparison of normalised pile end bearing capacities with trends from Klotz & Coop (2001)*

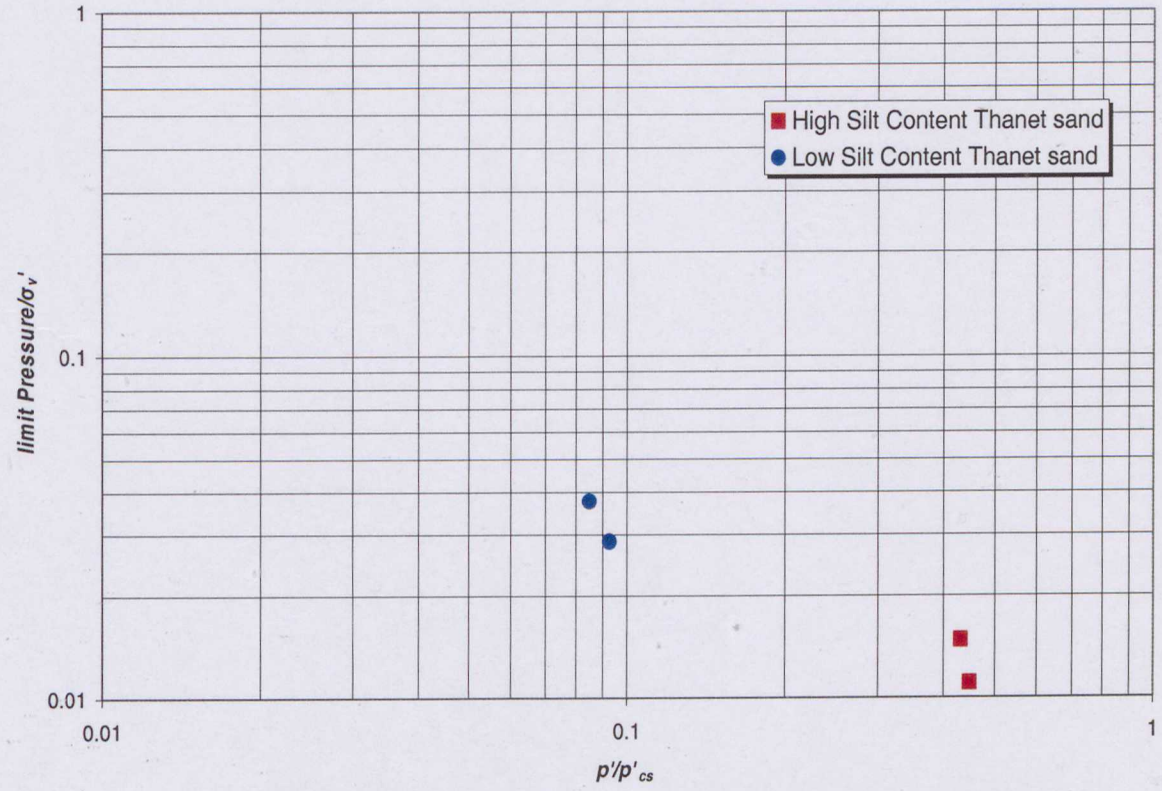


***Figure 5-72*** *Normalised Limit Pressures*

6 SMALL STRAIN BEHAVIOUR ..... 227

6.1 Introduction ..... 227

6.2 Bender Element Tests – Dynamic Shear Moduli ..... 227

6.3 Equivalent Monotonic Shear Moduli ..... 229

6.3.1 Trends ..... 229
6.3.2 Silt content effect ..... 230
6.3.3 Intact – reconstituted effect ..... 231
6.3.4 Glauconite effect ..... 233
6.3.5 Material Anisotropy ..... 233

6.4 Stiffness – Influence of Effective Confining Stress ..... 235

6.5 Yielding behaviour ..... 238

# 6 SMALL STRAIN BEHAVIOUR

## 6.1 Introduction

In this chapter, the small strain behaviour of Thanet sand will be examined and with the use of a series of cross-comparisons, the influencing factors on the material behaviour will be distinguished and identified. As discussed in Chapter 5, the main factors examined were: the amount of silt content contained within the sand, whether the soil was intact or reconstituted, the sampling method of the soil as well as anisotropy. As for the specific site a tested sample came from, it was shown in Chapter 5 that it has no detectable influence on the material behaviour at large strains, based on the data available for analysis and comparison. Therefore, the specific site of origin of a sample is not examined again in this chapter.

## 6.2 Bender Element Tests – Dynamic Shear Moduli

As discussed in Section 3.2.4, the high pressure triaxial cell was equipped with bender elements. This allowed the variation of the dynamic shear modulus ($G_{VH}$) with p' to be determined. In order for the effect of structure, if any, to be examined, the dynamic shear moduli from a series of paired intact and reconstituted samples are presented. Again, it must be emphasised that the target void ratio of the reconstituted samples was the void ratio calculated from their intact counterparts, even though that was not always achieved (refer to Section 3.4.3).

Figure 6-1 shows data from two experiments on high silt content samples; RS5, a test on an intact cored sample and RS9, a test on a reconstituted sample. As can be seen from the figure, the reconstituted sample appears to give marginally higher

dynamic shear moduli than the intact sample, at the same p'. This set of data is the opposite of what a structured soil is expected to give. As will be shown in the following two cross-comparisons, having the reconstituted sample being stiffer than the intact, is not a repeated observation and is solely isolated to experiments RS5 and RS9. The reason for this is believed to be an electrical fault in the bender element testing equipment during test RS9. An electrical leak between transmitter and receiver may have caused a systematic offset of stiffness readings for this test.

The same graph of dynamic shear modulus versus effective confining pressure is shown Figure 6-2 for low silt content Thanet sand. In this case, the intact sample (Test RS1) gives consistently slightly higher values of $G_{VH}$ compared to its reconstituted counterpart (Test RS2). The offset that is observed between the two data-series can be considered to be a measure of the effect of structure of the material.

Figure 6-3 shows results from two high silt content samples; CTRL17, an intact block sample and CTRL16, a reconstituted sample. Again, the intact soil appears to have a slightly stiffer response than the reconstituted soil. The offset observed between these two tests is of the same order of magnitude as that for the low silt content pair of tests in Figure 6-2.

Finally, Figure 6-4 contains all available bender element test data. With the exception of experiment RS9, it can be seen that all the intact samples gave higher dynamic shear moduli than the reconstituted samples. Re-plotting all experiments without RS9 (Figure 6-5) we can see that all tests appear to form a linear relationship between p' and dynamic shear modulus. They appear to lie within a narrow band, with each test parallel to one another, converging to a unique line, one per sample type, at higher confining pressures. This line is the Normal Compression Line of the soil. This pattern of behaviour was presented in Section 2.3.1 (Figure 2-4). Typically, denser samples tend to require higher confining pressures to reach the location of the NCL in $\log G_0$-$\log p'$ space. An example of the effect of delayed convergence due to different densities for Thanet sand can be seen for tests CTRL16 and RS2, where the latter needs much higher levels of p' to converge to the final straight line shown on the plot. Even though RS2 and

CTRL16 are tests of different silt content material, it will be shown in the following paragraph that this has little effect on the stiffness of the soil. Therefore, the behaviour is solely attributed to the different initial densities of the two samples.

The most important result from Figure 6-5 is that the derived trends for the intact and reconstituted material show a clear offset between them. This is a clear manifestation of a small effect of structure on the behaviour of the soil. Although a distinction between intact and reconstituted samples is evident, no detectable difference can be seen between intact block and intact cored samples. Additionally, silt content does not appear to have an effect on the soil's behaviour as all intact and all reconstituted tests converge to the two corresponding lines, regardless of silt content. This provides additional proof that test RS9 was indeed influenced by an electrical fault as it is the only one that does not agree with the general pattern observed both in terms of silt content and the effect of structure.

Additionally, on the 100mm Thanet sand sample that was tested, horizontal bender elements were taken in two directions: $G_{HH}$ and $G_{HV}$ (Section 3.3.4). First arrival readings taken in both directions gave values of 303MPa for $G_{HH}$ and 162MPa for $G_{HV}$ at in-situ stresses. The difference of almost a factor of two between these readings is a direct result of the anisotropy of Thanet sand.

## 6.3 *Equivalent Monotonic Shear Moduli*

### 6.3.1 *Trends*

The equivalent monotonic shear moduli based in internal axial strain measurements, have been calculated according to Equation 3-13, as discussed in Section 3.6. Despite the rather large regression intervals that were used on the raw data, the shear moduli plots produced still contained large amounts of scatter that complicated their understanding. To eliminate this scatter and make the data more

usable for comparisons, trend curves had to be used through the stiffness degradation curves of the specific tests selected. These trends were derived based on the author's judgement and interpolation through the data. It must be noted that not all available experiments presented in Table 4-1 were analysed, as not all experiments could be used for stiffness comparisons; those chosen for comparisons shown in the following subsections of Chapter 6 are presented in Figure 6-6 to Figure 6-18. These plots contain the scattered data obtained from the calculation based on regressions, the smooth trend that was selected to be used later for comparisons as well as the dynamic shear modulus obtained from bender elements ($G_{VH}$) at the same initial effective confining stress, whenever such a reading was available. Bender element readings were taken on the high pressure triaxial apparatus for some samples, but are not available for all high pressure tests due to various rather frequent operational difficulties and problems with the bender element system of the apparatus. It should be noted that at small strains the curve of the equivalent monotonic shear modulus ($G_{EQ}$) must not necessarily match the dynamic shear modulus obtained from bender element readings as the soil might not be isotropic. In Figure 6-6 for example, the selected curve does indeed match the bender element reading whereas in Figure 6-7 the equivalent monotonic shear modulus trend is in fact slightly higher than the $G_{VH}$ obtained at very small strains. By looking at all the data, there is no obvious trend between $G_{EQ}$ and Go at very small strains. For some tests one is larger than the other whereas for other tests we have the reverse situation. Strictly judging by these data alone, it could be concluded that the soil has a rather isotropic behaviour. As has been seen in Section 5.6 and will be shown in Section 6.3.5, this is not the case since Thanet sand was found to have a high degree of anisotropy.

### *6.3.2 Silt content effect*

In order to examine the effect the amount of silt has on the small strain behaviour of Thanet sand, two sets of tests shall be presented; a set of high and low silt content samples initially intact and another set of reconstituted samples

Figure 6-19 shows two experiments on intact Thanet sand samples sheared in drained compression at initial mean effective stress of 4MPa; RS1 is a low silt content sample with initial spesific volume of 1.714 and RS5 a high silt content sample with initial specific volume of 1.681. For shear strains up to 0.003%, the high silt content sample appears to be marginally stiffer than the low silt content sample, with the difference though not exceeding 10%. For shear strains larger than 0.003% both experiments show similar stiffness behaviour with strain. Given the difficulties in defining $G_{EQ}$ at low strains, these differences are not significant.

To complement the intact comparison, Figure 6-20 presents the results from two reconstituted samples sheared in drained compression at 4MPa. Here, the low silt content sample (RS2 – $v_0$=1.704) appears to have a slightly higher stiffness than the high silt content sample (RS9 – $v_0$=1.831). This may at first appear to contradict what was seen for the comparison of intact samples, but this difference is not attributed to the effect of silt content. The cause for this divergence in behaviour is more probably the different initial specific volumes experiments RS2 and RS9 were setup at. As can be seen from Table 4-1, the two experiments were set up at specific volumes of 1.704 and 1.831 respectively, hence the initially denser soil (RS2) would be expected to have a higher stiffness during shearing.

When looking at both pairs of tests, it can be said that the amount of silt does not appear have an impact on the small strain behaviour of the soil. The intact pair of high and low silt content samples have very similar stiffness characteristics, whereas for the reconstituted pair, due to their initial difference in density, it is not possible to isolate an effect of silt content alone.

### *6.3.3 Intact – reconstituted effect*

In order to assess and quantify the effect of structure on the small strain behaviour of Thanet sand, pairs of intact and reconstituted tests have been compared and are presented, just as was done in Chapter 5. In total, three pairs of comparative tests are presented; one from cored high silt content material, one from cored low silt content material, as well as a pair from the block sample of high silt content soil.

The differences in behaviour observed from the diagrams that follow may then be primarily attributed to the effect of structure of the soil.

Starting with the comparison of the high silt content cored material, Figure 6-21 shows the equivalent monotonic shear moduli variations with strain for experiments RS5 ($v_0$=1.681) and RS9 ($v_0$=1.831) sheared in drained compression at 4MPa. Here, the intact sample appears to be consistently slightly stiffer than the reconstituted until shear strains of about 2%. From that point onwards, both tests appear to converge to similar decreasing trends. This could be interpreted as a manifestation of the effects of structure in the soil's behaviour.

Figure 6-22 presents the comparison for the high silt content block sample sheared in drained compression at 3MPa. Experiment CTRL17 ($v_0$=1.744) is an intact high silt content sample extracted with the block method and experiment CTRL16 ($v_0$=1.939) is a reconstituted sample from the same high silt content material. A clear difference between the intact and the reconstituted experiments can be seen, with CTRL17 showing a significantly higher stiffness.

Finally, the last comparison is presented in Figure 6-23. Here, a low silt content cored sample RS1 ($v_0$=1.714) is compared with its reconstituted counterpart, test RS2 ($v_0$=1.704). Both tests have been sheared drained at initial $p_0'$ of 4MPa. They appear to follow almost identical trends and from these two low silt content tests, no difference can be seen in terms of stiffness variation with shear strain between intact and reconstituted samples.

Combining all three sets of experiments together, it can be seen that for the first two high silt content pairs, a difference between intact and reconstituted samples can be seen whereas, in the case of low silt content material, both intact as well as reconstituted samples gave the same variation of equivalent monotonic shear modulus with shear strain. However, when interpreting these results, one should also consider the potential effect that the difference of initial void ratio between the intact and the reconstituted samples being compared might have. As can be seen from Table 4-1, for both high silt content pairs, there was a small but

significant difference in initial void ratios between the intact and the reconstituted samples. On the other hand, the two low silt content samples compared in Figure 6-23 were set up at almost exactly the same initial void ratio. Therefore, it is not possible to distinguish clearly to what extent the differences in behaviour observed in the first two cases are an effect of initial soil density or to what extent they are an effect of the structure of the soil, if indeed it exists. Either way, it is clear that any effect of structure on equivalent monotonic shear moduli at these strain levels is small, as was the case for the dynamic shear moduli seen in Section 6.2.

### *6.3.4 Glauconite effect*

In order to assess how Glauconite affects the small strain behaviour of Thanet sand, results from two high silt content reconstituted samples both sheared drained at an initial effective confinement of 4MPa are presented in Figure 6-24. Test RS9 ($v_0$=1.831) is a normal high silt content reconstituted sample whereas RS10 ($v_0$=1.747) a Glauconite-free high silt content sample. As can be seen from the plot, the two experiments show no significant difference in terms of their shear modulus variation with strain, indicating once more that the Glauconite does not appear to have an impact on the engineering behaviour of Thanet sand.

### *6.3.5 Material Anisotropy*

In order to assess the anisotropy of Thanet sand, vertical and horizontal samples that were cut from a block (Figure 3-31) and in turn tested in drained compression, undrained compression as well as drained extension will be compared (Figure 2-58). As the samples that are presented in this section were all intact samples that came from the same block of sand, they have no difference in initial void ratios; their only difference is the direction in which they were cut. Therefore, any divergence in behaviour between them is purely due to the anisotropy of the material.

In Figure 6-25 the results from a vertical and a horizontal sample sheared in drained compression are presented. The initial effective confinement for both samples was 0.55MPa. This comparison does not show any consistent difference in behaviour between the vertical and the horizontal samples. Both tests do have their own distinct behaviour, at certain strains test CTRL4 ($v_0$=1.807) is stiffer than CTRL6 ($v_0$=1.800), whereas at other strain levels, the situation is reversed, but no definite conclusions can be drawn from this pair of tests.

A comparison of a vertical and a horizontal sample sheared undrained in compression is presented in Figure 6-26. In this case, a well defined difference between the horizontal and the vertical samples can be seen. For shear strains up to 0.8%, test CTRL15 ($v_0$=1.780), which is the horizontally cut sample, is stiffer than the vertically cut sample, test CTRL12 ($v_0$=1.789). For the initial part of the two curves, at shear strains of about 0.0025%, the horizontal sample develops almost double the stiffness of the vertical sample

The final pair of experiments examined to assess the anisotropy of Thanet sand is presented in Figure 6-27. Here, a vertical and a horizontal sample have both been sheared drained in triaxial extension. Just as was seen before, the horizontal sample gives distinctly higher stiffness than the vertical sample, until shear strains of approximately 0.08% in this case.

It can be therefore concluded from what has been presented here that Thanet sand is stiffer horizontally than vertically. This in effect contradicts the general trend that was seen in Section 6.3.1 where $G_{EQ} \approx$ Go at very small strains, but agrees with the observations in Section 5.6.2 that the horizontal samples were stiffer in the larger strain range. It also confirms that the higher horizontal stifffness could cause the difference in undrained stress paths seen in Figure 5-68.

Kuwano (1999), working on Ham River Sand, showed that under isotropic conditions HRS was stiffer in the vertical direction than the horizontal. The Thanet sand in this case, even though it is in almost isotropic conditions (see Figure 3-32), gives a higher horizontal than vertical stiffness. When comparing the two studies of anisotropy, though, one must consider that this study on Thanet

sand was based on intact samples whereas the Ham River sand was based on reconstituted samples which then had a selected stress history simulated in the apparatus.

## 6.4 *Stiffness – Influence of Effective Confining Stress*

In order to investigate how the stiffness of the soil varies at different levels of effective confinement, equivalent monotonic stiffnesses have been plotted against mean effective stress at two specific strain levels of 0.01% and 0.1% from all available reconstituted and vertical intact samples sheared in both drained as well as undrained compression. In order to incorporate both high as well as low stress experiments in the same plot, logarithmic scales were used for both axes. This does not distort in any way the shape of the potential trend formed but merely allows all results to be plotted and compared in a single graph.

Figure 6-28 shows the equivalent monotonic shear moduli at a shear strain of 0.01%. Here, the tests have been grouped based on the amount of silt in the specific sample tested. The stiffnesses lie within a narrow band that is almost linear and gently convergent to the trends for $G_0$ from Figure 6-4, with a tendency to converge and even cross at higher pressures. This pattern of behaviour was reported by Jovicic & Coop (1997) from tests on Dogs Bay sand (Figure 2-4), although they also saw a similar pattern for Ham River sand. The scatter is partially caused by the different initial densities of the samples. It must be noted that no normalisation for the initial density variation has been preformed. As for the effect of silt content, from an examination of the plot, a possible pattern of behaviour arises. The low silt content tests appear to have slightly higher stiffnesses than the high silt content samples. However, it must be taken into account that there is considerable scatter in the data. Figure 6-29 shows the trends from both the equivalent monotonic shear moduli as well as dynamic shear moduli. The linear trends are close but have a small difference in slope. It must be emphasised that trends from $G_0$ and $G_{EQ}$ at 0.001% should not cross if the soil is

isotropic and the fact that they tend to, as shown in Figure 6-29, could be argued to be an effect of anisotropy.

Figure 6-30 presents the equivalent monotonic shear moduli of all the selected tests at a shear strain of 0.1%. The data have been again grouped based on the silt content of the soil. Again, the results form a linear band, with the low silt content stiffnesses appearing to be slightly higher than those of the high silt content soil, within the scatter. The dynamic shear moduli data have again been added to the monotonic data and presented in Figure 6-31. Some difference in slope is observed as was seen before with a larger offset between the dynamic and monotonic shear moduli. This is due to stiffness degradation taking place during sample shearing. Figure 6-32 shows the dynamic shear moduli along with the monotonic shear data for both shear strain levels. It can be seen that the 0.01% and 0.1% shear strain equivalent monotonic shear moduli form parallel trends, with the dynamic moduli trends converging and crossing the first pair. It must be emphasised that silt content was been show to affect soil stiffness at small strains ($G_{EQ}$) and not at very small strains, i.e. dynamic shear moduli $G_0$. in Chapter 5 it was found that once the effect of state had been accounted for, there was little difference in the stess:strain behaviour at larger strains. The difference in state between the high and low silt content samples may to some extent explain the small difference in $G_{EQ}$ values, but in that case it would also be expected that $G_{VH}$ would also be different.

Moving from the effect of silt content to the effect of sample type and therefore effect of structure on stiffness, Figure 6-33 presents the equivalent monotonic shear moduli at a shear strain of 0.01%. On this plot though, the tests have been grouped based on whether the sample tested was intact or reconstituted. Additionally, a distinction among the intact samples has been made based on the specific sampling method. Within the scatter, the stiffnesses of the intact samples do appear to be slightly higher than those of the reconstituted samples, suggesting that structure again does indeed have a small impact on the soil stiffness. As for the two sampling methods, no apparent difference between the two can be seen in terms of stiffness. Again, Figure 6-34 shows the trends from both the equivalent monotonic shear moduli as well as dynamic shear moduli.

Finally, Figure 6-35 shows the equivalent monotonic shear moduli of all selected experiments at a shear strain of 0.1%. Again, the tests have been grouped based on whether the sample tested was intact or reconstituted. Just as was seen at 0.01% strain, the initially intact samples have slightly higher stiffnesses than the reconstituted samples. The offsets of the trend-lines for natural and reconstituted samples at 0.01% and 0.1% shear strain seem similar to those of the $G_0$ values, as shown in Figure 6-36. Figure 6-37 shows the dynamic shear moduli along with the monotonic shear data for both shear strain levels. It can be seen that, once again, the 0.01% and 0.1% shear strain equivalent monotonic shear moduli form parallel trends, with the dynamic moduli trends converging to and even crossing the dynamic data.

From the first two comparisons, it is clear that the amount of silt contained within Thanet sand does have a small impact on the monotonic stiffness behaviour ($G_{EQ}$) of Thanet sand, with the low silt content soil giving slightly higher stiffnesses than the high silt content soil, at both strain levels, but there is no measurable effect on the dynamic shear modulus, $G_0$. As for the effect of structure, it can be seen from the last two comparisons that intact samples appear to give slightly higher stiffnesses than reconstituted samples. It was not possible, though, to assess the effect of the sampling method on the stiffness variation of the soil, as too few experiments were available for the differences caused by different sampling methods, if any, to become visible.

Ideally, for a broader understanding of the stiffness behaviour of Thanet sand, four distinct categories should have been formed when examining the equivalent monotonic shear moduli; (a) intact low silt, (b) reconstituted low silt, (c) intact high silt and finally (d) reconstituted high silt. In the comparisons previousely presented in this sub-chapter, part of the scatter arises due to the fact that the data has not been separated in this way. Unfortunately though, such a separation was not possible as again there were insufficient data to cover the entire stress range for the four suggested categories. In the absence of data, the alternative grouping method was used as presented.

## 6.5 *Yielding behaviour*

In order to assess the yielding behaviour of Thanet sand, an experiment was performed on a 100mm by 200mm sample, as discussed in Section 3.5.4. This experiment allowed the identification of the Y1 and Y2 yield points for selected stress-paths starting from an estimated in situ stress state (see Table 6-1).

The data used for the selection of Y1 and Y2 yield points are presented in Figure 6-38 to Figure 6-47. Y1 points were identified based on a change in the gradient of the stress:strain curve. Most Y2 points were identified based on a change in the gradient of $\varepsilon_v$:$\varepsilon_s$ or $\Delta u$:$\varepsilon_s$ depending on whether the experiment was drained or undrained, indicating a change of the strain increment vector.

All derived Y1 points have been plotted in stress space as shown in Figure 6-48, along with a possible Y1 envelope. Similarly, all derived Y2 points have been plotted together in stress space in Figure 6-49, with a possible Y2 envelope. It must be noted that this is based on only one set of probes and, as can be seen on the two figures, the uneven distribution of available data points leaves the location of much of the envelope in question. In order for the location and shape of the Y1 and Y2 envelopes to be more clearly defined, additional experiments with different stress-paths on block samples would be needed.

In comparison with the envelopes of Kuwano (Figure 2-48 & Figure 2-49), the Y2 envelope for Thanet sand is apparently more circular, although a test in axial compression is really needed to confirm this. When compared in both dimension as well as general shape to what was derived by Kuwano (Figure 2-48 & Figure 2-49), the Thanet sand yield envelopes appear to be very different. Kuwano presents highly asymmetrical envelopes, with the Y1 radius reaching values of 15kPa and the Y2 radius values of 150kPa or more whereas the average stress change prior to reaching Y1 and Y2 for Thanet sand was no more than 5kPa and 20kPa respectively. Additionally, as mentioned before, the asymmetrical shape of the envelope shown in Figure 2-48 was attributed to the recent stress path history

which was not evident here. It is not known why the yield surfaces of Thanet sand are so much smaller than those that Kuwano determined. The reverse might have been expected as these tests were performed on intact samples whereas Kuwano tested reconstituted samples.

It was also intended for the elastic parameters of intact Thanet sand to be calculated. Unfortunately, as the quality of some of the probes performed (see Table 6-1) was not high enough, it has not been possible to calculate all the parameters presented in Section 3.6. Those parameters that were calculated include: the vertical Young's Modulus in compression $E_v^{comp}$ (Probe E), which was found to be 450MPa (Figure 6-41); the vertical Young's Modulus in extension $E_v^{ext}$ (Probe J), which was calculated at 460MPa (Figure 6-45); the poisons ratio in compression $\nu_{vh}$, which was found to be approximately 0.5. In order to achieve repeatability and to calculate the full set of elastic parameters for intact Thanet sand, another series of Y1 probes is required.

| *Probe Name* | *Type of Probe* | | *Strain Level Reached* |
|---|---|---|---|
| A | $\delta\sigma_h' = 0$ | $\sigma_v'$ drained loading | Y1 |
| B | $\delta\sigma_v' = 0$ | $\sigma_h'$ drained loading | Y1 |
| C | $\delta p' = 0$ | $q$ drained loading | Y1 |
| D | $\delta q = 0$ | $p'$ drained unloading | Y1 |
| E | $\delta\sigma_h' = 0$ | $\sigma_v'$ drained loading | Y1 & Y2 |
| F | $\delta\sigma_v' = 0$ | $\sigma_h'$ drained loading | Y1 & Y2 |
| H | $\delta q = 0$ | $p'$ undrained unloading | Y1 & Y2 |
| I | $\delta\sigma_h' = 0$ | $\sigma_v'$ undrained loading | Y1 & Y2 |
| J | $\delta\sigma_h' = 0$ | $\sigma_v'$ drained unloading | Y1 & Y2 |
| K | $\delta\sigma_v' = 0$ | $\sigma_h'$ drained loading | Y1 & Y2 |

***Table 6-1*** *Summary table of Y1 & Y2 probes*

A schematic representation of the probe directions in p'-q space is shown in Figure 3-33

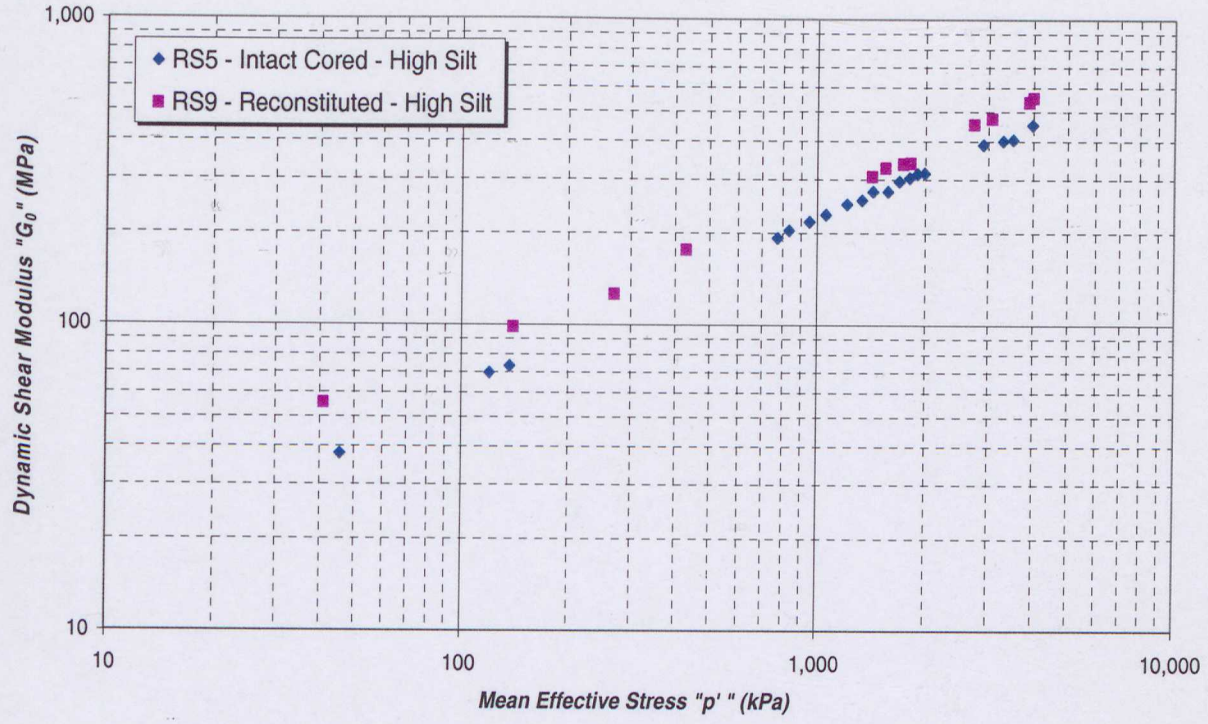


***Figure 6-1*** *Effect of structure – Cored sample – High Silt content material*

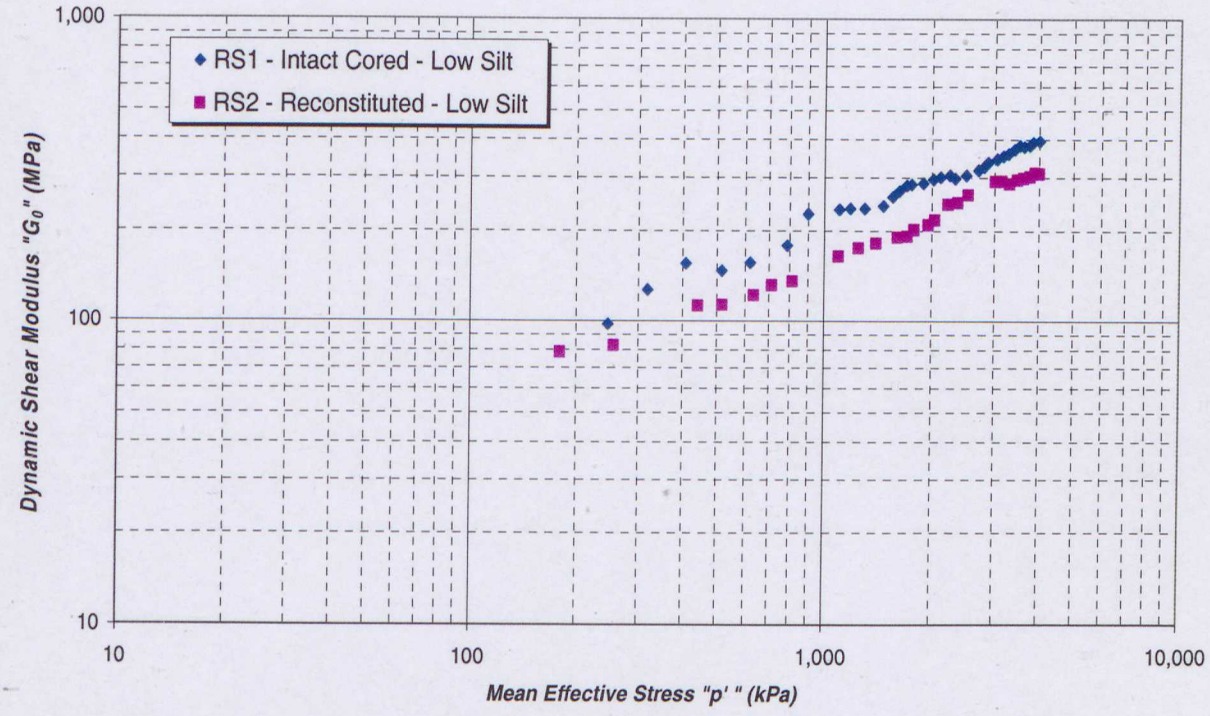


***Figure 6-2*** *Effect of structure – Cored sample – Low Silt content material*

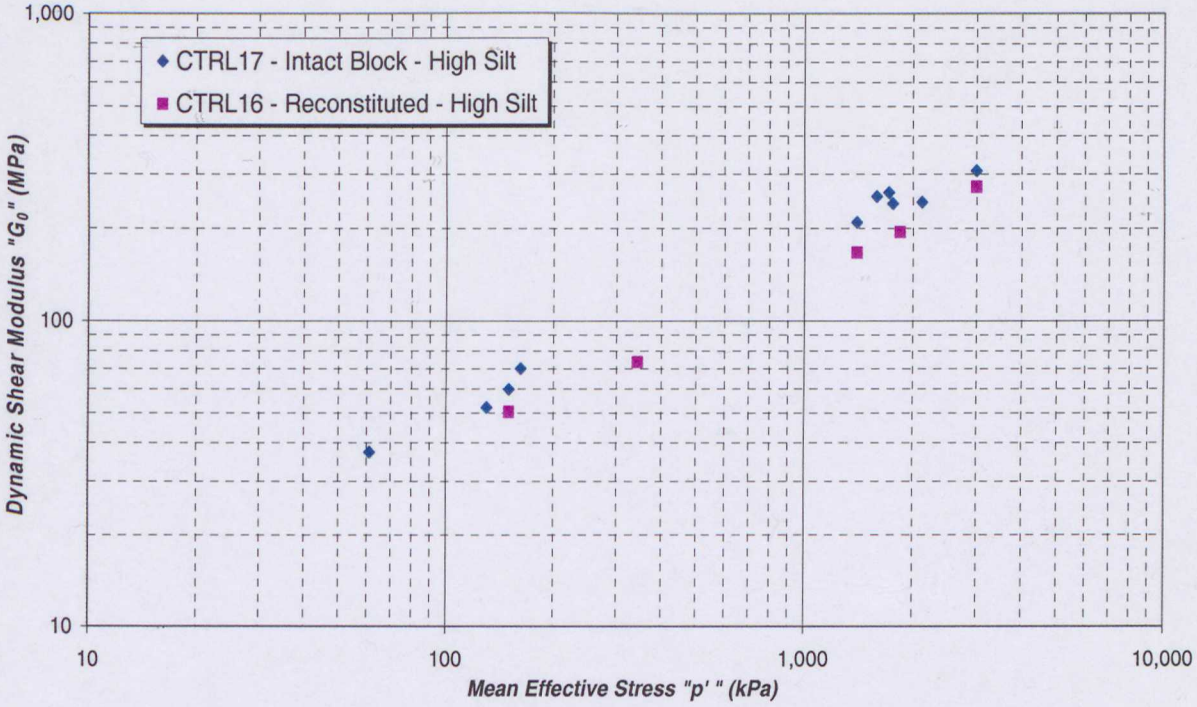


***Figure 6-3*** *Effect of structure – Block sample – High silt content material*

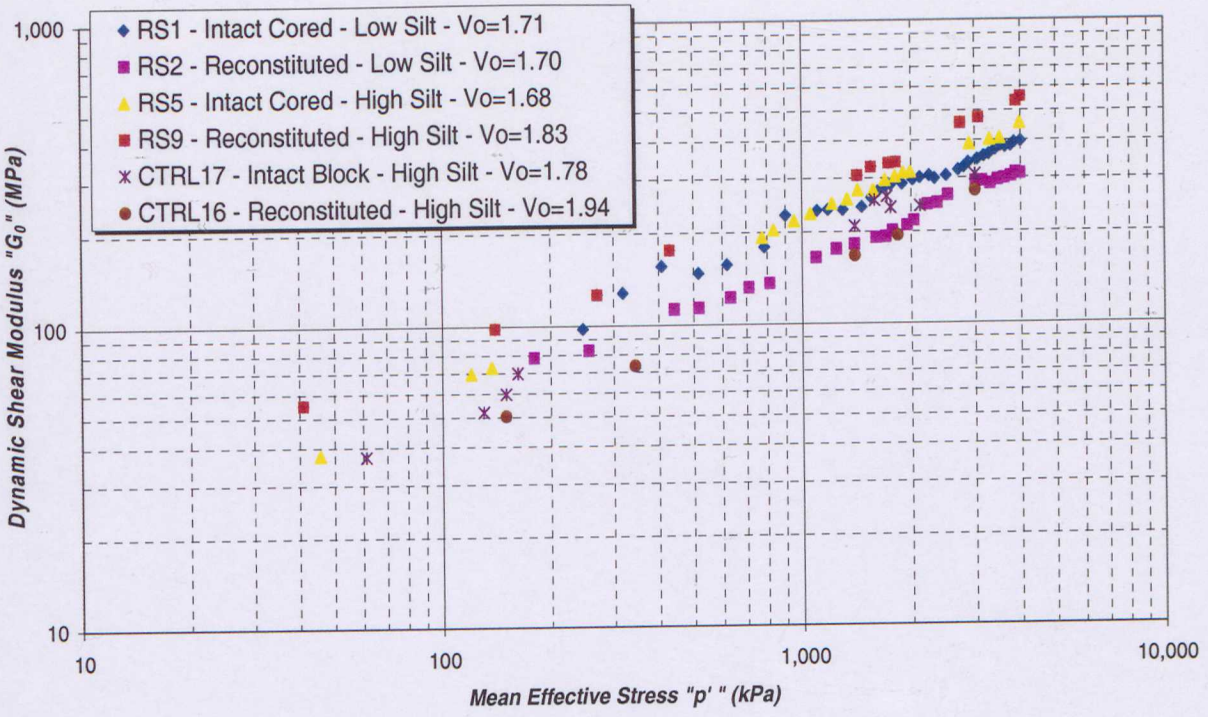


*Figure 6-4 Effect of structure – All bender element results*

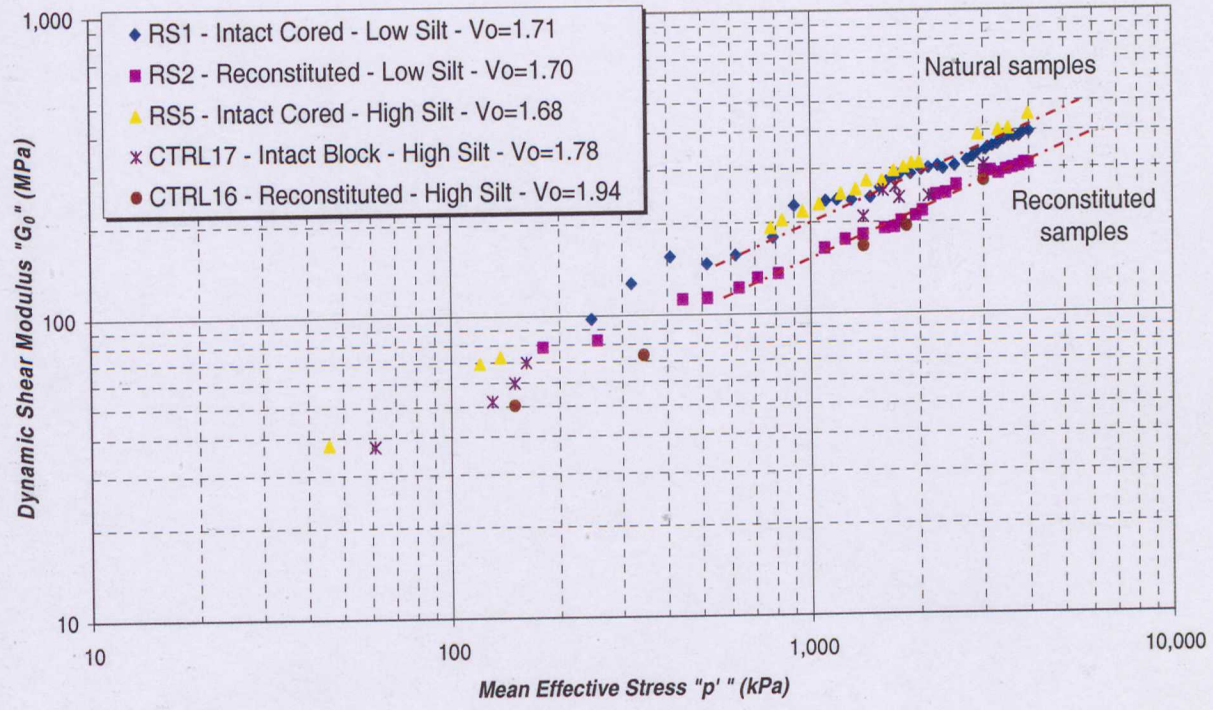


*Figure 6-5 Effect of structure –Bender element results with trends*

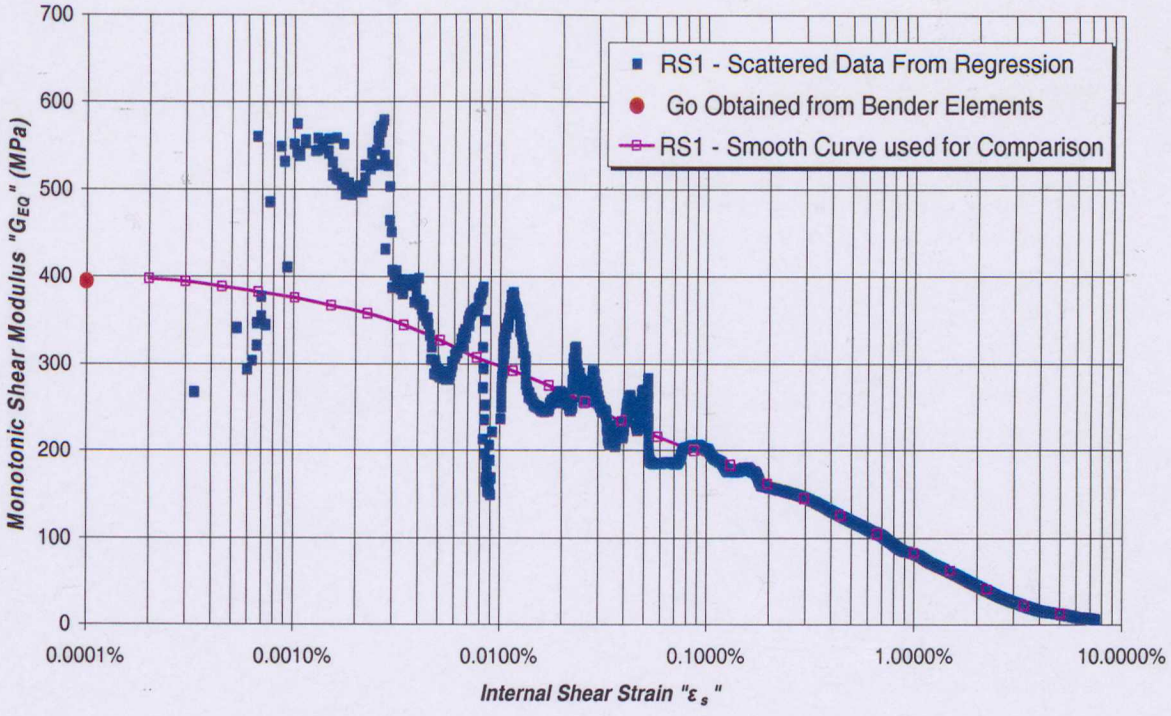


*Figure 6-6 Shear modulus trend for RS1*

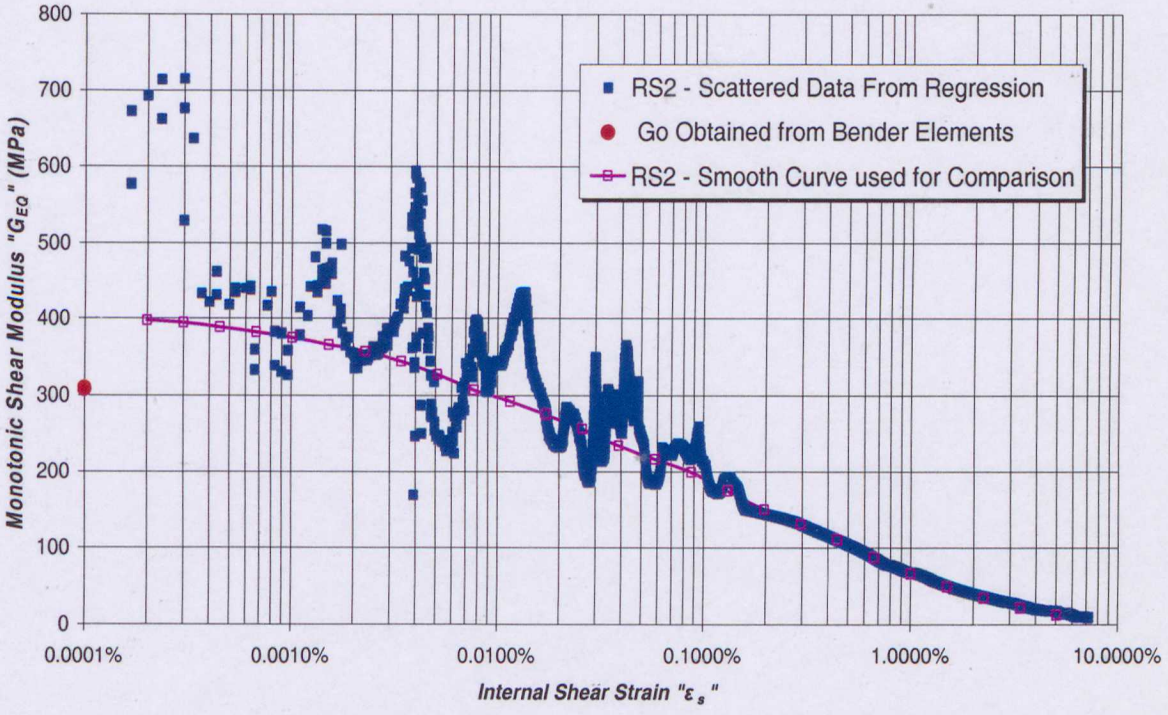


*Figure 6-7 Shear modulus trend for RS2*

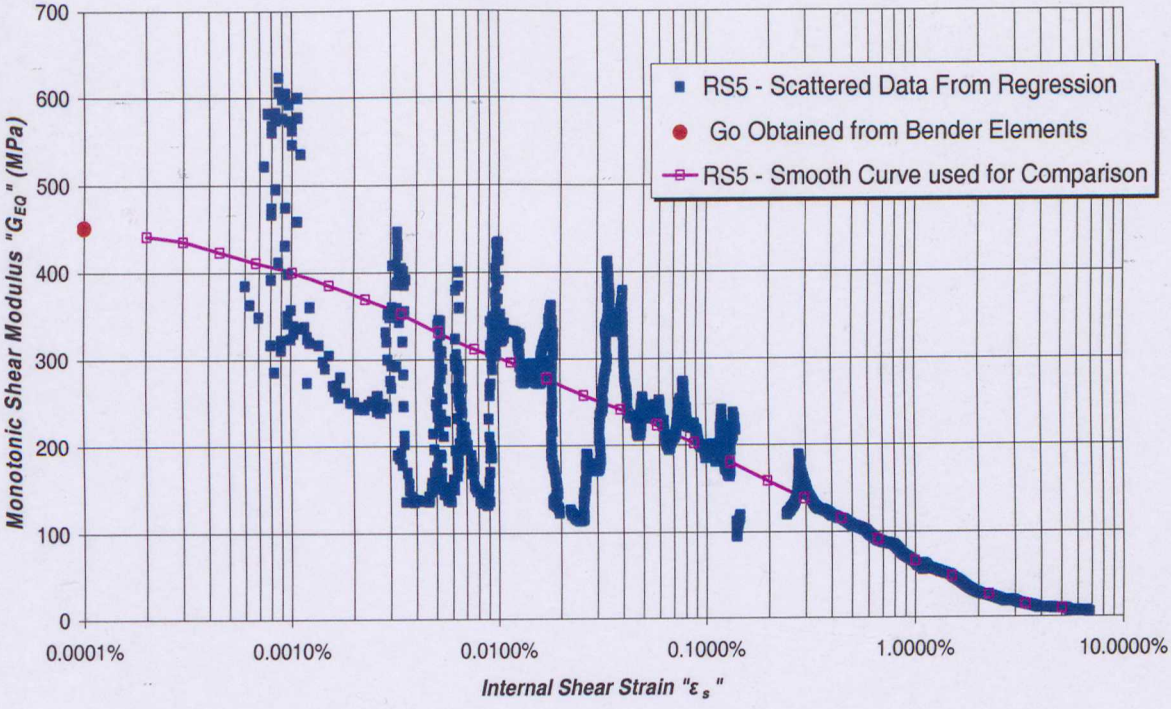


*Figure 6-8* Shear modulus trend for RS5

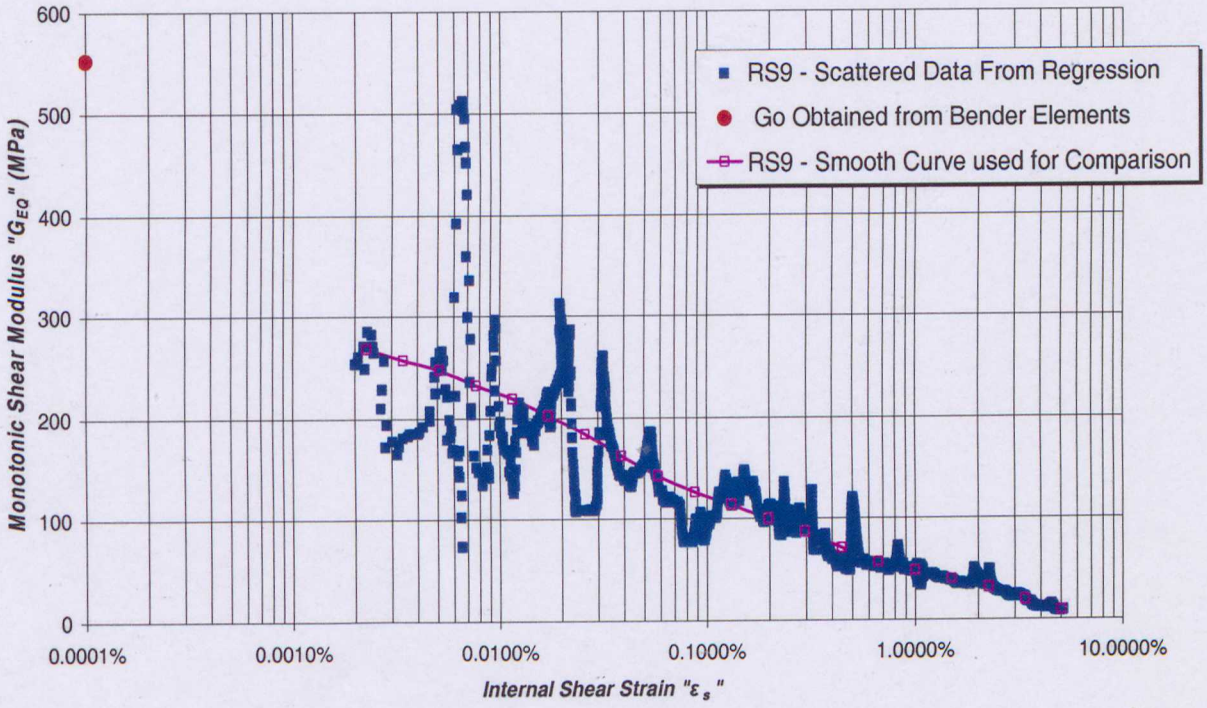


*Figure 6-9* Shear modulus trend for RS9

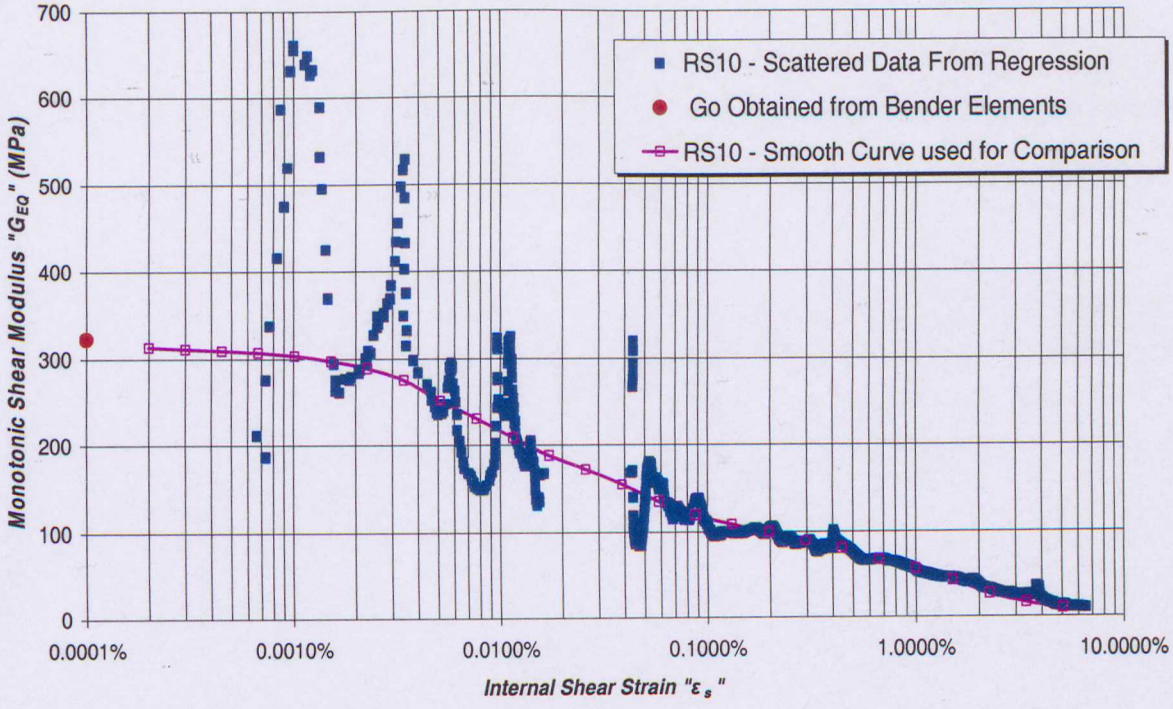


*Figure 6-10* Shear modulus trend for RS10

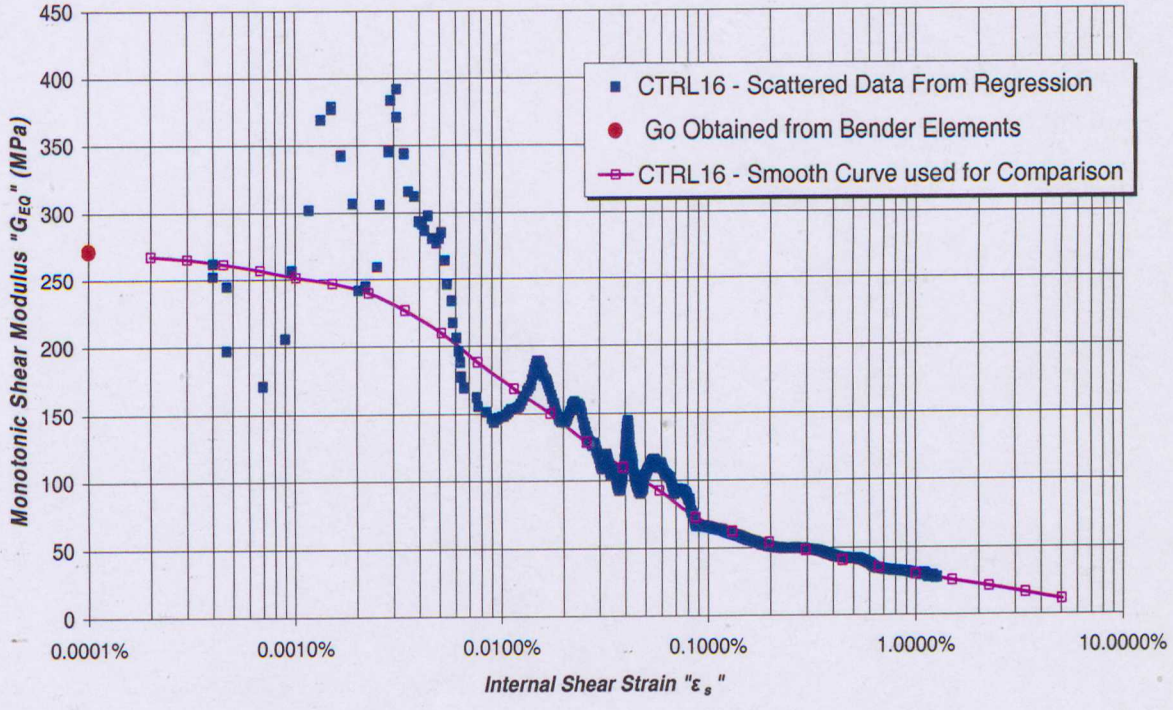


*Figure 6-11* Shear modulus trend for CTRL16

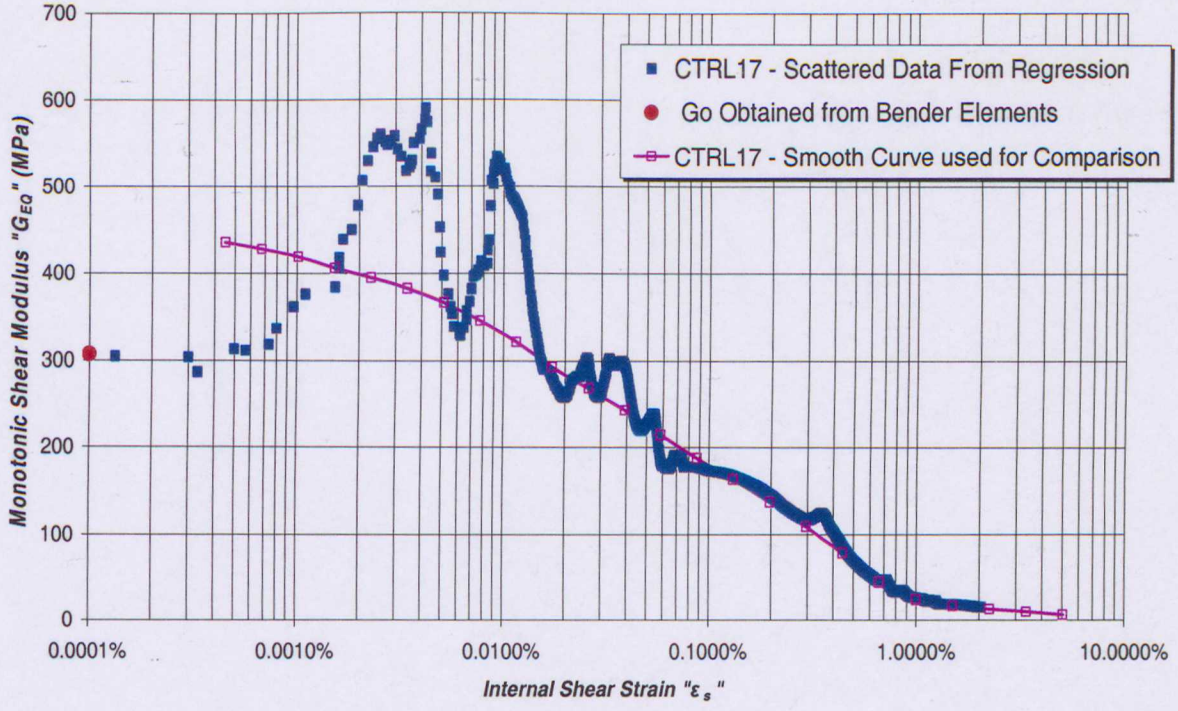


*Figure 6-12 Shear modulus trend for CTRL17*

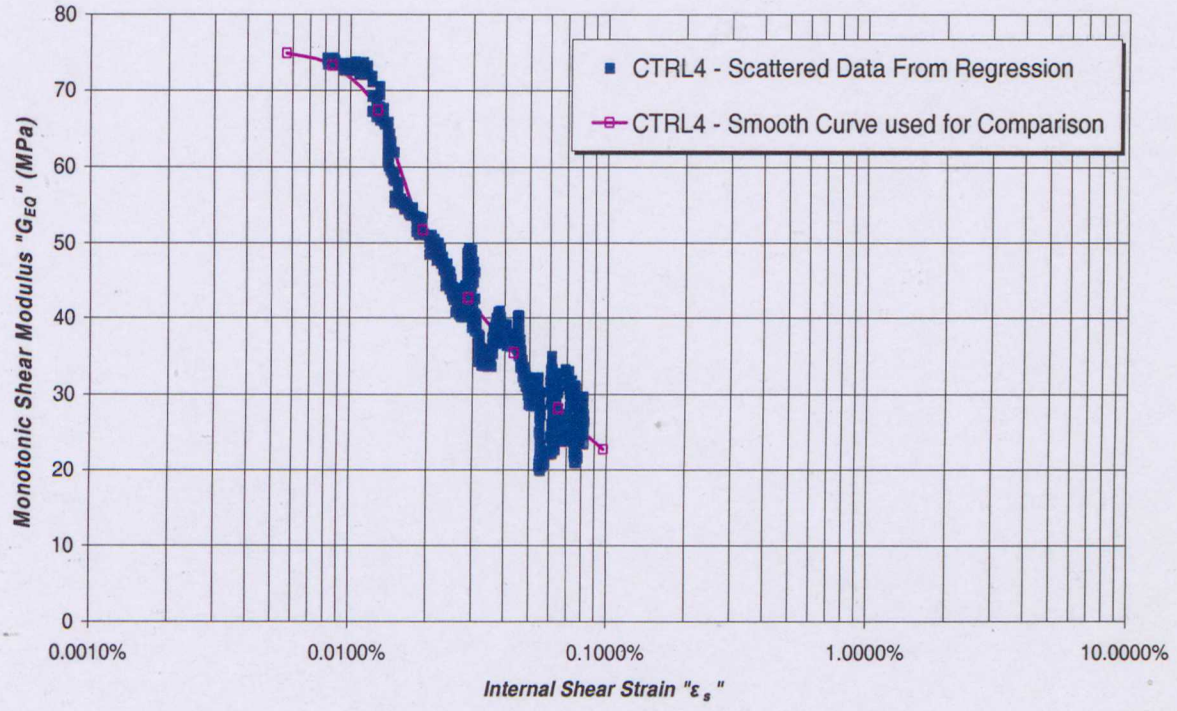


*Figure 6-13 Shear modulus trend for CTRL4*

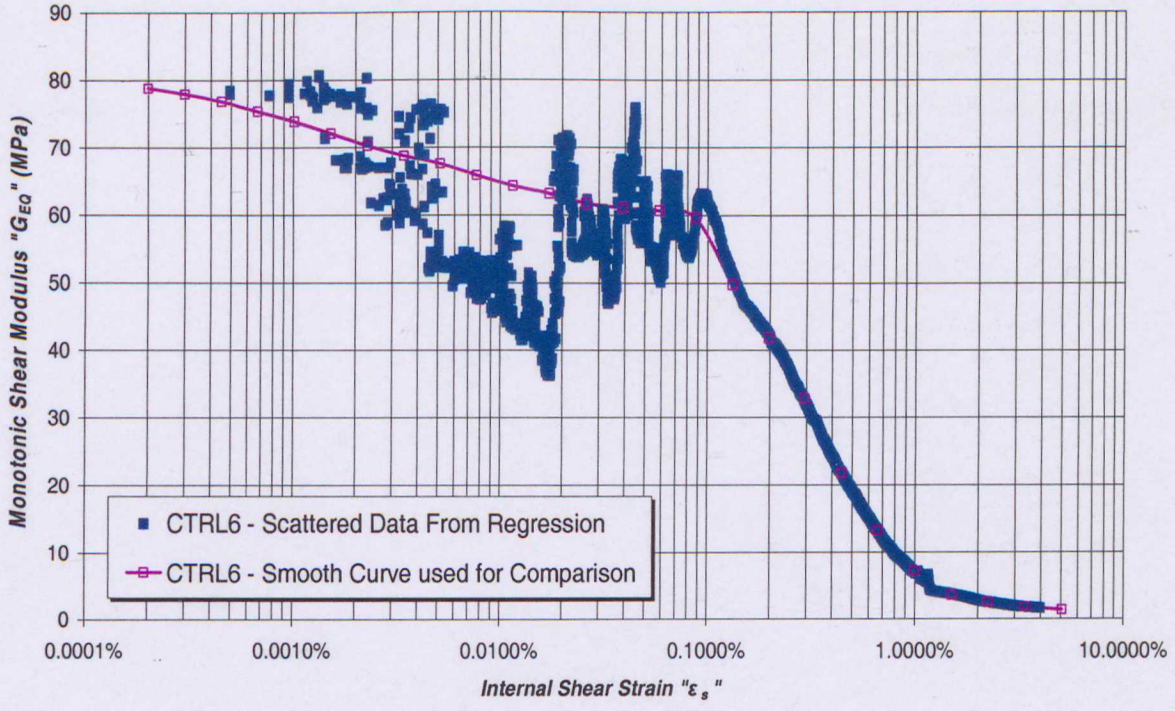


*Figure 6-14 Shear modulus trend for CTRL6*

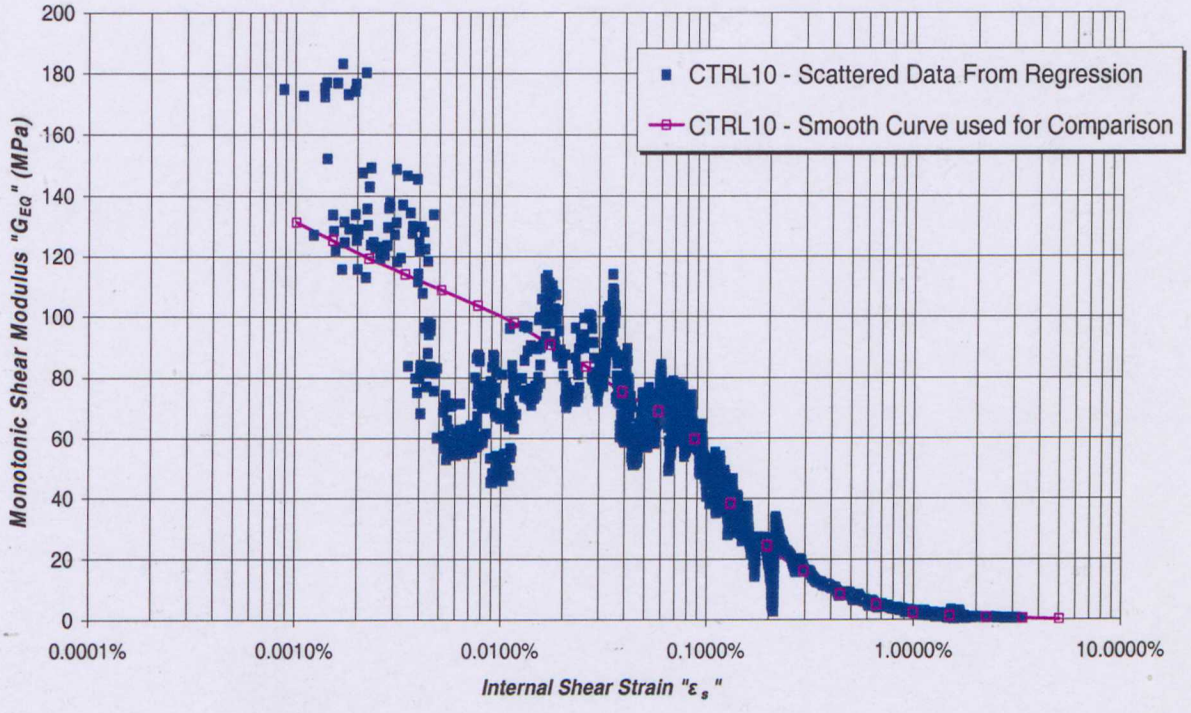


*Figure 6-15 Shear modulus trend for CTRL10*

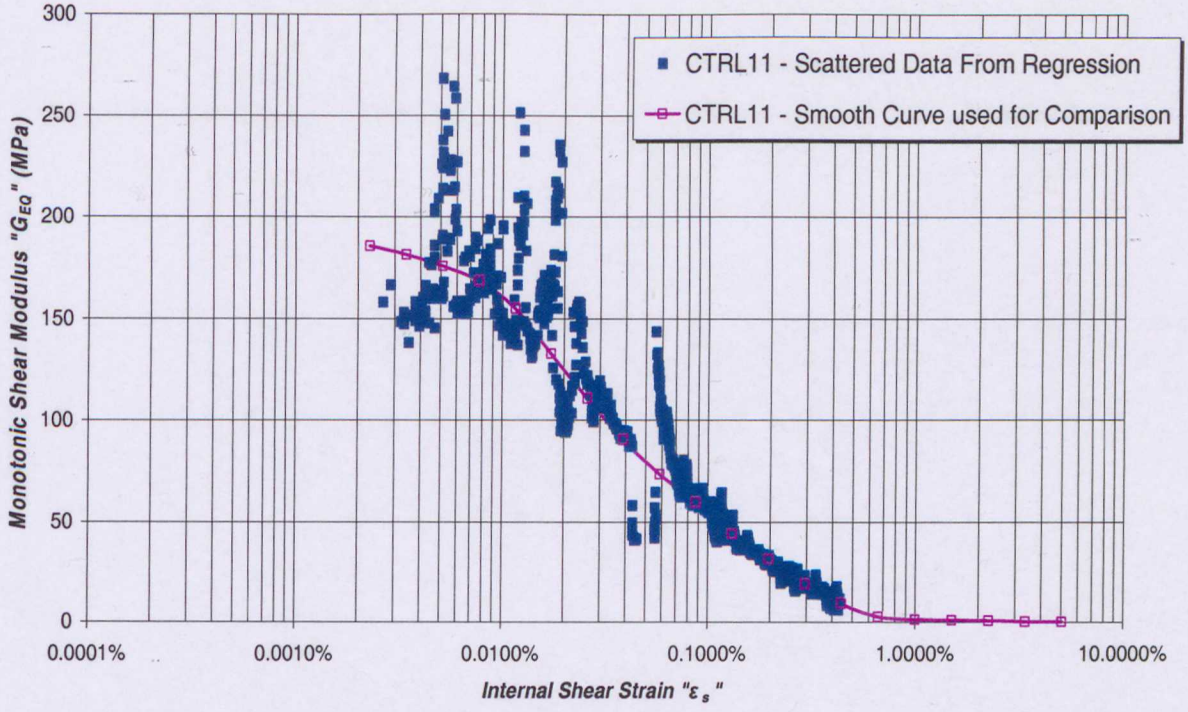


*Figure 6-16* Shear modulus trend for CTRL11

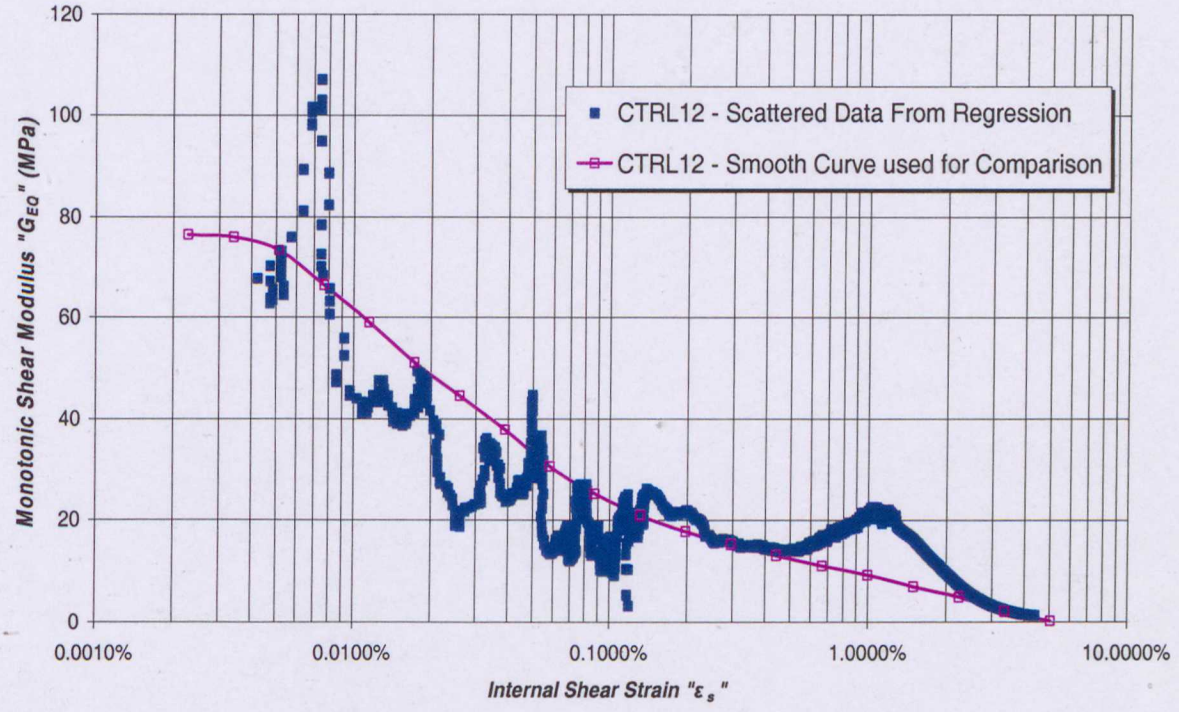


*Figure 6-17* Shear modulus trend for CTRL12

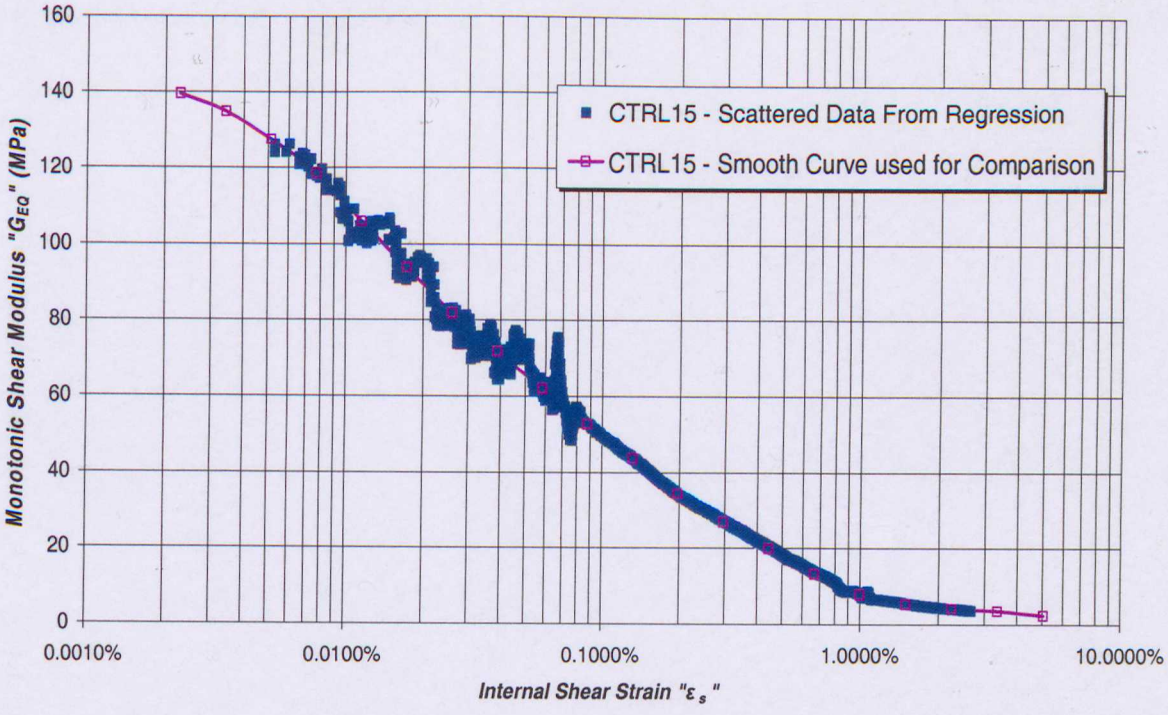


***Figure 6-18*** *Shear modulus trend for CTRL15*

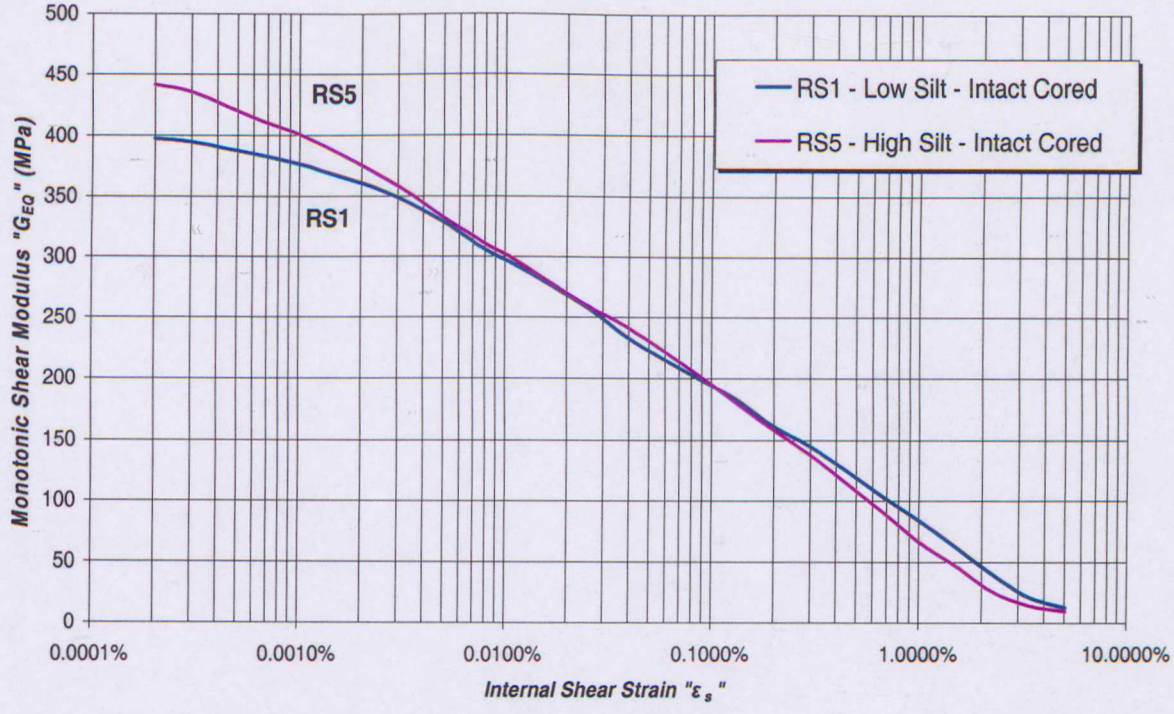


***Figure 6-19*** *High/low silt content comparison of stiffness for intact (cored) material*

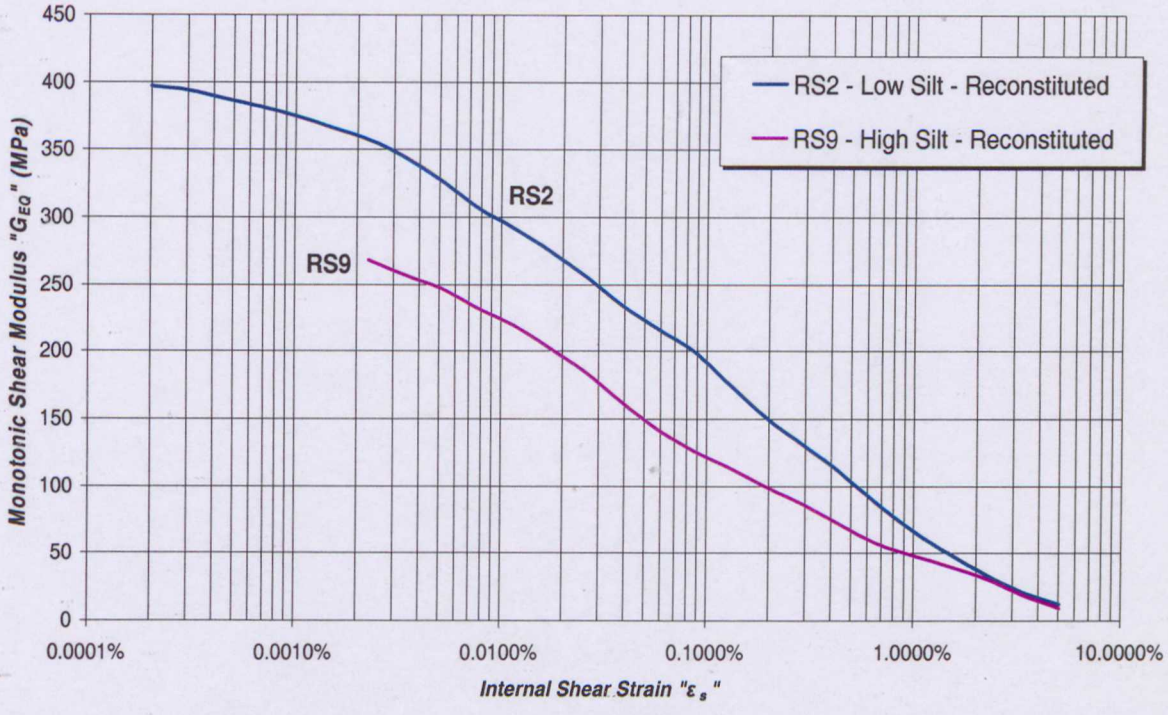


***Figure 6-20*** *High/low silt content comparison of stiffness for reconstituted material*

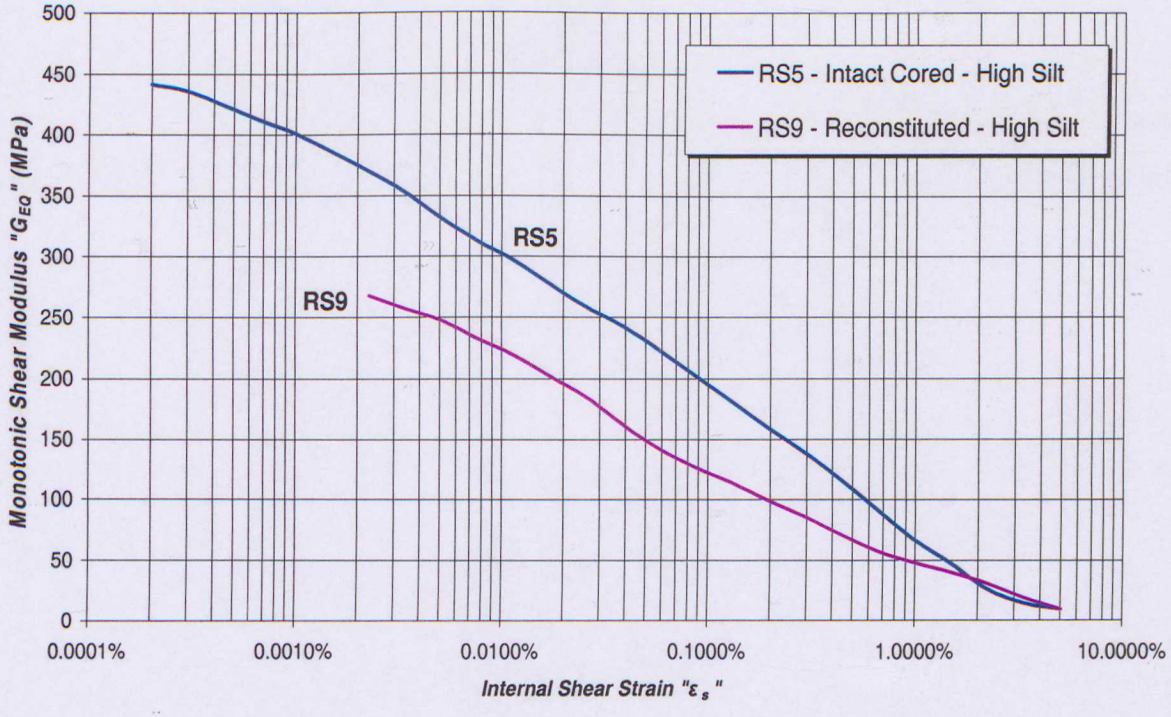


***Figure 6-21*** *Sample type comparison of stiffness for a high silt content cored sample*

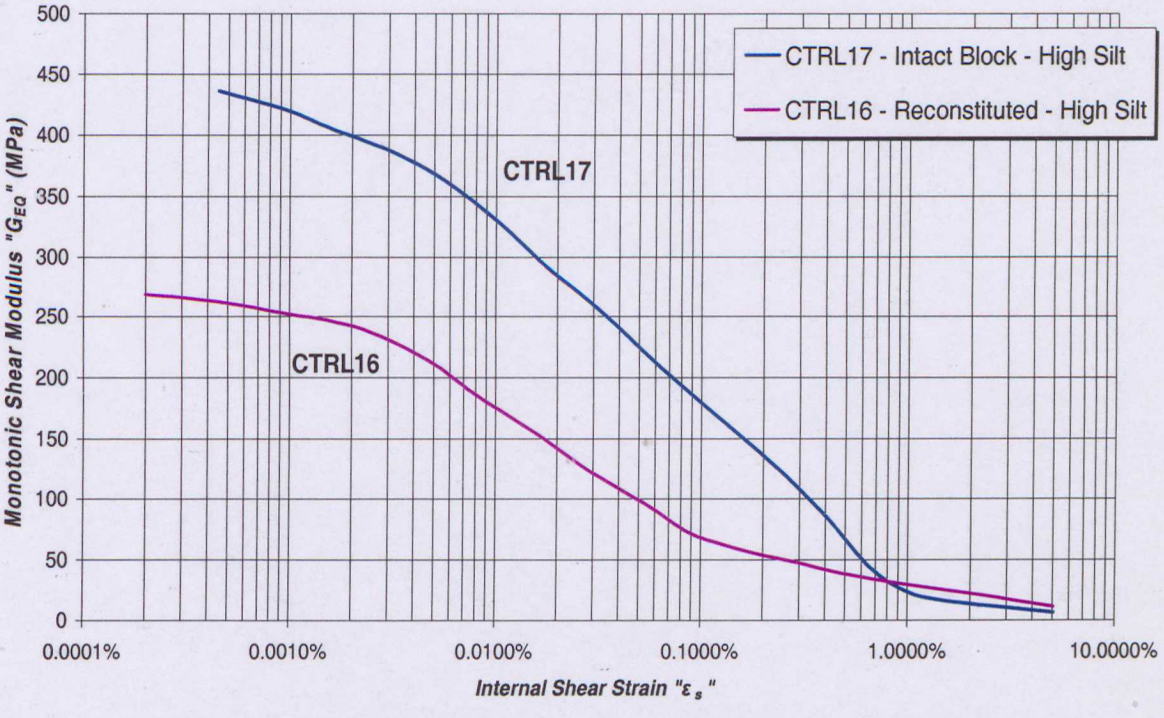


***Figure 6-22*** *Sample type comparison of stiffness for a high silt block sample*

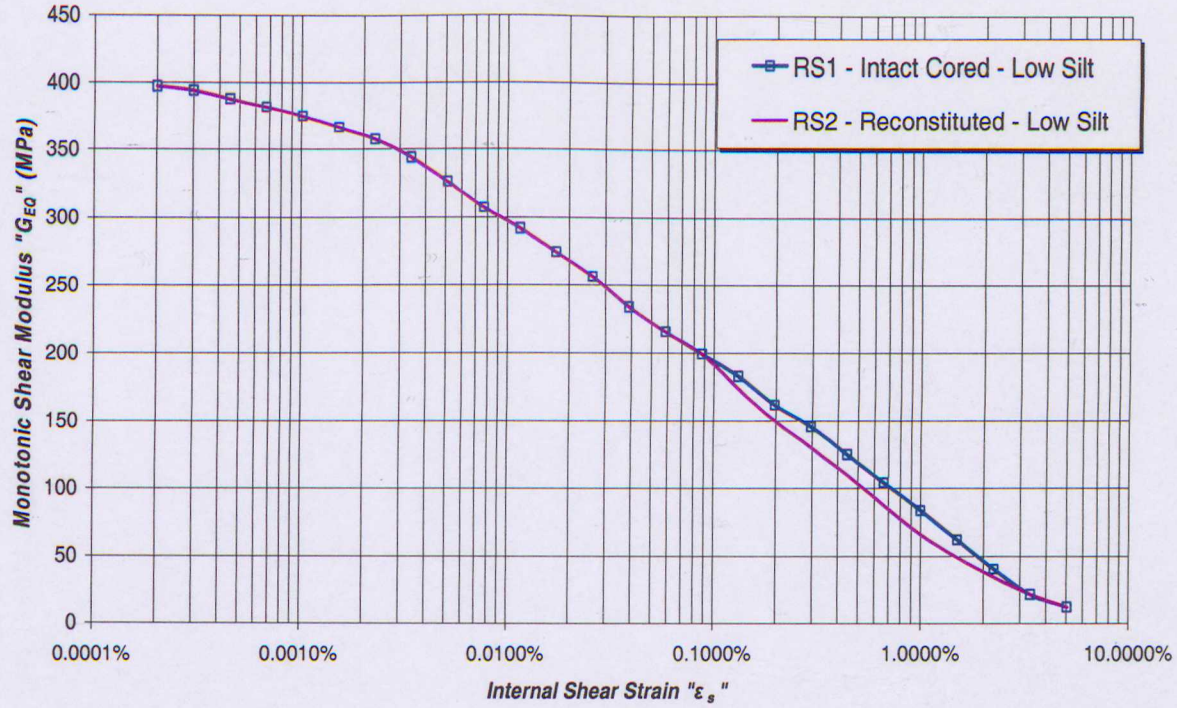


***Figure 6-23*** *Sample type comparison for stiffness of low silt cored sample*

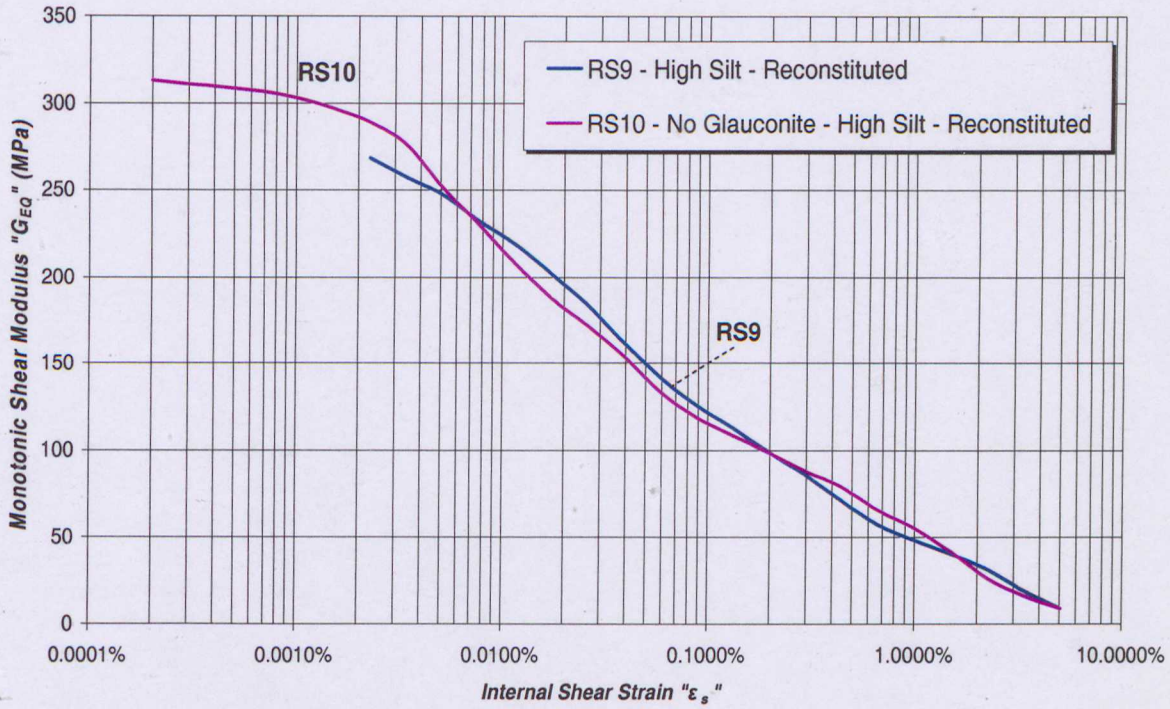


***Figure 6-24*** *Glauconite effect on stiffness for High silt content material*

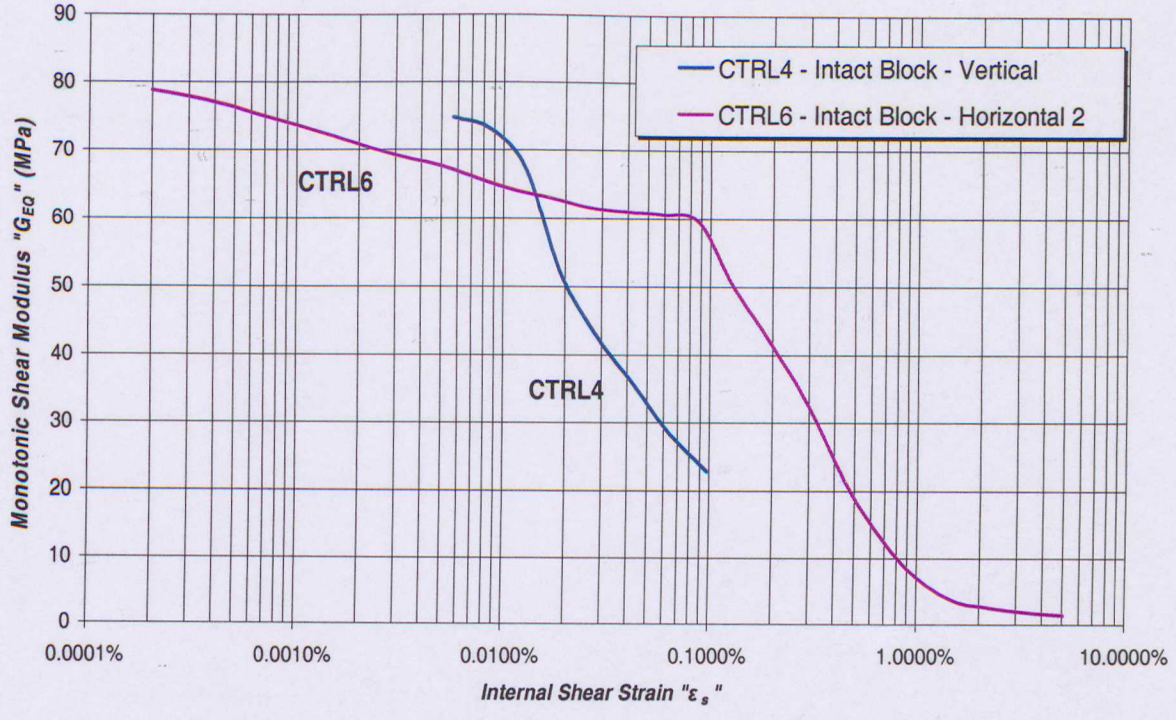


*Figure 6-25 Material anisotropy comparison – Drained Compression tests*

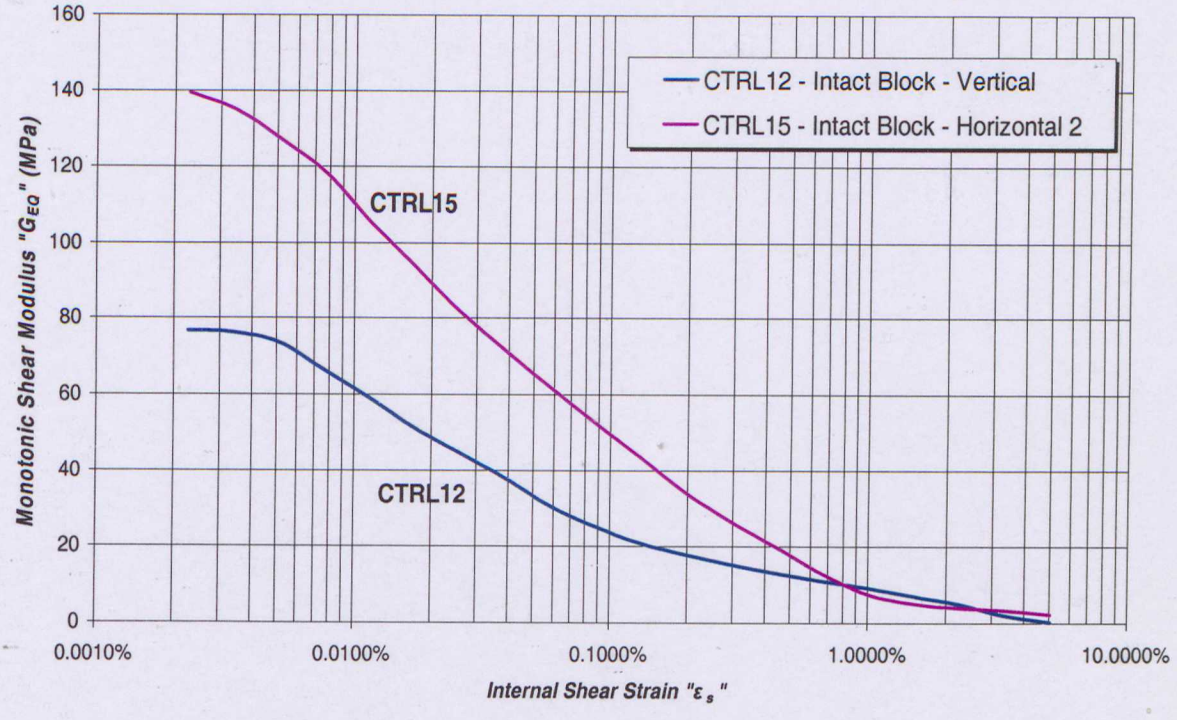


*Figure 6-26 Material anisotropy comparison – Undrained Compression tests*

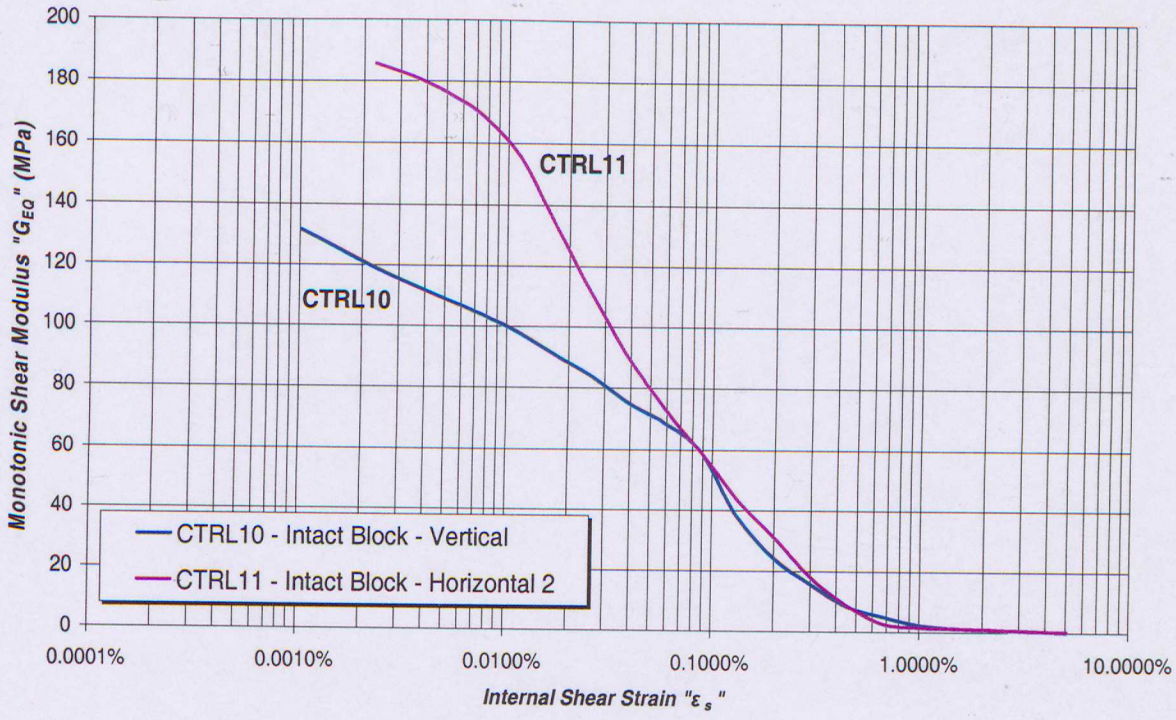


***Figure 6-27*** *Material anisotropy comparison – Drained Extension tests*

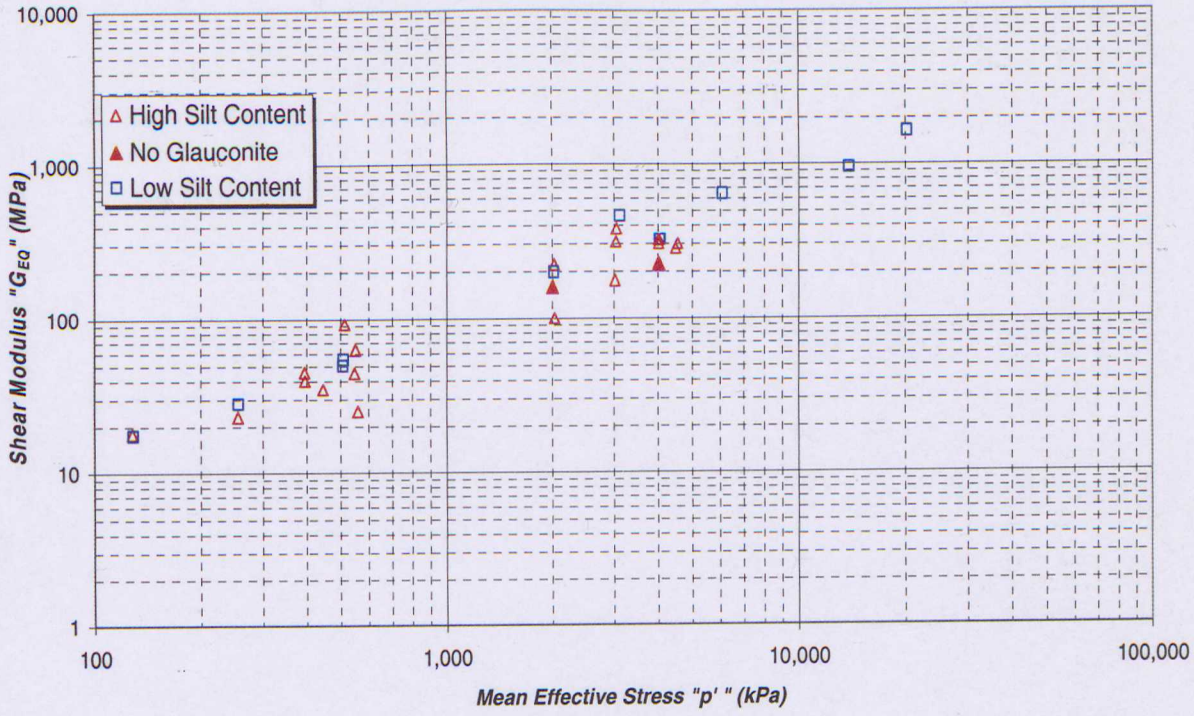


***Figure 6-28*** *Monotonic shear moduli @ 0.01% $\varepsilon_s$ – Silt content comparison*

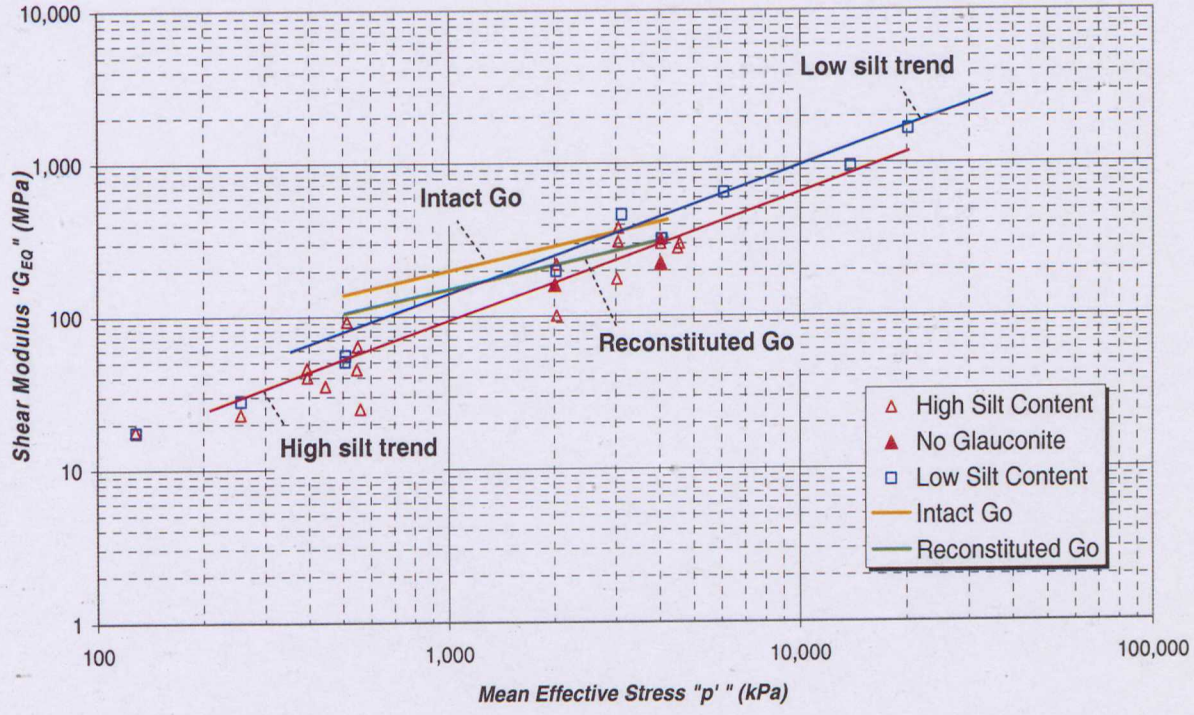


***Figure 6-29*** *Monotonic shear moduli @ 0.01% $\varepsilon_s$ – Silt content comparison – dynamic and monotonic stiffness trends added*

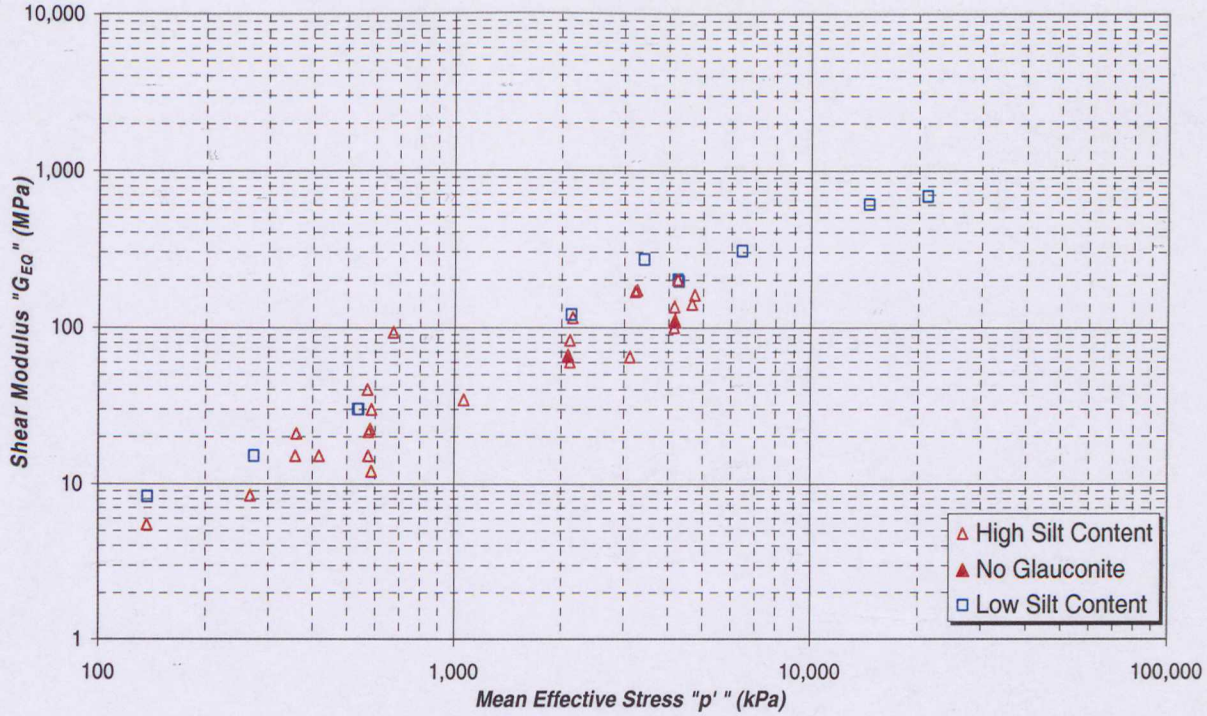


***Figure 6-30*** *Monotonic shear moduli @ 0.1% $\varepsilon_s$ – Silt content comparison*

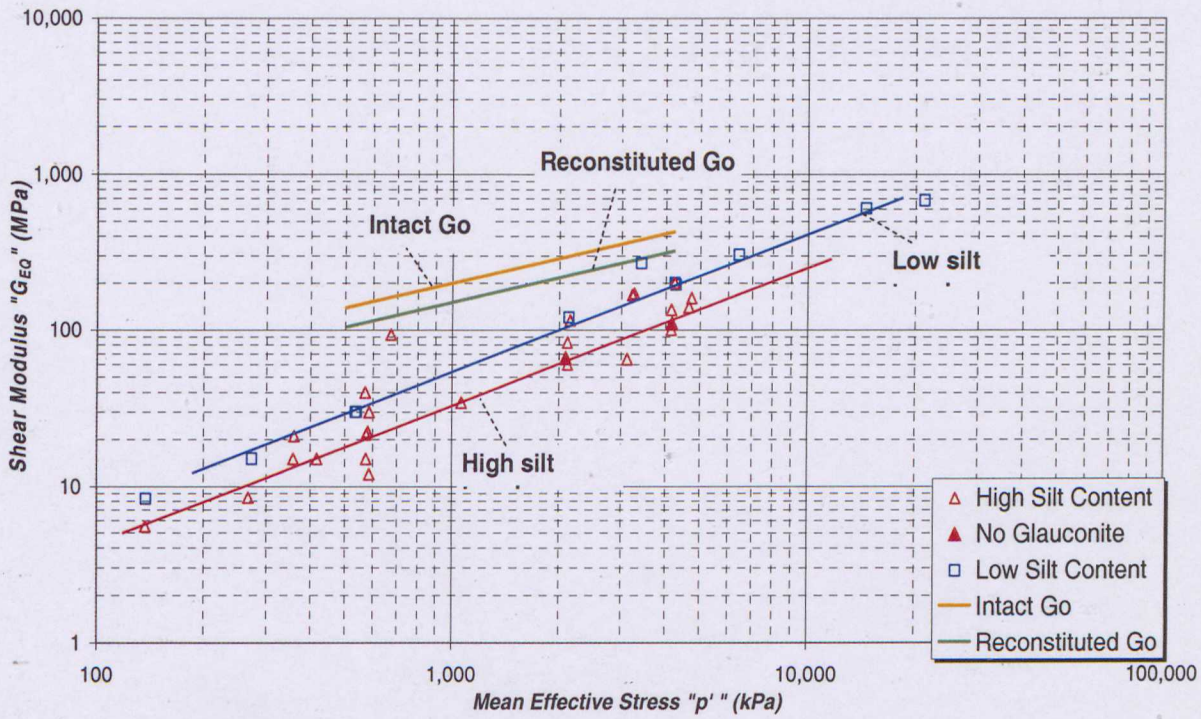


***Figure 6-31*** *Monotonic shear moduli @ 0.1% $\varepsilon_s$ – Silt content comparison - dynamic and monotonic stiffness trends added*

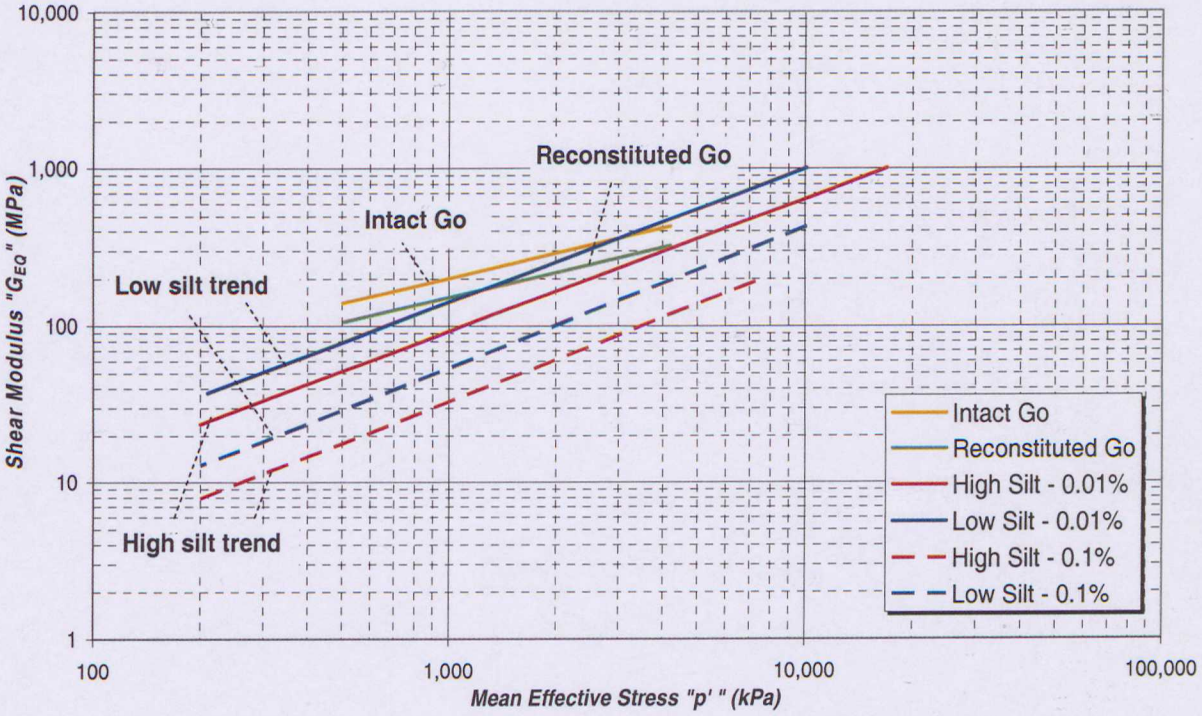


***Figure 6-32*** *Monotonic shear moduli @ 0.1% $\varepsilon_s$ and 0.01% $\varepsilon_s$ – Silt content comparison - dynamic and monotonic stiffness trends added*

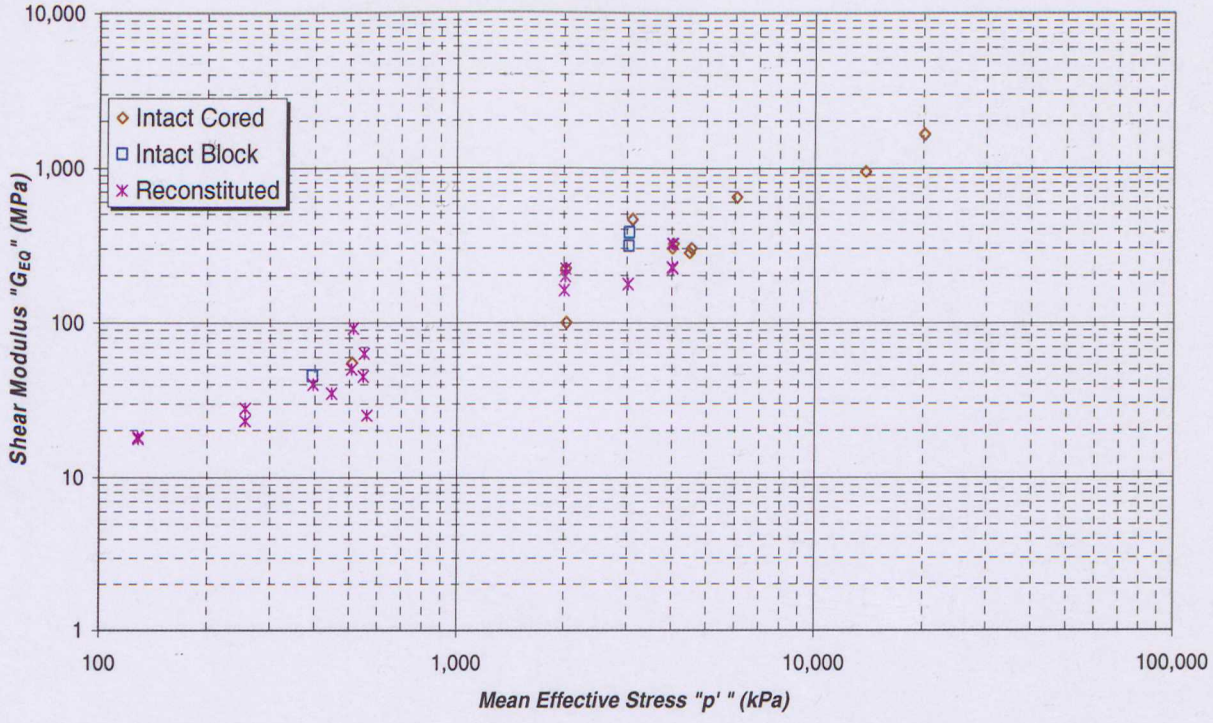


***Figure 6-33*** *Monotonic shear moduli @ 0.01% $\varepsilon_s$ – Sample type comparison*

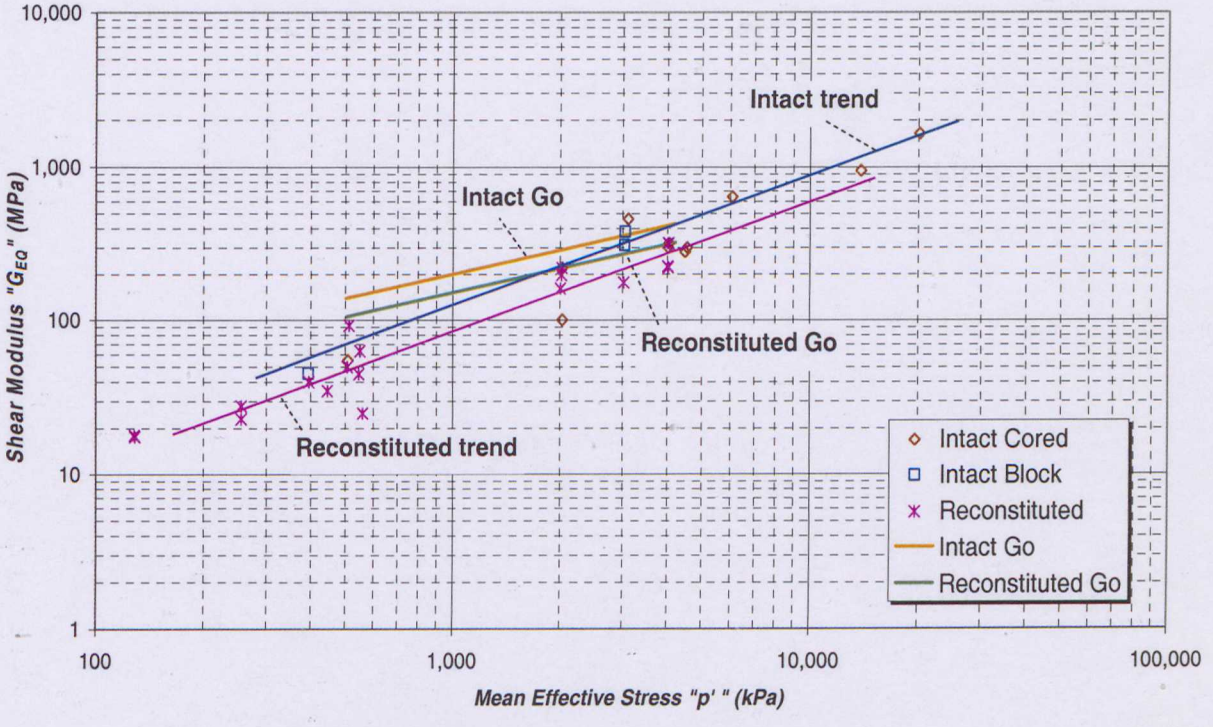


***Figure 6-34*** *Monotonic shear moduli @ 0.01% $\varepsilon_s$ – Sample type comparison - dynamic and monotonic stiffness trends added*

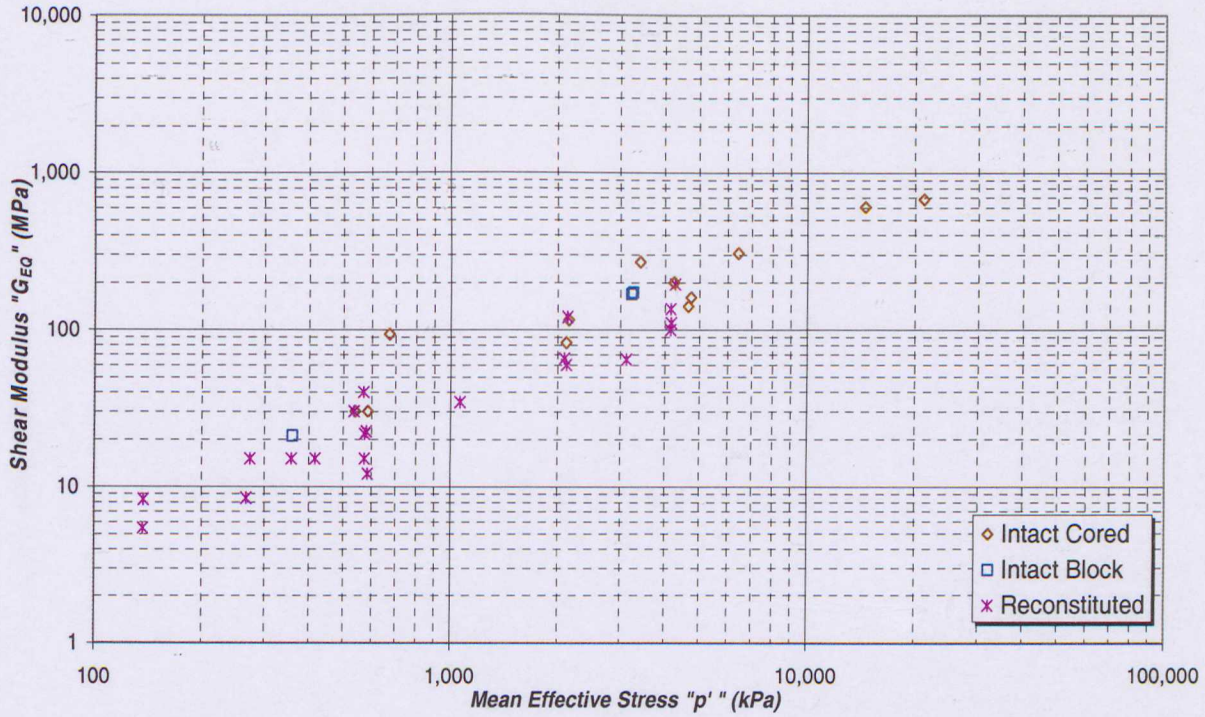


*Figure 6-35 Monotonic shear moduli @ 0.1% $\varepsilon_s$ – Sample type comparison*

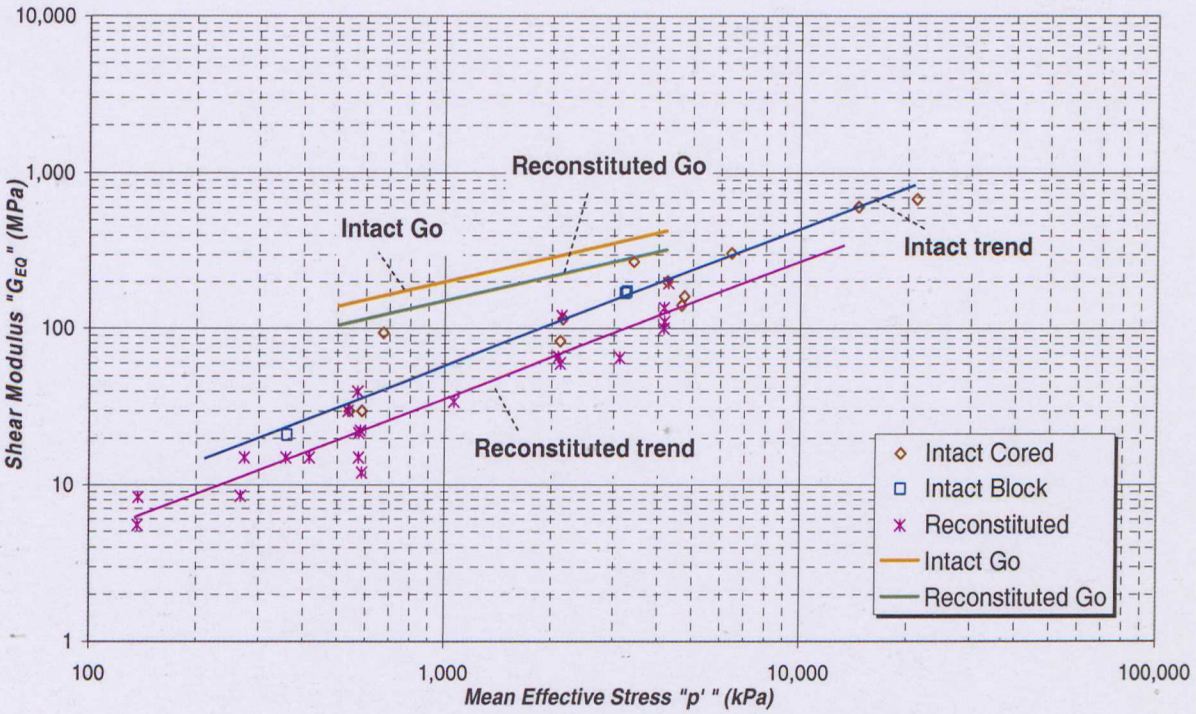


*Figure 6-36 Monotonic shear moduli @ 0.1% $\varepsilon_s$ – Sample type comparison - dynamic and monotonic stiffness trends added*

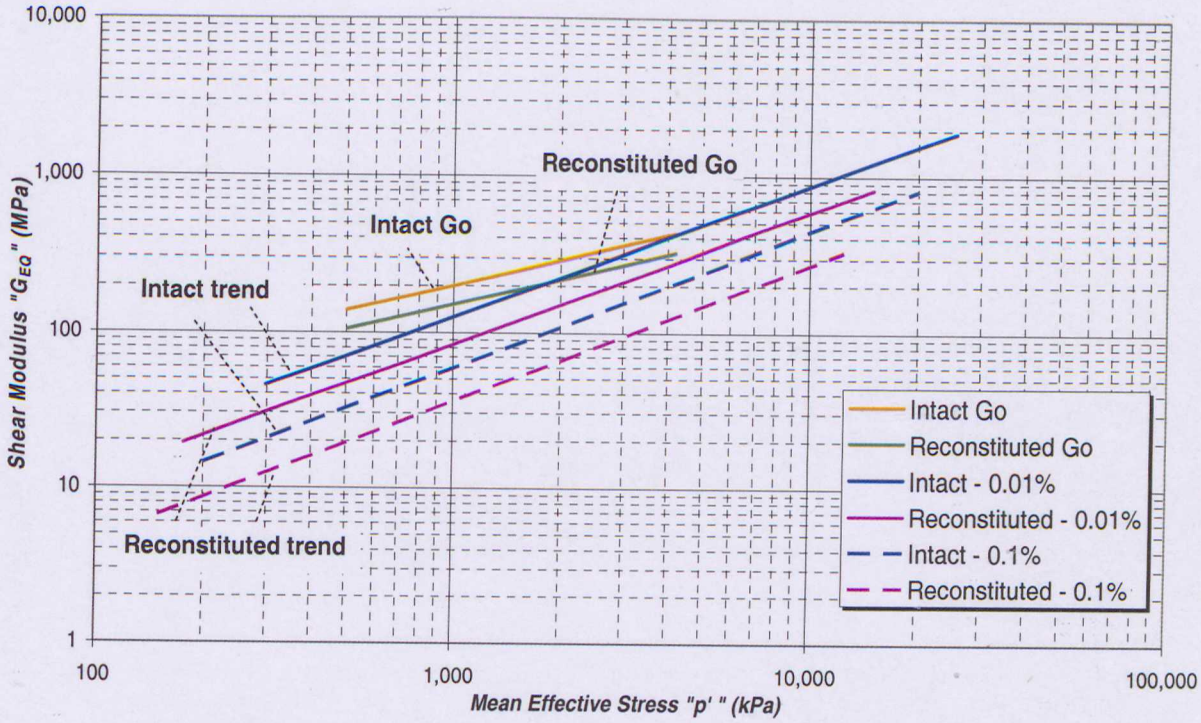


***Figure 6-37*** *Monotonic shear moduli @ 0.1% $\varepsilon_s$ and 0.01% $\varepsilon_s$ – Sample type comparison - dynamic and monotonic stiffness trends added*

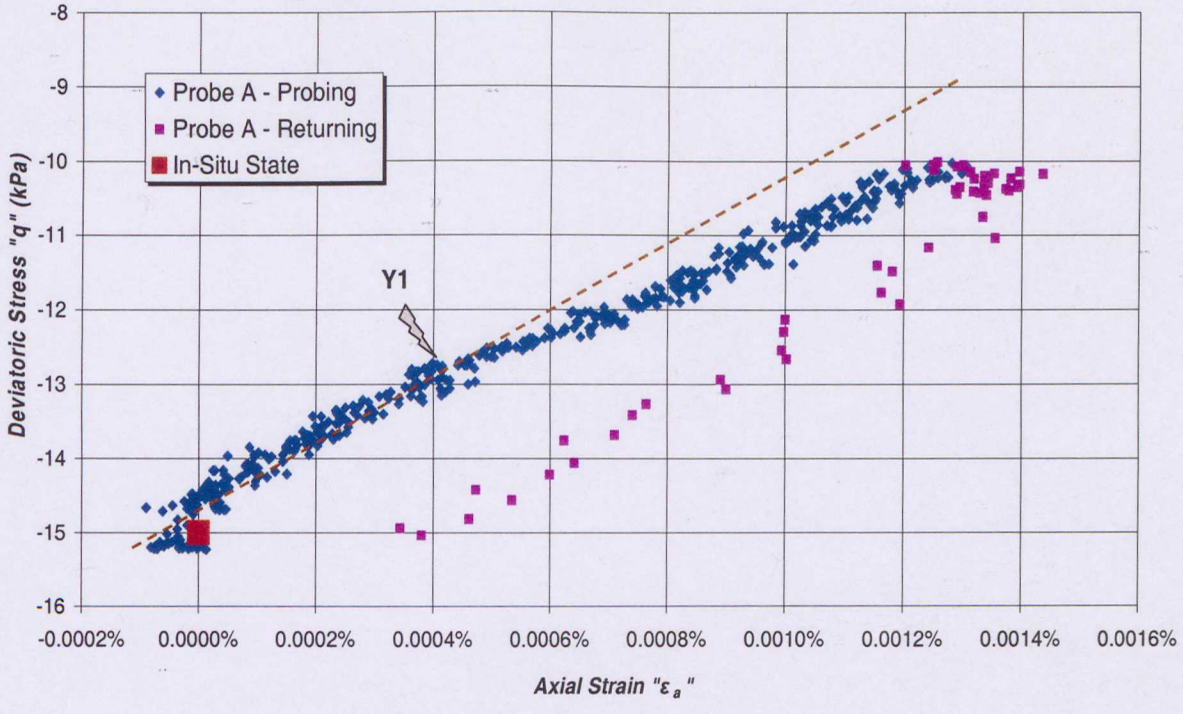


*Figure 6-38 Y1 location for probe A*

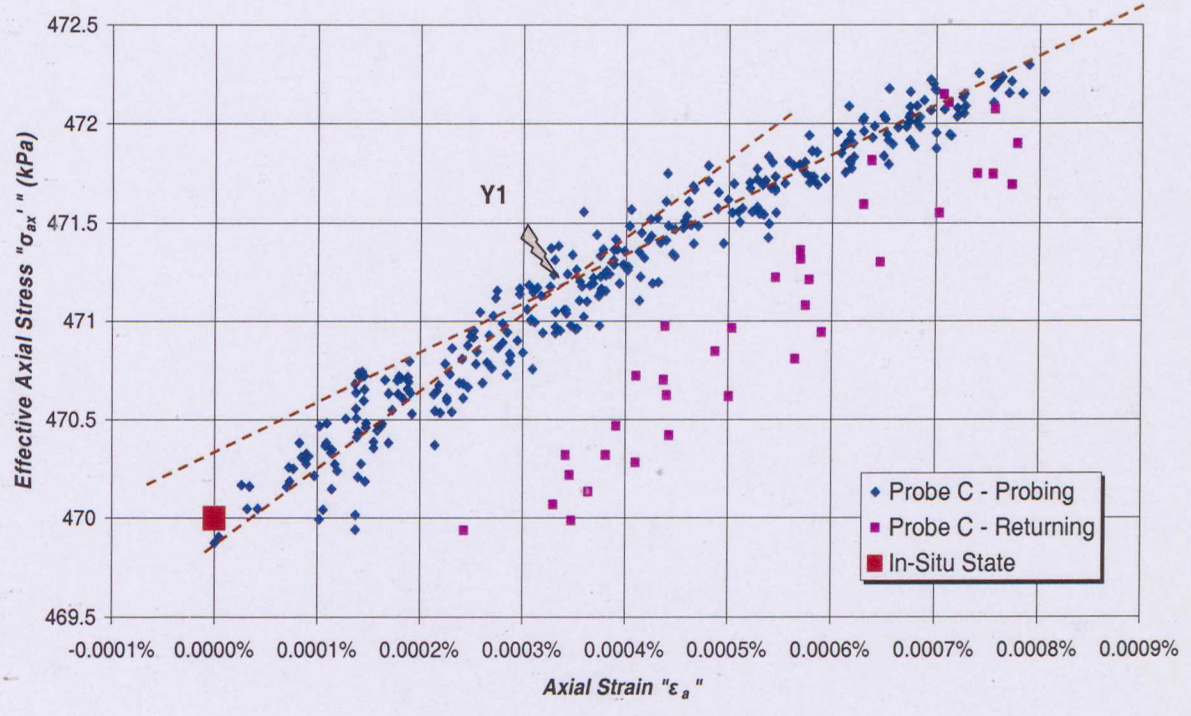


*Figure 6-39 Y1 location for probe C*

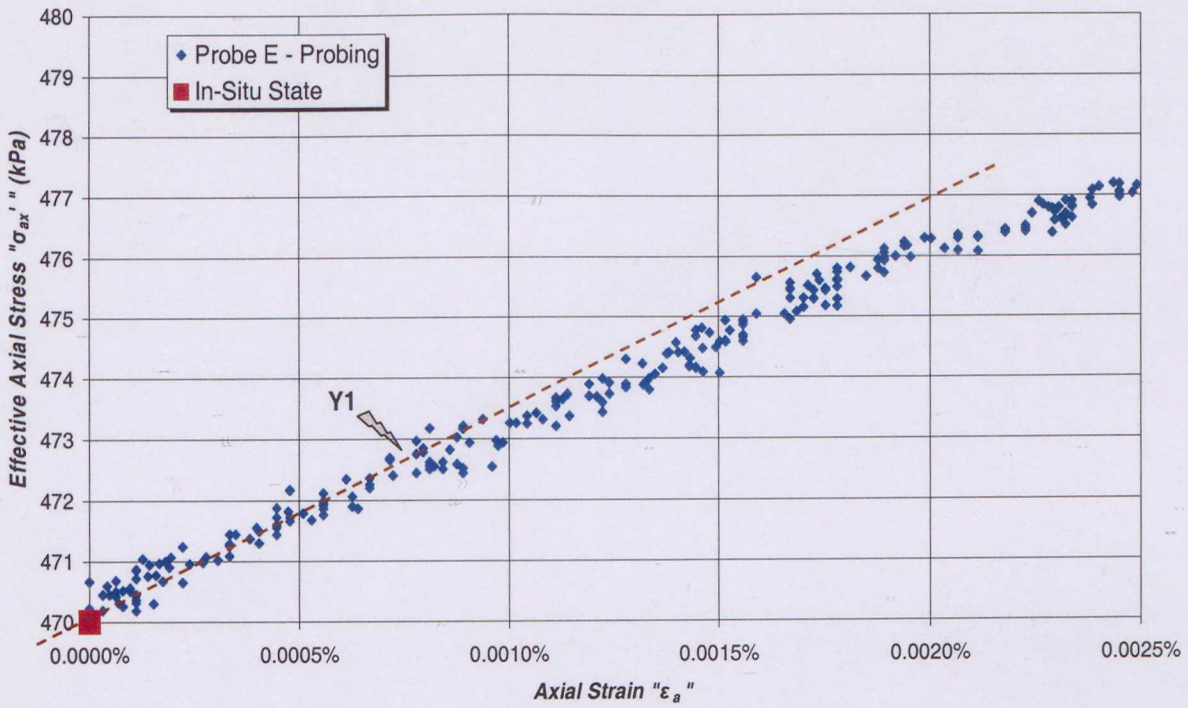


*Figure 6-40 Y1 location for probe E*

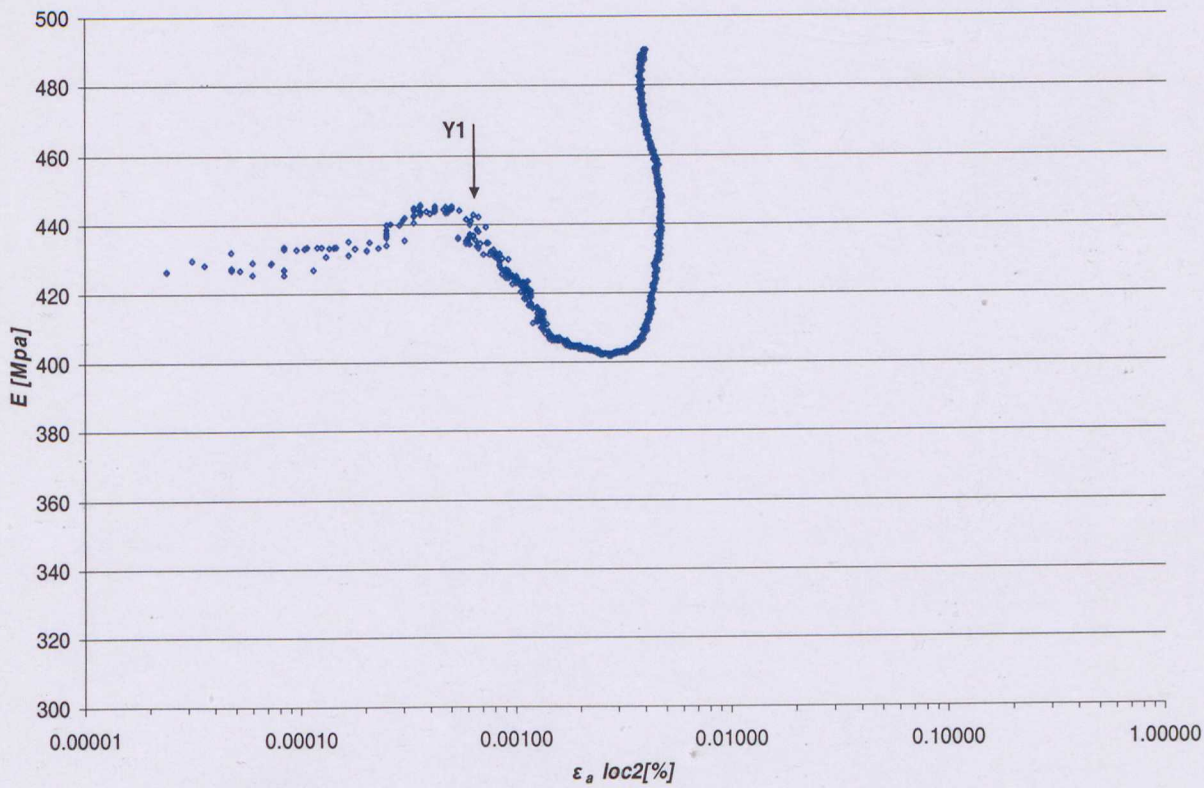


*Figure 6-41 Y1 location for probe E –Vertical Young's Modulus calculation*

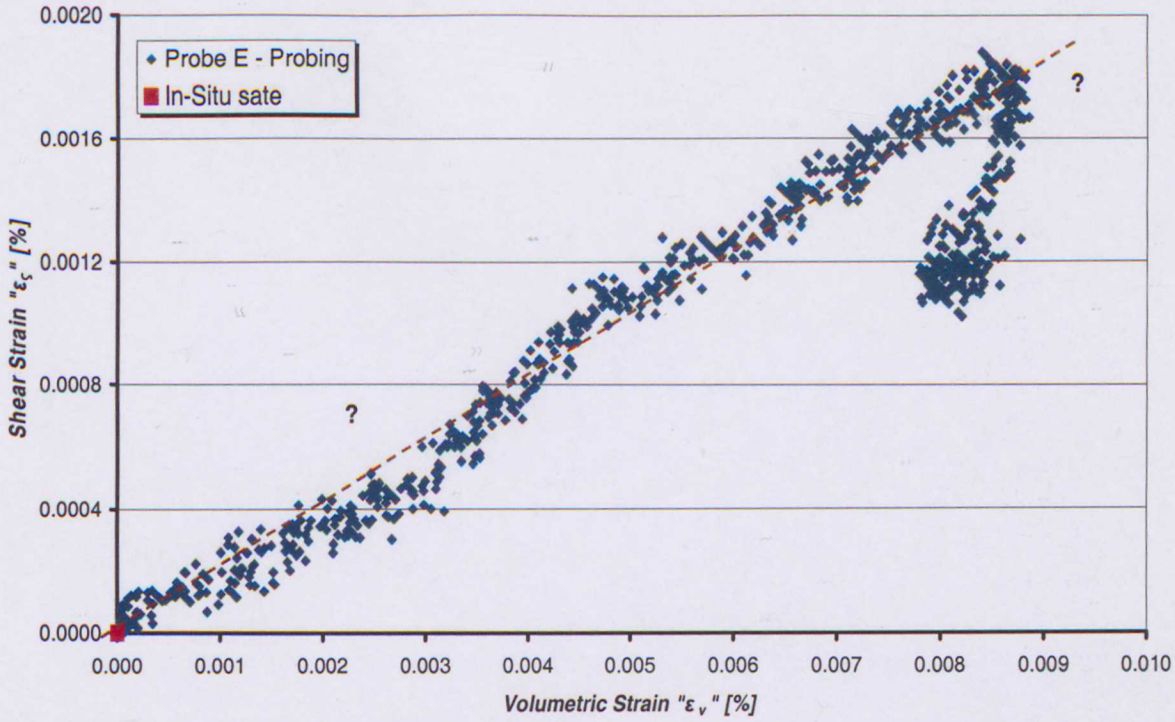


***Figure 6-42*** *Possible Y2 location for probe E*

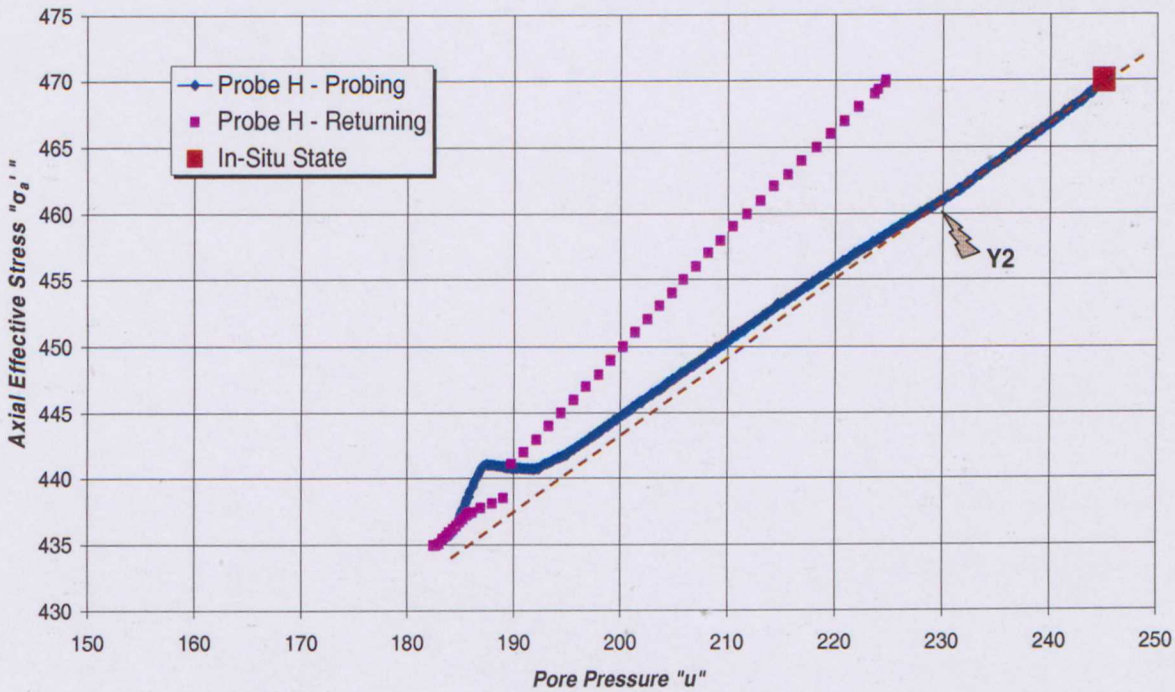


***Figure 6-43*** *Y2 location for probe H*

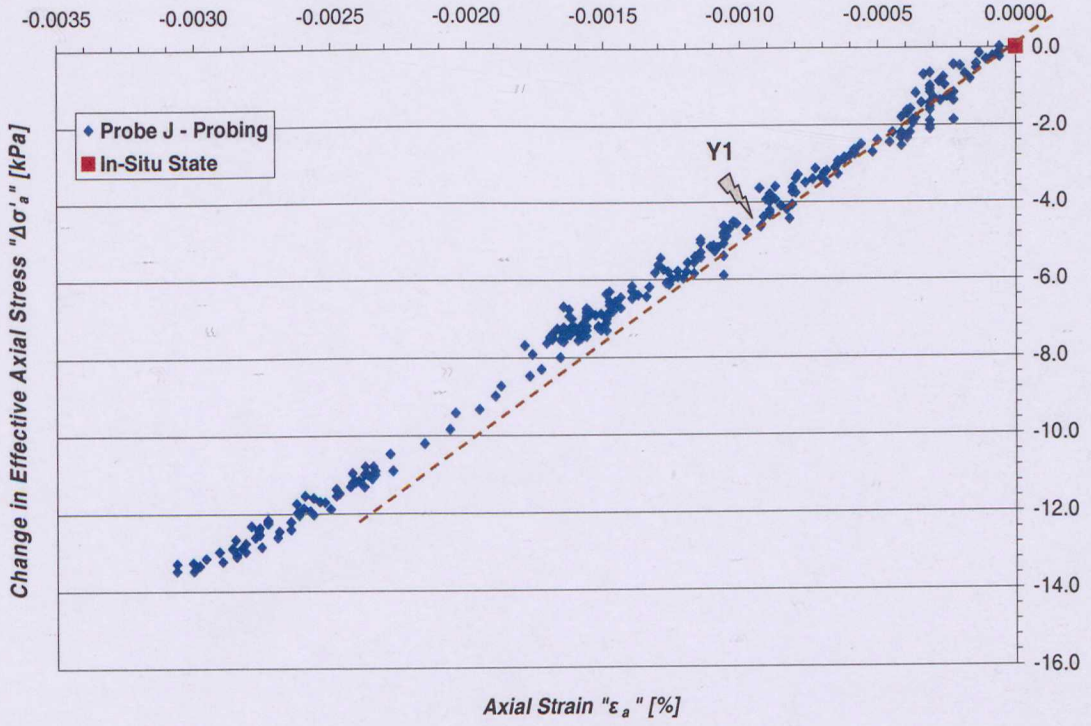


*Figure 6-44 Y1 location for probe J*

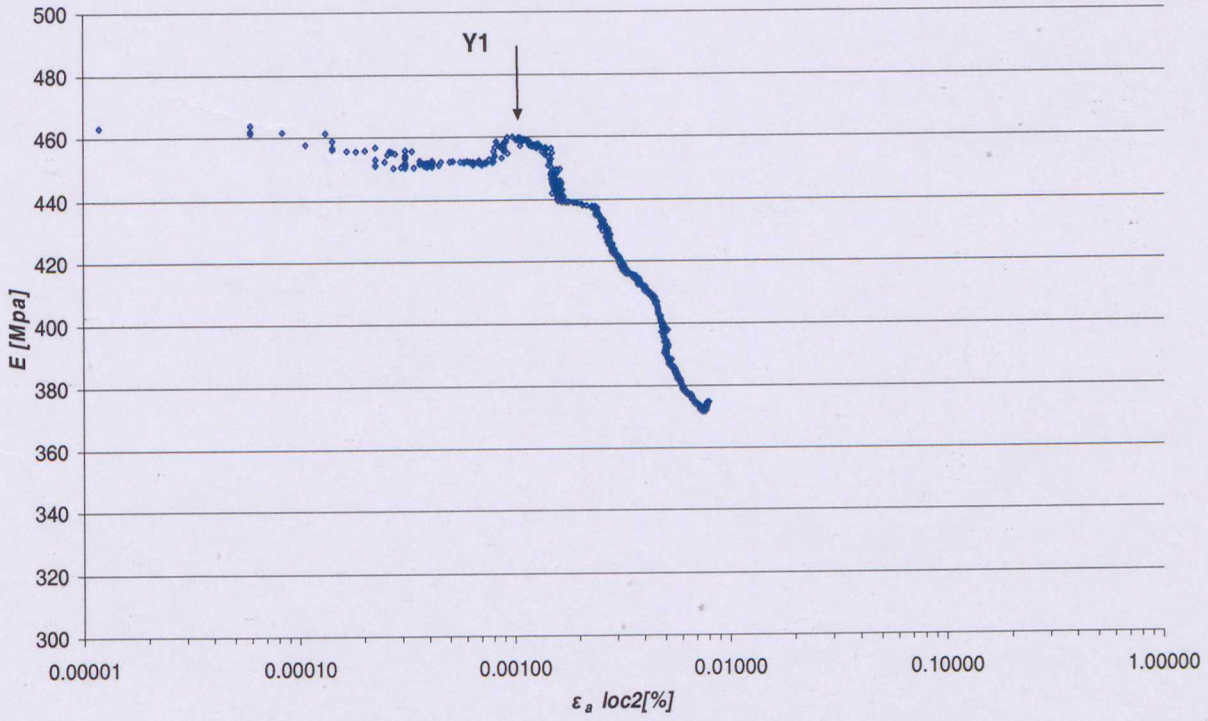


*Figure 6-45 Y1 location for probe J–Vertical Young's Modulus calculation*

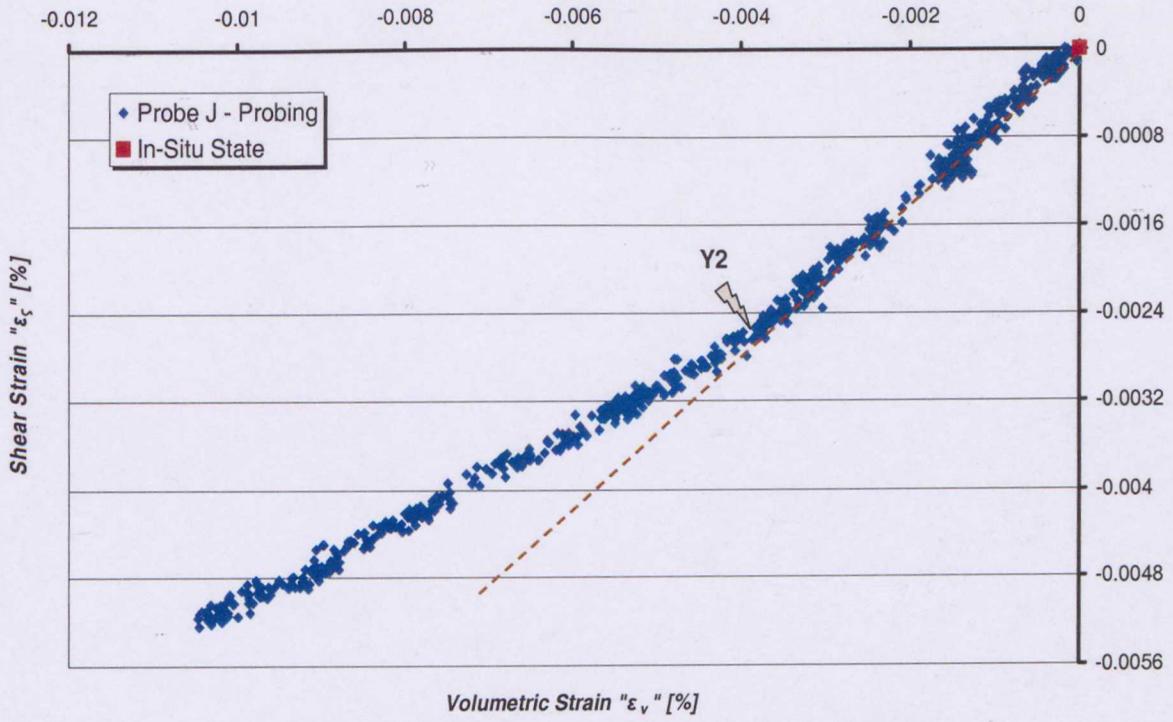


*Figure 6-46 Y2 location for probe J*

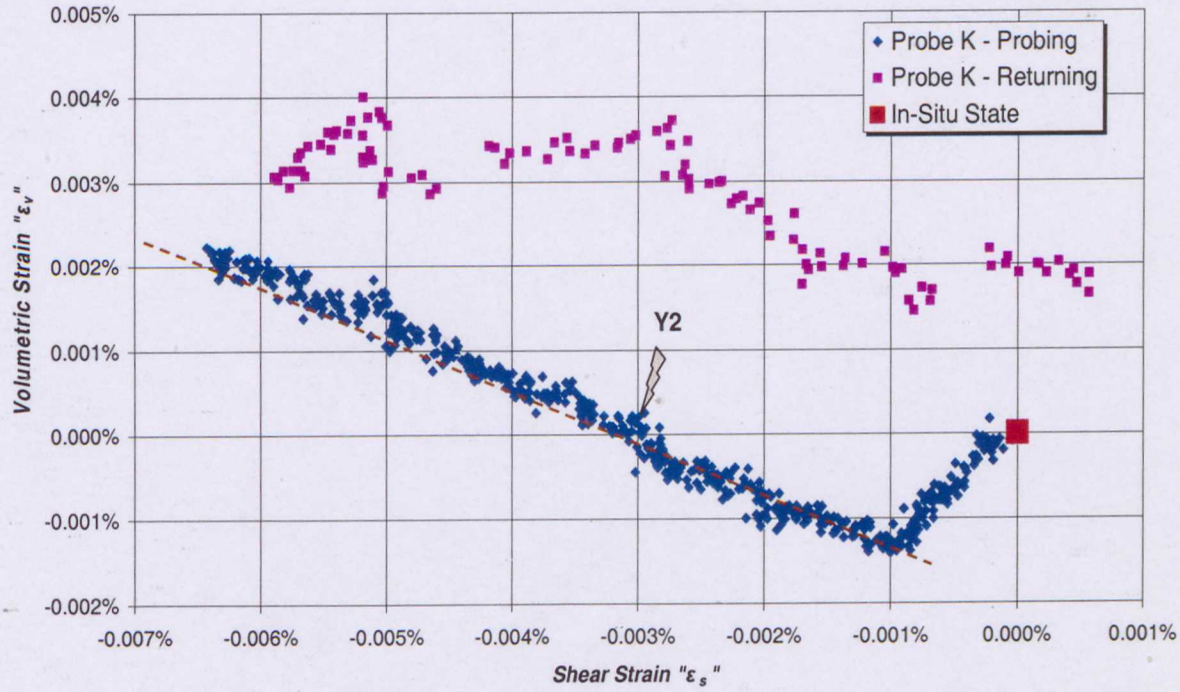


*Figure 6-47 Y2 location for probe K*

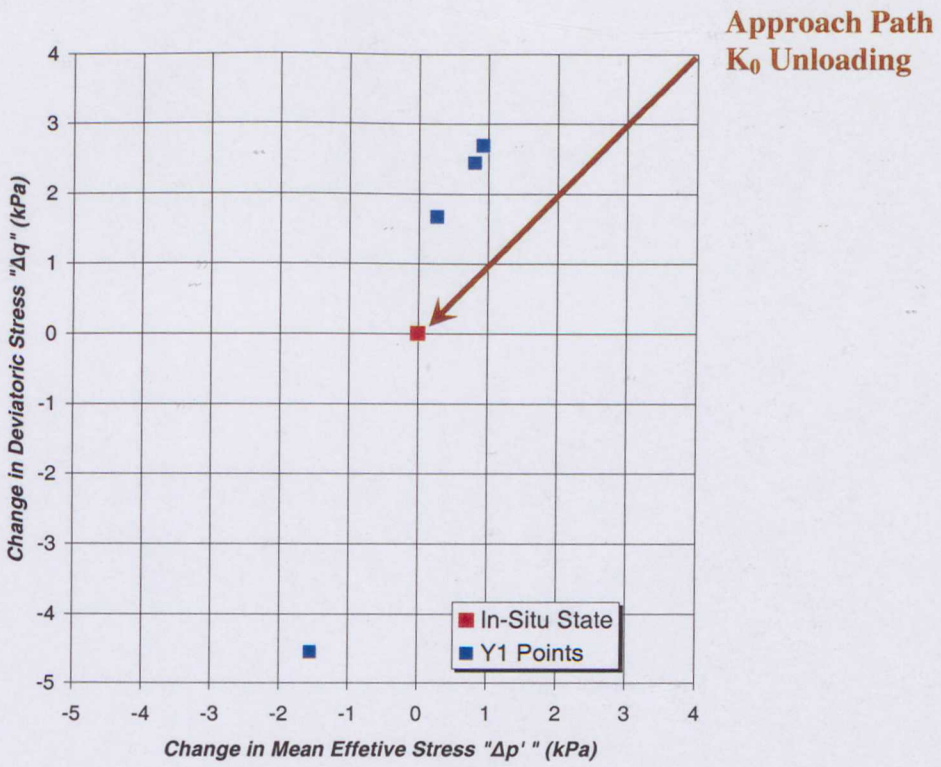


***Figure 6-48*** *Location of all Y1 points on stress-space*

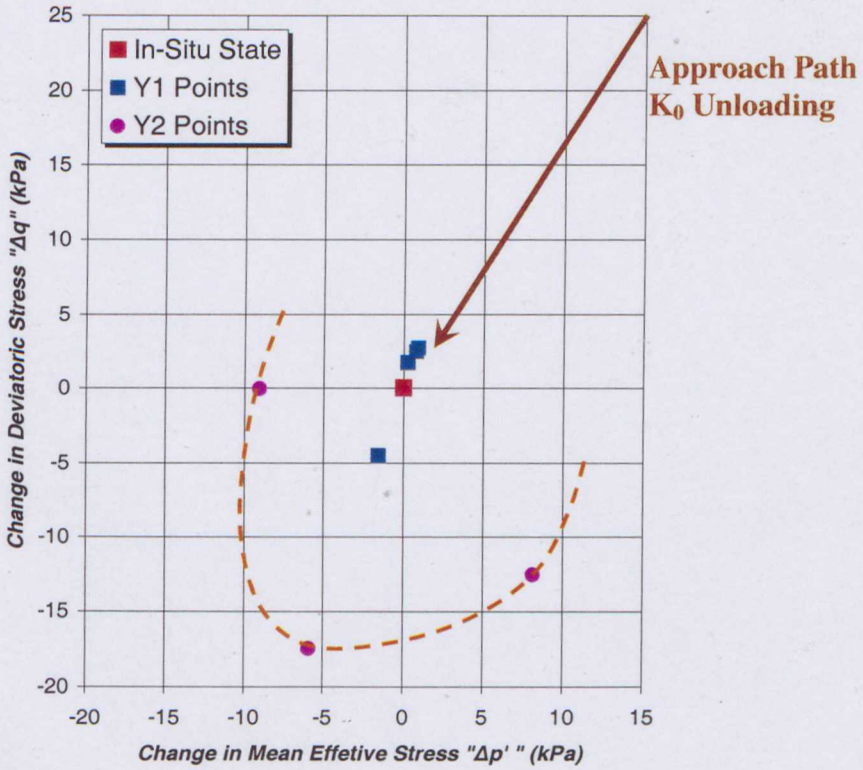


***Figure 6-49*** *Location of all Y1 & Y2 pSoints on stress-space*

7 SUMMARY, CONCLUSIONS & FURTHER RESEARCH ..... 268

7.1 Summary & Conclusions ..... 268

7.1.1 Silt Content effect ..... 268
7.1.2 Effect of structure ..... 269
7.1.3 Glauconite effect ..... 271
7.1.4 Influence of site location ..... 271
7.1.5 Anisotropy ..... 271
7.1.6 State parameter effect on stress-dilatancy ..... 273

7.2 Future Research ..... 273

# 7 SUMMARY, CONCLUSIONS & FURTHER RESEARCH

## 7.1 Summary & Conclusions

In this chapter, the influence of the dominant factors on both the small and large strain behaviour of Thanet sand are summarised and assessed, allowing a better overall understanding of how each of the factors affects the soil behaviour. Thanet sand based on its geophysical properties and experimental behaviour was sub-divided by ARUP Geothechnics into two sub-strata; the upper low silt content stratum and the lower high silt content stratum.

### 7.1.1 Silt Content effect

Starting with the isotropic compression behaviour, it has been shown that the silt content does indeed affect the behaviour of Thanet sand. From comparative tests presented in Section 5.2 it can be seen that high silt samples compress more than low silt samples taken to the same stress conditions.

When assessing how the amount of silt affects the critical state of the soil, two distinct Critical State Lines were found in v-lnp' space; one for the low silt and one for the high silt content Thanet sand. In terms of critical state stress ratios, it was shown that both the high silt and low silt content strata gave the same final stress ratio of M=1.3. In q-p' space this corresponds to one unique critical state line, as presented in Figure 5-14.

In terms of stress: strain behaviour during shearing, the low silt content samples reach higher stress-ratios during the test while still giving the same stress-ratio as the high silt content samples at the end of shearing (critical state). Additionally, the low silt

content samples give smaller volumetric strains during shearing compared with high silt content samples when sheared at the same initial effective confining stress. In terms of stress-dilatancy, both high as well as low silt content samples showed no difference in behaviour, giving a similar linear trends at higher stress-ratios. Therefore, much of the differences in peaks, stress-strain and volumetric-strain behaviour between the two is a result of the different states for the two strata at a given e and p' due to their different CSLs.

Finally, based on the two pairs of experiments that were compared, the amount of silt did not appear to have an impact on the elastic shear modulus. However, the equivalent shear moduli plots for all experiments sheared in compression at 0.01% $\varepsilon_s$ and 0.1% $\varepsilon_s$ (Figure 6-28 and Figure 6-30 respectively), revealed the low silt content sand samples to give slightly higher stiffnesses than the high silt content samples.

Therefore, it is clear that the behaviour of Thanet sand is indeed affected to a significant extent by the amount of silt contained within the sample tested and hence between the two sub-strata that have been identified.

### *7.1.2 Effect of structure*

Looking at the comparisons performed to examine the effect on the isotropic compression behaviour of the soil, as shown in Section 5.2, it can be seen that that when compressing an intact sample, there is a smaller volumetric strain than for a reconstituted sample.

For the critical state of the soil, no apparent difference could be detected, based on whether the sample sheared was either intact or reconstituted. In v-lnp' space no pattern arose and in q-p' space, all experiments lay on the same linear trend (Figure 5-16), with a critical state stress ratio of M=1.3. Structure was not expected to have any effect on the critical state of Thanet sand, as any form of structure within the soil would have been destroyed by the large distortions and particle rearrangements that take place during shearing till large strains.

When examining the shearing behaviour of the soil, the intact samples have been shown to give higher peak stress-ratios during the test while at the end giving the same stress-ratio as the reconstituted samples. Additionally, the reconstituted samples did generate higher volumetric strains during shearing compared to the intact samples tested. Considering that both intact and reconstituted samples have been shown to have the same CSL, these higher volumetric strains must be caused by the higher initial specific volumes of the reconstituted samples upon setup, compared to the intact samples (and therefore larger $\psi$ when compared to the location of the CSL). In general, the intact samples appeared to be slightly stiffer than the reconstituted samples at larger strains, as seen in Figure 5-58 and Figure 5-61.

For the stress-dilatancy plots, both intact as well as reconstituted tests form a unique straight line with a y-axis intercept equal to the critical state stress ratio of M=1.3, although the data were found to be quite scattered. However, no correlation between the state parameter and the stress:dilatancy relationship was found.

The equivalent monotonic shear moduli ($G_{EQ}$) comparisons that were described in Section 6.3.3 did not shed any light in the initial condition of the sample tested affects the stiffness characteristics of the soil. This was due to the higher initial void ratios that the reconstituted samples were set up at. When examining Figure 6-34, Figure 6-36 & Figure 6-37, the intact samples appear to have higher stiffnesses, compared with the reconstituted samples tested. It is however unclear to what extent this is due to the lower specific volume of the intact samples tested and to what extent it is a manifestation of the soil's structure on the shearing behaviour. Thetrends of $G_{EQ}$ with p' did however indicate a small effect of structure at small strain levels.

Unlike monotonic shear moduli, when examining the effect of structure on dynamic shear moduli ($G_0$) it was possible to see two distinct trends, one for intact and one for reconstituted material. The structure within Thanet sand is believed to have caused the offset between the two trends, as shown in Figure 6-5.

Finally, a manifestation of structure was seen when looking at the normalised stress path data for all experiments when grouped based on sample type (Figure 5-50 and

Figure 5-52), where the paths for intact samples are steeper and form sharper corners compared to the paths for to reconstituted samples

Thanet sand is therefore an interesting example of a sand that is showing effects of structure in its behaviour without though having traces of either cementation or locked fabric when closely examined under a microscope (Figure 4-15 & Figure 4-16).

### *7.1.3 Glauconite effect*

Glauconite was shown not to have a distinguishable impact on the behaviour of Thanet sand. When compared with a high silt content reconstituted sample with the same grading, the glauconite-free sample did not show any differences in either large or small strain behaviour.

### *7.1.4 Influence of site location*

The effect of the specific location a tested sample came from was examined in Sections 5.3 and 5.4.5. Because of the variation of other factors apart from the location of origin of each tested sample, such as silt content, effective confinement and initial void ratio upon setup, it was not possible for any clear patterns to be seen. Therefore, with the exception of the location of the CSL in v-lnp' where it was found that site location does not have a direct effect, it is not possible for any hard conclusions to be drawn regarding the effect of site on other aspects of the behaviour of Thanet sand such as stiffness and stress:strain behaviour.

### *7.1.5 Anisotropy*

As was seen in Section 5.6, the two horizontal samples gave very similar behaviour in terms of stress-strain behaviour for the drained compression experiments as well as stress paths for the undrained compression experiments. The vertical direction on the other hand gives a distinctly different behaviour compared with the two horizontal

directions in terms of peak stress-ratio and phase transformation point (Figure 2-58). At large strains, as the samples approach critical states, all the compression tests give a unique stress ratio of approximately 1.3 that corresponds to an angle of shearing resistance of about $32.3^0$.

Considering the two extension tests performed, due to sample necking the final stress-ratio at critical state could not be determined accurately. The $q/p':\varepsilon_a$ plot reached a plateau with peak stress ratio of 0.85 for both vertical and horizontal samples (Section 5.6.3). This corresponds to a peak angle of shearing resistance of $29^0$. It is possible that had necking not occurred a higher critical state $\varphi'$ might have been observed.

The effect of the intermediate stress factor "b" can be assessed by comparing a vertical sample sheared in triaxial compression ($\alpha=0$ & $b=0$) with a horizontal sample sheared in triaxial extension ($\alpha=0$ & $b=1$) (Figure 2-58). The two experiments give different angles of shearing resistance, with the sample sheared in compression giving higher values. In other words, $b = 0$ gives a higher $\phi'$ than $b = 1$.

When comparing a vertically cut with a horizontally cut sample sheared in drained compression (Figure 5-58) it can be seen that the vertical sample gives a higher peak stress ratio and therefore higher angle of shearing resistance than the horizontal. At critical state though, both samples give the same stress ratio of 1.3. Therefore, "$\alpha$" has an effect on the peak angle of shearing resistance but no effect on the critical state angle of shearing resistance with $\alpha=0$ giving higher values of $\phi'_{peak}$ compared to $\alpha=90^0$.

When looking at the small strain behaviour of the soil, the horizontal direction can be seen to produce higher equivalent monotonic shear moduli than the vertical direction. The high degree of soil anisotropy is also supported by the bender element readings that were taken from the 200mm by 100mm sample for both directions ($G_{HV}$ & $G_{HH}$), as shown in Section 6.2, that gave values of dynamic stiffness of 162MPa and 303MPa respectively.

When assessing all the results obtained, Thanet sand can be characterised as cross-anisotropic. As has been shown, the anisotropy of the soil does clearly affect its behaviour at small strains. As the shearing progresses, the initial particle structure is destroyed and its effect gradually diminishes, giving similar critical state behaviour for all samples sheared in either compression or extension, regardless of their initial orientation.

### *7.1.6 State parameter effect on stress-dilatancy*

Finally, for the stress-dilatancy of Thanet sand, all experiments presented in Figure 5-40 lie on a similar linear trend at higher stress ratios. Although there is some scatter within the plot, it is clear that there is no correlation between the location of the relationship and stress level, initial void ratio at the start of shearing ($e_s$), or state parameter. Therefore, stress-dilatancy models such as that suggested by Yang and Li (2004), as mentioned in Section 2.3.1, that consider a state dependant behaviour (Figure 2-24 & Figure 2-25) clearly do not apply to Thanet sand.

## *7.2 Future Research*

Two distinct sources of intact samples were available for this project. Samples from Moore House, Millennium Tower and River Side were extracted using rotary coring whereas, from the CTRL site at Stratford the block sampling method was used. To correctly asses what the effect of sampling method is, a cored sample and a block sample should be extracted from the same site and depth. This would allow a direct comparison of how truly "intact" the samples produced from these two methods really are, considering that unlike rotary coring, when extracting a block, one can limit to an absolute minimum the vibrations and strains on the soil prior to extraction and therefore the potential soil disturbance and structure degradation.

Towards the end of the project, a series of high pressure odometers were performed on reconstituted Thanet sand samples of both high as well as low silt contents (Figure

7-1). The aim of these tests was to derive the $K_0$ Normal Compression Line at higher confining pressures for Thanet sand. Based on the theory and what was found for other sands, as presented in Chapter 2, the Normal Compression Line should be a unique line that lies parallel to the Critical State Line. In the case of Thanet sand though, the unique $K_0$ NCL was not found. Instead, a series of parallel lines is formed at higher pressures. This type of behaviour has only been seen until now for silty clays, which are considered transitional soils (Martins et al.,2002). Transitional soils are soils that range between plastic clays and clean sands. Research on the compression behaviour of transitional soils has only very recently commenced as the general compression theory that has been verified for either clean sands or plastic clays was widely considered to be valid for all soils. It has been found that for transitional soils, the uniqueness of the NCL and CSL does not apply. It is rather unexpected that Thanet sand falls under this category as it is, after all, a predominatly quartzitic sand. Also, as shown in Figure 7-1, even the low silt content Thanet sand with a fines content that does not exceed 15% fails to reach a unique NCL. Considering that the specific volumes reached at maximum applied stresses tend towards the minimum theoretically achievable specific volume of one and any NCL must curve towards the horizontal as the pressures are increased pass about 40MPa - 50MPa (Figure 2-11), reaching a unique NCL by further increasing the pressures seems to be highly unlikely.

By analogy, if it is possible that if instead of a unique NCL a series of NCLs can be found, the same may apply for the CSL of Thanet sand. Ferreira et al. (to be published in 2006 in *Geotechnique*) have shown for a residual soil that reconstituted samples set up at different initial e values have different CSLs. This did not apply to the natural soil as this had only one initial e. the same may be true for Thanet sand, but to verify this, a much larger series of experiments would be needed; these experiments should not only have a wide range of confining pressures for the CSL to be defined, but would also require a variation of the initial specific volume samples would be set at that could in turn lead to the determination of the potential series of CSLs.

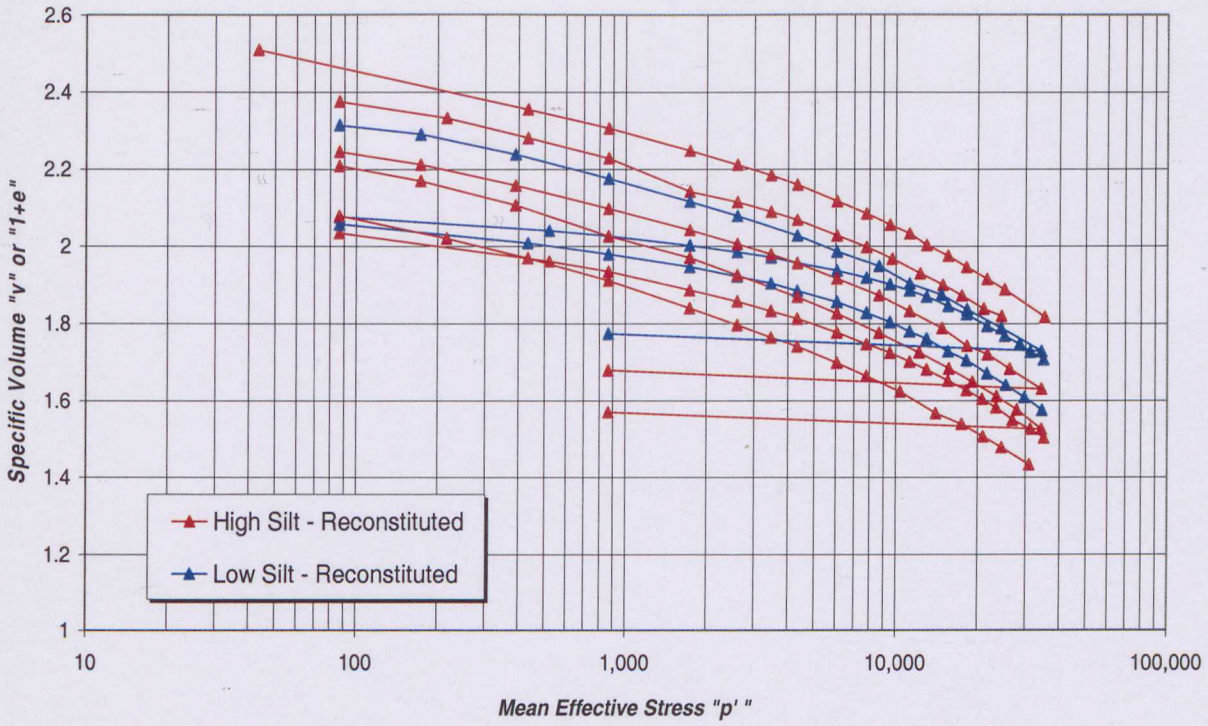


***Figure 7-1*** *High pressure odometer tests – silt comparison*

# REFERENCES

Arthur, J. R. F. & Menzies, B. K. (1972). Inherent anisotropy in a sand. *Geotechnique, 22, No. 1, 115-128.*

Arthur, J. R. F., Chua, K. S. & Dunstan, T. (1977). Induced anisotropy in a sand. *Geotechnique, 27, No. 1, 13-30.*

Barton, M. E. & Palmer S. N. (1989). The relative density of geologically aged, British fine and fine-medium sands. *Scottish Academic Press, Geological Society of London. Edinburgh, UK.*

Been, K. & Jefferies, M. G. (1985). A state parameter for sands. *Geotechnique, 35, No. 2, 99-112.*

Been, K., Jefferies, M. G. & Hachey, J. (1991). The critical state of sands. *Geotechnique, 41, No. 3, 365-381.*

Been, K., Jefferies, M. G., Crooks, J. H. A. & Rothenburg, L. (1987). The cone penetration test in sands : Part 2, general influence of state. *Geotechnique, 37, No. 3, 285-299.*

Bishop, A. W. & Wesley, L. D. (1975). A hydraulic apparatus for controlled stress path testing. *Geotechnique, 25, No. 4, 657-670*

Burland, J. B., Jardine, R. J. & Symes, M. J. (1984). The measurement of soil stiffness in the triaxial apparatus. *Geotechnique, 34, No. 3, 323-340*

Casagrande, A. & Carrillo, N. (1944). Shear failure on anisotropic materials. *Proc. Boston. Soc. Of Civil Engineers. Vol. 31, pp. 74-87.*

Chandler, H. W. (1985). A plasticity theory without Drucker's postulate, suitable for granular materials. *J. Mech Phys Of Solids, 33, 215-226.*

Coop, M. R. (1990). The mechanics of uncemented carbonate sands. *Geotechnique, 40, No. 4, 607-626.*

Coop, M. R. (1997). London Millennium tower. Bender element and high pressure tests on intact samples. *Geotechnical Engineering Research centre, Department of Civil Engineering - City University. Report Number GE/97/03*

Coop, M. R. (1999). The influence of particle breakage and state on the behaviour of sands. *International workshop on soil crushability, IWSC '99, Japan.*

Coop, M. R. (2003). On the mechanics of reconstituted and natural sands. *Keynote Lecture, in "Deformation Characteristics of Geomaterials", Di Benedetto, H.,*

*Doanh, T., Geoffroy, H. & Saueat, C. eds, Swets and Zeitlinger, Kisse, 2003, Vol.2, 29-58.*

Coop, M. R. & Atkinson, J. H. (1993). The mechanics of cemented carbonate sands. *Geotechnique, 43, No. 1, 53-67.*

Coop M. R. & Lee, I. K. (1993). The influence of pore water on the mechanics of granular soils. *Proc. 11th ECSMFE, Copenhagen, Danish Geotechnical Society, 1.63-1.72*

Coop, M.R. & Willson, S.M. (2003) On the Behavior of Hydrocarbon Reservoir Sands and Sandstones. *J. Geotech. Engng, ASCE, Vol.129, No.11, 1010-1019.*

Coop, M. R., Sorensen, K. K., Bodas Freitas, T. & Georgoutsos, G. (2004). Particle breakage during shearing of a carbonate sand. *Geotechnique 54, No. 3, 157-163.*

Cresswell, A. & Powrie, W. (2004). Triaxial tests on an unbonded locked sand. *Geotechnique 54, No. 2, 107-115.*

Cuccovillo, T. & Coop, M. R. (1997). The measurement of local axial strains in triaxial tests using LVDTs. *Geotechnique 47, No. 1, 167-171.*

Cuccovillo, T. & Coop, M. R. (1997). Yielding and pre-failure deformation of structured sands. *Geotechnique 47, No. 3, 491-508.*

Cuccovillo, T. & Coop, M. R. (1999). On the mechanics of structured sands. *Geotechnique 49, No. 6, 741-760.*

Dano, C. & Hitcher, P-Y. (2003). Behaviour of uncemented sands and grouted sands before peak strength. *Soils and Foundations, Japanese Geotechnical Society, Vol. 43, No. 4, 13-19.*

Desrues, J., Chambon, R., Mokni, M. and Mazerolle, F. (1996). Void ratio evolution inside shear bands in triaxial specimens studied by computed tomography. *Geotechnique, 46, No. 3, 529-546.*

Fleming W. G. K., (1992). A new method for single pile settlement prediction and analysis. *Geotechnique, 42, No. 3, 441-425.*

Fukumoto, T. (1992). Particle breakage characteristics of granular soils. *Soils and Foundations, Japanese Geotechnical Society, Vol. 32, No. 1, 26-40.*

Gasparre, L (2005). Advanced laboratory characterisation of London clay. *PhD Dissertation, Imperial College London*

Hardin, B. O. (1985). Crushing of soil particles. *J. Geotech Engng, ASCE, Pages 1177-1192*

Head, K. H. (1985). Manual of Soil Laboratory Testing Vol 3. Pentech Press, London

Hight, D. W. (1983). Laboratory investigations of sea bed clays. *PhD Dissertation, Imperial College London*

Jardine, R. J. (1992). Some observations on the kinematic nature of soil stiffness. *Soils and foundations, Japanese Geotechnical society, Vol. 32, No. 2, 111-124.*

Jovicic, V (1997). The measurement and interpretation of small strain stiffness of soils. *PhD Dissertation, City University, London*

Jovicic, V. & Coop, M. R. (1997). Pre-failure deformation behaviour of geomaterials. *Geotechnique 47, No. 3, 545-561.*

Klotz, E. U. (2000). The influence of state on the capacity of driven piles in sands. *Doctoral Dissertation, City University, London*

Klotz, E. U. & Coop, M. R. (2001). An investigation of the effect of soil state on the capacity of driven piles in sands. *Geotechnique 51, No. 9, 733-751.*

Klotz, E. U. & Coop, M. R. (2002). On the identification of critical state lines for sands. *Geotechnical testing journal, Sept. 2002, Vol. 25, No. 3.*

Konrad, J. M. (1988). Interpretation of flat plate dilatometer tests in sands in terms of the state parameter. *Geotechnique 38, No. 2, 263-277.*

Kuwano, R. (1999). The stiffness and yielding anisotropy of sand. *PhD Dissertation, Imperial College London*

Lee, K. L. & Seed, H. B. (1967). Drained strength characteristics of sands. *Proceedings of the American Society of Civil Engineers. 93; SM6, Pages 117-141.*

Martins, B. F., Bressani, L. A., Coop, M. R. & Bica, V. D (2002). Some aspects of the compressibility behaviour of a clayey sand. *Canadian Geotechnical Journal, 38, No. 6, pp 1177-1186.*

McDowell, G. R. & Bolton, M. D. (1998). On the micromechanics of crushable aggregates. *Geotechnique 48, No. 5, 667-679.*

Mimura, M. (2003). Characteristics of some Japanese natural sands – data from undisturbed frozen samples. *Disaster Prevention Research Institute of Kyoto University, Japan.*

Nakata, Y., Hyodo, M., Hyde, A. F. L., Kato Y. & Murata H. (2001). Microscopic particle crushing of sand subjected to high pressure one-dimensional compression. *Soils and Foundations, Japanese Geotechnical Society, Vol. 41, No. 1, 69-82.*

Nicholson, D., Chapman, T. & Morrison P. (2002). Pressuremeter proves its worth in London's Docklands. *Ground Engineering, March pages 32-34.*

Oda, M (1972). Initial fabrics and their relations to the mechanical properties of granular materials. *Soils and Foundations, Japanese Geotechnical Society, Vol. 12, No.4, pp45-63.*

Pascal D. (2002). Personal communication

Qadimi, A. (2005). The cyclic response of a carbonate sand through critical state soil mechanics. *PhD Dissertation, Imperial College London*

Rolo, R. (2003). The anisotropic stress-strain-strength behaviour of brittle sediments. *PhD Dissertation, Imperial College London*

Symes, M.J. (1983). Rotation of principal stresses in sands. *PhD Dissertation, Imperial College London.*

Takei, M. (2001). Time-dependent behaviour of geomaterials due to particle crushing. *Doctoral Dissertation, Tokyo Institute of Technology*

Verdugo, R., Ishihara, K. (1996). The steady state of sandy soils. *Soils and Foundations, Japanese Geotechnical Society, Vol. 36, No. 2, 81-91.*

Viggiani, G. & Atkinson, J. H. (1995). Interpretation of bender element tests. *Geotechnique 45, No. 1, 149-154.*

Yang, J., Li & X. S. (2004). State-dependent strength of sands from the perspective of unified modelling. *Journal of Geotechnical and Geoenvironmental Engineering, ASCE 1090-0241 page 186-198.*